REPORT DOCUMENTATION PAGE

Form Approved
OMB No. 0704-0188

Public reporting burden for this collection of information is estimated to average 1 hour per response, including the time for reviewing instructions, searching existing data sources, gathering and maintaining the data needed, and completing and reviewing this collection of information. Send comments regarding this burden estimate or any other aspect of this collection of information, including suggestions for reducing this burden to Department of Defense, Washington Headquarters Services, Directorate for Information Operations and Reports (0704-0188), 1215 Jefferson Davis Highway, Suite 1204, Arlington, VA 22202-4302. Respondents should be aware that notwithstanding any other provision of law, no person shall be subject to any penalty for failing to comply with a collection of information if it does not display a currently valid OMB control number. **PLEASE DO NOT RETURN YOUR FORM TO THE ABOVE ADDRESS.**

1. REPORT DATE *(DD-MM-YYYY)*
08/01/2002

2. REPORT TYPE
Conference Proceedings

3. DATES COVERED *(From - To)*
01/05/2001 - 31/10/2001

4. TITLE AND SUBTITLE
Workshop on Quantum Transport in Semiconductors

5a. CONTRACT NUMBER

5b. GRANT NUMBER
N00014-01-1-0115

5c. PROGRAM ELEMENT NUMBER

6. AUTHOR(S)
Ferry, David K.

5d. PROJECT NUMBER

5e. TASK NUMBER

5f. WORK UNIT NUMBER

7. PERFORMING ORGANIZATION NAME(S) AND ADDRESS(ES)
Arizona Board of Regents for and on behalf of
Arizona State University
Office for Research and Sponsored Projects Administration
270 Administration B Wing
PO Box 873503
Tempe, AZ 85287-3503

8. PERFORMING ORGANIZATION REPORT NUMBER
DWD 2651/TE (ARO)
DWA 0052/TE (ONR)
DWD 2652/TE (NASA)

9. SPONSORING / MONITORING AGENCY NAME(S) AND ADDRESS(ES)
Army Research Office, Research Triangle Park NC 27709-2211
Office of Naval Research, Arlington VA 22217-5660
National Aeronautics and Space Administration, Moffett Field CA 94035-1000

10. SPONSOR/MONITOR'S ACRONYM(S)
ARO, ONR, NASA

11. SPONSOR/MONITOR'S REPORT NUMBER(S)

12. DISTRIBUTION / AVAILABILITY STATEMENT
Approved for public release

13. SUPPLEMENTARY NOTES

14. ABSTRACT
A workshop was held on the topic of quantum transport in semiconductor devices. This workshop brought together 17 lecturers and 35 other attendees for this purpose.

20020405 085

15. SUBJECT TERMS
Semiconductor devices, transport, quantum mechanics

16. SECURITY CLASSIFICATION OF:			17. LIMITATION OF ABSTRACT	18. NUMBER OF PAGES	19a. NAME OF RESPONSIBLE PERSON
a. REPORT	b. ABSTRACT	c. THIS PAGE			David K. Ferry
Unclassified	Unclassified	Unclassified	None	256 plus CD	19b. TELEPHONE NUMBER *(include area code)* 480.965.2570

Advanced Research Workshop on Quantum Transport in Semiconductors

Hotel Villa del Mare, Maratea, Italy 17-22 June 2001

Session 1

Moderator: John Barker, Glasgow University, "Status of the physics and modeling of ultrasmall devices"

- 1A Greg Timp, University of Illinois, "Making small MOSFETs: ballistic and quantum effects"
- 1B Max Fischetti, IBM Research, "Modeling small MOSFETs-the role of quantum and many-body effects"
- 1C Steve Goodnick, Arizona State University, "Full Band Structure Calculations for Transport in Wide-Band-Gap Semiconductors"

Session 2

Moderator: Max Fischetti, IBM Research, "Semi-classical modeling of small semiconductor devices"

- 2A Asen Asenov, Glasgow University, "Discrete impurities and quantum potentials in MOSFET modeling"
- 2B Richard Akis, Arizona State University, "Effective potentials for quantum effects in MOSFETs"

Session 3

Moderator: Antti-Pekka Jauho, Danish University of Technology, "Introduction to Quantum Transport"

- 3A David Ferry, Arizona State University, "Wave function approaches for self-consistent computations of transport in quantum dots and arrays"
- 3B John Barker, Glasgow University, "Trajectories in quantum mechanics"
- 3C Michael Bonitz, Rostock University, "Non-equilibrium Green's functions: transient phenomena and the role of the initial state for devices"

Session 4

Moderator: Chihiro Hamaguchi, Osaka University, "The Metal-Insulator Transition"

- 4A Günther Bauer, University of Linz, "The metal-insulator transition in $d = 2$"
- 4B Jonathan Bird, Arizona State University, "The metal-insulator transistion in open quantum dots and arrays"

Session 5

Moderator: Michael Bonitz, Rostock University, "Spins and few particle problems in Semiconductors"

- 5A David Awschalom, UC Santa Barbara, "Spin coherence and optical measurements"
- 5B Daniel Loss, University of Basel, "Quantum computing in semiconductor systems"
- 5C Sankar Das Sarma, University of Maryland, "Few electron (and few impurity) systems-small system effects"

Session 6

Moderator: Gerhard Klimeck, Jet Propulsion Laboratory, "Applications of quantum transport in devices"

- 6A Carlo Jacoboni, Modena University, "The Wigner function and quantum transport"
- 6B Harold Grubin, SRA, Inc., "Modeling resonant tunneling diodes with Wigner functions and density matrices"
- 6C Dejan Jovanovic, Motorola, "Non-equilibrium Green's functions for MOSFET modeling"

Session 7

Moderator: Karl Hess, University of Illinois, "Applications of quantum transport in optics"

- 7A Tilmann Kuhn, University of Münster, "Quantum kinetics and the femtosecond time scale in optical excitation of semiconductors"
- 7B Rolf Haug, University of Hannover, "Single-electron charging effects in quantum dot arrays"

Session 8

Moderator: Anant Anantram, NASA Ames, "Novel New Concepts"

- 8A Karl Hess, University of Illinois, "EPR Experiments: the Assumptions, and the Failure of Bell's Theorem"
- 8B Antti-Pekka Jauho, Danish University of Technology, "Scanning probe measurements of biomolecules on silicon surfaces"
- 8C Mark Lundstrom, Purdue, "The Landauer approach in device modeling"
- 8D Wolfgang Windl, Motorola, "Diffusion and clustering of impurities-a problem that cannot be ignored"

Poster Presentations

Poster Group 1

- 1-1 "Analytical theory for the low frequency transport and noise in Q1D conductors," G. Gomilla and L. Reggiani, Universidad Polytechnica Catalunya.
- 1-2 "Monte Carlo simulations of Wigner function tunneling: Role of the effective potential," L. Shifren and D. K. Ferry, Arizona State University.
- 1-3 "3D device Monte Carlo modeling with discrete impurities," S. Barraud, S. Galdin, P. Dollfus, Institut d'Electronique Fondamentale.
- 1-4 "3D modeling of imperfect interfaces and edges in decanano MOSFETs," S. Kaya, Ohio

University, and A. R. Brown, S. Roy, and A. Asenov, Glasgow University.

- 1-5 "Comparison of first-order quantum correction schemes in 3D drift-diffusion simulations in sub-0.1 micron MOSFETs," J. R. Watling, A. R. Brown, A. Asenov, and D. K. Ferry, Glasgow University.
- 1-6 "Quantum potential in the presence of heterointerfaces," J. R. Watling, R. C. W. Wilkins, and J. R. Barker, Glasgow University.
- 1-7 "Performance of scaled double delta doped PHEMTs," K. Kalna, J. R. Watling, A. Brown, and A. Asenov, Glasgow University.
- 1-8 "Electron transport and infrared photoconductivity in quantum dot structures," V. Ryzhii and V. Mitin, University of Aizu.
- 1-9 "Photoluminescence from hot electrons in low dimensional systems," H. Momose, Y. Inui, M. Itoh, and C. Hamaguchi, Osaka University.
- 1-10 "Nonlinear transport through an array of quantum dots," G. Kiesslich, A. Wacker, and E. Schöll, Technische Universität Berlin.

Poster Group 2

- 2-1 "Quantum algorithms in the frame of a coupled-quantum-wires physical system," S. Reggiani, A. Bertoni, R. Brunetti, and M. Rudan, University of Bologna.
- 2-2 "Quantum waves in the coupled-wire Qubit," J. Harris, R. Akis, and D. K. Ferry, Arizona State University.
- 2-3 "Quantum mechanical study of nanoscale MOSFET," A. Svizhenko, M. P. Anantram, and T. R. Govindam, NASA Ames Research Laboratory.
- 2-4 "Effects of lead population on magnetic flux controlled dissipative electron transport through coupled quantum dots," N. Horing, Stevens Institute of Technology.
- 2-5 "Transport in quantum dot arrays," N. Mori, Y. Takamura, T. Ishida, and C. Hamaguchi, Osaka University.
- 2-6 "Non-equilibrium transport in nanostructures," J. Fransson, University of Uppsala.
- 2-7 "Tunneling spectroscopy of exchange-correlation interaction of electrons in Schottky barrier in quantizing magnetic field," A. Shulman, Institute of Radioengineering and Electronics.
- 2-8 "Stochastic simulation of the Barker-Ferry equation," M. Nedjalkov, Technical University of Vienna.
- 2-9 "Simulation of entanglement in semiconductor quantum wires," A. Bertoni, R. Ionicioiu, P. Zanardi, F. Rossi, and C. Jacoboni, University of Modena.
- 2-10 "Mesoscopic fluctuations of Coulomb drag between quasi-ballistic 1D wires," N. A. Mortensen, K. Flensburg, and A.-P. Jauho, Danish Technical University.

Poster Group 3

- 3-1 "Spin dynamics in III-V quantum wells using Monte Carlo simulation," A. Bournel and P. Hesto, Universite Paris Sud.
- 3-2 "Electron-spin-phonon coupling and relaxation dynamics in a double quantum dot," V. Puller, L. Mourokh, and N. Horing, Stevens Institute of Technology.
- 3-3 "Quantum computing with spin qubits in semiconductors structures," V. Privman, Clarkson University.
- 3-4 "High-field transport through semiconductor heterostructures," M. Morifuji, Osaka University.
- 3-5 "Effect of electronic disorder on the phonon-drag," V. Mitin, Wayne State University.
- 3-6 "Wigner function dynamics in presence of an infinite potential barrier," P. Bordone and C. Jacoboni, Modena University.
- 3-7 "Quantum transport in 2D MOSFETs," A. P. Anantram, A. Svizhenko, and T. R. Govindan,

NASA Ames Research Center.

- 3-8 "Density-matrix modeling of terahertz photon-assisted tunneling in resonant tunneling diodes," M. Asada, Tokyo Insitute of Technology.
- 3-9 "Hyperfine interaction between nuclear and electronic spins," I. D. Vagner, Holon Academic Institute of Technology.
- 3-10 "Metal-insulator transition in 2D few-electron systems," A. Filinov, M. Bonitz, and Yu. Lozovik, University of Rostock.
- 3-11 "Quantum dot modeling using NEMO-3D," G. Klimeck, F. Oyafuso, R. C. Bowen, T. B. Boykin, T. A. Cwik, E. Huang, and E. Vinyard, Jet Propulsion Laboratory.

Advanced Research Workshop
on

Quantum Transport in Semiconductors

Introduction and Overview

John Barker
University of Glasgow

Hotel Villa del Mare, Maratea, Italy
17-22 June, 2001

Advanced Research Workshop
on

Quantum Transport in Semiconductors

Organisation

David Ferry
John Barker
Carlo Jacoboni
Hal Grubin, Lino Reggiani, Bernd Lassen

Advanced Research Workshop
on

Quantum Transport in Semiconductors

Our long-suffering sponsors

Office of Naval Research
US Army Research Office
NASA

Origins

1 Day Workshop on Quantum Transport Theory
(Glasgow, May 2000)

Present state of play in the field

Encourage new workers

Map out new opportunities

Flag new directions

Format

Gordon Conference Style

- Introductory/tutorial material
- Advanced Topics
- Pre-publication ethics

Sessions

- Moderator: overview and introduction (5-10 minutes)
- Speakers: 45 minutes (questions welcomed in talks)
- Questions & Discussion:10-15 minutes per lecture

Time Table

- Breakfast 8 00
- Morning session: 9 00-12 30 (coffee 11 10)
- Lunch 13 00
- Ad hoc sessions
- Poster session: 16 00-17 00
- Evening session: 1700-1930
- Dinner: 20 00

Wednesday

- 14 00
- Excursion: Monastery visit + shopping in Maratea
- Please sign up: Rosella Brunetti
- Dinner: 20 00

Session 1: Moday, June 18

Ultra-small devices

Status of Physics and Modelling of ultra-small devices

- Moderator: John Barker, University of Glasgow
- Greg Timp, University of Illinois
- Max Fischetti, IBM T J Watson Research Lab
- Steve Goodnick, Arizona State University

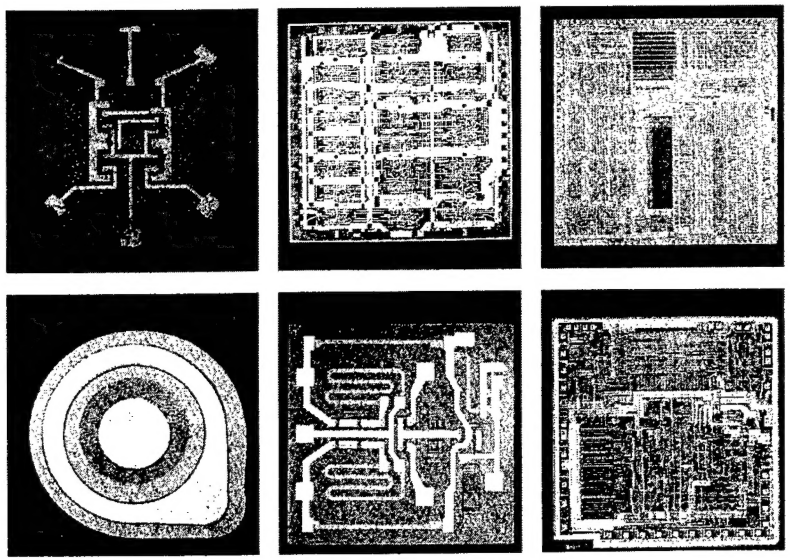

UNIVERSITY of GLASGOW

Status of the physics and modelling of ultra-small Semiconductor devices

John. R. Barker
Nanoelectronics Research Centre
Department of Electronics and Electrical Engineering
University of Glasgow

Advanced Research Workshop
on
Quantum Transport in Semiconductors

Moores Law

history
since
1970

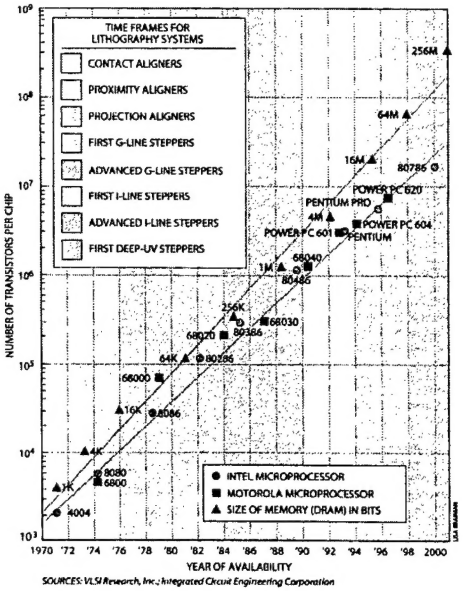

The dinosaur model: silicon will eventually become extinct

© J.R. Barker 2001
University of Michigan
This material is used with the author's permission
published without permission

.... due to impending catastrophe

© J.R. Barker 2001
University of Michigan
This material is used with the author's permission
published without permission

After the catastrophe, a long hiatus will occur and silicon's role will be replaced by new species : quantum, molecular…

QuickTime™ and a
Photo - JPEG decompressor
are needed to see this picture.

© J.R. Barker 2001
University of Michigan
This material is used with the author's permission
published without permission

Projected Breakdown of Moore's Law

1977

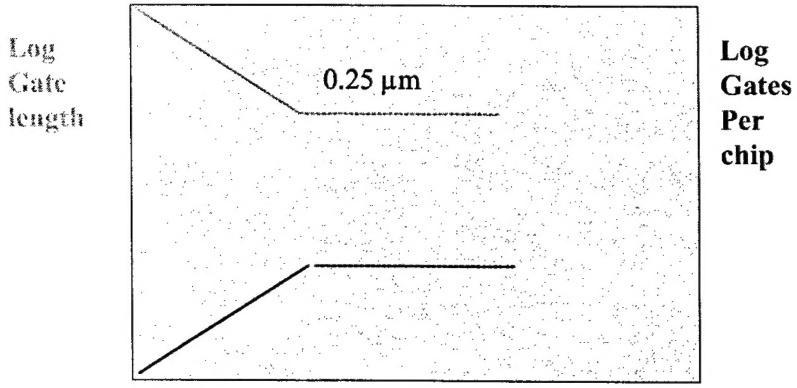

(challenged by JRB/DKF
In 1979- 25 nm)

© J.R. Barker 2001
University of Michigan
This material is used with the author's permission
published without permission

The guiding philosophy behind semiconductor quantum transport theory strategy has often been :

- Moore's empirical Law will eventually breakdown at small enough physical scales.
- Quantum effects will likely become dominant by then.
- Prepare for new devices based on novel quantum concepts:
  - discrete energy levels
  - wave interference devices
  - tunnel devices
  - single electronics
  - quantum computing…

The silicon MOSFET scene

Conventional device modelling:

Empirical
Drift Diffusion
Hydrodynamic
Monte Carlo

Self-consistent via Poisson equation

The first moves:

Ballistic transport
Serious
non-equilibrium effects

Schrödinger-Poisson
Quantum levels in
channel

Density gradient or
Quantum potential
Corrections
Tunnelling &
Keep charge away
from interfaces

What has actually happened

Year	1999	2001	2004	2008	2011	2014
MPU Gate Length *(nm)*	140	100	70			
Oxide thickness *(nm)*	1.9-2.5	1.5-1.9	1.2-1.5			
Drain extensions *(nm)*	42-70	30-50				

Solution exists
Solution Being Pursued
No Known Solutions

Scaling of MOSFETs to decanano dimensions

(International Roadmap for Semiconductors - 1999 Edition)

And very recently, the road map has speeded up by 5 years!!

Robert Chau (Intel) 2001

"High performance 30 nm gate length CMOS transistors operating at Vcc = 0.85 V demonstrated for 65 nm logic technology node, which will be ready for production in 2005."

Part of Intel Road Map:

Year	2001	2003	2005	2007	2009
Node	150	90	65	45	30
Gate Length	70	50	30	20	15

In production

Chau
Intel
2001

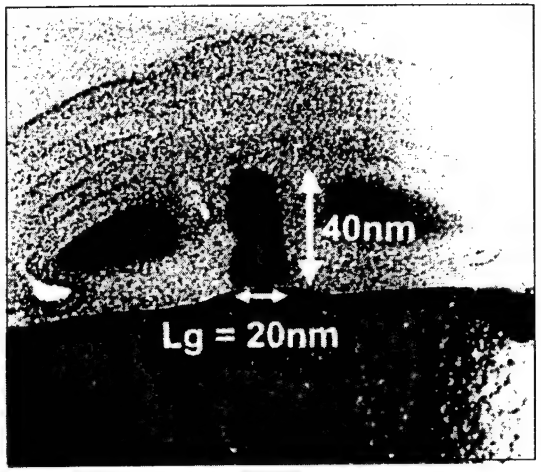

TEM Cross section of a 20 nm gate length NMOS transistor

Chau, Intel
2001

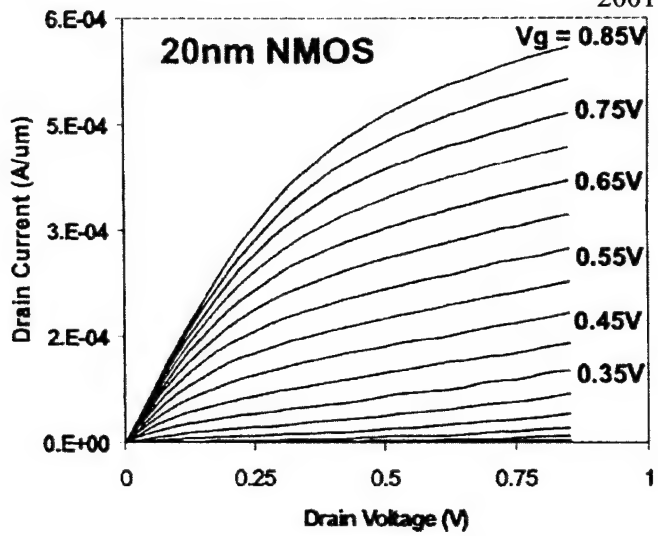

Single prototype MOSFETS devices have also been demonstrated with healthy I-V characteristics with gate lengths in 7-14 nm scales.

- **What quantum/many-body effects occur in these devices and how do we model them?**
- **What are the implications of the dinosaur refusing to die for quantum devices?**

Where is the limit and what QTT is needed if any?

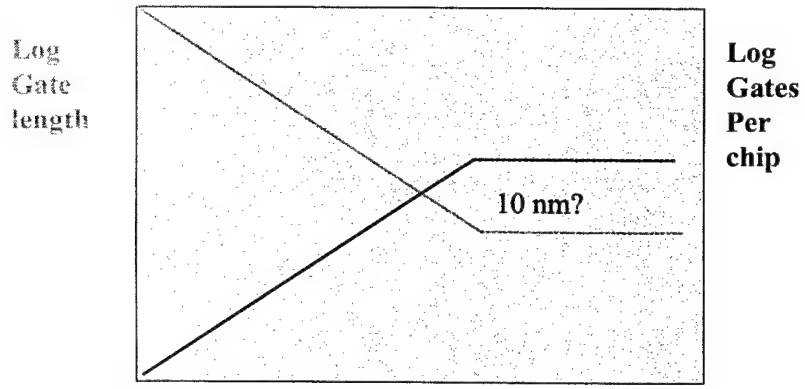

Certainly, below 50 nm we expect strong **atomistic effects**.
The predicted high carrier densities also suggest strong **many-body effects**: Coulombic, correlations/fluctuations.

But at what level do we need to move to a true atomistic model, and where does the need for computational **chemistry methods** come in?

These questions are addressed in today's sessions and the role of the fundamental theoretical frameworks that underpin true QTT and fully quantum devices are discussed later.

© J R Barker 2011
University of Glasgow
This work should not be reproduced or
published without permission

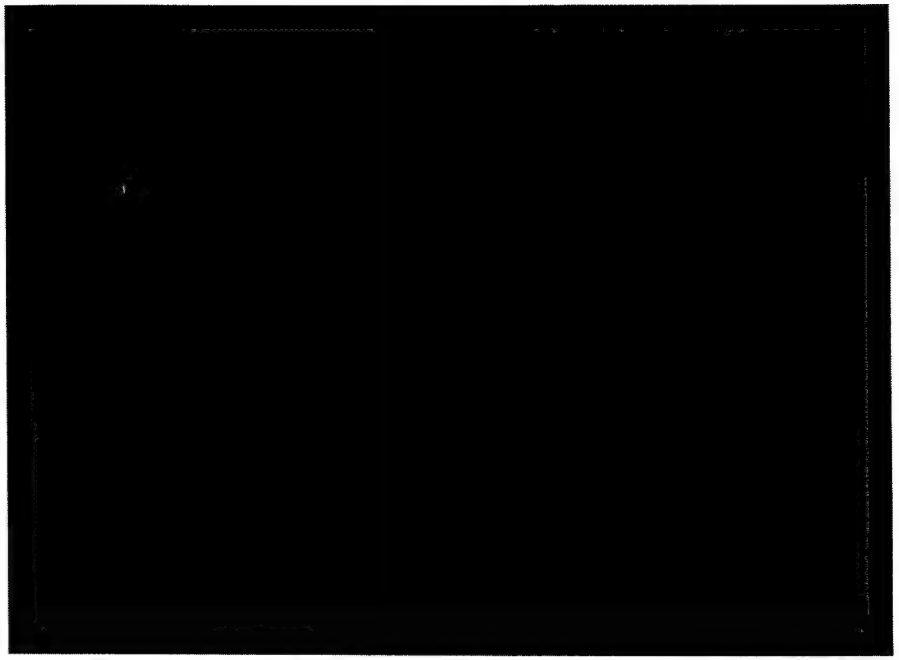

The Nano-transistor

J. Bude, F. Baumann‡, K. Evans-Lutterodt, A. Ghetti, S. Goodnick†, J. Grazul‡, M. Green, S. Hillenius,Y. Kim, J. Lyding+, W. Mansfield, D. Muller‡, T. Sorsch, K. Timp+, R. Timp+, J. Yu+.

Agere, Arizona State University†, Bell Laboratories, Lucent Technologies‡, University of Illinois+

G. Timp
University of Illinois

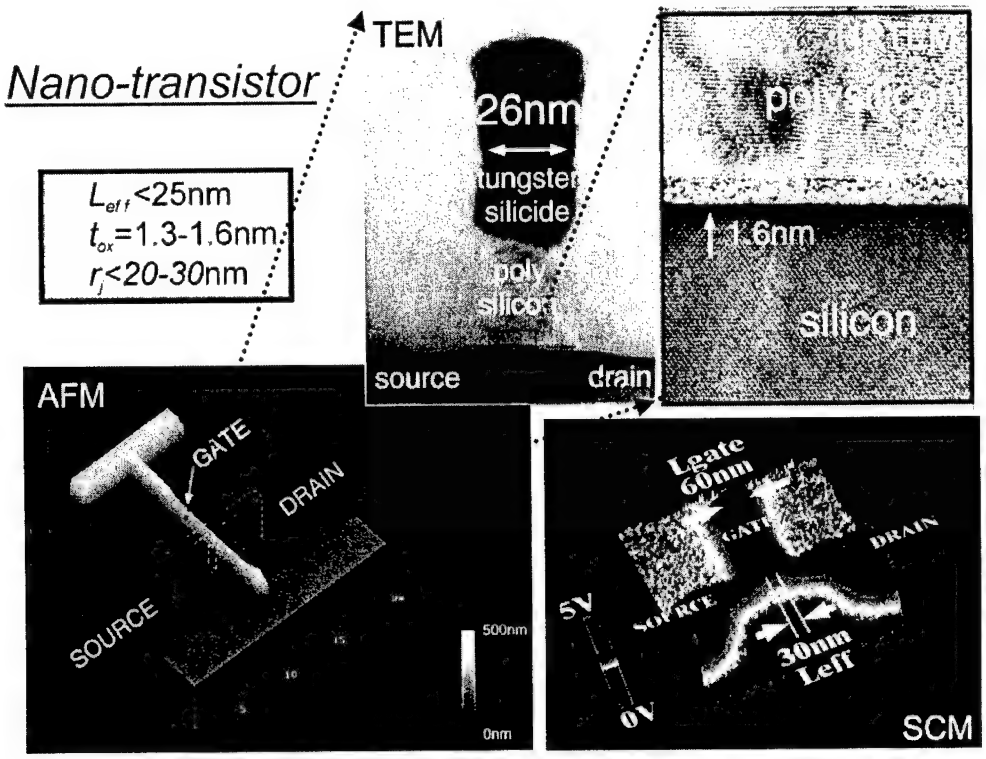
Nano-transistor
L_{eff}<25nm
t_{ox}=1.3-1.6nm
r_j<20-30nm
TEM
26nm
tungsten silicide
poly silicon
source
drain
1.6nm
silicon
AFM
GATE
DRAIN
SOURCE
500nm
0nm
Lgate 60nm
GATE
DRAIN
SOURCE
5V
0V
30nm Leff
SCM

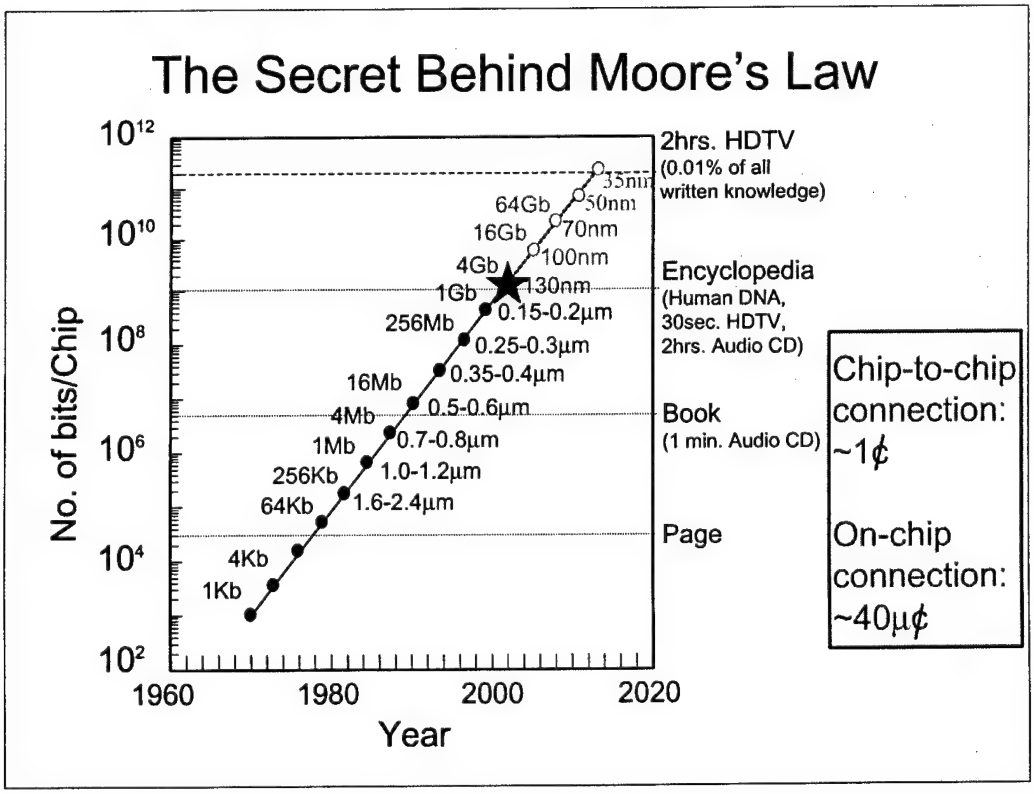
The Secret Behind Moore's Law
No. of bits/Chip
Year
10^{12}
10^{10}
10^{8}
10^{6}
10^{4}
10^{2}
1960
1980
2000
2020
1Kb
4Kb
64Kb
256Kb
1Mb
4Mb
16Mb
256Mb
1Gb
4Gb
16Gb
64Gb
1.6-2.4µm
1.0-1.2µm
0.7-0.8µm
0.5-0.6µm
0.35-0.4µm
0.25-0.3µm
0.15-0.2µm
130nm
100nm
70nm
50nm
35nm
2hrs. HDTV
(0.01% of all written knowledge)
Encyclopedia
(Human DNA, 30sec. HDTV, 2hrs. Audio CD)
Book
(1 min. Audio CD)
Page
Chip-to-chip connection: ~1¢
On-chip connection: ~40µ¢

2000 ITRS National Roadmap Projections

30nm research is targeted at a ~15 year horizon

Technology Generations

YEAR OF FIRST PRODUCT SHIPMENT	2001	2004	2008	2014
TECHNOLOGY GENERATIONS DENSE LINES (DRAM Half-Pitch) (nm)	130	90	60	30
Logic (High-Volume: MPU)				
Logic Transistors/chip (including SRAM)	67.3M	135M	539M	4.3B
Chip Frequency (GHz)				
On-chip local clock, high performance	2.1G	3.5G	7.1G	14.9G
TECHNOLOGY REQUIREMENTS				
Min. Logic Vdd(V) (desktop)	1.5	1.2	0.9	0.6
Nominal Ion (n/pMOS)@25C(mA/μm)	0.75/0.35		0.75/0.35	0.75/0.35
Nominal Ioff @25C (nA/μm)	5		80	160
tox equivalent (nm)	1.5-1.9		0.8-1.2	0.5-0.6
junction depth xj (nm)			16-26	8-13

Solutions exist — Solutions being pursued — No known solutions

*Drive current independent of technology

One of the Secrets Behind the Success of CMOS

Active Power Dissipation: $f_c C V_{DD}^2 \sim \eta V_{DD} I_{Dsat}$

Stand-by Power Dissipation: $V_{DD} I_{leakage}$

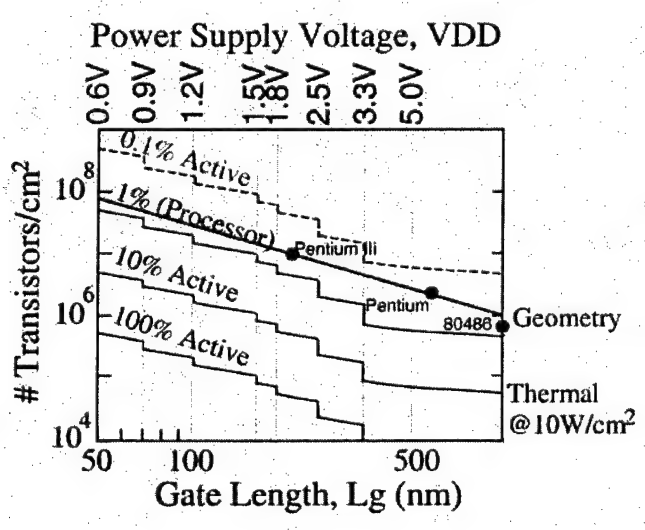

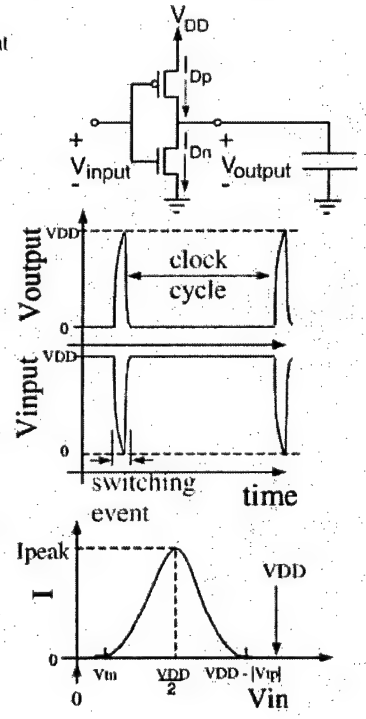

The Tyranny of Large Numbers

circuit margin M: $I_{D0}(1-M) < I_D < I_{D0}(1+M)$
process control: standard deviation $= \sigma\ I_{D0}$

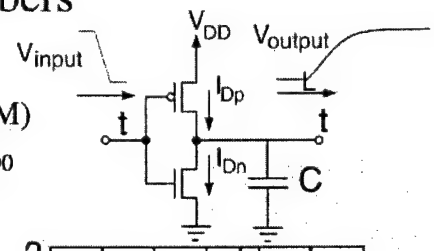

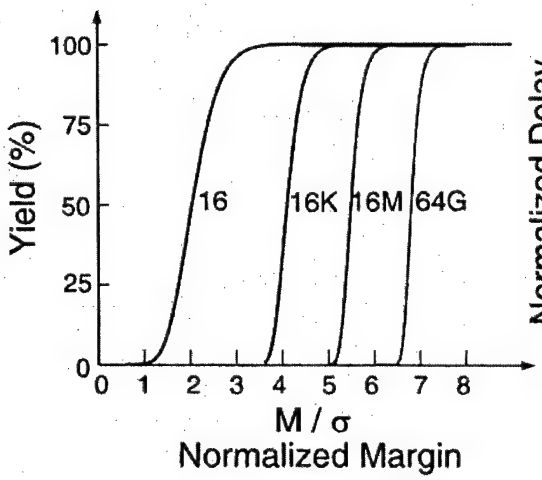

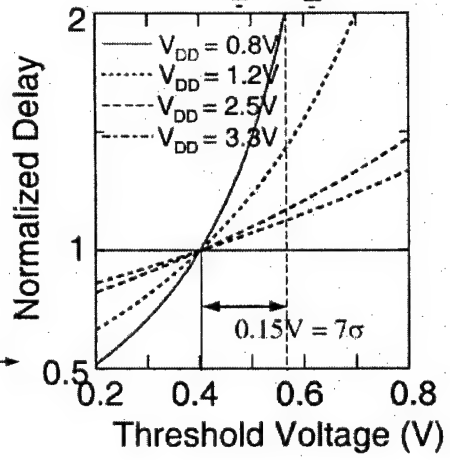

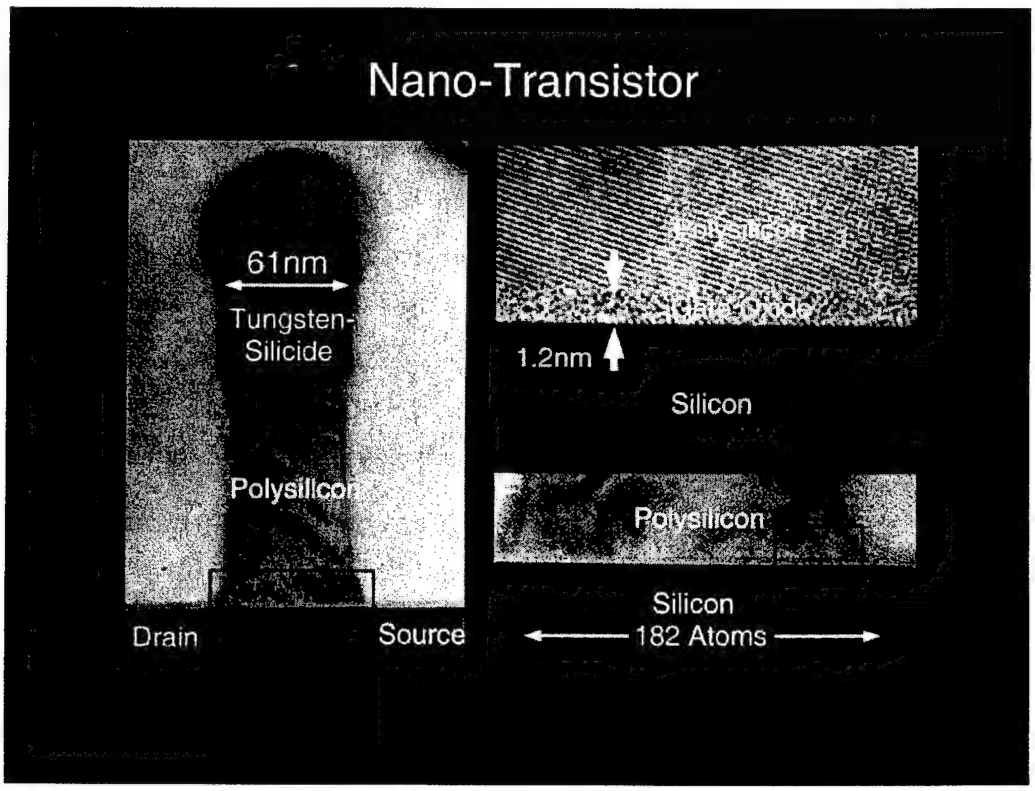

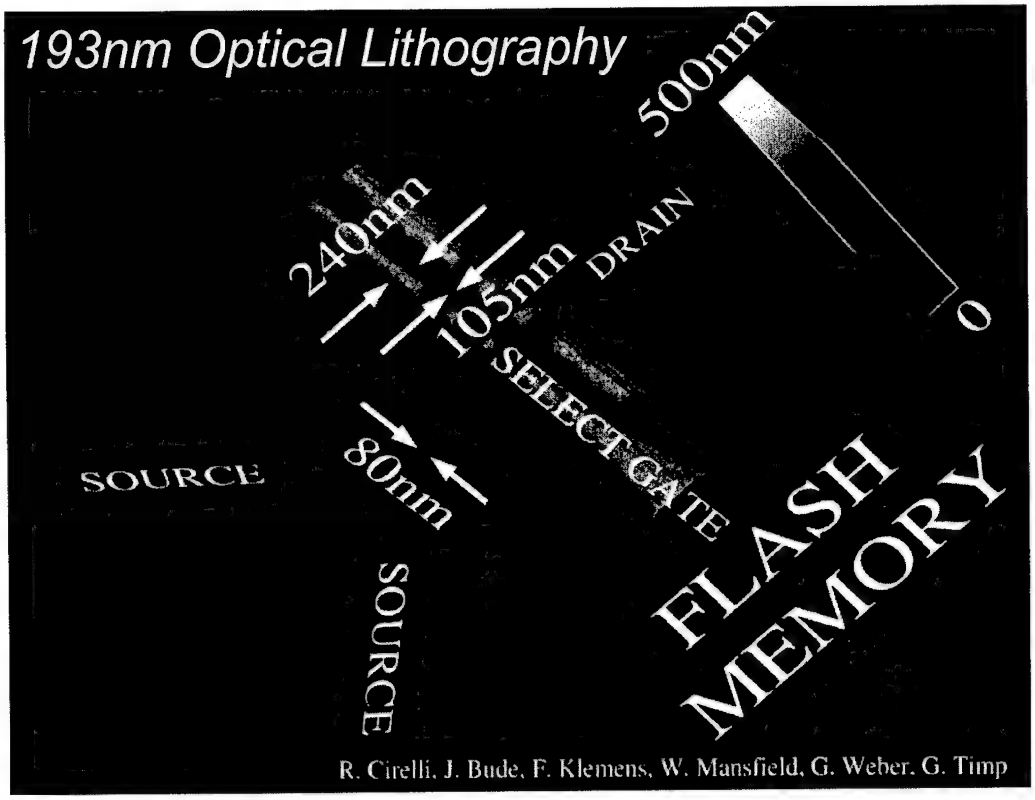
193nm Optical Lithography
500nm
0
240nm
105nm
DRAIN
SELECT GATE
80nm
SOURCE
SOURCE
FLASH
MEMORY
R. Cirelli, J. Bude, F. Klemens, W. Mansfield, G. Weber, G. Timp

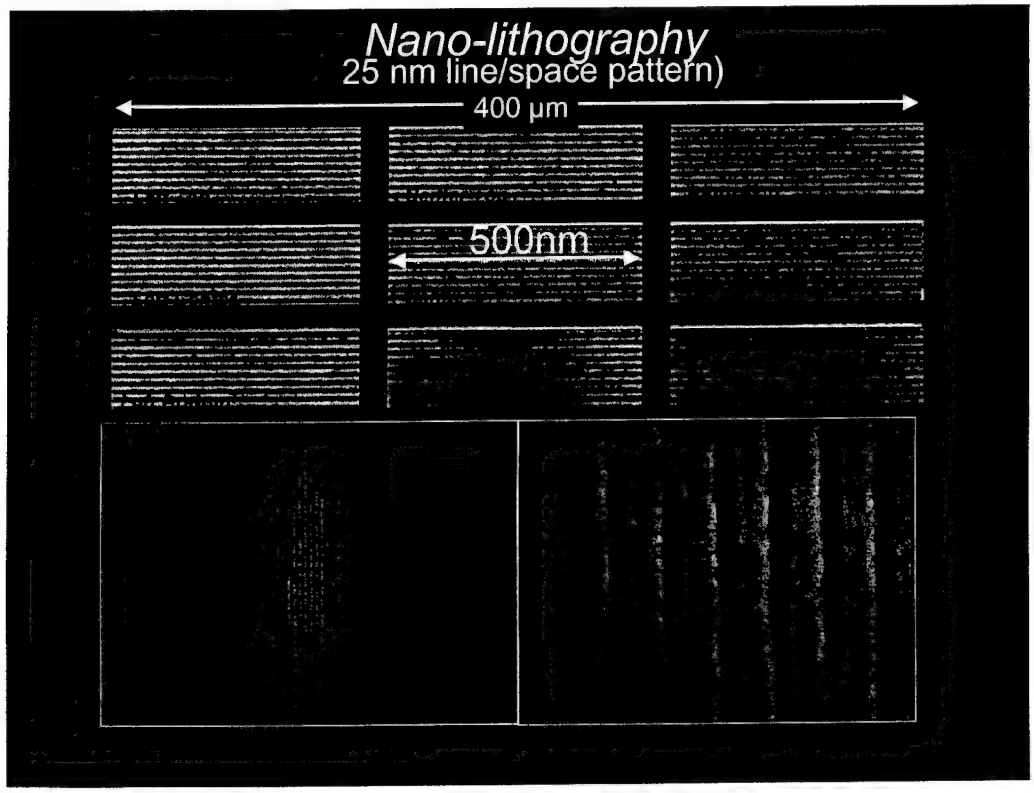
Nano-lithography
25 nm line/space pattern)
400 µm
500nm

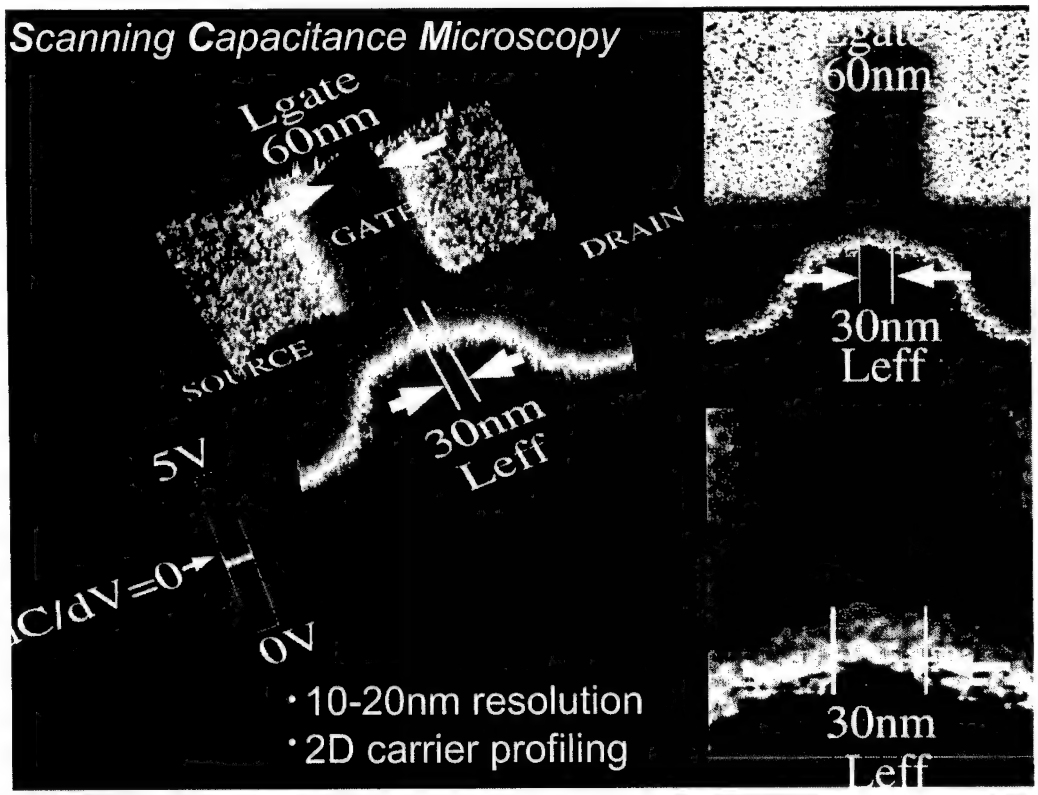
Scanning Capacitance Microscopy
Lgate
60nm
GATE
DRAIN
SOURCE
30nm
Leff
5V
dC/dV=0
0V
• 10-20nm resolution
• 2D carrier profiling
60nm
30nm
Leff
30nm
Leff

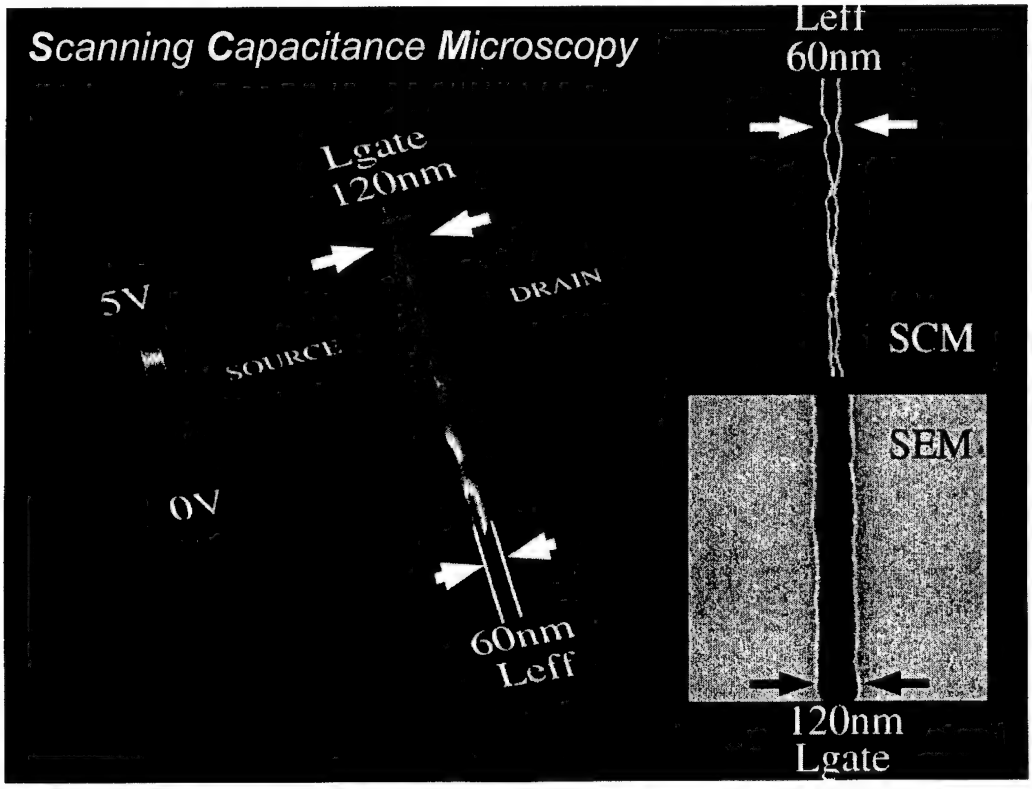
Scanning Capacitance Microscopy
Lgate
120nm
5V
DRAIN
SOURCE
0V
60nm
Leff
Leff
60nm
SCM
SEM
120nm
Lgate

The Nanotransistor: Hyper-thin Oxide

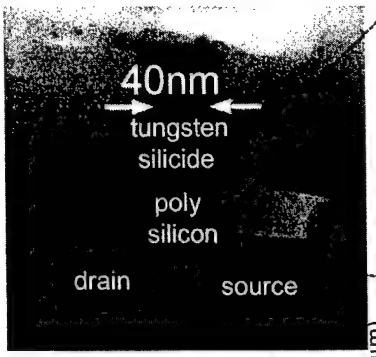

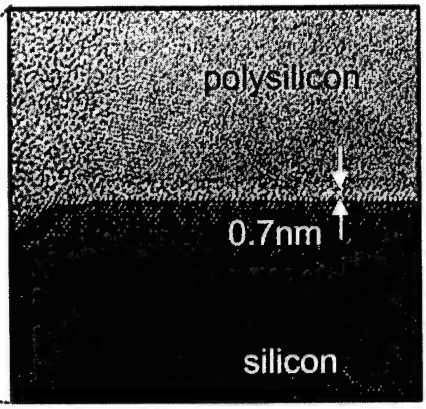

Gate leakage current comparable to drain current

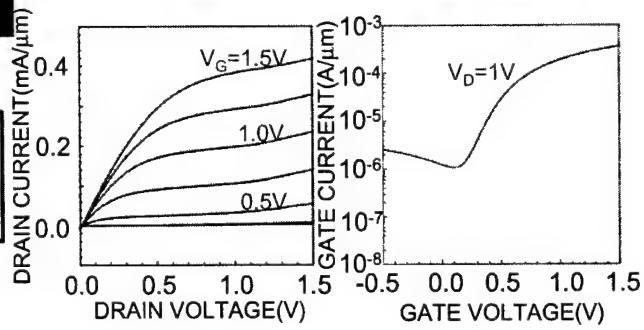

Capacitance Improvement with decreasing t_{ox}

$$I_D = WC_G(V_G - V_T)v_o$$

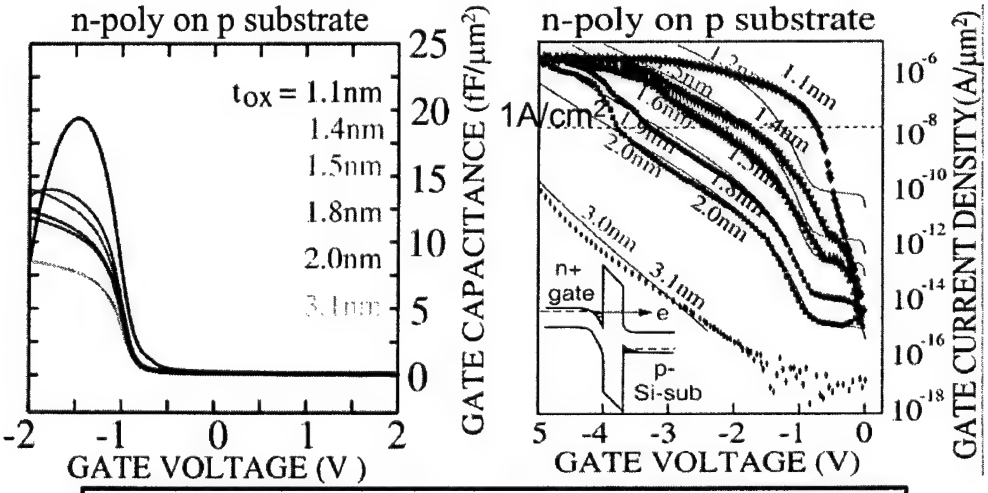

- exponential increase in leakage with increasing V_G
- exponential increase in leakage with t_{ox}

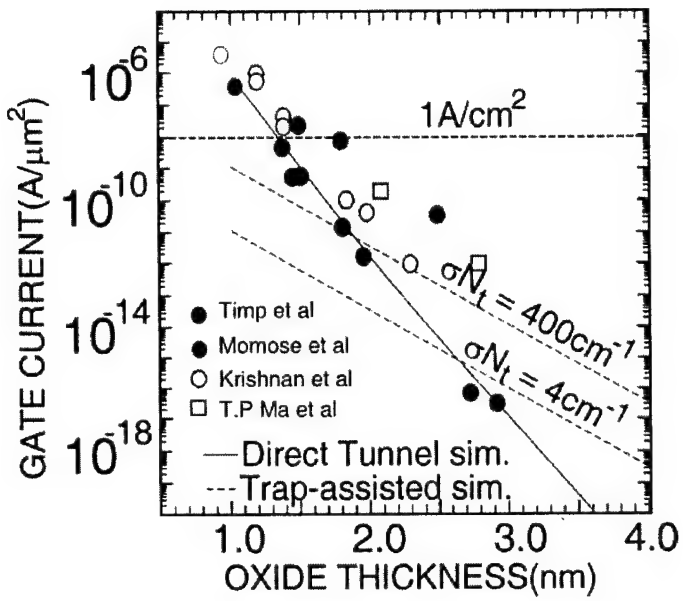

Specimen thickness:

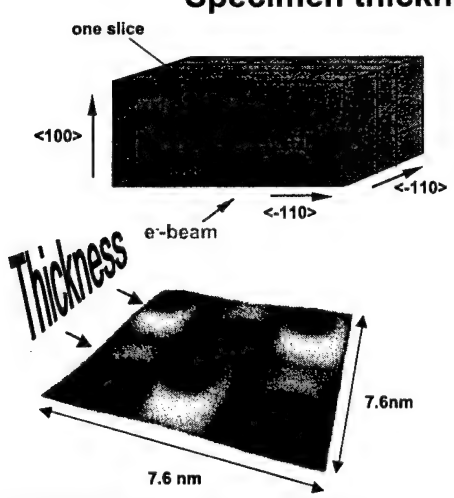

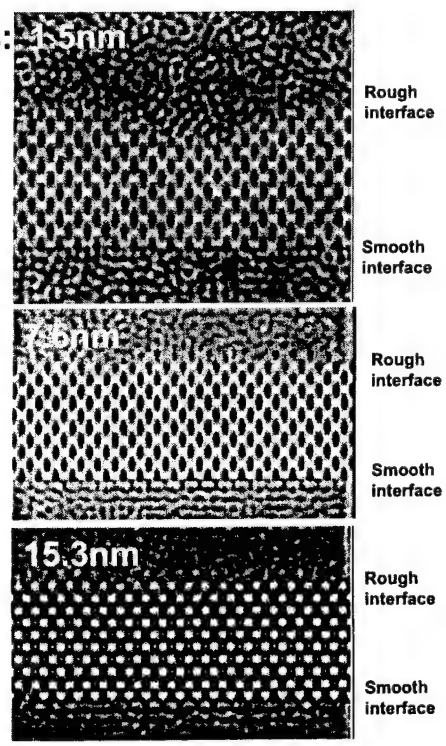

- **Apparently very sharp interface !!**
  Rough interface (11 Å pp) looks as smooth as atomically sharp interface. Minor intensity differences

- **Projection along electron beam smoothes the "apparent" interface**

Frieder Baumann et al.

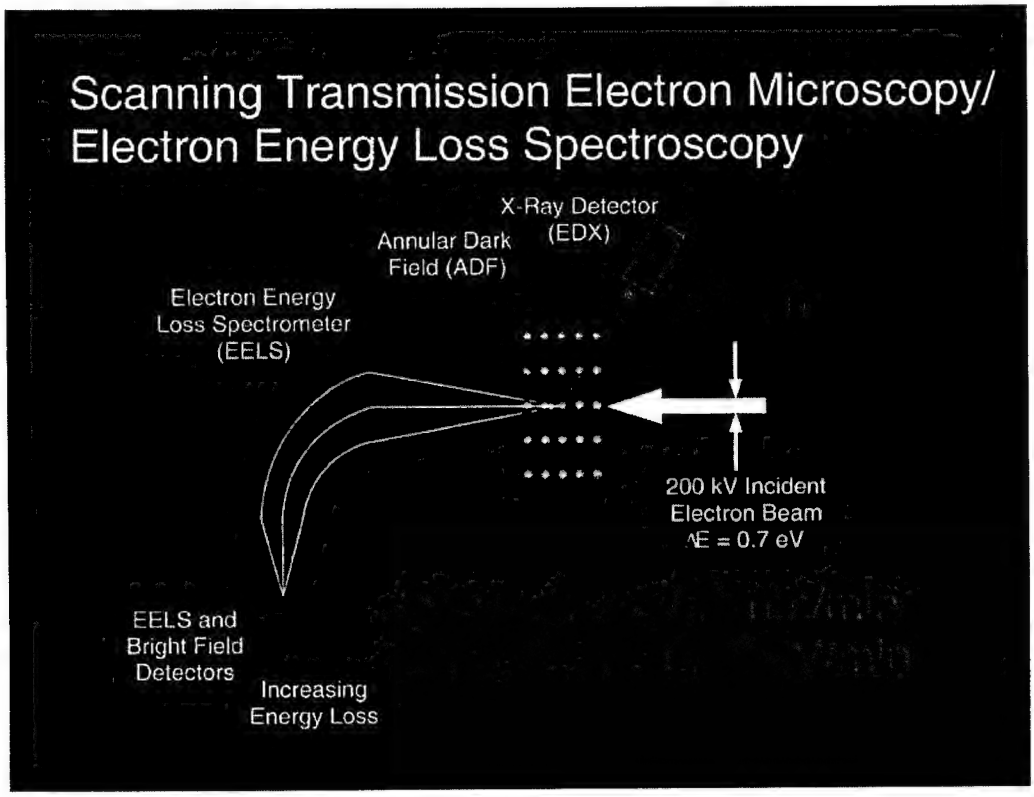

What does t_{ox}=1nm look like?

Nominally 1.3nm thick gate oxide

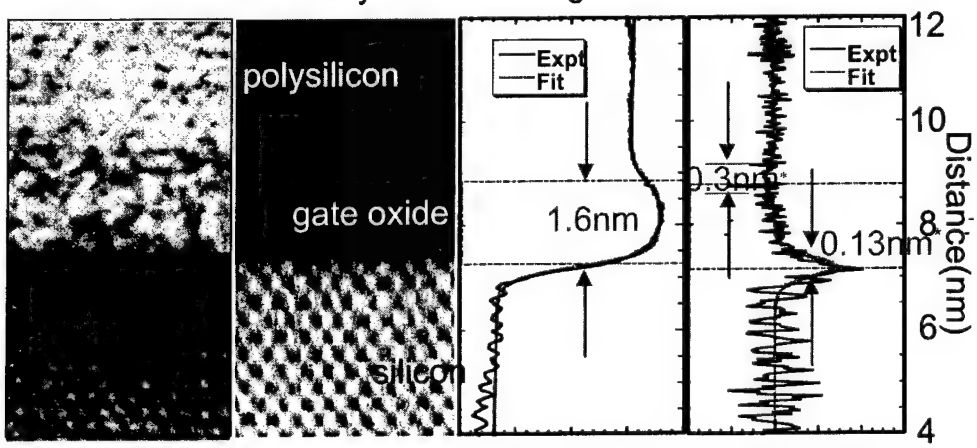

HREM | ADF STEM | Intensity Line Scan | Line Scan Derivative

Oxygen Bonding from STEM/EELS (Chemistry on an Atomic Scale)

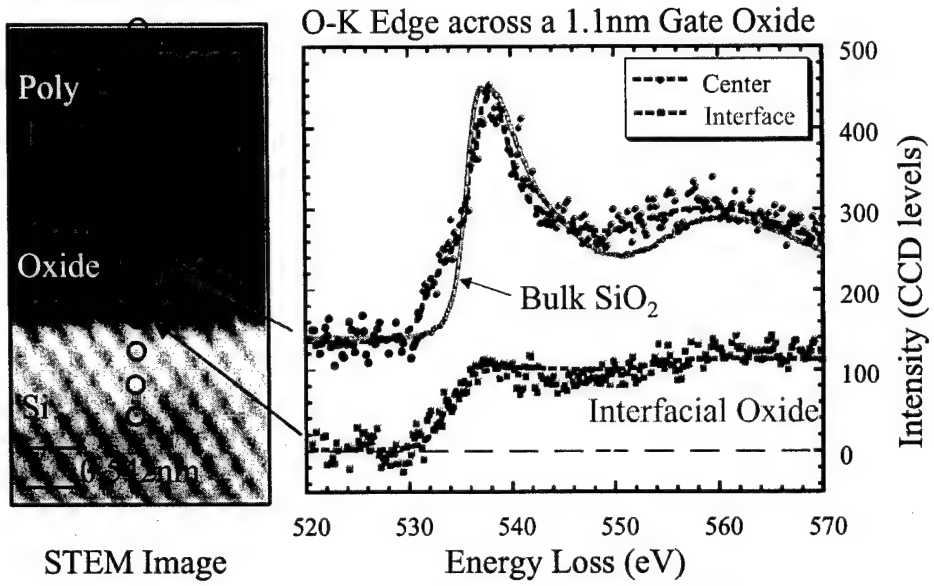

A Model Si/SiO_2 Interface

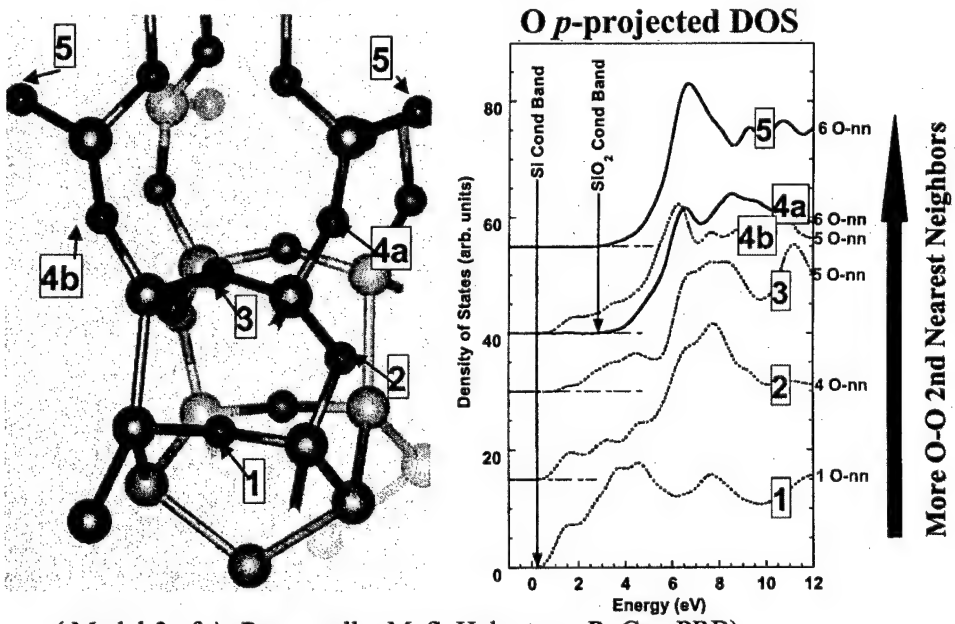

(Model-3 of A. Pasquarello, M. S. Hybertson, R. Car, PRB)

Jeff Neaton & David Muller

When is t_{ox}=1nm?

STEM/EELS

Nominally 1.1nm thick gate oxide: 0.8-1.0nm SiO_2

1.6nm wide oxygen profile

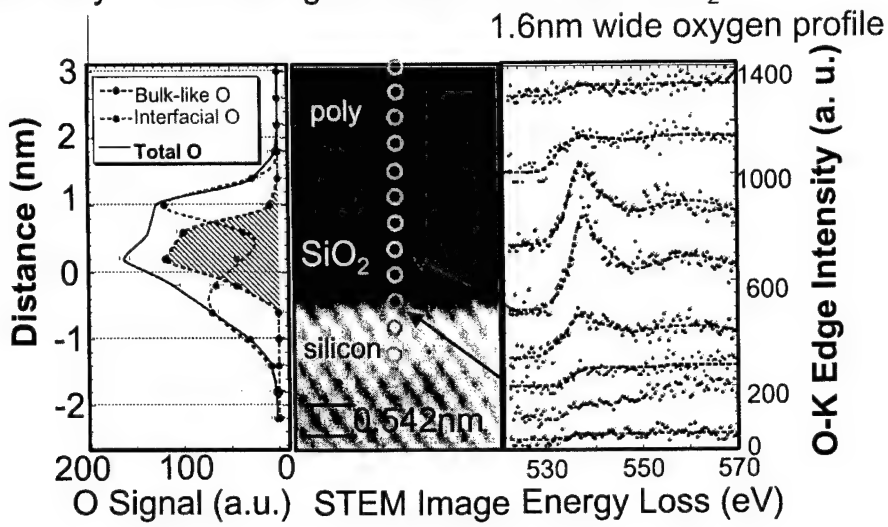

Evolution of the O-DOS from Si to SiO_2

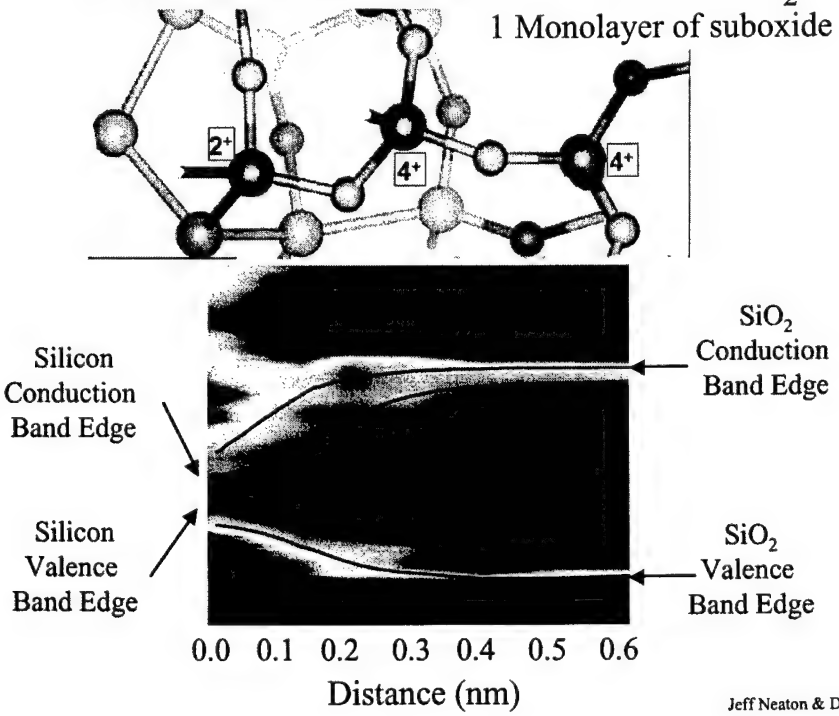

Jeff Neaton & David Muller

The End of the Roadmap for SiO_2

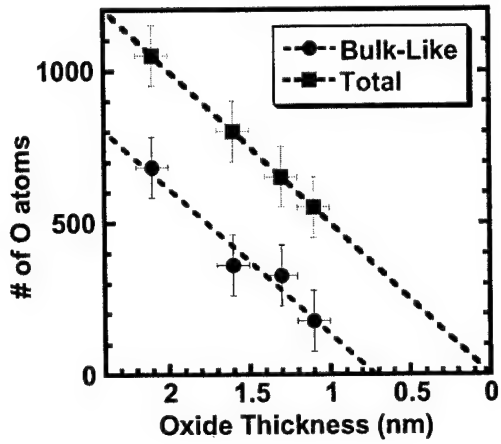

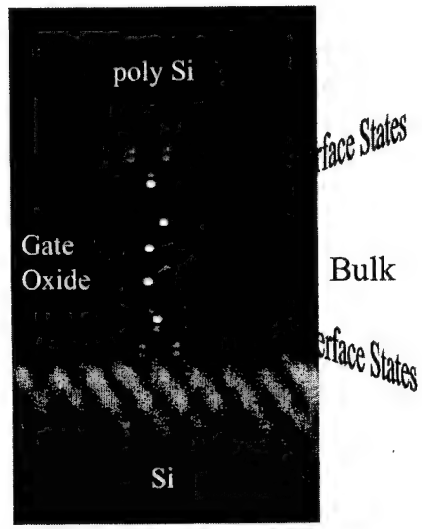

There will be no more bulk-like bonding
when the Oxide is less than 0.7 nm

The MOSFET from Landauer's Perspective

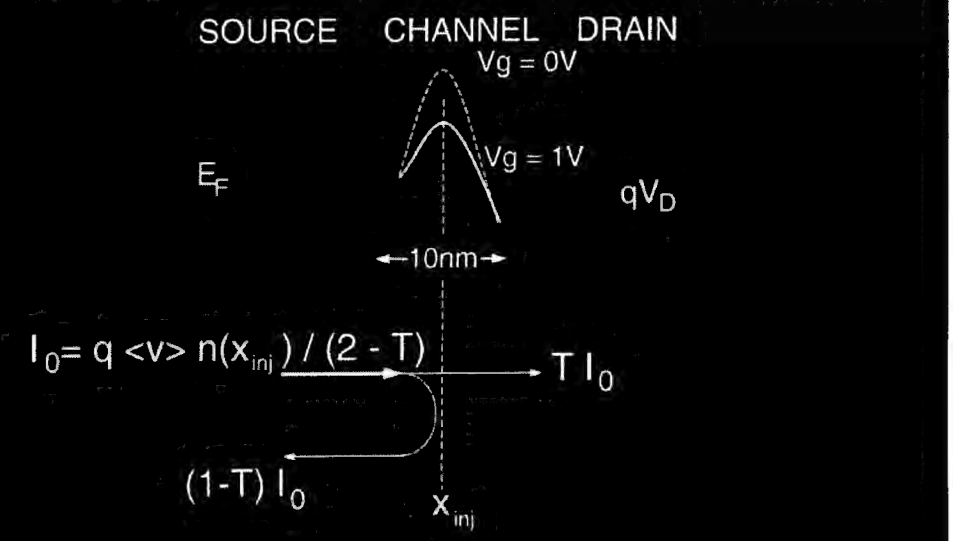

$$I_D/W = TI_0 = q\langle v\rangle n(x_{inj})T/(2-T)$$

Lundstrom, S. Datta, F. Assad; Frank, Laux and Fischetti

The Ballistic Nanotransistor

(Vg=Vds=1V)

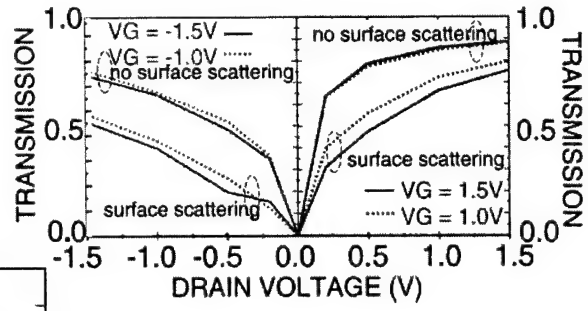

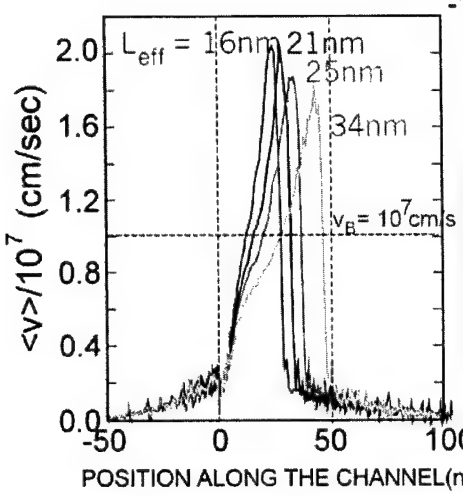

<v> exceeds bulk saturation

the velocity (averaged over L_{eff}) increases as L_{eff} decreases.

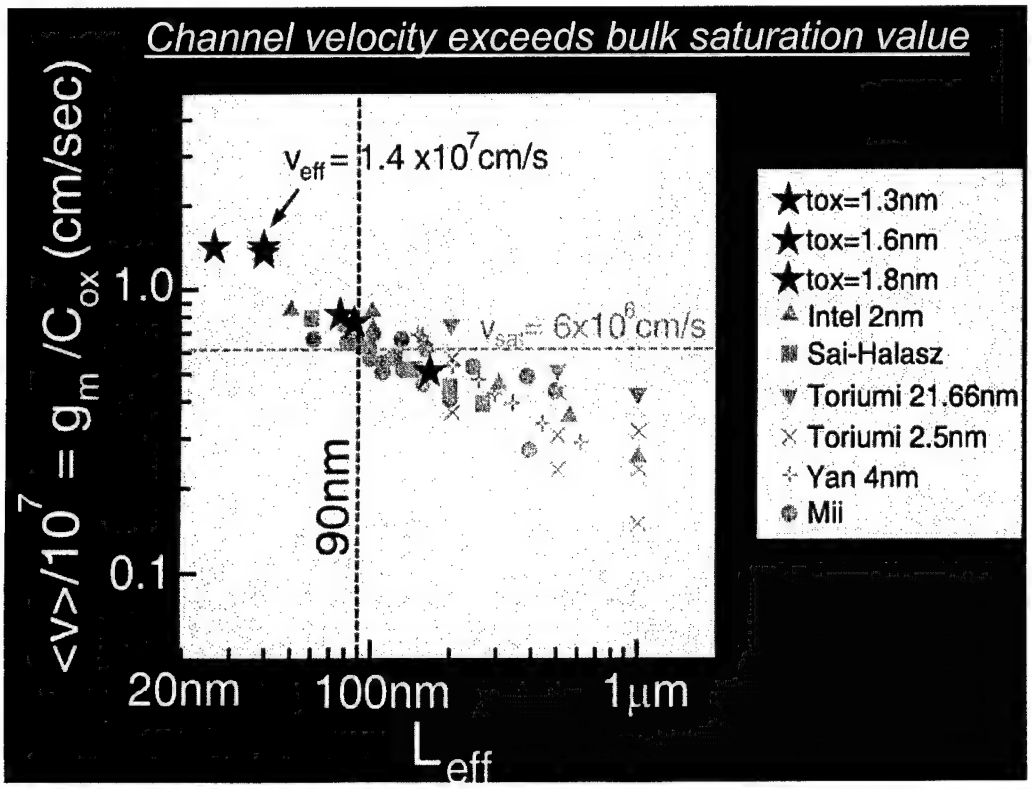

Nanotransistor DC Performance

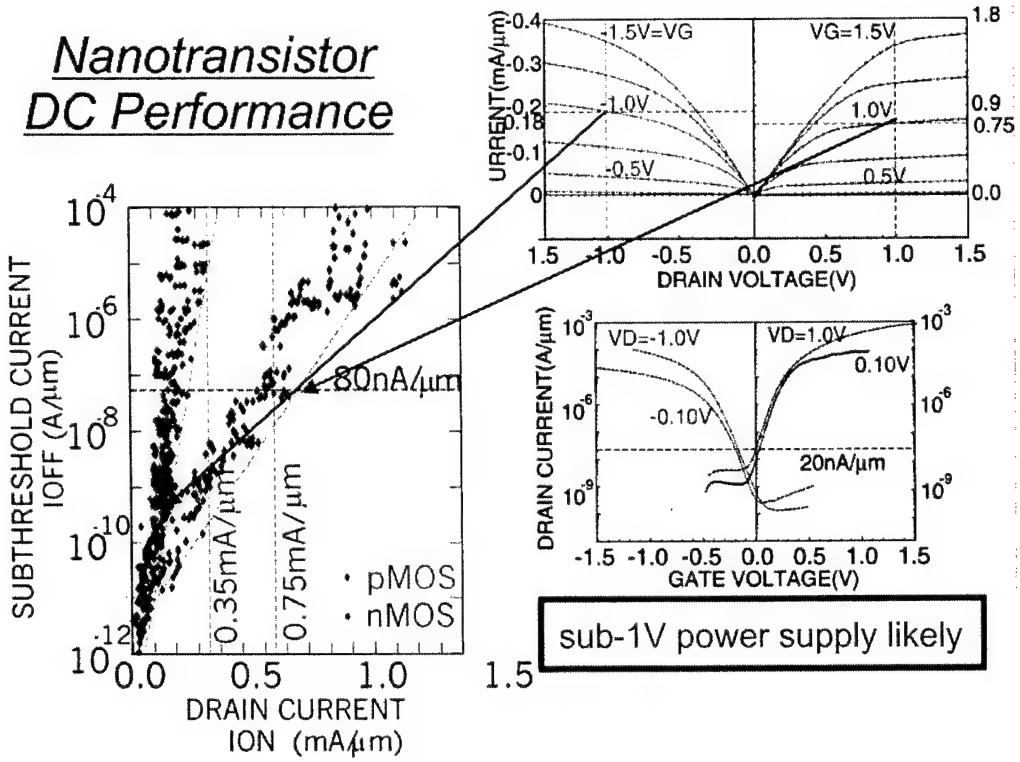

sub-1V power supply likely

Simulation versus Measurement

V_{DD} = 1V@ V_T=0.4V;
t_{ox}=1.5nm (ellips.)

nMOSFET DRIVE CURRENT

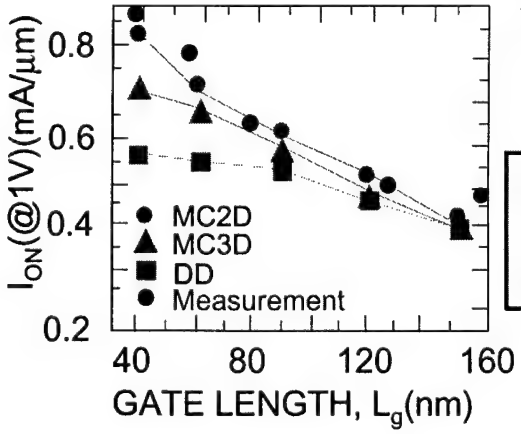

TRANSCONDUCTANCE

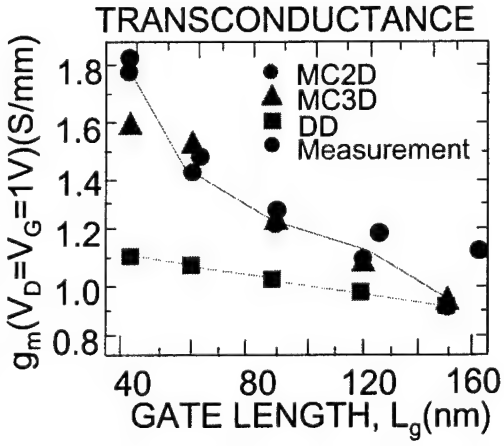

80% improvement in drive over DD prediction independent of t_{ox}

TECHNOLOGY TRENDS

60nm nMOS: f_T=265GHz
(measurement Momose et al.)

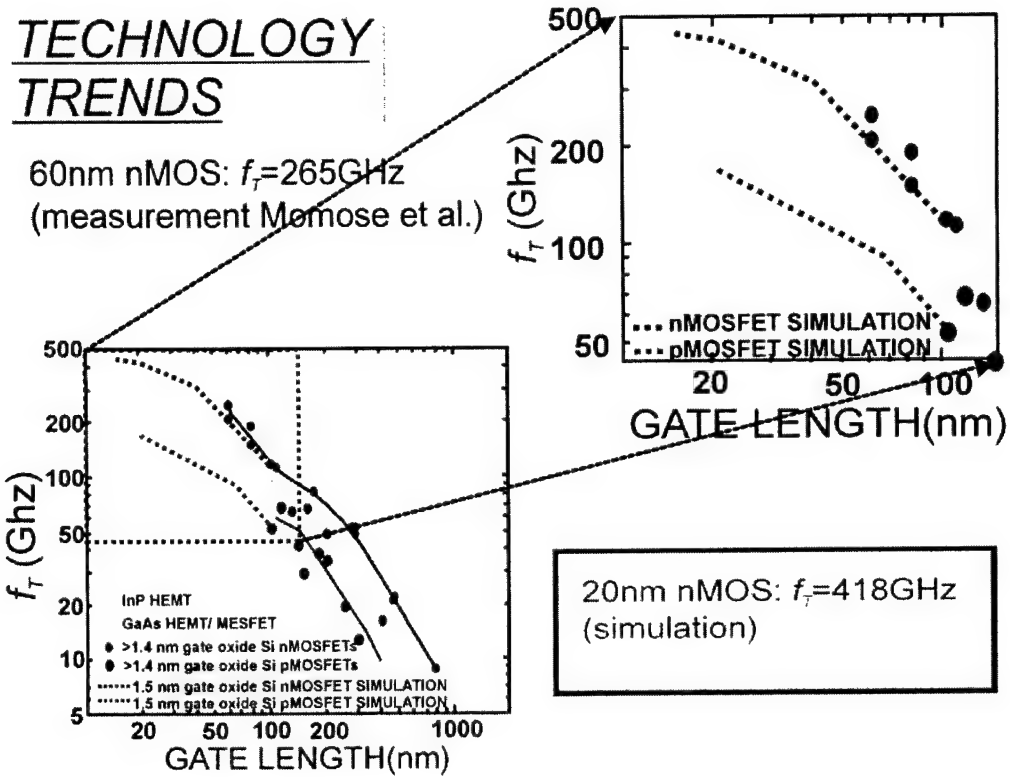

20nm nMOS: f_T=418GHz
(simulation)

Roughness Scattering and Mobility

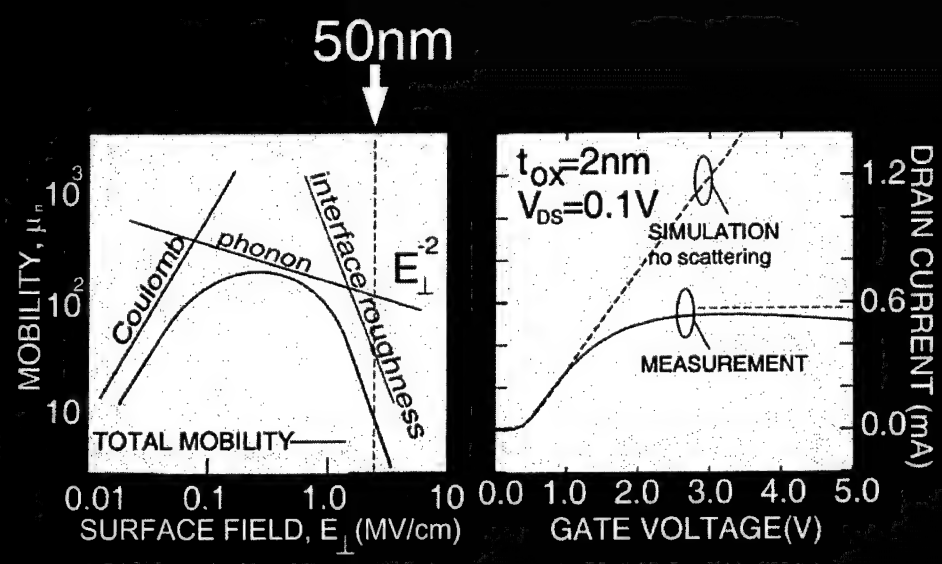

•ostensibly roughness scattering predominates for $E_\perp$>0.5MV/cm

MOBILITY RESOLVED

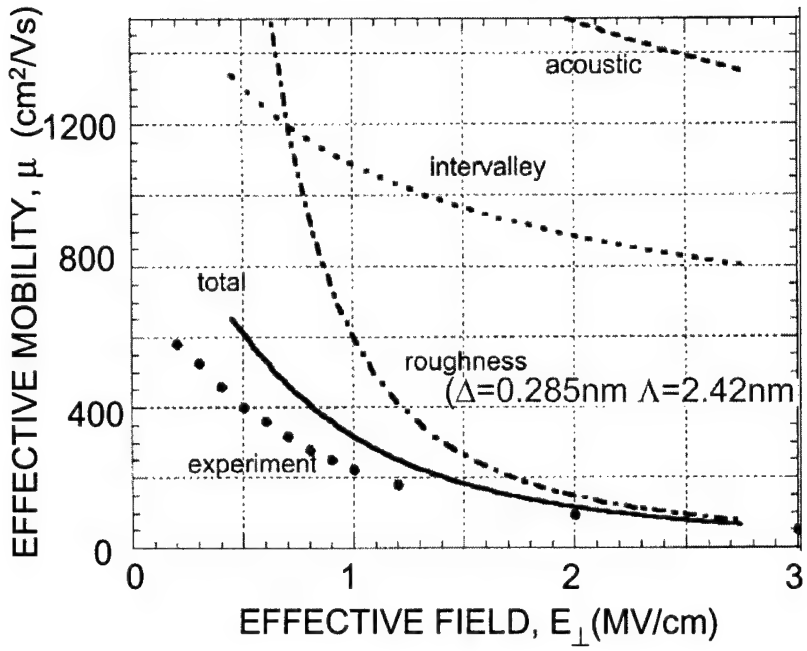

S. Goodnick

Roughness limited mobility decreases as inverse square of surface field, and as $(\Delta\Lambda)^2$:

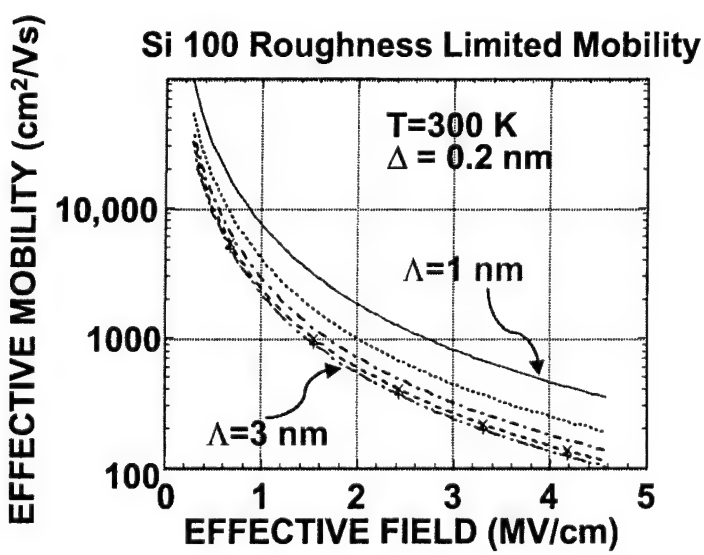

S. Goodnick

Scanning Tunneling Microscopy THROUGH *the Oxide* (for t_{ox}<1.5nm, d_{gap} <0.3-0.5nm)

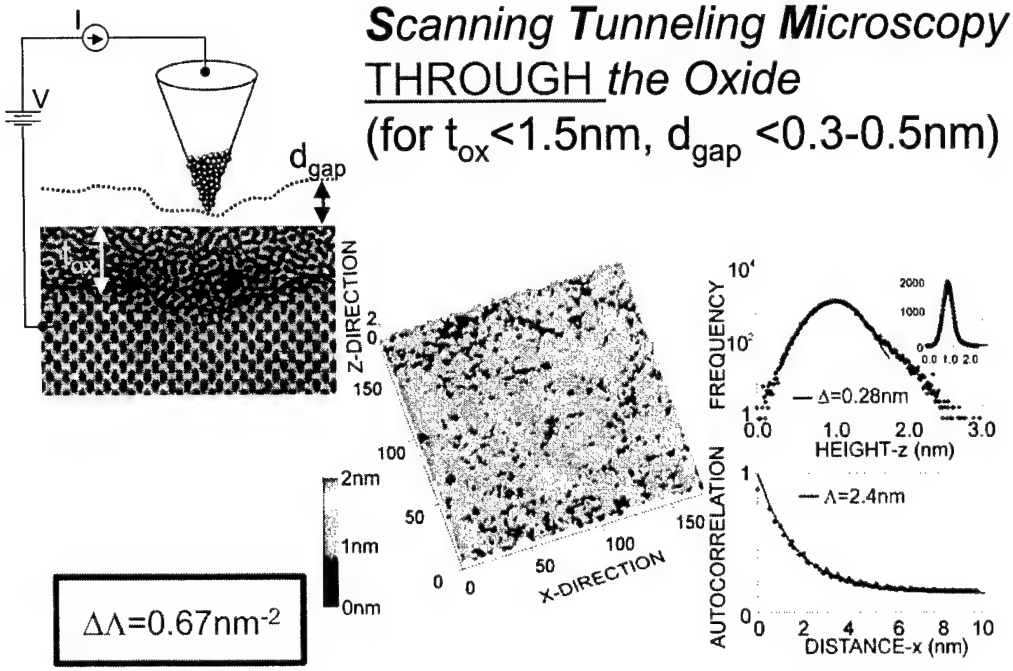

$\Delta\Lambda$=0.67nm^{-2}

J. Yu and J. Lyding

Scanning Tunneling Microscopy THROUGH *the Oxide*

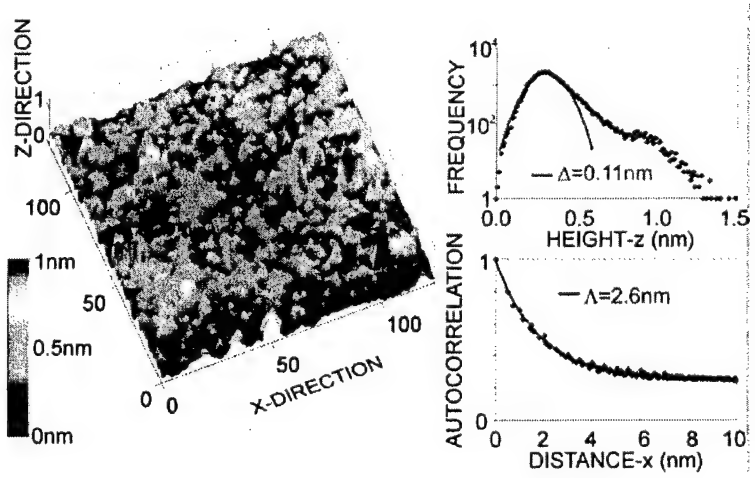

$\Delta\Lambda$=0.29nm^{-2}

X-ray DIFFRACTION

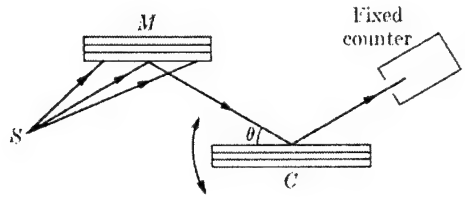

$\Delta\Lambda$=0.67nm^{-2} ⟹ 0.35nm^{-2}

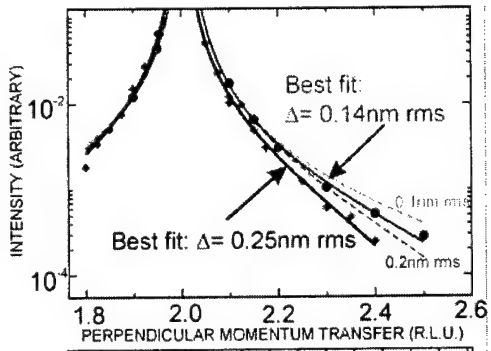

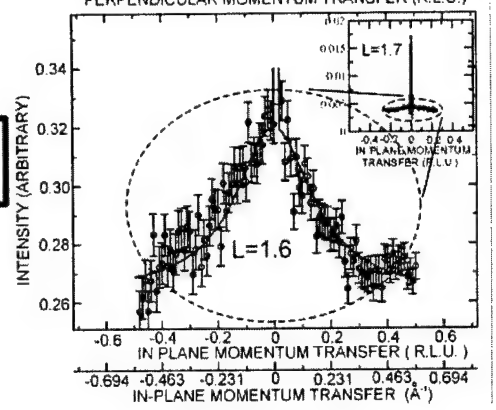

K. Evans-Lutterodt

MOBILITY MEASUREMENTS VS. CALCULATION

Δ=0.28nm, Λ=2.4nm

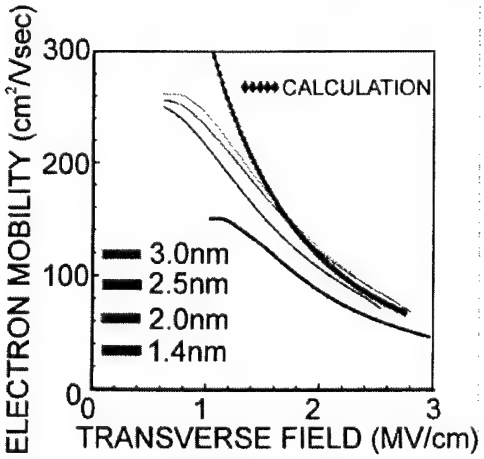

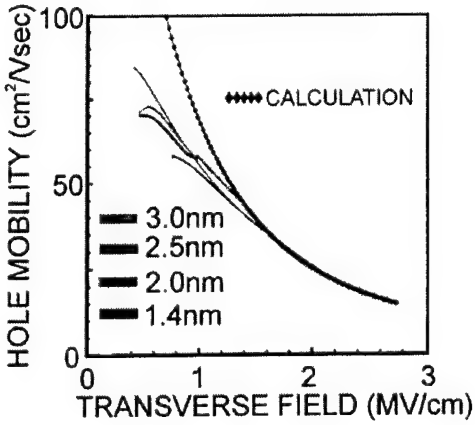

Completely constrained mobility Calculation on"rough" MOSFETS correlates well with measurements.

The Highlights

- *Homeric challenges face bulk silicon technology, but the same is true of all the pretenders to the throne.*
- *Some of these challenges stem from "atomic" sensitivity (e.g. the gate oxide)*
- *As process control decreases; circuit margins must increase at an even faster rate.*

Long-range Coulomb interactions, coupled plasmon/insulator-TO-phonon modes, and electron mobility in Si inversion layers

Max Fischetti

IBM Research Division
T. J. Watson Research Center
Yorktown Heights, NY 10598
in collaboration with Deborah Neumayer and Eduard Cartier

June 2001

MVF

Outline

- Long-range Coulomb interactions (a short review):
  - g_m and v_{eff} degradation in short-channel/thin-oxide MOSFETs (semiclassical)
  - mobility degradation in thin-oxide MOSFETs (quantum)
- High-κ insulators:
  - Simple picture
  - Dispersion of coupled insulator-TO-phonons/plasmon modes
  - Material parameters
  - Scattering strength
  - Electron mobility in inversion layers
  - Effect of SiO_2 interfacial layers

Long-range Coulomb interactions in small MOSFETs

- Source, drain, and gate regions are high-density electron gases
- S/D separation (*i.e.*, channel length) is shrinking below the Debye length of the channel
- Gate needs to be 1 nm (or less!) away from the channel
- Collective 'fluctuations' in S/D perturb electrons in the channel (electron/bulk-plasmon interactions)
- Collective fluctuations in gate (interface plasmons) cause Coulomb drag

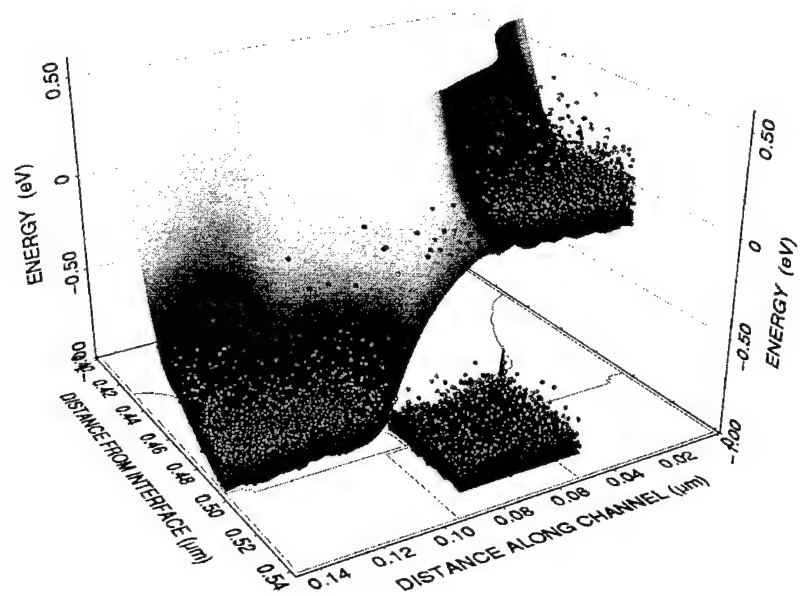

Coulomb interactions and device speed

- S/D interactions thermalize carriers, build high-energy tails, increase momentum-loss *indirectly*
- Gate-induced Coulomb-drag subtracts momentum *directly*
- Lower transconductance, lower mobility

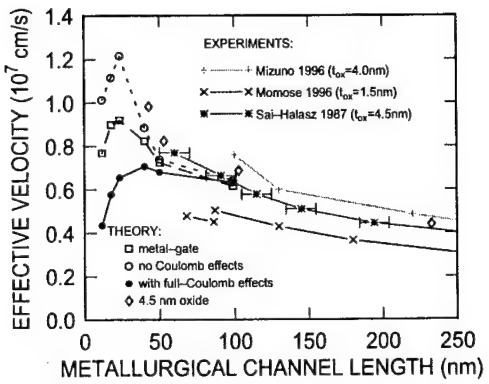

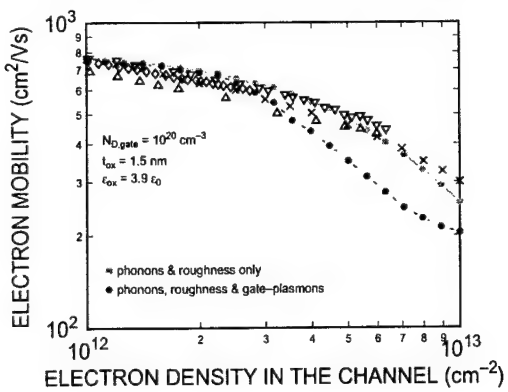

High-κ insulators

- VLSI scaling demands insulator thicknesses t approaching 1 nm for (near) future devices. But it's hard to go below 1.5 nm:
  - Gate tunneling draws too much stand-by power
  - Reliability (wear-out, breakdown) is a debated issue, but 1 nm seems to be 'too much' even to the optimist
- Lot of activity on insulators with high dielectric constant ($\epsilon^0_{ox} = \kappa\epsilon_0$), so that the gate capacitance

$$C_g = \frac{\epsilon^0_{ox}}{t} = \frac{\epsilon^0_{SiO_2}}{t_{eq}}$$

  corresponds to the required small t_{eq}.
- Materials considered:
  - Metal-oxides (HfO_2, ZrO_2, Al_2O_3...), with $\kappa \approx$ 10-30
  - Silicates ($ZrSiO_4$, $HfSiO_4$), with $\kappa \approx$ 15-25
  - Perovskites, rare-earth oxides, with $\kappa \approx 100$
  - Nitrides (AlN, Si_3N_4), with $\kappa \approx 10$
  - Ferroelectrics ($\kappa \sim 10^3$)... but that's another story...

High-κ insulators: A simple picture

- $\epsilon^0_{ox} = \epsilon^0_{ion} + \epsilon^0_{el}$
- $\epsilon^0_{el} \propto E^{-1}_{gap}$ ... so, not much room left for insulators (must have large E_{gap}!)
- Large ϵ^0_{ion} due to polarizable bonds (typically, metal-oxygen), 'soft' bonds associated with 'soft' TO-phonons
- ϵ^∞_{ion} not too large (ions move slowly)
- So, for large-κ materials, ϵ^0_{ox} much larger than ϵ^∞_{ox}
- Insulator-TO-modes at interface (surface-optical modes, SO) scatter electrons with strength $\propto$:

$$\hbar\omega_{SO}\left[\frac{1}{\epsilon^\infty_{Si}+\epsilon^\infty_{ox}} - \frac{1}{\epsilon^\infty_{Si}+\epsilon^0_{ox}}\right]$$

(Fröhlich + images, Wang-Mahan, 72)

- Small effect ($\sim$ 5%) in SiO_2:
  - ϵ^0_{ox} ($\approx$ 3.9) not much larger than ϵ^∞_{ox} ($\approx$ 2 to 2.5) because Si-O bond is 'hard'
  - Small Fröhlich-like coupling constant
  - Hard bonds imply 'stiff' TO-modes, $\hbar\omega_{TO} >> k_BT$: too energetic to be emitted by thermal electrons, too energetic to be thermally excited (no absorption).
- But large effects in high-κ materials:
  - Large ϵ^0_{ox} due to polarization of 'soft' bonds
  - Large Fröhlich-like coupling constant
  - Soft bonds imply 'soft' TO-modes, $\hbar\omega_{TO} \sim k_BT$: energy low enough to allow emission by thermal electrons, low enough to be thermally excited (absorption possible).

High-κ insulators: A simple picture

- Use Wang-Mahan (Hess-Vogl, 79; Moore-Ferry, 80) matrix element
- Single insulator/Si interface (infinitely-thick insulator)
- No electronic screening
- Add Si-phonons and (shamelessly) empirical surface-roughness (Matthiessen's rule to fit experiments for SiO_2 at $n_s = 10^{13}$ cm^{-2})

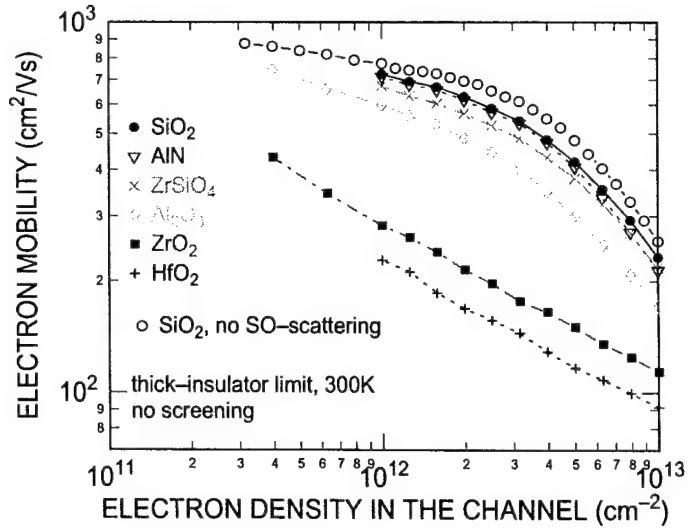

Interface modes:
A better model for thin-insulator MOSFETs

- Consider a depleted-Si/insulator/inverted-Si MOS system
- Look for longitudinal eigenmodes (TM-modes or p-waves) of Maxwell's equations: $\epsilon_{tot}(\mathbf{Q},\omega) = 0$.
  These give $\mathbf{E} \neq 0$ even when $\mathbf{D} = 0$, while transverse modes ($\epsilon_{tot}(\mathbf{Q},\omega) = \infty$) give $\mathbf{E} = 0$ for any $\mathbf{D}$, so no scattering field.
- Use non-retarded limit (OK for wavelength $\sim \lambda_F$), so unknown is electrostatic potential satisfying Laplace equation.
- Chose model dielectric functions (long-wavelength-limit, two insulator TO modes).
- Impose continuity of $\mathbf{E}_{\parallel}$ and $\mathbf{D}_{\perp}$ at two interfaces
  $\rightarrow$ homogeneous linear problem of 4 equations in 4 unknowns
  $\rightarrow$ 3 unknowns expressed in terms of the remaining one (to be fixed).
- Secular equation (*i.e.* vanishing of determinant) gives dispersion of coupled modes (4+2 of them).
- Determine phonon- and plasmon-content of each mode.
- Normalize potential (*i.e.* determine last unknown) somehow... (semiclassically). This defines the scattering potential.
- Account for Landau-damping (lost in taking a real ϵ in the long-wavelength limit).
- Determine the subband structure (triangular-well).
- Compute the mobility (Kubo-Greenwood).

Interface modes

- Consider MOS system:
  - (poly-)Si gate, $\epsilon_g(\mathbf{q},\omega)$, for $z \leq 0$
  - insulator, $\epsilon_{ox}(\omega)$, for $0 < z \leq t$
  - Si 2DEG, $\epsilon_s(\mathbf{Q},\omega)$, for $z > t$
- Write electrostatic potential (non-retarded limit):

$$\phi(\mathbf{R},z,t) \;=\; \sum_{\mathbf{Q}} \phi_{\mathbf{Q},\omega}(z)\, e^{i\mathbf{Q}\cdot\mathbf{R}}\, e^{i\omega t}$$

with

$$\phi_{Q,\omega}(z) \;=\; \begin{cases} a_{Q,\omega}\, e^{Qz} & (z<0) \\ b_{Q,\omega}\, e^{-Qz} + c_{Q,\omega}\, e^{Qz} & (0 \leq z < t_{ox}) \\ d_{Q,\omega}\, e^{-Qz} & (z \geq t_{ox}) \end{cases}$$

- Solve Laplace equation:

$$\frac{d^2\phi_{\mathbf{Q},\omega}(z)}{dz^2} - Q^2\phi_{\mathbf{Q},\omega}(z) \;=\; 0$$

with boundary-conditions (BCs):

$$\begin{cases} E_{\parallel,\omega}(\mathbf{R},z=0^-,t) & = & E_{\parallel,\omega}(\mathbf{R},z=0^+,t) \\ E_{\parallel,\omega}(\mathbf{R},z=t_{ox}^-,t) & = & E_{\parallel,\omega}(\mathbf{R},z=t_{ox}^+,t) \\ D_{z,\omega}(\mathbf{R},z=0^-,t) & = & D_{z,\omega}(\mathbf{R},z=0^+,t) \\ D_{z,\omega}(\mathbf{R},z=t_{ox}^-,t) & = & D_{z,\omega}(\mathbf{R},z=t_{ox}^+,t) \end{cases}$$

- BCs become:

$$\begin{cases} a_{Q,\omega} & = & b_{Q,\omega} + c_{Q,\omega} \\ b_{Q,\omega}\, e^{-Qt} + c_{Q,\omega}\, e^{Qt} & = & d_{Q,\omega}\, e^{-Qt} \\ \tilde{\epsilon}_g(Q,\omega)\, a_{Q,\omega} & = & \epsilon_{ox}(\omega)\,(c_{Q,\omega} - b_{Q,\omega}) \\ \epsilon_{ox}(\omega)\,[\, b_{Q,\omega}\, e^{-Qt} - c_{Q,\omega}\, e^{Qt}] & = & \tilde{\epsilon}_s^{(2D)}(Q,\omega)\, d_{Q,\omega}\, e^{-Qt}\,, \end{cases}$$

- Eigenmodes $\omega(\mathbf{Q})$ given by secular equation:

$$e^{Qt}[\tilde{\epsilon}_g(Q,\omega) + \epsilon_{ox}(\omega)][\tilde{\epsilon}_s^{(2D)}(Q,\omega) + \epsilon_{ox}(\omega)]$$
$$- e^{-Qt}[\tilde{\epsilon}_g(Q,\omega) - \epsilon_{ox}(\omega)][\tilde{\epsilon}_s^{(2D)}(Q,\omega) - \epsilon_{ox}(\omega)] \;=\; 0$$

"Effective" dielectric functions

- Gate:
  - RPA:

$$\tilde{\epsilon}_g(Q,\omega) = \frac{1}{\pi}\int_{-\infty}^{+\infty} d\left(\frac{q_z}{Q}\right)\frac{\epsilon_g(\mathbf{Q},q_z;\omega)}{1+(q_z/Q)^2} \approx \epsilon_g(q=\sqrt{2}Q,\omega)$$

  - Long-wavelength limit:

$$\epsilon_g(\omega) = \epsilon_{Si}^{\infty}\left(1 - \frac{\omega_{p,g}^2}{\omega^2}\right)$$

Getting $\omega_{p,g}$ is not trivial: Electron density in the depleted gate is *at least* z-dependent. Use either surface-density or Q-dependent average.

- Substrate:
  - RPA:

$$\tilde{\epsilon}_s^{(2D)}(Q,\omega) = \epsilon_{Si}^{\infty}\left\{1 + e^{2Qt}\sum_{\mu\mu'}\frac{\beta_{\mu\mu'}(Q,\omega)}{2Q}\,\Phi_{Q,\omega;\mu\mu'}\,\Phi^{(0)}_{Q,\mu\mu'}\right\}$$

  - Long-wavelength limit:

$$\epsilon_s^{(2D)}(Q,\omega) = \epsilon_{Si}^{\infty}\left[1 - \frac{\omega_{p,s}(Q)^2}{\omega^2}\right]$$

- Insulator (taking only 2 TO modes):

$$\epsilon_{ox}(\omega) = \epsilon_{ox}^{\infty} + (\epsilon_{ox}^{i}-\epsilon_{ox}^{\infty})\frac{\omega_{TO2}^2}{\omega_{TO2}^2-\omega^2} + (\epsilon_{ox}^{0}-\epsilon_{ox}^{i})\frac{\omega_{TO1}^2}{\omega_{TO1}^2-\omega^2}$$

RPA vs long-wavelength-limit for $Si/SiO_2/Si$

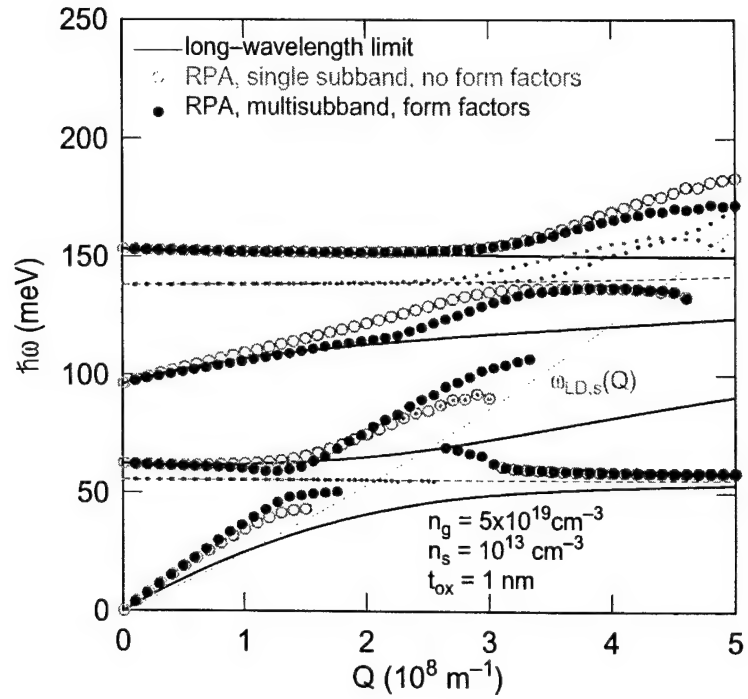

Coupled modes for $Si/SiO_2/Si$ system: Effect of coupling

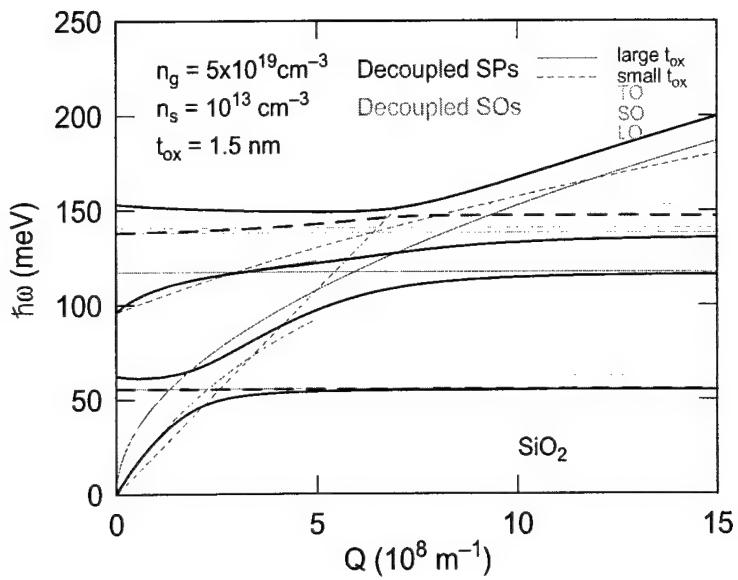

Coupled modes for $Si/SiO_2/Si$ system: Thickness dependence

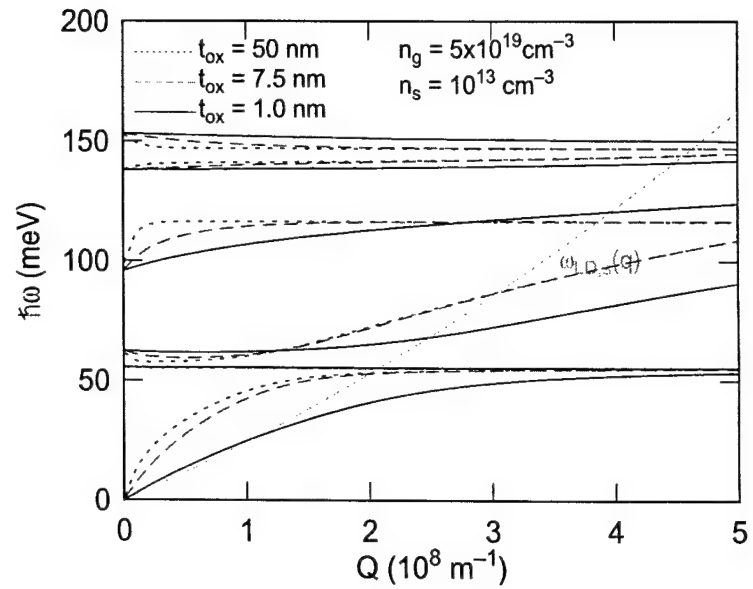

Coupled modes for $Si/Al_2O_3/Si$ system

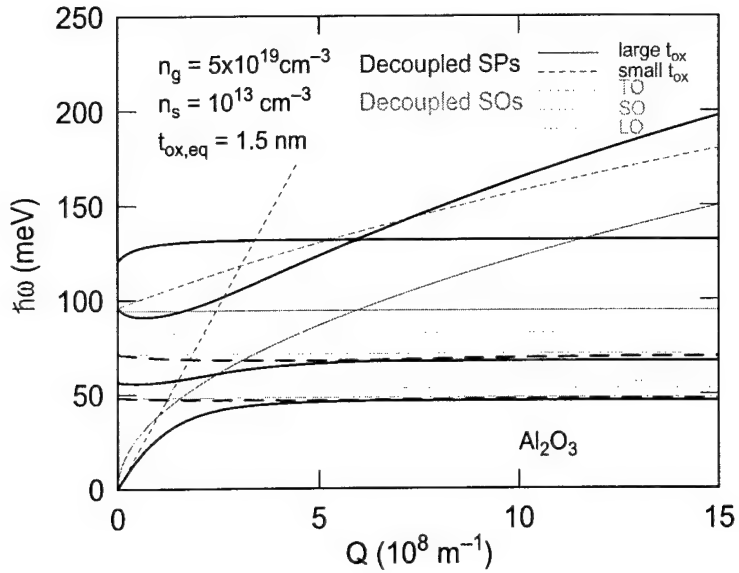

Coupled LO-plasmons modes for Si/AlN/Si system

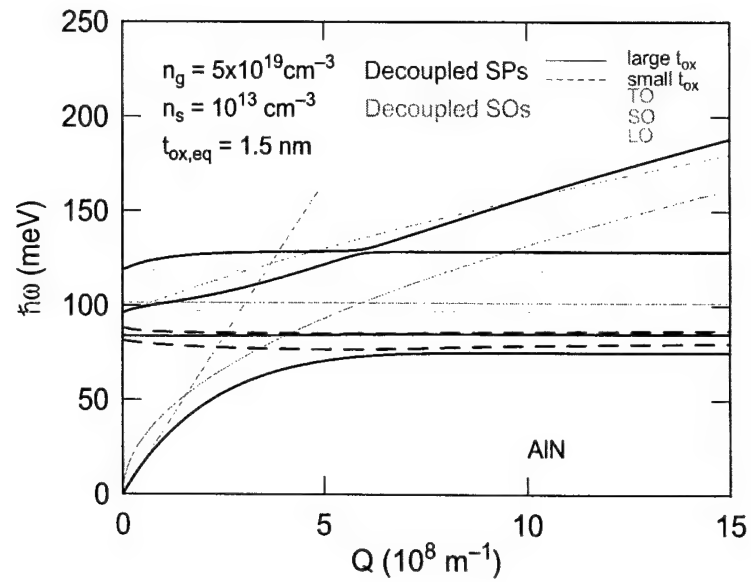

Coupled LO-plasmons modes for $Si/ZrO_2/Si$ system

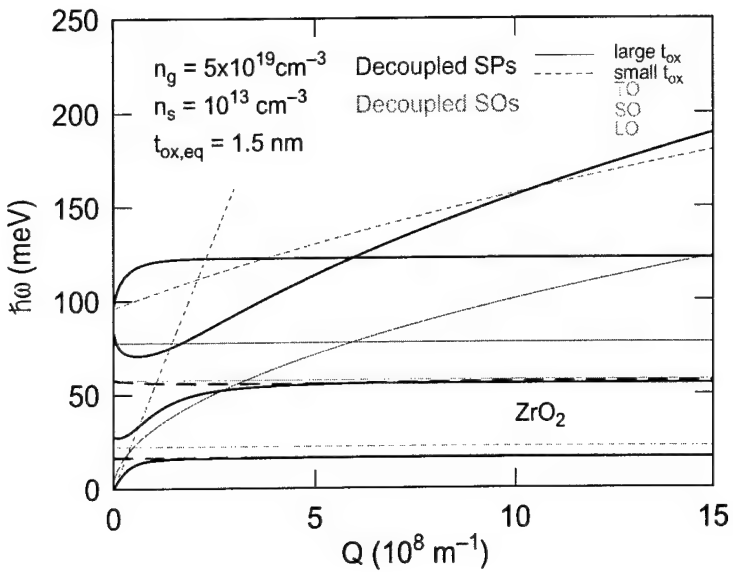

TO- and plasmon content Landau damping

- Define 3 dispersions $\omega_Q^{(-\alpha,j)}$ (j=1,3) by ignoring mode α (α = TO1, TO2, gate-plasma, substrate-2D-plasma)
- Mode-α content of mode $\omega_Q^{(i)}$ (for 4 modes):

$$\Pi^{(\alpha)}(\omega_Q^{(i)}) \approx$$

$$\left| \frac{(\omega_Q^{(i)^2} - \omega_Q^{(-\alpha,1)^2})\,(\omega_Q^{(i)^2} - \omega_Q^{(-\alpha,2)^2})\,(\omega_Q^{(i)^2} - \omega_Q^{(-\alpha,3)^2})}{(\omega_Q^{(i)^2} - \omega_Q^{(j)^2})\,(\omega_Q^{(i)^2} - \omega_Q^{(k)^2})\,(\omega_Q^{(i)^2} - \omega_Q^{(l)^2})} \right|$$

with i, j, k, l cyclical.

- Content normalized so that:

$$\sum_{i=1}^{4} \Pi^{(\alpha)}(\omega_Q^{(i)}) = 1$$

$$\Pi^{(G)}(\omega_Q^{(i)}) + \Pi^{(S)}(\omega_Q^{(i)}) + \Pi^{(TO1)}(\omega_Q^{(i)}) + \Pi^{(TO2)}(\omega_Q^{(i)}) = 1$$

- Landau damping (poor man's way): Ignore response of gate-plasma when gate-plasmon-like mode is in Landau-damped region; same for substrate plasma

Scattering strength

- Field $\phi_{Q,\omega_Q^{(i)}}(z)$ defined up to a multiplicative constant $a_{Q,\omega_Q^{(i)}}$:

$$b_{Q,\omega_Q^{(i)}} = \frac{\epsilon_{ox}(\omega_Q^{(i)}) - \epsilon_g(\omega_Q^{(i)})}{2\epsilon_{ox}(\omega_Q^{(i)})} a_{Q,\omega_Q^{(i)}}$$

$$c_{Q,\omega_Q^{(i)}} = \frac{\epsilon_{ox}(\omega_Q^{(i)}) + \epsilon_g(\omega_Q^{(i)})}{2\epsilon_{ox}(\omega_Q^{(i)})} a_{Q,\omega_Q^{(i)}}$$

$$d_{Q,\omega_Q^{(i)}} = \frac{\epsilon_{ox}(\omega_Q^{(i)}) - \epsilon_g(\omega_Q^{(i)})}{\epsilon_{ox}(\omega_Q^{(i)}) + \epsilon_s(Q,\omega_Q^{(i)})} a_{Q,\omega_Q^{(i)}}$$

- Fix $a_{Q,\omega_Q^{(i)}}$ via second-quanization or semiclassically.
- Semiclassically (not-so-trivial extension of Kittel 63):
  - Re-write potential as:

$$\phi_Q^{(i)}(\mathbf{R},z,t) = \phi^{(i)}_{Q,\omega_Q^{(i)}}(z)\ \cos(\mathbf{Q}\cdot\mathbf{R} - \omega_Q^{(i)}t)$$

  - Write interface charge-density as:
    $\rho_Q^{(i)}(\mathbf{R},z,t)$

$$= \{\delta(z)\,[\,\epsilon_{gate}(\omega_Q^{(i)})\,a_{Q,\omega_Q^{(i)}} + \epsilon_{insulator}(\omega_Q^{(i)})\,(b_{Q,\omega_Q^{(i)}} - c_{Q,\omega_Q^{(i)}})\,]$$

$$+\ \delta(z-t)\,[\,\epsilon_{insulator}(\omega_Q^{(i)})(c_{Q,\omega_Q^{(i)}}e^{Qt} - b_{Q,\omega_Q^{(i)}}e^{-Qt})$$

$$+\ \epsilon_{substrate}(Q,\omega_Q^{(i)})\,d_{Q,\omega_Q^{(i)}}e^{-Qt}\,]\,\}\ Q\ \cos(\mathbf{Q}\cdot\mathbf{R} - \omega_Q^{(i)}t)\ .$$

    $\epsilon_{gate}(\omega)$, $\epsilon_{insulator}(\omega)$, and $\epsilon_{substrate}(Q,\omega)$ to be determined: whatever response is accounted for by these functions, is not accounted for by the potential

  - Get total energy (potential+kinetic, including self-energy):
    $< W_Q^{(i)} > = 2\ < U_Q^{(i)} >$

$$= \frac{2}{\Omega}\left\langle \int_\Omega d\mathbf{R} \int_{-\infty}^{\infty} dz\ \phi_Q^{(i)}(\mathbf{R},z,t)\ \rho_Q^{(i)}(\mathbf{R},z,t)\right\rangle$$

$$= Q\,\epsilon_{TOT}(Q,\omega_Q^{(i)})\left[\frac{\epsilon_{ox}(\omega_Q^{(i)}) - \epsilon_g(\omega_Q^{(i)})}{\epsilon_{ox}(\omega_Q^{(i)}) + \epsilon_s(Q,\omega_Q^{(i)})}\right]^2 a^2_{Q,\omega_Q^{(i)}}\,e^{-2Qt}$$

with

$$\epsilon_{TOT}(Q,\omega) = \epsilon_{gate}(\omega)\left[\frac{\epsilon_{ox}(\omega) + \epsilon_s(Q,\omega)}{\epsilon_{ox}(\omega) - \epsilon_g(\omega)}\right]^2 e^{2Qt}$$

$$+\ \epsilon_{insulator}(\omega)\left\{\left[\frac{\epsilon_{ox}(\omega) + \epsilon_s(Q,\omega)}{2\epsilon_{ox}(\omega)}\right]^2 (e^{2Qt} - 1)\right.$$

$$\left. +\ \left[\frac{\epsilon_{ox}(\omega) - \epsilon_s(Q,\omega)}{2\epsilon_{ox}(\omega)}\right]^2 (1 - e^{-2Qt})\right\}$$

$$+\ \epsilon_{substrate}(Q,\omega)$$

  - Finally:

$$\phi^{(i)}_{Q,\omega_Q^{(i)}} = \left[\frac{\hbar\omega_Q^{(i)}}{2\ Q\ \epsilon_{TOT}(Q,\omega_Q^{(i)})}\right]^{1/2} e^{-Q(z-t)}$$

  - Setting:
    * $\epsilon_{gate}(\omega) = \epsilon_g(\omega)$
    * $\epsilon_{insulator}(\omega) = \epsilon_{ox}(\omega)$
    * $\epsilon_{substrate}(Q,\omega) = \epsilon_s^{(2D)}(Q,\omega)$

    the secular equation is equivalent to
    $\epsilon_{TOT}(Q,\omega) = 0$

- Scattering field due to plasmon- and phonon-components:
  - Plasmon: Set
    * $\epsilon_{substrate}(Q,\omega) = \epsilon_{Si}$, $\epsilon_{gate}(\omega) = \epsilon_{Si}$
      (full plasma response lumped into the field)
    * $\epsilon_{insulator}(\omega) = \epsilon^0_{ox}$
      (TO-response excluded from the field and fully lumped into the dielectric function) in $\epsilon_{TOT}(Q,\omega)$
    * Call it $\epsilon^{(PL)}_{TOT}(Q,\omega)$

    Then, field due to gate-plasmons:

$$\phi^{(i,g,PL)}_{Q,\omega^{(i)}_Q}(z) \;=\; \left[\frac{\hbar\omega^{(i)}_Q}{2\,Q\,\epsilon^{(PL)}_{TOT}(Q,\omega^{(i)}_Q)}\,\Pi^{(G)}(\omega^{(i)}_Q)\right]^{1/2} e^{-Q(z-t)}$$

  - TO1-mode:
    * Let substrate and gate plasmas respond:
      $\epsilon_{substrate}(Q,\omega) = \epsilon_s(Q,\omega)$, $\epsilon_{gate}(\omega) = \epsilon_g(\omega)$ (so excluding plasmas from the potential)
    * Define $\epsilon^{(TO1)}_{TOT,high}(Q,\omega^{(i)}_Q)$ by setting

$$\epsilon_{insulator}(\omega) \;=\; \epsilon^{\infty}_{ox}\,\frac{\omega^2_{LO2}-\omega^2}{\omega^2_{TO2}-\omega^2}$$

      (phonon 2 responds at the frequency ω, while phonon 1 does not respond).
    * Define $\epsilon^{(TO1)}_{TOT,low}(Q,\omega^{(i)}_Q)$ by setting

$$\epsilon_{insulator}(\omega) \;=\; \epsilon^{\infty}_{ox}\,\frac{\omega^2_{LO2}-\omega^2}{\omega^2_{TO2}-\omega^2}\left(\frac{\omega_{LO1}}{\omega_{TO1}}\right)^2$$

      (phonon 2 responds at the frequency ω, while phonon 1 responds fully).

    Then, amplitude of (scattering) field due *only* to TO1 is:

$$\phi^{(i,PH1)}_{Q,\omega^{(i)}_Q}(z) \;=\; e^{-Q(z-t)}\;\times$$

$$\left\{\frac{\hbar\omega^{(i)}_Q}{2Q}\left[\frac{1}{\epsilon^{(TO1)}_{TOT,high}(Q,\omega^{(i)}_Q)}-\frac{1}{\epsilon^{(TO1)}_{TOT,low}(Q,\omega^{(i)}_Q)}\right]\Phi^{(TO1)}(\omega^{(i)}_Q)\right\}^{1/2}$$

  - Note: Modes 5 and 6 are SO-modes at the far (gate-insulator) interface. At small K_F, large n_g, they are screened by gate-electrons, at large K_F their effect on the mobility is depressed by a factor $\exp(-2K_F t)$... so, ignore them.

- Interesting limits:
  - TO-mode (no plasma) in bulk: Scattering field $\propto$

$$\left[\frac{\hbar\omega_{LO}}{2q^2}\left(\frac{1}{\epsilon^\infty}-\frac{1}{\epsilon^0}\right)\right]^{1/2}$$

    (usual Fröhlich coupling)
  - Coupled TO-plasma modes in bulk:

$$\epsilon_{TOT}(Q,\omega)=\epsilon^\infty[(\omega^2-\omega_{LO}^2)/(\omega^2-\omega_{TO}^2)-(\omega_P/\omega)^2]$$

    with dispersion:

$$\omega_\pm^2=\frac{1}{2}\{\omega_{LO}^2+\omega_P^2\pm[(\omega_{LO}^2+\omega_P^2)^2-4\omega_{TO}^2\omega_P^2]^{1/2}\}$$

    and scattering field:

$$\left\{\frac{\hbar\omega_\pm}{2q^2}\left[\frac{1}{\epsilon^\infty-\epsilon^\infty\omega_P^2/\omega_\pm^2}-\frac{1}{\epsilon^0-\epsilon^\infty\omega_P^2/\omega_\pm^2}\right]\left|\frac{\omega_\pm^2-\omega_P^2}{\omega_+^2-\omega_-^2}\right|\right\}^{1/2}$$

    (cf. Varga 65, Kim-Das-Senturia 78, Ridley 88, Sanborn 95)
- Single TO-mode at Si-insulator interface:

$$\epsilon_{TOT}=\epsilon_{ox}(\omega)+\epsilon_{Si}^\infty$$

  with dispersion

$$\omega_{SO}=\omega_{TO}\left[\frac{\epsilon_{ox}^0+\epsilon_{Si}^\infty}{\epsilon_{ox}^\infty+\epsilon_{Si}^\infty}\right]^{1/2}$$

  and scattering strength $\propto$

$$\phi_{Q,\omega_{SO}}^{(PH)}(z)=\left\{\frac{\hbar\omega_{SO}}{2Q}\left[\frac{1}{\epsilon_{Si}^\infty+\epsilon_{ox}^\infty}-\frac{1}{\epsilon_{Si}^\infty+\epsilon_{ox}^0}\right]\right\}^{1/2}e^{-Q(z-t)}$$

  (cf Wang-Mahan 72) which is also the unscreened $Qt\to\infty$-limit of the general formula

Insulator parameters

- Select/compromise:
  - from literature (theory, experiments: FTIR, Raman, tunneling spectroscopy)
  - From 'in-house' FTIR
- Complications:
  - several modes: lump 2 stronger groups/bands into 2 discrete TO modes
  - several forms (cubic, hexagonal, monoclinic, amorphous): find closest to 'in-house' FTIR-measured films
  - process dependence (*e.g.*, Al-ions in non-stoichiometric Al_2O_3): assume 'ideal' films
  - interfacial layers (SiO_2 for oxides and silicates, Si_3N_4 for nitrides and oxynitrides): estimate effect

Material Quantity (units)	SiO_2	Al_2O_3	AlN	ZrO_2	HfO_2	$ZrSiO_4$
ϵ_{ox}^0 (ϵ_0)	3.90	12.53	9.14	24.0	22.00	11.75
ϵ_{ox}^i (ϵ_0)	3.05	7.27	7.35	7.75	6.58	9.73
ϵ_{ox}^∞ (ϵ_0)	2.50	3.20	4.80	4.00	5.03	4.20
ω_{TO1} (meV)	55.60	48.18	81.40	16.67	12.40	38.62
ω_{TO2} (meV)	138.10	71.41	88.55	57.70	48.35	116.00
α_1	0.0248	0.0788	0.0248	0.2504	0.3102	0.0322
α_2	0.0113	0.0814	0.0423	0.0779	0.0362	0.2942

$$\alpha_i=\frac{e^2}{4\pi\hbar}\left(\frac{m_t}{2\hbar\omega_{SOi}}\right)^{1/2}\left(\frac{1}{\epsilon_{Si}^\infty+\epsilon_{ox}^\infty}-\frac{1}{\epsilon_{Si}^\infty+\epsilon_{ox}^0}\right)$$

FTIR spectra (D. Neumayer)

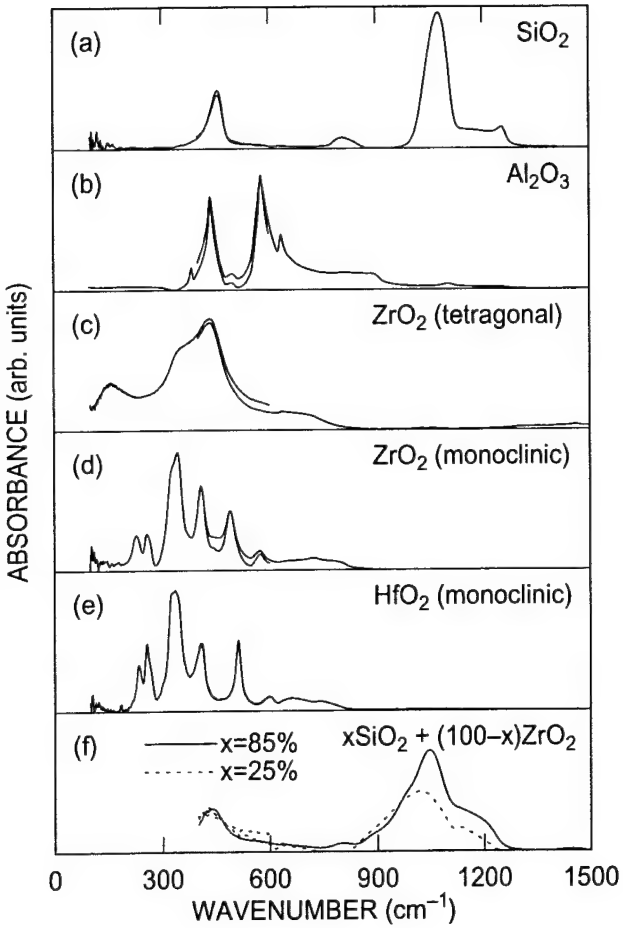

Mobility

- Scattering rate:

$$\frac{1}{\tau_{\mu\nu}(\mathbf{K})} = \frac{2\pi}{\hbar} \sum_{\mathbf{Q}} |V_{\mu\nu}(\mathbf{Q})|^2 \, \delta[E_\mu(\mathbf{K}) - E_\nu(\mathbf{K}+\mathbf{Q}) \pm \Delta E(\mathbf{Q})]$$

$$V_{\mu\nu}(\mathbf{Q}) = \int_0^\infty dz \, \zeta_\mu^*(z) \, \phi_{\mathbf{Q}}(z) \, \zeta_\nu(z)$$

- Momentum relaxation rate (along x-axis):

$$\frac{1}{\tau_{\mu\nu}^{(p,x)}(\mathbf{K})} \approx \frac{2\pi}{\hbar} \sum_{\mathbf{Q}} |V_{\mu\nu}(\mathbf{Q})|^2 \left(\frac{Q_x}{K}\right)$$

$$\times \delta[E_\mu(\mathbf{K}) - E_\nu(\mathbf{K}+\mathbf{Q}) \pm \Delta E(\mathbf{Q})]$$

- Mobility along x-axis (assuming spherical dispersion):

$$\mu_{x,x} = \sum_\nu \mu_\nu \frac{n_\nu}{n_s} =$$

$$\sum_\nu \frac{e n_\nu}{m_{x,\nu} k_B T n_s} \int_{E_\nu}^\infty dE \, (E - E_\nu) \, \rho_\nu(E) \, \tau_\nu^{(p,x)}(E) \, f_\nu(E)[1 - f_\nu(E)]$$

- Screening (dynamic):

$$V_{\mu\nu}^{(s)}(\mathbf{Q},\omega) = V_{\mu\nu}(\mathbf{Q}) - \sum_{\lambda\lambda'} \frac{\beta_\lambda(\mathbf{Q},\omega)}{Q} \, \mathcal{G}_{\mu\nu;\lambda\lambda'}(\mathbf{Q}) \, V_{\lambda\lambda'}^{(s)}(\mathbf{Q},\omega)$$

$$\mathcal{G}_{\mu\nu;\lambda\lambda'}(\mathbf{Q}) = \int_0^\infty dz \int_0^\infty dz' \, \zeta_\mu^*(z) \zeta_\nu^*(z') \, G_{\mathbf{Q}}(z,z') \, \zeta_\lambda(z) \zeta_{\lambda'}(z')$$

where $G_{\mathbf{Q}}(z,z')$ is the Poisson Green's function.

In matrix form:

$$V^{(s)}(\mathbf{Q},\omega) = [1 - \mathbf{\Pi}(\mathbf{Q},\omega)]^{-1} \, V(\mathbf{Q})$$

Scattering processes

- Bulk Si phonons:

$$|V_{\mu\nu}(\mathbf{Q})|^2 \propto \frac{\Delta_Q^2}{\hbar\omega_Q} F_{\mu\nu}(Q)$$

  - Example: for acoustic, intravalley, one-subband, variational wavefunction

$$\frac{1}{\tau^{(p)}} \approx \frac{3m_z b}{64\hbar^3}\frac{\Delta_{ac}^2}{\rho c_s^2} \rightarrow \mu_{ph} \propto b^{-1} \propto n_s^{-1/3}$$

  - In general, more complicated:
    1. Deformation potential is anisotropic:

$$\Delta_{LA} \rightarrow \Xi_d + \Xi_u \cos^2 \eta_Q$$

$$\Delta_{TA} \rightarrow \Xi_u \cos \eta_Q \sin \eta_Q$$

    2. Subband dispersion is nonparabolic
    3. Subband dispersion is non-spherical
    4. Intervalley scattering (projected onto 2D BZ)
    5. Are bulk Si phonons OK near the interface?
    6. What about screening?

- Coulomb scattering (with dopants, oxide charges, etc):

$$V_{\mu\nu}(\mathbf{Q}) \propto \frac{e^2 N_C^{1/2}}{Q^2} \tilde{\mathcal{G}}_{\mu\mu;\nu\nu}(Q)$$

(must be screened!) and

$$\mu_C \propto \frac{n_s^{4/3}}{N_C}$$

- Surface roughness:
Ando's model assumes 1st-order pertubation given by steps at interface of rms height Δ and correlation-distance Λ.

$$V_{\mu\nu}(\mathbf{Q}) \propto \Delta\ \Lambda\ F_s \begin{cases} e^{-Q^2\Lambda^2/4} \\ (1+Q^2\Lambda^2/2)^{-1} \end{cases}$$

(must be screened) and

$$\mu_{SR} \propto \Delta^2 \Lambda^2\ n_s^{-2}$$

Subbands

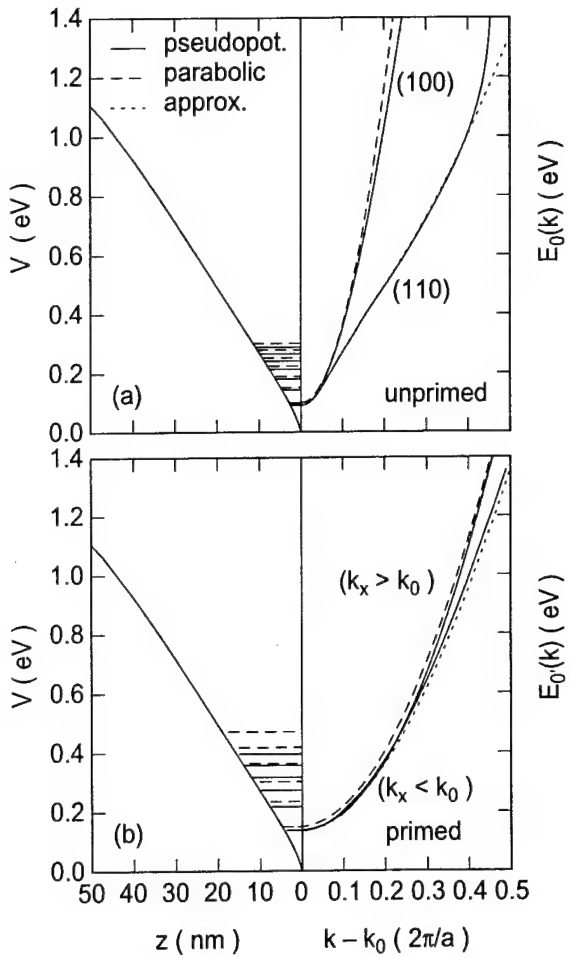

Triangular-well approximation

- Energy levels:

$$E_\mu = \left(\frac{\hbar^2}{2m_z}\right)^{1/3} \left[\frac{3\pi F_s}{2}\left(\mu + \frac{3}{4}\right)\right]^{2/3}$$

- Wavefunctions:

$$\zeta_\mu(z) = N\, Ai\left[\left(\frac{2m_z e F_s}{\hbar^2}\right)^{1/3}\left(z - \frac{E_\mu}{eF_s}\right)\right]$$

- Variational ground-state wavefunction:

$$\zeta_0(z) \approx \left(\frac{b^3}{2}\right)^{1/2} z\, e^{-bz/2}$$

with

$$b = \frac{3}{z_0} \propto n_s^{1/3}$$

Phonon-assisted intervalley scattering

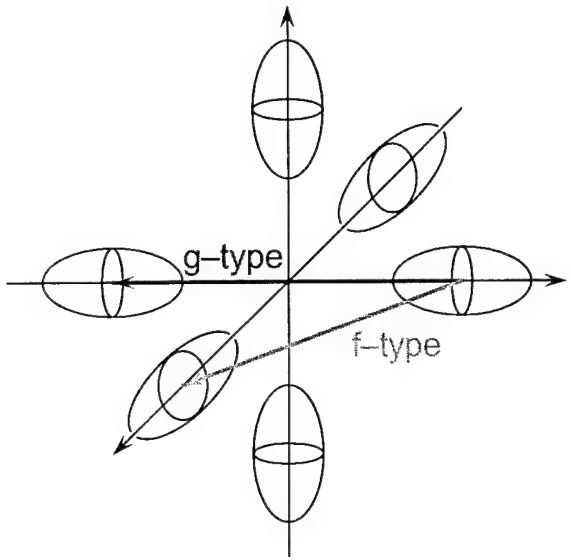

Mobility split into various components

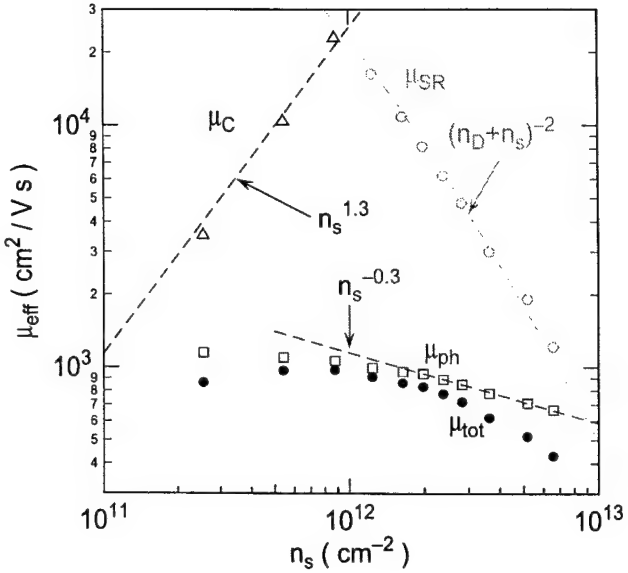

The fight for the right phonon-limited mobility

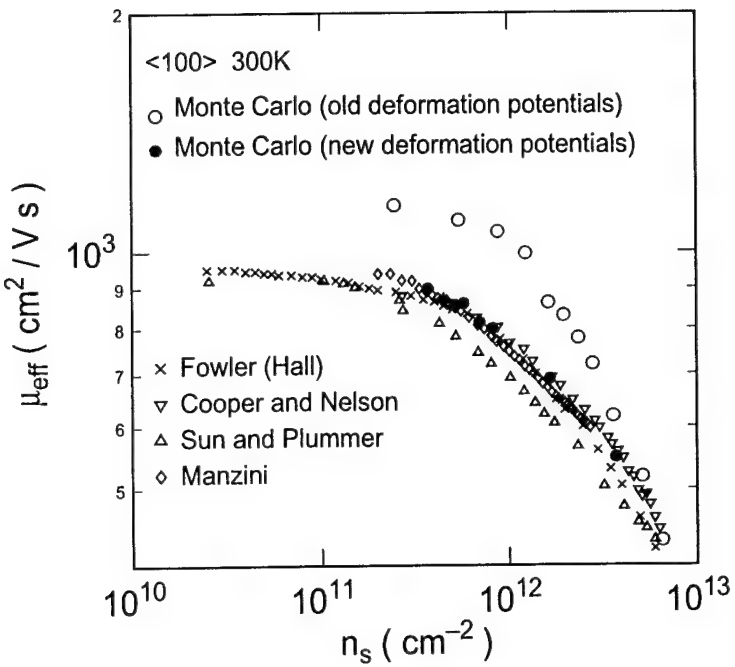

The $Si/SiO_2/Si$ system

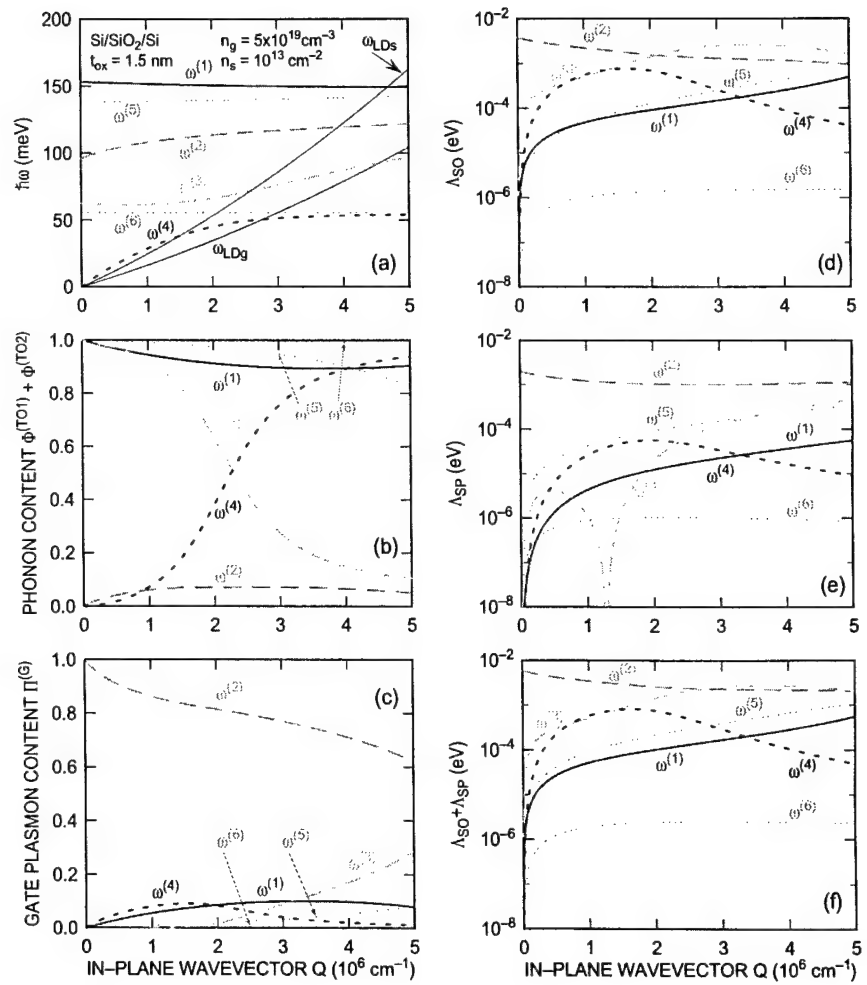

The Si/ZrO_2/Si system

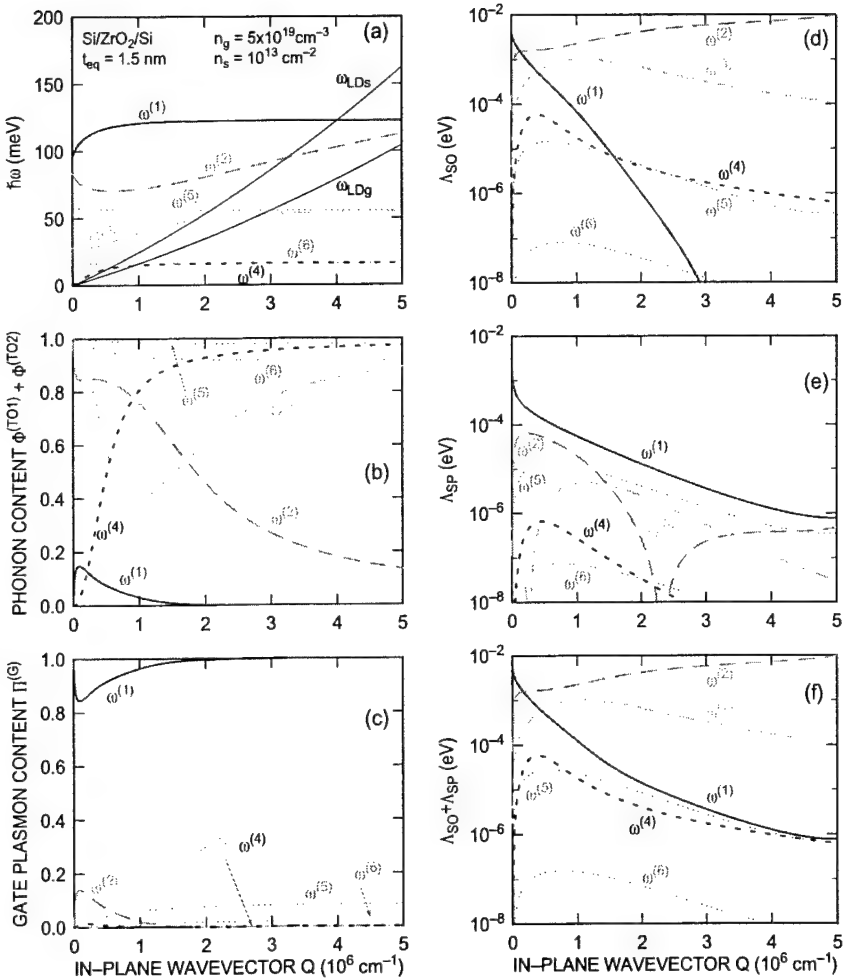

Effective mobility I (average n_g)

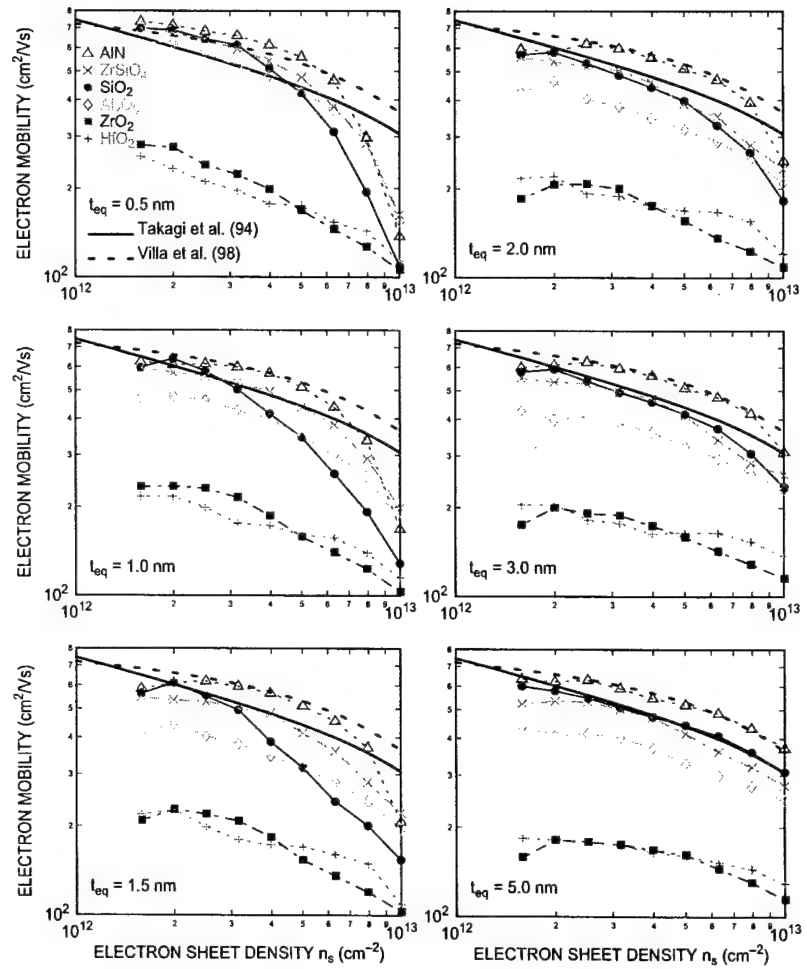

Effective mobility II (Q-dependent n_g)

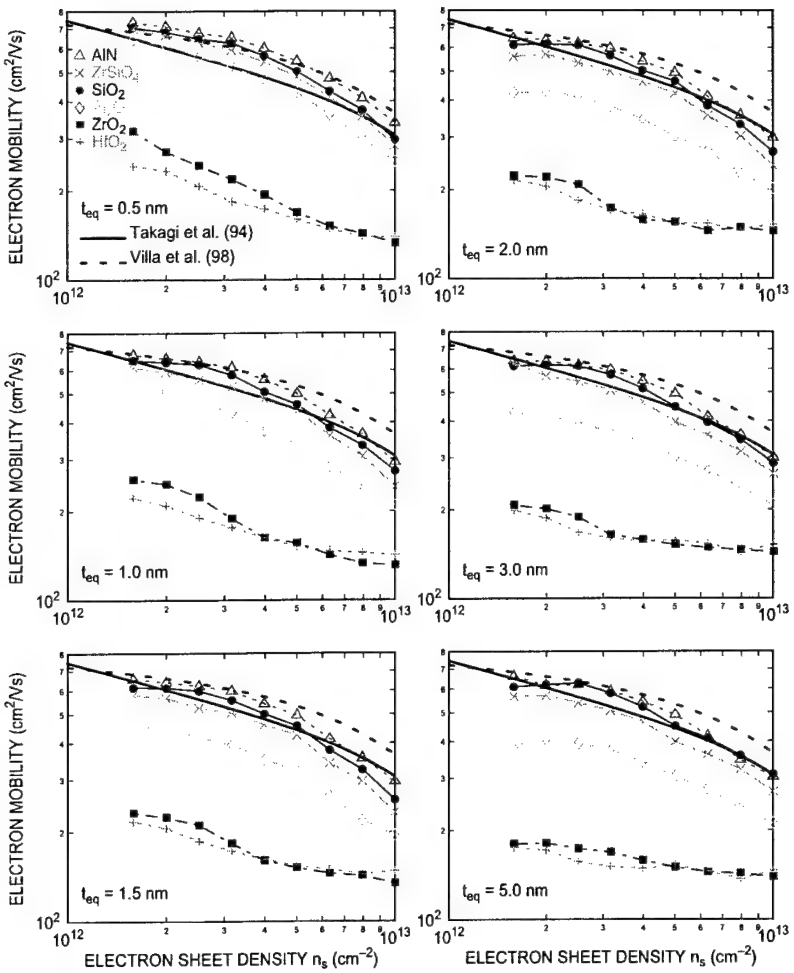

Components of the mobility (low density)

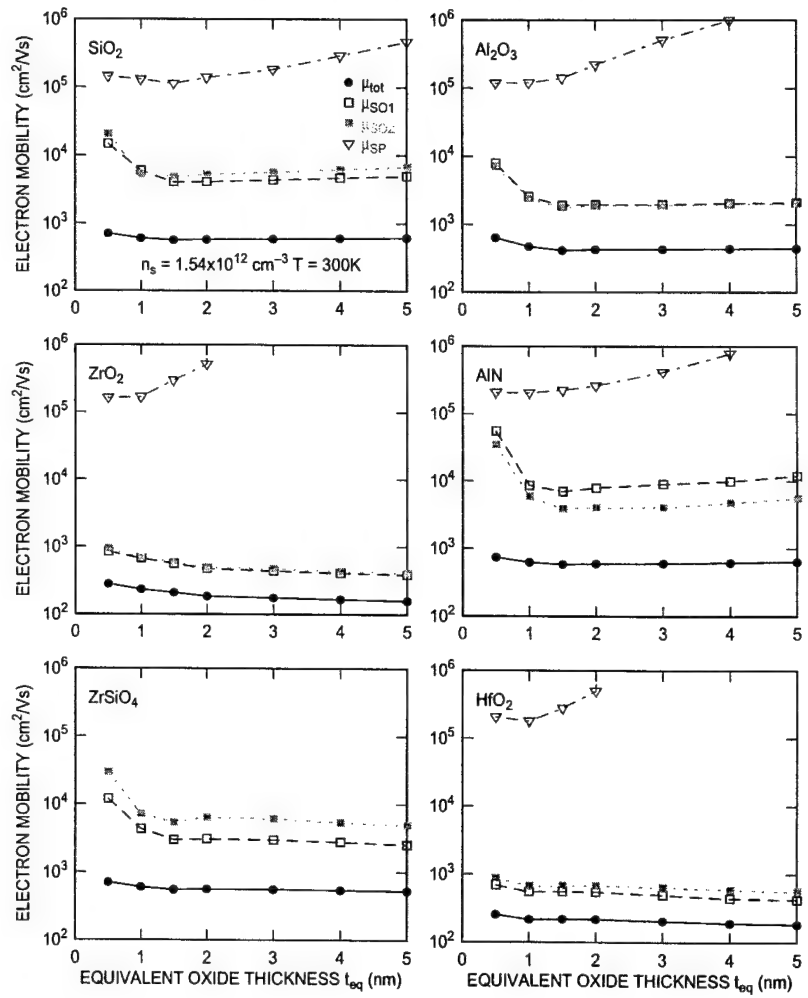

Components of the mobility (high density)

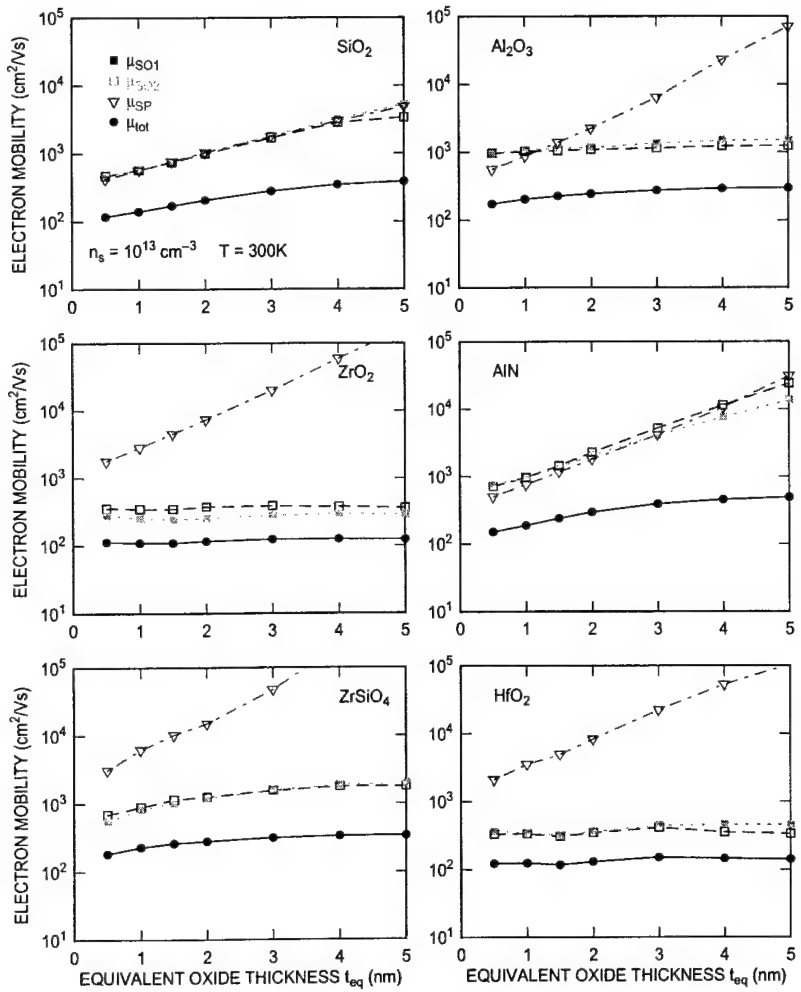

Mobility vs static dielectric constant

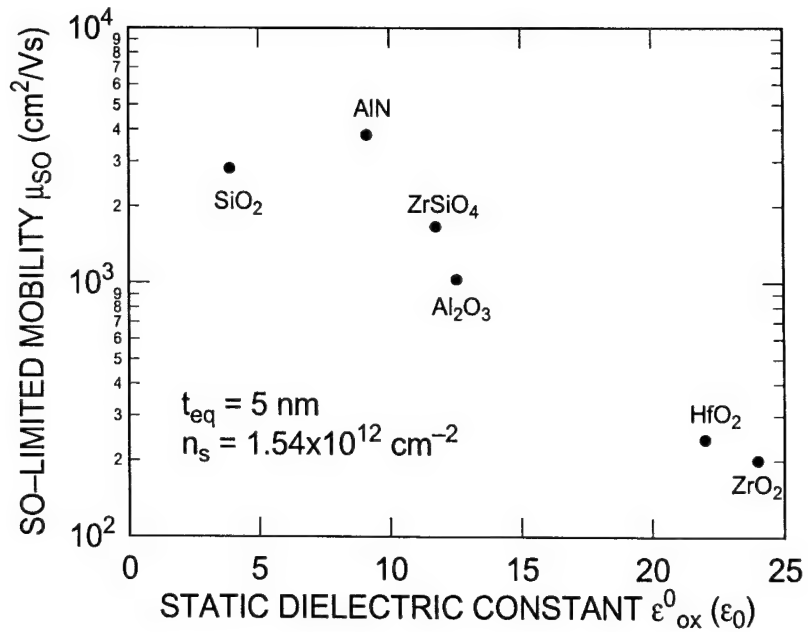

Effect of SiO_2 interfacial layer

- Interfacial layer probably unavoidable, possibly desirable (with moderation...)
- Full system Si/high-κ/SiO_2/Si too cumbersome...
  secular equation

$$(\epsilon_g+\epsilon_\kappa)(\epsilon_s+\epsilon_{ox})(\epsilon_{ox}+\epsilon_\kappa) + (\epsilon_g-\epsilon_\kappa)(\epsilon_s+\epsilon_{ox})(\epsilon_{ox}-\epsilon_\kappa)\, e^{-2Qt_\kappa}$$
$$- (\epsilon_g - \epsilon_\kappa)(\epsilon_s - \epsilon_{ox})(\epsilon_{ox} + \epsilon_\kappa)\, e^{-2Q(t_\kappa+t_{ox})}$$
$$- (\epsilon_g + \epsilon_\kappa)(\epsilon_s - \epsilon_{ox})(\epsilon_{ox} - \epsilon_\kappa)\, e^{-2Qt_{ox}} = 0$$

  (16 coupled modes!)
- Consider instead 'unscreened' high-κ/SiO_2/Si system and only one TO-mode in each insulator.
  3 modes with high-Q-frequencies:
  1. SiO_2 mode Ω_{TO} localized at the Si/SiO_2 interface:

$$\omega_Q^{(-)} \approx \Omega_{TO}\left[\frac{\epsilon_{ox}^0 + \epsilon_{Si}^\infty}{\epsilon_{ox}^i + \epsilon_{Si}^\infty}\right]^{1/2}$$

  2. SiO_2 mode Ω_{TO} localized at the high-κ/SiO_2 interface:

$$\omega_Q^{(+)} \approx \Omega_{TO}\left[\frac{\epsilon_{ox}^0 + \epsilon_\kappa^\infty}{\epsilon_{ox}^i + \epsilon_\kappa^\infty}\right]^{1/2}$$

     (negligible, as for modes 5 and 6 before)
  3. remote) high-κ mode ω_{TO} localized at the Si/SiO_2 interface:

$$\omega_Q^{(\kappa)} \approx \omega_{TO}\left[\frac{\epsilon_\kappa^0 + \epsilon_{Si}^\infty}{\epsilon_\kappa^i + \epsilon_{Si}^\infty}\right]^{1/2}$$

Effect of the SiO_2 interfacial layer

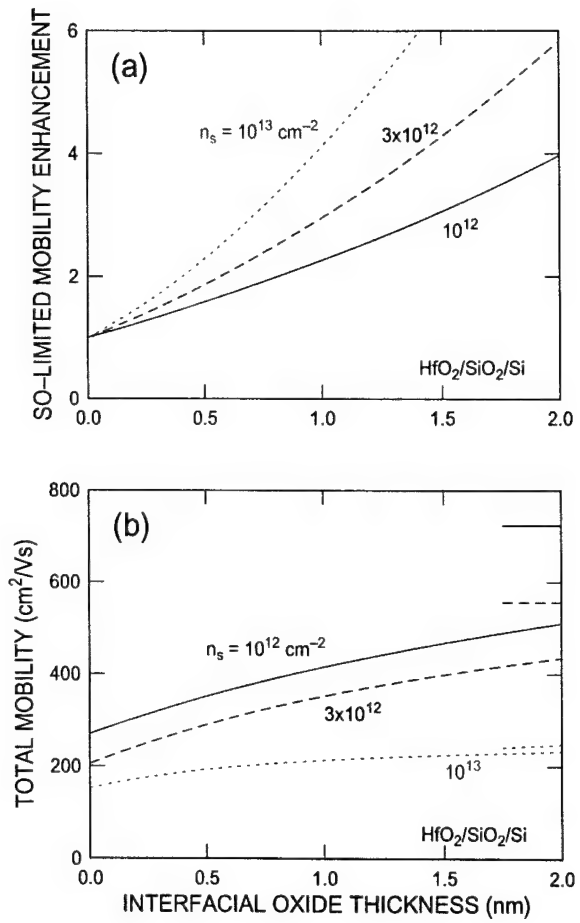

Conclusions

- Experimental confirmation?
  - Poor mobility observed almost always, but mainly due to poor material quality (traps, interface states, non-stochiometry, interfacial layers). Must solve these problems first! n_s hard to measure accurately.
  - Parameters: what material do we really have? How far from 'ideal'?
  - Still...trends show HfO_2 and ZrO_2 yield worst mobility (Ragnarsson, Callegari, 00-01), $ZrSiO_4$ somewhat better than ZrO_2 (Qi, 00), Al_2O_3 in-between, AlN very poor (but Si_3N_4 interfacial layer present)
- If theory is right:
  - Interfacial and many-body effects paramount in small devices:
    - Coulomb effects make 'ballistic limit' only a theoretical dream (metal contacts?)
    - there's no more 'bulk', only 'interfaces', in small devices
  - Must pay for high κ with poor mobility
  - Metal-oxides worst
  - Silicates promising
  - AlN promising (if we only could get rid of the Si_3N_4 interfacial layer!)
  - Thin SiO_2 interfacial layer desirable
  - Assessing whether this low mobility is a fatal flaw or not is up to the circuit designers. Alternatives to high-κ are even riskier propositions.

Full Bandstructure Calculations for Transport in Wide-Band-Gap Semiconductors*

Stephen M. Goodnick

Department of Electrical Engineering
Arizona State University
stephen.goodnick@asu.edu
www.eas.asu.edu/~goodnick

*Supported by ONR and the DARPA/Phophor Technology Center of Excellence

Outline

1. Wide-Bandgap Materials
2. Electronic Structure Calculations
3. Impact Ionization Rate
4. Electron-Phonon Interaction
5. Full-band Monte Carlo Simulation
6. Experimental Results

Collaborators

- Richard Akis, Joy Barker, Manfred Dür*, David Ferry, Trevor Thornton, *Arizona State University*
- Shankar Pennathur*, John Wager, *Oregon State University*
- Marco Saraniti, *Illinois Inst. Tech.*
- Niels Fitzer, Ronald Redmer, Martin Reigrotzki*, *Universität Rostock*
- Martin Städele* and Peter Vogl, *Technische Universität München*
- Randy Shul, *Sandia National Labs*
- Daniel Koleske, *Naval Research Labs*

Wide-Bandgap Semiconductors

Column IV
- SiC

III-V Nitrides
- GaN, AlN, InN

II-VI Compounds
- ZnS, ZnSe, MnS, SrS, CeS

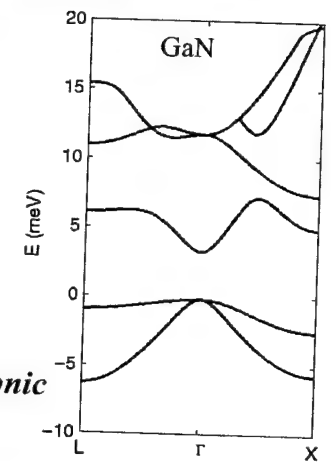

Compound Semiconductors: *ionic zincblende→wurzite →rocksalt*
E_G~ 3-5 eV
Breakdown field ~ 1 MV/cm

Wide-Bandgap Semiconductor Applications

High-Frequency Power Amplifiers

- GaN MESFETS
- AlGaN/InGaN HEMTs

Optical Sources

- ZnS/ZnSe, AlGaN/InGaN LEDs/Lasers (Green-Blue-uv)
- Phosphor materials (ZnS:Mn, SrS:Ag, CeS:Mn)-FED, TFEL

High Field Transport in TFEL Devices

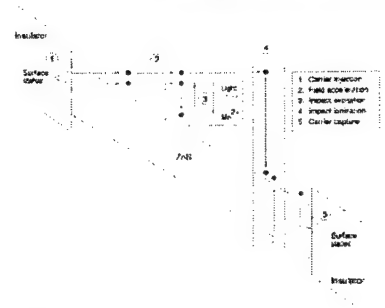

High field phenomena affecting TFEL performance:

- **Impact excitation of luminescent impurities**
- **Band to band impact ionization of electrons and holes**

Issues

- **Average carrier energies at 1-2 MV/cm are 2-3 eV, several conduction bands occupied: Full bandstructure must be considered**
- **Band to band impact ionization process in wide bandgap materials not well understood**
- **Electron-phonon interaction at high fields is unknown experimentally in phosphor materials**

General Modeling Approach

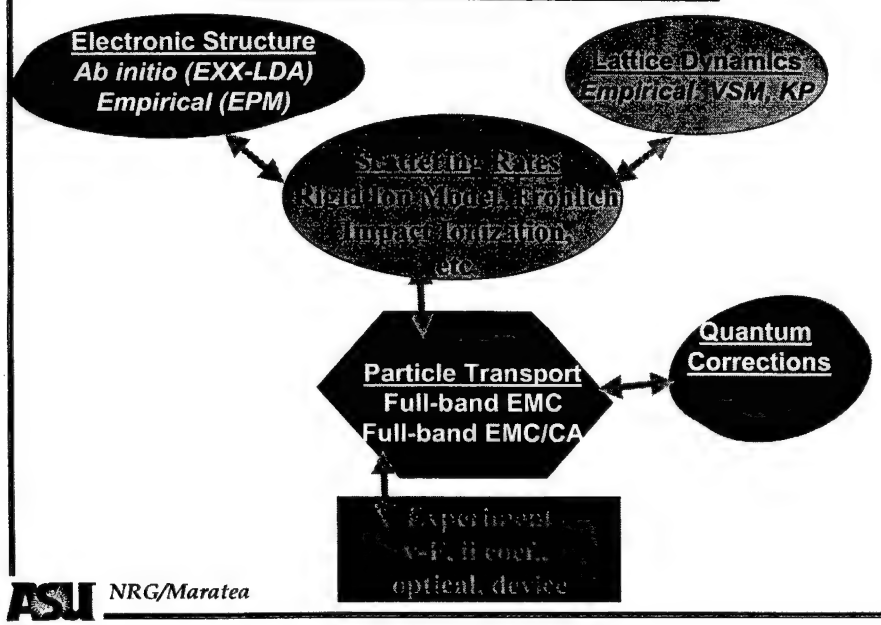

Bandstructure for Cubic GaN, ZnS, and SrS

Empirical Pseudopotential Method

Local and nonlocal bandstructures for cubic GaN, ZnS and SrS are calculated either from formfactors in literature, or derived using least squares fit to existing critical point data.

- ZnS
  - **-Local: Walter and Cohen, *Phys. Rev.* 183, 763 (1969)**
  - **-Nonlocal: M. Dür *et al.*, *JAP* 83, 3176 (1998)**
- SrS
  - **-Nonlocal- Reigrotski *et al*, *JAP* 86, 4458, (1999)**
- GaN
  - **-Oguzman *et al.*, *JAP* 80,4429 (1996)**
  - **-Xia *et al.*, *Phys. B* 59,10119 (1999)**

Ab Initio Bandstructure

EXX-LDA (exact exchange-local density approximation) Method[1]

- **Kohn-Sham method is particular, exact realization of density functional theory which maps interacting system onto non-interacting system of the same density**
- **LDA approximates BOTH exchange and correlation potential within the Kohn-Sham model**
  - **–Good ground state properties but poor band gaps**
- **EXX-LDA is a systematic step beyond LDA which treats the exchange potential EXACTLY**
  - **–EXX+LDA yields excellent ground state properties AND band gaps**

[1]M. Städele, J. A. Majewski, P. Vogl, and A. Görling, *Phys. Rev. Lett.* 79, 2089 (1997)

EXX Results for Cubic Semiconductors

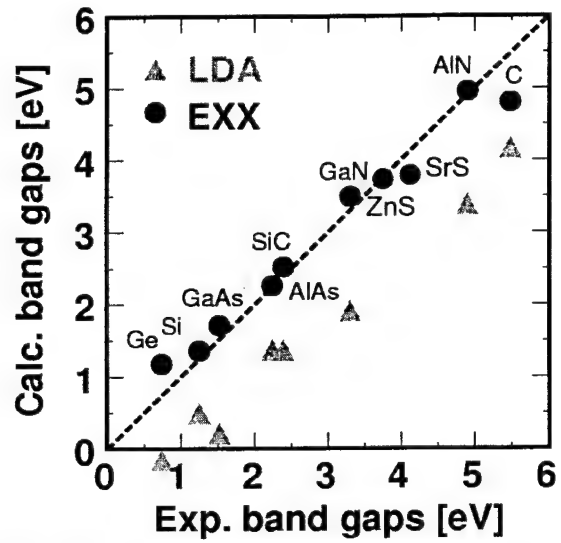

Band Structure Based on EXX and Empirical Pseudopotential Method (EPM)

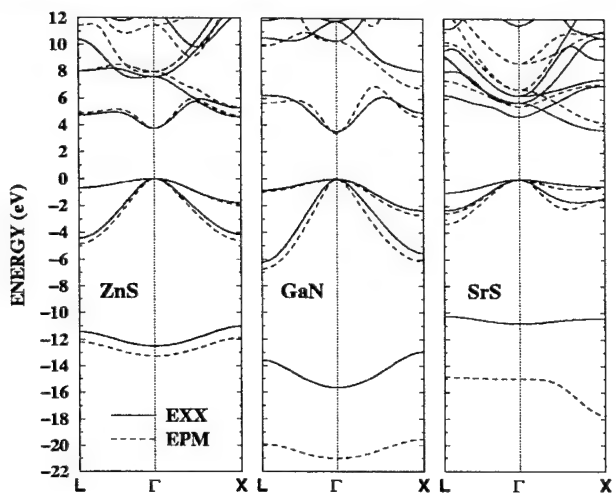

SrS Band Structure Based on EXX and Empirical Pseudopotential Method (EPM)

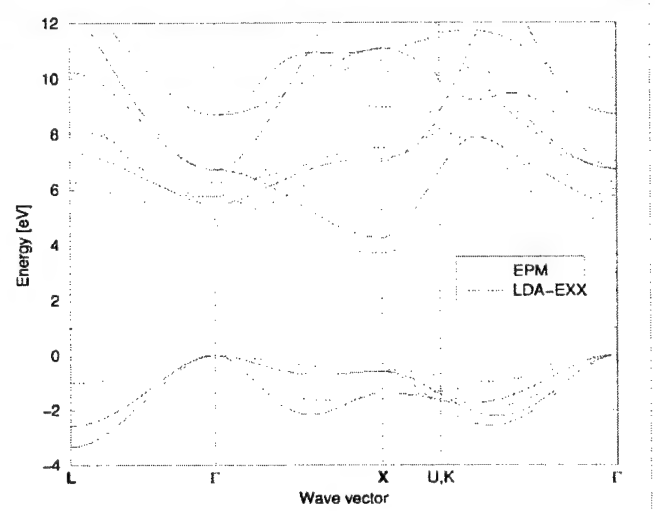

Comparison of EXX and EPM Results for SrS and ZnS to Experimental Data (in eV)

SrS: indirect

SrS	EXP	EXX	EPM
$E(\Gamma_v\text{-}X_c)$	4.32	3.69	4.26
$E(\Gamma_v\text{-}\Gamma_c)$	5.33	4.67	5.45
$E(X_v\text{-}X_c)$	4.83	4.21	4.86

EXP: Kaneko and Koda, *J. Cryst. Growth* **86**, 72 (1988)

ZnS: direct

ZnS	EXP	EXX	EPM
$E(\Gamma_v\text{-}\Gamma_c)$	3.68	3.73	3.73
$E(L_v\text{-}L_c)$	5.73	5.45	5.59
$E(X_v\text{-}X_c)$	6.31	6.43	6.58

EXP: Walter and Cohen, *Phys. Rev.* **183**, 763 (1969)

EXX Density of States for SrS, Zns, and GaN

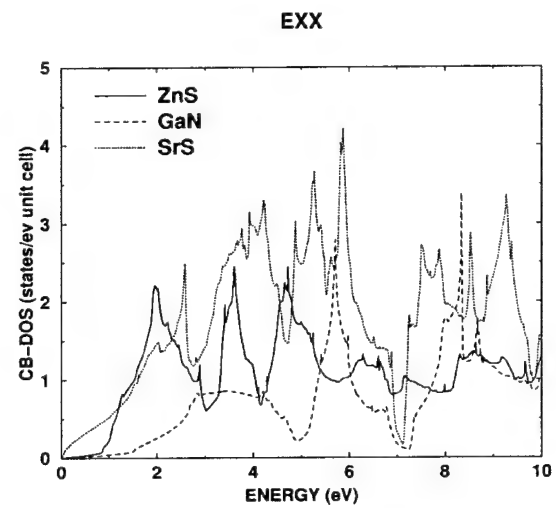

Impact Ionization Rate in Wide-Bandgap Materials

- **Band to band impact ionization rate calculated directly from pseudopotential bandstructure (M. Reigrotzki *et al.*, *Phys. Rev. B* 52, 1456 [1995]).**
- **Energy dependent scattering rate is fit to $R(E) = P\,(E-E_{th})^a$**

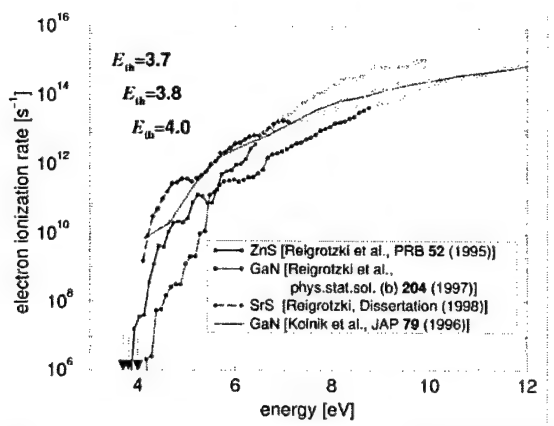

Impact Ionization Rate for Holes

Cut-off in hole rate due to finite VB width

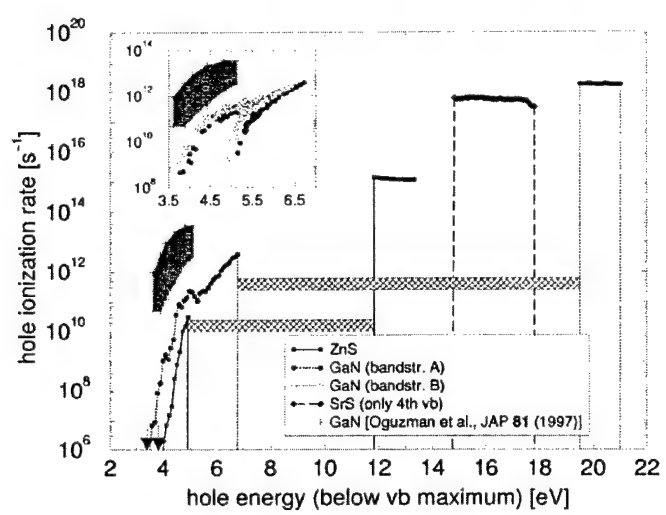

Intercollisional Field Effect in Impact Ionization

- Quade et al. (PRB 50, 7398, 1994) ICFE in parabolic band approximation based on density matrix approach
- Redmer et al (JAP 87, 781, 2000) Extension of Quade et al. to full bandstructure, widebandgap materials using Zubarev nonequilibrium statistical operator approach.

$$\frac{\partial}{\partial t} f_{\upsilon,\mathbf{k}}(t) + e\vec{E}_0(t) \bullet \frac{\partial}{\partial \mathbf{k}} f_{\upsilon,\mathbf{k}}(t) = J_e(\upsilon,\mathbf{k},t)$$

- Treating only electron-electron interactions,

$$r_{ii}(\varepsilon_1, E_0) = C\int_0^\infty dE \left(\frac{E}{E_{th}}\right)^a \frac{1}{E_F^{ii}} Ai\left(\frac{E_{th} - \varepsilon_1 + E}{E_F^{ii}}\right)$$

$$E_F^{ii} = \left[\frac{(1+\alpha)(eE_0)^2}{8m_e\hbar}\right]^{1/3}$$

Intercollisional Field Effect in Impact Ionization

- Softening of threshold field is main effect, little effect at high energy

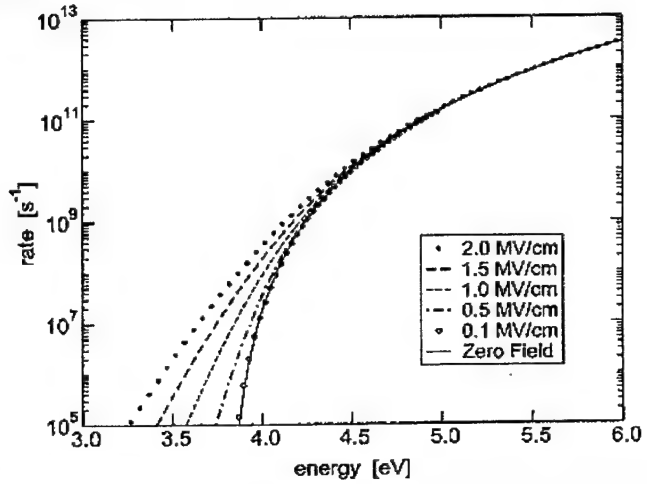

Direct Calculation of Electron-Phonon Scattering Rate

MOTIVATION

- The electron-phonon coupling is the dominant scattering process controlling the high field distribution
- Deformation potential model relies on constants which are not known experimentally for phosphor materials of interest
- A method is required to obtain the electron-phonon coupling directly from the electronic and vibrational properties of the crystal

METHOD

- Rigid-ion model (RIM) used[2] in which the rigid displacement of the atomic pseudo-potential (from EPM calculation) due to lattice vibrations gives the interaction potential

 [2]M. V. Fischetti and J. M. Higman, 1991

Scattering Mechanisms

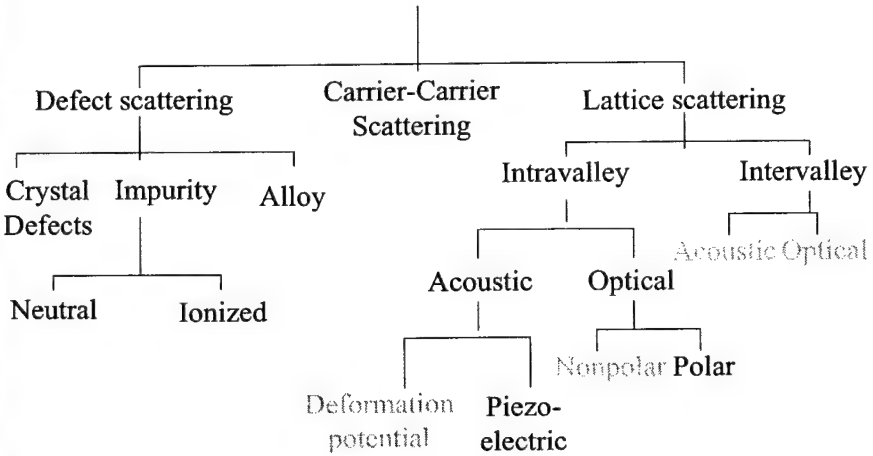

RIM electron-phonon coupling constant that enters into the scattering rate

$$\Delta_j(n\mathbf{k};n'\mathbf{k}') = -\frac{i}{2}(M_1+M_2)^{1/2}$$
$$\times\sum_{\mathbf{GG}'}[\,C^n_{\mathbf{G}}(\mathbf{k})C^n_{\mathbf{G}'}(\mathbf{k}')^*(\mathbf{Q}-\mathbf{G}+\mathbf{G}'-\mathbf{G_u})$$
$$\sum_\alpha \mathbf{e}^\alpha_{Qj}M_\alpha^{-1/2}\,\underline{V_\alpha(\mathbf{Q}-\mathbf{G}+\mathbf{G}'-\mathbf{G_u})} \longrightarrow$$
$$\times e^{-i(\mathbf{G}+\mathbf{G}'-\mathbf{G_u})\cdot\tau_\alpha}\delta_{\mathbf{k}-\mathbf{k}'+\mathbf{Q},\mathbf{G_u}}\,]$$

Important complication: require the electron potential for arbitrary q values, not just the reciprocal lattice vectors

To calculate this quantity, you need the band structure, the pseudo wavefunctions and the phonon dispersion relations

Phonon Spectrum of ZnS

Phonon modes calculated using an empirical valence-shell model for the lattice dynamics with parameters fit to measured phonon dispersion (Vagelatos *et al.*, *J. Phys. Chem.* 60, 3613 [1974]).

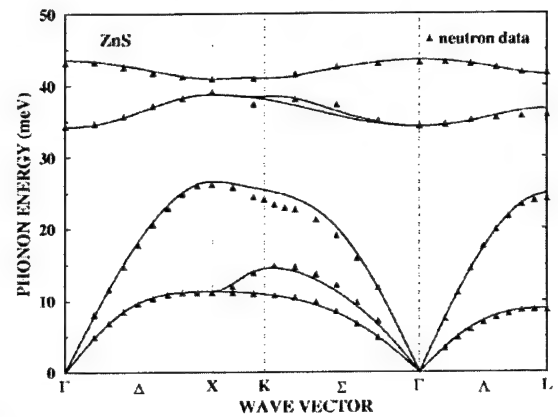

Interpolation of Local Pseudopotentials for ZnS

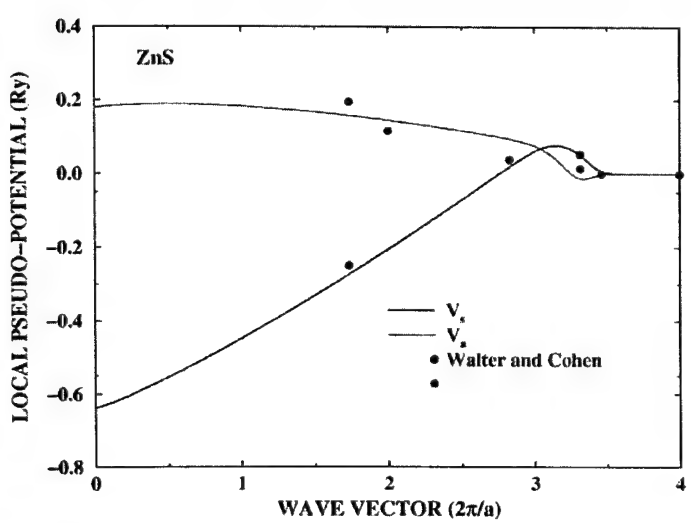

Calculated average electron-phonon scattering rate versus energy for ZnS using the rigid-ion model compared to density of states.

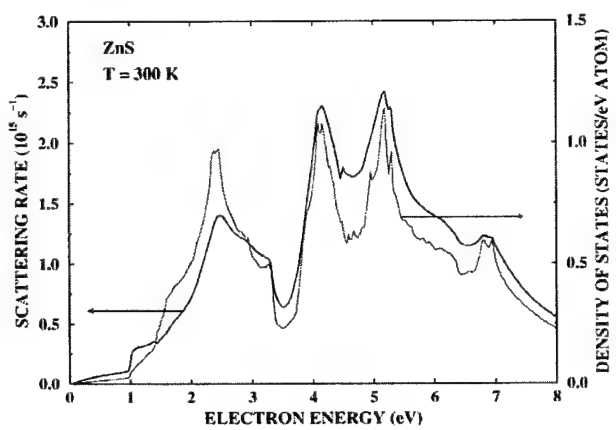

Phonon dispersion for zincblende GaN obtained using a ten parameter empirical Shell model[1]

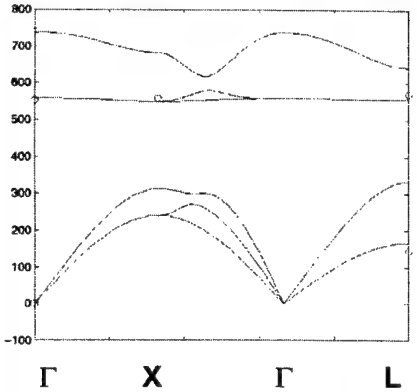

To fit the parameters of the model, experimentally determined phonon frequencies[2], as well as several theoretically values calculated using a Keating model[3] were used

[1] K Kunc, OH Neilson, Comput. Phys. Comm. 17, 413 (1979)

[2] T. Azuhata *et al.* J. Phys. Condens. Matter 7, L129 (1995)

[3] J. Zi *et al.* J. Phys. Condens. Matter 8, 6323 (1996)

GaN band structures used based on the Empirical Pseudopotential Method (EPM)

IH Oguzman *et al.*, J. Appl. Phys. 80,4429 (1996)

J-B Xia *et al.*, Phys. B 59,10119 (1999)

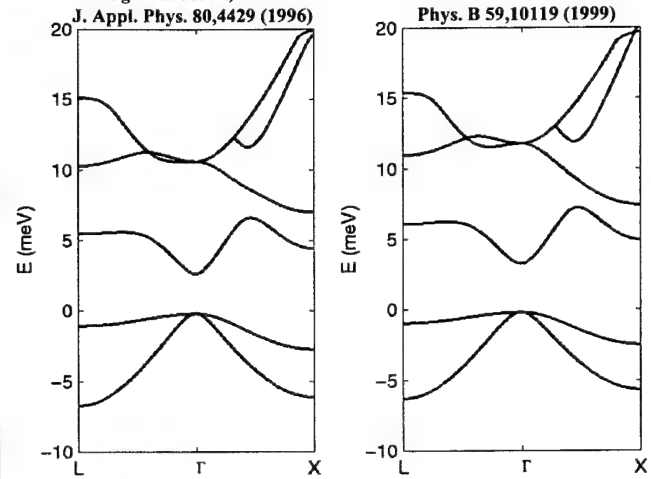

The EPM uses fitted form factors to represent the atomic potentials $V_{Ga}(G)$, $V_N(G)$, for a limited set of reciprocal lattice points, G

Only local potentials were used in both cases

Density of states for the two cases:

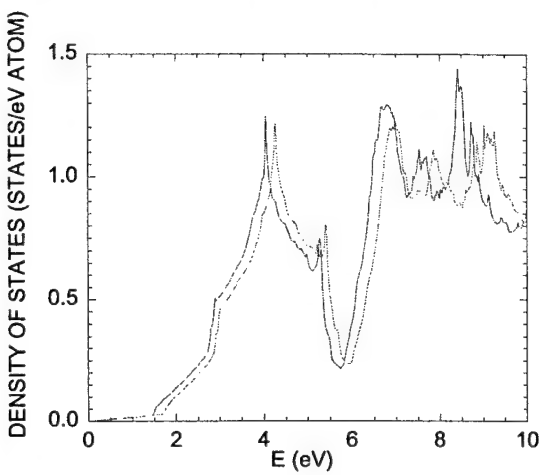

Oguzman *et al.*

J-B Xia *et al.*

Interpolation schemes for the pseudopotentials

Model 1: use polynomial interpolation to fit the form factors of Oguzman *et al.* (J. Appl Phys. 80, 4429, 1996) but impose the condition:

$$V_1(0) = V_2(0) = 0$$

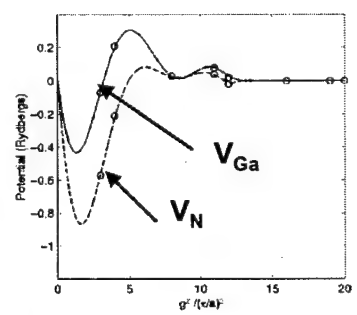

Circles represent actual factors used by Oguzman *et. al.*

Model 2: Use the same functional form and fits used by Xia *et al.* (Phys. Rev. B 59, 10119, 1999) :

$$V_i(g) = a_1\left(g^2 - a_2\right)/\left[1 + \exp\left(a_3\left(g^2 - a_2\right)\right)\right]$$

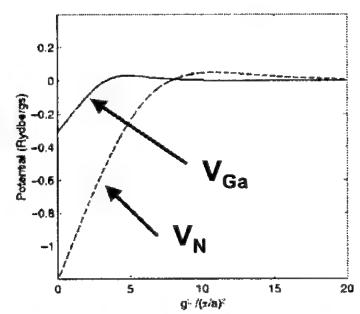

Note that model 2 takes on more extreme values near zero

Phonon scattering rate results for the two models

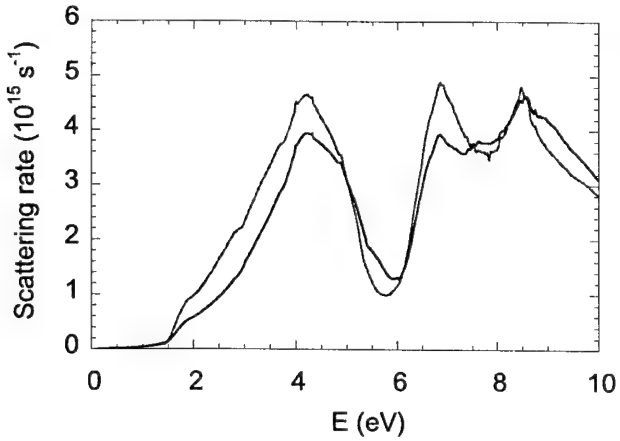

Previous work on ZnS has suggested that the high field scattering rate in wide band gap materials is dominated by optical phonon deformation potential scattering : $R(E) \sim K_{fit}^{2} N(E')$

K_{fit} **is a fitted deformation potential constant and** $N(E')$ **the final density of states**

Comparison between fit and full calculations:

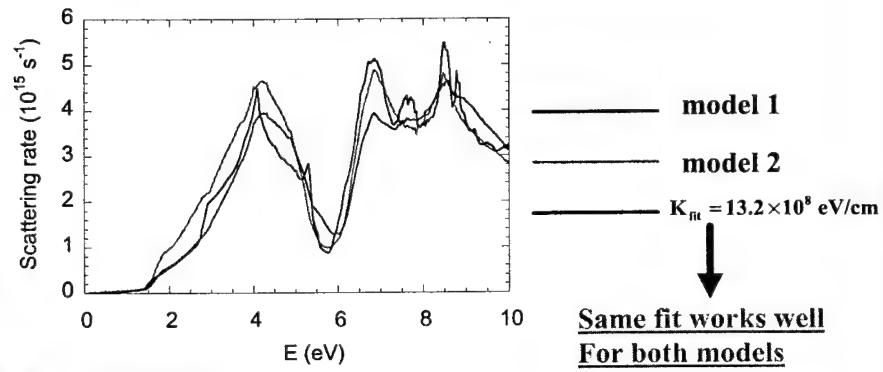

Same fit works well For both models

Second phonon dispersion model for zincblende GaN was also considered

valence shell fit to the data of
K. Karch, J.-M. Wagner, and F. Bechstedt, Phys. Rev. B **57**, 7043 (1998)

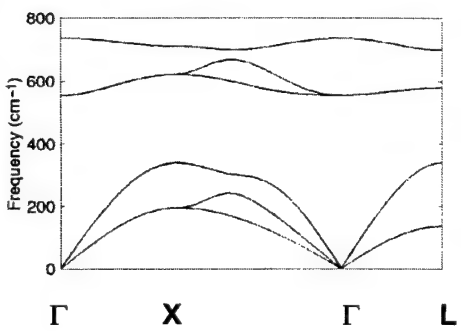

The data of Karch *et al.* was calculated within the framework of self-consistent density functional perturbation theory.

differences:
More dispersion shown TO branches than with the Zi *et al.* fit.

The frequencies attained by the TA branchs are significantly lower than for the Zi *et al.* case.

Phonon scattering rate results for the two phonon models

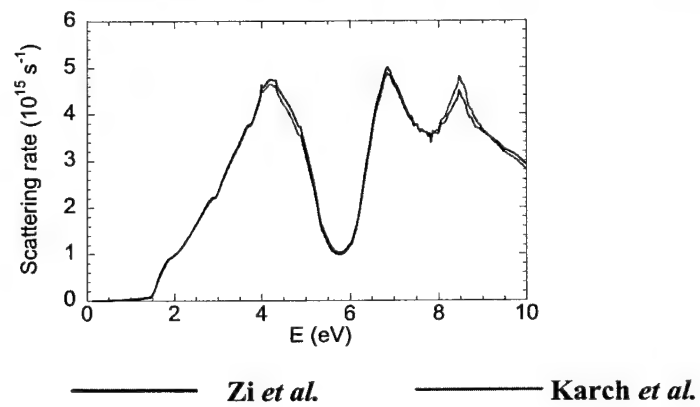

using Oguzman *et al.* pseudopotential parameters

Full Band Ensemble Monte Carlo Model

- Full band dispersion used for particle dynamics
- Scattering treated a) pseudo isotropic, energy averaged rates from full band model b) full anisotropic rates in CA model
- Deformation potential Ansatz assumed, with values chosen either from fit to experimental data or extracted from RIM calculation
- Polar optical assuming Fröhlich coupling
- Ionized impurity, other elastic mechanisms included for low energies

Impact Ionization Coefficient for Electrons

- Thompson and Allen (J. Phys. C 1989) measured the impact ionization coefficient in ZnS from multiplication measurements on photoinjected carriers in reverse biased Schottky barriers
- They assumed the the e and h impact ionization rates were equal in order to relate multiplication to the ii coefficient

- Assuming the hole ionization rate is negligible, the expression relating carrier multiplication to the ionization coefficient is given by

$$\ln M_n = \int_0^W \alpha_n dx = \alpha_n(E_m) W_{eff}$$

- Using this relation, we re-evaluated the impact ionization coefficient derived by Thompson and Allen assuming equal electron and hole coefficients

Re-Evaluation of Experimental Impact ionization coefficient assuming only electrons

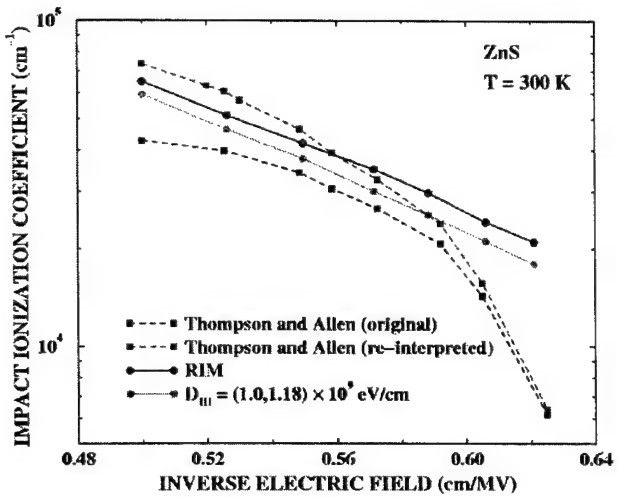

Comparison of steady-state particle distributions in ZnS at 2 MV/cm and 300 K using rigid-ion model and deformation potential sets D_{II} and D_{III}.

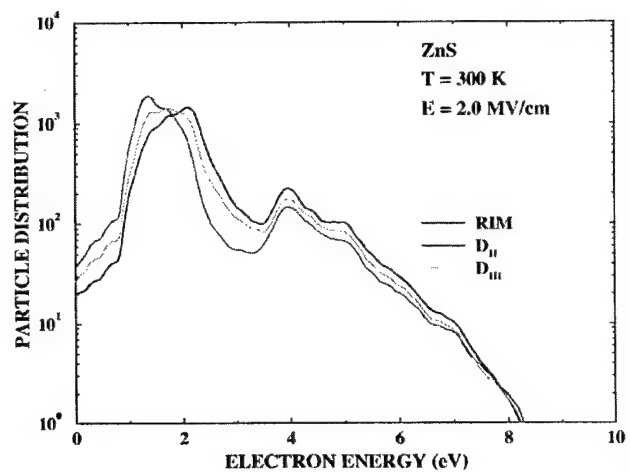

Effect of ICFE on Distribution Function and Impact Ionization Coefficient

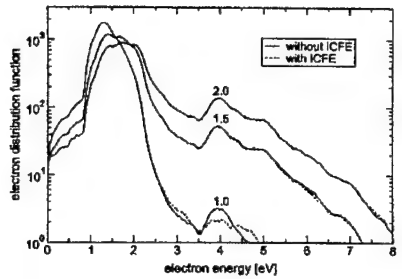

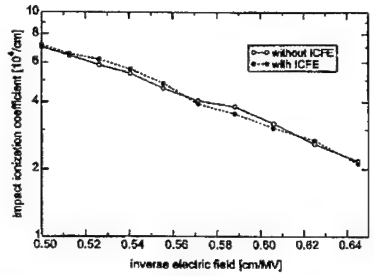

Calculated Brightness-Field Characteristics for $ZnS:Mn^{+2}$ assuming zero space charge

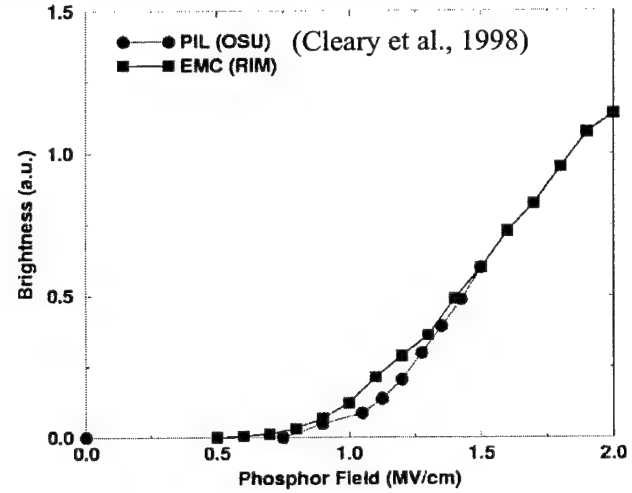

Calculated Velocity Field Characteristics

Drift velocity results of full-band Monte Carlo simulations using the fitted deformation potential at 300 K

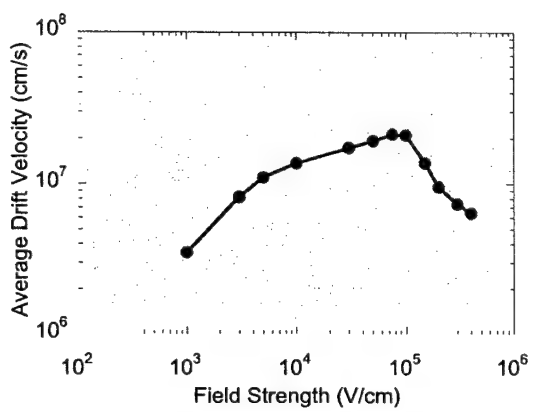

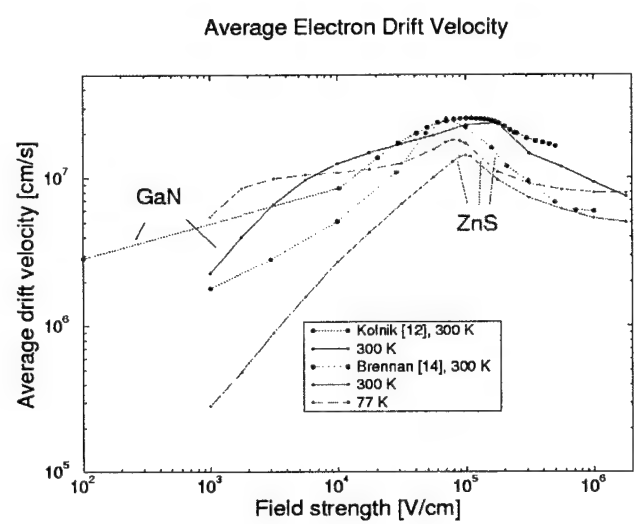

High Field Transport in GaN: Experimental

Pulse I-V measurements of velocity field characteristics

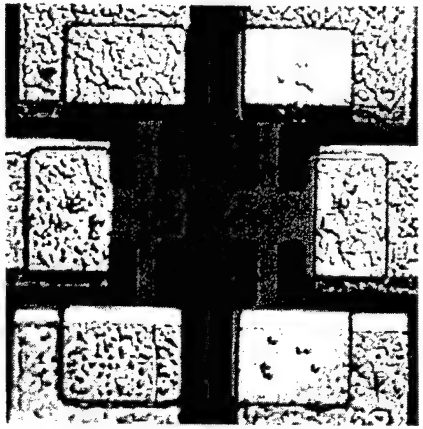

GaN Test Structure Process Flow

i) Mesa Etch
   ICP (Sandia)
   Photo-chemical etching

ii. Ti/Al Ohmic Contacts

iii) Ti/Au Bond Pads

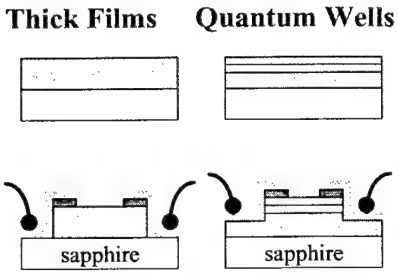

Pulsed Measurements

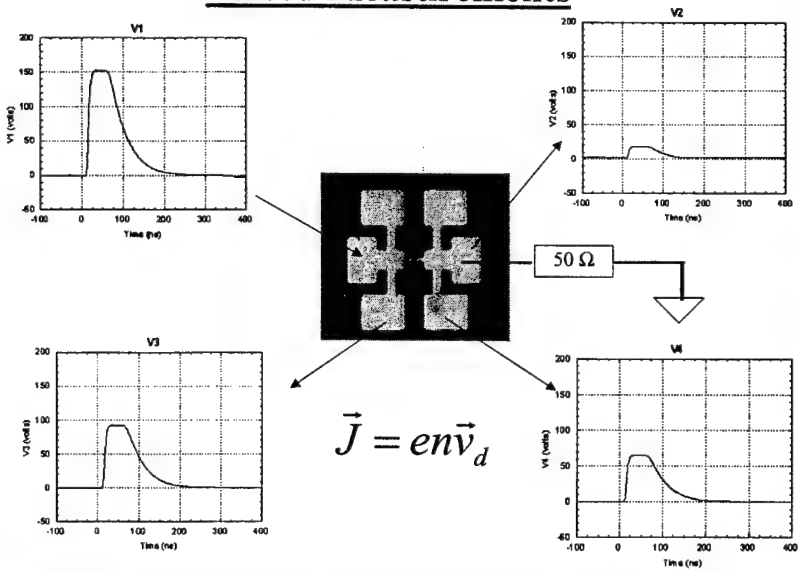

$$\vec{J} = en\vec{v}_d$$

Results at low electric fields from GaN thick films

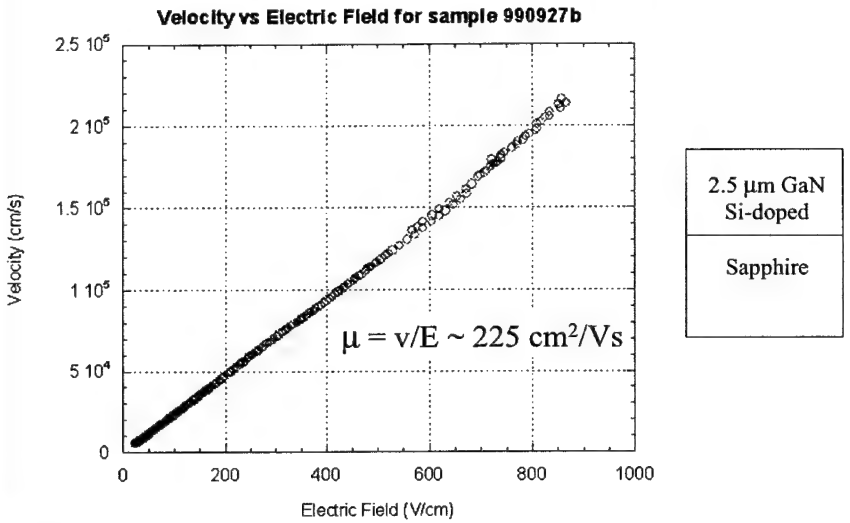

High Field Pulse Measurements in Bulk GaN

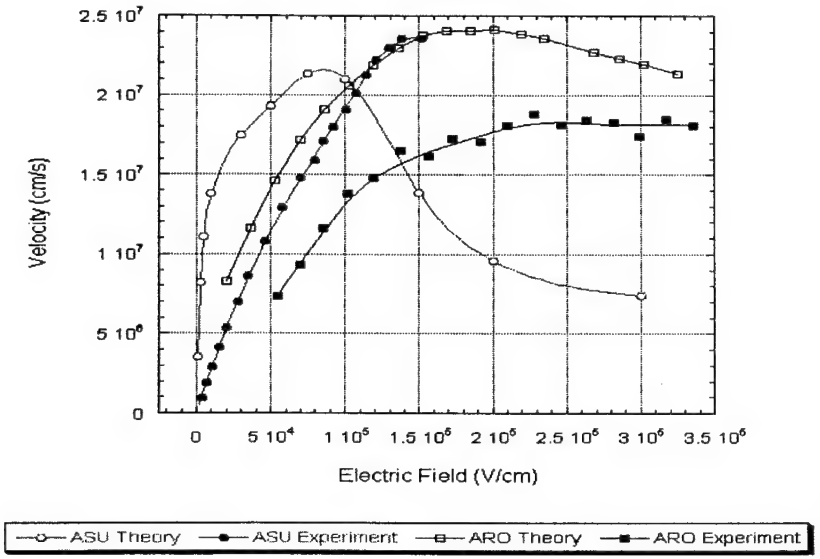

Summary

Bandstructure Calculations

- Ab initio techniques more accurate, but not necessarily better than empirical methods for transport

Impact Ionization Rate for Holes in Phosphors

- Narrow valence band structure for ZnS and SrS implies impact ionization due to holes should be weak process
- Re-evaluation of Thompson-Allen data, comparable to theory
- No effect of ICFE on impact ionization

Velocity Field Characteristics

- Deformation potential of 1.3×10^9 eV/cm fits RIM calculation well: dominant mechanism above intervalley threshold
- Comparison to experimental measurement by different techniques

Semiclassical modeling of small semiconductor devices

Max Fischetti

IBM Research Division
T. J. Watson Research Center
Yorktown Heights, NY 10598

June 2001

Semiclassical modeling of small semiconductor devices

- Asen Asenov, Glasgow University,
  Discrete impurities and quantum potentials in MOSFET modeling
- Richard Akis, Arizona State University,
  Effective potentials for quantum effects in MOSFETs

Semiclassical modeling

- Various flavors:
  - Strict: may use the **bulk (3D)** Boltzmann Transport Equation (BTE), *à la* Kohn-Luttinger (Liouville-von Neumann with infinitely-may randomly-distributed impurities), even if Quantum Mechanics is pervasive (bands, collisions, etc.)
  - Somewhat looser: may use a lower-dimensional BTE (quantum confinement), or any Master equation (dots). No transport 'in the quantized direction'
  - Very loose ('psychologically' classical): Approximate quantum effects so to allow the concept of 'particle' or 'trajectory' (Bohm trajectories, quantum potentials, effective potentials, Wigner paths/trajectories...)
- Anticipated failures:
  - Quantum confinement (strict): channels, wires, dots
  - Tunneling (somewhat looser): band-to-band, across barrier, resonant, ...
  - Interference effects (somewhat looser): Bohm-Aharonov, current oscillations in FN-tunneling and channel current (?!), ...
  - 2D/3D confinement-effects (somewhat-looser/very-loose?): narrow channels in double-gate, point contacts, strongly-coupled dots
  - High-energy, high-field, short-time effects (Somewhat/very loose): Collisional broadening, intracollisonal-field, coherent phenomena,..
- Virtues of semiclassical modeling:
  - We have survived so far...
  - 'Intuitive', leading to deeper understanding
  - Simpler (or just...doable?), allowing more accurate description of effects which *may* be dominant in many real-life experiments/devices
  - Determination of 'bulk quantum properties' (band-structures, strain, electron-phonon coupling constants, Auger/impact processes)
  - Collective/many-body effects (Coulomb effects, quantum or MD)

Dopant fluctuations

- Important (threshold control a crucial element in VLSI)...
- but complicated:
  - BTE suspect
  - Scatterers closer than mean-free-path:
    - no rigorous use of mobility possible
    - multiple-scattering, interference, non phase-breaking
  - What's the scattering potential?
- So far limited to drift-diffusion and to electrostatics (probably good enough)

Quantum/effective potentials

- From Wigner or Bohm
- 'Phsychologically easy', mathematically hard
- So far approximated (equilibrium) or of a heuristic nature
- Of high appeal because of their 'intuitive' nature

Session 4
The Metal-Insulator Transition

- Moderator: Chihiro Hamaguchi, Osaka University
- 4A: Guenther Bauer, University of Linz,
  "The metal-insulator transition in d=2"
- 4B: Jonathan Bird, Arizona State University,
  "The metal-insulator transition in open quantum dots and arrays"

Metal-insulator transition in two dimensions

Guenther Bauer, University of Linz

- No metallic state in two dimensions in B = 0 (Abrahams et al. in 1979: Scaling theory).
- With decreasing temperature the resistance should rise logarithmically (weak localization) or even exponentially (strong localization) with R→ • •for T→0.
- In the limit of weak localization R should grow logarithmically for T→0.

- For strong interactions it should end up as a Wigner crystal (or pinned Wigner crystal).
- Therefore, neither in the limit of weak nor in the limit of strong interactions, 2D systems should conduct for T→0.
- Early experiments confirmed these predictions.
- However, experiments with very clean high mobility samples contradict it.
  - A non zero conductivity was found.
  - Evidence for a metal-insulator transition

- A critical density was found::
  - Below the system is insulating
  - Above the system shows metallic behaviors
- Many explanations were put forward
- Si-MOS
  - Experiments: weak localization
    → onset of metal-insulator transition: classical effect (screening, ionized impurity scattering,.....)

The metal-insulator transition in open quantum dots and arrays

Jonathan Bird, Arizona State University

- Much recent interest in the observation of a Kondo effect in Coulomb blockaded quantum dots.
- In open quantum dots the Coulomb blockade is suppre4ssed.
- Transport is found to be mediated by strongly scarred wavefunction states.
- The scars correspond to quasi-bound resonant states of the open system which are characterized by long trapping times at specific energies.
- The quasi-bound nature is expected to give rise to novel signatures in transport due to electron interactions.
- The behavior of the quasi-bound states will be explored in this presentation.

Intrinsic Fluctuations and Quantum Potentials in MOSFET Modelling

"The tyranny of the large numbers"
G. Timp

A. Asenov
A. R. Brown, S. Kaya, J. Watling, J. H. Davies, G. Slavcheva
Department of Electronics and Electrical Engineering
University *of* Glasgow

Sponsored by NASA NAB SHEFC

© A. Asenov 2001

Summary

- ☐ Introduction
- ☐ Quantum corrections
- ☐ Random Dopant Fluctuations
- ☐ Oxide Thickness Fluctuations
- ☐ Conclusions

© A. Asenov 2001

Scaling of MOSFETs to decanano dimensions

(International Roadmap for Semiconductors - 1999 Edition)

International Technology Roadmap

Year	1999	2001	2004	2008	2011	2014
MPU Gate Length *(nm)*	140	100	70			
Oxide thickness *(nm)*	1.9-2.5	1.5-1.9	1.2-1.5			
Drain extensions *(nm)*	42-70	30-50				

Intel Roadmap

Year	1998	2000	2003	2005	2007	2009
Technology node *(nm)*	130	130	90	65	45	30
Gate length *(nm)*	130	70	50	30	20	

Solution exists
Solution Being Pursued
No Known Solutions

Vertical confinement
Direct oxide tunnelling
S-to-D tunnelling

© A. Asenov 2001

Conventional MOSFET with 20 nm gate length

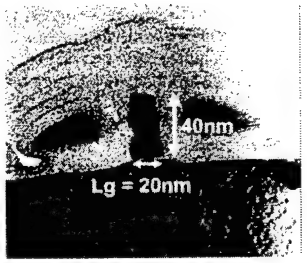

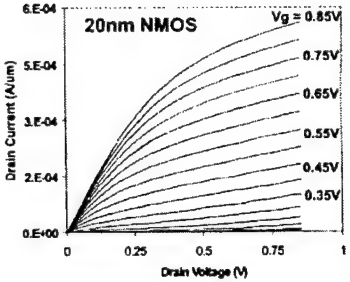

Robert Chaw
Si Nanoel. Workshop 01

© A. Asenov 2001

Double gate MOSFET with 8 nm gate length

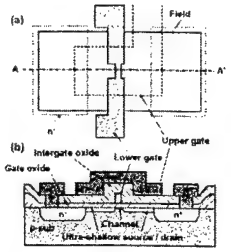

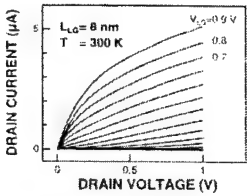

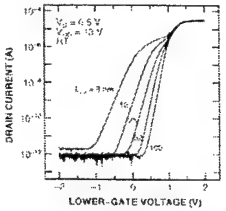

H. Kawagura et al.
Si Nanoel. Workshop 99

© A. Asenov 2001

Random Dopants Fluctuations (RDF)

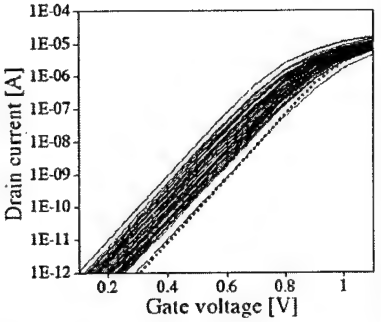

© A. Asenov 2001

Numbers and position fluctuations

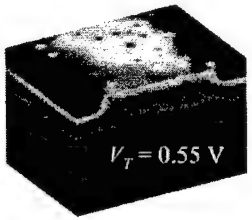

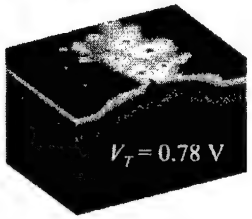

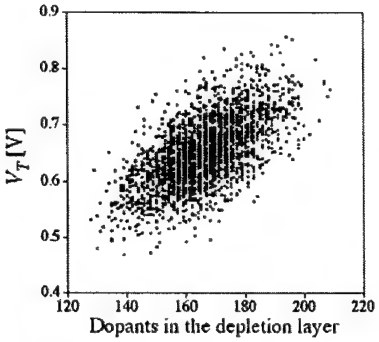

© A. Asenov 2001

Threshold voltage asymmetry in a 50×50 nm MOSFET

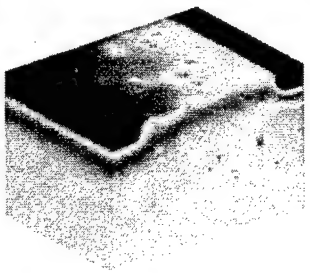

V_T = 0.67 V

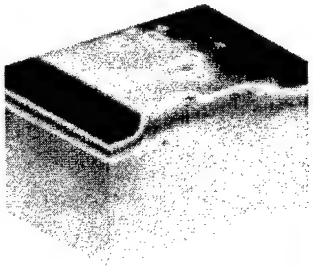

V_T = 0.80 V

© A. Asenov 2001

The poly-Si gate
(A 50×50 nm MOSFET)

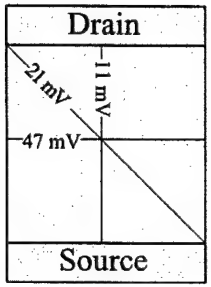

Grain boundaries

© A. Asenov 2001

Single charge trapping

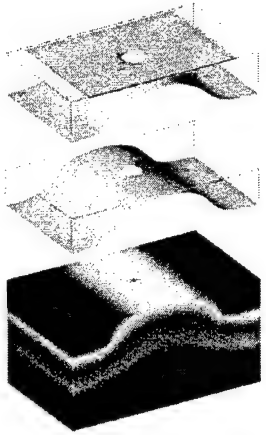

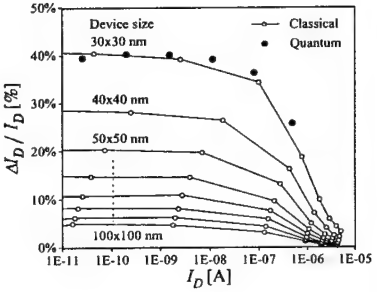

© A. Asenov 2001

Single charge trapping
(A 50×50 nm MOSFET with discrete dopants)

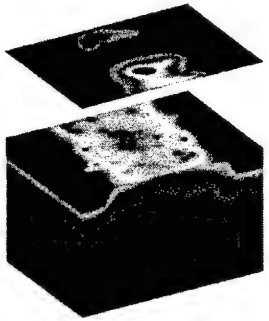

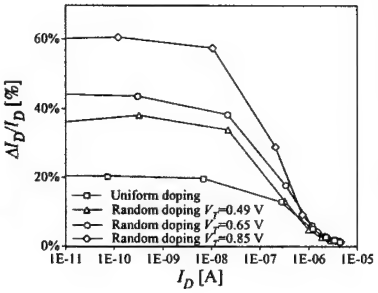

© A. Asenov 2001

Oxide Thickness Fluctuations (OTF)

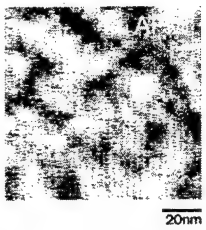

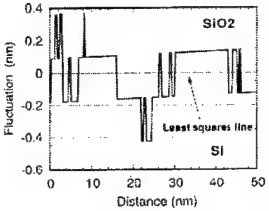

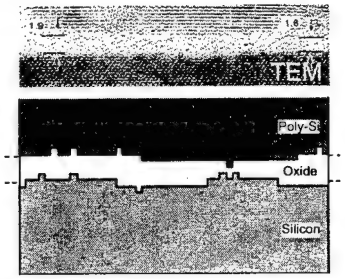

M. Niva et al.
Jpn. J. Appl. Phys

© A. Asenov 2001

OTF induced MOSFET parameter fluctuations

(A 30×30 nm MOSFET)

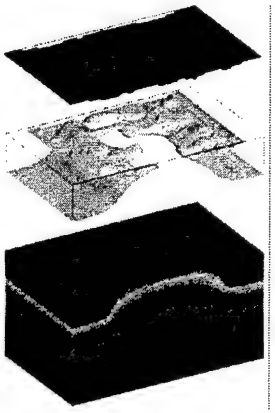

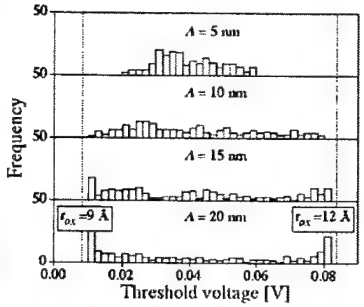

© A. Asenov 2001

Line edge roughness (LER)

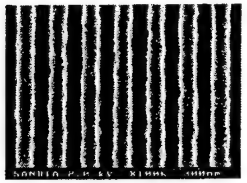

Sandia Labs – EUV

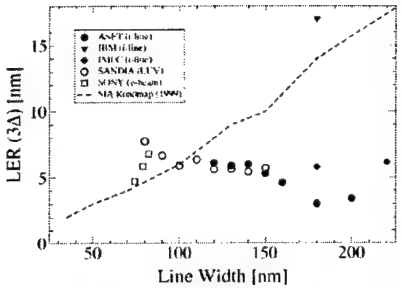

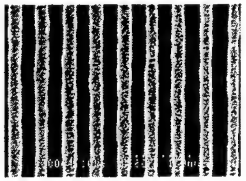

Glasgow – E-beam

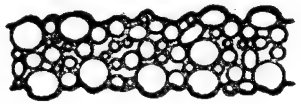

© A. Asenov 2001

Line edge roughness (LER)

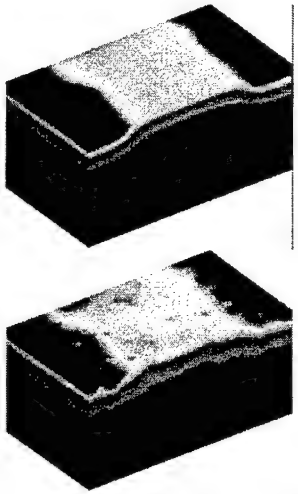

(A 30×30 nm MOSFET)

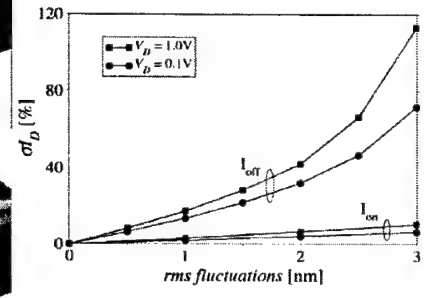

© A. Asenov 2001

Summary

- ☐ Introduction
- ☐ Quantum corrections
- ☐ Random Dopant Fluctuations
- ☐ Oxide Thickness Fluctuations
- ☐ Conclusions

© A. Asenov 2001

Solution domain in 3D 'atomistic' simulation

- 3D DD simulations + quantum corrections
- Fine grain discretisation
- Statistical ensembles of microscopically different devices
- Estimation of averages and standard deviations

50×50 nm MOSFET

The Density Gradient (DG) approach

(C.S. Rafferty et al., SISPAD'98)

DG introduces QM corrections by introducing an extra term into carrier flux expression

$$F_n = n\mu_n \nabla\psi - D_n \nabla n + 2\mu\nabla\left(b_n \frac{\nabla^2 \sqrt{n}}{\sqrt{n}} \right)$$

where

$$b_n = \hbar / (12 q m_n^*)$$

Generalised quasi-Fermi potential

$$F_n = n\mu_n \nabla\phi_n$$

DD with DG corrections for unipolar device

(C.S. Rafferty et al., SISPAD'98)

The system

$$\nabla.(\varepsilon\nabla\psi) = -q(p - n + N_D^+ - N_A^-)$$

$$\nabla.(n\mu_n\nabla\phi_n) = 0$$

$$2b_n \frac{\nabla^2\sqrt{n}}{\sqrt{n}} = \phi_n - \psi + \frac{kT}{q}\ln\frac{n}{n_i}$$

The variables

$$\psi,\ \phi_n,\ \sqrt{n}$$

Quantum mechanical threshold voltage shift

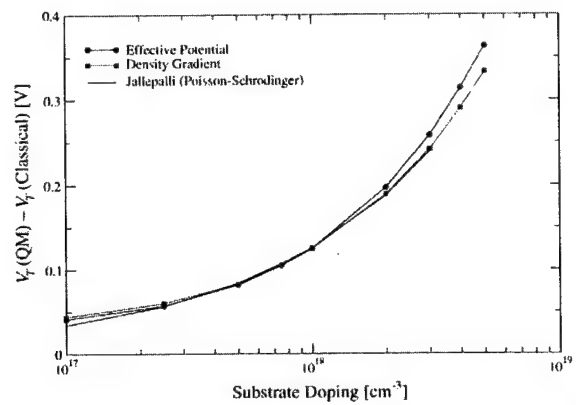

Quantum mechanical charge distribution

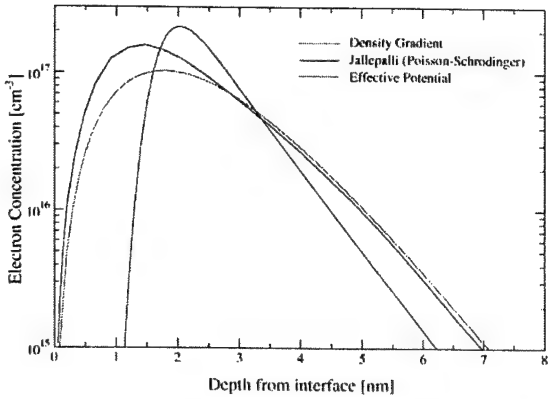

© A. Asenov 2001

m^* is a fitting parameter

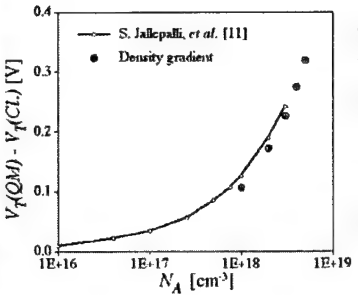

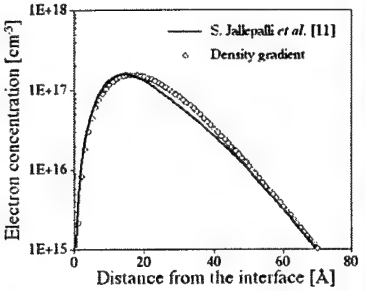

$m^* = 0.18m_o$

© A. Asenov 2001

Double gate MOSFET

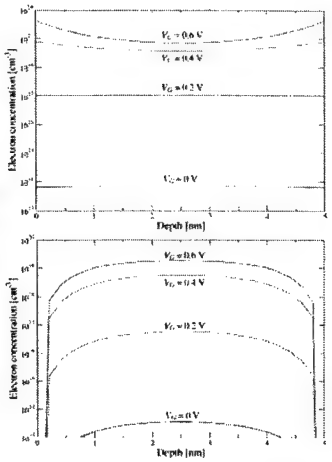

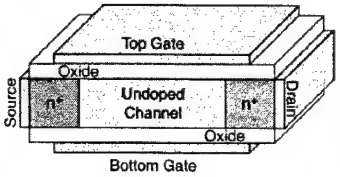

© A. Asenov 2001

Source-to-drain tunnelling

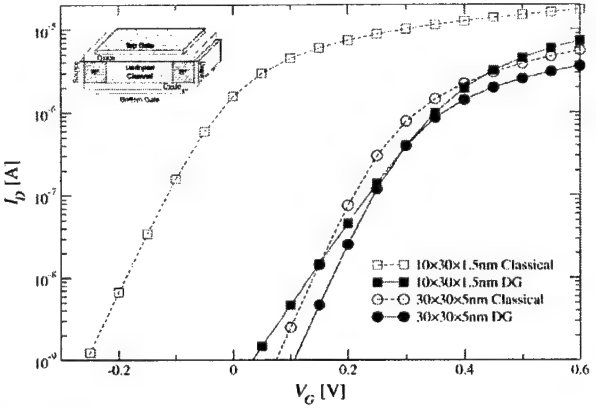

© A. Asenov 2001

Summary

- ☐ Introduction
- ☐ Quantum corrections
- ☐ Random Dopant Fluctuations
- ☐ Oxide Thickness Fluctuations
- ☐ Conclusions

Potential and electron distribution

(A 50×50 nm MOSFET)

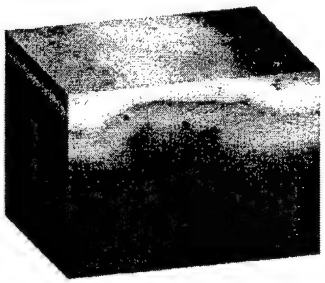

Potential

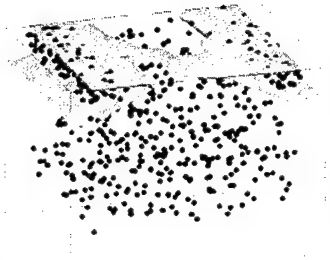

Electron concentration

Electron equiconcentration distribution

(A 50×50 nm MOSFET)

QuickTime™ and a decompressor are needed to see this picture.

Threshold voltage as a function of the gate length

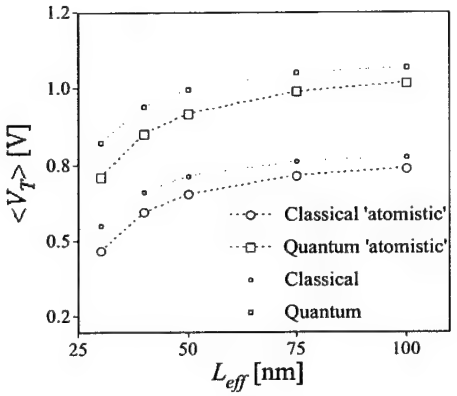

W_{eff} = 50 nm
N_A = 5×10^{18} cm^{-3}
t_{ox} = 3 nm

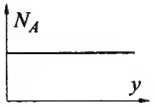

Threshold voltage standard deviation as a function of the gate length

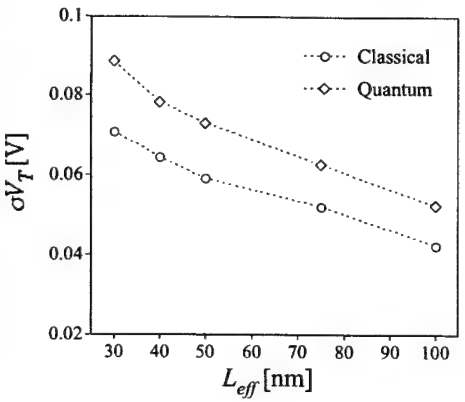

$W_{eff} = 50$ nm
$N_A = 5\times10^{18}$ cm^{-3}
$t_{ox} = 3$ nm

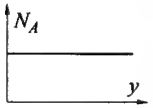

© A. Asenov 2001

Threshold voltage as a function of the oxide thickness

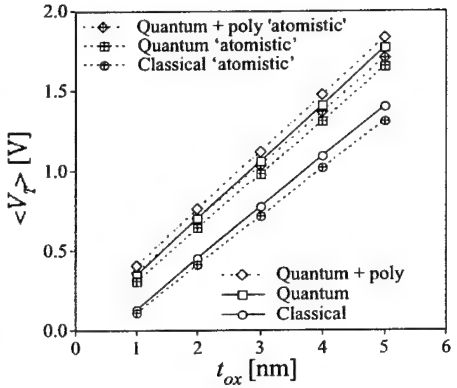

$L_{eff} = 50$ nm
$W_{eff} = 50$ nm
$N_A = 5\times10^{18}$ cm^{-3}

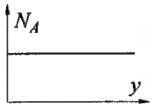

© A. Asenov 2001

Threshold voltage standard deviation as a function of the oxide thickness

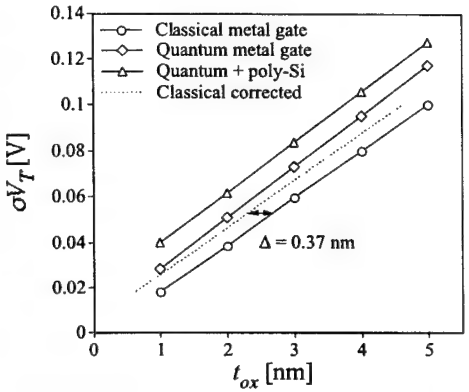

$L_{eff} = 50$ nm
$W_{eff} = 50$ nm
$N_A = 5\times10^{18}$ cm^{-3}

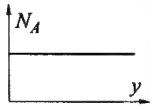

© A. Asenov 2001

Summary

- ☐ Introduction
- ☐ Quantum corrections
- ☐ Random Dopant Fluctuations
- ☐ Oxide Thickness Fluctuations
- ☐ Conclusions

© A. Asenov 2001

Threshold voltage as a function of the period of oxide thickness superlattice

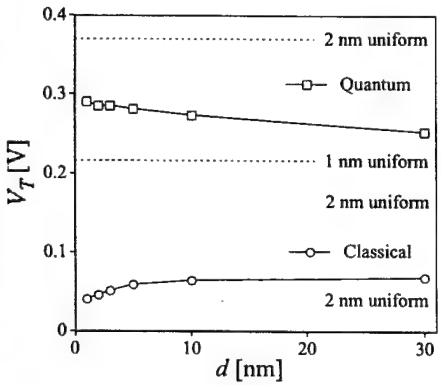

Channel width

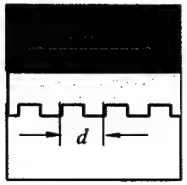

© A. Asenov 2001

Classical and quantum mechanical charge distribution in the oxide superlattice

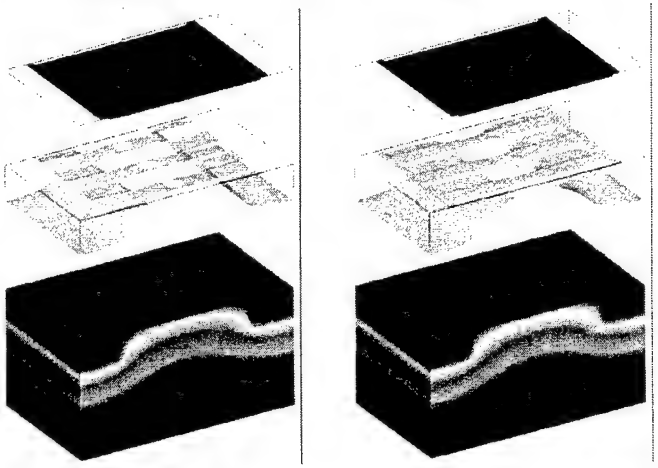

Classical QM

© A. Asenov 2001

Reconstruction of the Si/SiO_2 interface

Exponential power spectrum

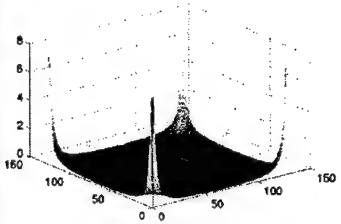

$$C_E(r) = \Delta^2 e^{-r/\Lambda}$$

$$S_E(q) = \frac{2\pi\Delta^2\Lambda^2}{\left(1+q^2\Lambda^2\right)^{3/2}}$$

Gaussian power spectrum

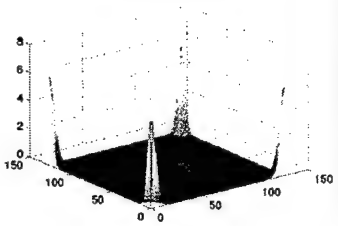

$$C_G(r) = \Delta^2 e^{-r^2/\Lambda^2}$$

$$S_G(q) = \pi\Delta^2\Lambda^2 e^{-\frac{q^2\Lambda^2}{4}}$$

© A. Asenov 2001

Reconstruction of the Si/SiO_2 interface

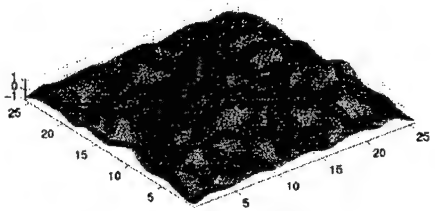

Gaussian power spectrum

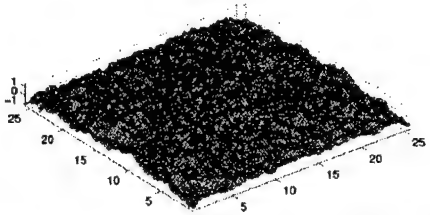

Exponential power spectrum

© A. Asenov 2001

Digitisation of the Si/SiO_2 interface

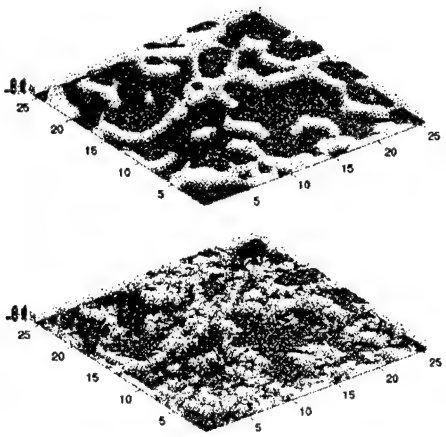

Gaussian power spectrum

Exponential power spectrum

© A. Asenov 2001

OTF induced MOSFET parameter fluctuations

(A 30×30 nm MOSFET)

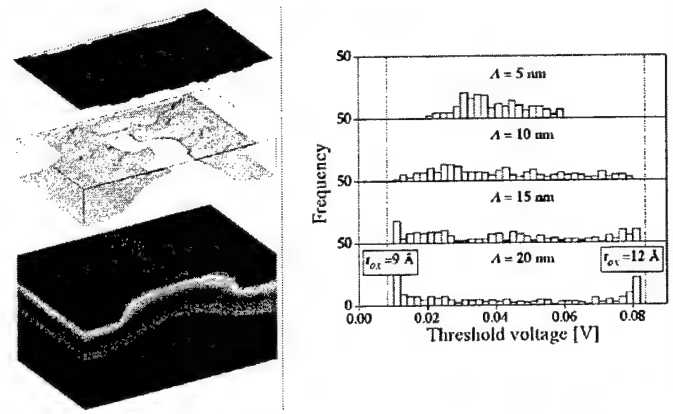

© A. Asenov 2001

Threshold voltage standard deviation as a function of the correlation length

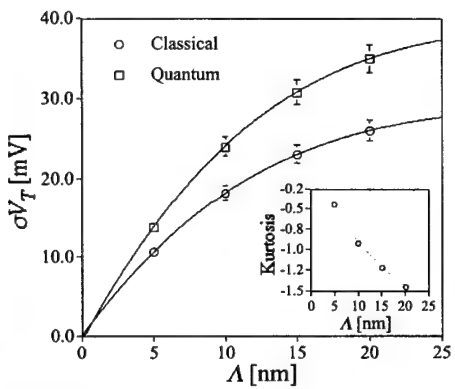

L_{eff} = 30 nm
W_{eff} = 30 nm
$N_A = 5\times10^{18}$ cm^{-3}
$\langle t_{ox} \rangle$ = 10.5 Å

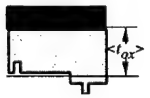

© A. Asenov 2001

Threshold voltage as a function of the average oxide thickness

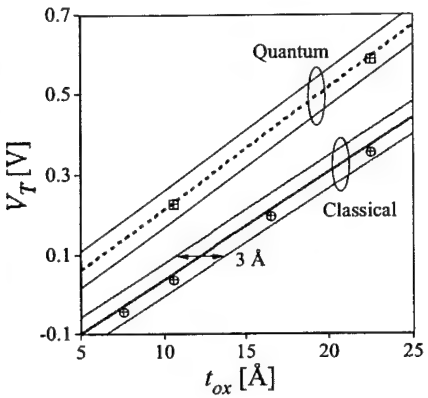

L_{eff} = 30 nm
W_{eff} = 30 nm
$N_A = 5\times10^{18}$ cm^{-3}
Λ = 12 nm

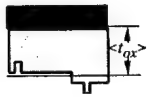

© A. Asenov 2001

Threshold voltage standard deviation as a function of the oxide thickness

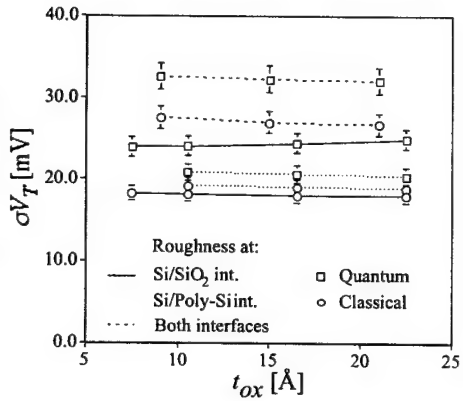

L_{eff} = 30 nm
W_{eff} = 30 nm
$N_A = 5\times10^{18}$ cm^{-3}
Λ = 12 nm

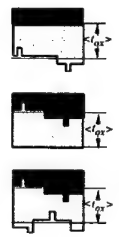

© A. Asenov 2001

Threshold voltage standard deviation as a function of the doping concentration

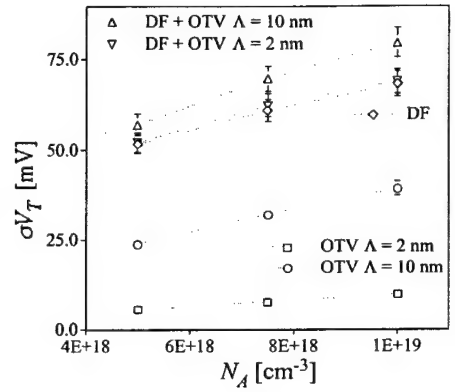

L_{eff} = 30 nm
W_{eff} = 30 nm
$<t_{ox}>$ = 10.5 Å

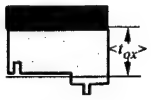

© A. Asenov 2001

Conclusions

- The DG approach provides relatively simple means to include quantum correction in the 3D DD 'atomistic' MOSFET simulation.
- The inclusion of the QM corrections increases the intrinsic parameter fluctuations associated with discrete random dopants and oxide thickness variation.

© A. Asenov 2001

Effective Potentials for Quantum Effects in MOSFETs

Dr. Richard Akis
Department of Electrical Engineering
Arizona State University

Who else is to blame:

L. Shifren
S. Ramey
S. N. Milicic
D. Vasileska
and, in particular
D. K. Ferry

Work supported by ONR, NSF, and SRC

Outline

Introduction
the effective potential- what is it and why should you care

Including the effective potential in device simulations
1D simulation of a MOSFET channel
2D simulation of a "standard" MOSFET
simulation of SOI devices
simulation of a quantum point contact

Conclusions

A Major Concern for Future ICs

While current production devices are only at 0.18 μm, predictions are that they will be at 50 nm by year 2012. At these sizes, we should begin to see **quantum effects**, as λ_D~3-5 nm at 300 K. The questions are:

- In quantum mechanics, electrons no longer behave as point particles. How "large" is the electron wave packet?
- How can we include space quantization effects efficiently into what are otherwise classical device simulators?

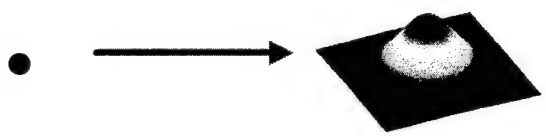

The smallest size will be determined by the effective size of the electron wave packet.

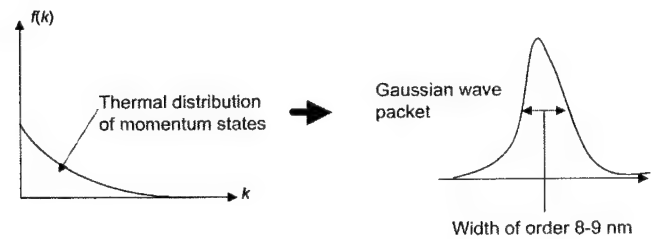

$$\psi(r) = \frac{\pi}{\left(\sqrt{2}\lambda_D\right)^{3/2}} \exp\left(-\frac{\pi r^2}{\lambda_D^2}\right)$$

MOSFET conduction band profile along the growth direction

inversion layer formed carriers at interface trapped in a triangular well → **creation of 1D subbands that leads to charge set back**

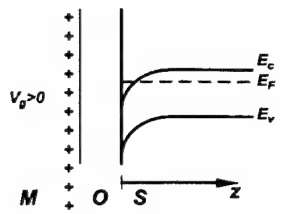

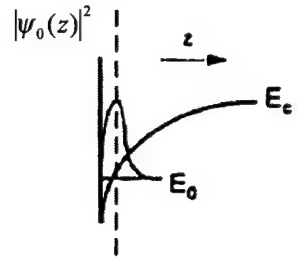

Quantization in the Channel of the MOSFET

The electrons in the inversion layer are quantized—their motion normal to the interface is quantized by the potential well between the oxide and the conduction band. The actual width of the inversion layer is found from the Schrödinger equation.

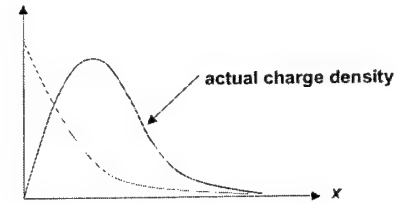

$$n_s = \frac{mk_BT}{\pi\hbar^2}\ln\left[1+\exp\left(\frac{E_F-E_0}{k_BT}\right)\right]$$

Quantum method of finding the wave functions and energy levels

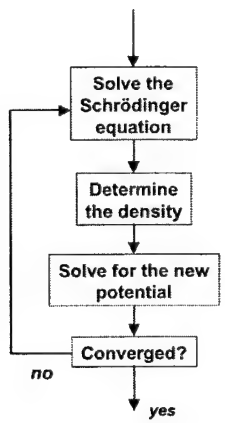

$$-\frac{\hbar^2}{2m}\frac{d^2\psi}{dx^2}+V(x)\psi(x)=E\psi(x)$$

$$n(x)=-e\sum_i|\psi_i(x)|^2$$

$$\frac{d^2V(x)}{dx^2}=-e\frac{e}{\varepsilon}[n(x)-N_A]$$

Extra factors, as V(x) is potential energy, not electrostatic potential.

✔ **The concept of the effective potential was introduced by Feynman, and has been extended by several authors.**

Classically, we use $e^{-\beta V}$; thus, the idea of the effective potential is to seek a modified potential V_{eff} by which we can write the density as

$$n = n_0 e^{-\beta V_{eff}}$$

➔ **Sharp potentials no longer appear in the problem. Rather, these are "smoothed" by a Gaussian function, here derived from the effective minimal size of the electron wave packet in the system under study.**

By replacing the sharp potentials by smoothed potentials, we can return to using quasi-classical point charges in our simulations, confident that the results will be quite appropriate.

$$V_{eff}(x)=\frac{1}{\sqrt{2\pi}\,a_0}\int_{-\infty}^{\infty}V(x')\exp\left(-\frac{(x-x')^2}{2a_0^2}\right)dx'$$

Effective Potential Approach

In principle, the effective role of the potential can be rewritten in terms of the non-local density as (Ferry *et al.*[1]):

$$\bar{V} = \int d\mathbf{r} V(\mathbf{r}) \sum_i n_i(\mathbf{r})$$

$$\sim \int d\mathbf{r} V(\mathbf{r}) \sum_i \int d\mathbf{r}' \exp\left(-\frac{|\mathbf{r}-\mathbf{r}'|^2}{\alpha^2}\right) \delta(\mathbf{r}'-\mathbf{r}_i)$$

$$\sim \sum_i \int d\mathbf{r} \delta(\mathbf{r}-\mathbf{r}_i) \int d\mathbf{r}' V(\mathbf{r}') \exp\left(-\frac{|\mathbf{r}-\mathbf{r}'|^2}{\alpha^2}\right)$$

$$\sim \sum_i \int d\mathbf{r} \delta(\mathbf{r}-\mathbf{r}_i) V_{eff}(\mathbf{r})$$

Classical density

Smoothed, effective potential

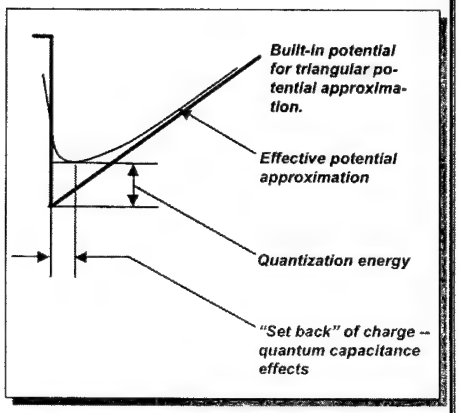

[1] D. K. Ferry, *Superlatt. Microstruc.* **27**, 59 (2000); *VLSI Design*, in press.

Use of the Effective Potential

$$V_{eff}(x) = \frac{V_0}{2}\left[1 - erf\left(\frac{x}{\sqrt{2}a_0}\right)\right] + \frac{Fx}{2}\left[1 + erf\left(\frac{x}{\sqrt{2}a_0}\right)\right] + \frac{Fa_0}{\sqrt{2\pi}}\exp\left(-\frac{x^2}{2a_0^2}\right)$$

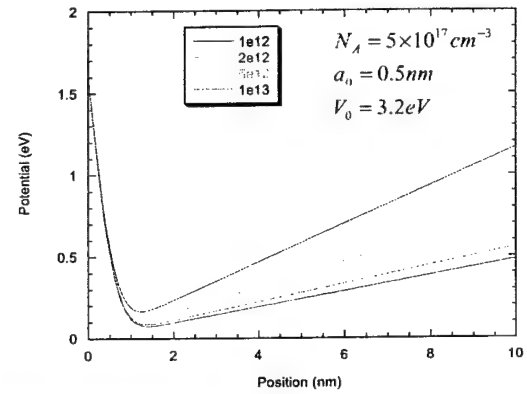

$$F = \frac{e}{\varepsilon}\left(N_A d_A + \frac{n_s}{2}\right)$$

Use of the Effective Potential

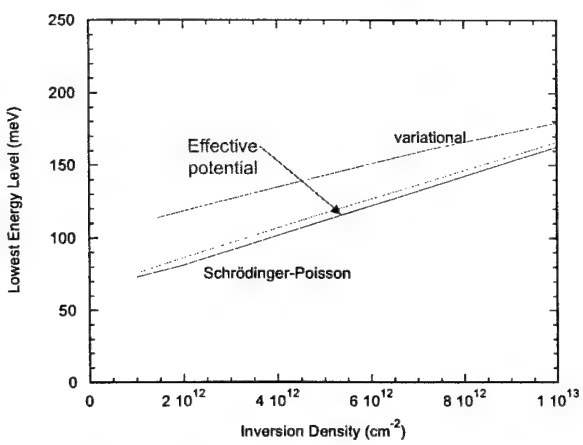

$N_A = 5\times10^{17} cm^{-3}$

Use of the Effective Potential

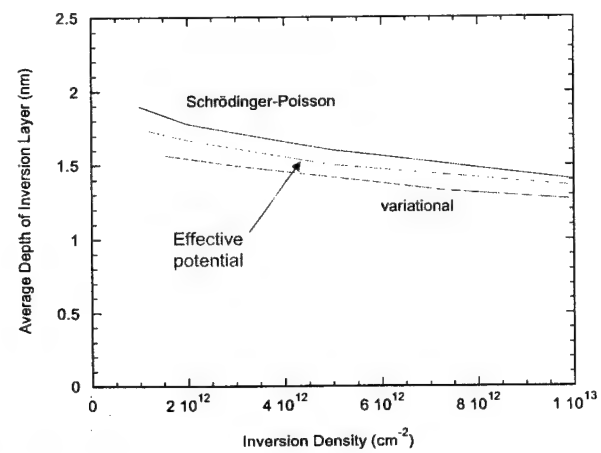

$N_A = 5\times10^{17} cm^{-3}$

Description of the Existing 2D/3D Device Simulators

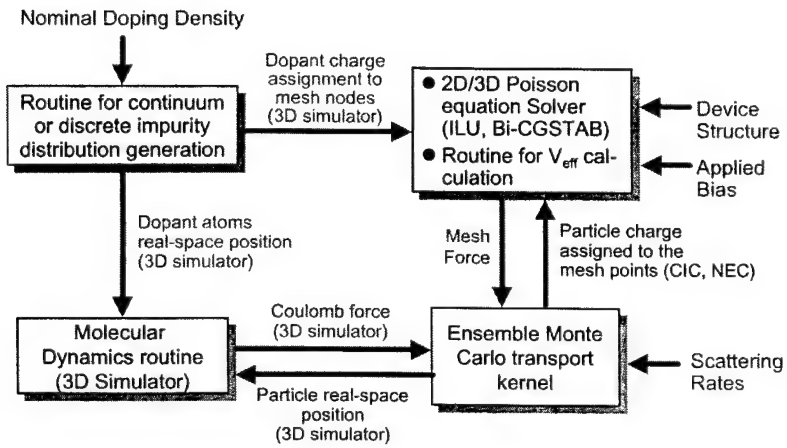

Simulation of a 50 nm MOSFET Device

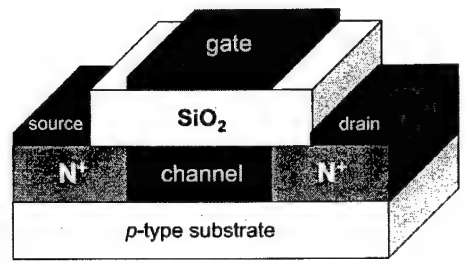

Device specification:

- Oxide thickness = 2 nm
- Channel length = 50 nm
- Channel width = 0.8 μm
- Junction depth = 36 nm
- Substrate doping: $N_A=10^{18}$ cm^{-3}
- Doping of the source-drain regions: $N_D = 10^{19}$ cm^{-3}

Conduction Band Profile

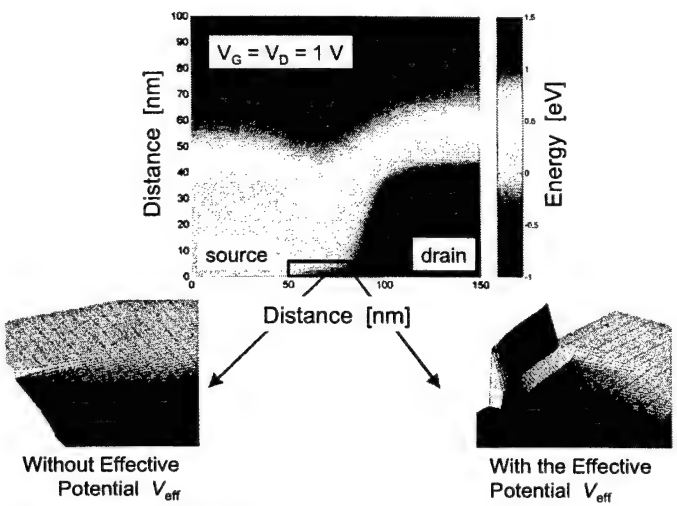

Electric Field Profile

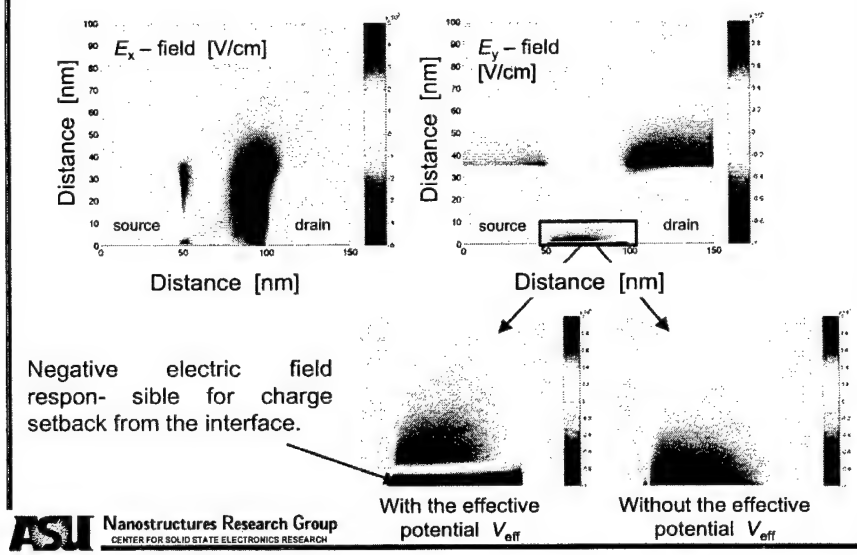

Carrier Density and Average Distance

Applied bias: $V_G = 1$ V

Electron sheet density reduction due to quantum-mechanical band-gap widening effect

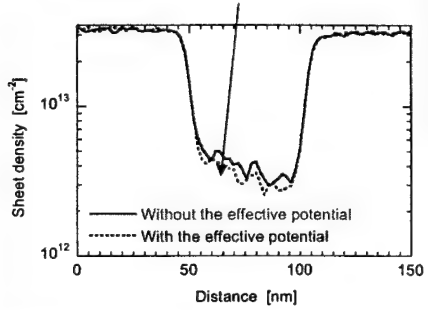

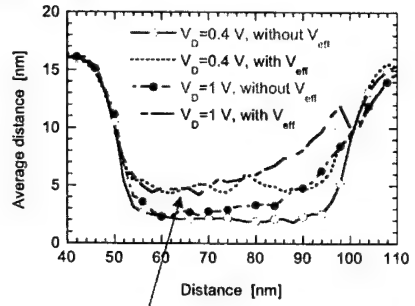

Additional 2-3 nm charge set-back from the interface due to quantum-mechanical space-quantization effect

Transfer and Output Characteristics

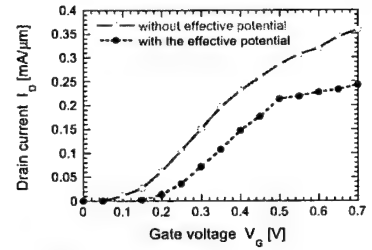

- The observed threshold voltage shift is mainly due to the degradation of the device transconductance and is not due to mobility degradation in the channel.
- The shift in the threshold voltage leads to a reduction in the on-state current.

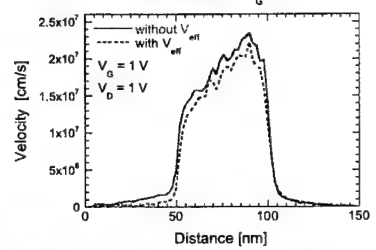

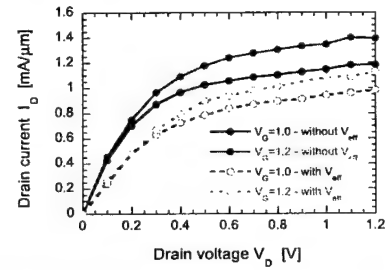

SOI Device Structure

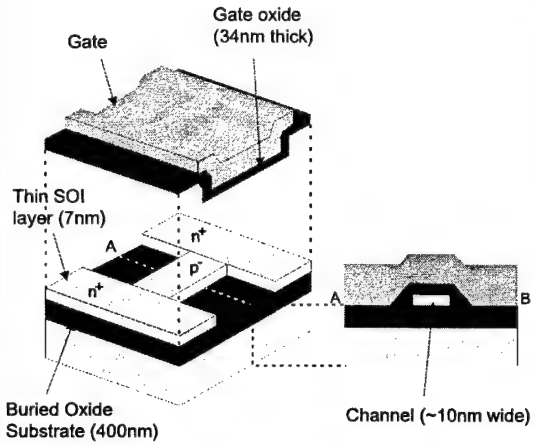

Experimental data[1]:

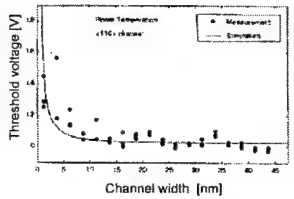

- Simulate this structure using full 3D Poisson solver coupled with 2D Schrödinger solver.
- Do same calculation with effective potential

[1] Majima, Ishikuro, Hiramoto, *IEEE El. Dev. Lett.* **21**, 396 (2000).

Conduction Band Edge and Electron Density

Classical Simulation | Effective Potential

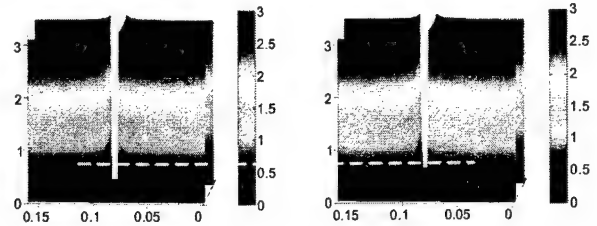

Smoothing of the potential rises its value in the channel and this influences electron density.

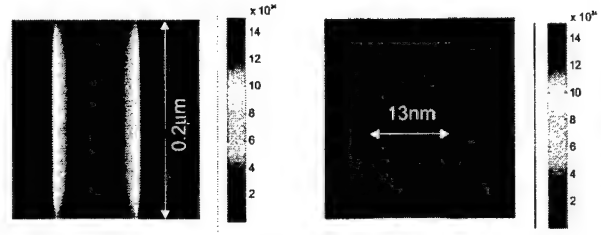

The electron density in the case of the effective potential approach is moved away from the edges of the channel, which gives a more physical description.

Number of Electrons in the Channel

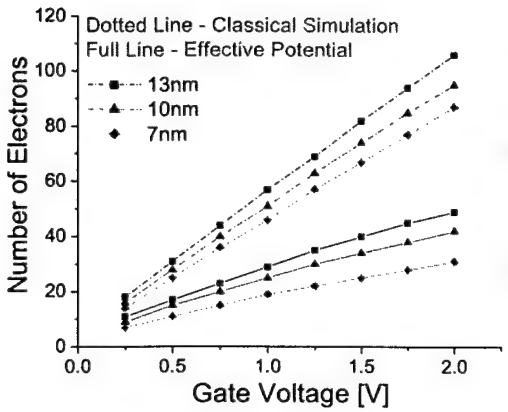

Change in the number of electrons under the gate for classical vs. effective potential method shows the shift in the threshold voltage due to the quantum-mechanical effects.

Effective potential vs. 2D Schrodinger

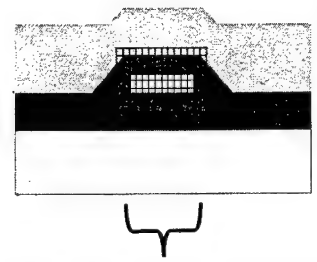

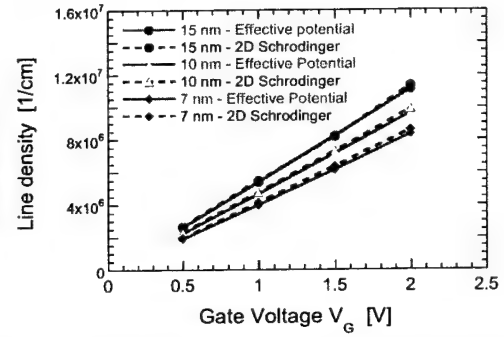

2D Schrodinger equation solved in cross section

effective potential results match full calculation rather well

SOI MOSFET Structure

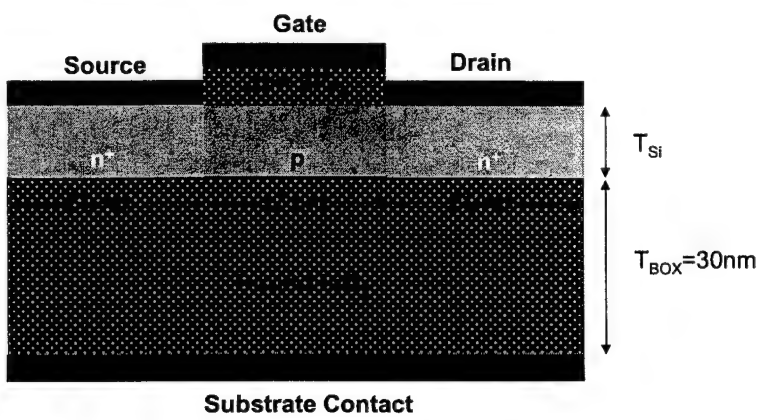

Potential Profile Under Gate

T_{OX}= 2nm, V_D=0.1V,
V_{sub}=0.0V, N_A=5x10^{18} cm^{-3}

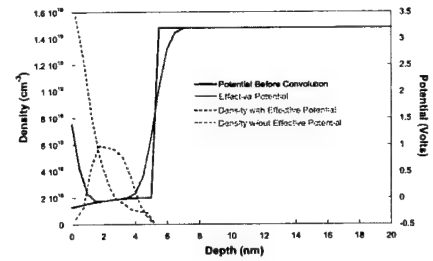

Results of Effective Potential on V_T

N_A=5x10^{18}cm^{-3}, V_G=0.6V,
V_D=0.1V, T_{OX}=2nm

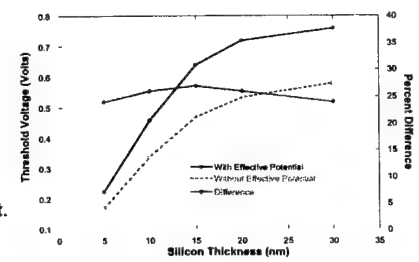

Neglecting quantum underestimates V_T and therefore overestimates drive current.

Electron Density Distribution

Fully Depleted

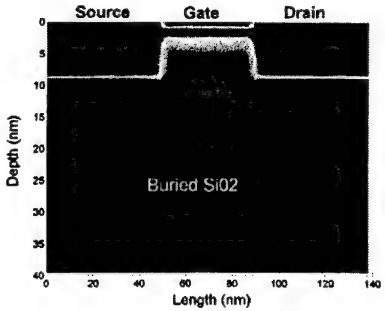

Partially Depleted

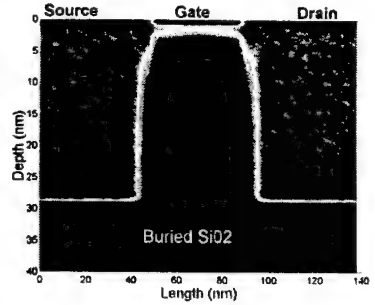

Gate Voltage = 1.0 Volt Drain Voltage = 0.1 Volts $N_A=5\times10^{18}\ cm^{-3}$

I_D-V_D Characteristics

T_{Si}=30 nm

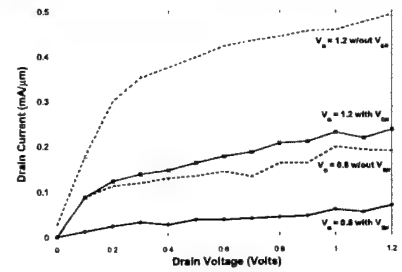

T_{Si}=10 nm

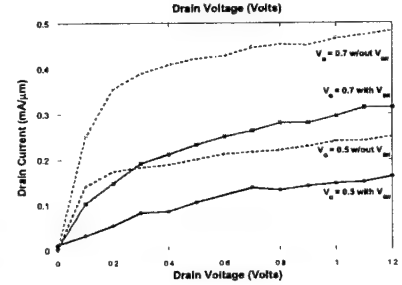

Decreasing silicon film thickness increases drive current and reduces V_T.

Madelung and Bohm's reformulation of quantum mechanics

insert $\psi = Re^{iS/\hbar}$, $R=\sqrt{n}=|\psi|$ ➟ $-\frac{\hbar^2}{2m}\nabla^2\psi + V\psi = i\hbar\frac{\partial\psi}{\partial t}$

real part yields the quantum Hamilton-Jacobi equation: $$\frac{\partial S}{\partial t}+\frac{(\nabla S)^2}{2m}+V+Q=0$$

where $S \rightarrow$ action, and $Q=-\frac{\hbar^2}{2m^*}\frac{\nabla^2|\psi|}{|\psi|}$ is the "quantum potential"

equations of motion: $$\mathbf{v}(\mathbf{x},t)=\frac{\nabla S(\mathbf{x},t)}{m^*}=\frac{\hbar}{m^*}\frac{\mathrm{Im}(\psi\nabla\psi)}{|\psi|^2}$$

$$\mathbf{a}(\mathbf{x},t)=-\frac{\nabla(V+Q)}{m^*}$$

Connection with the effective potential

$$V_{eff}(x)=\frac{1}{\sqrt{2\pi}\alpha}\int_{-\infty}^{\infty}V(x+\xi)e^{-\xi^2/2\alpha^2}d\xi$$

$$\cong\frac{1}{\sqrt{2\pi}\alpha}\int_{-\infty}^{\infty}\left[V(x)+\xi\frac{\partial V}{\partial x}+\frac{\xi^2}{2}\frac{\partial^2 V}{\partial x^2}+\ldots\right]e^{-\xi^2/2\alpha^2}d\xi.$$

$$V_{eff}(x)=V(x)+\alpha^2\frac{\partial^2 V}{\partial x^2}+\ldots.$$

$$V_{eff}(x)=V(x)-\frac{2\alpha^2}{\beta}\frac{\partial^2\ln(\sqrt{n/n_0})}{\partial x^2}+\ldots$$

$$=V(x)-\frac{2\alpha^2}{\beta\sqrt{n}}\frac{\partial^2\sqrt{n}}{\partial x^2}+\ldots.$$

$$Q=\frac{\hbar^2}{2m^*}\frac{\nabla^2|\psi|}{|\psi|}$$

In semiconductors, typically the dependence of the density upon the potential is as a factor *exp(-βV)*

Within a factor of 2, the second term is now recognized as the density gradient term, but is more commonly known as the Bohm potential

quantum point contact

1. We start by consider a quantum wire with constriction
2. We solve the system with and without self-consistently
3. We smooth the self-consistent solution to obtain the effective potential
4. We use the effective potential to generate classical trajectories and the self-consistent solution to generate quantum trajectories

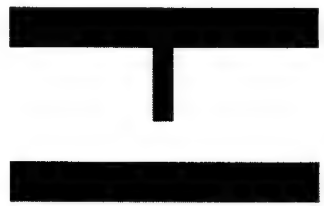

Self-Consistent Solutions

Solving Schrödinger's Equation

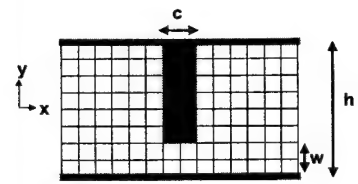

- Solution obtained via finite difference scattering matrix cascade
- We assume:
  1. *that the wire extends to $\pm\infty$*
  2. *the reflected waves do not interfere with the boundary*

- Therefore, solutions have continuous boundary conditions
- This is our criteria for boundary conditions

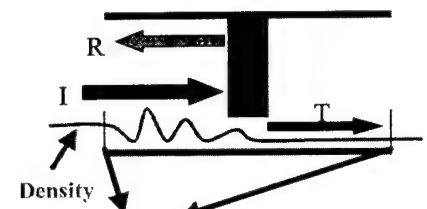

$$\frac{dn}{dx} = 0$$

Self-Consistent Solutions

1. Boundary conditions for the Poisson solver and the Schrödinger solver
2. Calculating the Hartree potential (via the Poisson solver) and included the exchange and correlation potentials
3. Maintaining a constant density in the system. A build up of density occurs due to the inclusion of the correlation potential which drops the conduction band edge
4. Using the correct electron density in the Poisson solver. (Taking into account the contributions of the positive ions in the system)

Self-Consistent Solutions

Dealing with the dynamic density

- Solving the self-consistent problem introduces a potential profile into the device → **Self-consistent potential**
- The correlation energy lowers the conduction band edge, and therefore allows a build up of charge which increases the number of propagating modes and density in the device → **Density**
- To keep density constant, the Fermi energy is adjusted with the lowering conduction band edge during iteration to maintain a constant density (propagating modes)

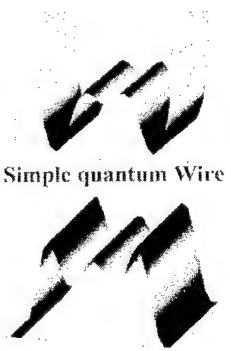

$$N = \frac{2}{\pi} \sum_{E_l < E_F} \left[\frac{2m^*(E_F - E_l)}{\hbar^2} \right]^{\frac{1}{2}}$$

Self-Consistent Solutions

Positive Ion Contribution

When solving the Poisson equation, we need to make sure we do not over-count free electron charges in the system

$$\nabla^2\phi(\mathbf{r}) = -\frac{e}{\varepsilon}\rho(\mathbf{r})$$

$$\rho(\mathbf{r}) = n(\mathbf{r}) - n_{eq}$$

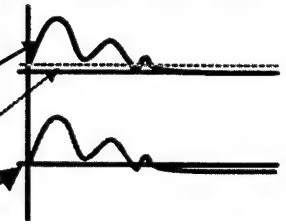

- We know there is a potential drop after the constriction
- We can interpret the drop in the Hartree potential to be the expected drop in the Fermi level

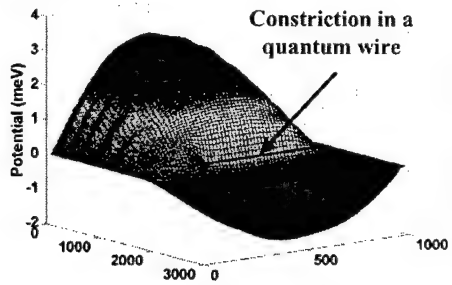

Effective Potential

Densities

(a) No potential
(b) Self-consistent potential
(c) Effective Potential

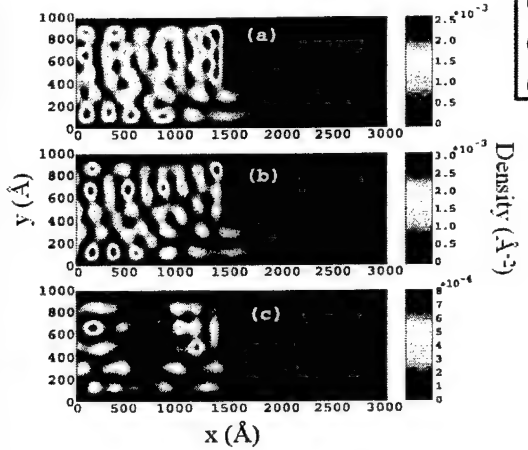

- As we begin to include higher levels of potential into the system [from (a)-(c)], we see the density move further from the walls of the device

Bohm trajectories flowing through the QPC. The background is the self-considtent potential.

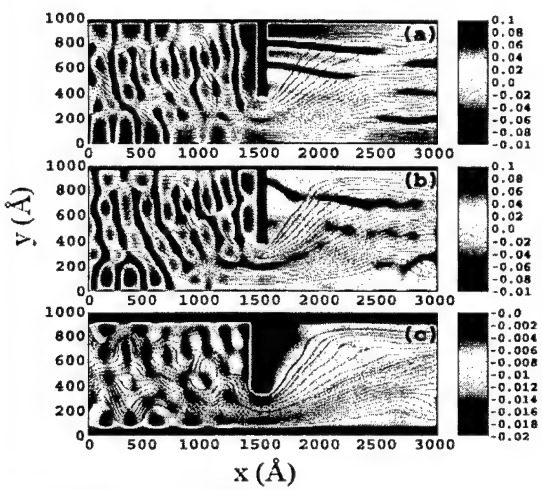

Calculation involving no self-consistency, background is the quantum potential

Calculation with self-consistency, background is the quantum + self-consistent potential

Calculation with the effective potential, background is the self-consistent potential

Electron density

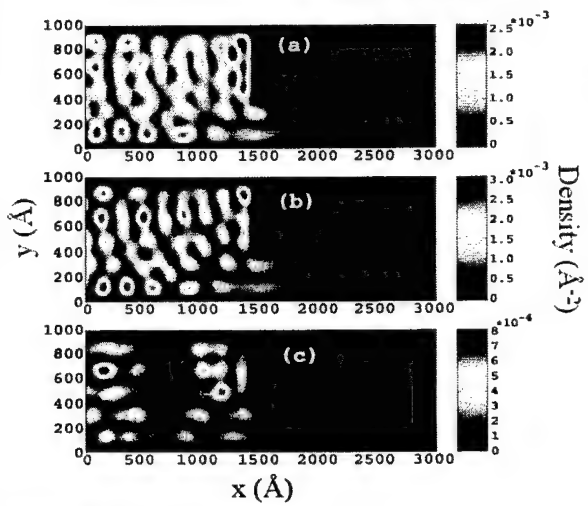

Calculation involving no self-consistency

Calculation with quantum + self-consistent potential

Calculation with the effective potential

Classical particles moving in the effective potential

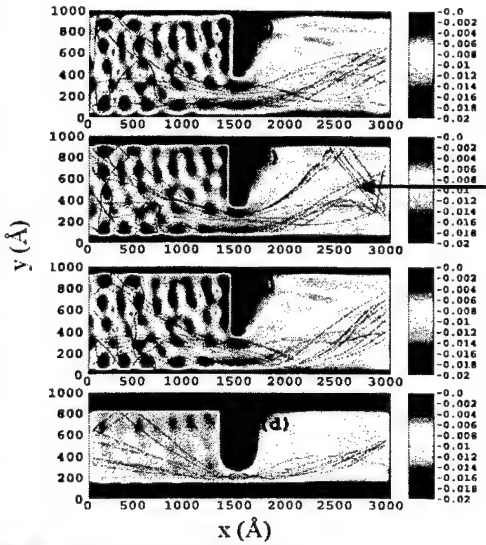

Only with the proper value of the "smoothing" constant in the effective potential do the classical particles refract in the proper quantum mechanical manner!

Conclusions

- The effective potential approach in many cases allows for a quite accurate approximation of the quantization effects in real semiconductor devices

- The numerical cost of including the effective potential is low – "more bang for the buck"

Some challenges remain....

▷ Model valid only within the random phase approximation.

▷ It is still "quasi-local", so it does not allow proper treatment phase interference effects

Wave function approaches for self-consistent computations of transport in quantum dots and arrays

D. K. Ferry

Center for Solid State Electronics Research and Department of Electrical Engineering
Arizona State University, Tempe, AZ 85287-5706

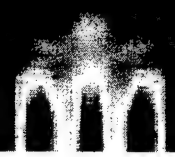

Outline

- Discretization of the Schrödinger equation
- The Usuki mode matching technique
- Application to quantum dots
- Incorporation of Poisson's equation
- Further application to quantum dots

Special thanks to R. Akis, L. Shifren, J. Harris for their contributions, without which there would be no content to this talk. Also, discussions with C. Jacoboni on quantum computing have been most helpful.

- Throughout this discussion, we will consider the region of interest to be the quasi-two-dimensional electron gas at the interface of a GaAs/AlGaAs heterojunction: all parameters will be for electrons in GaAs and confining potentials will be imposed upon this 2D gas.

The Schrödinger equation, in 2D, can be written as

$$-\frac{\hbar^2}{2m^*}\left(\frac{d^2}{dx^2}+\frac{d^2}{dy^2}\right)\psi(x,y)+V(x,y)\psi(x,y)=E\psi(x,y)$$

where V(x,y) is the local "site potential." This potential will be the self-consistent potential in later usage.

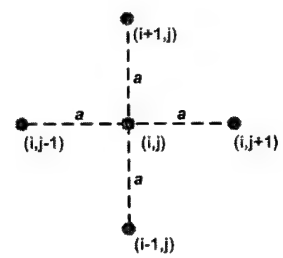

We now discretize the Schrödinger equation, using the 5-point scheme shown at left. This is a form of central differencing, that will introduce some unfortuante byproducts that will have to be addressed.

The Schrödinger equation, in its discretized form, now takes the shape of

$$-t\left[\psi(i+1,j)+\psi(i-1,j)+\psi(i,j+1)+\psi(i,j-1)\right]$$
$$+\left[V(i,j)+4t\right]\psi(i,j)=E\psi(i,j)$$

$$t=\frac{\hbar^2}{2m^*a^2}$$ is the "hopping" energy.

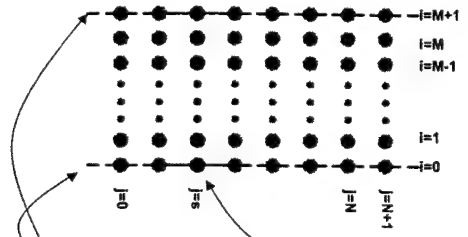

There is an automatic assumption that

$$\psi(0,j)=\psi(M+1,j)=0$$

On slice s, we may write the wave function as

$$\vec{\psi}(s)=\begin{bmatrix}\psi(M,s)\\ \psi(M-1,s)\\ \bullet\\ \bullet\\ \bullet\\ \psi(1,s)\end{bmatrix}$$

In general, this discretized Schrödinger equation can now be written in the form of coupled "slices" (columns *j*) as

$$\mathbf{H}_0(s)\vec{\psi}(s)-t\mathbf{I}\vec{\psi}(s+1)-t\mathbf{I}\vec{\psi}(s-1)=E\vec{\psi}(s)$$

with

$$\mathbf{H}_0(s)=\begin{bmatrix}[V(M,s)+4t] & -t & 0 & \dots & & & \\ -t & [V(M-1,s)+4t] & -t & \dots & & & \\ & & & \dots & & & \\ & & & \dots & -t & [V(2,s)+4t] & -t \\ & & & \dots & 0 & -t & [V(1,s)+4t]\end{bmatrix}$$

There are two approaches that can be developed now to "iterate" the solutions from one end to the other. These are:

- The "recursive" Green's function, in which a Green's function is developed for each slice, and coupling from one slice to the next is carried out by use of Dyson's equation.
- We use the wave functions directly, matching the wave and its derivative from one slice to the next--unstable, but can be stabilized by use of the scattering matrix.

These two approaches are very nearly identical in procedure and in central iterations. They differ somewhat in the end-point processing and in extraction of the density and wave function.

We use the latter approach, since it allows us to actually follow individual modes.

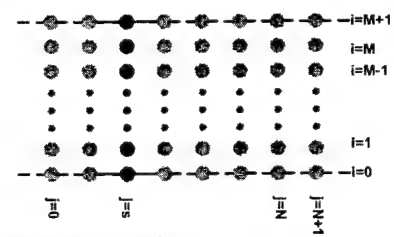

The general approach is to begin with slice "0" and propagate the excited modes toward the end of the device, as slice "N+2"

We then back propagate the density at slice "N+1" to the beginning at slice "0" in order to determine the wave function and the density in the structure.

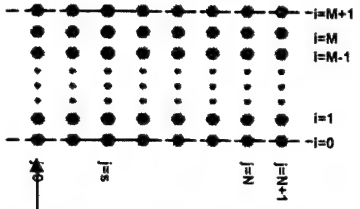

Matrix of the modes (columns) and their amplitude at each site (rows)

At slice "0", we must first determine the 2M modes (left and right propagating) by solving an eigenvalue equation:

$$\begin{bmatrix} 0 & 1 \\ -\mathbf{H}_{0,1}^{-1}\mathbf{H}_{0,-1} & \mathbf{H}_{0,1}^{-1}[E_F\mathbf{I}-\mathbf{H}_0(0)] \end{bmatrix}\begin{bmatrix} \mathbf{U}(\pm) \\ ?\mathbf{U}(\pm) \end{bmatrix} = ?\begin{bmatrix} \mathbf{U}(\pm) \\ ?\mathbf{U}(\pm) \end{bmatrix}$$

hopping matrix $\left(\mathbf{H}_{s,s-1}\right)_{rk} = -te^{ir\phi}\delta_{rk}$

$\mathbf{H}_{s,s+1} = \mathbf{H}_{s,s-1}^{+}$ $\qquad \phi = \dfrac{eBa^2}{\hbar}$

eigenvalues $? = \lambda_m \delta_{mm}$

This creates the first "problem" as the discretization introduces an artificial band structure:

The energy diverges from the expected parabolic band

The artificial band has a width of $4t$ and here t = 21.5 meV.

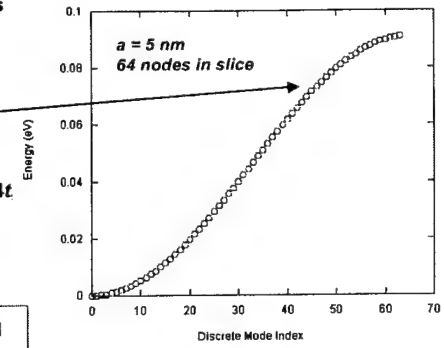

As a result, it is imperative that all relevant energies in the problem be < t in magnitude.

The general propagation scheme for the sth slice follows:

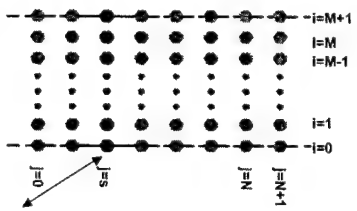

$$\begin{bmatrix} \mathbf{C}_1^{s+1} & \mathbf{C}_2^{s+1} \\ \mathbf{0} & \mathbf{1} \end{bmatrix} = \mathbf{T}_s \begin{bmatrix} \mathbf{C}_1^{s} & \mathbf{C}_2^{s} \\ \mathbf{0} & \mathbf{1} \end{bmatrix}\begin{bmatrix} \mathbf{1} & \mathbf{0} \\ \mathbf{P}_1^{s} & \mathbf{P}_2^{s} \end{bmatrix}$$

$$\mathbf{T}_s = \begin{bmatrix} \mathbf{0} & \mathbf{1} \\ -\mathbf{H}_{s,s+1}^{-1}\mathbf{H}_{s,s-1} & \mathbf{H}_{s,s+1}^{-1}[E_F\mathbf{I}-\mathbf{H}_0(s)] \end{bmatrix}$$

The LHS condition leads to:

$$\mathbf{P}_2^s = \left[\mathbf{T}_{21}^s\mathbf{C}_2^s + \mathbf{T}_{22}^s\right]^{-1}$$

$$\mathbf{P}_1^s = -\mathbf{P}_2^s\mathbf{T}_{21}^s\mathbf{C}_1^s$$

This term is the $G_0^{-1} - VG$ that appears in the recursive Green's function approach. This is Dyson's equation.

We have to initialize at slice "0" with a different scheme which converts from the mode basis to the site basis:

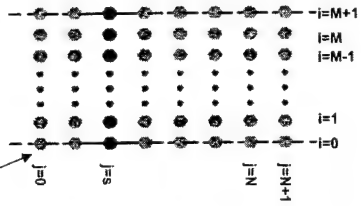

$$\begin{bmatrix} \mathbf{C}_1^{1} & \mathbf{C}_2^{1} \\ \mathbf{0} & \mathbf{1} \end{bmatrix} = \mathbf{T}_0 \begin{bmatrix} \mathbf{1} & \mathbf{0} \\ \mathbf{0} & \mathbf{1} \end{bmatrix}\begin{bmatrix} \mathbf{1} & \mathbf{0} \\ \mathbf{P}_1^{0} & \mathbf{P}_2^{0} \end{bmatrix}$$

$$\mathbf{T}_0 = \begin{bmatrix} \mathbf{U}(+) & \mathbf{U}(-) \\ \mathbf{U}(+)?(+) & \mathbf{U}(-)?(-) \end{bmatrix}$$

The LHS condition leads to:

$$\mathbf{P}_2^0 = \left[\mathbf{T}_{21}^0\cancelto{0}{\mathbf{C}_2^0} + \mathbf{T}_{22}^0\right]^{-1}$$

$$\mathbf{P}_1^0 = -\mathbf{P}_2^0\mathbf{T}_{21}^0\cancelto{1}{\mathbf{C}_1^0}$$

This part remains unchanged.

Finally, we have to convert back to the mode basis at the "N+2" slice:

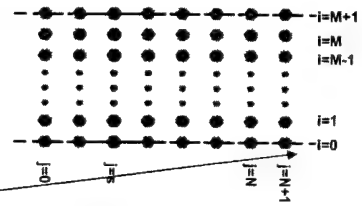

$$\begin{bmatrix} \mathbf{C}_1^{N+2} & \mathbf{C}_2^{N+2} \\ \mathbf{0} & \mathbf{1} \end{bmatrix} = \mathbf{T}_{N+1} \begin{bmatrix} \mathbf{C}_1^{N+1} & \mathbf{C}_2^{N+1} \\ \mathbf{0} & \mathbf{1} \end{bmatrix} \begin{bmatrix} \mathbf{1} & \mathbf{0} \\ \mathbf{P}_1^{N+1} & \mathbf{P}_2^{N+1} \end{bmatrix}$$

$$\mathbf{T}_{N+1} = \begin{bmatrix} \mathbf{0} & [\mathbf{U}(+)?(+)]^{-1} \\ \mathbf{1} & -\mathbf{U}(+)[\mathbf{U}(+)?(+)]^{-1} \end{bmatrix}$$

$$\mathbf{t} = \mathbf{C}_1^{N+2}$$

The LHS condition leads to:

$$\mathbf{P}_2^s = \left[\mathbf{T}_{21}^s \mathbf{C}_2^s + \mathbf{T}_{22}^s\right]^{-1}$$

$$\mathbf{P}_1^s = -\mathbf{P}_2^s \mathbf{T}_{21}^s \mathbf{C}_1^s$$

This part remains unchanged.

We then back propagate from a density near the "N+2" slice in order to get the density at each point in the structure.

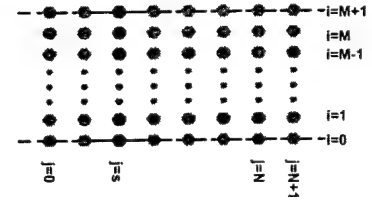

Once we know the wave function at slice s, near the end, we can back propagate, using:

$$\mathbf{F}^{(N+2,s)}(i,w) = \mathbf{P}_1^s + \mathbf{P}_2^s \mathbf{F}^{(N+2,s+1)}(i,w)$$

The "propagated" wave function connecting slice "s" to the output modes

Site "*i*" in the slice

Mode "*w*" in the density.

$$n_w(i,s) = \left|\Phi^{(N+2,s)}(i,w)\right|^2$$

$$n(i,s) = \sum_w \left|\Phi^{(N+2,s)}(i,w)\right|^2$$

Let us consider a simple example--that of a quantum point contact embedded in a wider wire:

a = 5 nm
width = 64 sites
QPC opening = 12 sites

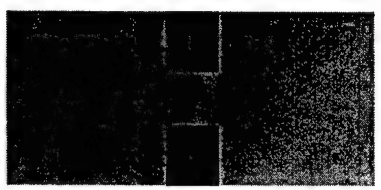

Because we initialize at one end of the structure, the result is *not* symmetric in the long axis. Thus, there is a definite input side and a definite output side, which is not often recognized.

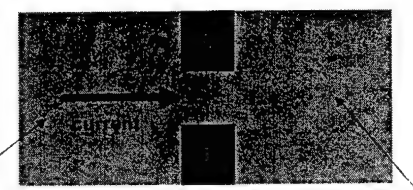

Input

Output

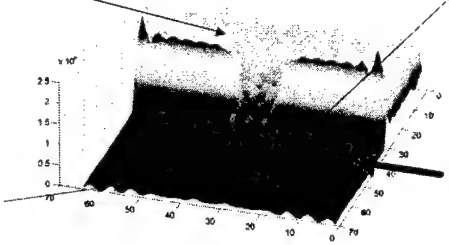

QPC region

Ripples caused by side wall reflections (mode structure) of hard wall boundary conditions

An Interesting Experiment:

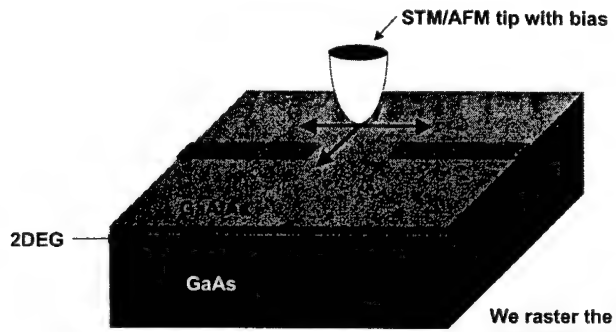

We raster the biased tip across the surface. The bias affects the 2DEG and changes the transmission through the QPC. We plot the transmission change as a function of the tip position.

simulation

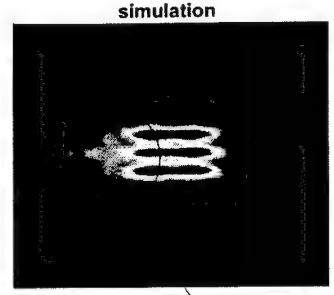

experiment

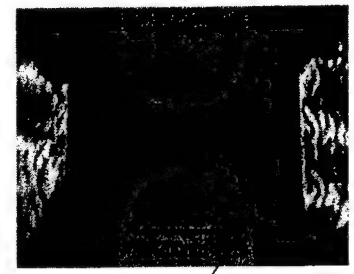

M. A. Topinka *et al.*, Science 289, 2323 (2000).

The three-fold pattern of the conduction change is seen only on the *input* side of the QPC (experiment is done in a.c. fashion rather in d.c. fashion assumed in the calculations).

As a second example, we consider an open quantum dot.

Dots can be of many shapes, even multiple dots:

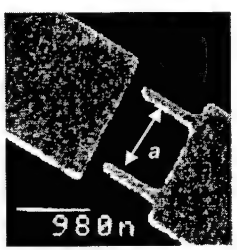

Typical fluctuations as B or V_G is varied:

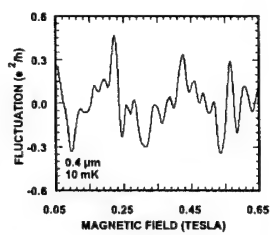

THE CLOSED DOT

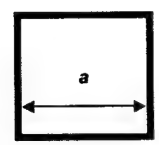

$$\psi_{nm}(x,y) = \frac{2}{a}\sin\left(\frac{n\pi x}{a}\right)\sin\left(\frac{m\pi y}{a}\right)$$

$n,m = 1,2,\ldots..$

- A magnetic field mixes the states and produces an *entangled* state.

Spectrum for a closed 0.3 μm dot

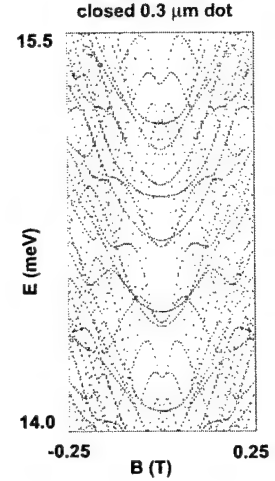

The Open Dot

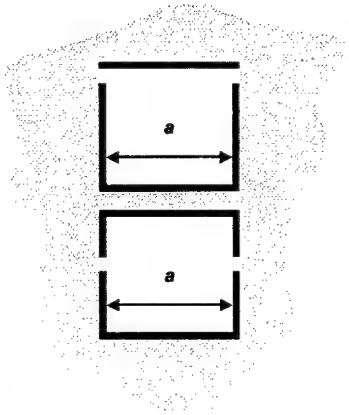

- Opening the dot does NOT destroy the quantization within the dot!
- The dot states hybridize (entangle) with the environment states.

Dot: *states* $\{|\alpha_d\rangle\}$
parameters (ops., var.)

Environment: *states* $\{|\alpha_e\rangle\}$
parameters (ops., var.)

$$H = H_d + H_e + H_{ed}$$

The Open Dot

Define the *system* density matrix ρ_s

and the *reduced, device* density matrix $\rho_d = Tr_e\{\rho_s\}$

$$H = H_d + H_e + H_{ed}$$

Use a projection super-operator $\hat{P}$ to remove the environment variables

This leads to the new Liouville equation for the device density matrix:

$$i\hbar \frac{\partial \rho_d}{\partial t} = \left(\hat{H}_d + \hat{H}_{ed} + \hat{\Sigma}(t \to \infty)\right)\rho_d$$

Where (in Laplace transform notation):

$$\hat{H}_{ed}\rho_d(s) \equiv Tr\left\{\hat{P}\hat{H}_{ed}\hat{P}\rho_s(s)\right\}$$

$$\hat{\Sigma}(s) = \hat{P}\hat{H}\hat{Q}(i\hbar s - \hat{Q}\hat{H}\hat{Q})^{-1}\hat{Q}\hat{H}\hat{P}$$

Modifications of spectrum by the environment

Superlattice effects from device array

Environmental Effects

We can understand how the QPCs and the dot work together to provide the "spectrum" of conductance.

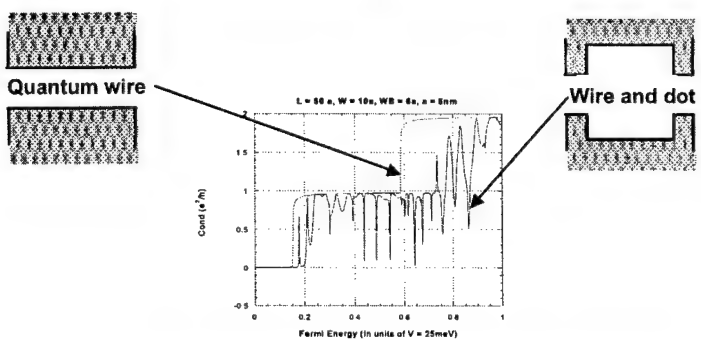

Dot modes, which are excited, work to provide modulation of the overall transmission.

The Open Dot

⇨ We determine the "spectrum" of the open dot from the conductance through the dot:

G ~ density of states

DOS ~ energy levels

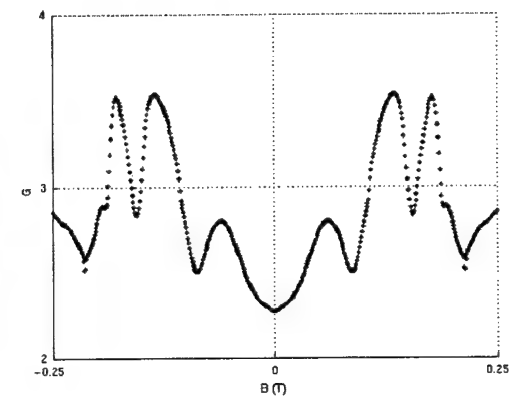

Decoration by "Scars"

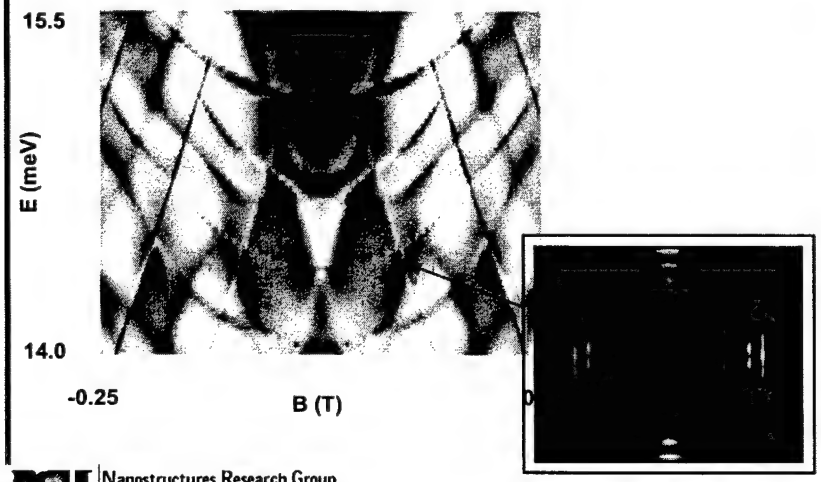

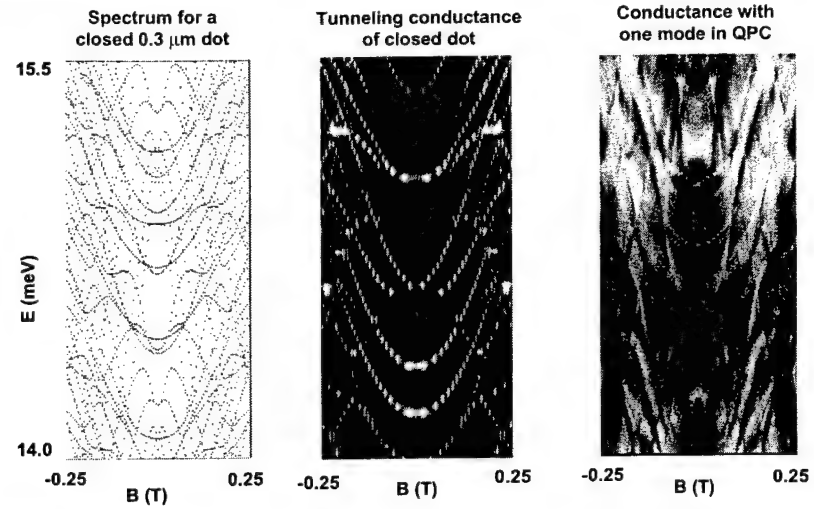

Four modes propagating through the quantum point contact:

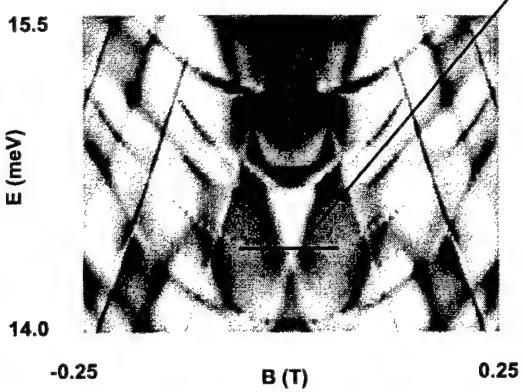

Basic structure arises from density of states: back-scattered trajectories (the various *trace* formulas)

The "back-scattered" trajectories are the FUNDAMENTAL trajectories, not additional structure!

Hence, there is nothing like *weak localization* in these dots!

Role of Averaging on the Spectra

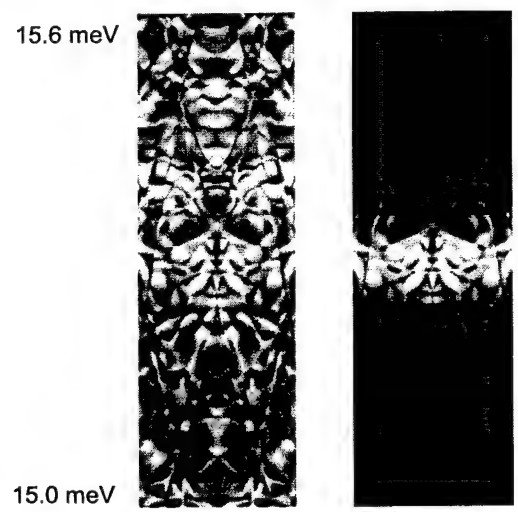

Role of Averaging on the Spectra

Moving average

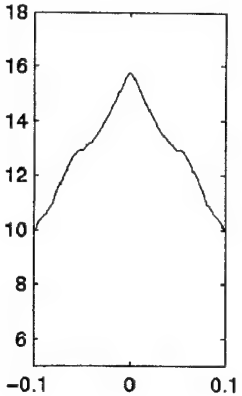

Let us now turn to the problem of self-consistency of the potential in the calculation--

The potential that is included in the site energy *V(i,j)* can be included as a self-consistent quantity. Here, the charge density is

$$\rho(x,y) = -\frac{e}{\varepsilon_s}\left(|\psi(x,y)|^2 - 1\right)n_0$$

Uniform electron density set by remote dopants in AlGaAs

For simple systems, we can generate a relatively straight-forward loop to find the solutions:

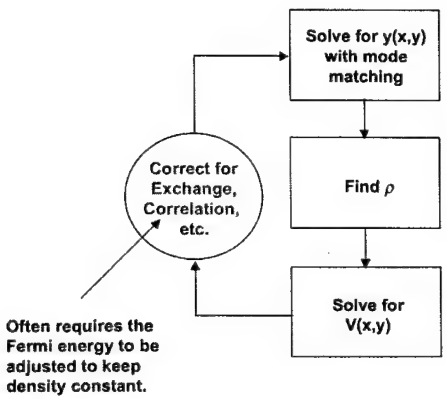

Consider a simple quantum wire with an embedded QPC. Here, we move the QPC to one side of the wire:

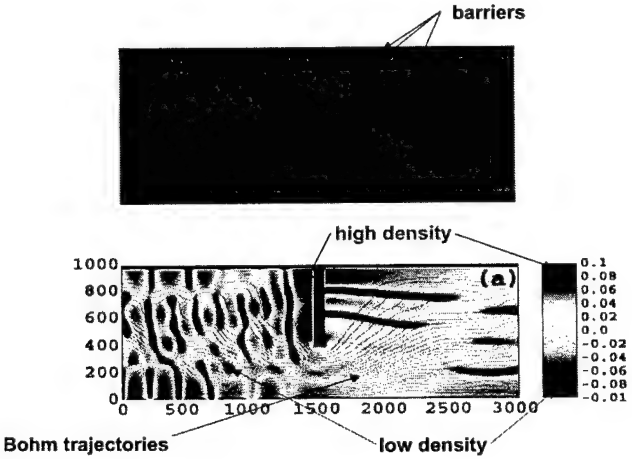

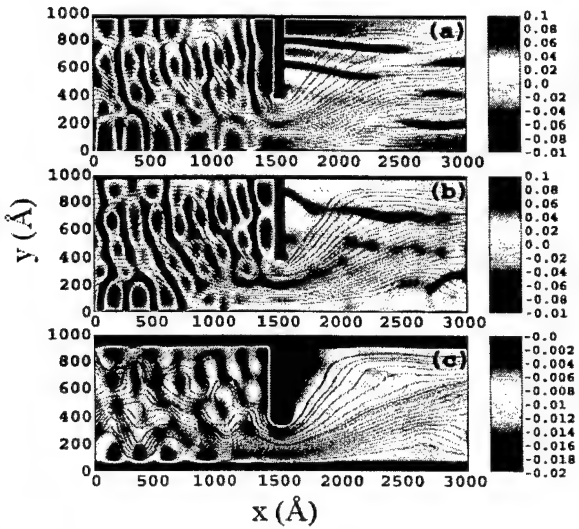

Calculation involving no self-consistency, background is the quantum potential

Calculation with self-consistency, background is the quantum + self-consistent potential

Calculation with the effective potential, background is the self-consistent potential

Electron density

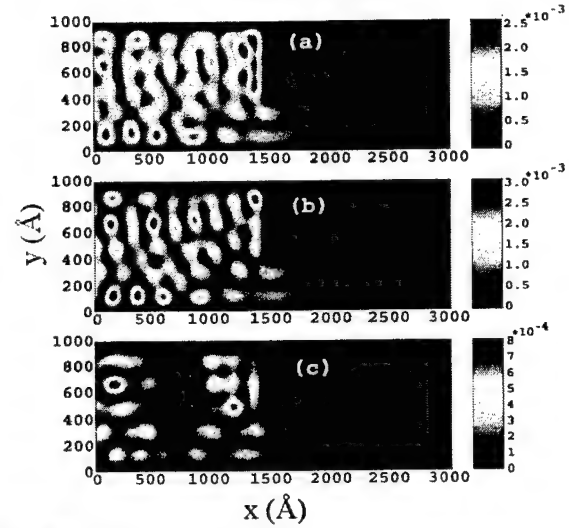

Calculation involving no self-consistency

Calculation with quantum + self-consistent potential

Calculation with the effective potential + self-consistent potential

For our dots, we embed everything in a 3D Poisson solver. However, the mode-matching is only a 2D quantum transport solver in the plane.

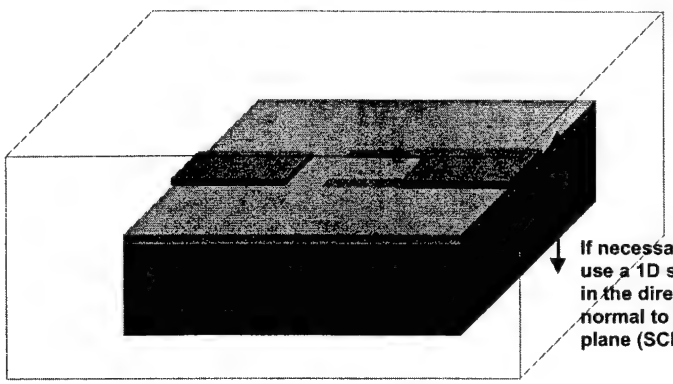

If necessary, we use a 1D solver in the direction normal to the plane (SCHRED).

Double dots:

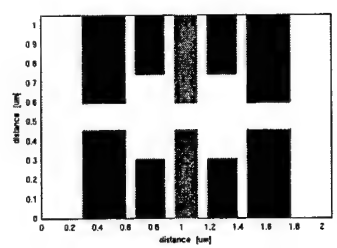

Typically, the center gate voltage is varied

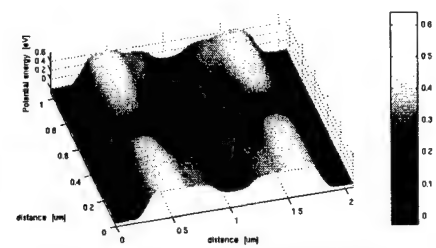

Determine the confining dot potential from a numerical solution of the three-dimensional (3D) Poisson equation:

$$\nabla \cdot (\varepsilon \nabla V(x,y,z)) = -e\left(p - n + N_D^+ - N_A^-\right)$$

coupled with the 1D Schrödinger equation:

$$\left[-\frac{\hbar^2}{2}\frac{\partial}{\partial z}\left(\frac{1}{m_z^*}\frac{\partial}{\partial z}\right) + V_{eff}(z)\right]\psi_n(z) = E_n\psi_n(z)$$

eigenfunctions ← eigenvalues

Problems with simple mode matching when:

- ❖ V(x,y) is not a simple function
- ❖ A magnetic field is applied

Then the modes can no longer be expressed as well characterized analytical functions.

Example: <u>a realistic quantum dot potential obtained by a self-consistent calculation</u>

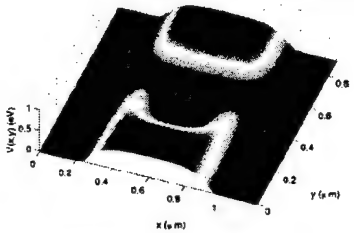

For better flexibility and accuracy it is advantageous to do the problem on a <u>discrete lattice.</u>

Our use of a solver for the modes, with a lattice representation solves this problem.

Confining potential has the form of a [illegible] parabolas

Split gate pattern

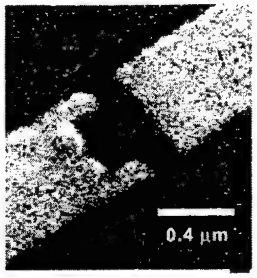

Measured conductance

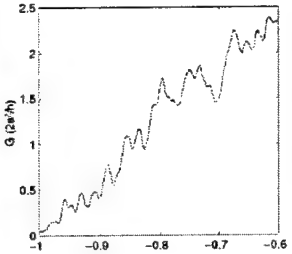

In the normal direction, the Exchange and correlation corrections to the ground state energy of the are included by using the Local Density Approximation.

V_g= -1.0 V V_g= -0.9 V V_g= -0.7 V

Gate voltage comparison revisited

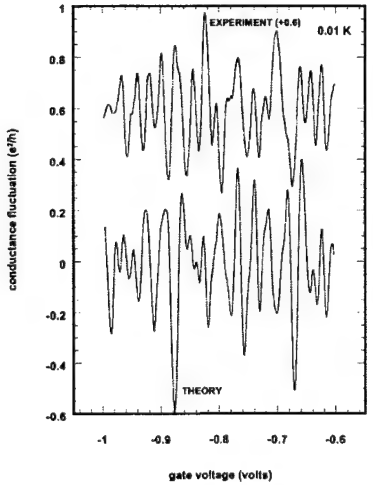

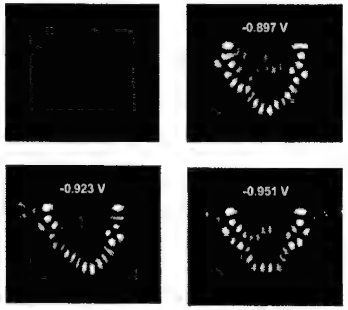

Simulations also reveal that certain scars may RECUR as gate voltage is varied. The resulting periodicity agrees WELL with that of the conductance oscillations

Persistence of the scarring at zero magnetic field indicates its INTRINSIC nature

The scarring is NOT induced by the application of the magnetic field

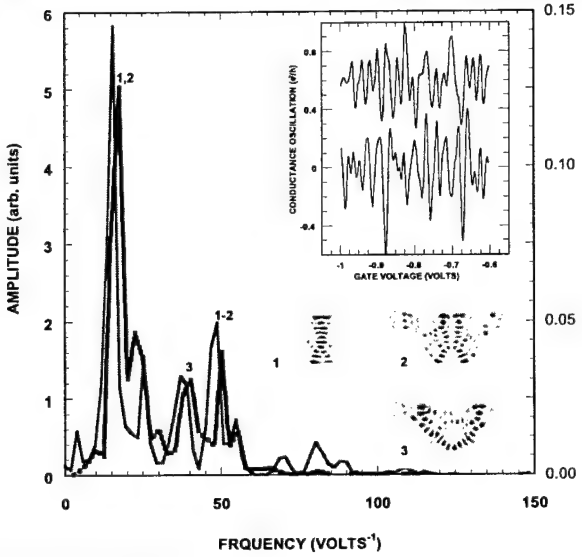

- Mode matching approaches are a viable method of computing the conduction in mesoscopic systems.
- This can easily be incorporated with the Poisson equation for self-consistent solutions.

- In addition, the energy dependence can be converted to a temperature dependence for near-equilibrium systems. It is also possible to do non-equilibrium approaches with only slight changes in the program (in principle).

Trajectories in quantum mechanics

John. R. Barker
Nanoelectronics Research Centre
Department of Electronics and Electrical Engineering
University of Glasgow

Advanced Research Workshop
on
Quantum Transport in Semiconductors

© J R Barker 2001, University of Glasgow. This material is not to be reproduced or published without permission

Conventional device modelling:semi-classical

Empirical
Drift Diffusion
Hydrodynamic ← Velocity flows, Particle trajectories
Monte Carlo

Self-consistent via Poisson equation

Can we obtain a trajectory description of quantum transport?

In principle, the the surprising answer is yes

© J R Barker 2001, University of Glasgow. This material is not to be reproduced or published without permission

1. Without any extension of quantum theory we may define velocity flows.
2. With special assumptions we may define trajectories
3. Bohm has also proposed deterministic extension to QM which uses trajectories calculated in 1 or 2.
4. Others have defined stochastic trajectories in extensions to QM

- Position- momentum uncertainty relations
- Non-locality of quantum mechanics

© J R Barker 2001, University of Glasgow. This material is not to be reproduced or published without permission

cloud chamber

Wigner trajectories

(stationary states only)
no compact support

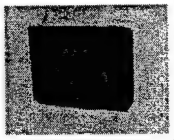

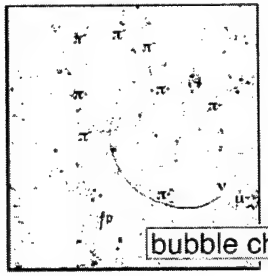

bubble chamber

Feynman paths

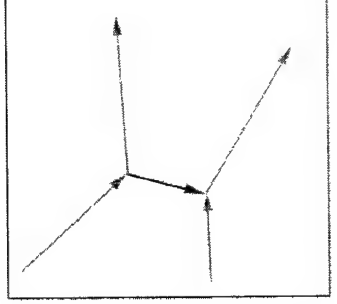

© J R Barker 2001, University of Glasgow. This material is not to be reproduced or published without permission

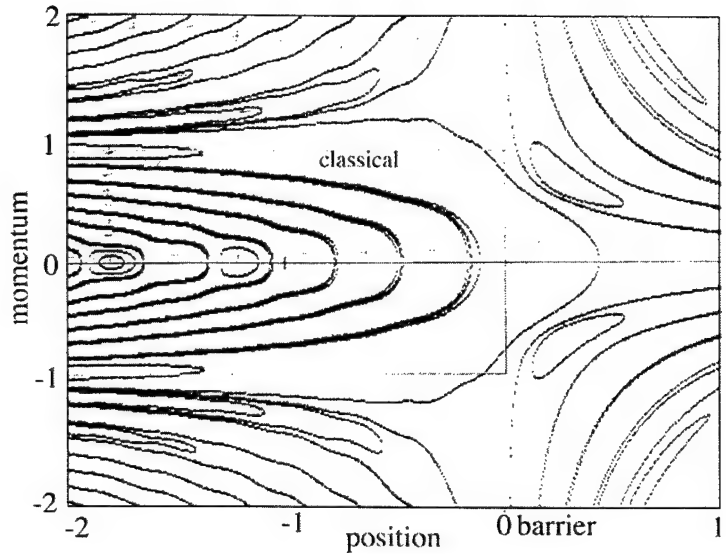

© J R Barker 2001, University of Glasgow. This material is not to be reproduced or published without permission

What do we want from a quantum transport theory?

A self-consistent treatment of the local charge and current density fields which describe

- tunnelling
- scattering
- interference effects
- size quantisation
- time-dependence
- de-coherence effects
- many-body issues

FOR FINITE REGIONS OF OPEN SYSTEMS

© J R Barker 2001, University of Glasgow. This material is not to be reproduced or published without permission

A rigorous approach to trajectories

Velocity Flow Picture

Probability density $n(\mathbf{x},t)$

Particle Current density $\mathbf{j}(\mathbf{x},t)$

Define a velocity field:

$$\mathbf{v}(\mathbf{x},t) = \mathbf{j}(\mathbf{x},t)/n(\mathbf{x},t)$$

© J R Barker 2001, University of Glasgow. This material is not to be reproduced or published without permission

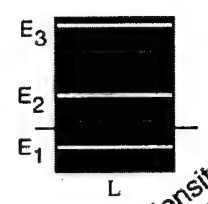

particle in box

$$\Psi(x,t) = \cos|\phi|\,\Psi_1 + \sin|\phi|\,\Psi_2$$

$$\langle x\rangle = (L/2)(1 - (32/9\pi^2)\sin[2\phi]\cos[\omega t])$$

$$\langle v\rangle = (16L/9\pi 2)\sin[2\phi]\sin[\omega t]$$

$$\langle E\rangle = \cos^2|\phi|E_1 + \sin^2|\phi|E_2$$

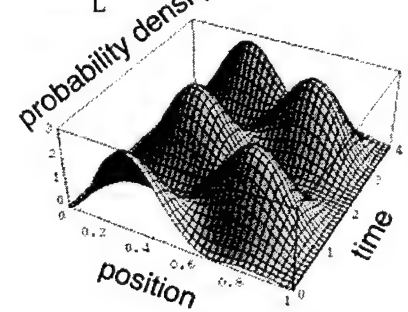

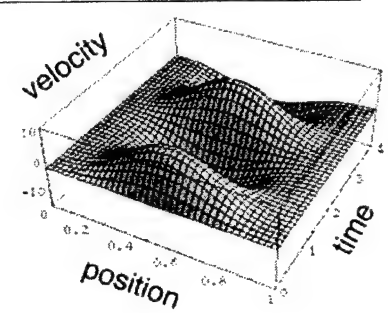

Non-stationary states show trajectories

© J R Barker 2001, University of Glasgow. This material is not to be reproduced or published without permission

Schrödinger Equation

$$i\hbar\frac{\partial\Psi}{\partial t} = H\Psi(x,t)$$

$$H = -\frac{\hbar^2}{2m}\nabla^2 + \Phi$$

$$n(x,t) = \Psi^*(x,t)\Psi(x,t)$$

$$\mathbf{j}(x,t) = \frac{-i\hbar}{2m}\{\Psi^*\nabla\Psi - \Psi\nabla\Psi^*\}$$

© J R Barker 2001, University of Glasgow. This material is not to be reproduced or published without permission

A posteriori quantum hydrodynamics

Express wave function in polar form: $\Psi = R\exp(iS/\hbar)$

$$\frac{\partial n}{\partial t} + \nabla.n\mathbf{v} = 0$$

$$\frac{\partial S}{\partial t} + \frac{\nabla S.\nabla S}{2m} + \Phi(x,t) + V_Q(x,t) = 0$$

$$V_Q = -\frac{\hbar^2}{2m}\frac{\nabla^2\sqrt{n}}{\sqrt{n}} \qquad n = R^2 \qquad m\mathbf{v} = \nabla S$$

Quantum potential

© J R Barker 2001, University of Glasgow. This material is not to be reproduced or published without permission

Take the gradient of the phase equation

mdv/dt

$$m\frac{\partial\mathbf{v}}{\partial t} + m\mathbf{v}.\nabla\mathbf{v} = -\nabla\Phi(\mathbf{x},t) - \nabla V_Q(\mathbf{x},t)$$

Quantum Euler Eqn

$$\frac{\partial n}{\partial t} + \nabla.n\mathbf{v} = 0$$

Continuity Equation

The first equation is not quite correct and we need further constraints as we shall see

$$V_Q = -\frac{\hbar^2}{2m}\frac{\nabla^2\sqrt{n}}{\sqrt{n}} \qquad n = R^2 \qquad m\mathbf{v} = \nabla S$$

© J R Barker 2001, University of Glasgow. This material is not to be reproduced or published without permission

Quantum corrected Drift - diffusion

n, **v**, ψ

Newton's 2nd law for carriers:

$$m^*\frac{d\mathbf{v}}{dt} = q\nabla(\psi - \varphi) - \frac{D}{n\mu}\nabla n - q\frac{\mathbf{v}}{\mu}$$

electrostatic potential

chemical potential

diffusion coefficient
mobility
effective mass

Density gradient model

$$\varphi \rightarrow \varphi - 2b\frac{\nabla^2\sqrt{n}}{\sqrt{n}}$$

Poisson-**Schrödinger** equation

© J R Barker 2001, University of Glasgow. This material is not to be reproduced or published without permission

Quantum potential causes repulsion from boundaries
But also lowers barrier energies to allow tunnelling

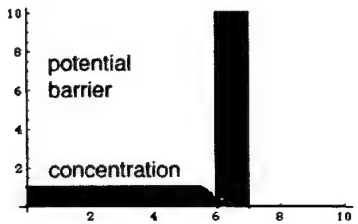

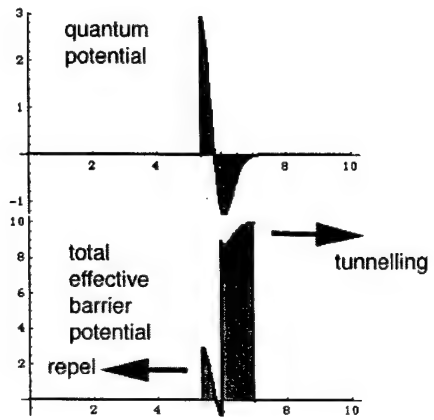

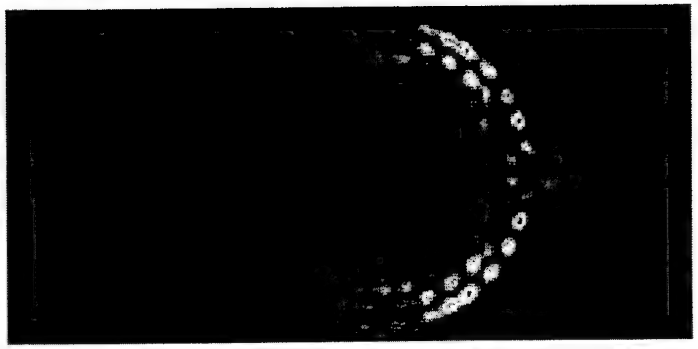

2-slit interference

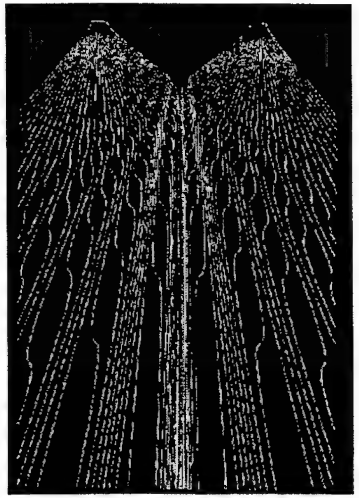

Trajectories equivalent to streamlines in steady state

First reported by Dewdney et al

Interpretation: discover a trajectory

Quantum Potential

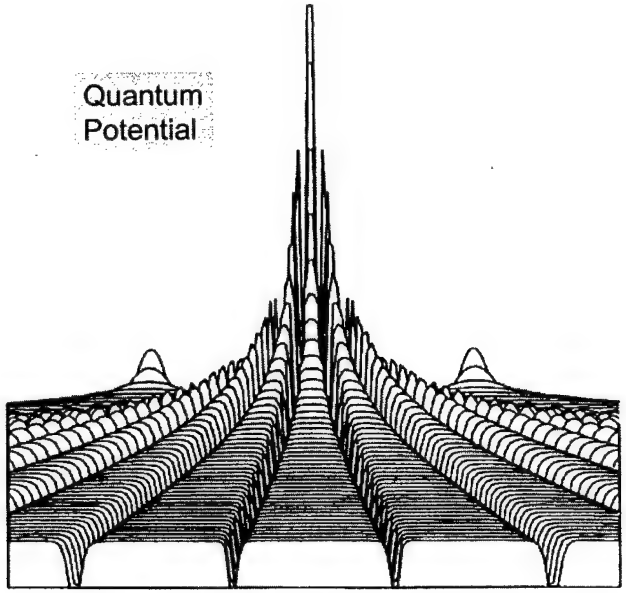

Uncertainty Relations

$$\Delta x \Delta p \geq \hbar / 2$$

$$\Delta x = <(x - <x>)^2>^{1/2} = \{ \int x^2 n(x) dx - [\int x \; n(x) dx]^2 \}^{1/2}$$

$$\Delta p = <(p - <p>)^2>^{1/2} =$$

$$\{ \int (p^2(x) + 2mV_Q(x)) n(x) dx - [\int p(x) \; n(x) dx]^2 \}^{1/2}$$

$$p = \partial S / \partial x$$

Barker (1992)

© J.R. Barker 2001, University of Glasgow. This material is not to be reproduced or published without permission

Entanglement

Factorisable wave-function -> physical independence

Sum of factorisable wave-functions :

1. Effective statistical mixture
2. Entangled state: correlation

© J.R. Barker 2001, University of Glasgow. This material is not to be reproduced or published without permission

Configuration Space

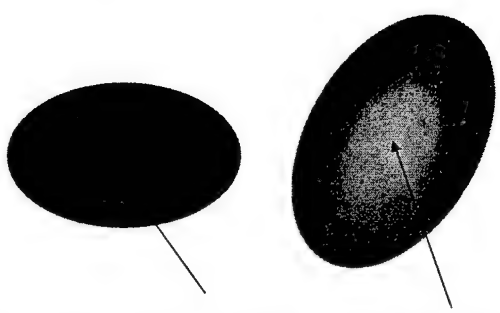

$$\Psi(\mathbf{r}_1, \mathbf{r}_2) = C[\Psi_\alpha(\mathbf{r}_1)\Psi_\beta(\mathbf{r}_2) + \Psi_\gamma(\mathbf{r}_1)\Psi_\delta(\mathbf{r}_2)]$$

No overlap: effective statistical mixture,
System point is in one or the other sub-state

© J.R. Barker 2001, University of Glasgow. This material is not to be reproduced or published without permission

Configuration Space

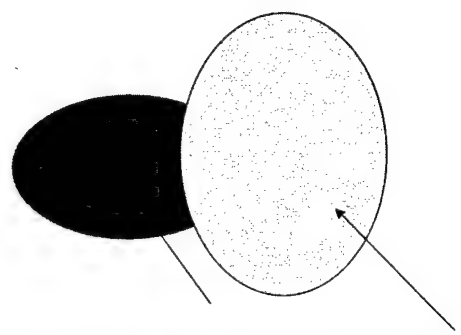

$$\Psi(\mathbf{r}_1, \mathbf{r}_2) = C[\Psi_\alpha(\mathbf{r}_1)\Psi_\beta(\mathbf{r}_2) + \Psi_\gamma(\mathbf{r}_1)\Psi_\delta(\mathbf{r}_2)]$$

Overlap: entangled state,
Correlation

© J.R. Barker 2001, University of Glasgow. This material is not to be reproduced or published without permission

Fermions

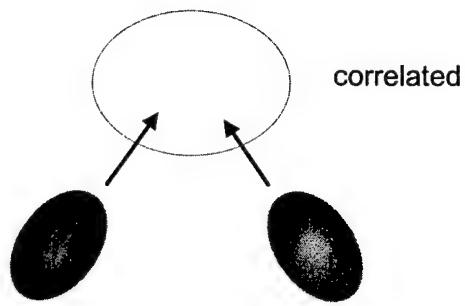

$$\Psi(\mathbf{r}_1,\mathbf{r}_2) = C[\Psi(\mathbf{r}_1,\mathbf{r}_2) - \Psi(\mathbf{r}_2,\mathbf{r}_1)]$$

Effectively factorisable at long distances

© J R Luther 2001, University of Glasgow. This material is not to be reproduced or published without permission

2 fermions in a harmonic oscillator potential

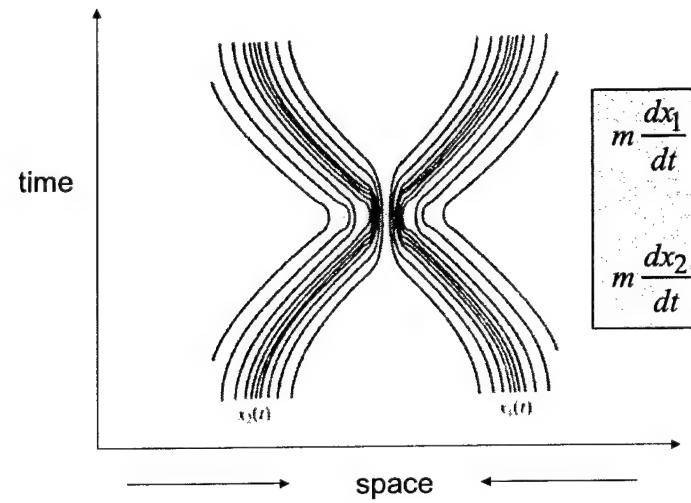

$$m\frac{dx_1}{dt} = \frac{\partial S}{\partial x_1}$$

$$m\frac{dx_2}{dt} = \frac{\partial S}{\partial x_2}$$

Vigier, Dewdney, Holland and Kypriandis (1987)

© J R Luther 2001, University of Glasgow. This material is not to be reproduced or published without permission

Topological properties of quantum flows

Velocity **v** derived from gradient of phase S

Wave function R exp(iS/h) is single-valued

Streamlines do not cross

Velocity circulation is quantised

Position coordinates form an autonomous system:
flow determined topologically by fixed points in the flow.

© J R Luther 2001, University of Glasgow. This material is not to be reproduced or published without permission

2D example

$$\frac{dx}{dt} = v_x = m^{-1}\frac{\partial S}{\partial x}; \quad \frac{dy}{dt} = v_y = m^{-1}\frac{\partial S}{\partial y}$$

$$\frac{dy}{dx} = \frac{\dfrac{\partial S(x,y)}{\partial y}}{\dfrac{\partial S(x,y)}{\partial x}}$$

© J R Luther 2001, University of Glasgow. This material is not to be reproduced or published without permission

Flow near singularities

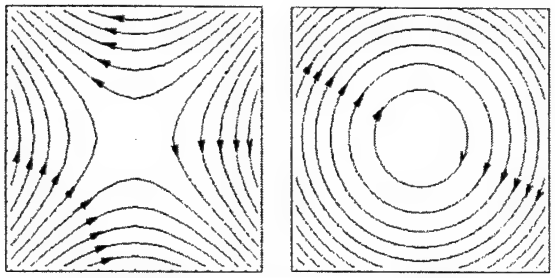

hyperbolic vortex

At velocity nodes At density nodes

© J R Barker 2001, University of Glasgow. This material is not to be reproduced or published without permission

The quantisation of velocity circulation

The *a posteriori* QHD equations automatically satisfy the velocity circulation theorem:

$$\oint \nabla S.dr = Nh \quad (N: \text{ integer})$$

$$\oint \mathrm{v}.d\mathrm{r} = Nh/m$$

© J R Barker 2001, University of Glasgow. This material is not to be reproduced or published without permission

Vortices occur at strong nodal points/lines (Barker 2001)

$$R \approx |\mathbf{r} - \mathbf{x}_i|^{N_i}$$

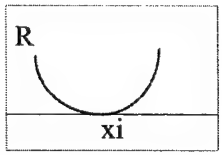

Or generally,

$$R \approx [(\mathbf{r} - \mathbf{x}_i).\Lambda.(\mathbf{r} - \mathbf{x}_i)]^{N_i/2}$$

$$\boxed{V_Q = -(\hbar^2/2m)\nabla^2 R/R \approx -(\hbar^2/2m)N_i^2/|\mathbf{r} - \mathbf{x}_i|^2}$$

© J R Barker 2001, University of Glasgow. This material is not to be reproduced or published without permission

Vortex line

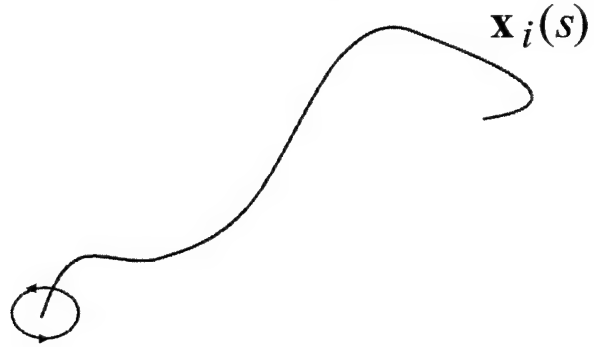

$$\nabla \times \mathbf{v} = N_i(h/m)\int \delta(\mathbf{r} - \mathbf{x}_i(s))(d\mathbf{x}_i/ds)ds$$

© J R Barker 2001, University of Glasgow. This material is not to be reproduced or published without permission

Near the strong nodal point:

$$\frac{1}{2}mv^2 \approx -V_Q = (\hbar^2/2m)\nabla^2 R/R$$
$$\approx (\hbar^2/2m)N_i^2/|\mathbf{r}-\mathbf{x}_i|^2$$

Singular velocity

$$\mathbf{v} = \frac{N_i\hbar}{m\,|\mathbf{r}-\mathbf{x}_i|}$$

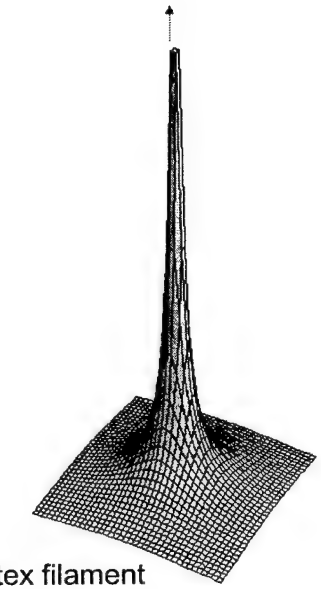

Analogous to classical Eulerian vortex filament

Non-singular current density

$$\mathbf{J} \propto |\mathbf{r}-\mathbf{x}_i|^{2N_i-1}$$

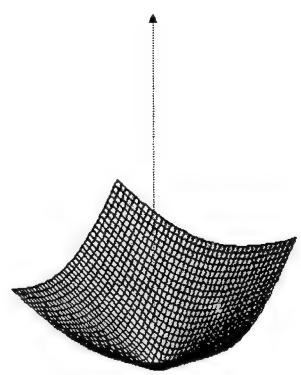

Phase $S = N_k ArcTan(y/x) \quad x,y \neq 0$

$$\Psi \approx |\mathbf{r}-\mathbf{x}_k|^{N_k} \exp[iN_k\phi]$$

Re-constructed wave-function

$$\oint \nabla S.d\mathbf{r} = N_k h$$

Traversal Time

requires Bohm interpretation

$$t = \int_{r_1}^{r_2} \frac{\mathbf{v}.\mathbf{dr}}{\mathbf{v}^2}$$

$$= \int_{r_1}^{r_2} \frac{\mathbf{p}.\mathbf{dr}}{2T}$$

Kinetic energy appears as metric

On a vortex, one loop executed in time $t=Nh/2T$

Barker (1992)

© J.R. Barker 2001. University of Glasgow. This material is not to be reproduced or published without permission.

To describe vortex motion with ***ab initio*** **quantum hydrodynamics**
we need to introduce a **vector** quantum potential $\mathbf{a_Q}(r,t)$

$$\oint_C \mathbf{a}_Q .\mathbf{dr} = nh$$

$$\boxed{m\frac{\partial \mathbf{v}}{\partial t} + m\mathbf{v}.\nabla\mathbf{v} = -\nabla\Phi(\mathbf{x},t) - m\mathbf{v}\times\nabla\times\mathbf{a}_Q(\mathbf{x},t) - \nabla V_Q(\mathbf{x},t)}$$

where

$$\nabla\times\mathbf{a}_Q = \sum_i N_i(h/m)\int \delta(\mathbf{r}-\mathbf{x}_i(s))(d\mathbf{x}_i/ds)ds$$

© J.R. Barker 2001. University of Glasgow. This material is not to be reproduced or published without permission.

Ballistic flow in open quantum dots

© J.R. Barker 2001. University of Glasgow. This material is not to be reproduced or published without permission.

Quantum smoke ring

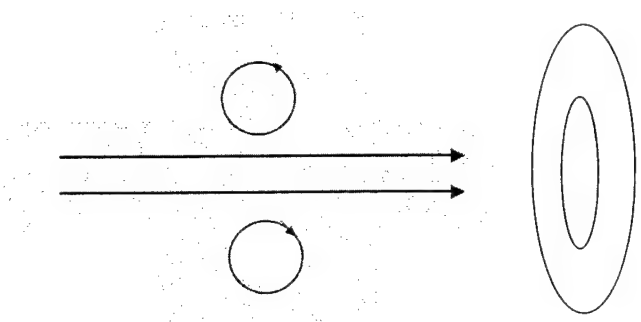

Compare Lord Kelvin's cigar box!

© J.R. Barker 2001. University of Glasgow. This material is not to be reproduced or published without permission.

Density evolution

QuickTime™ and a
Animation decompressor
are needed to see this picture.

Travelling wave in single transverse mode

© J R Butler 2001, University of Glasgow. This material is not to be reproduced or published without permission

Current density evolution

4 vortices formed

QuickTime™ and a
Animation decompressor
are needed to see this picture.

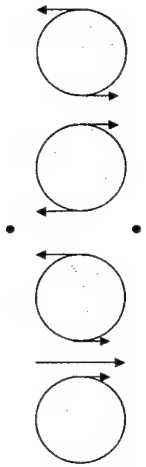

2 saddles

© J R Butler 2001, University of Glasgow. This material is not to be reproduced or published without permission

Transmission
Maximum

Density plot

QuickTime™ and a
Animation decompressor
are needed to see this picture.

Lower energy, transmission minimum (reflection)

© J R Butler 2001, University of Glasgow. This material is not to be reproduced or published without permission

Current
Density
And
Particle
density

QuickTime™ and a
Animation decompressor
are needed to see this picture.

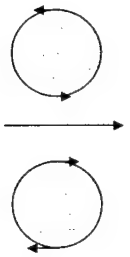

Smoke ring

2 vortices
formed

© J R Butler 2001, University of Glasgow. This material is not to be reproduced or published without permission

Transmission Coefficient

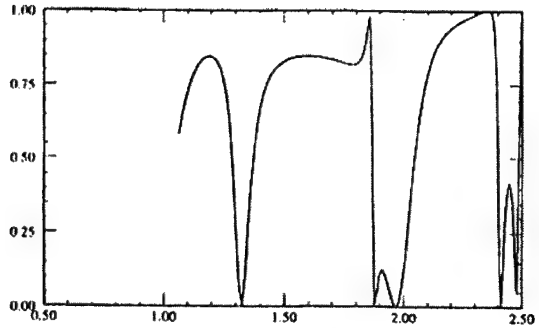

Total wave-vector

Compare Lent (1990)

© J R Barker 2001, University of Glasgow. This material is not to be reproduced or published without permission

Current density magnitude transverse across the cavity

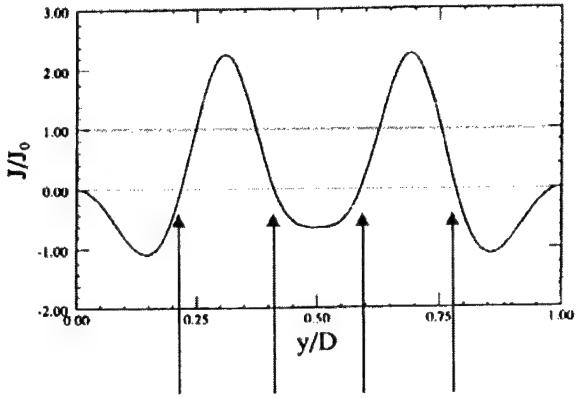

4 vortex cores

Compare Lent (1990)

© J R Barker 2001, University of Glasgow. This material is not to be reproduced or published without permission

Quantum potential

Confining

Reflecting wall

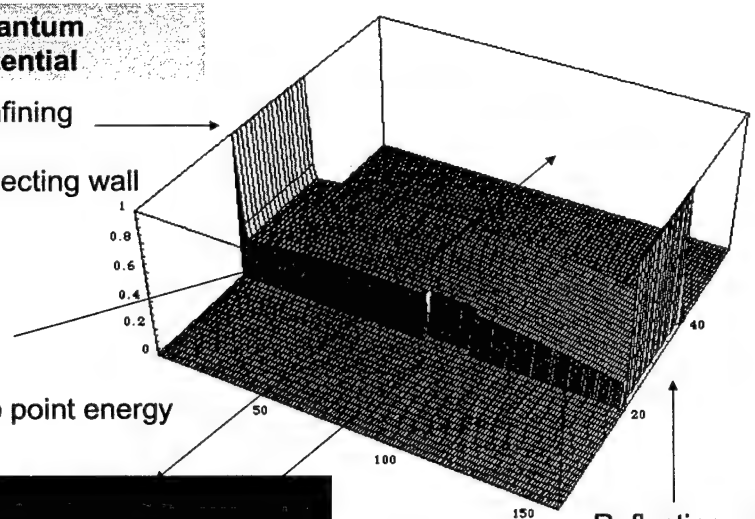

Zero point energy

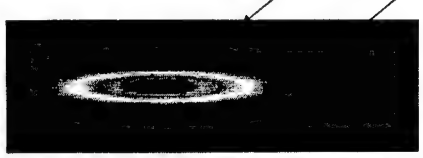

Reflecting wall

Note long range of V_Q

© J R Barker 2001, University of Glasgow. This material is not to be reproduced or published without permission

Rapid development of V_Q with time

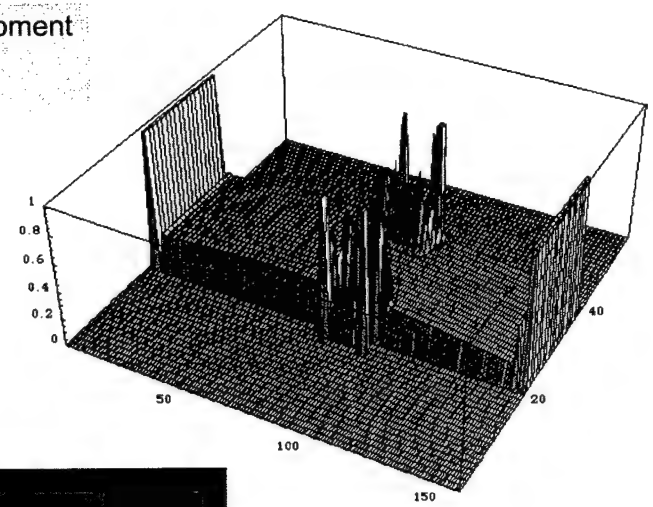

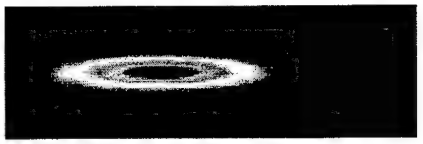

© J R Barker 2001, University of Glasgow. This material is not to be reproduced or published without permission

Attractive V_Q heralds start of vortex motion

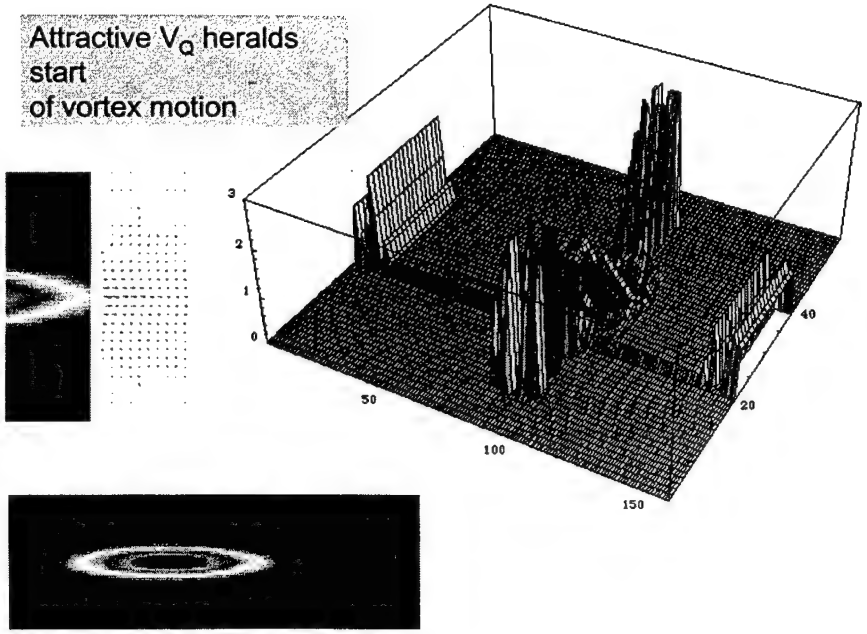

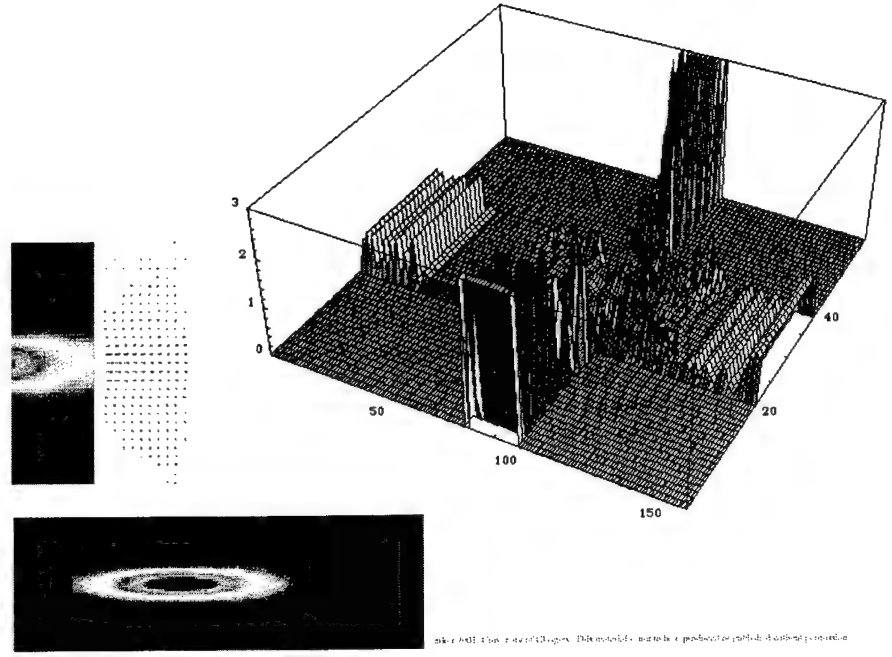

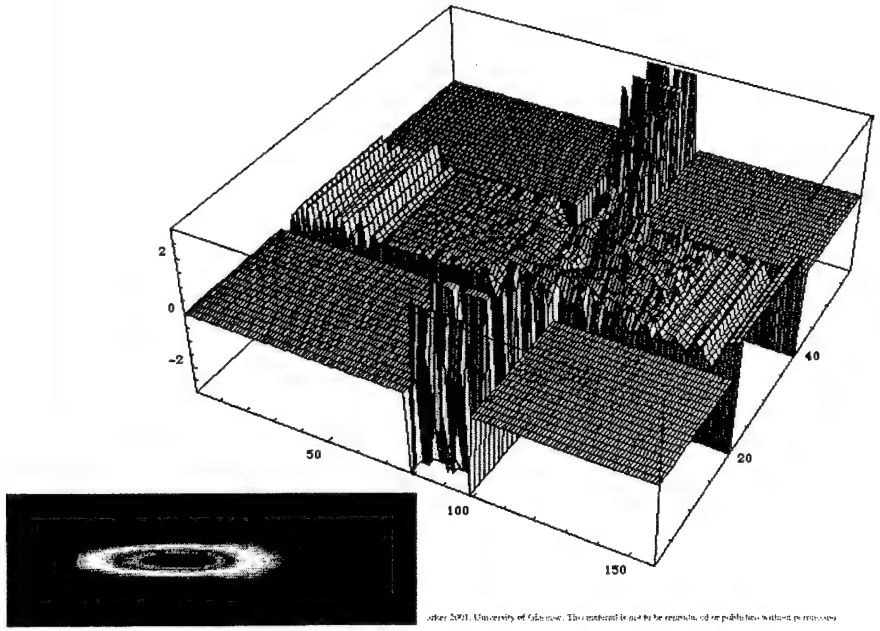

Vortex flow develops around attractor basins of V_Q.

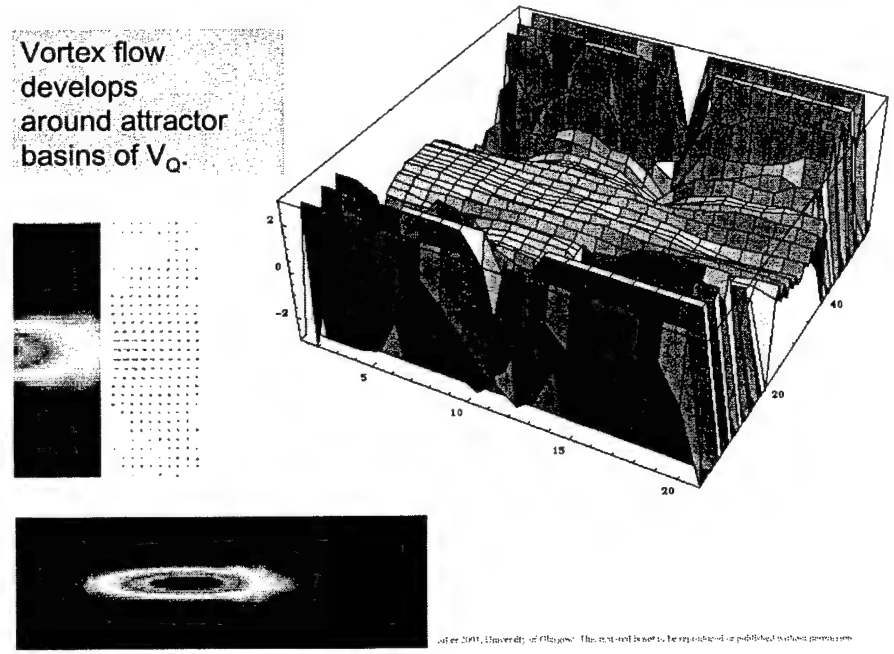

Full vortices developed

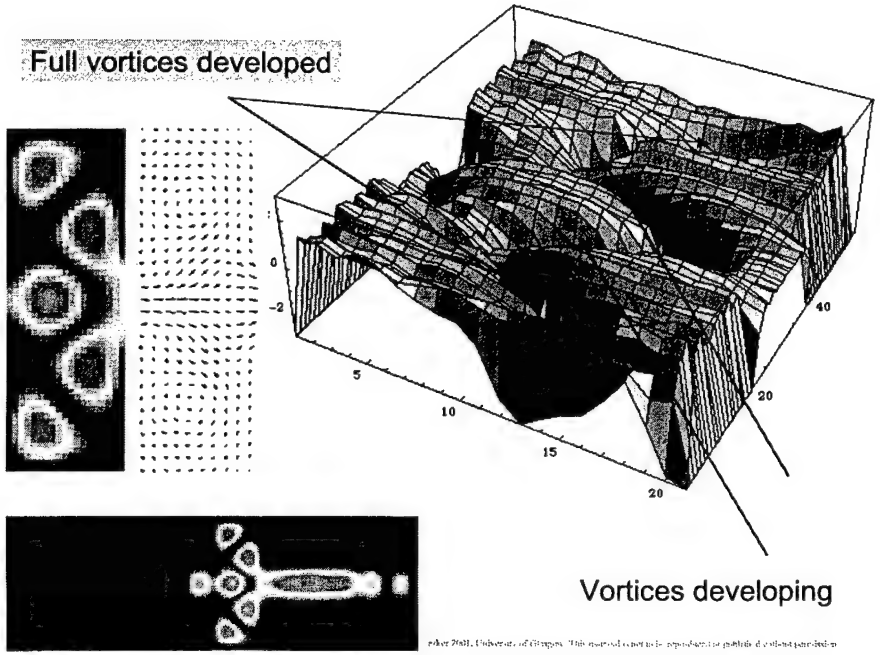

Vortices developing

© J R Butler 2001, University of Glasgow. This material is not to be reproduced or published without permission

Non-locality of full quantum potential

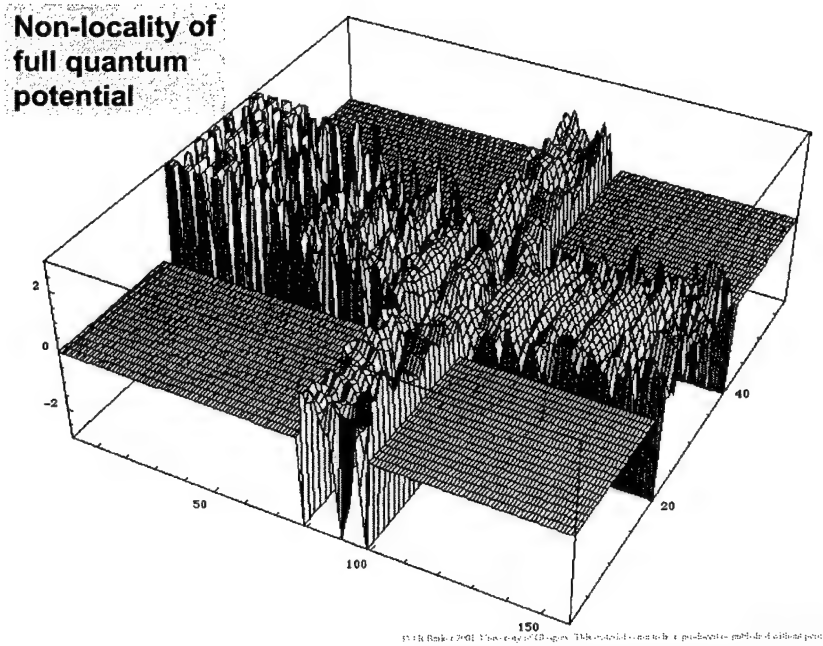

© J R Butler 2001, University of Glasgow. This material is not to be reproduced or published without permission

Angular momentum

$$\mathbf{l} = \mathbf{r} \times \nabla S$$

$$\mathbf{l_z} = N\hbar$$

$$\mathbf{L^2} = l^2 + L_Q^2$$

Leads to stability

© J R Butler 2001, University of Glasgow. This material is not to be reproduced or published without permission

Example: Wave incident on a 2DEG throttle

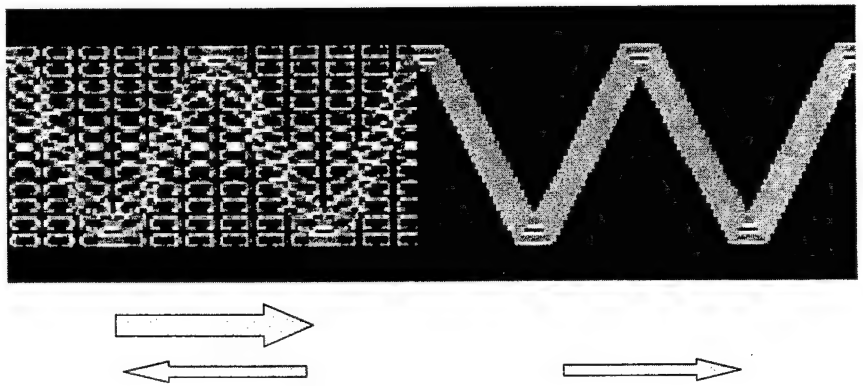

Incident travelling wave in high transverse mode

© J R Butler 2001, University of Glasgow. This material is not to be reproduced or published without permission

Detail of upstream density and velocity flow

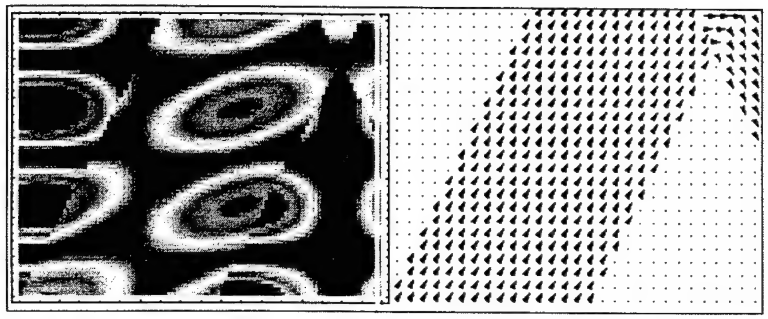

density | velocity field

Scarred wave-function | Ray approximation

© J.R. Barker 2001, University of Glasgow. This material is not to be reproduced or published without permission

Upstream flow: full form

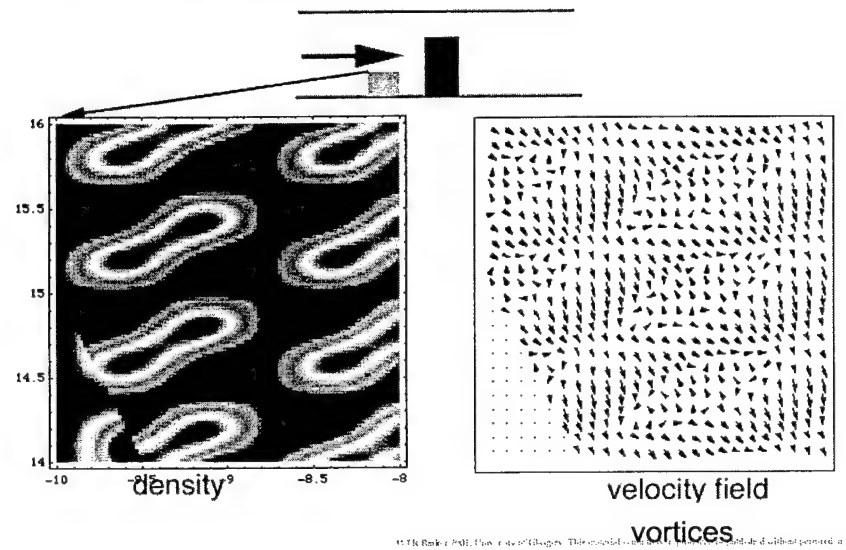

© J.R. Barker 2001, University of Glasgow. This material is not to be reproduced or published without permission

Quantum Flows

Barker
Ferry & Akis (2000)

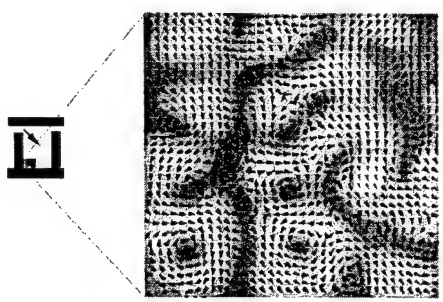

- Velocity field in quantum dot
- Meandering open orbits
- Trapped flows - vortices

© J.P. Barker 2001, University of Glasgow. This material is not to be reproduced or published without permission

Flow of an extended wave packet in a double throttle = open quantum dot

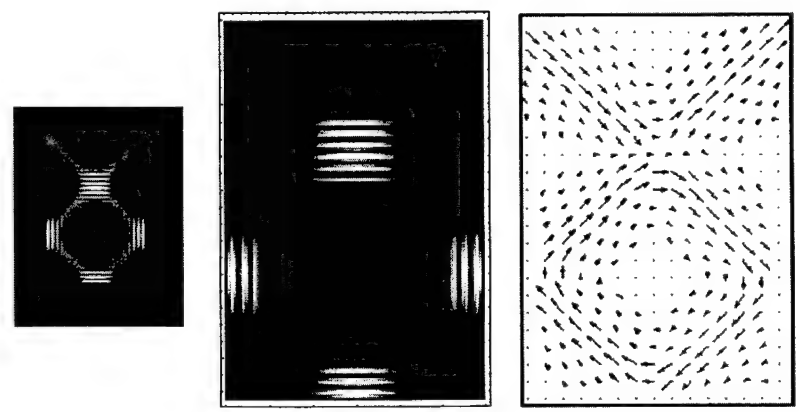

A posteriori quantum hydrodynamics

Calculate **J** and n, form **v**

Quantum Euler equations automatically satisfied, including quantization of circulation.

Ab initio quantum hydrodynamics

To be of predictive power rather than purely explanatory the velocity flow approach must become *ab initio*.

Quantum Euler equations ,+ scalar & vector quantum potentials
A neat way to put QM in Monte Carlo, Hydrodynamic, DD models.
Difficult to solve in general.

conjecture

The open quantum dot analysis suggests:
Can we construct the quantum flow by first constructing the classical flow and then replacing any trajectory crossing points by flow separation?

Classical and quantum ray paths

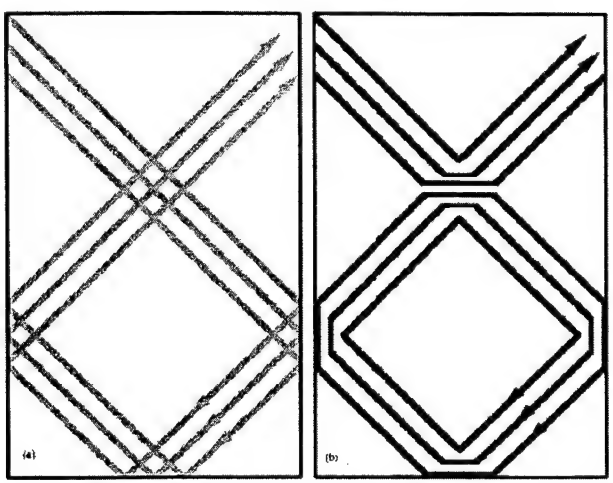

Spatially correlated virtual particles

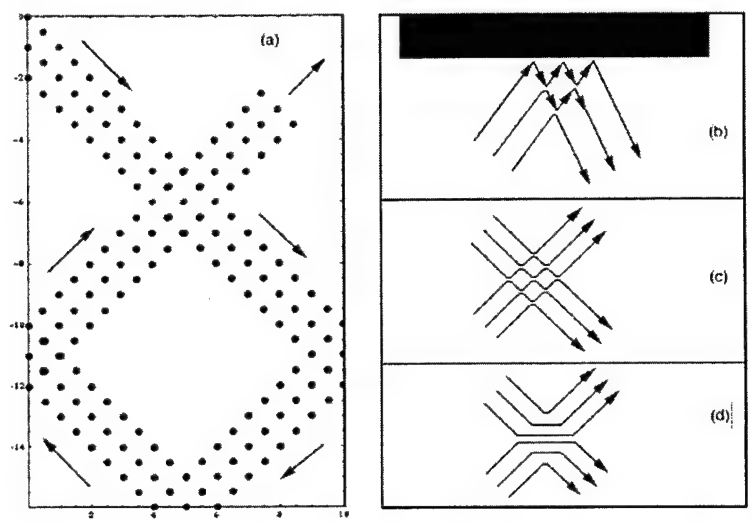

Dissipative quantum hydrodynamics

Conventional QHD has used classical HD model for scattering processes.
Less empirical approach

Use transient scattered wave or use non-hermitian Hamiltonian:
leads to description of trapping/de-trapping, elastic and inelastic scattering with extended collision zones and intra-collisional field effect

Barker and Ferry, APL 74 582 (1999),
Barker and Watling, Superlattices and microstructures, 27, 347 (2000)

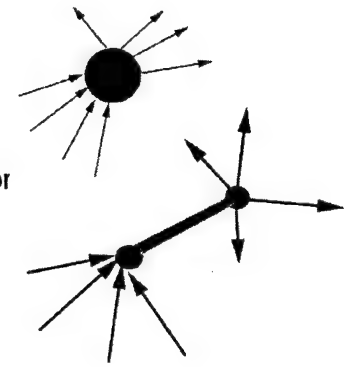

New Topological features

© J R Barker 2001, University of Glasgow. This material is not to be reproduced, or published without permission

Inelastic Scattering

Flow occurs in configuration space
Electron coordinate **r**
Scatterer generalised coordinate(s) X,...

Trajectories cannot cross in configuration space.

But trajectories may now cross in real space PROVIDED.... Scatterer coordinates are different - a new result.

© J R Barker 2001, University of Glasgow. This material is not to be reproduced, or published without permission

Inelastic Scattering

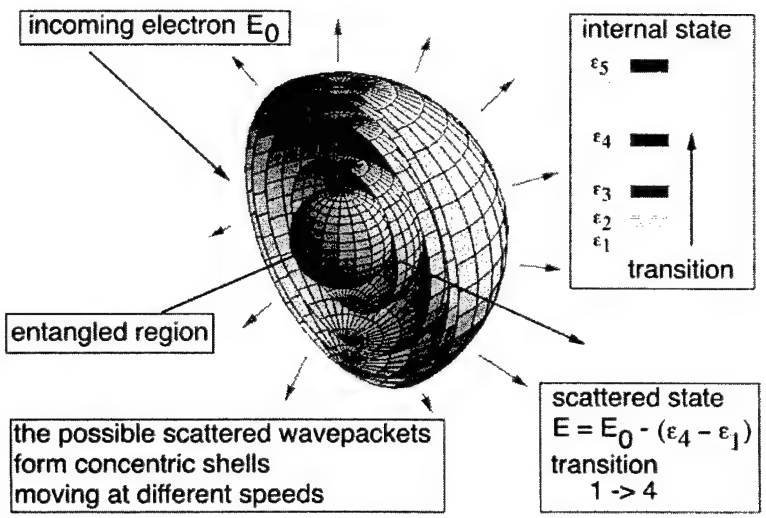

© J R Barker 2001, University of Glasgow. This material is not to be reproduced, or published without permission

Inelastic Scattering

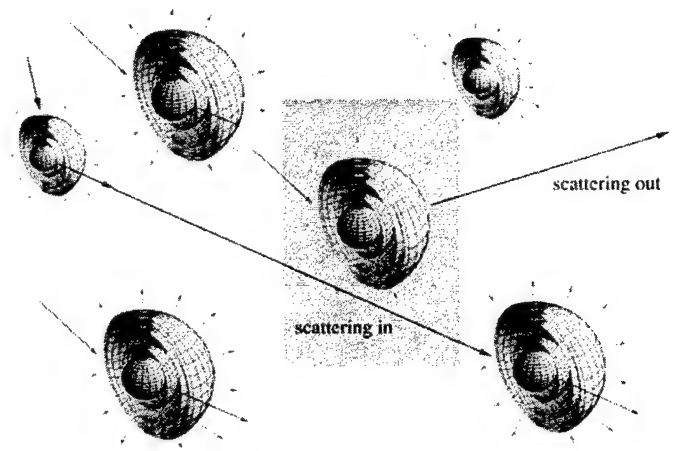

superposition of randomly selected output trajectories -> Boltzmann transport theory

© J R Barker 2001, University of Glasgow. This material is not to be reproduced, or published without permission

Dissipation may be shown to leads to crossings of quantum trajectories in the carrier space.

The trajectories in the full phase space do not cross.

Pure state, coherent

$$f(x,p;t) = n(x,t)\delta(p - \nabla S)$$

Pure state developing incoherence

f -> solution of a BTE-like transport eqn.

corresponds to evolution of mixed states

Comparison between finite temperature mixed state quantum hydrodynamics and pure state QHD (vortex free)

$$\frac{\partial(nP)}{\partial t} + \frac{\partial(nU)}{\partial x} + n\frac{\partial}{\partial x}(\varphi + \boxed{\frac{1}{3}V_Q}) = 0 \qquad U = mV^2 + \boxed{kT}$$

$$\frac{\partial(nP)}{\partial t} + \frac{\partial(nU_0)}{\partial x} + n\frac{\partial}{\partial x}(\varphi + V_Q) = 0 \qquad U_0 = mV^2$$

Paradox: Pure state is not zero temperature limit?

Recall the temperature tensor: the covariance matrix of the velocity

$$k\mathbf{T} = m < (\mathbf{v} - \mathbf{V})(\mathbf{v} - \mathbf{V}) >$$

Taking quantum mechanical averages this is just:

$$k\mathbf{T}_Q = m < \mathbf{vv} > - m < \mathbf{V} >< \mathbf{V}) >$$

$$NkT_Q = mV^2 + 2V_Q - mV^2 = 2V_Q$$

$$(N = 1,2,3)$$

Choosing N = 3 we get

$$\frac{\partial(nP)}{\partial t} + \frac{\partial(n[U_0 + kT_Q))}{\partial x} + n\frac{\partial}{\partial x}(\varphi + \frac{1}{3}V_Q) = 0$$

$$U = U_0 + kT_Q$$

which is essentially the finite temperature QHD result

A more detailed examination of the closure relations indicates further reconciliation of the two pictures although the finite temperature case involves coupling to a full hierarchy of moment equations.

Mixed states

For mixed states, existing quantum hydrodynamic and density gradient models are not complete.

If vortex formation may be ignored then empirical quantum potential Is the most pragmatic approach.

However, if coherent flow occurs with scattering off more than one obstacle we expect vortex flows and QHD and DD needs to be solved under the constraint of a generalised velocity circulation theorem By solving for nodal lines and computing the Vector quantum potential.

© J R Barker 2003, University of Glasgow. This material is not to be reproduced or published without permission

Application to MOS device modelling

At Glasgow, we have begun a systematic inclusion of quantum effects into finite MOSFET models at decanano dimensions.

The first level uses a phenomenological quantum potential model.

The effect is to keep charge away from interfaces and to induce some tunnelling effects.

© J R Barker 2003, University of Glasgow. This material is not to be reproduced or published without permission

Digitisation of the Si/SiO_2 interface topology

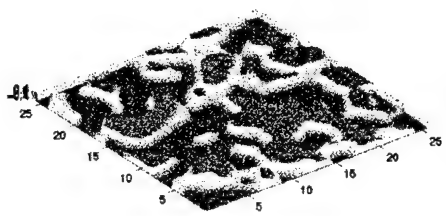

Gaussian power spectrum

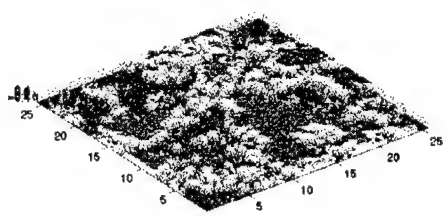

Exponential power spectrum

© J R Barker 2003, University of Glasgow. This material is not to be reproduced or published without permission

The fluctuation landscape admits flows which involve multiply-connected paths:

Possibility of
Diffraction, interference effects-> vortex flows
And meandering orbits.

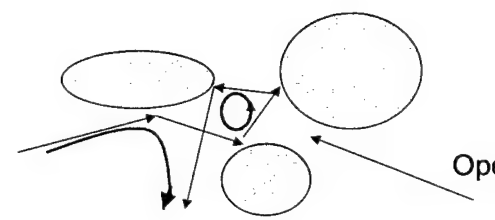

Open channels

Classical ---------->
Quantum ---------->

© J R Barker 2003, University of Glasgow. This material is not to be reproduced or published without permission

Conclusions

- Quantum flow formalism is close to spirit of drift diffusion and hydrodynamic models.
- Vortex motion is ubiquitous
- In the immediate future, density gradient QHD may be parameterised from deeper quantum simulations in analogy with using BTE to re-parameterise Drift Diffusion and HD models beyond their normal range of validity.

© UK Research Council, University of Glasgow. This material is not to be reproduced or published without permission.

Coulomb correlations in semiconductors and transient phenomena.
Nonequilibrium Greens functions and beyond

Michael Bonitz, Universität Rostock

Workshop „Quantum Transport in Semiconductors"

Maratea, June 17-22 2001

© Michael Bonitz, all rights reserved

Outline

1. Introduction: Coulomb correlations in semiconductors
2. Short-time phenomena and Initial correlations
3. Nonequilibrium Greens functions:
   - main ideas
   - application to optics and high field transport
4. Strong correlations in semiconductors:
   - excitons, biexcitons, electron-hole liquid
   - Wigner crystal
5. Summary and Outlook

In collaboration with

1. Dirk Semkat (Rostock), Nai Kwong, Sigurd Köhler, Rolf Binder (Tucson)
2. Antigoni Alexandrou (Paliseaou)
3. Hartmut Haug (Frankfurt), Ronald Redmer, Justino Madureira (Rostock)
4. Vladimir Filinov (Moscow), Stephan Koch, Walter Hoyer (Marburg)
5. Alexei Filinov, Yuri Lozovik (Moscow)

1. Introduction: Coulomb correlations in semiconductors

Coulomb correlations in semiconductors

Coulomb interaction between electrons / holes $U(r) = \pm e^2 / r$

Coupling strength: Ratio of Interaction energy/kinetic energy

$$\Gamma \equiv \langle U(r) \rangle / k_B T \qquad r_s \equiv \langle U \rangle / E_F \propto \langle r \rangle / a_B$$

E_F - Fermi energy $\quad a_B$ - exciton Bohr radius

Quantum degeneracy: $\chi \equiv n\lambda^d$ $\quad \lambda$ - electron quantum wave length, d - dimension

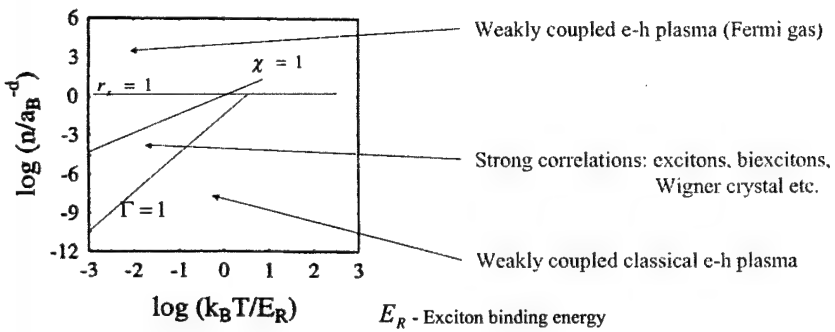

E_R - Exciton binding energy

Coulomb correlations in

$$\Gamma \equiv \langle U(r) \rangle / k_B T \qquad r_s \equiv \langle U \rangle / E_F \propto \langle r \rangle / a_B$$

$\chi \equiv n\lambda^3$ $\quad E_F$ - Fermi energy $\quad a_B$ - exciton Bohr radius

λ - electron quantum wave length

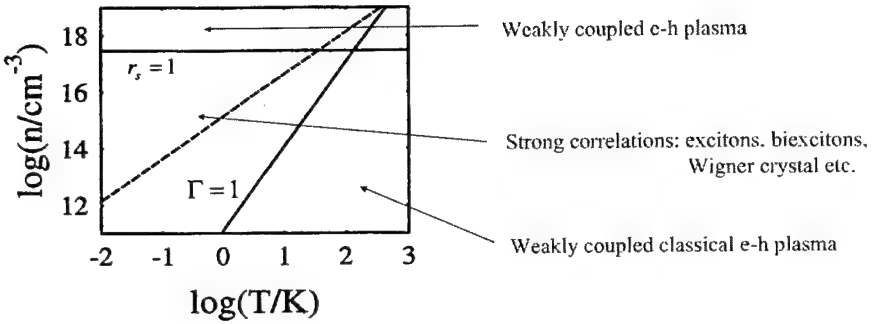

Statistical treatment of correlations

➡ Pair distribution function $g_{ab}(r)$; a,b – electrons, holes

= probability of finding particle a at distance r from particle b

Normalization: $\int g_{ab}(r)\,dV = 1$ $\qquad$ Interaction energy: $\langle U \rangle = \int U(r)\, g_{ab}(r)\,dV$

Non-interacting particles

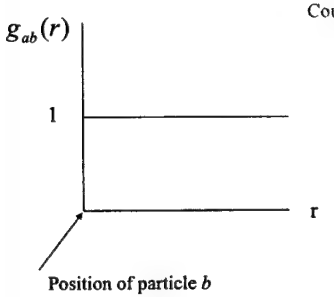

Interacting 2D e-h plasma

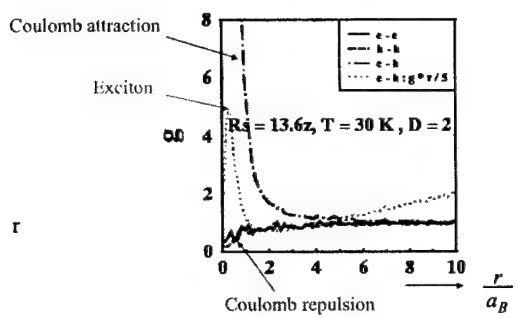

Pair correlation function: $c_{ab}(r) \equiv g_{ab}(r) - 1$

2. Short-time phenomena and initial correlations

Relaxation processes in electron-hole systems

Pre-excited e-h plasma (doping/prepulse, correlated contacts etc.) — *Initially correlated e-h ensemble* — $t = t_0$

↓

Excitation: e.g. optical or electric field — Finite duration — $\Delta\tau_{exc}$

↓

Creation of nonequilibrium electrons/holes — *Decay of initial correlations*, Correlation buildup — $t \le \tau_{cor}$

↓

Relaxation towards equilibrium/stationary state due to scattering processes (collisions) — Formation of stationary distribution $f^{EQ}{}_{e,h}$: $t \le t_{rel}$

$f^{EQ}{}_{e,h}$ – Fermi distribution or correlated Wigner function

$t_{rel} \sim 100\,fs \ldots 1\,ps$

$$\tau_{cor} \propto \frac{2\pi}{\omega_{pl}}; \frac{2\pi}{\omega_{ph}} \sim 20 \ldots 100\,fs$$

Example: buildup of Coulomb correlations/screening
e-h pairs created uncorrelated

$$\tau_{cor} \sim r_D / v_{th} \propto 2\pi / \omega_{pl}$$

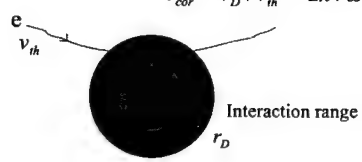

When are initial correlations important?

➡ *Transient processes before stationary state*

1. Short times: $t_0 \le t \le \tau_{corr}$ (Or high-frequency switching: $\omega_s \ge 2\pi / \tau_{cor}$)

2. Strongly correlated initial state: $|\langle U_{corr}\rangle|(t_0) \ge \langle E_{kin}\rangle(t_0)$
   - materials with strong electron-phonon coupling
   - materials with strong Coulomb interaction

   In this case also: $\tau_{corr} \ge t_{rel}$

3. „bottel neck" situations, threshold processes:
   - carrier excitation below phonon energy, impact ionization etc.
   - modified plasmon spectrum in p-doped semiconductors

4. Long-living initial correlations: e.g. bound states (excitons, impurities etc.), Wigner crystal, Bose condensate etc.
   - weak damping (slow decay) of initial correlations

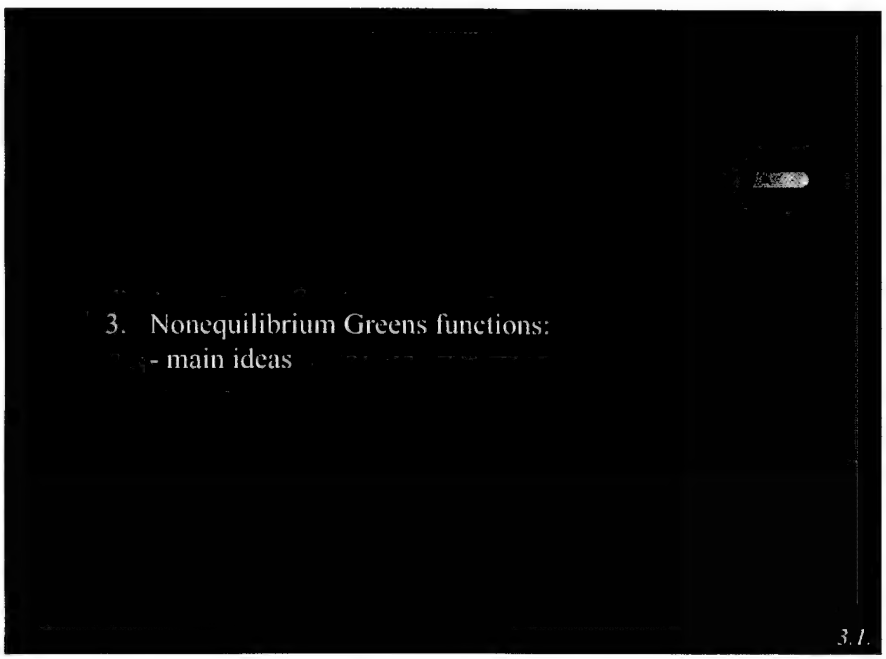

Idea of Green's functions

1. Classical N-body system: statistical properties given by distribution function $f(r,p,t)$

$$\int \frac{d^3p}{(2\pi h)^3} f(r,p,t) = n(r,t), \quad \int d^3r\, n(r,t) = N(t)$$

2. Quantum N-body system:
   - Wigner („quasi")-distribution function $f(r,p,t)$
   - Wave properties, energy „spectrum" *A(E)*

Idea: combine into „generalized distribution" $g(r,p,t;E)$ — E- independent variable

⟶ Green's function

Equilibrium: $g(p;E) = if(E)A(p,E), \quad f(E) = 1/(e^{\beta(E-\mu)}+1)$

- non-interacting particles: $A(p,E) = 2\pi\,\delta(E - p^2/2m)$
- interacting (correlated) particles: $A(p,E) \propto \dfrac{\gamma/2}{(E - p^2/2m + \Delta)^2 + \gamma^2}$

  Correlated Wigner distribution *g(p)*

  Finite line width (finite life time), related to pair correlations *c(r)*

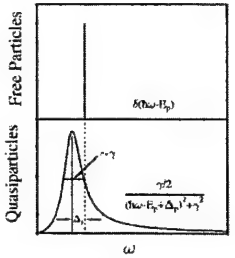

⟶ Correlations included into single-particle properties (quasi-particle)

Nonequilibrium Green's functions

$g(r,p,t;E)$ Equivalent to function of *two-times*:

I. Fourier transform: $\int dE\, g(r,p,t;E)\, e^{iE\tau/\hbar} \rightarrow g(r,p,t,\tau)$

II. Define $t_{1,2} = t \pm \tau/2 \rightarrow g(r,p,t_1,t_2)$

III. Build in spin: relate g to fermion field operators: $\psi^+(r,t),\ \psi(r,t)$

Anticommutation: $\psi^+(r_1,t)\psi(r_2,t) + \psi(r_2,t)\psi^+(r_1,t) = \delta(r_1 - r_2)$

IV. Two-operator averages – two possibilities: (two independent functions)

$\langle\psi^+(2)\psi(1)\rangle \rightarrow g^<(1,2);\quad 1 \equiv r_1, t_1, s_1$

$\langle\psi(1)\psi^+(2)\rangle \rightarrow g^>(1,2)$

V. Physical contents: *on time diagonal*: $g^<(r_1,t,r_2,t) \propto f(r_1,r_2,t)$ Density matrix, Wigner distribution etc.

Across diagonal: $g^>(1,2) - g^<(1,2) \propto A(1,2)$ Spectral function, Density of states etc.

VI. Heisenberg equations for ψ^+, ψ ➡ (Kadanoff-Baym/Keldysh) equations of motion for $g^>, g^<$

➡ Fully selfconsistent treatment of relaxation, correlations and energy spectrum

➡ Clear recipe for treatment of complex processes and systematic approximations

Spectral function of interacting electrons

E_p - Kinetic (quasiparticle) energy

γ, Δ_p imaginary and real part of selfenergy

Exponential damping Lorentzian power-law tail, wrong at large frequency!

Solution of the two-time Kadanoff-Baym equations. Zero slope at tau=0!

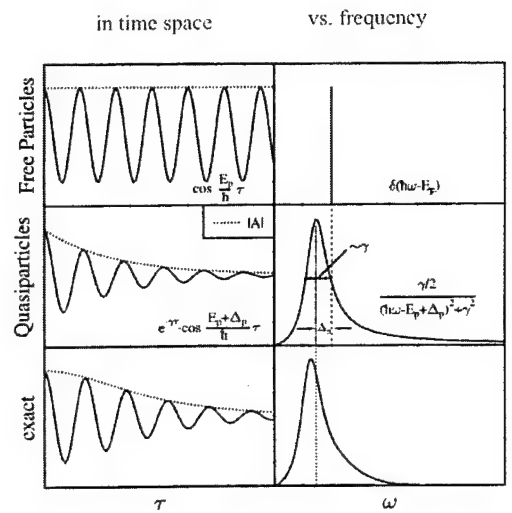

Direct Solution of the Kadanoff-Baym equations

Imaginary part of $g^<(k,t_1,t_2)$ for fixed momentum k

1. Relaxation of nonequilibrium electron distribution (peaked at k=3.9/ao)
2. Build up of electron spectrum (of Coulomb correlations) across time diagonal

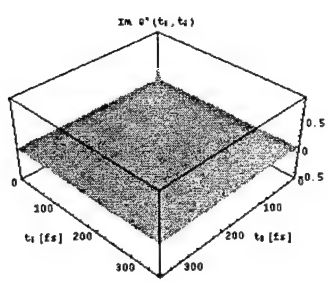

k=2.7/ao

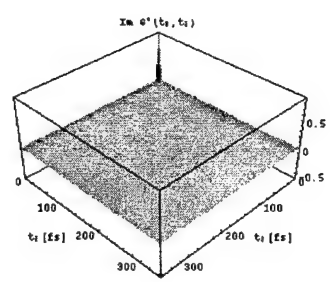

k=3.9/ao

Homogeneous bulk GaAs $n = 10^{17}\,cm^{-3}$

Dirk Semkat/Michael Bonitz

Exact spectral function with Coulomb scattering

$$A(t,t') = i\hbar[g^>(t,t') - g^<(t,t')]$$

Spektralfunktion

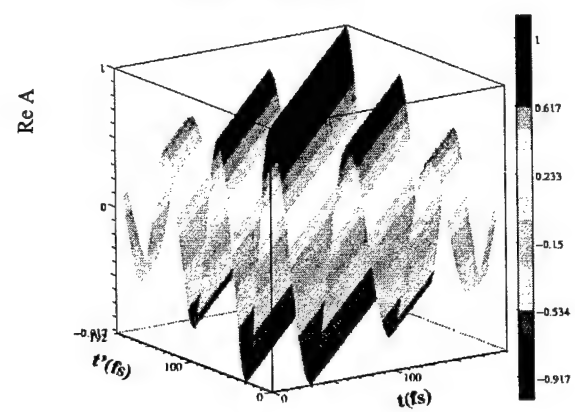

Semkat/Kwong/Köhler/Binder/MB

Kadanoff-Baym equations with initial correlations

N-particle system, binary interaction V(r), external potential U(r)

Nonequilibrium: Greens functions on time contour C *(Keldysh, Schwinger)*

G. Baym [*]

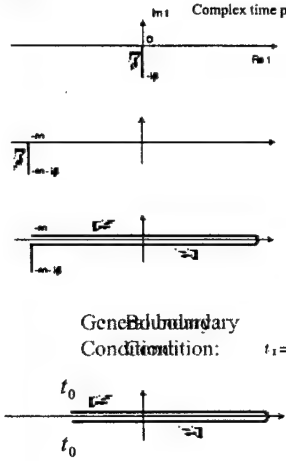

$$g_{1\ldots s}(1\ldots s,1'\ldots s') = \left(\frac{1}{i}\right)^s \langle T_{\mathcal{C}}\left[\Psi(1)\ldots\Psi(s)\Psi^+(s')\ldots\Psi^+(1')\right]\rangle$$

Equation of motion for $g_1(t_1,t_1')$: *(Martin/Schwinger)*

$$\int_{\mathcal{C}} d\bar{1}\left\{g_1^{0^{-1}}(1,\bar{1}) - U(1,\bar{1})\right\} g_1(\bar{1},1';U) = \delta(1-1') \pm i\int d2\, V(1-2) g_{12}(12,1'2^+)$$

with $$g_1^{0^{-1}}(1,1') = \left(i\frac{\partial}{\partial t_1} + \frac{\nabla_1^2}{2m}\right)\delta(1-1')$$

Generalized Boundary Condition:

$$\lim_{t_1=t_0\to-\infty} g_{12}(12,1'2')|_{t_0} = [g_1(1,1')g_1(2,2') \pm g_1(1,2')g_1(2,1')]|_{t_0} + c(\mathbf{r}_1\mathbf{r}_2,\mathbf{r}_1'\mathbf{r}_2';t_0)$$

Correlated initial state: e.g. Fujita, Hill, Danielewicz, Wagner

* *In: „Progress in Nonequilibrium Green's functions", M. Bonitz (Ed.), 2000*

Semkat, Kremp, Bonitz 1999, 2000

Haug/Jauho „Quantum Kinetics...."

Kadanoff-Baym equations with initial correlations, contd.

Formal closure of hierarchy (generalized*): introduce selfenergy

$$\int_{\mathcal{C}} d\bar{1}\,\Sigma(1,\bar{1})g_1(\bar{1},1') = \pm i\int d2\, V(1-2) g_{12}(12,1'2^+)$$
$$= \pm i\int d2\, V(1-2)\left\{\pm\frac{\delta g_1(1,1';U)}{\delta U(2^+,2)} + g_1(1,1')g_1(2,2^+)\right\}$$

Boundary condition:

$$\lim_{t_1=t_1'\to t_0}\int_{\mathcal{C}} d\bar{1}\,\Sigma(1,\bar{1})g_1(\bar{1},1') = \pm i\int d\mathbf{r}_2\, V(\mathbf{r}_1-\mathbf{r}_2)\,[c(\mathbf{r}_1\mathbf{r}_2,\mathbf{r}_1',\mathbf{r}_2';t_0)$$
$$+ g_1(\mathbf{r}_1\mathbf{r}_1',t_0)g_1(\mathbf{r}_2\mathbf{r}_2',t_0) \pm g_1(\mathbf{r}_1\mathbf{r}_2',t_0)g_1(\mathbf{r}_2\mathbf{r}_1',t_0)]$$

Binary correlations at t=to

Result: additional selfenergy contribution

$$\Sigma(1,1') = \Sigma^{HF}(1,1') + \Sigma^c(1,1') + \Sigma^{in}(1,1')$$
$$\Sigma^{in}(1,1') = \Sigma^{in}(1,\mathbf{r}_1't_0)\delta(t_1'-t_0)$$

*Semkat, Kremp, MB, J. Math. Phys., **41**, 7458 (2000)

Generalized Kadanoff-Baym equations

Result:

$$\int_{\mathcal{C}} d\bar{1}\left[g_1^{0^{-1}}(1\bar{1}) - U(1\bar{1}) - \Sigma^{HF}(1\bar{1})\right] g_1(\bar{1}1')$$
$$= \delta(1-1') + \int_{\mathcal{C}} d\bar{1}\left[\Sigma^c(1\bar{1}) + \Sigma^{in}(1\bar{1})\right] g_1(\bar{1}1')$$

Matrix equations on the time contour

Result on the physical (real) time axis:

$$\left(i\frac{\partial}{\partial t_1} + \frac{\nabla_1^2}{2m}\right) g_1^{\gtrless}(11') - \int d\bar{1}\, U(1\bar{1}) g_1^{\gtrless}(\bar{1}1') - \int d\bar{r}_1\, \Sigma^{HF}(1\bar{1}) g_1^{\gtrless}(\bar{1}1')$$
$$= \int_{t_0}^{\infty} d\bar{1}\, \Sigma^R(1\bar{1}) g_1^{\gtrless}(\bar{1}1') + \int_{t_0}^{\infty} d\bar{1}\left[\Sigma^{\gtrless}(1\bar{1}) + \Sigma^{in}(1\bar{1})\right] g_1^A(\bar{1}1')$$

Result for selfenergy:

$$\Sigma^{in}(11') = \pm i\int d2\, V(1-2)\int d\bar{r}_1 d\bar{r}_2 d\bar{\bar{r}}_1 d\bar{\bar{r}}_2$$
$$\times\, g_{12}^R(12,\bar{r}_1t_0,\bar{r}_2t_0)c(\bar{r}_1t_0,\bar{r}_2t_0,1',\bar{\bar{r}}_2t_0)g_1^A(\bar{\bar{r}}_2t_0,2^+)\delta(t_1'-t_0).$$

➡ Selfconsistent evolution and decay of initial correlations

Short-time relaxation with initial correlations

Solution of KB-equations with initial correlation selfenergy

Example: bulk GaAs, *uncorrelated* vs. over-correlated initial state

- **Correct conservation** of total energy (kinetic + correlation)
- Energy relaxation reflects correlation build up/decay for $t \le \tau_{cor}$

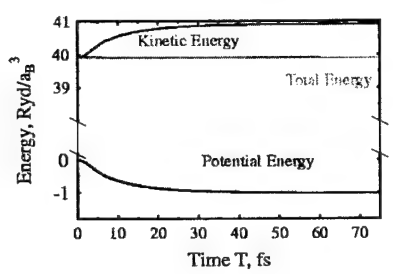

$n = 2.77a_B^{-3}$ (weak coupling)

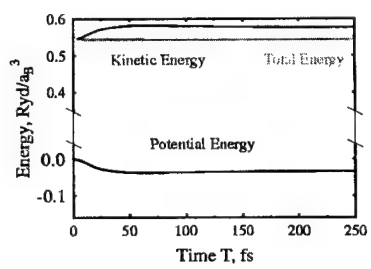

$n = 0.277a_B^{-3}$ (intermediate coupling)

Dynamic Structure factor of interacting electrons

Solution of inhomogeneous Kadanoff-Baym Equations

Start from correlated initial state

At t=0 monochromatic perturbation

Density fluctuation

(Landau plus collisional damping)

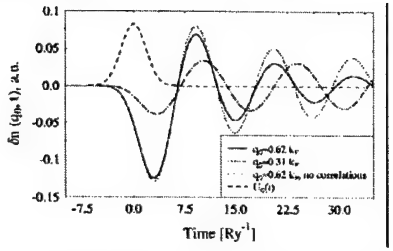

Selfconsistent dynamic Structure factor with Correlations (Born approximation plus vertex corrections)

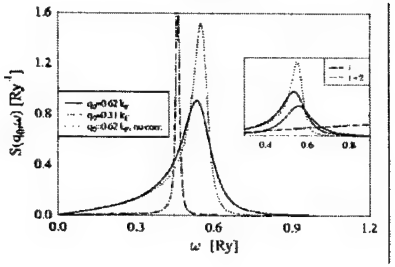

Kwong, Bonitz, Phys. Rev. Lett. 84, 1768 (2000)

3. Nonequilibrium Greens functions:

- application to optics and high field transport

3.2.

Electron dynamics in semiconductors

Example: Optical Excitation

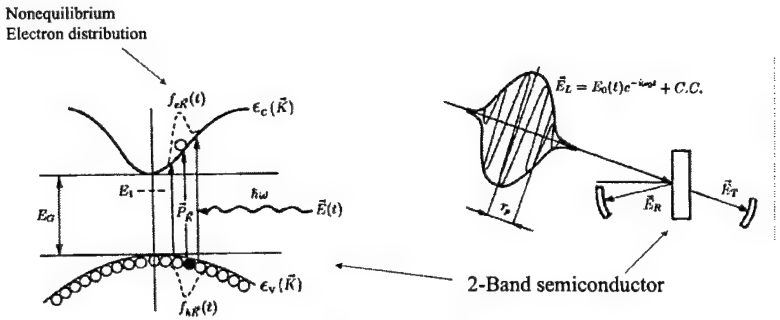

Laserpuls excitation

Evolution of electron and hole distributions $f_e(p,t)$, $f_h(p,t)$

Time evolution of energy spectrum $E_c(p,t)$, $E_v(p,t)$

Effective E/B-field in the semiconductor (Maxwell's equations)

Interband-Kadanoff-Baym equations

μ_1, μ_2 – Band indices, $E_\mu(p)$ – Semiconductor band structure

$$\left\{i\hbar\frac{\partial}{\partial t_1} - \epsilon_{\mu_1}\right\} g^{\gtrless}_{\mu_1\mu_2}(t_1t_2) - \sum_{\bar\mu} \hbar\Omega_{\mu_1\bar\mu}(t_1) g^{\gtrless}_{\bar\mu\mu_2}(t_1t_2) = I^{\gtrless}_{\mu_1\mu_2}(t_1t_2)$$

$$\left\{-i\hbar\frac{\partial}{\partial t_2} - \epsilon_{\mu_2}\right\} g^{\gtrless}_{\mu_1\mu_2}(t_1t_2) - \sum_{\bar\mu} g^{\gtrless}_{\mu_1\bar\mu}(t_1t_2)\hbar\Omega_{\bar\mu\mu_2}(t_2) = -I^{\gtrless}_{\mu_2\mu_1}(t_2t_1)$$

$$\hbar\Omega_{\mu_1\mu_2}(t) = -\mathbf{d}_{\mu_1\mu_2}\mathcal{E}(t)(1-\delta_{\mu_1\mu_2}) + i\hbar\sum_{k'} g^{<}_{\mu_1\mu_2}(k't t)V_{\mu_1\mu_2}(k-k')$$

Dipole moment Laser field Hartree-Fock mean field

Correlations (collisions)

(with phonons, electrons, defects etc.)

$$I^{\gtrless}_{\mu_1\mu_2}(t_1t_2) = \sum_{\bar\mu}\int_{t_0}^{t_1} d\bar t\,[\sigma^{>}_{\mu_1\bar\mu}(t_1\bar t) - \sigma^{<}_{\mu_1\bar\mu}(t_1\bar t)]\, g^{\gtrless}_{\mu_1\bar\mu}(\bar t t_2)$$

$$-\sum_{\bar\mu}\int_{t_0}^{t_2} d\bar t\,\sigma^{\gtrless}_{\mu_1\bar\mu}(t_1\bar t)\,[g^{>}_{\mu_1\bar\mu}(\bar t t_2) - g^{<}_{\mu_1\bar\mu}(\bar t t_2)]$$

σ – self energies

Kwong, Bonitz, Binder, Köhler, phys. stat. sol. (b) **206**, 197 (1998)

Laser pulse excitation of a s.c. quantum well

50fs-laser pulse

Electron density

Interband-Polarization

Kinetic energy

Correlation energy

Hartree-Fock energy
(mean field, coherent excitons)

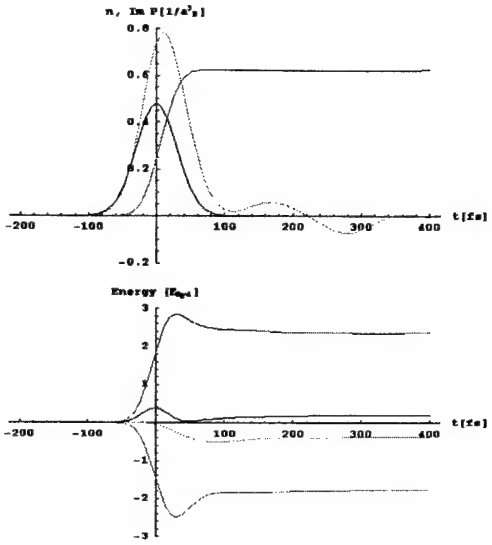

Electron dynamics in a semiconductor

Laser „lifts“ Electrons from valence band to conduction band

(50fs-Pulse, Maximum at t=0)

Valence band, v

Conduction band, c

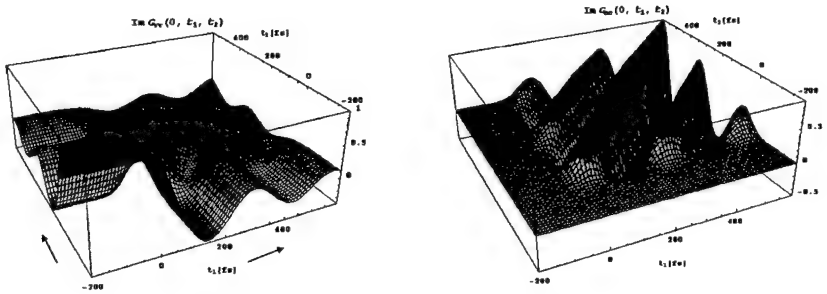

Information in the Green‘s functions:

Electron Wigner distribution f
(along time diagonal)

Electron spectrum
(across diagonal)

Damping of the Electrons and Renormalization of the energy bands

Valence band, v

Conduction band, c

Momentum k=0

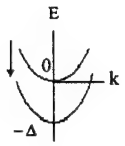

k=2/a_B

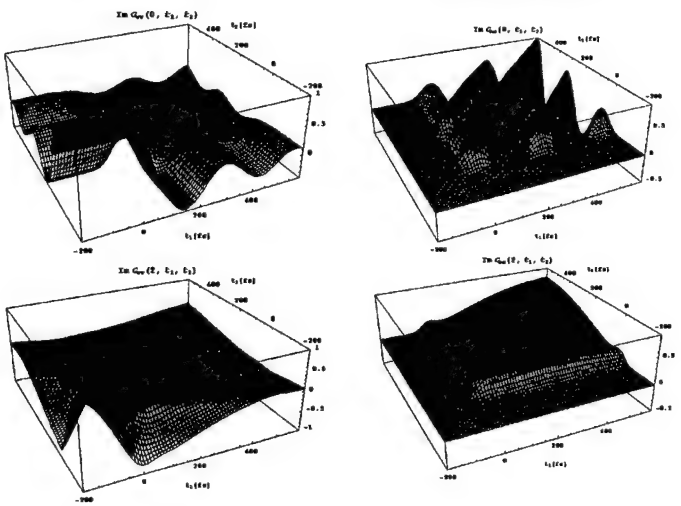

Relaxation in the presence of preexcited electrons/holes

Bulk GaAs

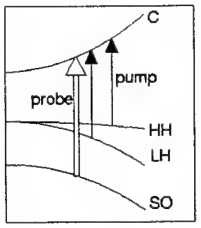

Drastically accelerated thermalization
In the presence of prepump or p-doping

Reason: pre-existing carriers
qualitatively modify plasmon
spectrum and e-e/e-h scattering rates
-> *Pre-existing Coulomb correlations*

Lampin, Alexandrou et al. 1999, Bonitz et al. PRB **62**, *15724 (2000)*

Differential absorption spectra

T=15K

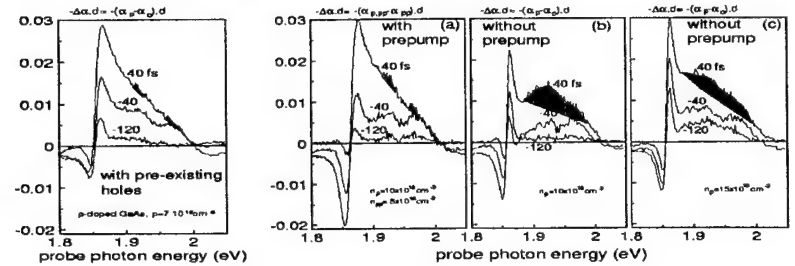

Impact Ionization rates in semiconductors

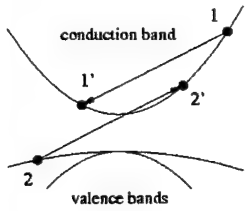

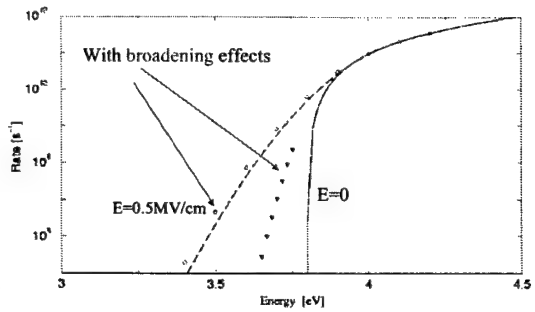

Account for correlation effects (collisional broadening):

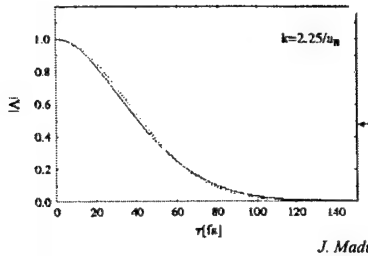

ZnS: $T = 300K$, $n = 10^{17}\ cm^{-3}$

Damped spectral function from solution of the Kadanoff-Baym equations (full line)

Dots: analytical fit $|A(\tau)| = 1/\cosh^{\alpha} \omega_{pl}\tau$

(M. Bonitz, D. Semkat and H. Haug, Europ.J.Phys.B 9, 309(1999)

J. Madureira, D. Semkat, M. Bonitz., R. Redmer, J. Appl. Phys. **90**, *829 (2001)*

4. Strong correlations in semiconductors:
   - excitons, e-h liquid

4.1.

Strong Coulomb correlations

$\Gamma \equiv \langle U \rangle / k_B T$ $\qquad r_s \equiv \langle U \rangle / E_F \propto \langle r \rangle / a_B$

E_F - Fermi energy $\qquad a_B$ - exciton Bohr radius

Expected behavior:

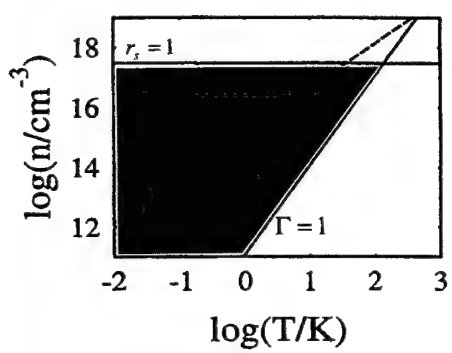

$r_s << 1$ Fermi gas

$r_s \sim 1$ Fermi liquid, Electron-hole liquid

$r_s > 1$ Excitons, biexcitons

$r_s \geq 37$ Electron Wigner crystal

Non-perturbative theories needed

- Greens functions: ladder diagrams
- Path integral Monte Carlo
- Quantum Molecular Dynamics

Greens functions treatment of Strong Coulomb correlations

Problem: strong Coulomb correlations, bound states, exciton formation etc. not possible in Born approximation

→ Need selfenergies in T-matrix (ladder) approximation
Electron spectrum: continuum and bound states

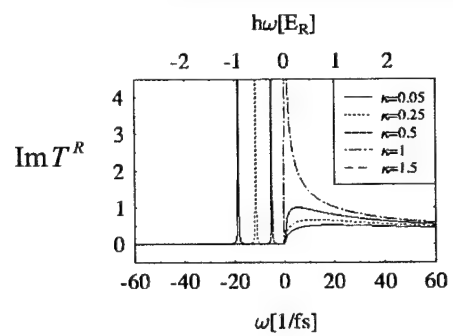

Bound state (peak) modified by surrounding e-h-plasma (Mott Effekt)

Screening parameter $\kappa = 4\pi n e^2 / kT$

Semkat, Bonitz, Kremp (2001)

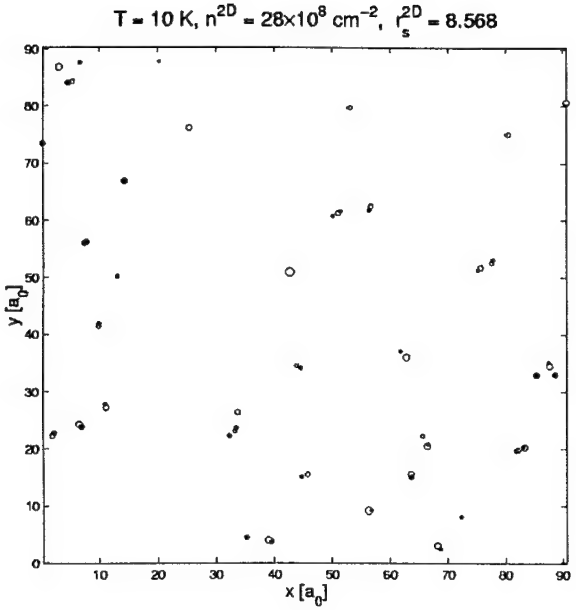

Rigorous Path integral
Monte Carlo simulations

Start with electrons and holes,
Full inclusion of
- Coulomb interaction
- Quantum effects
- Spin

Dots: [illegible] and hole
Location (wave function
squared) in quantum well

V. Filinov, W. Hoyer,
S.W. Koch, and M. Bonitz 2001

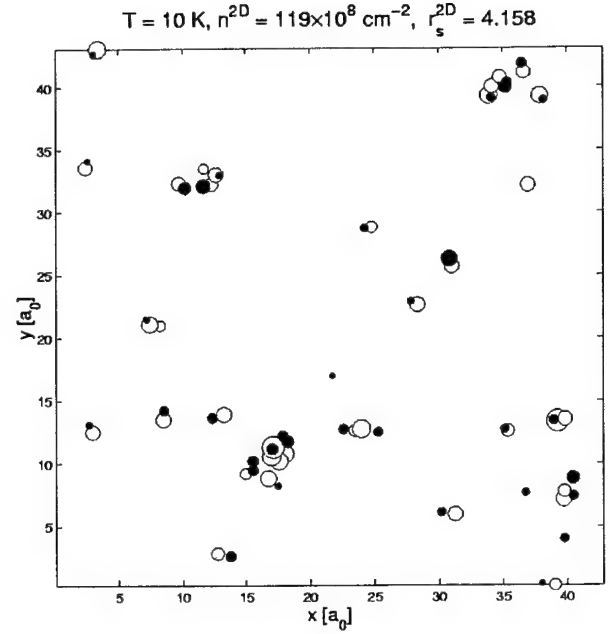

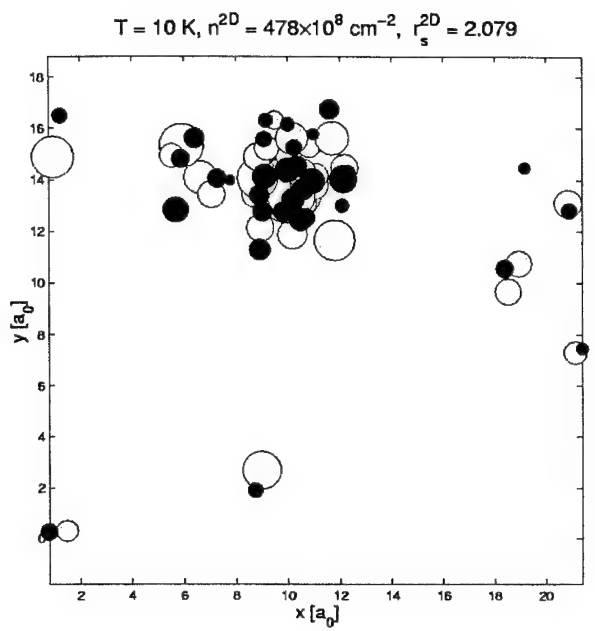

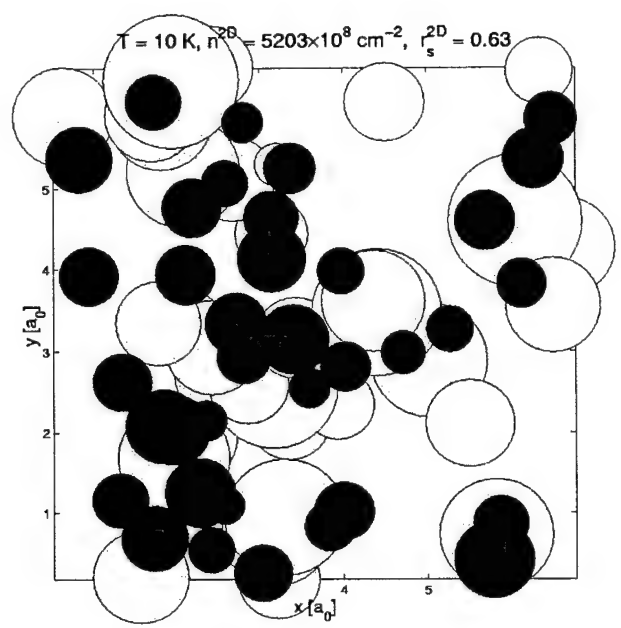

4. Strong correlations in semiconductors:

- Wigner crystal

4.2.

Mesoscopic electron clusters

Easy realization of strong correlations
Question: possibility of Wigner crystallization?
Is there a metal-insulator transition?

Problem: simultaneous account of correlations, quantum and spin effects
many-body approaches (including NGF) not applicable
⟶ Path integral Monte Carlo

Model: 2D electron clusters
in spherical trap, N=1...100
T=const, B=0

Results: - Shell structure,
- pronounced symmetry effects
- Strong N-dependence

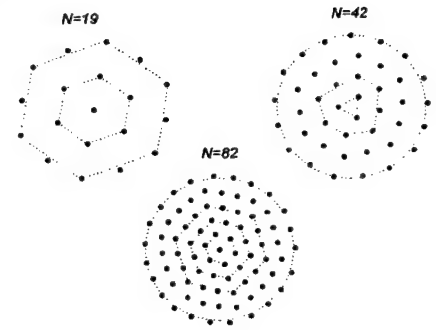

Wigner crystallization of electron clusters

Variation of temperature or density (confinement)

Existence of two crystal phases: *intra*-shell and *inter*-shell ordering

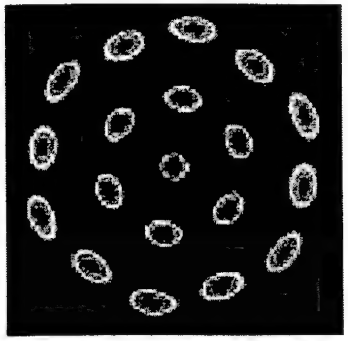

A. Filinov, M. Bonitz, and Yu. Lozovik, Phys. Rev. Lett. **86**, 3851 (2001)

Phase diagram of the mesoscopic Wigner crystal

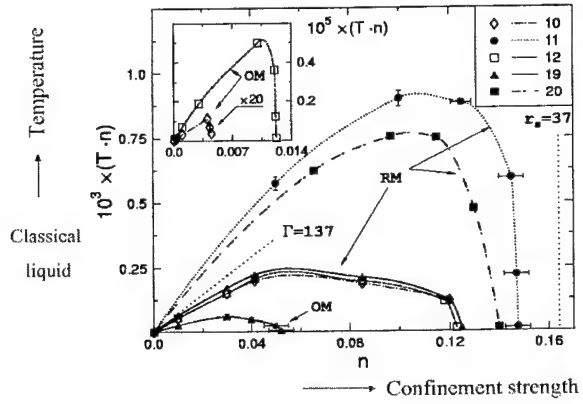

⟶ See poster !

Quantum liquid
(Wigner molecule)

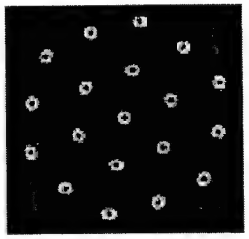

RM - Radial melting, OM – Orientational melting

Crystal melting and mobility increase

At the melting point: drastic increase of angular and radial distance fluctuations

→ Mobility and conductivity increase

Relative distance fluctuations

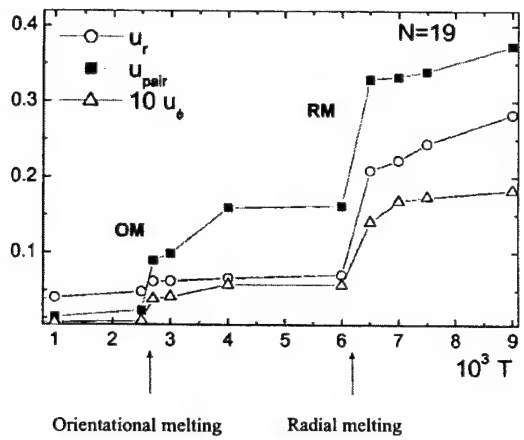

Summary and Outlook

I. Nonequilibrium Greens functions powerful tool
- extended to arbitrary initial correlations
- well applicable to ultrafast/transient phenomena
- useful for high field transport

II. Strong correlations in semiconductors
- excitons, droplets, Wigner crystal
- quantum Monte Carlo and molecular dynamics

III. Future: combination of NGF and quantum simulations

References

1. Quantum kinetic theory with density operators and Greens functions, see M. Bonitz „Quantum Kinetic Theory", B.G. Teubner, Stuttgart/Leipzig 1998
2. An overview (review articles) on Kadanoff-Baym equations can be found in „Progress in Nonequilibrium Greens Functions", M. Bonitz (ed.), World Scientific, Singapore 2000
3. Kadanoff-Baym equations with initial correlations: see D. Semkat, D. Kremp, and M. Bonitz, J. Math. Phys. **41**, 7458 (2000) and references therein
4. Greens functions applications to high-field transport, see e.g. Madureira, Semkat, Bonitz, Redmer, JAP 90, 829 (2001)
5. Greens functions applications to semiconductor optics, see e.g. Kwong, Bonitz, Binder, Köhler, phys.stat.sol. (b) **206**, 197 (1998)
6. Fermionic path integral Monte Carlo (bound state formation etc.): see V.S. Filinov, M. Bonitz, W. Ebeling, and V.E. Fortov, Plasma Phys. Contr. Fusion **43**, 743 (2001) and references therein
7. Wigner crystallization in mesoscopic electron clusters (open quantum dots): A. Filinov, M. Bonitz, and Yu. Lozovik, Phys. Rev. Lett. **86**, 3851(2001); Physical Review Focus April 19 (2001)

For updated references, please look at http://ehle.mpg.uni-rostock.de/mb

Gunther Bauer, University of Linz, "The metal-insulator transition in d=2"

Content

- Motivation
  - The observation of the 'metal-insulator transition' in 2D
- Scaling theory of localization
  - Scaling Function and phase coherence length
  - Importance electron-electron interaction
- Experiments
  - Measurement technique and Si-MOSFET devices
  - Standard transport measurements with and without magnetic field
- Weak localization
  - The role of quantum interference on the MIT
- The trap model
  - The capability and the limits
- Conclusions

Motivation

The observation of the 'metal-insulator transition' in 2D

Temperature dependence of the resistivity

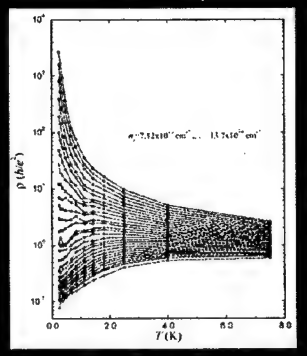

Resistivity vs T/T_0

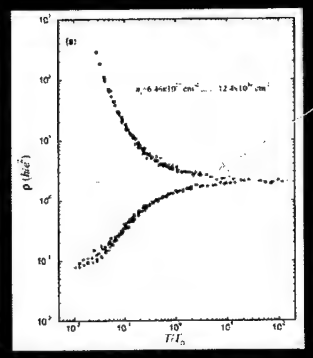

mirror-reflection symmetry

Scaling parameter T_0

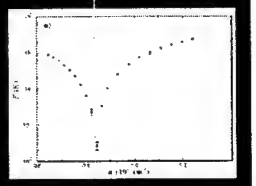

Kravchenko, Pudalov et al. PRB51 (1995)

Motivation

Suppression of the conducting phase by a parallel magnetic field

Resistivity vs parallel magnetic field

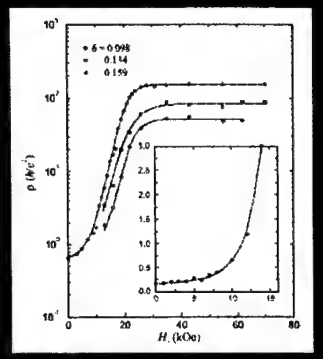

Temperature dependence of the resistivity in a parallel magnetic field

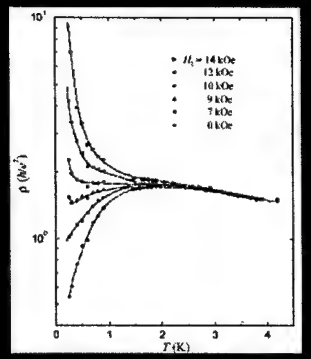

Simonian et al., PRL79, 2304 (1997)

Scaling function β(g)

for non-interacting electrons and for T=0K

$$\beta(g) = \frac{d\ln g}{d\ln L} = \frac{L}{g}\frac{dg}{dL}$$

g ... conductance in e^2/h,
L ... system size

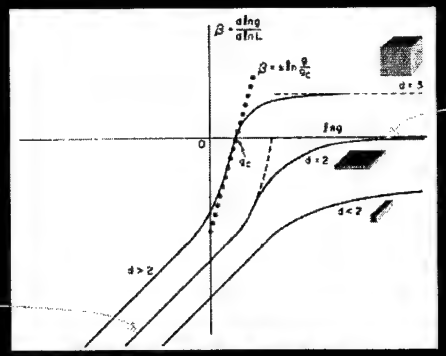

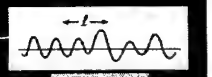

$g(L) = \sigma L^{d-2}$

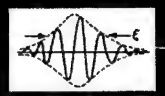

$g(L) \propto \exp(-L/\xi)$

Fig.1, PRL 42, 673 (1979)

Importance Electron-Electron Interaction

Coulomb energy versus Fermi energy:

$$r_s = \frac{E_{Coul}}{E_F} \propto \frac{1}{r} \propto \frac{\sqrt{n_{sp}}}{n_{sp}} \propto \frac{m^*}{\varepsilon_r} \frac{1}{\sqrt{n_{sp}}}$$

Material	m^*	ε_r	n (10^{11} cm^{-2})
n-Si-MOS	0.19	7.8	6.7
p-SiGe/Si	0.3	12.6	6.4
n-Si/SiGe	019	11.7	3.0
p-GaAs/AlGaAs	0.32	10.9	9.8
n-GaAs/AlGaAs	0.067	10.9	0.43

Possible explanations for the phenomenon

Failure of the quasi-particle picture of Landau due to EEI

⬇

new groundstate: Non-Fermi liquid

⬇

Superconductivity

or just a 'classical' effect ?

Transport measurements in zero B-field

Temperature dependence of the resistivity

Comparison of different samples

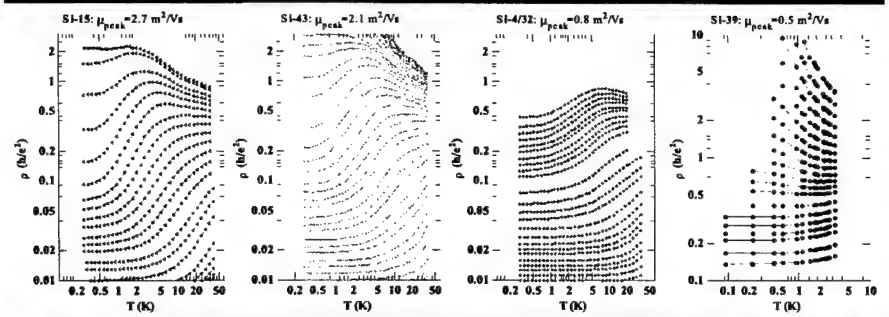

The exponential drop increases with the peak mobility !

Weak Localization

Overview

Quantum mechanical interference enhances back scattering

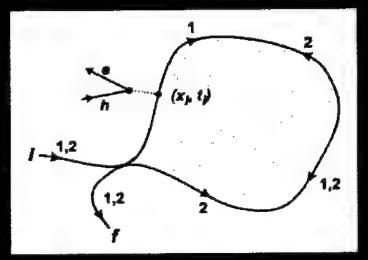

2 features of weak localization are important :

(1) logarithmic temperature dependence of the conductivity

(2) negative magnetoresistance

Weak Localization
electron density regime ($n>10^{12}$ cm^{-2})

Phase coherence time & momentum relaxation time vs T

Si-43

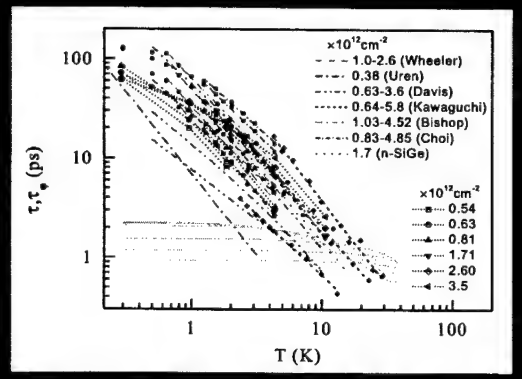

Weak Localization
Low electron density regime ($n<10^{12}$ cm^{-2})

Magnetoresistivity for $n=0.37\times10^{12}$ cm^{-2}

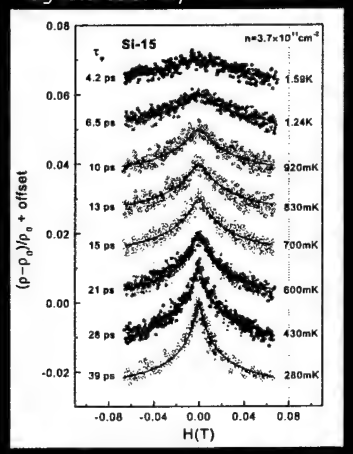

Temperature dependence of resistivity for $n=0.37\times10^{12}$ cm^{-2}

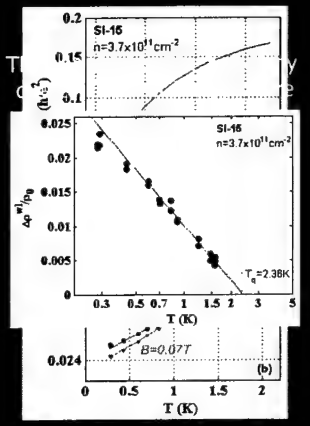

Weak Localization
Low electron density regime ($n<10^{12}$ cm^{-2})

Temperature dependence of the phase coherence time

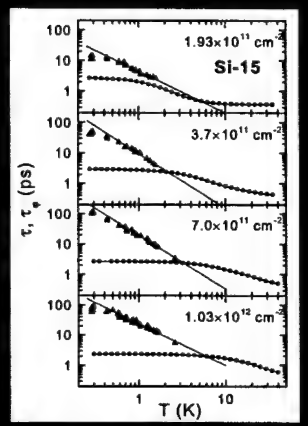

Single particle interference cease to effect resistivity for $\tau_\varphi<\tau$

Weak Localization
Result of the weak localization analysis

Temperature dependence of resistivity with 'critical' borders

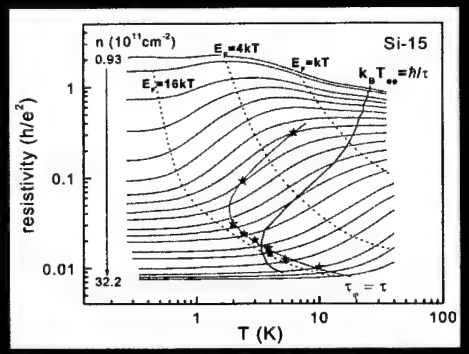

red curve ... disappearance of the weak localization
... border for the EEI

Trap Model after B.L. Altshuler and D.L. Maslow

Overview

Assumptions:

- traps are distributed homogenously in the oxide
- all the traps have the same energy ε_t
- traps are due to weak Si-Si bonds (occupied by $1e^-$ or $2e^-$)
- traps can be easily charged and discharged

Charge state of the trap depends on the Fermi energy of the 2D electron gas

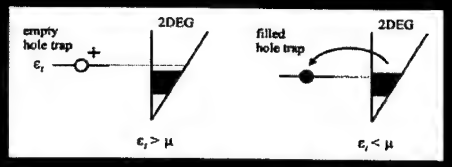

Trap Model

The effect of the magnetic field

Splitting of the trap energy levels in a magnetic field

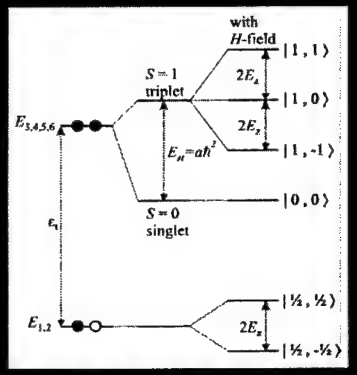

Conclusions

- The experimentally determined **phase coherence time** is about 10 smaller than theoretically predicted, but is in agreement with prior works on low-mobility samples
- From analysis of the weak localization, **quantum interference** can be excluded as an origin for the metallic state and the MIT
- There is no indication of a non-Fermi liquid in the metallic regime → **no quantum phase**
- The trap model can explain qualitatively certain feature of the MIT, but fails to give quantitative results

The "Metal-Insulator Transition" in Open Quantum Dots & Dot Arrays

Jonathan P. Bird
Department of Electrical Engineering &
Center for Solid State Electronics Research
Arizona State University
Tempe, AZ 85287-5706

S4700 15.0kV 12.3mm x11.0k SE(U) 5/31/00 15:31 5.00um

This Research is the result of a joint collaboration with:

A. S. S. - Aoki - Chiba University

M. Elhassan - ASU L. H. Lin - Chiba University

D. K. Ferry - ASU Y. Ochiai - Chiba University

C. Prasad - ASU Y. Aoyagi - RIKEN

A. Stallos - ASU K. Ishibashi - RIKEN

L. Shifren - ASU

Work at ASU is Supported By:

Office of Naval Research

National Science Foundation

OUTLINE

- INTRODUCTION
- TRANSPORT IN QUANTUM DOTS
- DEVICE FABRICATION & BASIC CHARACTERIZATION
- EXPERIMENTAL RESULTS
- CONCLUSIONS

- The study of the transport properties of LOW-DIMENSIONAL systems has lead to the discovery of a number of novel MANY-BODY effects in recent years

  * Striking examples include the recent discovery of COMPOSITE FERMIONS in the fractional quantum-Hall effect and the METAL-INSULATOR TRANSITION in two dimensions

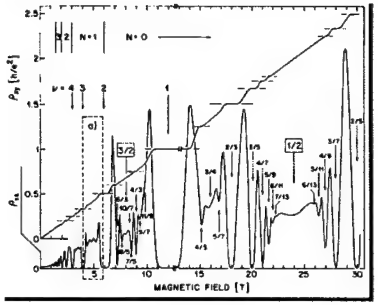

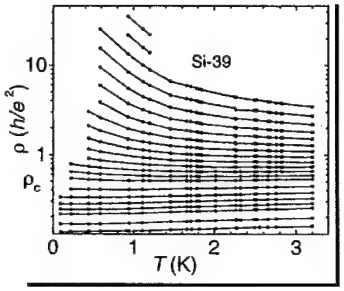

R. Willet *et al.*
Phys. Rev. Lett. 59, 1776 (1987)

V. M. Pudalov *et al.*
Physica E 3, 79 (1998)

- In mesoscopic QUANTUM DOTS electron interactions are known to play an important role when the dots are coupled to their reservoirs by means of weakly transmitting TUNNEL BARRIERS

  * In this regime the COULOMB BLOCKADE of transport gives rise to SINGLE-ELECTRON behavior which can be used to demonstrate SHELL-LIKE filling of electron states

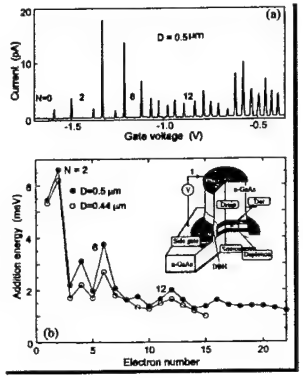

S. Tarucha *et al.*
Phys. Rev. Lett. 77, 3613 (1996)

- When the dots are coupled to their external reservoirs by means of WEAK tunnel barriers many-body effects have been argued to give rise to KONDO-LIKE behavior

  * Here electrons confined WITHIN the dot play the role of the magnetic impurity in the more conventional Kondo effect

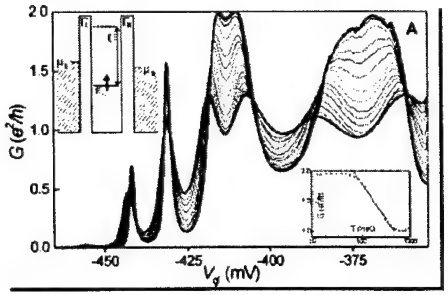

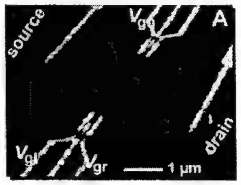

D. Goldhaber-Gordon *et al.*
Nature 391, 156 (1998)
J. Schmid *et al.*
Phys. Rev. Lett. 84, 5824 (2000)
W. G. van der Wiel
Science 289, 2105 (2000)

- In contrast to these studies our interest will lie in a discussion of transport in OPEN quantum dots

  * These dots are coupled to their external reservoirs by means of quantum-point-contact LEADS that are configured to support a SMALL number of PROPAGATING modes

  * Since transport through these structures is typically BALLISTIC in nature their electrical properties strongly reflect the details of the electron BOUNDARY scattering they generate

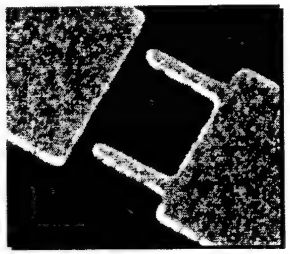

- While the Coulomb blockade is QUENCHED in open dots electrons may still be confined for LONG times in such structures
  - We might therefore expect that the transport properties of open dots should exhibit NOVEL signatures that arise due to the MANY-BODY interactions of carriers trapped within them
  - FEW studies to date appear to have explored this possibility however

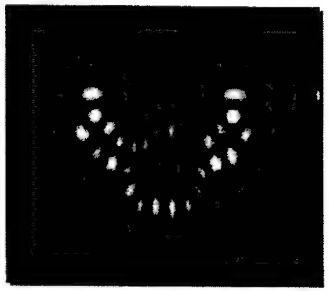

R. Akis *et al.*
Physica E 7, 745 (2000)

- We investigate evidence for MANY-BODY interactions in open quantum dots and quantum-dot arrays by studying the variation of their resistance with TEMPERATURE
  - We find evidence for novel LOCALIZATION behavior that we speculate arises due to an ENHANCED electron-electron interaction in these mesoscopic structures

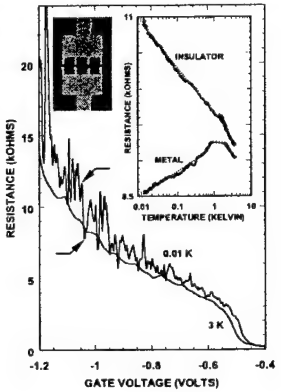

A. Shailos *et al.*
Phys. Rev. B 63, 241302 (2001)

OUTLINE

- *INTRODUCTION*
- *TRANSPORT IN QUANTUM DOTS*
- *DEVICE FABRICATION & BASIC CHARACTERIZATION*
- *EXPERIMENTAL RESULTS*
- *CONCLUSIONS*

- It is well known that at low temperatures the DISCRETE level spectrum of ISOLATED quantum dots can be RESOLVED in experiment
  - When the dot is OPENED to the outside world the coupling between to the reservoirs gives rise to a NON-UNIFORM broadening of the dot states
  - Discrete states that SURVIVE the coupling can be driven past the Fermi level by applying a magnetic field or gate voltage which gives rise to OSCILLATIONS in the conductance

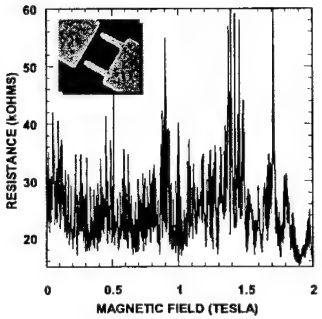

J. P. Bird *et al.*
Europhys. Lett. 35, 529 (1996)

• The particular states that persist in the open dots are found to correspond to strongly SCARRED wavefunctions

* The conductance oscillations observed in experiment therefore represent MEASURABLE signatures associated with these wavefunction scars

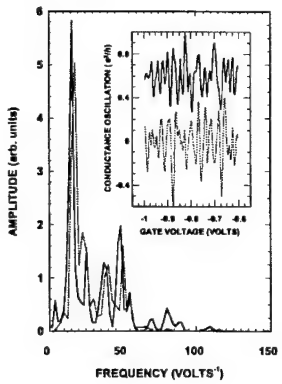

R. Akis *et al.*
Phys. Rev. Lett. 79, 123 (1997)
J. P. Bird *et al.*
Phys. Rev. Lett. 82, 4691 (1999)
R. Akis *et al.*
Physica E 7, 745 (2000)

• By changing the ORIENTATION of the leads that couple the dot to the reservoirs DIFFERENT groups of states can be selected to mediate the transport behavior

* Evidence for this process of SCAR SELECTION can be observed directly in experiment

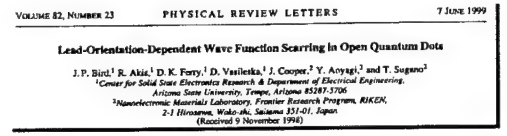
VOLUME 82, NUMBER 23 PHYSICAL REVIEW LETTERS 7 JUNE 1999

Lead-Orientation-Dependent Wave Function Scarring in Open Quantum Dots

J. P. Bird,[1] R. Akis,[1] D. K. Ferry,[1] D. Vasileska,[1] J. Cooper,[2] Y. Aoyagi,[2] and T. Sugano[2]
[1]*Center for Solid State Electronics Research & Department of Electrical Engineering, Arizona State University, Tempe, Arizona 85287-5706*
[2]*Nanoelectronic Materials Laboratory, Frontier Research Program, RIKEN, 2-1 Hirosawa, Wako-shi, Saitama 351-01, Japan*
(Received 9 November 1998)

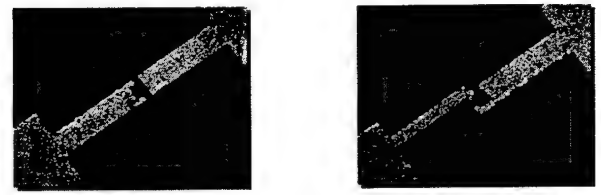

• From an analysis of the magneto-conductance fluctuations we can determine the electron PHASE-BREAKING time which is a measure of the time over which the coherent WAVE-LIKE nature of the electron is PRESERVED within the dot

* At low temperatures this time scale is several ORDERS of magnitude longer than the time required to traverse the dot thus allowing confinement effects to be strongly RESOLVED

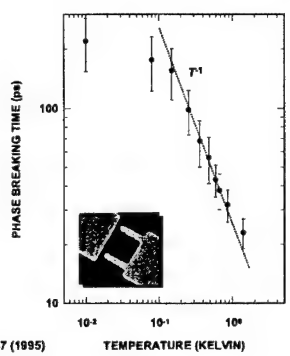

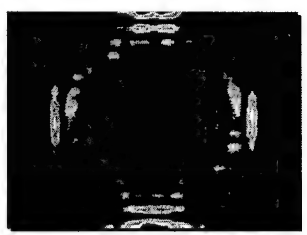

J. P. Bird *et al.*
Phys. Rev. B 51, 18037 (1995)
D. P. Pivin, Jr. *et al.*
Phys. Rev. Lett. 82, 4687 (1999)

R. Akis *et al.*
Phys. Rev. B 54, 17705 (1996)
Phys. Rev. Lett. 79, 123 (1997)

OUTLINE

- *INTRODUCTION*
- *TRANSPORT IN QUANTUM DOTS*
- *DEVICE FABRICATION & BASIC CHARACTERIZATION*
- *EXPERIMENTAL RESULTS*
- *CONCLUSIONS*

- In this report we discuss the transport properties of multiply-coupled QUANTUM-DOT ARRAYS
  - The arrays are realized using the SPLIT-GATE technique in which a depleting voltage is applied to lithographically-defined Schottky gates to induce LATERAL confinement of the high-mobility two-dimensional electron gas formed at the heterointerface

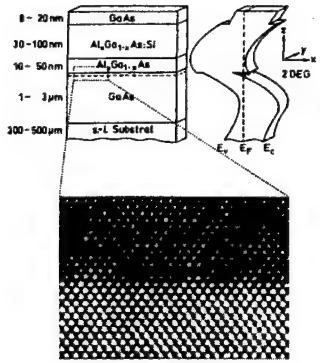

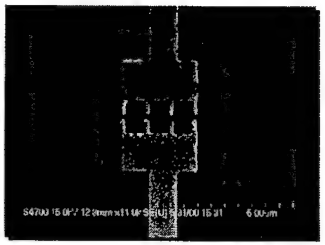

- Measurements of the carrier density of the underlying two-dimensional electron gas indicate a value for the INTERACTION PARAMETER r_s that is close to UNITY
  - Electron transport within the two-dimensional layer is therefore expected to exhibit WEAKLY-INTERACTING behavior

$$E_{ee} = \frac{e^2}{4\pi\varepsilon}\frac{1}{\bar{r}} = \frac{e^2}{4\pi\varepsilon}\sqrt{\pi n_s} \qquad E_F = \frac{\hbar^2 k_F^2}{2m} = \frac{\pi n_s \hbar^2}{m}$$

$$r_s = \frac{E_{ee}}{E_F} = \frac{m^* e^2}{4\pi\varepsilon\hbar^2}\frac{1}{\sqrt{\pi n_s}}$$

$$r_s(GaAs) = \frac{0.067\times 9.1\times 10^{-31}\times 2.6\times 10^{-38}}{12.6\times(12.4\times 8.854\times 10^{-12})\times 1.1\times 10^{-68}}\frac{1}{\sqrt{3.1\times 5\times 10^{15}}} \approx 0.9$$

- Some further COMMENTS on the transport characteristics of the arrays
  - The carrier density within the arrays is found to remain UNCHANGED with gate voltage
  - The transport mean free path (>10 μm) is very much LONGER than the size of the arrays so that transport within them is expected to be highly BALLISTIC in nature
  - At low temperatures the electron phase-breaking length is of order 100 ps corresponding to a TOTAL coherent path length in EXCESS of 50 μm

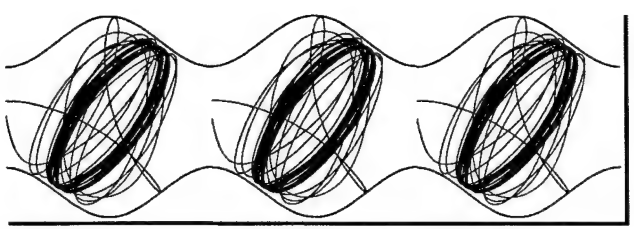

OUTLINE

- *INTRODUCTION*
- *TRANSPORT IN QUANTUM DOTS*
- *DEVICE FABRICATION & BASIC CHARACTERIZATION*
- *EXPERIMENTAL RESULTS*
- *CONCLUSIONS*

• The details of quantum transport in the arrays are investigated by studying the TEMPERATURE dependence of their resistance

* These studies reveal evidence for behavior reminiscent of a METAL-INSULATOR transition

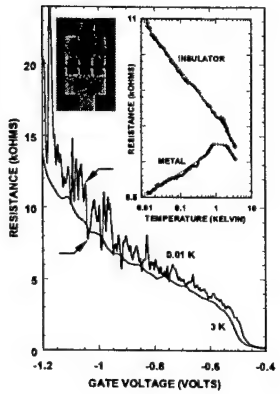

A. Andresen *et al.*
Phys. Rev. B 60, 16050 (1999)
A. Shailos *et al.*
Phys. Rev. B 63, 241302 (2001)

• NO evidence for the temperature-dependent variations found in the arrays is seen in studies performed with the gates GROUNDED

* This indicates that these variations are INTRINSIC to the dot ARRAYS rather than being a property of the two-dimensional electron-gas layer

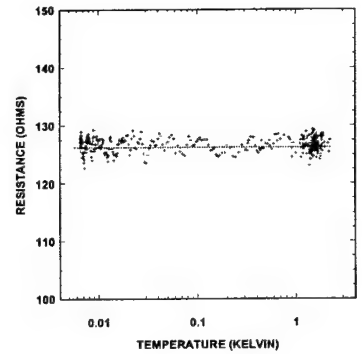

A. Andresen *et al.*
Phys. Rev. B 60, 16050 (1999)
L.-H. Lin *et al.*
Phys. Rev. B 60, R16299 (1999)
A. Shailos *et al.*
Phys. Rev. B 63, 241302 (2001)

• The main characteristics of the metal-insulator behavior are an EXPONENTIAL increase of the resistance at intermediate temperatures and for ALL gate voltages

* This gives way to a LOGARITHMIC variation of the resistance at lower temperatures that may be either METALLIC or INSULATING in nature

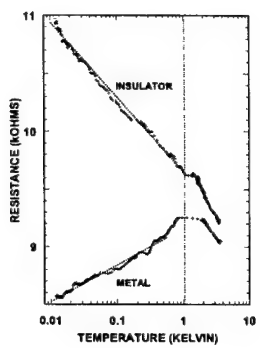

A. Andresen *et al.*
Phys. Rev. B 60, 16050 (1999)
A. Shailos *et al.*
Phys. Rev. B 63, 241302 (2001)

• An important clue as to the origin of the exponential variation is provided by numerical studies where the conductance is CONVOLVED with the derivative of the Fermi function

* This reveals a regime of increasing resistance with decreasing temperature PRIOR to the emergence of conductance oscillations

$$G(T, E_F) = \int G(E)\left[-\frac{df(T, E-E_F)}{dE}\right]dE$$

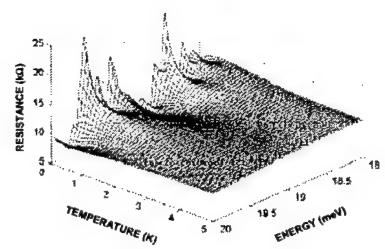

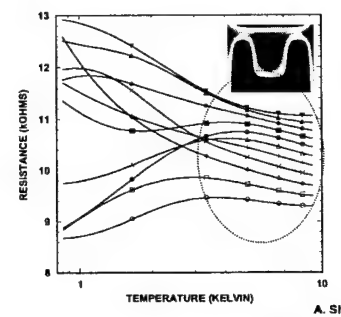

A. Shailos *et al.*
submitted for publication

• We suggest the exponential regime indicates a transition from THERMALLY-BROADENED to ENERGETICALLY-DISCRETE levels in the dots with decreasing temperature

* This assertion is further supported by studies of the temperature dependence of the MAGNETO-RESISTANCE which show a large change in amplitude in the exponential regime

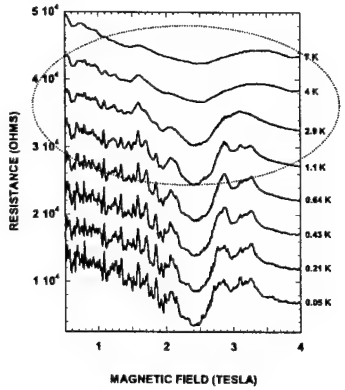

A. Shailos *et al.*
submitted for publication

• While our simulations show features reminiscent of the exponential regime found in experiment they are UNABLE to reproduce the LOGARITHMIC behavior seen at much lower temperatures

* To further investigate the properties of this term we have fabricated quantum dot arrays of DIFFERENT size

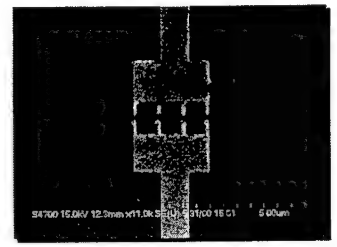

ARRAY	DOT SIZE (μm^2)
A	0.8 x 1.3
B	0.6 x 1.0
C	0.4 x 0.7

• The amplitude of the logarithmic term is found to be LARGER in the arrays composed of smaller dots

* We quantify this effect in terms of the SLOPE of the logarithmic variation (γ) in this regime

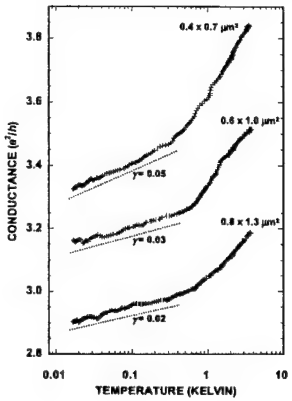

A. Shailos *et al.*
Phys. Rev. B 63, 241302 (2001)

• Averaging the results of measurements performed at a NUMBER of different gate voltages we find that the logarithmic terms scales INVERSELY with dot size

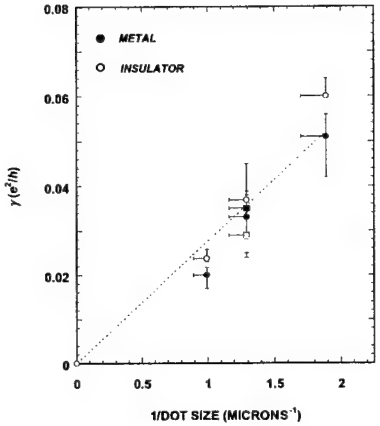

A. Shailos *et al.*
Phys. Rev. B 63, 241302 (2001)

• We also find that the magnitude of the logarithmic term is INSENSITIVE to the application of a magnetic field sufficient to BREAK time-reversal symmetry

* This indicates that this term is NOT associated with a weak-localization effect in the dots

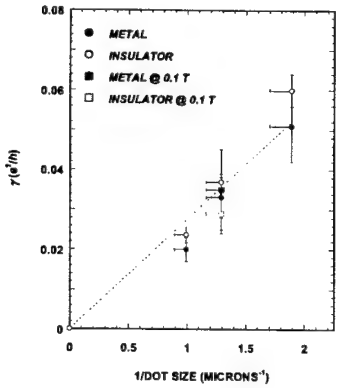

A. Shailos *et al.*
Phys. Rev. B 63, 241302 (2001)

• Logarithmic conductance variations are well known from studies of DISORDERED mesoscopic systems in which they can result from WEAK LOCALIZATION or ELECTRON INTERACTIONS

* In order to distinguish between these two effects it is necessary to apply a sufficient MAGNETIC FIELD to break time-reversal symmetry and so quench weak localization

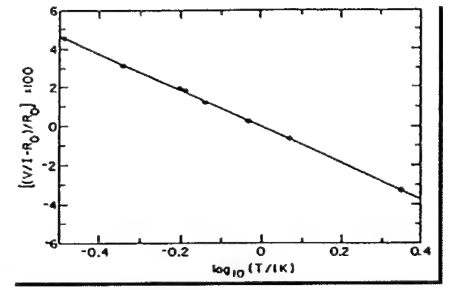

G. J. Dolan and D. C. Osheroff
Phys. Rev. Lett. 43, 721 (1979)

• Based on experiment we have suggested that the logarithmic term in the conductance results from an ENHANCEMENT of the electron-electron interaction inside the dots

* The basic idea is that confining electrons within the ballistic dots should AMPLIFY the Coulomb many-body interaction by SUPPRESSING the tendency for charge separation

* In fact the SCALING of the logarithmic term with INVERSE dot size is consistent with an interaction that scales in inverse proportion to the PERIMETER LENGTH

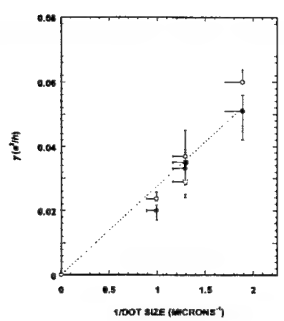

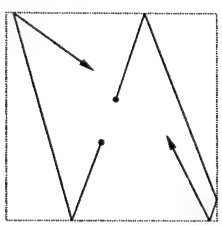

A. Shailos *et al.*
Phys. Rev. B 63, 241302 (2001)

• In the absence of any formal theory we consider it INTRIGUING that a logarithmic variation of the conductance has also been found in studies of the KONDO EFFECT in tunnel-coupled dots

* While there are important DIFFERENCES with the behavior we observe in open dots this comparison appears to SUPPORT our assertion that the logarithmic term we observe does result from MANY-BODY effects

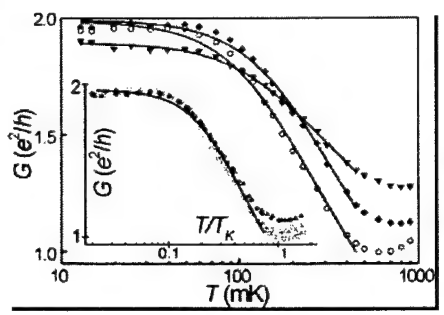

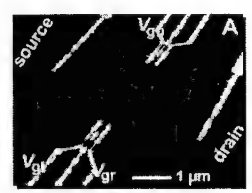

W. G. van der Wiel
Science 289, 2105 (2000)

- We therefore arrive at the following MODEL to account for the different temperature variations
  - At temperatures in EXCESS of a few Kelvin the discrete dot states are thermally OBSCURED
  - Lowering the temperature in this regime allows the dot states to become RESOLVED and it is this transition that is reflected in the EXPONENTIAL resistance

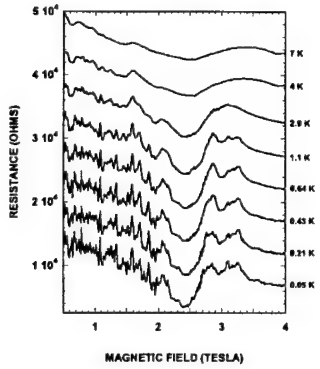

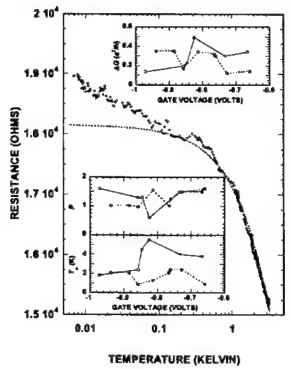

A. Shailos *et al.*
submitted for publication

- As the temperature is lowered below a KELVIN we enter the regime of strongly-resolved dot states and it is here that the LOGARITHMIC variation of resistance is observed
  - An INTRIGUING issue concerns whether this variation signals the emergence of some NOVEL many-body state once the quantum nature of these structures is well resolved?

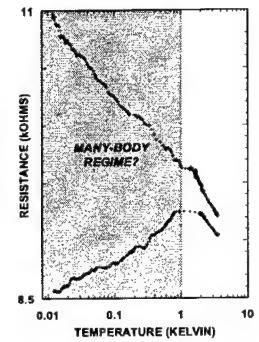

CONCLUSIONS

- *WE HAVE STUDIED THE TEMPERATURE-DEPENDENT TRANSPORT IN COUPLED QUANTUM-DOT ARRAYS AND FIND VERY DIFFERENT BEHAVIOR COMPARED TO THAT OF THE UNDERLYING TWO-DIMENSIONAL ELECTRON GAS*

- *THE REGIME OF EXPONENTIAL RESISTANCE VARIATION IS SUGGESTED TO SIGNIFY THE EMERGENCE FROM THERMALLY-BROADENED TO ENERGETICALLY-RESOLVED DOT LEVELS WITH DECREASING TEMPERATURE*

- *THE LOGARITHMIC VARIATION SEEN AT EVEN LOWER TEMPERATURES CANNOT BE ACCOUNTED FOR BY EXISTING THEORIES AND MAY SIGNIFY THE EMERGENCE OF A NOVEL MANY-BODY STATE AT LOW TEMPERATURES THAT RESULTS FROM AN ENHANCEMENT OF ELECTRON INTERACTIONS IN THE CONFINED DOTS*

- *IT IS OUR HOPE THAT THIS WORK WILL STIMULATE RENEWED THEORETICAL INTEREST IN THE STUDY OF ELECTRON INTERACTIONS IN OPEN MESOSCOPIC SYSTEMS*

Wedenesday, June 20
Session 5:

1. David Awschalom. „Spin coherence and optical measurements"
2. Daniel Loss. „Quantum Computing in semiconductor systems"
3. Sankar Das Sarma. „Few electron (and few impurity) systems"

Also related posters Thursday: 3-1 Bournel et al.
3-2 Puller et al.
3-3 Privman
3-9 Vagner
3-10 Filinov et al.

Workshop „Quantum Transport in Semiconductors"

Maratea, June 17-22 2001

Introduction to Spins and few particle problems in semiconductors

Michael Bonitz, Universität Rostock

Workshop „Quantum Transport in Semiconductors"

Maratea, June 17-22 2001

© Michael Bonitz

Welcome to the spin doctors!

I. What desease?

II. Who is sick?

III. What is the cure?

Workshop „Quantum Transport in Semiconductors"

Maratea, June 17-22 2001

B

Spintronics (alternative medicine ?)

Idea: control devices by controling the electron spin (instead of the charge)

Spin already in use: M-RAMS, read heads of hard drives etc.

But: metal based. Challenge: semiconductors (integrability)

I. Improve *classical* devices (computers)

→ *Many*-electron problem

→ Replace current $j \to j_\uparrow$ voltage $U = \varphi_+ - \varphi_- \to N_\uparrow - N_\downarrow$

Gate field $E \to B$

Example: $j_\uparrow + j_\downarrow$

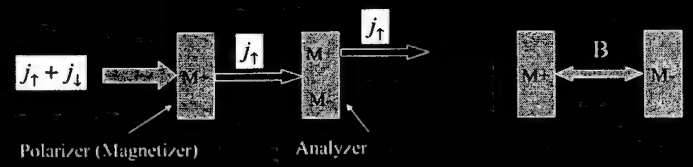

Problems: creation/injection/transport/storage..... (possible side effects?)

Spintronics II.

II. Create new *quantum* computers (*few-body* problem)

1. Instead of classical states (bit) „0 1"

Use quantum states („qubits"): $|0\rangle, |1\rangle, \ldots$

And their linear combinations $C = a|0\rangle + b|1\rangle + \ldots$

2. Build a linear computer U and perform U „vector" operation U C
n scalar (classical) operations at once

3. Build qubits from ↑↓

4. Mix qubits by designing

→ True quantum-mechanical approach (use amplitude)

→ Optical analogue: holography

Semiconductor electrons in E/B fields

E-Field (couples to charge)

1. $e: e\vec{E} \to \vec{v} \to \vec{j}$ *current*

→ Transport (intraband)

2. Interband transport (optics)

$$e \to d_{cv} \sim e\int dV \psi_c^*(r)\, r\, \psi_v(r)$$

Interband current (polarization) P

$$\left[\frac{\partial}{\partial t} + i\frac{\tilde{\varepsilon}_{cv}(k)}{\hbar}\right] P_k = -i\tilde{d}_{cv} E(t)\left[f_{ck}(t) - f_{vk}(t)\right]$$

- Coherent oscillations of P, Rabi flops, photon echo etc., coherent excitons, biexcitons
- Dephasing due to scattering $\sim -\frac{P_{cv}}{T_2}$

B-Field (couples to mag. moment)

$\vec{s} \to \vec{m}$: $\vec{m}\vec{B} \to \omega_L = g\mu_B B/\hbar$

→ Larmor precession

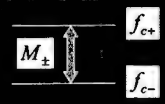

M-magnetization

$$\left[\frac{\partial}{\partial t} + i\frac{\tilde{\varepsilon}_{\pm}(k)}{\hbar}\right] M_\pm = ig\tilde{\mu}_\pm B(t)\left[f_{c+}(t) - f_{c-}(t)\right]$$

$\tilde{\varepsilon}_{\pm k}$ HI-renormalized gap Zeeman splitting

- Coherent oscillations of M, „Larmor flops" spin echos ?
- very long dephasing times
- bound states (cooper pairs) ??

Electrons in E/B-fields, contd.

3. Spin meets optics

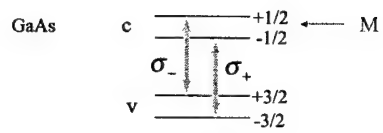

-spin-sensitive absorption/emission of circular-polarized light (old)

-spin-modulated polarization of laser emission [Hallstein et al. PRB **56**, R7076 (1997)]
Experiment and theory

$$\left[\frac{\partial}{\partial t} + i\frac{\tilde{\varepsilon}_{\pm}(k)}{\hbar}\right] M_\pm = ig\tilde{\mu}_\pm B(t)\left[f_{c+}(t) - f_{c-}(t)\right]$$

4. Spin meets intraband transport

- „Conversion of spin into directed electric current in Quantum Wells", Ganichev et al. PRL **86**, 4356 (2001)
- B-field induced separation of +3/2 and −3/2 hh bands *in k-space*
- current direction determined by helicity of light polarization

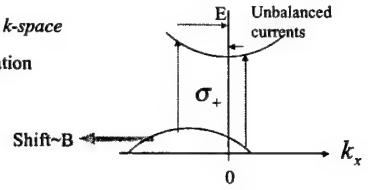

Outlook

Number of quantum computing papers (title and abstract): from 1994-2001 (June14): 1, 6, 10, 15, 38, 59, 81, 122

→ On track with Moore's law

Number of spintronics papers: from 1999-2001 (June 14 11.32 a.m. ET): 2, 8, 10

→ Way ahead of Moore's law

⇒ True reason for Intel's rush ahead of the road map

Workshop „Quantum Transport in Semiconductors"

Maratea, June 17-22 2001

Listen to (and interrupt!) the spin doctors!

Workshop „Quantum Transport in Semiconductors"

Maratea, June 17-22 2001

SPIN ELECTRONICS

Group of Sankar Das Sarma, University of Maryland
Igor Žutić, Jaroslav Fabian, Xuedong Hu, et al.

- theory of bipolar spin-polarized transport in inhomogeneous semiconductors (magnetic and nonmagnetic) and their heterostructures
- spin devices: proposal and modeling of spin-polarized and magnetic p - n junctions and solar cells, magnetic field sensors, spin transistors, ...
- dynamical mean field theory for critical temperature in ferromagnetic semiconductors (e.g., GaMnAs)
- spin entangelment and interactions in quantum dots: assessment of feasibility for spin-based quantum computing

Group Publications (partial list):

Theory of spin-polarized transport in inhomogeneous magnetic semiconductors, LANL preprint cond-mat/0106085

Spin Electronics and Spin Computation, to appear in Solid State Commun., LANL preprint cond-mat/0105247

A proposal for spin-polarized solar battery. to appear in Appl. Phys. Lett. (8/27/01); LANL preprint cond-mat/0104416

Spin transport in ihomogeneous magnetic fields: a proposal for Stern-Gerlach-like experiments with conduction electrons, LANL preprint cond-mat/0104146

Spin injection throught the depletion layer: a theory of spin-polarized p-n junctions and solar cells, to appear in Phys. Rev. B. Rapid Commun. (8/15/01) ; LANL preprint cond-mat/0103473

Issues, Concepts, and Challenges in Spinronics, IEEE 58th DRC Device Research Conference Digest, p. 95 (2000)

Theoretical Perspectives on Spintronics and Spin-Polarized Transport. IEEE Trans. Magn. 36, 2821 (2000)

Issues Concepts, and Challenges in Spintronics, Superlatice Microst. 27, 289 (2000)

Spin-polarized transport and Andreev reflection in semiconductor/superconductor hybrid structures. Phys. Rev. B 60 Rapid Commun., R16 322 (1999).

publicatioons also available at :
http://www.physics.umd.edu/rgroups/spin/papers.html

Spin - Polarized p - n Junction

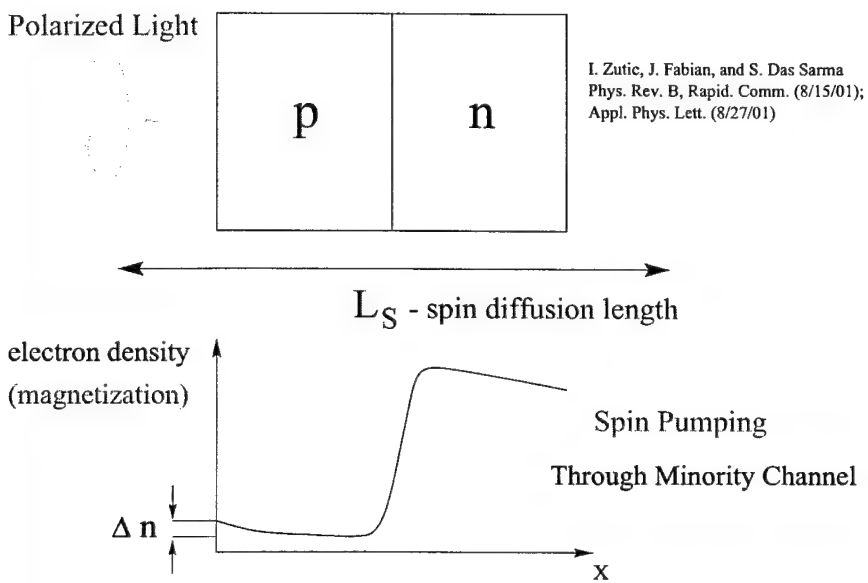

I. Zutic, J. Fabian, and S. Das Sarma
Phys. Rev. B, Rapid. Comm. (8/15/01);
Appl. Phys. Lett. (8/27/01)

Spin-Polarized and Magnetic p - n Junctions and Solar Batteries

spin-polarized p - n junction -- building block for semiconductor spin electronics , feasible with the current technology and available materials (e.g., GaAs with the appropriate doping)

spin polarization can be created by circularly polarized light, electrical spin injection, applied magnetic field, ...

Example: Spin-Polarized Solar Battery

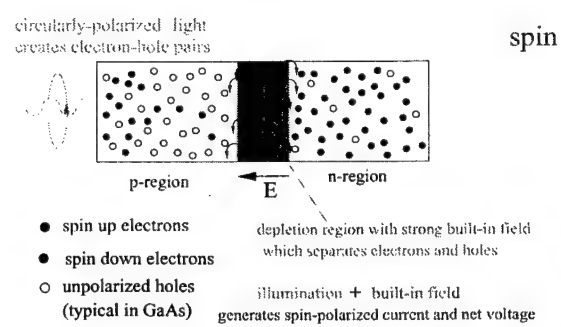

Spin Amplification

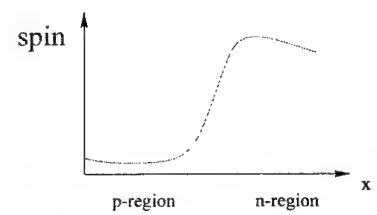

Near the depletion region, electron population increases

↓

spin (magnetization) increases in the interior of nonmagnetic material !

Spin - Polarized Drift - Diffusion Equations

$$\nabla^2\phi = -\frac{e}{\varepsilon}(p - n + N_A - N_D)$$

and

4 Continuity equations for $n_\uparrow$, $n_\downarrow$, $p_\uparrow$ and $p_\downarrow$

Generation - Recombination (τ_n, τ_p)

Spin Relaxation (T_1)

Results based on realistic GaAs parameters

$p_\uparrow = p_\downarrow$

$(n_\uparrow - n_\downarrow) / n$ ← max polarization 50% (with circularly-polarized light)

$T_1 \sim 0.2$ns

Continuity Equation for $n_\uparrow$

$$J_{n_\uparrow} = -n_\uparrow \mu_{n_\uparrow} E - D_{n_\uparrow} \nabla n_\uparrow$$

particle current (for nonmagnetic p - n junction)

$$\frac{dn_\uparrow}{dt} + \nabla \cdot J_{n_\uparrow} = -w_{n_\uparrow}\left(n_\uparrow p - \frac{n_0 p_0}{2}\right) - \frac{n_\uparrow - n_\downarrow}{2T_1} + G_\uparrow$$

$w_{n_\uparrow}$ - Generation -Recombination rate

$G_\uparrow$ - Photo-excitation rate for $n_\uparrow$

Spin Injection through the p - n junction

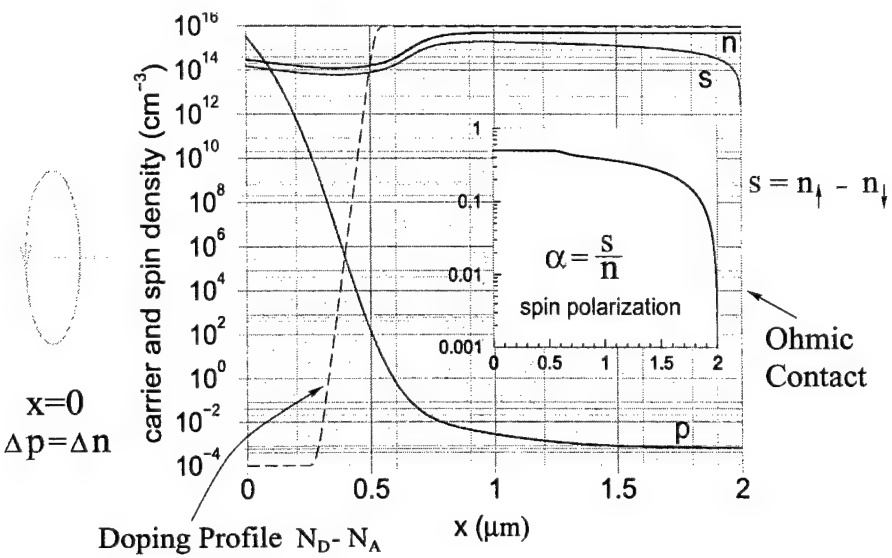

Spin Polarization Profiles for different voltages

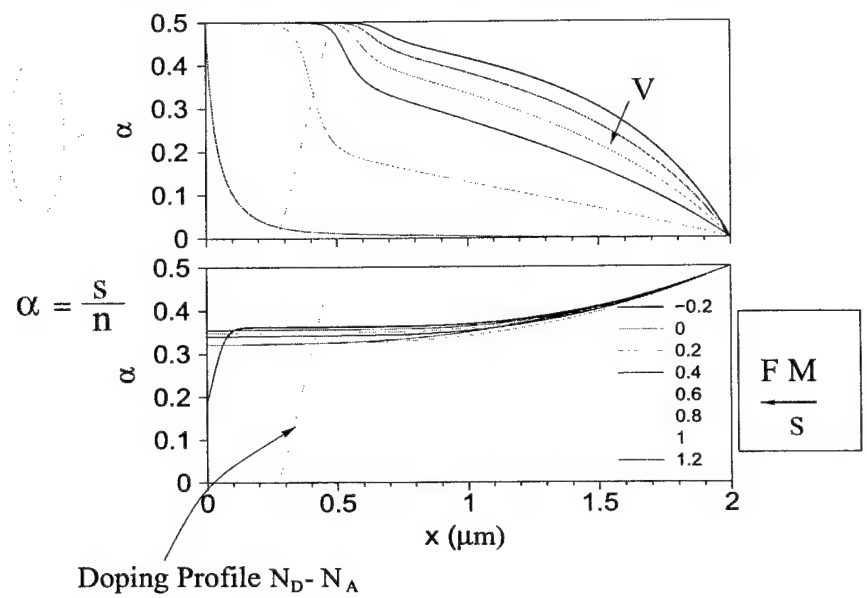

Magnetic / Nonmagnetic p - n Junctions

I. Zutic, J. Fabian, and S. Das Sarma, LANL preprint cond-mat/0106085

Band energy scheme

Zeeman spliting

$q\zeta(x) = g(x)\mu_B B$

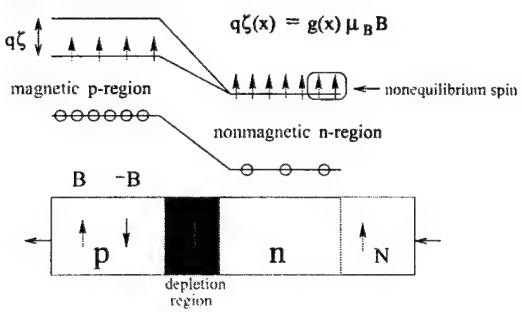

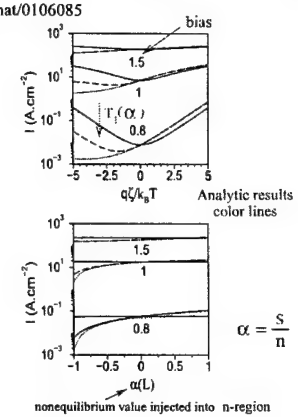

p-region: $n_0 \approx (n_i^2 / N_A)\cosh(q\zeta/kT)$

at low bias: current ~ minority carriers -> exponentially large magnetoresistance with the increase in |B| (i.e. |ζ|)

$J = J_n + J_p + J_n'$ -> nonequilibrium spin-induced current

$J_{n,p} \sim (e^{(qV/kT)} - 1)$ $\quad J_n' \sim \alpha \sinh(q\zeta/kT)\, e^{(qV/kT)}$

next to depletion region

zero bias current changes sign with the change of α and / or B

I (V,B) characteristics

electrical probe for B, α, T_1

current can flow at zero bias!

spinvoltaic effect

(spin analogue of photovoltaic effect)

Aplications of Spin-Polarized and Magnetic p - n Junctions and Solar Batteries

- Generation of spin and charge currents
- Spin injection through the depletion layer
- Electronically tunable spin polarization
- Amplification of spin density
- Extension of the spin-diffusion range
- Exponentional magnetoresistance and spinvoltaic effect
- Magnetic field sensors
- Electrical detection of spin polarization and spin relaxation

Applications of quantum transport in devices

Gerhard Klimeck

Jet Propulsion Laboratory,
California Institute of Technology

gekco@jpl.nasa.gov, 818-354-2182
http://hpc.jpl.nasa.gov/PEP/gekco

Application of Quantum Transport in Devices

- **What is the focus of the research?**
  - **Quantum Transport**
    => Devices/Structures are a tool to explore the needed theory
    - Relevant Theories:
      Green Functions, Wigner Functions, Rate Equations
    - Relevant Structures:
      quantum dots/wires, molecules, RTDs (for time dependence only)
  - **Devices / Applications**
    => Quantum transport is a tool to design/optimize devices
    - Relevant devices: super-scaled FETs, RTDs, Esaki diodes
    - Need quantitative agreement between experiment and theory
      - DC, high bias performance
      - AC / time-dependent high bias performance
    - Need realistically sized devices - contacts/reservoirs.
    - Need realistic electron interactions with environment:
      phonons, light, bandstructure.

Quantitative Modeling of Devices

Quick review of DC transport simulations in RTDs - NEMO 1-D

- **Realistic contacts:**
  - **Quantized and continuous states in the emitter**
- **Realistic bandstructure:**
  - **Band-non parabolicity - emitter states and RTD state alignment**
- **Putting it together:**
  - **Valley current at high temperatures due to bandstructure effects (thermionic emission)**
  - **Bistability (in symmetric structures) a numerical problem due to limited device models**
  - **Test matrix - comparison to experiment**

 Work on this slide performed by NEMO team at Texas Instruments / Raytheon 1995-1997

Realistic Devices have Extended Contacts

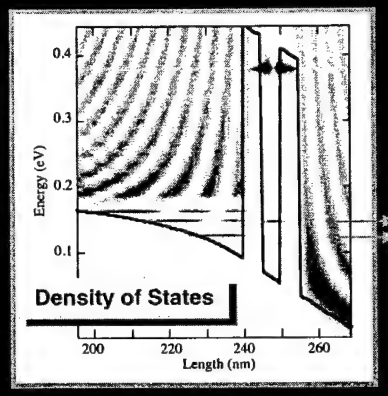

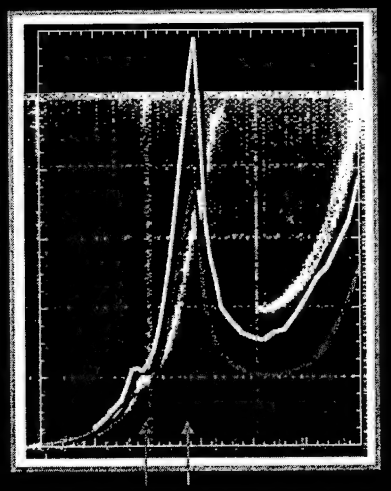

	Potential	Current
—	1 Band	1 Band
—	2 Bands	2 Bands
—	1 Band	10 Bands

Quantum selfconsistent potential

 Work on this slide performed by NEMO team at Texas Instruments / Raytheon 1995-1997

Band non-parabolicity modifies momentum dependence in emitter-RTD coupling

Density of States (k_x=0.00)

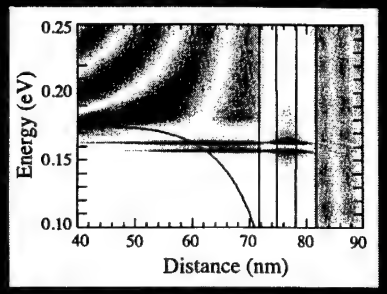

Density of States (k_x=0.03)

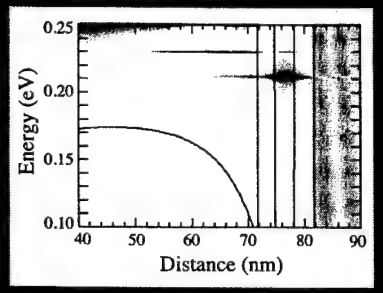

Resonance coupling depends on the transverse momentum

Full Band Simulation of Electron Transport

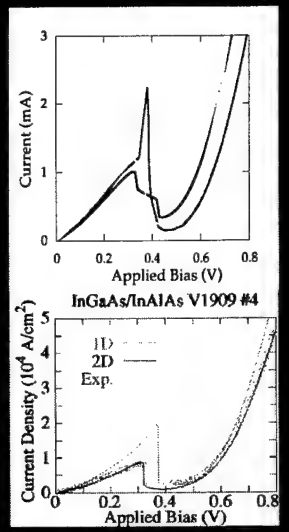

- 1D integration assuming parabolic subbands can lead to unphysical current overshoots.
- **2 Examples on InGaAs/InAlAs simulations:**
  - **Sp3s* simulation with partial charge self-consistency -> sharp spike at turn-off**
  - **Parameterized single band simulation which incorporates the band-non-parabolicity -> overall current overshoot.**

-> 2D integration with good bandstructure fixes these unphysical results.

Spurious Bistability: More Physics -> Better results

Full band integration + Exchange&Correlation

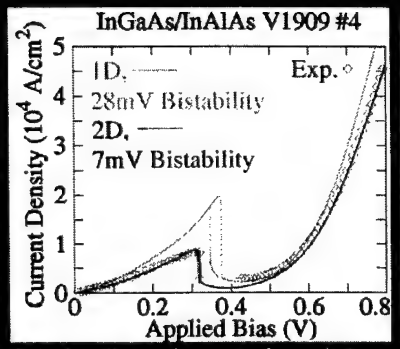

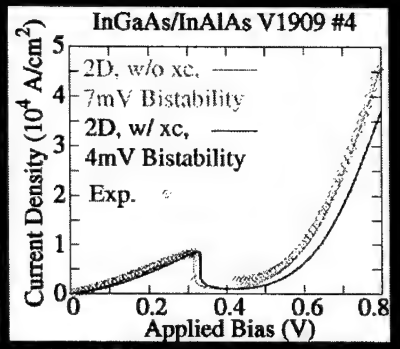

- **Calculate the exchange and correlation potential in LDA.**
- **Exchange and correlation energy does not eliminate (in general) the bistability, it does reduce it however.**
- **Inclusion of scattering in the simulation reduces the bistability region as well.**

Scattering also reduces the numerical bi-stability

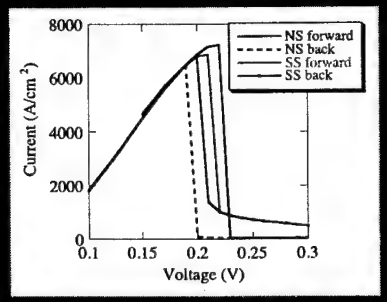

- **Current Model:**
  - self-consistent elastic and single tridiagonal POP scattering
- **Potential Models: Hartree self-consistency**
  - no scattering
  - selfconsistent elastic and tridiagonal POP scattering
- **Compare forward to reverse bias sweep:**
  - Scattering reduces the width of the bistability region.
  - not shown: inclusion of exchange correlation does not change the width of the bistability in this device.

Testmatrix-Based Verification (room temperature)

Strained InGaAs/AlAs 4 Stack RTD with Asymmetric Barrier Variation

Vary One Barrier Thickness

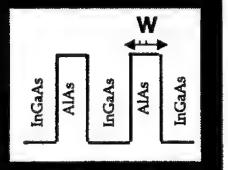

Four increasingly asymmetric devices:
20/50/20 Angstrom
20/50/23 Angstrom
20/50/25 Angstrom
20/50/27 Angstrom

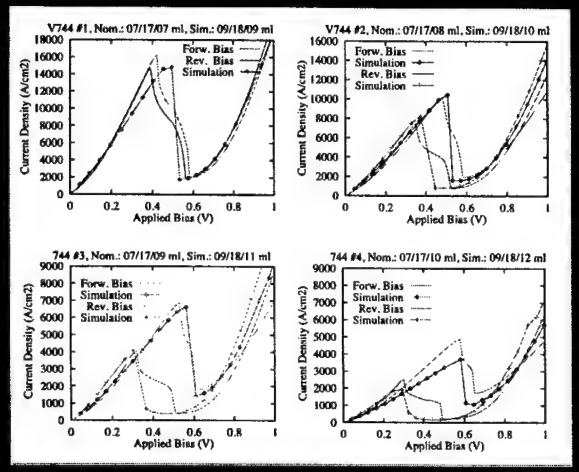

Presented at IEEE DRC 1997

Work on this slide performed by NEMO team at Texas Instruments / Raytheon 1995-1997

Tow Temperature: Polar Optical Phonon and Interface Roughness Scattering

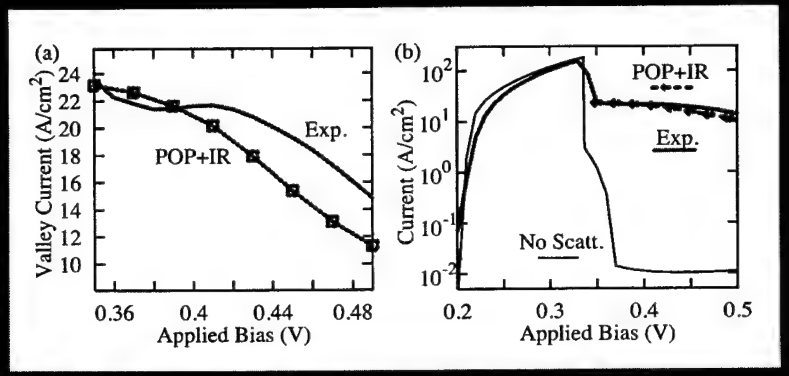

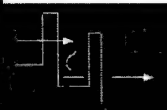

scattering raises valley current by several orders of magnitude

Work on this slide performed by NEMO team at Texas Instruments / Raytheon 1995-1997

Nano-scale Device Analysis / Synthesis

Development of a Bottom-Up Nanoelectronic Modeling Tool (NEMO-3D)

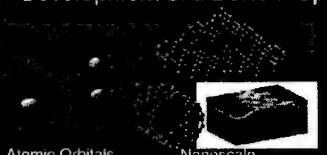

Atomic Orbitals size: 0.2nm — Nanoscale Structures (~20nm)

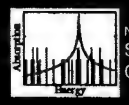

New Devices for Sensing and Computing

Analyze Devices Environment and Failures

Assertions / Problems:
- Nanoscale structures are built today! The design space is huge: choice of materials, compositions, doping, size, shape
- Radiation on today's sub-micron devices modifies the electronics on a nanoscale.

Approach:
- Deliver a 3-D atomistic simulation tool
- Enable analysis of arbitrary crystal structures, particles, atom compositions and bond/structure at arbitrary temperatures and ambient electric and magnetic fields.

Collaborators:
- U. of Alabama, Ames, Purdue, Ohio State, NIST

NASA Relevance:
- Enable new devices needed for NASA missions beyond existing industry roadmap:
  - Water detection -> 2-5μm Lasers and detectors.
  - Avionics -> High density, low power computing.
- Analyze state-of-the-art devices for non-commercial environments:
  - Europa -> Radiation and low temperature effects. Aging and failure modes.
  - Jovian system -> Magnetic field effects
  - Venus -> high temperature materials: SiGe

Impact:
- Low cost development of revolutionary techn.

Modeling will narrow the empirical search space!

Speakers in the Program

- **Carlo Jacoboni, Modena University, "The Wigner function and quantum transport"**
- **Harold Grubin, SRA, Inc., "Modeling resonant tunneling diodes with Wigner functions and density matrices"**
- **Dejan Jovanovic, Motorola, "Non-equilibrium Green's functions for MOSFET modeling"**

Advanced Research Workshop on
QUANTUM TRANSPORT IN SEMICONDUCTORS
Maratea, Italy, 17-22 June 2001

WIGNER-FUNCTION AND QUANTUM TRANSPORT IN SEMICONDUCTORS

Carlo Jacoboni

INFM - Istituto Nazionale per la Fisica della Materia
Dipartimento di Fisica - Università di Modena
Via Campi 213/A - I 41100 Modena, ITALY

Partially supported by O.N.R. and MURST

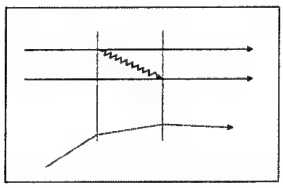

Rossella Brunetti
Paolo Bordone
Andrea Bertoni
Stefano Monastra

Antonio Abramo
Marco Pascoli
Fausto Rossi

Contents

Elementary definition and properties

Dynamical equations
- Classical force
- Infinite potential barrier

Electron - phonon interaction

Wigner paths and MC simulation
- Paths and diagrams
- Multiplicity of Wigner paths
- Quantum self scattering

Two-time Wigner function $f_w(p, \omega)$

- Spectral density

THE WIGNER FUNCTION

The Wigner-function approach is a phase-space formulation of quantum mechanics that allows to establish many analogies with the semiclassical theory based on the concept of distribution function

Elementary definition:

$\rho(\mathbf{r}_1,\mathbf{r}_2)$

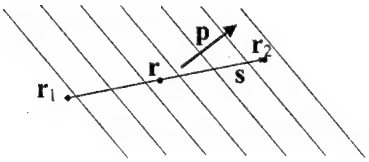

$$f_w(\boldsymbol{r},\boldsymbol{p},t)=\int ds\, e^{-ips/\hbar}\overline{\Psi(\boldsymbol{r}+\boldsymbol{s}/2,t)\Psi^*(\boldsymbol{r}-\boldsymbol{s}/2,t)}$$

Properties of the Wigner function

$$\frac{1}{h^3}\int f_w(\boldsymbol{r},\boldsymbol{p},t)\,d\boldsymbol{p} = \left|\Psi(\boldsymbol{r},t)\right|^2$$

$$\frac{1}{h^3}\int f_w(\boldsymbol{r},\boldsymbol{p},t)\,d\boldsymbol{r} = \left|\Phi(\boldsymbol{p},t)\right|^2$$

$$\langle A\rangle = \frac{1}{h^3}\int d\boldsymbol{r}\int d\boldsymbol{p}\; f_w(\boldsymbol{r},\boldsymbol{p},t)\;\; A_w(\boldsymbol{r},\boldsymbol{p})$$

$$A_w(\boldsymbol{r},\boldsymbol{p}) = \int d\boldsymbol{s}\; e^{-i\boldsymbol{p}\cdot\boldsymbol{s}/\hbar}\,\langle \boldsymbol{r}+\boldsymbol{s}/2|A|\boldsymbol{r}-\boldsymbol{s}/2\rangle$$

Linear in f

NOT positive definite

Strong oscillations

$\neq 0$ also where $\Psi = 0$

WIGNER FUNCTION

Ground state in a box:

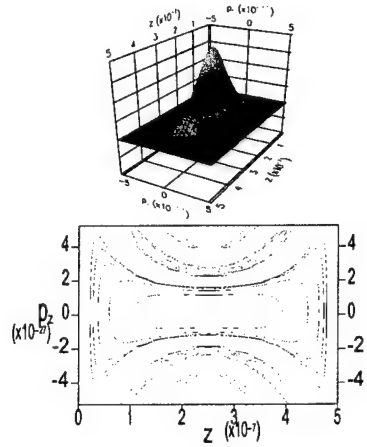

WIGNER FUNCTION

Potential step with scattering states:

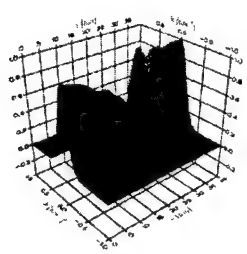

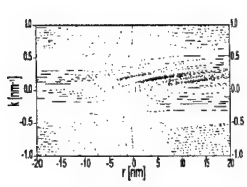

WIGNER FUNCTION FOR A DOUBLE BARRIER

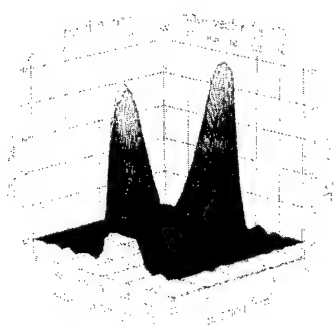

COHERENT PROPAGATION OF THE W.F.

If

$$\mathbf{H}|\varphi_n\rangle = \hbar\omega_n|\varphi_n\rangle$$

then

$$f_w(\boldsymbol{r},\boldsymbol{p},t) = \sum_{n,m} f_{n,m}(\boldsymbol{r},\boldsymbol{p})e^{-i(\omega_n-\omega_m)(t-t_o)}\frac{1}{h^3}\int d\boldsymbol{r}'\int d\boldsymbol{p}' f^*_{n,m}(\boldsymbol{r}',\boldsymbol{p}')f_w(\boldsymbol{r}',\boldsymbol{p}',t_o)$$

Linear

where

$$f_{n,m}(\boldsymbol{r},\boldsymbol{p}) = \int ds\, e^{-ips/\hbar}\langle \boldsymbol{r}+\boldsymbol{s}/2|\varphi_n\rangle\langle\varphi_m|\boldsymbol{r}-\boldsymbol{s}/2\rangle$$

DYNAMICAL EQUATION OF THE W.F. (1)

From the Liouville – Von Neumann

$$i\hbar\frac{d}{dt}\rho = [\mathbf{H},\rho]$$

with

$$\mathbf{H} = \mathbf{H}_o + \mathbf{V}(\boldsymbol{r})$$

$$\mathbf{H}_o = -\frac{\hbar^2}{2m}\nabla^2$$

Obtain

$$\frac{\partial}{\partial t}f_w(\boldsymbol{r},\boldsymbol{p},t) = \int ds\, e^{-ips/\hbar}\times\langle \boldsymbol{r}+\boldsymbol{s}/2|\tfrac{1}{i\hbar}[\mathbf{H}_o+\mathbf{V}(\boldsymbol{r}),\rho]|\boldsymbol{r}-\boldsymbol{s}/2\rangle$$

With standard elaboration:

$$\int ds\, e^{-ips/\hbar}\langle \boldsymbol{r}+\boldsymbol{s}/2|\tfrac{1}{i\hbar}[\mathbf{H}_o,\rho]|\boldsymbol{r}-\boldsymbol{s}/2\rangle = -\frac{\boldsymbol{p}}{m}\nabla f_w$$

and

$$\int ds\, e^{-ips/\hbar}\langle \boldsymbol{r}+\boldsymbol{s}/2|\tfrac{1}{i\hbar}[\mathbf{V}(\boldsymbol{r}),\rho]|\boldsymbol{r}-\boldsymbol{s}/2\rangle = \int d\boldsymbol{p}' V_w(\boldsymbol{r},\boldsymbol{p}-\boldsymbol{p}')f_w(\boldsymbol{r},\boldsymbol{p}',t)$$

where

$$V_w(\boldsymbol{r},\boldsymbol{p}) = \frac{1}{i\hbar}\frac{1}{h^3}\int ds\, e^{ips/\hbar}\left[V(\boldsymbol{r}-\boldsymbol{s}/2)-V(\boldsymbol{r}+\boldsymbol{s}/2)\right]$$

DYNAMICAL EQUATION OF THE W.F. (2)

Collecting the above:

$$\frac{\partial}{\partial t}f_w(\boldsymbol{r},\boldsymbol{p},t) + \frac{\boldsymbol{p}}{m}\frac{\partial}{\partial \boldsymbol{r}}f_w = \left.\frac{\partial f_w}{\partial t}\right|_V$$

For "regular" potential (up to quadratic):

$$\frac{\partial}{\partial t}f_w(\boldsymbol{r},\boldsymbol{p},t) + \frac{\boldsymbol{p}}{m}\frac{\partial}{\partial \boldsymbol{r}}f_w + \boldsymbol{F}\frac{\partial}{\partial \boldsymbol{p}}f_w = 0$$

as in Liouville theorem.

WIGNER PATHS:

The Wigner function of electrons in presence of potentials up to quadratic evolves as an ensemble of classical particles: each point follows a classical path in the Wigner phase space (Wigner path)

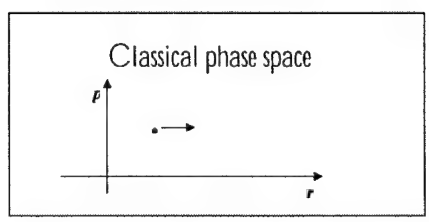

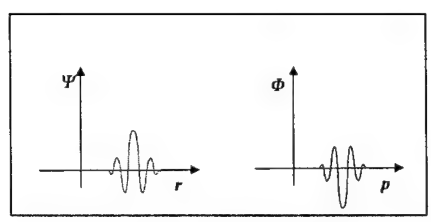

Quantum mechanics

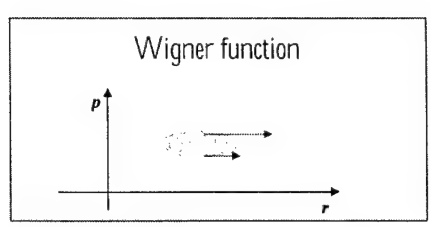

Time evolution of the Wigner Function of a wave packet

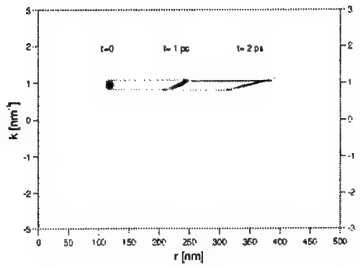

Time evolution of the Wigne Function reflected by an infinite potential barrier

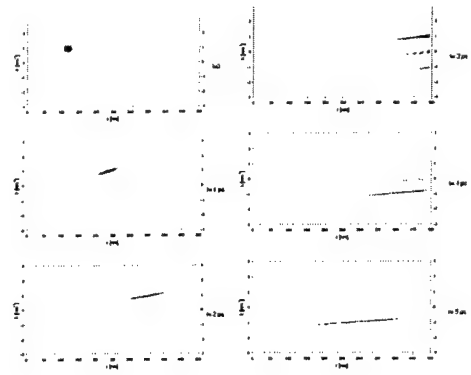

WIGNER PATHS WITH POTENTIAL SCATTERING

$$V = V_o + V' \qquad F = -\nabla V_o$$

V_o linear or quadratic - Integro-differential equation

$$\frac{\partial}{\partial t} f_w(\boldsymbol{r},\boldsymbol{p},t) + \frac{\boldsymbol{p}}{m}\frac{\partial}{\partial \boldsymbol{r}} f_w + \boldsymbol{F}\frac{\partial}{\partial \boldsymbol{p}} f_w = \int d\boldsymbol{p}'\, V_w(\boldsymbol{r},\boldsymbol{p}-\boldsymbol{p}') f_w(\boldsymbol{r},\boldsymbol{p}',t)$$

where

$$V_w(\boldsymbol{r},\boldsymbol{p}) = \frac{1}{h^3}\int d\boldsymbol{s}\, e^{-i\boldsymbol{p}\boldsymbol{s}/h}[V'(\boldsymbol{r}+\boldsymbol{s}/2) - V'(\boldsymbol{r}-\boldsymbol{s}/2)]$$

path variables:

$$\boldsymbol{r}(\tilde{t}) = \boldsymbol{r} - \int_t^{\tilde{t}} dt'\, \boldsymbol{p}(t')/m \qquad \boldsymbol{p}(\tilde{t}) = \boldsymbol{p} - \int_t^{\tilde{t}} \boldsymbol{F}(\boldsymbol{r}(t')\, dt'$$

time integration:

$$f_w(\boldsymbol{r},\boldsymbol{p},t)$$

$$= f_w(\boldsymbol{r}(t_o),\boldsymbol{p}(t_o),t_o) + \int_{t_o}^{t} dt' \int d\boldsymbol{p}'\, V_w(\boldsymbol{r}(t'),\boldsymbol{p}'-\boldsymbol{p}(t'))\, f_w(\boldsymbol{r}(t'),\boldsymbol{p}',t')$$

as in Chambers kinetic integral equation, without scattering "out", with similar interpretation:

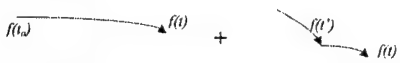

Neumann expansion

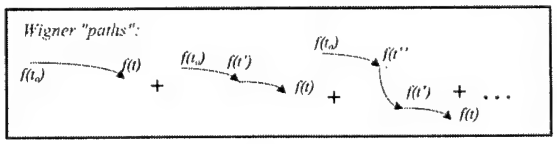

Boundary conditions

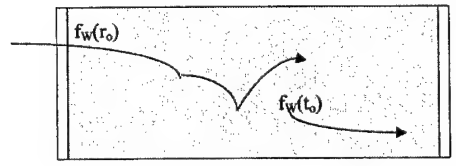

Phys.Rev.B 58, 3503 (1998)

Phys.Rev.B 59, 3060 (1999)

Single barrier (4nm x .05eV)

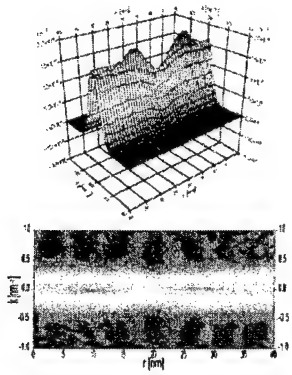

Obtained by means of W. Paths with potential scattering in a Monte Carlo approach

Wigner Function confined by an infinite potential barrier

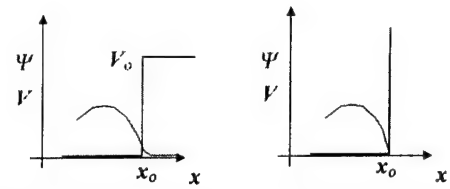

For the infinite barrier the Schroed. eq. holds only inside.
For a box (a,b)

$$f_w(x,p,t)=\int_{-\xi(x)}^{\xi(x)} ds\, e^{-ips/\hbar}\overline{\Psi(x+s/2,t)\Psi^*(x-s/2,t)}$$

where

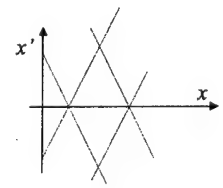

$$\xi(x)=V(r+s/2)\begin{cases}2(x-a) & if \quad x<(a+b)/2\\ 2(b-x) & if \quad x\geq(a+b)/2\end{cases}$$

Wigner Function confined by an infinite potential barrier(ii)

In the derivation of the dynamical eqiation, the derivatives at the boundaries do not vanish, and we have an extra integral term

$$\frac{\partial f_w}{\partial t}+\frac{p}{m}\frac{\partial f_w}{\partial x}=\frac{1}{h}\int dp' V_w(x,p-p')f_w(x,p',t)$$
$$+\frac{1}{h}\int dp' B(x,p-p')\frac{\partial}{\partial x}f_w(x,p',t)$$

where

$$B(x,p)=\frac{2\hbar}{m}\sin\left[\frac{p}{\hbar}\xi(x)\right]$$

simulation …

SEPARATION BETWEEN CLASSICAL FORCE AND QUANTUM EFFECTS

$$\frac{\partial f_w}{\partial t}+\frac{\boldsymbol{p}}{m}\frac{\partial f_w}{\partial \boldsymbol{r}}=\frac{1}{h^3}\int_{-\infty}^{\infty} d\boldsymbol{p}' V_w(\boldsymbol{r},\boldsymbol{p}-\boldsymbol{p}')f_w(\boldsymbol{r},\boldsymbol{p}',t)$$

where

$$V_w(\boldsymbol{r},\boldsymbol{p})=\frac{1}{i\hbar}\int ds\, e^{-ips/\hbar}\beta(\boldsymbol{r},\boldsymbol{s})$$
$$\beta(\boldsymbol{r},\boldsymbol{s})=V(\boldsymbol{r}+\boldsymbol{s}/2)-V(\boldsymbol{r}-\boldsymbol{s}/2)$$

or

$$\frac{\partial f_w}{\partial t}+\frac{\boldsymbol{p}}{m}\frac{\partial f_w}{\partial \boldsymbol{r}}+\boldsymbol{F}\frac{\partial f_w}{\partial \boldsymbol{p}}=\frac{1}{h^3}\int_{-\infty}^{\infty} d\boldsymbol{p}' \tilde{V}_w(\boldsymbol{r},\boldsymbol{p}-\boldsymbol{p}')f_w(\boldsymbol{r},\boldsymbol{p}',t)$$

where

$$\boldsymbol{F}=-\frac{\partial V f_w}{\partial \boldsymbol{r}}$$
$$\tilde{V}_w(\boldsymbol{r},\boldsymbol{p})=\frac{1}{i\hbar}\int ds\, e^{-ips/\hbar}\tilde{\beta}(\boldsymbol{r},\boldsymbol{s})$$
$$\tilde{\beta}(\boldsymbol{r},\boldsymbol{s})=\left[V(\boldsymbol{r}+\boldsymbol{s}/2)-\frac{\partial V}{\partial \boldsymbol{r}}\boldsymbol{s}/2\right]-\left[V(\boldsymbol{r}-\boldsymbol{s}/2)+\frac{\partial V}{\partial \boldsymbol{r}}\boldsymbol{s}/2\right]$$

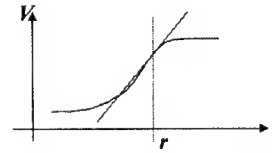

ELECTRON-PHONON SCATTERING WITH THE WIGNER FUNCTION

Extend the definition of Wigner function:

$$f_w(\mathbf{r},\mathbf{p},\{n_q\},\{n'_q\},t)$$

$$= \int d\mathbf{s}\, e^{-ip\mathbf{s}/\hbar}\left\langle \mathbf{r}+\mathbf{s}/2,\{n_q\}\middle|\rho(t)\middle|\mathbf{r}-\mathbf{s}/2,\{n'_q\}\right\rangle$$

Hamiltonian:

$$\mathbf{H} = \mathbf{H}_o + \mathbf{H}_{ph} + \mathbf{H}_{e-p} + \mathbf{V}_o(\mathbf{r}) + \mathbf{V}'(\mathbf{r})$$

where

$$\mathbf{H}_o = -\frac{\hbar^2}{2m}\nabla^2 \qquad \mathbf{H}_{ph} = \sum_q \mathbf{b}_q^+\mathbf{b}_q\hbar\omega_q$$

$$\mathbf{H}_{e-p} = \sum_q i\hbar F(q)(\mathbf{b}_q e^{i\mathbf{q}\cdot\mathbf{r}} - \mathbf{b}_q^+ e^{-i\mathbf{q}\cdot\mathbf{r}}) \qquad \mathbf{V}_o(\mathbf{r}) = e\mathbf{E}\cdot\mathbf{r}$$

$\mathbf{V}'(\mathbf{r})$ *= potential profile*

Differentiate the definition above and use

$$i\hbar\frac{d}{dt}\rho = [\mathbf{H},\rho]$$

Obtain

$$\frac{\partial}{\partial t} f_w(\mathbf{r},\mathbf{p},\{n_q\},\{n'_q\},t) = \int d\mathbf{s}\, e^{-ip\mathbf{s}/\hbar} \times$$

$$\left\langle \mathbf{r}+\mathbf{s}/2,\{n_q\}\middle|\tfrac{1}{i\hbar}[\mathbf{H}_o + \mathbf{H}_{ph} + \mathbf{H}_{e-p} + \mathbf{V}_o(\mathbf{r}) + \mathbf{V}'(\mathbf{r}),\rho]\middle|\mathbf{r}-\mathbf{s}/2,\{n'_q\}\right\rangle$$

ELECTRON-PHONON SCATTERING WITH THE WIGNER FUNCTION- II

Several terms:

$$\int d\mathbf{s}\, e^{-ip\mathbf{s}}\left\langle \mathbf{r}+\mathbf{s}/2,\{n_q\}\middle|\tfrac{1}{i\hbar}[\mathbf{H}_o,\rho]\middle|\mathbf{r}-\mathbf{s}/2,\{n'_q\}\right\rangle = -\frac{\mathbf{p}}{m}\nabla f_w$$

$$\int d\mathbf{s}\, e^{-ip\mathbf{s}}\left\langle \mathbf{r}+\mathbf{s}/2,\{n_q\}\middle|\tfrac{1}{i\hbar}[\mathbf{H}_{ph},\rho]\middle|\mathbf{r}-\mathbf{s}/2,\{n'_q\}\right\rangle = -\tfrac{1}{i\hbar}[\varepsilon(\{n_q\}) - \varepsilon(\{n'_q\})]\, f_w$$

$$\int d\mathbf{s}\, e^{-ip\mathbf{s}}\left\langle \mathbf{r}+\mathbf{s}/2,\{n_q\}\middle|\tfrac{1}{i\hbar}[\mathbf{V}_o(\mathbf{r}),\rho]\middle|\mathbf{r}-\mathbf{s}/2,\{n'_q\}\right\rangle = -\mathbf{F}\frac{\partial}{\partial \mathbf{p}} f_w$$

$$\int d\mathbf{s}\, e^{-ip\mathbf{s}}\left\langle \mathbf{r}+\mathbf{s}/2,\{n_q\}\middle|\tfrac{1}{i\hbar}[\mathbf{V}'(\mathbf{r}),\rho]\middle|\mathbf{r}-\mathbf{s}/2,\{n'_q\}\right\rangle$$

$$= \int d\mathbf{p}'\, V_w(\mathbf{r},\mathbf{p}-\mathbf{p}')\, f_w(\mathbf{r},\mathbf{p}',\{n_q\},\{n'_q\},t)$$

Electron-phonon term:

$$\int d\mathbf{s}\, e^{-ip\mathbf{s}}\left\langle \mathbf{r}+\mathbf{s}/2,\{n_q\}\middle|\tfrac{1}{i\hbar}[\mathbf{H}_{e-p},\rho]\middle|\mathbf{r}-\mathbf{s}/2,\{n'_q\}\right\rangle =$$

$$\sum_{q'} \mathrm{F}(q')\{e^{i\mathbf{q}'\mathbf{r}}\sqrt{n_{q'}+1}\, f_w(\mathbf{r},\mathbf{p}-\tfrac{\hbar\mathbf{q}'}{2}),n_1\ldots n_{q'}+1\ldots,\{n'_q\},t)$$

$$-e^{-i\mathbf{q}'\mathbf{r}}\sqrt{n_{q'}}\, f_w(\mathbf{r},\mathbf{p}+\tfrac{\hbar\mathbf{q}'}{2}),n_1\ldots n_{q'}-1\ldots,\{n'_q\},t)$$

$$-e^{i\mathbf{q}'\mathbf{r}}\sqrt{n'_{q'}}\, f_w(\mathbf{r},\mathbf{p}+\tfrac{\hbar\mathbf{q}'}{2}),\{n_q\},n'_1\ldots n'_{q'}-1\ldots,t)$$

$$+e^{-i\mathbf{q}'\mathbf{r}}\sqrt{n'_{q'}+1}\, f_w(\mathbf{r},\mathbf{p}-\tfrac{\hbar\mathbf{q}'}{2}),\{n_q\},n'_1\ldots n'_{q'}+1\ldots,t)\}$$

Path pariables, time integration, Neumann expansion ...

PHONON AVERAGE

Reduction to electron Wigner function

Trace over phonon variables:

$$f_w\langle \mathbf{p},t\rangle = \sum_{\{n_q\}} f_w\langle \mathbf{p},\{n_q\},\{n_q\},t\rangle$$

Assume separate equilibrium initial density matrix:

$$f_w\langle \mathbf{p},\{n_q\},\{n_q\},t=0\rangle \propto \prod_q P_{eq}\langle n_q\rangle$$

For final diagonal terms, with initial diagonal W.f., each Monte Carlo term contains a phonon mode twice and has factors like

$$\Delta f_w\langle \mathbf{p},\{n_q\},\{n_q\},t\rangle \propto n_{q_1}\ldots\langle n_{q_2}+1\rangle\ldots f_w\langle \mathbf{p},\{n_q\},\{n_q\},t\rangle$$

The simulation must be thought of as repeated a 'large number' of times for each $\{n_q\}$. Then, if hot-phonon effects are ignored,

⇨ ***for absent q:***

$$\sum_{\{n_q\}} P_{eq}\langle n_q\rangle = 1$$

⇨ ***for real or virtual absorptions:***

$$\sum_{n_q}\langle n_q+1\rangle P_{eq}\langle n_q\rangle = \langle n_q\rangle \qquad \sum_{n_q}\langle n_q\rangle P_{eq}\langle n_q\rangle = \langle n_q\rangle$$

⇨ ***for real or virtual emissions:***

$$\sum_{n_q} n_q P_{eq}\langle n_q-1\rangle = \langle n_q+1\rangle \qquad \sum_{n_q}\langle n_q+1\rangle P_{eq}\langle n_q\rangle = \langle n_q+1\rangle$$

Phonon scattering

Real emission ("in")

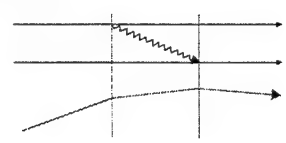

Virtual emission ("out")

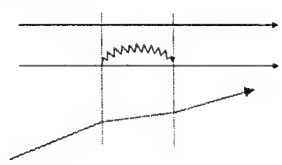

Multiple scattering

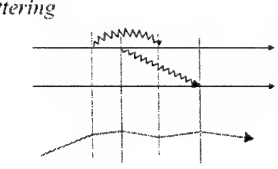

Intracollisional field effect, interference with potential scattering, ...

MONTE CARLO

Multiplicity of Wigner paths

Each multiple path can be obtained with different diagrams

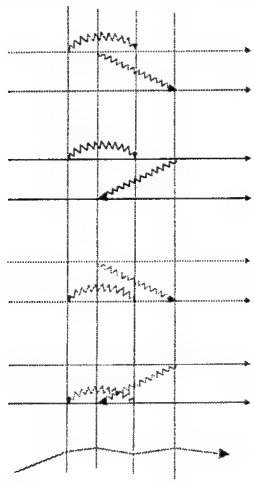

Each graph contributes with a factor

$$e^{i(qr_{ij}-\omega t_{ij})}$$

Summing up all terms, the contribution becomes

$$2\cos(qr_{ij}-\omega t_{ij})2\cos(q'r_{kl}-\omega' t_{kl}) \rightarrow 2^n \prod \cos$$

Potential step – one phonon scattering

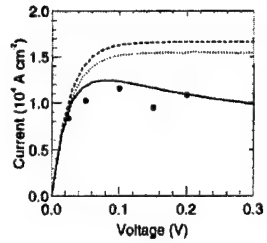

Double barrier – one phonon scattering

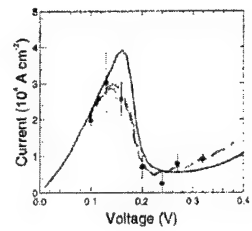

Quantum self-scattering

IN STRICT FORMAL ANALOGY WITH SELF SCATTERING IN SEMICLASSICAL TRANSPORT SIMULATION

Define:

$$\tilde{f}_w\left(\boldsymbol{r},\boldsymbol{p},\{n_q\},\{n'_q\},t\right)=e^{\Gamma(t-t_0)}f_w$$

By substitution into the dynamical equation, an extra term is added to the interaction, proportional to Γ.

Each "free flight" in the Wigner paths is multiplied by a factor

$$e^{-\Gamma(t_i-t_j)}$$

corresponding to an approximate constant life-time of the electron state (imaginary part of the self energy).

At each "scattering event" a choice is made between self or actual scattering, thus correcting, at each order, the approximate self energy with the exact one.

TWO-TIME WIGNER FUNCTION

$\rho(\mathbf{r}_1,t_1;\mathbf{r}_2,t_2)$

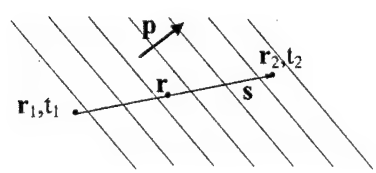

$$\boldsymbol{r}=\frac{\boldsymbol{r}_1+\boldsymbol{r}_2}{2} \qquad \boldsymbol{s}=\boldsymbol{r}_2-\boldsymbol{r}_1$$

$$t=\frac{t_1+t_2}{2} \qquad \tau=t_2-t_1$$

$$f_w(\boldsymbol{r},\boldsymbol{p},\omega,t)=$$
$$=\int d\tau\, e^{i\omega\tau}\int d\boldsymbol{s}\, e^{-i\boldsymbol{p}\boldsymbol{s}/\hbar}\langle \boldsymbol{r}+\boldsymbol{s}/2|\Psi(t+\tau/2)\rangle\langle\Psi(t-\tau/2)|\boldsymbol{r}-\boldsymbol{s}/2\rangle$$

TWO-TIME WIGNER F. WITH PHONONS (1)

$$G^<(\boldsymbol{r}_1,t_1;\boldsymbol{r}_2,t_2)=\frac{i}{\hbar}\langle\Psi^\dagger(\boldsymbol{r}_2,t_2)\Psi(\boldsymbol{r}_1,t_1)\rangle$$

$$=\frac{i}{\hbar}\overline{\langle\Phi(t_2)|\Psi^\dagger(\boldsymbol{r}_2)U(t_2,t_1)\Psi(\boldsymbol{r}_1)|\Phi(t_1)\rangle}$$

$$\Phi(\boldsymbol{r},\{n_q\},t)=\langle\boldsymbol{r},\{n_q\}|\Phi(t)\rangle$$

$$\mathbb{H}=\mathbb{H}_e+\mathbb{H}_p+\mathbb{H}_{ep}$$

$$G^<=\frac{i}{\hbar}\overline{\sum_{\{n_q\}}\sum_{\{n'_q\}}\langle 0,\{n_q\}|e^{-i\mathbb{H}_p(t_2-t_1)/\hbar}|0,\{n'_q\}\rangle\Phi^*(\boldsymbol{r}_2,\{n_q\},t_2)\Phi(\boldsymbol{r}_1,\{n'_q\},t_1)}$$

$$=\frac{i}{\hbar}\sum_{\{n_q\}}e^{-i\omega_p(t_2-t_1)}\Phi^*(\boldsymbol{r}_2,\{n_q\},t_2)\Phi(\boldsymbol{r}_1,\{n_q\},t_1)$$

Put

$$g(\boldsymbol{r},\{n_q\},t)=e^{i\omega(\{n_q\})t}\Phi(\boldsymbol{r},\{n_q\},t)$$

Then

$$G^<(\boldsymbol{r}_1,t_1;\boldsymbol{r}_2,t_2)=\frac{i}{\hbar}\overline{\sum_{\{n_q\}}g^*(\boldsymbol{r}_2,\{n_q\},t_2)g(\boldsymbol{r}_1,\{n_q\},t_1)}$$

TWO-TIME WIGNER F. WITH PHONONS (2)

Performe traditional transformation:

$$t=\frac{t_1+t_2}{2},\quad \tau=t_2-t_1\quad \boldsymbol{r}=\frac{\boldsymbol{r}_1+\boldsymbol{r}_2}{2},\quad \boldsymbol{r}'=\boldsymbol{r}_2-\boldsymbol{r}_1$$

and Fourier transform:

$$f_w(\boldsymbol{r},\boldsymbol{p},t,\omega)=-i\hbar G^<(\boldsymbol{r},\boldsymbol{p},t,\omega)=\sum_{\{n_q\}}\int_{-\infty}^{\infty}e^{i\boldsymbol{p}\boldsymbol{r}'/\hbar}d\boldsymbol{r}'$$

$$\int_{-\infty}^{\infty}e^{-i\omega\tau}d\tau\,\overline{g(\boldsymbol{r}-\boldsymbol{r}'/2,\{n_q\},t-\tau/2)g^*(\boldsymbol{r}+\boldsymbol{r}'/2,\{n_q\},t+\tau/2)}$$

For dynamical equation generalize to non diagonal phonon states:

$$f_w(\boldsymbol{r},\boldsymbol{p},\{n_q\},\{n'_q\},t,\omega)=\int_{-\infty}^{\infty}e^{i\boldsymbol{p}\boldsymbol{r}'/\hbar}d\boldsymbol{r}'$$

$$\int_{-\infty}^{\infty}e^{-i\omega\tau}d\tau\,\overline{g(\boldsymbol{r}-\boldsymbol{r}'/2,\{n_q\},t-\tau/2)g^*(\boldsymbol{r}+\boldsymbol{r}'/2,\{n'_q\},t+\tau/2)}$$

and

$$f_w(\boldsymbol{r},\boldsymbol{p},t,\omega)=\sum_{\{n_q\}}f_w(\boldsymbol{r},\boldsymbol{p},\{n_q\},\{n_q\},t,\omega)$$

TWO-TIME WIGNER F. WITH PHONONS (3)

Dynamical equation

$$\frac{\partial}{\partial t}f_w(\boldsymbol{r},\boldsymbol{p},\{n_q\},\{n'_q\},t,\omega)=\int_{-\infty}^{\infty}e^{i\boldsymbol{p}\boldsymbol{r}'/\hbar}d\boldsymbol{r}'$$

$$\int_{-\infty}^{\infty}e^{-i\omega\tau}d\tau\overline{\left\{\left[\frac{\partial}{\partial t}g(\boldsymbol{r}-\boldsymbol{r}'/2,\{n_q\},t-\tau/2)\right]g^*(\boldsymbol{r}+\boldsymbol{r}'/2,\{n'_q\},t+\tau/2)+g\frac{\partial}{\partial t}g^*\right\}}$$

$$\frac{\partial}{\partial t}g(\boldsymbol{r},\{n_q\},t)=i\omega(\{n_q\})g+\frac{1}{i\hbar}\mathbb{H}g$$

If

$$\mathbb{H}=\mathbb{H}_e+\mathbb{H}_p+\mathbb{H}_{ep}$$

with

$$\mathbb{H}_p=\sum_q\mathbb{b}_q^\dagger\mathbb{b}_q\hbar\omega_q$$

then

$$\frac{\partial}{\partial t}g(\boldsymbol{r},\{n_q\},t)=i\omega(\{n_q\})g+\frac{1}{i\hbar}(\mathbb{H}_e+\mathbb{H}_p+\mathbb{H}_{ep})g$$

$$=\cancel{i\omega(\{n_q\})g}+\frac{1}{i\hbar}(\mathbb{H}_e+\mathbb{H}_{ep})g+\cancel{\frac{1}{i\hbar}\hbar\omega(\{n_q\})g}$$

<u>Thus the free-phonon dynamics is eliminated</u>

TWO-TIME WIGNER F. WITH PHONONS (4)

The various terms in the dynamical equations are treated as in the standard case:

$$\mathbb{H}_o=-\frac{\hbar^2}{2m}\nabla^2$$

yelds

$$\left.\frac{\partial}{\partial t}\right|_o f_w(\boldsymbol{r},\boldsymbol{p},\{n_q\},\{n'_q\},t,\omega)=-\frac{\boldsymbol{p}}{m}\nabla_r f_w$$

$$\mathbb{V}=V(\boldsymbol{r})$$

yelds

$$\left.\frac{\partial}{\partial t}\right|_V f_w(\boldsymbol{r},\boldsymbol{p},\{n_q\},\{n'_q\},t,\omega)$$

$$=\int_{-\infty}^{\infty}d\boldsymbol{p}'V_w(\boldsymbol{r},\boldsymbol{p}-\boldsymbol{p}')f_w(\boldsymbol{r},\boldsymbol{p}',\{n_q\},\{n'_q\},t,\omega)$$

where

$$V_w(\boldsymbol{r},\boldsymbol{p})=\frac{1}{i\hbar}\frac{1}{(2\pi\hbar)^3}\int d\boldsymbol{r}'e^{i\boldsymbol{p}\boldsymbol{r}'/\hbar}\left[V(\boldsymbol{r}-\boldsymbol{r}'/2)-V(\boldsymbol{r}+\boldsymbol{r}'/2)\right]$$

For a constant or harmonic force F

$$\left.\frac{\partial}{\partial t}\right|_F f_w(\boldsymbol{r},\boldsymbol{p},\{n_q\},\{n'_q\},t,\omega)=-\boldsymbol{F}\frac{\partial}{\partial\boldsymbol{p}}f_w$$

TWO-TIME WIGNER F. WITH PHONONS (5)

Taking into account that

$$\mathbf{b}_{q'} g\left(\boldsymbol{r}-\boldsymbol{r}'/2,\{n_q\},t-\tau/2\right)$$
$$= e^{i\omega(\{n_q\})(t-\tau/2)}\left\langle \boldsymbol{r}-\boldsymbol{r}'/2,\{n_q\}\right|\mathbf{b}_{q'}\left|\Psi(t-\tau/2)\right\rangle$$
$$= e^{-i\omega_{q'}(t-\tau/2)}\sqrt{n_{q'}+1}\,g\left(\boldsymbol{r}-\boldsymbol{r}'/2,\{n_1,\ldots,n_{q'}+1,\ldots\},t-\tau/2\right)$$

and similar,

the electron-phonon interaction

$$\mathbb{H}_{ep} = i\hbar\sum_{q'} F(\boldsymbol{q}')\left(\mathbb{b}_{q'}e^{i\boldsymbol{q}'\boldsymbol{r}} - \mathbb{b}^{\dagger}_{q'}e^{-i\boldsymbol{q}'\boldsymbol{r}}\right)$$

yields

$$\left.\frac{\partial}{\partial t}\right|_{ep} f_w\left(\boldsymbol{r},\boldsymbol{p},\{n_q\},\{n'_q\},t,\omega\right) = \sum_{q'} F(\boldsymbol{q}')\Big\{$$
$$e^{i(\boldsymbol{q}'\boldsymbol{r}-\omega_{q'}t)}\sqrt{n_{q'}+1}\,f_w\left(\boldsymbol{r},\boldsymbol{p}-\hbar\boldsymbol{q}'/2,\{n_1,\ldots,n_{q'}+1,\ldots\},\{n'_q\},t,\omega-\omega_{q'}/2\right)$$
$$-e^{-i(\boldsymbol{q}'\boldsymbol{r}-\omega_{q'}t)}\sqrt{n_{q'}}\,f_w\left(\boldsymbol{r},\boldsymbol{p}+\hbar\boldsymbol{q}'/2,\{n_1,\ldots,n_{q'}-1,\ldots\},\{n'_q\},t,\omega+\omega_{q'}/2\right)$$
$$+e^{-i(\boldsymbol{q}'\boldsymbol{r}-\omega_{q'}t)}\sqrt{n'_{q'}+1}\,f_w\left(\boldsymbol{r},\boldsymbol{p}-\hbar\boldsymbol{q}'/2,\{n_q\},\{n'_1,\ldots,n'_{q'}+1,\ldots\},t,\omega-\omega_{q'}/2\right)$$
$$-e^{i(\boldsymbol{q}'\boldsymbol{r}-\omega_{q'}t)}\sqrt{n'_{q'}}\,f_w\left(\boldsymbol{r},\boldsymbol{p}+\hbar\boldsymbol{q}'/2,\{n_q\},\{n'_1,\ldots,n'_{q'}-1,\ldots\},t,\omega+\omega_{q'}/2\right)\Big\}$$

TWO-TIME WIGNER F. WITH PHONONS (6)

The general equantion

$$\frac{\partial}{\partial t} f_w\left(\boldsymbol{r},\boldsymbol{p},\{n_q\},\{n'_q\},t,\omega\right) + \frac{\boldsymbol{p}}{m}\frac{\partial}{\boldsymbol{r}} f_w + \boldsymbol{F}\frac{\partial}{\partial \boldsymbol{p}} f_w = \left.\frac{\partial f_w}{\partial t}\right|_{v} + \left.\frac{\partial f_w}{\partial t}\right|_{ep}$$

here

$$\left.\frac{\partial}{\partial t}\right|_{v} f_w\left(\boldsymbol{r},\boldsymbol{p},\{n_q\},\{n'_q\},t,\omega\right) = \int d\boldsymbol{p}'\,V_w(\boldsymbol{r},\boldsymbol{p}-\boldsymbol{p}')\,f_w\left(\boldsymbol{r},\boldsymbol{p}',\{n_q\},\{n'_q\},t,\omega\right)$$
$$V_w(\boldsymbol{r},\boldsymbol{p}) = \frac{1}{i\hbar}\frac{1}{(2\pi\hbar)^3}\int d\boldsymbol{r}'e^{i\boldsymbol{p}\boldsymbol{r}'/\hbar}\left[V(\boldsymbol{r}-\boldsymbol{r}'/2)-V(\boldsymbol{r}+\boldsymbol{r}'/2)\right]$$

and

$$\left.\frac{\partial}{\partial t}\right|_{ep} f_w\left(\boldsymbol{r},\boldsymbol{p},\{n_q\},\{n'_q\},t,\omega\right) = \sum_{q'} F(\boldsymbol{q}')\Big\{$$
$$e^{i(\boldsymbol{q}'\boldsymbol{r}-\omega_{q'}t)}\sqrt{n_{q'}+1}\,f_w\left(\boldsymbol{r},\boldsymbol{p}-\hbar\boldsymbol{q}'/2,\{n_1,\ldots,n_{q'}+1,\ldots\},\{n'_q\},t,\omega-\omega_{q'}/2\right)$$
$$-e^{-i(\boldsymbol{q}'\boldsymbol{r}-\omega_{q'}t)}\sqrt{n_{q'}}\,f_w\left(\boldsymbol{r},\boldsymbol{p}+\hbar\boldsymbol{q}'/2,\{n_1,\ldots,n_{q'}-1,\ldots\},\{n'_q\},t,\omega+\omega_{q'}/2\right)$$
$$+e^{-i(\boldsymbol{q}'\boldsymbol{r}-\omega_{q'}t)}\sqrt{n'_{q'}+1}\,f_w\left(\boldsymbol{r},\boldsymbol{p}-\hbar\boldsymbol{q}'/2,\{n_q\},\{n'_1,\ldots,n'_{q'}+1,\ldots\},t,\omega-\omega_{q'}/2\right)$$
$$-e^{i(\boldsymbol{q}'\boldsymbol{r}-\omega_{q'}t)}\sqrt{n'_{q'}}\,f_w\left(\boldsymbol{r},\boldsymbol{p}+\hbar\boldsymbol{q}'/2,\{n_q\},\{n'_1,\ldots,n'_{q'}-1,\ldots\},t,\omega+\omega_{q'}/2\right)$$

- The left hand side of the above equation is the same Liouvillian as in the Boltzann equation
- Path variables and integral form of the transport equation
- Neumann expansion
- Wigner Paths
- Monte Carlo

- At each interaction "vertex" half phonon momentum and half phonon energy is trasferred to or taken from the electron

Spectral Density
A(p,ω)=fw(p,ω)/fw(p)

GaAs
Polar optical phonons
T=300 K
up to 3 scattering
t=150 fs

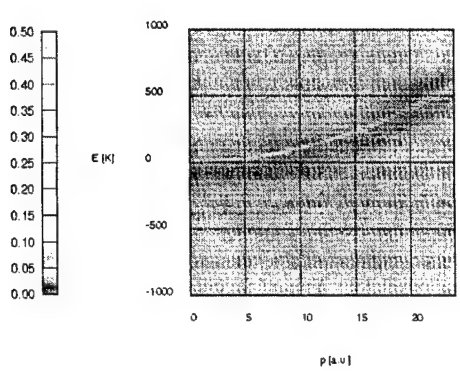

Conclusions

The Wigner-function approach allows a description of quantum transport in terms of phase-space analogous to the semiclassical case

Wigner paths can be defined as ballistic "flights" separated by scattering processes

A Monte Carlo algorithm can be implemented that accounts for given initial and boundary conditions

Momentum and frequency can be considered as independent variables in a two-time Green function approach, maintaining the path Monte Carlo approach

PROBLEMS ...

Modeling Resonant Tunneling Devices With Wigner Functions and Density Matrices

H. L. Grubin
Scientific Research Associates, Inc
hal@srassoc.com

- Collaborators:
  R.C. Buggeln and J. P. Kreskovsky
- Supported by Office of Naval Research

Quantum Transport RTD Studies

- Use Wigner Function (primarily) and Density Matrix to describe ***transient*** transport in nanoscale devices
- Go beyond using switching speed as a primary characteristic of a device. Instead we also determine the ***recovery*** time.
- We do this within the framework of an RTD as a self-excited sustained relaxation oscillator (RTD/RO) and seek the highest frequency of oscillation.

Simulation Requirements

- Suitable transient quantum transport equation—Wigner equation/Density Matrix
- Poisson's equation + flat band boundary conditions
- Circuit equations/transmission line equations—treated as boundary conditions
- Suitable description of reservoirs and dissipation

WF/DM Equation

- Can be obtained in simple cases directly from Schrodinger's equation or formally as follows:

Density Operator

$$\rho_{op}(t) = \sum_i |i(t)> P(i) < i(t)|$$

Single time
Density Operator

Density Operator

$$\rho_{op}(t) = \sum_i |i(t)> P(i) < i(t)|$$

Coordinate representation

$$<\mathbf{x}|\rho_{op}(t)|\mathbf{x}'> = \sum_i <\mathbf{x}|i(t)> P(i) < i(t)|\mathbf{x}'>$$

$$= \sum_i P(i)\Psi_i^*(\mathbf{x}',t)\Psi_i(\mathbf{x},t)$$

SRA
Nanostructures & Transients

Time Dependence/Liouville Eq.

$$i\hbar \frac{d\rho_{op}(t)}{dt} = \left[H(t), \rho_{op}(t)\right]$$

$$i\hbar \frac{\partial <\mathbf{x}|\rho(t)|\mathbf{x}'>}{\partial t}$$

$$= \left\{ -\frac{\hbar^2}{2m}\left(\frac{\partial^2}{\partial \mathbf{x}^2} - \frac{\partial^2}{\partial \mathbf{x}'^2}\right) + V(\mathbf{x}) - V(\mathbf{x}') \right\} <\mathbf{x}|\rho(t)|\mathbf{x}'>$$

dissipation $\longrightarrow + i\hbar \left\{ \frac{\partial <\mathbf{x}|\rho|\mathbf{x}'>}{\partial t} \right\}_{\text{scattering}}$

SRA
Nanostructures & Transients

Density & Current Density Matrix

$$\rho(\mathbf{x},\mathbf{x}') = <\mathbf{x}|\rho_{op}(t)|\mathbf{x}'>$$

Density $\rho(\mathbf{x}) = <\mathbf{x}|\rho_{op}(t)|\mathbf{x}>$

$$\mathbf{j}(\mathbf{x},\mathbf{x}') = \frac{\hbar}{2mi}(\nabla_{\mathbf{x}} - \nabla_{\mathbf{x}'}) <\mathbf{x}|\rho_{op}(t)|\mathbf{x}'>$$

Current Density $\mathbf{j}(\mathbf{x}) = \lim_{\mathbf{x} \to \mathbf{x}'} \mathbf{j}(\mathbf{x},\mathbf{x}')$

SRA
Nanostructures & Transients

Density Matrix Flat Profile

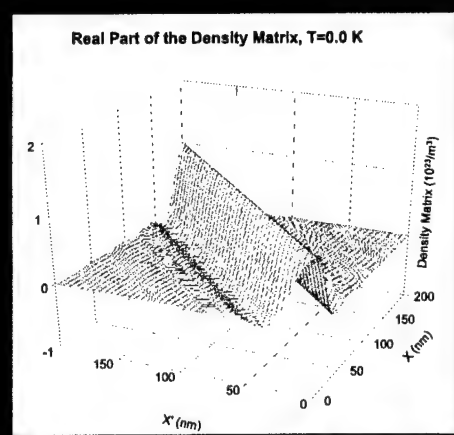

SRA
Nanostructures & Transients

Density Matrix Hetero-structure

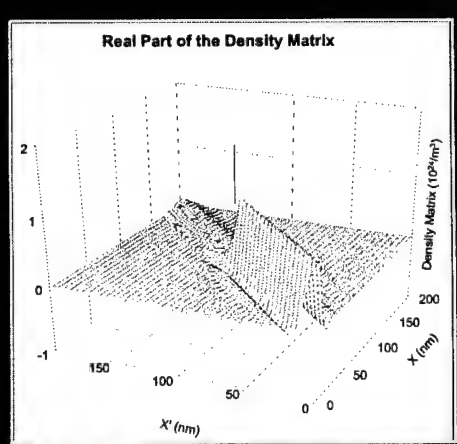

SRA
Nanostructures & Transients

Real Part Flat Profile, 300K

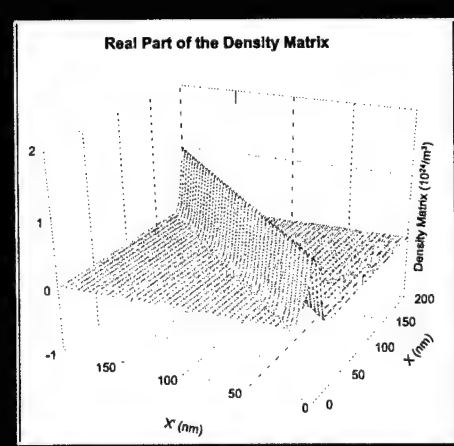

SRA
Nanostructures & Transients

Imag. Part Flat Profile, 300K

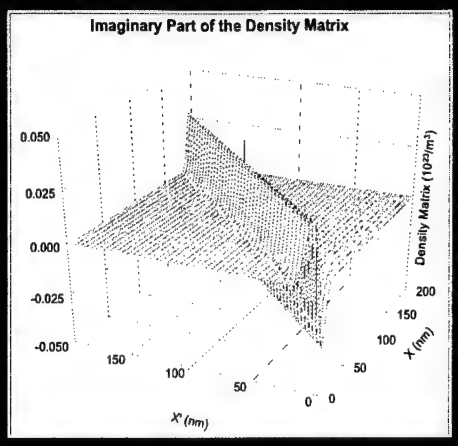

SRA
Nanostructures & Transients

IV Double Barrier RTD

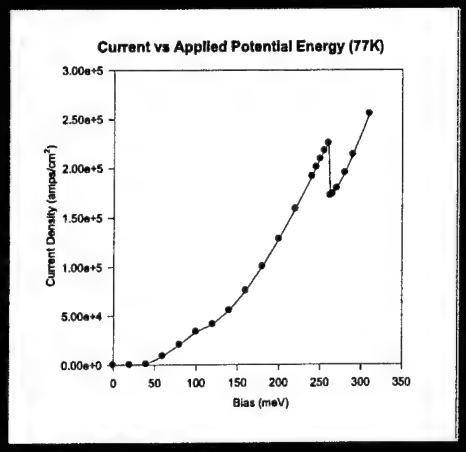

SRA
Nanostructures & Transients

What do we do with the RTD?

- Switching device!
  - There are many of these
- Logic device-particularly multiple value logic elements
- Quantum Van der Pol oscillator
  - Negative differential resistance can (sometimes) yield sustained oscillations.

SRA
Nanostructures & Transients

RTD as a Relaxation Oscillator:

(Verghese, C. D. Parker, E.R. Brown APL 1998)

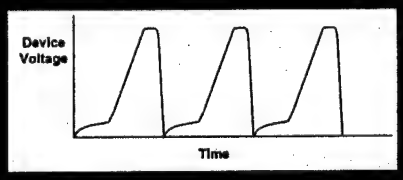

Transmission Line

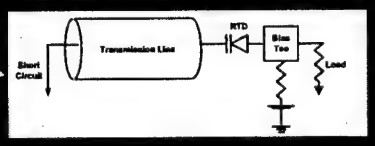

SRA
Nanostructures & Transients

Quantum Van der Pol Oscillator

- It should be of interest to physicists because it is capable of providing a practical measure of the speed and response time of resonant tunneling diode.
  - How?
    - Determine the maximum frequency of a controlled oscillation that can ***drive or affect*** the total system
    - Use the RTD/RO as a clock.

SRA
Nanostructures & Transients

There are non-Van der Pol Oscillations

- We have observed weak (above threshold) voltage oscillations at frequencies near 700 GHz!

SRA
Nanostructures & Transients

We will concentrate on the Wigner Function

- More success than with using the DM.
- Not as fast as the DM.

Wigner Function/Equation from the Density Matrix through the Weyl Transformation

$$f_W(\mathbf{k},\mathbf{r}) = \frac{1}{2}\int d\mathbf{s} < \mathbf{r}+\frac{\mathbf{s}}{2} | \rho_{\ldots}(t) | \mathbf{r}-\frac{\mathbf{s}}{2} > \exp -i\mathbf{k}\bullet\mathbf{s}$$

The Wigner Equation

Transient — Dissipation — Diffusion

$$0 = \frac{\partial f_W(\mathbf{k},x)}{\partial t} + \frac{f_W(\mathbf{k},x) - f_{W0}(\mathbf{k},x)}{\tau(x)} + \frac{\hbar k_x}{m}\frac{\partial f_W(\mathbf{k},x)}{\partial x}$$

$$-\frac{1}{\pi\hbar}\lim_{L\to\infty}\int_{-L}^{L} d\zeta \begin{bmatrix} V(x+\zeta) \\ -V(x-\zeta) \end{bmatrix} \int dk_x' f_W(k_x', k_y, k_z, \eta_t) \sin[2(k_x'-k_x)\zeta]$$

Quantum Mechanics: The Wigner integral represents a correlation of states in the coordinate representation.

The Wigner Integral Treated Analytically-Highlights Correlations

$$\lim_{L\to\infty}\int_{-L}^{L} dy \begin{bmatrix} V(x+y) \\ -V(x-y) \end{bmatrix} \sin[2(k_x'-k_x)y]$$

$$= \frac{2V_0 \sin[2(k_x'-k_x)(x_0-x)]\sin[(k_x'-k_x)\Delta]}{i(k_x'-k_x)}$$

V(x)-V(x') for a single asymmetrically placed barrier

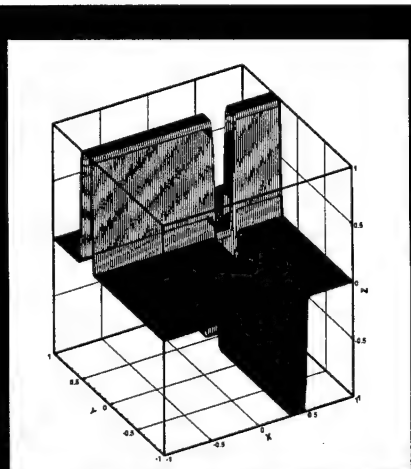

The Five Zone Structure

- Five zone structure:
  - The end regions (two) represent the contact regions;
  - The central region (one)-- incorporates the quantum barriers and wells;
  - The transition region (two)
- Variable scattering time, smallest in contact region.

Device Geometry

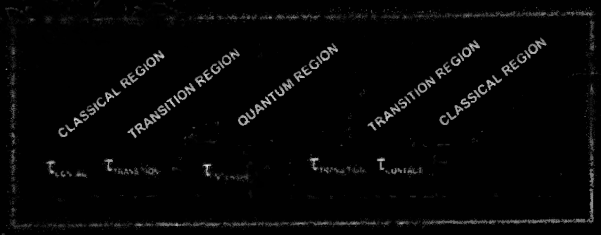

Structure Emphasized
The Baseline Studies

- 200 nm, DBRTD, 250/300mev-5nm-5nm-5nm, low doped central region
- DC and transient studies
- Hysteresis studies
- (Note: In the absence of barriers can compute IV of an NIN structure as well as linear resistor)

Structure Emphasized
The Baseline Study, cont.

- New derivative boundary conditions on Wigner function show flat-band and qualitative displacement momentum contributions.
- Do not need to assert displaced Fermi boundary conditions.
- Equilibrium distribution obtained first.

Structure Emphasized
The Baseline Study, cont.

- Converged dc solutions via small bias increments show ***no hysteresis***!
- Large signal transients show hysteresis.
- Relaxation to steady state occurs within a pico-sec and is bias dependent
- Devices sustain steady relaxation oscillations!

Wigner Function NIN

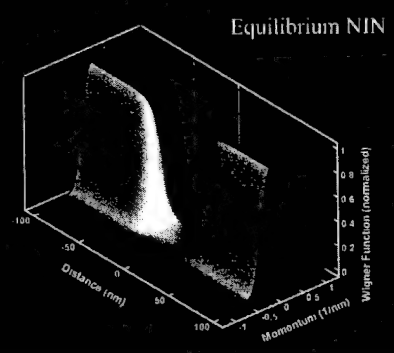

Wigner Function RTD

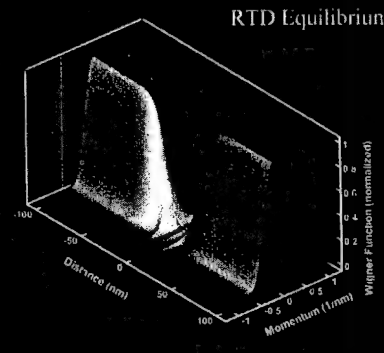

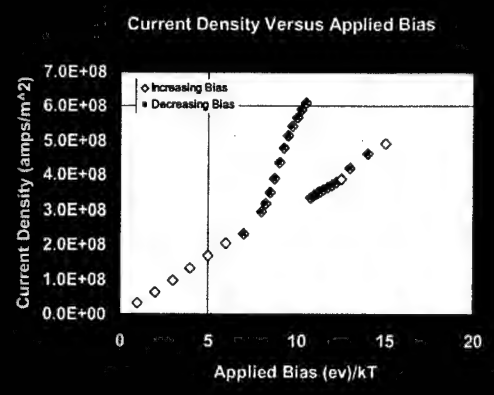

SRA
Nanostructures & Transients

RTD as a Relaxation Oscillator

(Lumped Circuit Elements, RTD Represented by Wigner Equation)

Wigner Equation Represents the RTD

Realistic Device Response

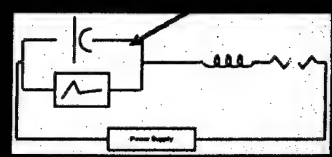

SRA
Nanostructures & Transients

RO Equations

$$\frac{dv_D}{dt} = \frac{2\pi Z_0}{R_D}\left\{i(t) - i_D(v_D)\right\}$$

$$\frac{di}{dt} = \frac{R_D}{2\pi Z_0}\left\{v_{APPLIED}(t) - v_D(t) + i(t)\frac{R_{LOAD}}{R_D}\right\}$$

SRA
Nanostructures & Transients

RO Equations

$$\frac{dv_D}{dt} = \frac{2\pi Z_0}{R_D}\left\{i(t) - i_D(v_D)\right\}$$

$$\frac{di}{dt} = \frac{R_D}{2\pi Z_0}\left\{v_{APPLIED}(t) - v_D(t) + i(t)\frac{R_{LOAD}}{R_D}\right\}$$

$$v_D = V_D / V_P, \quad i = I / I_P, \quad t = \tau / T_{ref}$$

SRA
Nanostructures & Transients

RO Equations

$$\frac{dv_D}{dt} = \frac{2\pi Z_0}{R_D}\left\{i(t) - i_D(v_D)\right\}$$

$$\frac{di}{dt} = \frac{R_D}{2\pi Z_0}\left\{v_{APPLIED}(t) - v_D(t) + i(t)\frac{R_{LOAD}}{R_D}\right\}$$

$$v_D = V_D / V_P, \quad i = I / I_P, \quad t = \tau / T_{ref}$$

$$Z_0 = \sqrt{L / C_D}, \; T_{ref} = 2\pi\sqrt{LC_D}, \; R_D = V_P / I_P$$

SRA
Nanostructures & Transients

RO Equation Parameters

$$Z_0 = \sqrt{L / C_D}$$
$$T_{ref} = 2\pi\sqrt{LC_D}$$
$$R_D = V_P / I_P$$

Observation: For a fixed Z, oscillation characteristics are the same for all oscillatory periods provided the NDR is not dynamic.

SRA
Nanostructures & Transients

RO at 11.5 GHz: Total Current Density and Potential Energy Drop

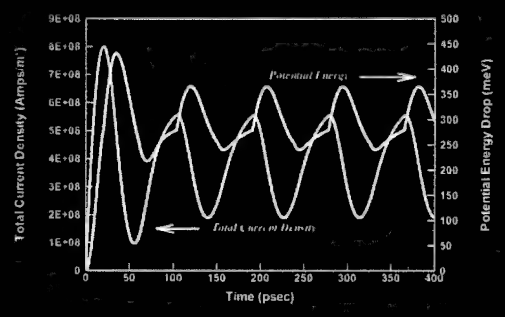

SRA
Nanostructures & Transients

RO at 11.5 GHz: Particle Current Density and Potential Energy Drop

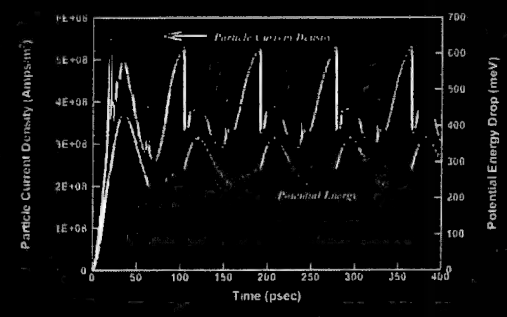

SRA
Nanostructures & Transients

Details of the RO at 11.5 GHz: Particle Current Density and Potential Energy Drop

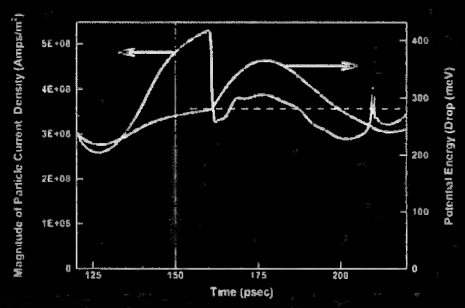

SRA
Nanostructures & Transients

Details of the RO at 11.5 GHz: Particle Current Density and Potential Energy Drop

- First part of the oscillation
  - Linear I versus V, L/R rise time
- Second part of the oscillation
  - Drop in particle current and increase in potential drop
- Third part of the oscillation
  - Decrease in potential drop, particle current remains below values associated with first part of the oscillation

SRA
Nanostructures & Transients

RO at 11.5 GHz: Dynamic 'IV'

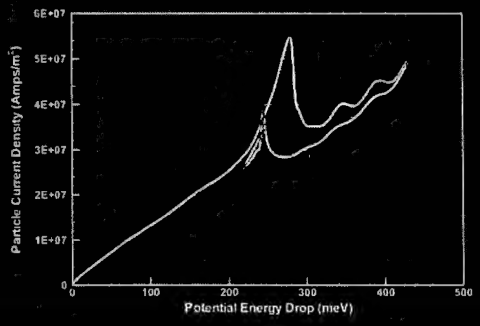

SRA
Nanostructures & Transients

'Temporal Invariance'

When the device oscillates, its characteristics are independent of oscillatory period!

SRA
Nanostructures & Transients

RO at 11.5 GHz: Total Current Density and Potential Energy Drop

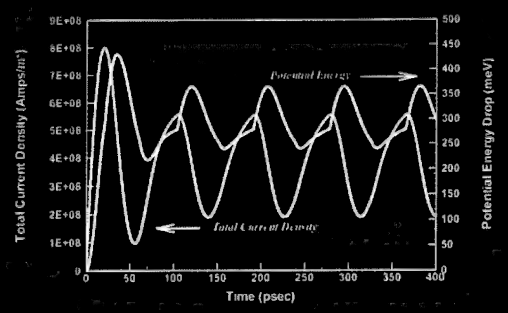

SRA
Nanostructures & Transients

RO at 22.0 GHz: Total Current Density and Potential Energy Drop

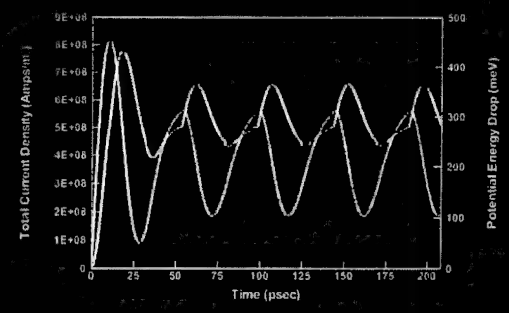

SRA
Nanostructures & Transients

RO at 41.8 GHz: Total Current Density and Potential Energy Drop

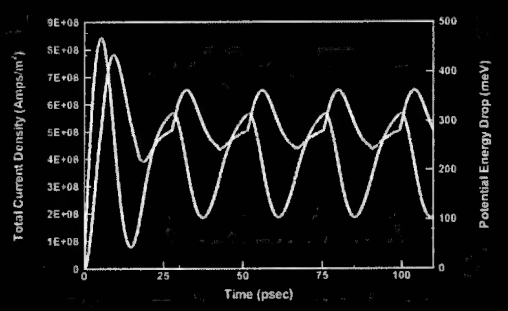

SRA
Nanostructures & Transients

RO at 113.7 GHz: Total Current Density and Potential Energy Drop

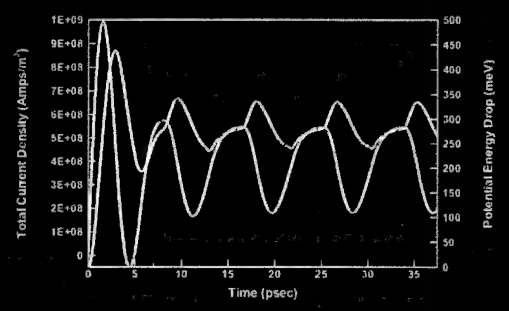

SRA
Nanostructures & Transients

Dynamic 'IV'

SRA
Nanostructures & Transients

RO at 6 GHz: Dynamic 'IV'

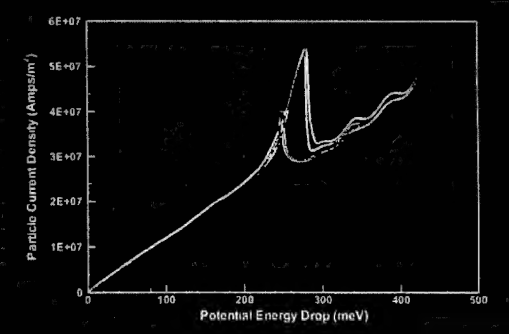

SRA
Nanostructures & Transients

RO at 11.5 GHz: Dynamic 'IV'

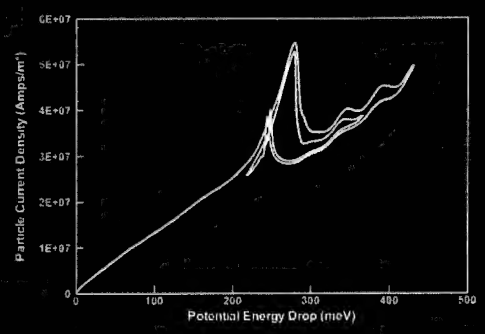

SRA
Nanostructures & Transients

RO at 22.0 GHz: Dynamic 'IV'

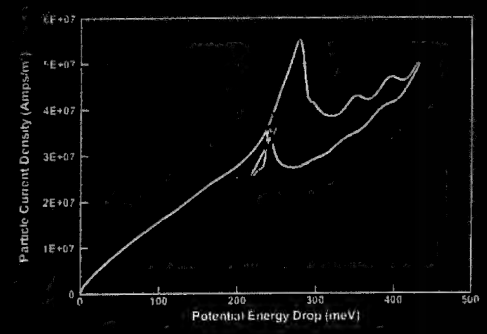

SRA
Nanostructures & Transients

RO at 41.8 GHz: Dynamic 'IV'

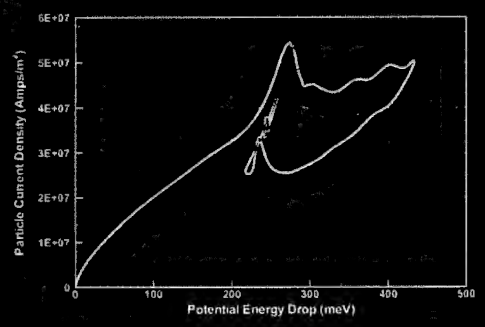

SRA
Nanostructures & Transients

Total and Dynamic 'IV'

SRA
Nanostructures & Transients

RO at 6 GHz: Total and Dynamic 'IV'

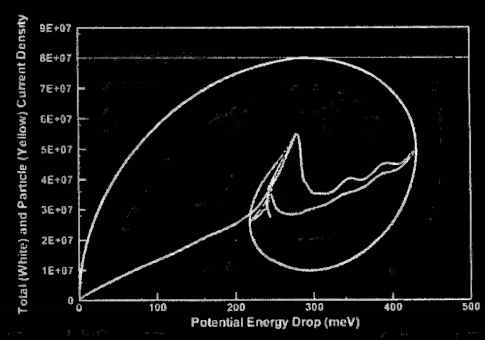

SRA
Nanostructures & Transients

RO at 113.72 GHz: Total and Dynamic 'IV'

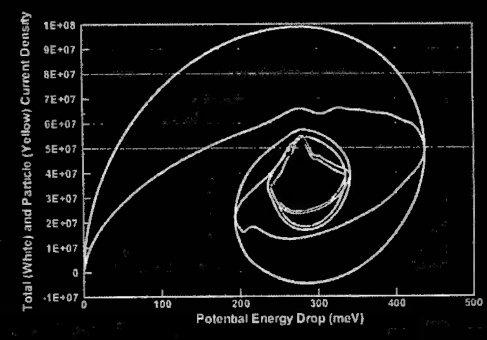

SRA
Nanostructures & Transients

Summary of Charge and Current for the 22.0 GHz RO

SRA
Nanostructures & Transients

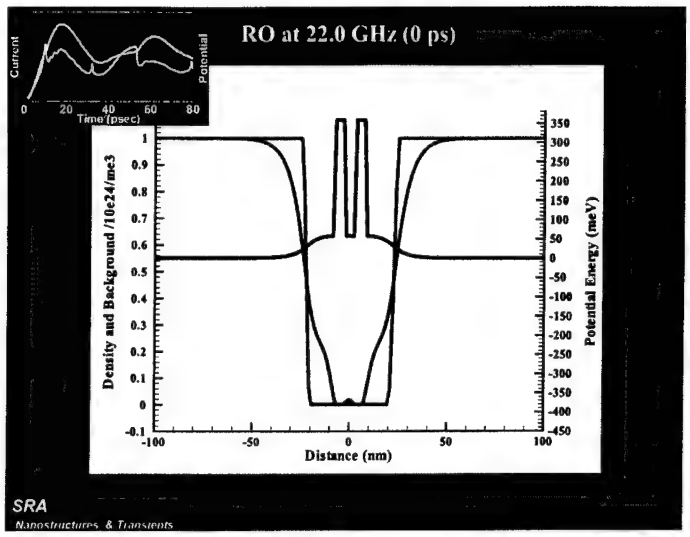

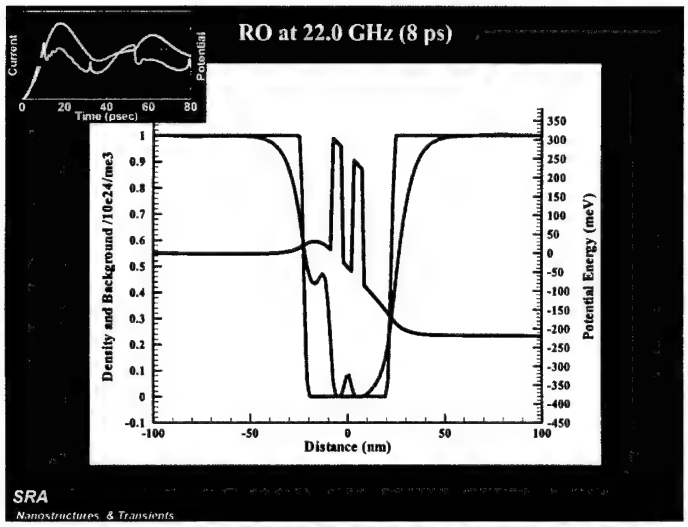

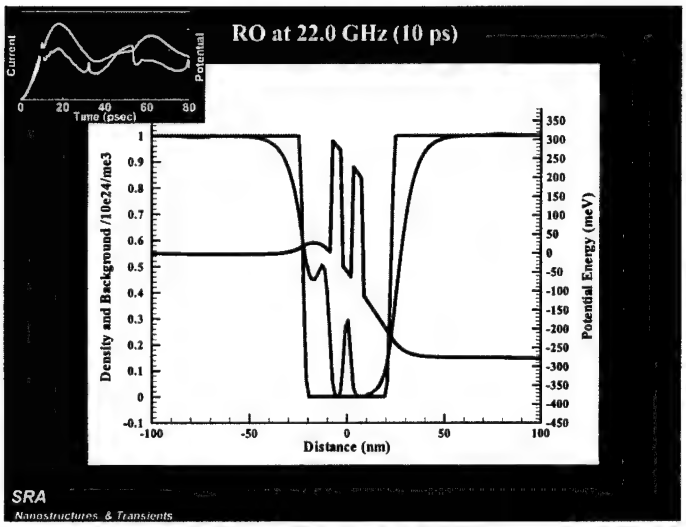

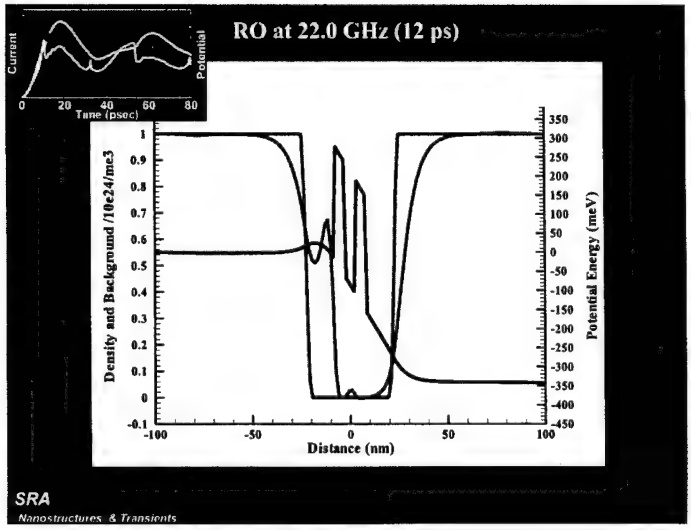

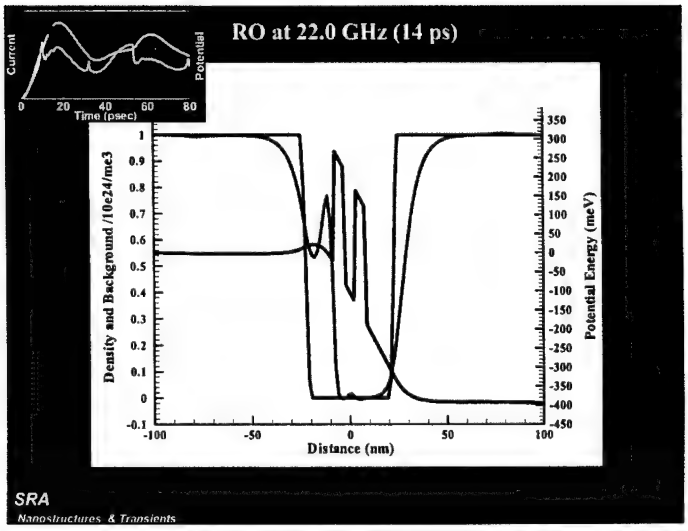

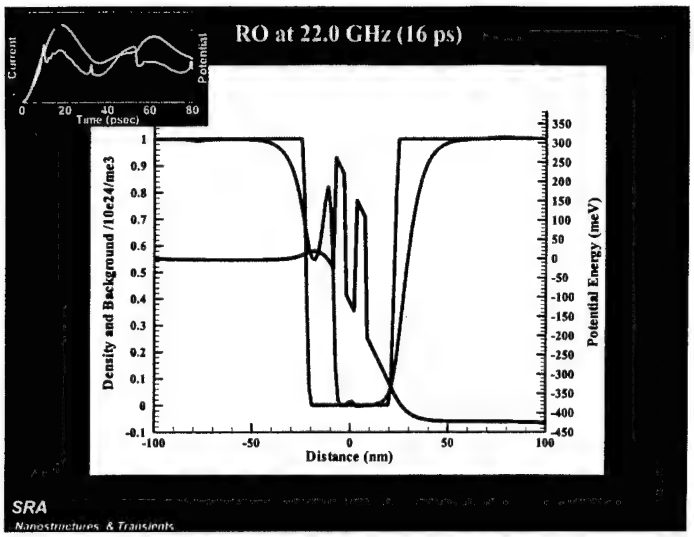
RO at 22.0 GHz (16 ps)
Current
Potential
Time (psec)
Density and Background /10e24/me3
Potential Energy (meV)
Distance (nm)
SRA
Nanostructures & Transients

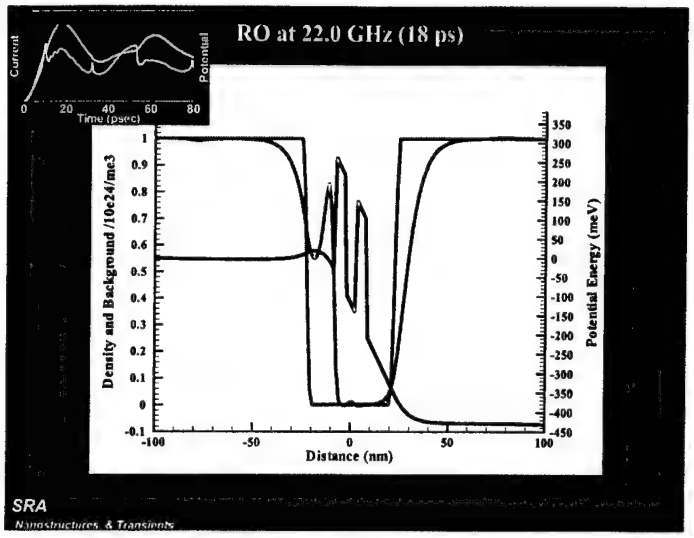
RO at 22.0 GHz (18 ps)
Current
Potential
Time (psec)
Density and Background /10e24/me3
Potential Energy (meV)
Distance (nm)
SRA
Nanostructures & Transients

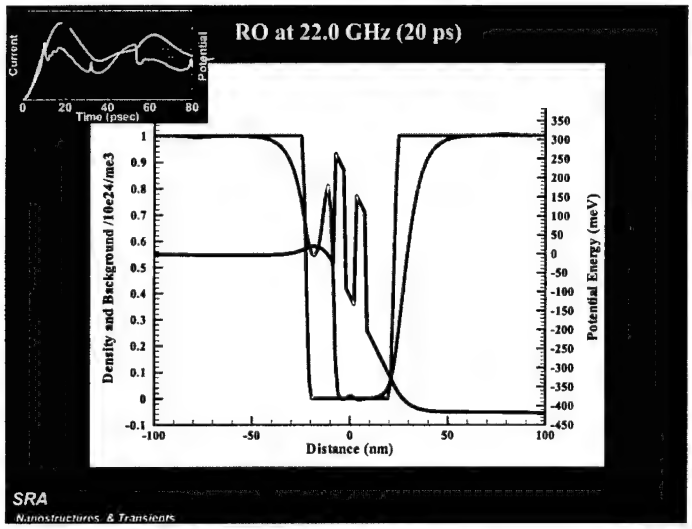
RO at 22.0 GHz (20 ps)
Current
Potential
Time (psec)
Density and Background /10e24/me3
Potential Energy (meV)
Distance (nm)
SRA
Nanostructures & Transients

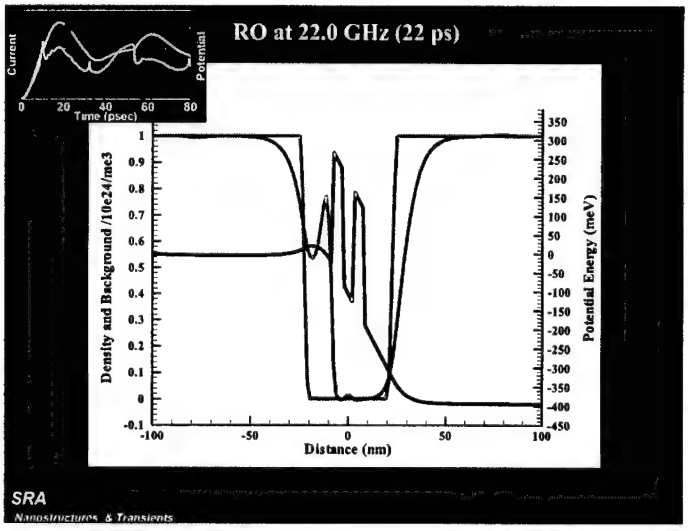
RO at 22.0 GHz (22 ps)
Current
Potential
Time (psec)
Density and Background /10e24/me3
Potential Energy (meV)
Distance (nm)
SRA
Nanostructures & Transients

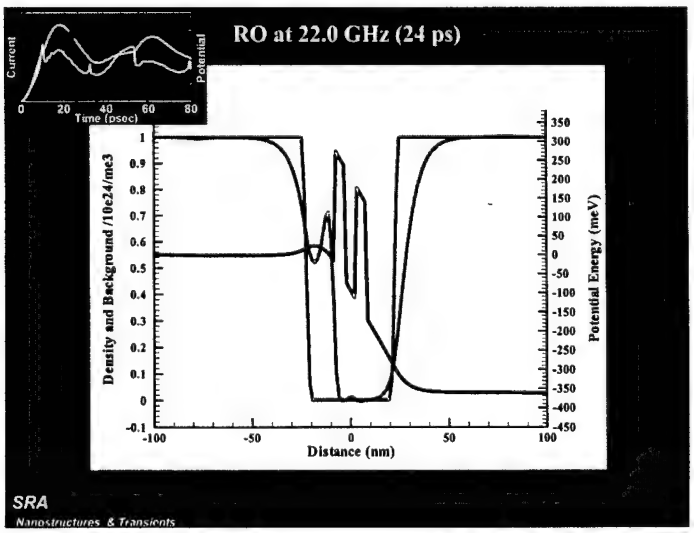
RO at 22.0 GHz (24 ps)
Current
Potential
Time (psec)
Density and Background /10e24/me3
Potential Energy (meV)
Distance (nm)
SRA
Nanostructures & Transients

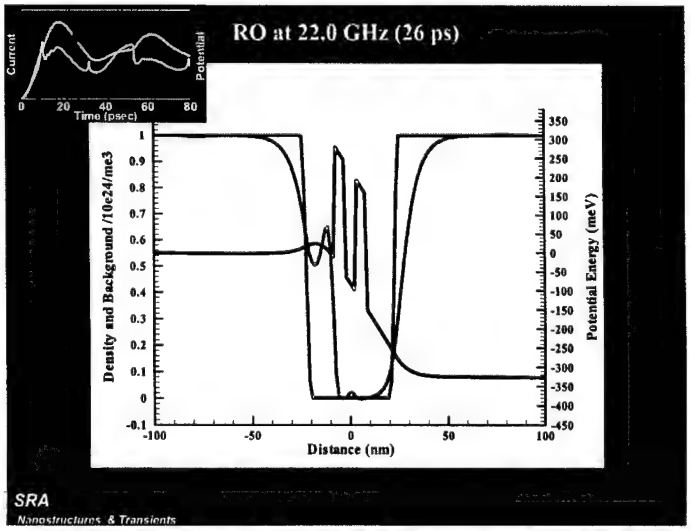
RO at 22.0 GHz (26 ps)
Current
Potential
Time (psec)
Density and Background /10e24/me3
Potential Energy (meV)
Distance (nm)
SRA
Nanostructures & Transients

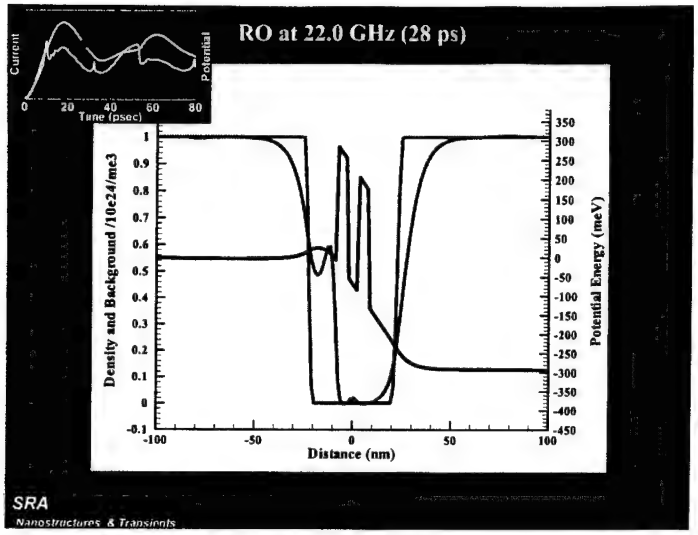
RO at 22.0 GHz (28 ps)
Current
Potential
Time (psec)
Density and Background /10e24/me3
Potential Energy (meV)
Distance (nm)
SRA
Nanostructures & Transients

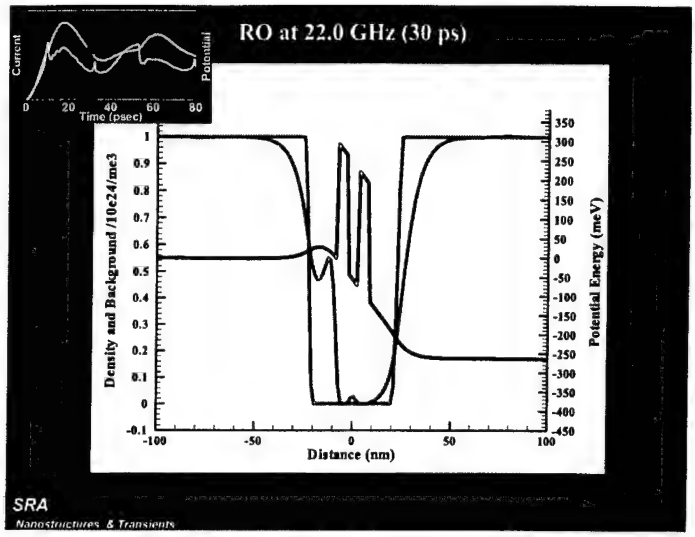
RO at 22.0 GHz (30 ps)
Current
Potential
Time (psec)
Density and Background /10e24/me3
Potential Energy (meV)
Distance (nm)
SRA
Nanostructures & Transients

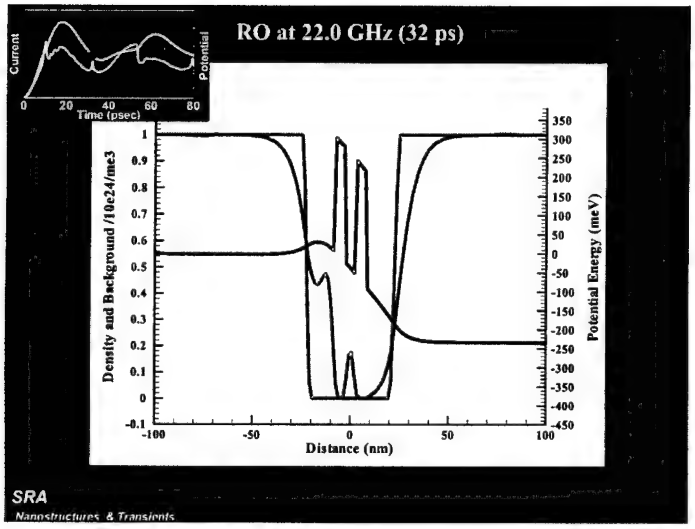
RO at 22.0 GHz (32 ps)
Current
Potential
Time (psec)
Density and Background /10e24/me3
Potential Energy (meV)
Distance (nm)
SRA
Nanostructures & Transients

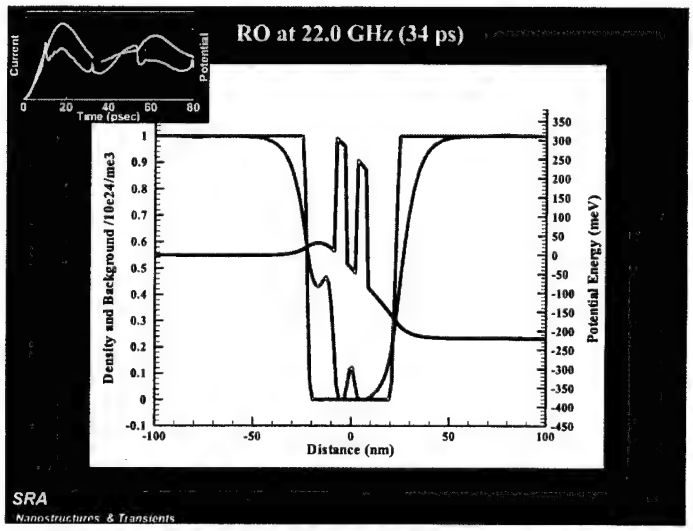
RO at 22.0 GHz (34 ps)
Current
Potential
Time (psec)
Density and Background /10e24/me3
Potential Energy (meV)
Distance (nm)
SRA
Nanostructures & Transients

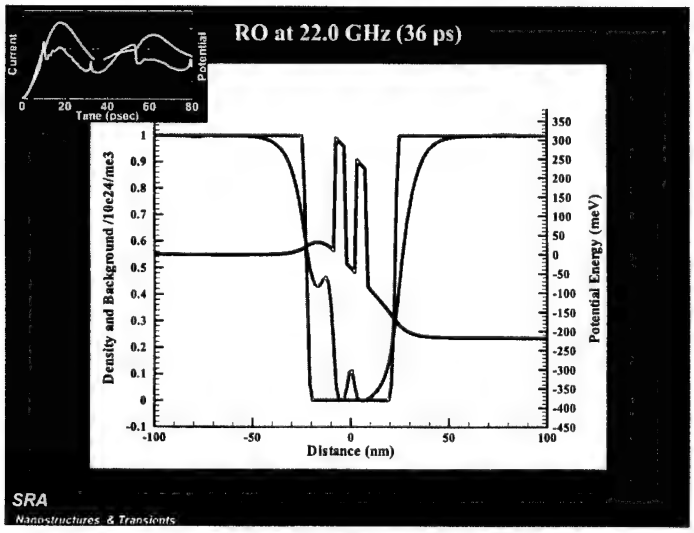
RO at 22.0 GHz (36 ps)
Current
Potential
Time (psec)
Density and Background /10e24/me3
Potential Energy (meV)
Distance (nm)
SRA
Nanostructures & Transients

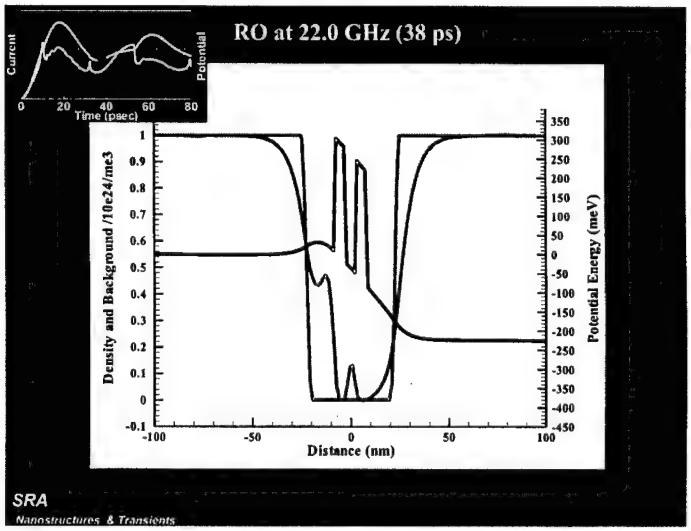
RO at 22.0 GHz (38 ps)
Current
Potential
Time (psec)
Density and Background /10e24/me3
Potential Energy (meV)
Distance (nm)
SRA
Nanostructures & Transients

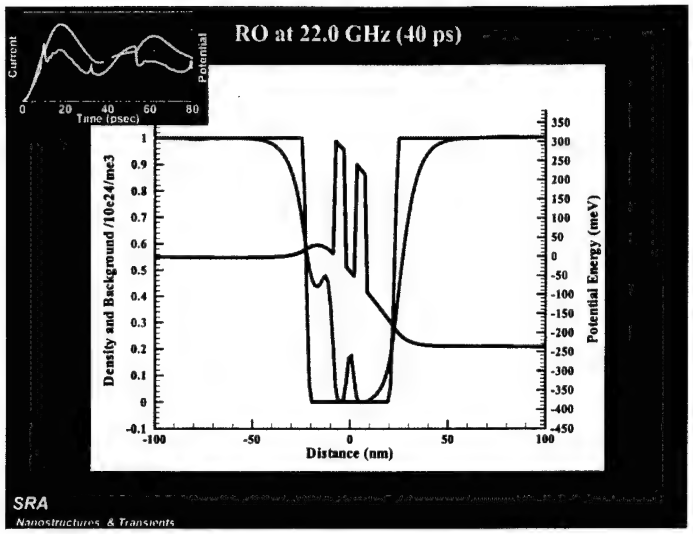
RO at 22.0 GHz (40 ps)
Current
Potential
Time (psec)
Density and Background /10e24/me3
Potential Energy (meV)
Distance (nm)
SRA
Nanostructures & Transients

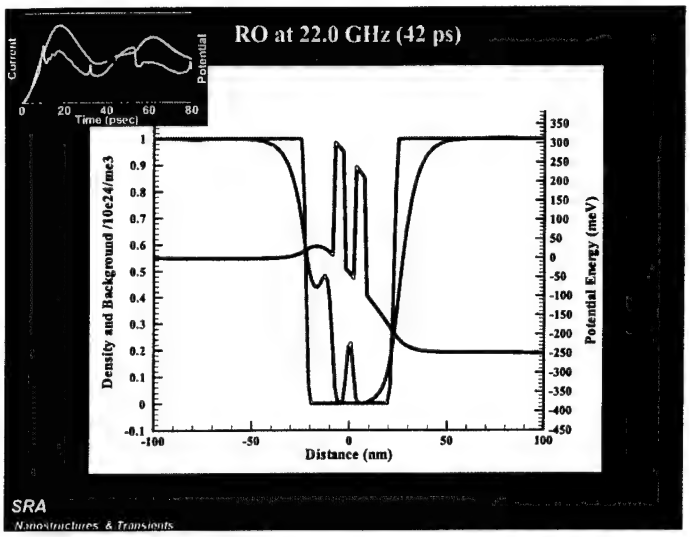
RO at 22.0 GHz (42 ps)
Current
Potential
Time (psec)
Density and Background /10e24/me3
Potential Energy (meV)
Distance (nm)
SRA
Nanostructures & Transients

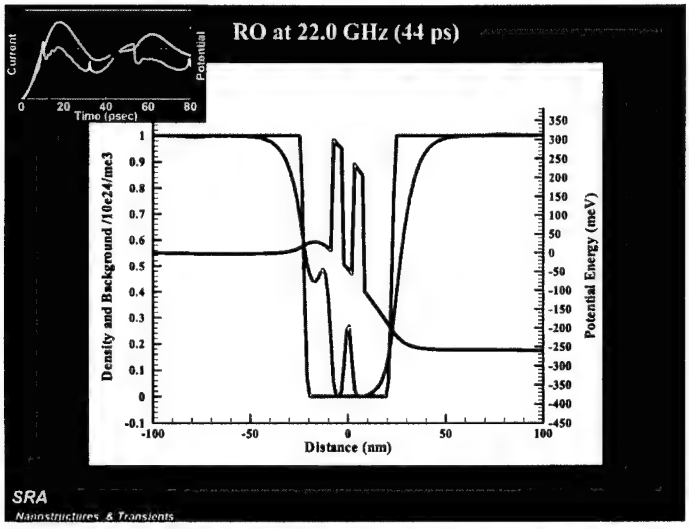
RO at 22.0 GHz (44 ps)
Current
Potential
Time (psec)
Density and Background /10e24/me3
Potential Energy (meV)
Distance (nm)
SRA
Nanostructures & Transients

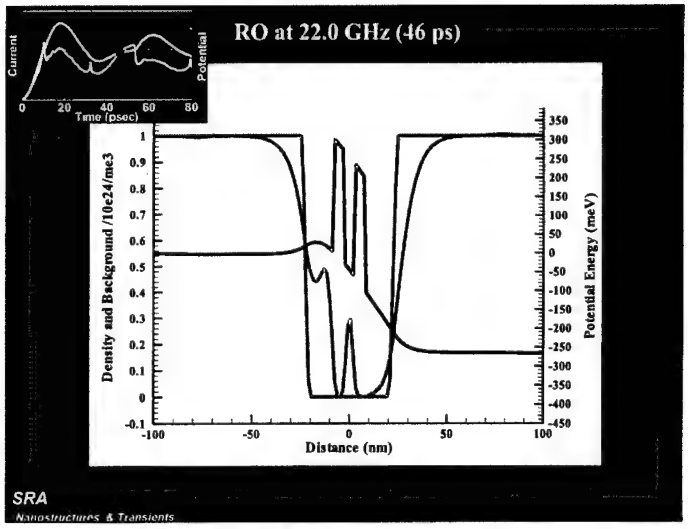
RO at 22.0 GHz (46 ps)
Current
Potential
Time (psec)
Density and Background /10e24/me3
Potential Energy (meV)
Distance (nm)
SRA
Nanostructures & Transients

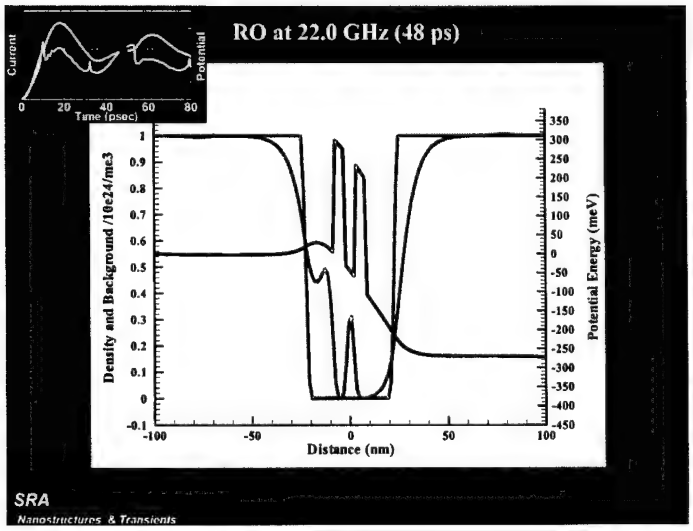
RO at 22.0 GHz (48 ps)
Current
Potential
Time (psec)
Density and Background /10e24/me3
Potential Energy (meV)
Distance (nm)
SRA
Nanostructures & Transients

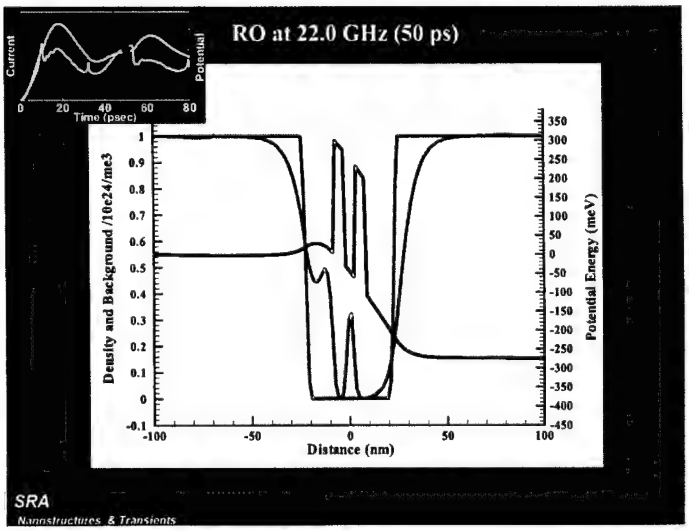
RO at 22.0 GHz (50 ps)
Current
Potential
Time (psec)
Density and Background /10e24/me3
Potential Energy (meV)
Distance (nm)
SRA
Nanostructures & Transients

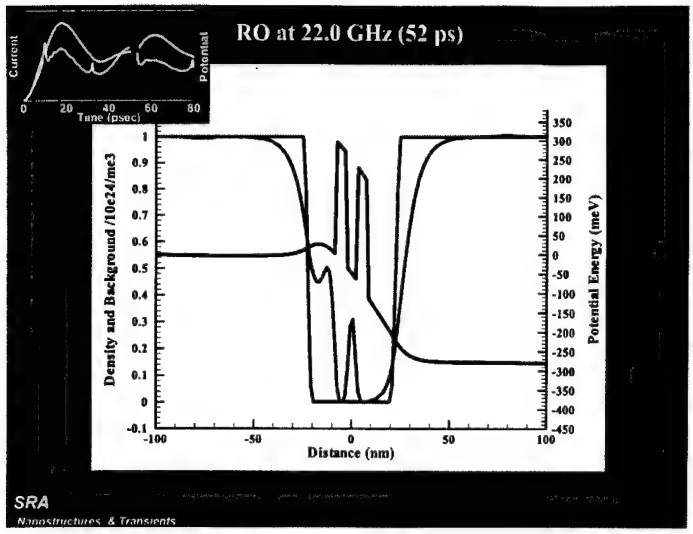

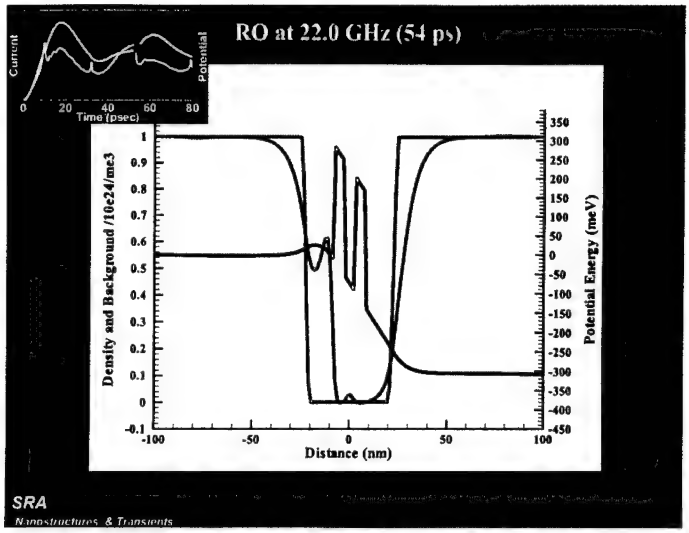

Contour and Surface Plots

SRA
Nanostructures & Transients

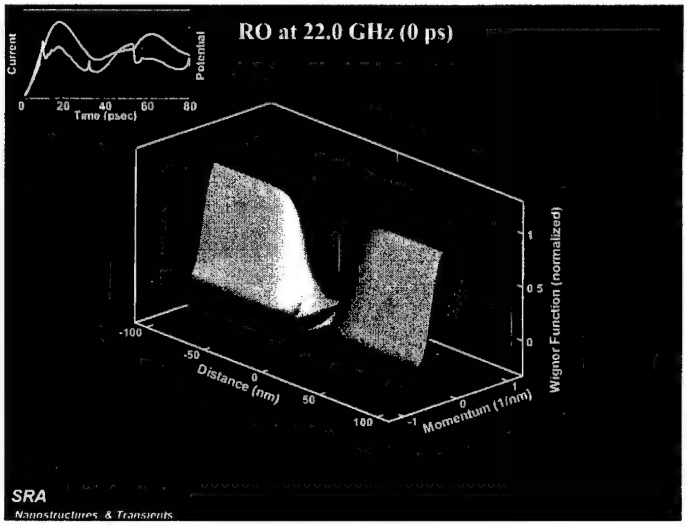

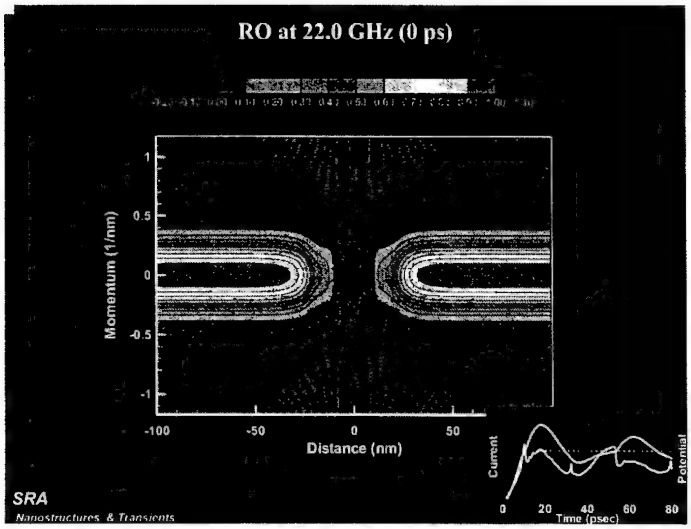

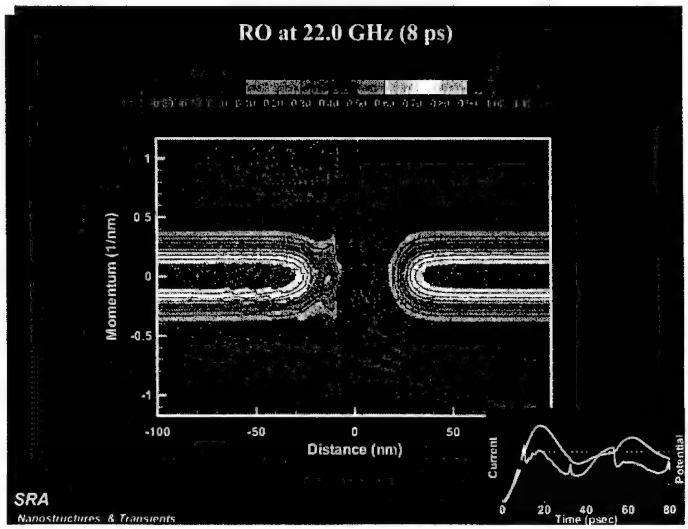

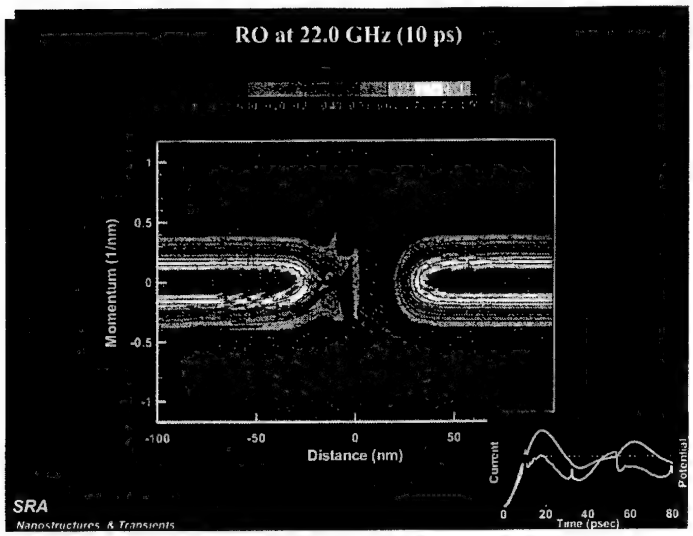

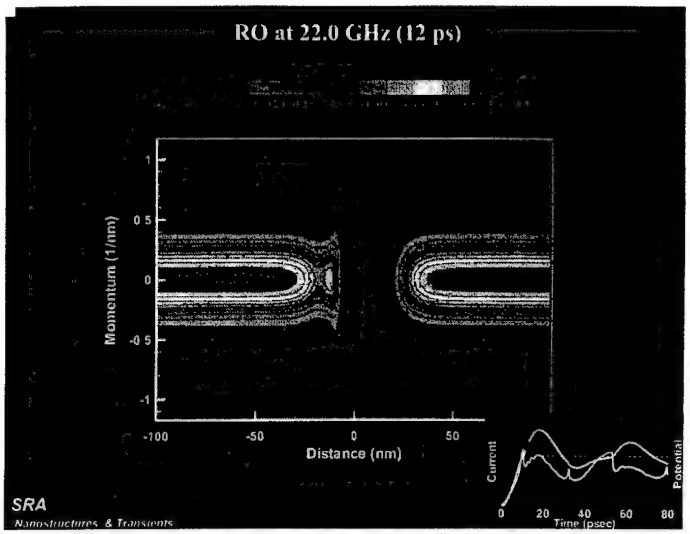

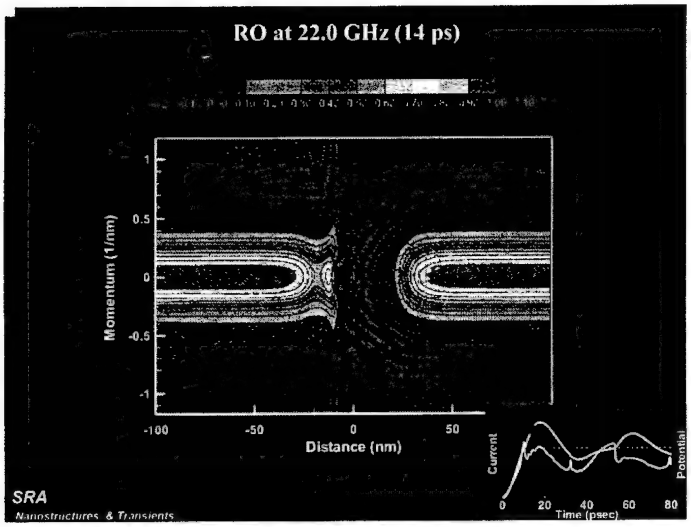

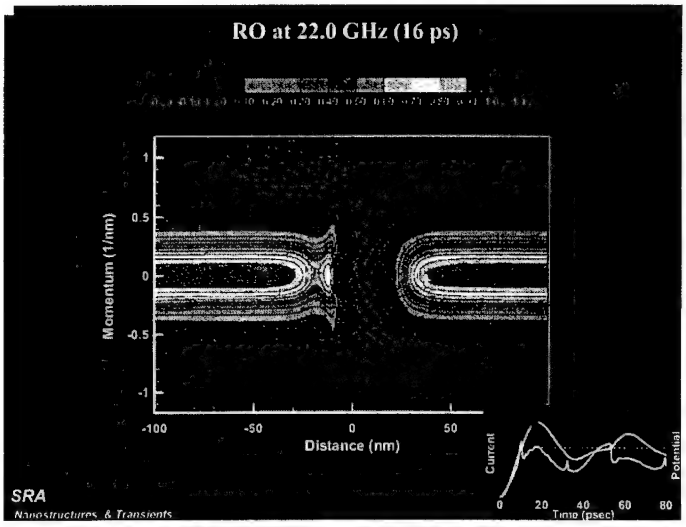

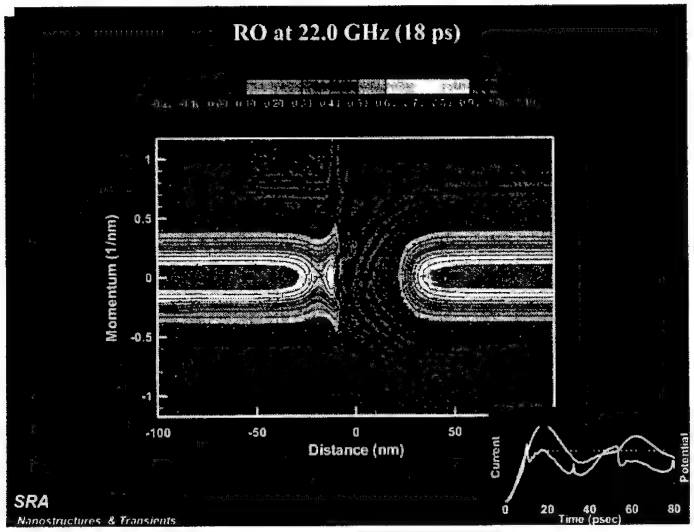

Observations

- Increasing circuit frequency results in increased looping of IV.
- Oscillations cease at approximately 120GHz for these device parameters.
- There is an invariant quantity prior to the current drop-back. This quantity is the "Bohm Quantum Potential".
- Oscillations are stable to circuit noise and device fluctuations.
- Noise characteristics can probably be explained by early discussions of M. Lax.

SRA
Nanostructures & Transients

The Bohm Quantum Potential and the Steady State Schrodinger Equation

$$-\frac{\hbar^2}{2m}\frac{\partial^2\psi}{\partial x^2}+V(x)\psi=E\psi$$

$$\psi(x)=R\exp\left[iS(x)/\hbar\right]$$

Quantum Potential

a. $$\frac{(\partial_x S)^2}{2m}+V+Q=E$$

b. $$\frac{\partial}{\partial x}\left(R^2\frac{\partial_x S}{m}\right)=0$$

c. $$Q=-\frac{\hbar^2}{2m}\frac{\partial_{xx}R}{R}$$

Q represents the ground state for simple double barrier problems

From Simulations (Post Processed): Quantum Potential, Within and to the Left of the Barrier—For Different Values of Bias

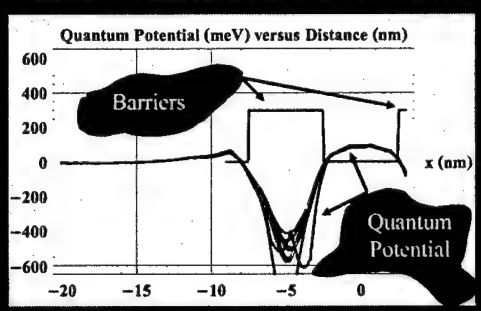

Conclusions Suggested by the Quantum Potential

- Simulations are consistent with the filling of a well defined quantum state prior to the drop-back in current.
- Quantum potential is not well defined after the drop-back.

  Certainly there are computational difficulties with small values of charge. But we may be dealing with a mixture of a large number of quantum states, scattering states and dissipation.

Noise Considerations

- For nonlinear systems amplitude noise is not an issue (M. Lax and our studies)
- Phase noise is additive.
- Amount of phase noise depends on time of disturbance.
- Recovery from disturbance occurs within one cycle.
- Illustrate with ODE and Quantum RO

Injected Current Source at a Particular Instant of Time

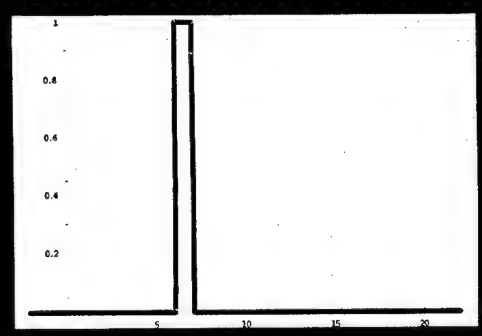

Same type of current source: different time

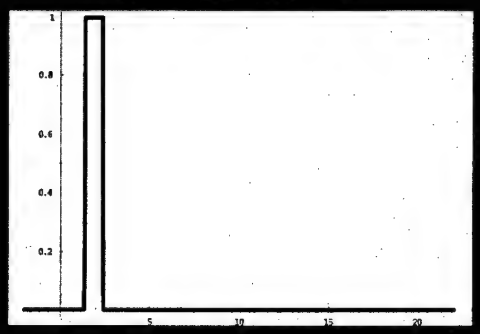

SRA
Nanostructures & Transients

ODE/RO Circuit Response

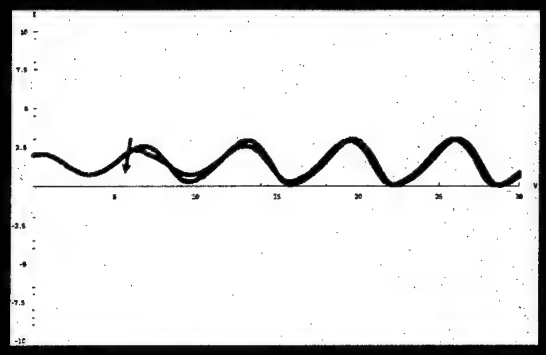

SRA
Nanostructures & Transients

ODE/RO Circuit Response

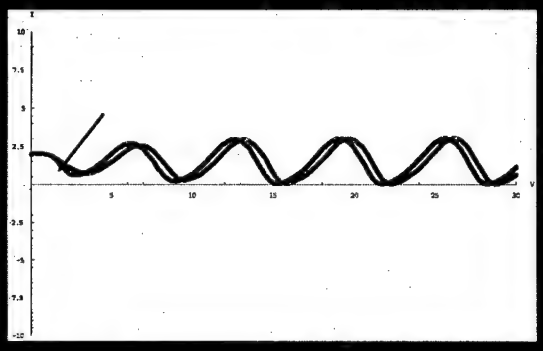

SRA
Nanostructures & Transients

Quantum RO at 113.7 GHz: Fluctuation Response of Particle Current and Potential Energy

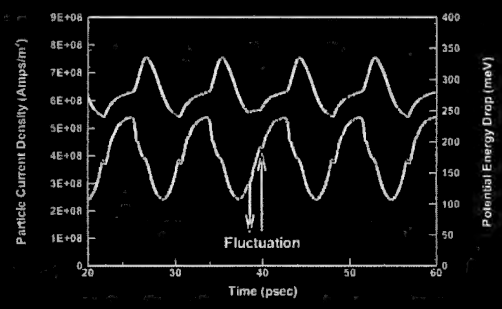

SRA
Nanostructures & Transients

Conclusions

- Quantum Van der Pol oscillator provides quantitative values for the large signal switching and recovery times of RTD.
- Large signal frequencies near 120 GHz for non-optimized structure.
- Small signal oscillations sustained at higher frequencies. (f>670 GHz).
- Quantum Van der Pol oscillators recover from fluctuations within one cycle.
- Phase noise dominates.

SRA
Nanostructures & Transients

Speculations

- Periodic invariance is probably due to time increments. If use was made of femtosecond increments would probably see high frequency contributions.
- Quantum potential interpretation not as simple for higher (>300 meV) barriers.

SRA
Nanostructures & Transients

Non-Equilibrium Green's Functions for MOSFET Modeling

Dejan Jovanovic
Benjamin Liu
Roland Stumpf
Keith Beardmore
Ramesh Venugopa (Purdue)
Mark Lundstrom (Purdue)
Supriyo Datta (Purdue)

Motorola
Computational Materials Group
4200 W. Jemez Rd., Suite 300
Los Alamos, NM 87544

Conventional TCAD

- **Process-Device simulation (TCAD) is used by the semiconductor industry to expedite and optimize process development**
- **TCAD enables the efficient use of experimental cycles and provides major cost/time savings during early design iterations**
- **TCAD device models are based on semi-classical transport theory which relies on approximations to facilitate performance efficiency**
- ***Semiclassical transport models will become increasingly inaccurate with decreasing L_{gate} due to the onset of quantum effects***

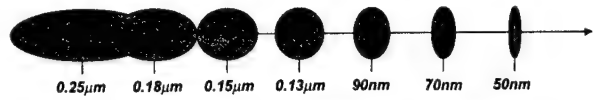

Experimental calibration will be increasingly required to calibrate TCAD device simulators which will undermine their usefulness

Device Model Deployment

CALIBRATION

Advanced Models

PURPOSE: Calibrate TCAD models for sub-0.1μm Tech. Nodes and provide platform for novel structures research

- **Full physics models with emphasis on global accuracy**
- **Provide detailed transport and material understanding**
- ***Minimal calibration required***

Monte-Carlo
Quantum Transport

TCAD

PURPOSE: Create Rev. 0 compact models and support lot design

- **Physics-based device models with emphasis on performance**
- **Provide interface between process and device behavior**
- ***Will require experimental (~100 days) or advanced model (~7 days) calibration***

Drift-diffusion
Hydrodynamic
Density Gradiant

Compact Models

PURPOSE: Enable circuit-level simulation

- **High-performance device models based on analytic equations**
- **Provide interface between devices and circuits**
- ***Requires experimental (~100 days) or TCAD-based (~30 days) calibration***

SPICE: BSIM3, SSIM, etc.

DESIGN

Comparison of Contemporary Device Simulators

Device Simulator	Transport Model	Scattering	Quantum Effects	Leakage	Material Properties	Biasing $V_G<V_T$	Biasing $V_G>V_T$	Performance
Drift-Difusion	Semi-Classical	Mobility based		Sub-threshold				~1 min/bias
Hydro-Dynamic	Semi-Classical	Mobility based		Sub-threshold				~10 min/bias
Density Gradient	Semi-Classical	Mobility based	Quantum Potentials	Sub-threshold				~10 min/bias
Monte Carlo	Semi-Classical	Detailed	Subband		Advanced			~1 hr/bias
Quantum Transport	Quantum Mechanical	Empirical or Detailed	Full Quantum Effects	Full Sub-threshold quantum				

Good
Average
Poor

Nonequilibrium Quantum Field Theory

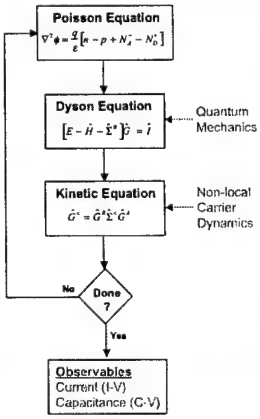

- NQFT is the most comprehensive theoretical framework for device simulation
- Within a single numerical platform, NQFT can encompass
  - Quantum transport
  - Scattering
  - Atomic-scale material properties
- The semi-classical Boltzmann equation is an approximate form of the NQFT kinetic equation
- Boltzmann Equation

$$\frac{\partial}{\partial t} f(\vec{v},\vec{r},t) + \vec{v}\cdot\nabla f(\vec{v},\vec{r},t) + \frac{1}{m}\vec{F}\cdot\nabla_{\vec{v}} f(\vec{v},\vec{r},t) = \sum_{\vec{v}'}\left[f(\vec{v}',\vec{r},t)S(\vec{v}',\vec{v}) - f(\vec{v},\vec{r},t)S(\vec{v},\vec{v}')\right]$$

- NQFT Kinetic Equation

$$\left\{\left[\frac{\partial}{\partial t} + \frac{\partial}{\partial t'}\right] + \frac{i}{\hbar}\left[H_o(\vec{r}) - H_o(\vec{r}')\right]\right\} G^<(\vec{x},\vec{x}') = \frac{i}{\hbar}\int_\Omega d\vec{x}_1\left[\Sigma^R(\vec{x},\vec{x}_1)G^<(\vec{x}_1,\vec{x}') - G^<(\vec{x},\vec{x}_1)\Sigma^A(\vec{x}_1,\vec{x}')\right] + \frac{i}{\hbar}\int_\Omega d\vec{x}_1\left[\Sigma^<(\vec{x},\vec{x}_1)G^A(\vec{x}_1,\vec{x}') - G^R(\vec{x},\vec{x}_1)\Sigma^<(\vec{x}_1,\vec{x}')\right]$$

- **Principal Equations**

$$\left[E - \hat{H}_o(\vec{k}_\perp) - \hat{\Sigma}^R(E,\vec{k}_\perp)\right]\hat{G}^R(E,\vec{k}_\perp) = \hat{I} \quad \longleftarrow \text{Impulse response}$$

$$G^<_{i,j}(E,\vec{k}_\perp) = \sum_{k,l} G^R_{i,k}(E,\vec{k}_\perp)\Sigma^<_{k,l}(E,\vec{k}_\perp)G^A_{l,j}(E,\vec{k}_\perp) + g^<_{i,j}(E,\vec{k}_\perp) \quad \longleftarrow \text{Convolution Integral}$$

- **Scattering**

$$\Sigma^R_{i,j}(E,\vec{k}_\perp) = \frac{1}{(2\pi)^3}\sum_k \int dE' \int d\vec{k}'_\perp V_{i,k}(E,\vec{k}_\perp,E',\vec{k}'_\perp)G^R_{k,j}(E',\vec{k}'_\perp)$$

$$\Sigma^<_{i,j}(E,\vec{k}_\perp) = \frac{1}{(2\pi)^3}\sum_k \int dE' \int d\vec{k}'_\perp V_{i,k}(E,\vec{k}_\perp,E',\vec{k}'_\perp)G^<_{k,j}(E',\vec{k}'_\perp)$$

$$\frac{1}{\tau^{tot}_{ij}(E)} \Leftrightarrow -\frac{2}{\hbar}\mathrm{Im}\left[\Sigma^R_{ij}(E,\vec{k}_\perp)\right]$$

Scattering is both the key and impediment to numerical quantum transport simulation

- **Definitions**

$\hat{H}_o(\vec{k}_\perp)$ - Tight-binding Hamiltonian
$\hat{\Sigma}^R(E,\vec{k}_\perp)$ - Retarded self-energy (out-scattering)
$\hat{G}^R(E,\vec{k}_\perp)$ - Retarded Green Function (Propagator)
$g^<_{ij}(E,\vec{k}_\perp)$ - Zero-order correlation function
$\Sigma^<_{ij}(E,\vec{k}_\perp)$ - Causal Self-Energy (in-scattering)
$G^<_{ij}(E,\vec{k}_\perp)$ - Full correlation function
$V_{ij}(E,\vec{k}_\perp,E',\vec{k}'_\perp)$ - Interaction Potential (Green Function)

Nonequilibrium Quantum Field Theory
Physical Observables

- **Density of States**

$$A_{ij}(E,\vec{k}_\perp) = -2\,\mathrm{Im}\left[G^R{}_{ij}(E,\vec{k}_\perp)\right] \quad \text{(quantum mechanical DOS)}$$

- **Electrons**

$$G^<_{ii}(E,\vec{k}_\perp) = if(E,\phi_F)A_{ii}(E,\vec{k}_\perp) \quad \text{(equilibrium)}$$

$$= if(E,\phi_F^L)A^L_{ii}(E,\vec{k}_\perp) + if(E,\phi_F^R)A^R_{ii}(E,\vec{k}_\perp) \quad \text{(non-equilibrium)}$$

$$n_i = -2i\int\frac{dE}{2\pi}\int\frac{d\vec{k}_\perp}{(2\pi)^2}G^<_{ii}(E,\vec{k}_\perp) \quad \text{(electron density)}$$

$$J_i = \frac{2e}{\hbar}\int\frac{dE}{2\pi}\int\frac{d\vec{k}_\perp}{(2\pi)^2}\left[H_{i,i+1}(\vec{k}_\perp)G^<_{i+1,i}(E,\vec{k}_\perp) - G^<_{i,i+1}(E,\vec{k}_\perp)H_{i+1,i}(\vec{k}_\perp)\right] \quad \text{(electron current)}$$

- **Holes**

$$G^>_{ii}(E,\vec{k}_\perp) = -i\left[1-f(E,\phi_F)\right]A_{ii}(E,\vec{k}_\perp) \quad \text{(equilibrium)}$$

$$= -i\left[1-f(E,\phi_F^L)\right]A^L_{ii}(E,\vec{k}_\perp) - i\left[1-f(E,\phi_F^R)\right]A^R_{ii}(E,\vec{k}_\perp) \quad \text{(non-equilibrium)}$$

$$p_i = -2i\int\frac{dE}{2\pi}\int\frac{d\vec{k}_\perp}{(2\pi)^2}G^>_{ii}(E,\vec{k}_\perp) \quad \text{(hole density)}$$

$$J_i = \frac{2e}{\hbar}\int\frac{dE}{2\pi}\int\frac{d\vec{k}}{(2\pi)^2}\left[H_{i,i+1}(\vec{k}_\perp)G^>_{i+1,i}(E,\vec{k}_\perp) - G^>_{i,i+1}(E,\vec{k}_\perp)H_{i+1,i}(\vec{k}_\perp)\right] \quad \text{(hole current)}$$

Nonequilibrium Quantum Field Theory
Spatial Discretization

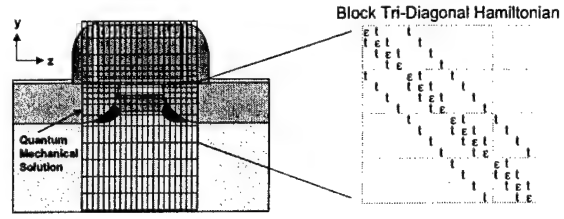

- Presently using multi-valley effective-mass based discretization
- Simulated bandstructure is intrinsically linked to grid morphology in lateral (z) direction

$$E(k_z) = \frac{\hbar^2}{m_z^*\Delta_z}\left[1-\cos(k_z\Delta_z)\right]$$

- Uniform grid is required for the lateral (z) direction to avoid spurious reflections
- Non-uniform grid can be used in vertical (y) direction

Nonequilibrium Quantum Field Theory
Boundary Conditions for Green's and Correllation Functions

- Boundary condition assumptions
  - Contacts are modeled as translationally invariant open boundaries and are assumed to be in local equilibrium
  - Closed boundaries are set where G^R and $G^<$ can be safely assumed to be negligible

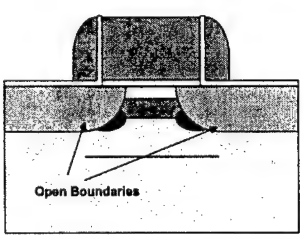

- Boundary eigenvalue problem

$$\left[Z_m + (Z_m)^{-1} - \frac{E-\varepsilon_j}{t_j}\right]\phi_{j,m} = 0$$

- Boundary Green's function

$$\tilde{g}^R_{0,1} = QZQ^{-1}\tilde{g}^R_{0,0}$$

$$\tilde{g}^R_{0,0} = \left[E - \hat{\varepsilon} - \hat{t}QZQ\right]^{-1}$$

$$\tilde{g}^<_{0,0} = -i2f(\phi_F^S)\,\mathrm{Im}\left[\tilde{g}^R_{0,0}\right]$$

Nonequilibrium Quantum Field Theory
Recursive Solution of Dyson and Kinetic Equations

- **General Dyson equations for G^R and $G^<$**

$$\hat{G}^R_{i,i'} = \hat{g}^R_{i,i'} + \sum_{j,k}\hat{g}^R_{i,j}\hat{\Sigma}^R_{j,k}\hat{G}^R_{k,i'}$$

$$\hat{G}^<_{i,i'} = \hat{g}^<_{i,i'} + \sum_{j,k}\hat{g}^<_{i,j}\hat{\Sigma}^A_{j,k}\hat{G}^A_{k,i'} + \sum_{j,k}\hat{g}^R_{i,j}\Sigma^<_{j,k}\hat{G}^A_{k,i'} + \sum_{j,k}\hat{g}^R_{i,j}\Sigma^R_{j,k}\hat{G}^<_{k,i'}$$

- **Recursive Greens Function (RGF) Technique**
  - Direct solution of the Green's functions is computationally prohibited $(N_zN_y)^3$
  - Physical observables are clustered along the Green's function diagonals
  - Dyson equations can be used to recursively construct Green and correlation function diagonals in a two-step manner $N_zN_y^3$
  - Perturbative elements are the off-diagonal elements of the Hamiltonian

$$\tilde{g}^R_{i,i'} = g^R_{i,i'} + \sum_{j,k}g^R_{i,j}t_{j,k}\tilde{g}^R_{k,i'}$$

$$\tilde{g}^<_{i,i'} = g^<_{i,i'} + \sum_{j,k}g^<_{i,j}t_{j,k}\tilde{g}^A_{k,i'} + \sum_{j,k}g^R_{i,j}t_{j,k}\tilde{g}^<_{k,i'}$$

  - Self-consistent scattering can be efficiently incorporated into the RGF approach

Nonequilibrium Quantum Field Theory
Recursive Solution of Semi-infinite Green/Correlation Functions

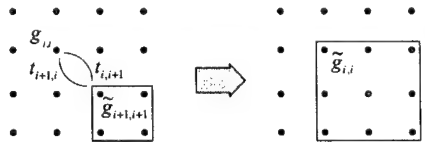

$$\tilde{g}^R_{i,i} = g^R_{i,i} + g^R_{i,i}t_{i,i+1}\tilde{g}^R_{i+1,i}$$

$$= g^R_{i,i} + g^R_{i,i}t_{i,i+1}\tilde{g}^R_{i+1,i+1}t_{i+1,i}\tilde{g}^R_{i,i}$$

$$\tilde{g}^<_{i,i} = g^<_{i,i} + g^<_{i,i}t_{i,i+1}\tilde{g}^A_{i+1,i} + g^R_{i,i}t_{i,i+1}\tilde{g}^<_{i+1,i}$$

$$= g^<_{i,i} + g^<_{i,i}t_{i,i+1}\tilde{g}^A_{i+1,i+1}t_{i+1,i}\tilde{g}^A_{i,i} + g^R_{i,i}t_{i,i+1}\tilde{g}^<_{i+1,i+1}t_{i+1,i}\tilde{g}^A_{i,i} + g^R_{i,i}t_{i,i+1}\tilde{g}^R_{i+1,i+1}t_{i+1,i}\tilde{g}^<_{i,i}$$

$$\tilde{g}^R_{i,i} = \left[\left(g^R_{i,i}\right)^{-1} - t_{i,i+1}\tilde{g}^R_{i+1,i+1}t_{i+1,i}\right]^{-1}$$

$$\tilde{g}^<_{i,i} = \tilde{g}^R_{i,i}\left[\sigma^<_{i,i} + t_{i,i+1}\tilde{g}^<_{i+1,i+1}t_{i+1,i}\right]\tilde{g}^A_{i,i}$$

Nonequilibrium Quantum Field Theory
Recursive Solution of Full Green/Correlation Functions

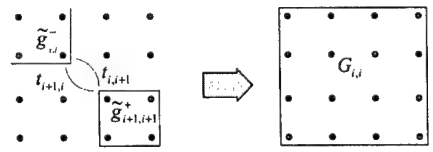

$$G^R_{i,i} = \tilde{g}^{R-}_{i,i} + \tilde{g}^{R-}_{i,i}t_{i,i+1}G^R_{i+1,i+1}t_{i+1,i}\tilde{g}^{R-}_{i,i}$$

$$= \left[\left(\tilde{g}^{R-}_{i,i}\right)^{-1} - t_{i,i+1}\tilde{g}^{R+}_{i+1,i+1}t_{i+1,i}\right]^{-1}$$

$$G^<_{i,i} = \tilde{g}^{<-}_{i,i} + \tilde{g}^{<-}_{i,i}t_{i,i+1}G^A_{i+1,i+1}t_{i+1,i}\tilde{g}^{A-}_{i,i} + \tilde{g}^{R-}_{i,i}t_{i,i+1}G^R_{i+1,i+1}t_{i+1,i}\tilde{g}^{<-}_{i,i} + \tilde{g}^{R-}_{i,i}t_{i,i+1}G^<_{i+1,i+1}t_{i+1,i}\tilde{g}^{A-}_{i,i}$$

$$= G^R_{i,i}\left[\sigma^<_{i,i} + t_{i,i-1}\tilde{g}^{<-}_{i-1,i-1}t_{i-1,i} + t_{i,i+1}\tilde{g}^{<+}_{i+1,i+1}t_{i+1,i}\right]G^A_{i,i}$$

Nonequilibrium Quantum Field Theory

Parallel Implementation of the Recursive Green's Function Method

- Parallel energy integration
  - Green's function calculations at each energy are distributed to slave processors
  - *Found to be highly inefficient for scattering simulations due to varying execution time per node*
- Parallel Recursive Green's function algorithm
  - Spatial grid topology is distributed across processors
  - Cross element coupling terms are calculated in parallel
  - Boundary Green's functions are calculated and distributed to enable parallel calculation of G^R
  - Correlation functions are then iteratively calculated until scattering self-consistency is achieved

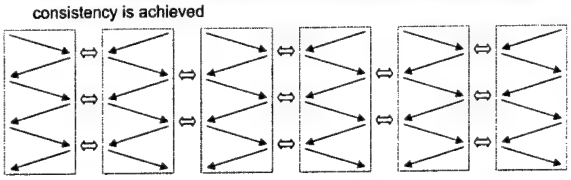

~ 80% parallel efficiency is exhibited for 60 processor simulations

Quantum Mechanical Simulation of MOSFETs

Numerical Issues and Computational Platforms

- **Algorithms**
  - Numerical NQFT solutions rely heavily on matrix inversion and multiplication
- **Computing Platforms**
  - *Commodity clusters are the enabling platforms for 2D NQFT simulation*
  - *All runs were performed on a 110 node 2xPII! 450MHz Linux cluster which cost under $250,000*
- **Performance**
  - 90nm Ballistic simulations: ~1 hour/bias point
  - 90nm Scattering simulations: ~8 hour/bias point

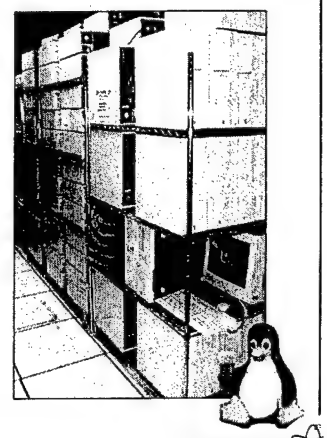

Scattering Model

- **Kinetic Equation**

$$\left\{\left[\frac{\partial}{\partial t}+\frac{\partial}{\partial t'}\right]+\frac{i}{\hbar}\left[H_o(\vec{r})-H_o(\vec{r}')\right]\right\}G^<(\vec{x},\vec{x}')$$
$$=\frac{i}{\hbar}\int_\Omega d\vec{x}_1\left[\Sigma^R(\vec{x},\vec{x}_1)G^<(\vec{x}_1,\vec{x}')-G^<(\vec{x},\vec{x}_1)\Sigma^A(\vec{x}_1,\vec{x}')+\Sigma^<(\vec{x},\vec{x}_1)G^A(\vec{x}_1,\vec{x}')-G^R(\vec{x},\vec{x}_1)\Sigma^<(\vec{x}_1,\vec{x}')\right]$$

- **Current Continuity**

$$\left\{\left[\frac{\partial}{\partial t}+\frac{\partial}{\partial t'}\right]+\frac{i}{\hbar}\left[H_o(\vec{r})-H_o(\vec{r}')\right]\right\}G^<(\vec{x},\vec{x}')=\frac{\partial}{\partial t}n(\vec{r},t)+\vec{\nabla}\cdot\vec{J}(\vec{r},t)=0$$

$$\int_\Omega d\vec{x}_1\left[\Gamma(\vec{x},\vec{x}_1)G^<(\vec{x}_1,\vec{x}')-\Sigma^<(\vec{x},\vec{x}_1)A(\vec{x}_1,\vec{x}')\right]=0$$

- **Rate-Based Scattering Model**

$$\Sigma^R_{i,j,i',j'}(E,\vec{k})\equiv i\delta_{i,i'}\delta_{j,j'}\int\frac{dE'}{2\pi}\int\frac{dk'}{2\pi}\lambda_{i,j}(E,\vec{k},E',\vec{k}')\equiv -i\frac{\Gamma_{i,j}(E,\vec{k})}{2}$$

$$\Sigma^<_{i,j,i',j'}(E,\vec{k})=-2\delta_{i,i'}\delta_{j,j'}\frac{G^<_{i,j}(E,\vec{k})}{A_{i,j}(E,\vec{k})}\int\frac{dE'}{2\pi}\int\frac{dk'}{2\pi}\lambda_{i,j}(E',\vec{k}',E,\vec{k})\equiv\frac{\tilde{\Gamma}_{i,j}(E,\vec{k})}{A_{i,j}(E,\vec{k})}G^<_{i,j}(E,\vec{k})$$

Approximation:

$$\Gamma_{i,j}(E,\vec{k})=\tilde{\Gamma}_{i,j}(E,\vec{k})\equiv\Gamma^o_{i,j}(E_z)\delta_{i,j}$$

- Enables efficient self-consistent scattering calculation
- Simple calibration
- *Accounts for resistive effects (e.g. L_{eff} scaling)*

Empirical Scattering Model

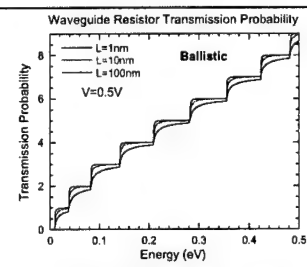

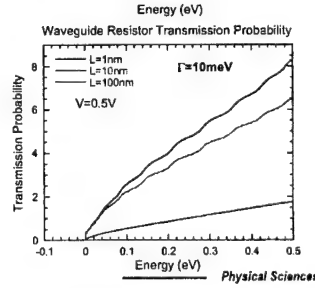

- Resistive electron wave-guide

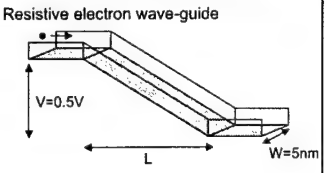

- Ballistic Case
  - Subband structure is apparent and retained up to 100nm
  - Variation in L causes subband smearing but no change in transmission envelope
  - ***Resistive effects are not accounted for***
- Constant-Rate model
  - Accounts for incoherence effects and back-scattering
  - Subband structure disappears for L=100nm
  - Attenuation of transmission envelope occurs for increasing L
  - ***Can account for resistive effects with proper calibration***

MIT Reference MOSFETs

MIT 90nm MOSFET
- L_{poly}=0.13μm
- t_{ox}=4.5nm

MIT 50nm MOSFET
- L_{poly}=85nm
- t_{ox}=2.0 nm

MIT 25nm MOSFET
- L_{poly}=50nm
- t_{ox}=1.5 nm

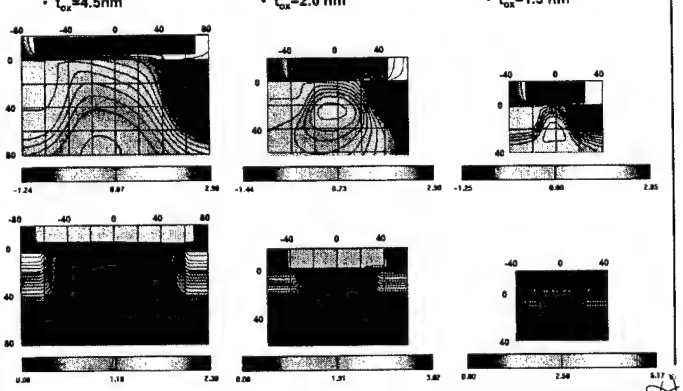

MOSFET Quantum Mechanical Effects

Sub-bands

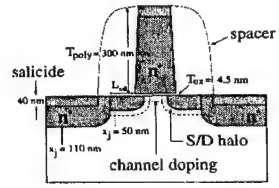

- **Quantum mechanical DOS (spectral function) data taken at Si-SiO_2 interface**
- **Striations in DOS plots are sub-bands**
- **Spectral shift evident near source barrier**
- **Multiple sub-bands are required for accurate scattering calculations**

25nm MIT MOSFET

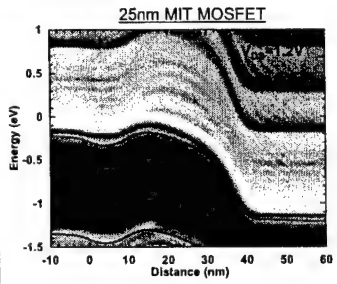

90nm MIT MOSFET

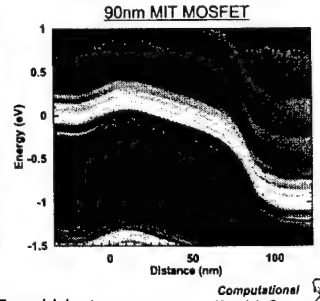

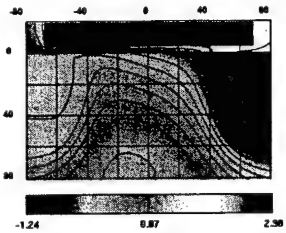

MOSFET Quantum Mechanical Effects
Sub-bands

- Intersubband scattering processes facilitate carrier capture under drain bias
- Back-scattering is effectively suppressed in the post source barrier region by coupling into high-barrier subbands
- As a result, scattering in the vicinity of the source barrier dominates transport
- This effect is captured in our empirical scattering model despite the lack of relaxation

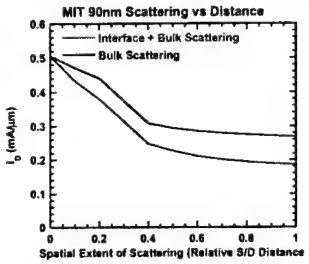

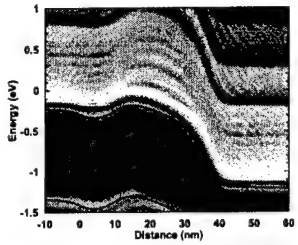

Quantum Mechanical Effects in MOSFETs
Subbands

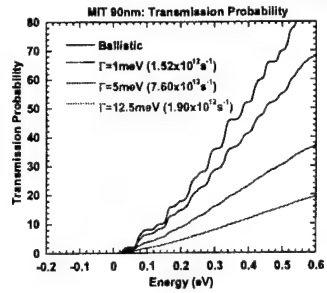

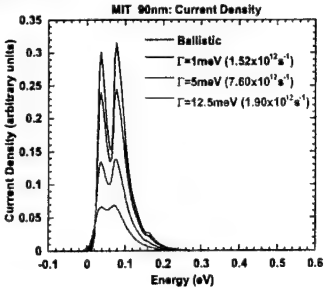

- Ballistic transmission probability shows steps at the onset of primed (4-fold degenerate) and unprimed (2-fold degenerate) sub-band conduction
- Spatial localization of Γ induces coupling between sub-bands which smears the transmission characteristics
- Increase in Γ causes decline in transmission envelope due to back-scattering

Quantum Mechanical Effects in MOSFETs
Charge Centroid Shift

- Charge centroid shift is the predominant quantum effect in MOSFETs with highly scaled t_{ox}
- Inversion layer charge shift increases effective t_{ox}, reduces C_{ox}, induces V_t shift and degrades sub-threshold performance
- Source/Drain centroid shift induces the formation of an interface dipole with a corresponding charge build-up to satisfy macroscopic charge neutrality

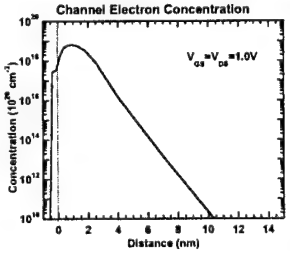

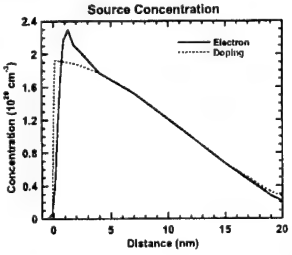

Quantum Mechanical Effects in MOSFETs
Charge Centroid Shift

- Source/Drain centroid shift induced dipole creates a large electric field along the extension interface
- Current density is tightly distributed along the interface implying that current crowding may be exaggerated in conventional series resistance calculations

MIT 25nm MOSFET Electric Field

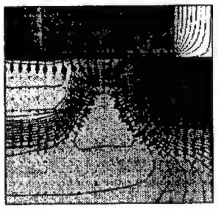

MIT 25nm MOSFET Current Density

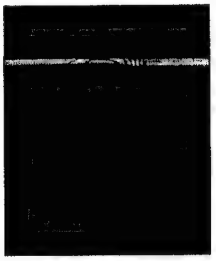

Quantum Mechanical Effects in MOSFETs
Ballistic Sub-band Mixing

- Schrodinger Equation in Spatial Representation

$$\left[\frac{-\hbar^2}{2m}\left(\nabla_y^2+\nabla_z^2\right)+E_c(y,z)\right]\psi(y,z)=E\psi(y,z)$$

- Discretized Schrodinger Equation in Mode Representation

$$\left(E-\varepsilon_i-E_i^m\right)\eta_i^m-t_{i,i+1}\sum_n r_{i,i+1}^{mn}\eta_{i+1}^n-t_{i,i-1}\sum_n r_{i,i-1}^{mn}\eta_{i-1}^n=0$$

$$r_{ij}^{mn}=\int dy\,\phi_i^{m*}(y)\phi_j^n(y)$$

- Double-Gate MOSFET

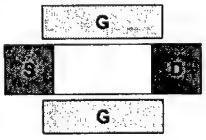

Modes are de-coupled

- Bulk MOSFET

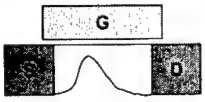

Modes are coherently coupled

Intrinsic Mode Coupling in MOSFETs

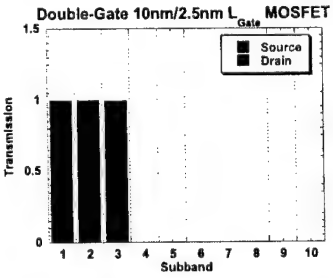

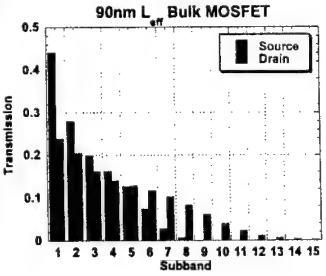

Double-Gate MOSFETs

- Minimal mode coupling occurs due to uniformity of channel
- Well approximated by de-coupled subband models

Bulk MOSFETs

- Significant intrinsic mode coupling into high-order modes occurs under on-state biasing
- *Effect is not captured by semiclassical transport models incorporating sub-bands*

Quantum Mechanical Effects in MOSFETs
Sub-Threshold Tunneling

- Sub-threshold tunneling through the source barrier enhances off-state leakage and compromises the I_{on}-I_{off} trade-off
- 50nm L_{eff} MOSFET exhibits a ~25% I_{off} increase
- 25nm L_{eff} MOSFET exhibits a ~40% I_{off} increase
- Further complications may arise from trap-assisted tunneling due to S/D extension lateral dopant diffusion into the channel

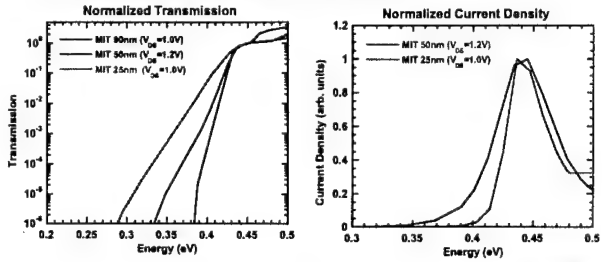

Si Spectral DOS

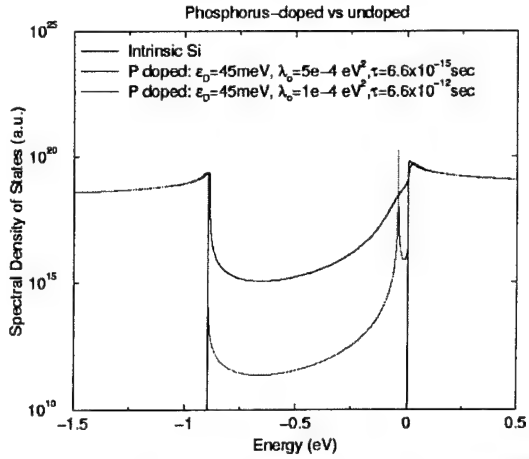

Quantum Mechanical Effects in MOSFETs
I_D-V_{GS} Saturation

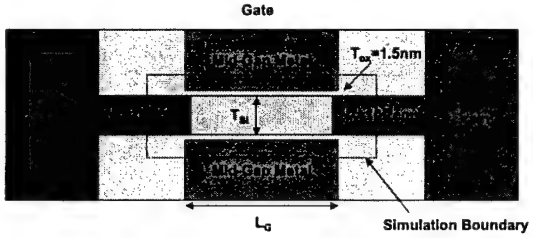

- Double-Gate MOSFETs are predicted to display optimal scaling properties and carry the potential of realizing (sub?) 10nm L_G technologies
- However, electrostatics dictates that L_G/T_{Si} remain roughly constant to suppress short-channel effects and achieve target $I_{on}/_{off}$

Scaling Study

- Set L_G/T_{si} = 4 to control SCE … keeping t_{ox}=1.5nm constant
- Evaluate device performance for 10nm < L_G < 80nm

Double-Gate SOI Simulation Study
Saturation of Gate Control

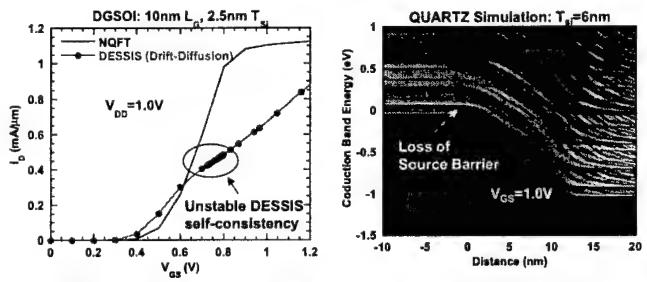

- Drift-diffusion simulations show an instability in self-consistency for V_{GS}>0.8V due to breakdown of macroscopic charge neutrality at the source boundary
- Boundary charge neutrality is maintained for quantum transport simulations by invoking the equilibrium approximation in the S/D extensions
- Quantum transport simulation predicts current saturation with V_{GS}=0.8V due to elimination of source barrier

Double-Gate SOI Simulation Study
Impact of Current Saturation on Device Scaling

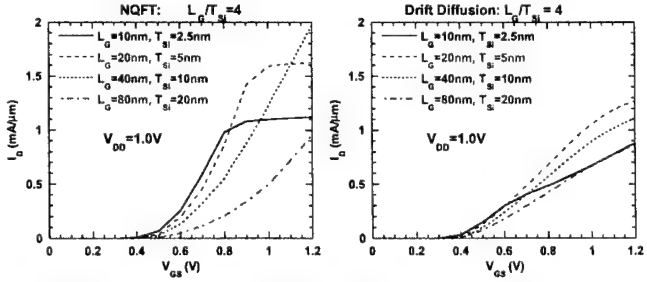

- Cases studied have L_G/T_{si} = 4 to maintain control of SCE with L_G scaling
- QUARTZ predicts I_{dsat} @ V_{DD}=1.0V increases with decreasing L_G down to ~30-40nm
- Subsequent reductions in L_G lead to reduced I_{dsat} @ V_{DD}=1.0V due to elimination of source barrier and current bottleneck with decreasing T_{si}
- A technology with V_{DD}=0.6V show increasing I_{dsat} with L_G for all cases studied
- DESSIS shows reduction of I_{Dsat} at L_G=10-20nm

Double-Gate SOI Simulation Study

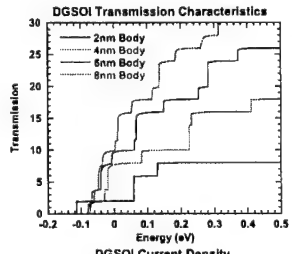

- Decreasing T_{si} is predicted to enhance mobility by breaking valley degeneracy and preferentially occupying low m_{eff} valleys
- Macroscopic charge neutrality must be satisfied in the source
- Velocity enhancement is cancelled out by decrease in density of states in transmission characteristics

Decreasing T_{si} degrades max I_D … cannot scale T_{si} indefinitely

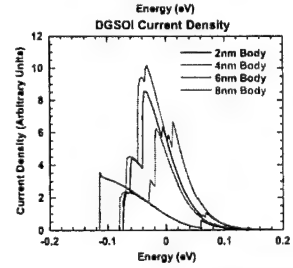

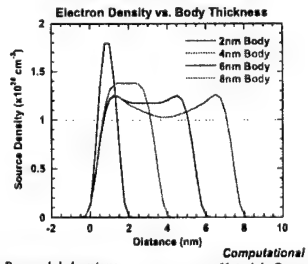

Quantum Transport Simulations of MOSFETs
Scattering Model Calibration

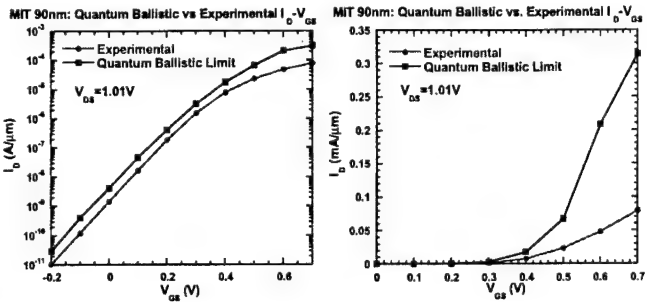

- Discrepancy in quantum mechanical sub-threshold current is due to non-locality of self-consistent charge
- ***Device drive current is 25% of theoretical limit***

MIT 90nm Device
Quantum Mechanical vs Semiclassical Transport

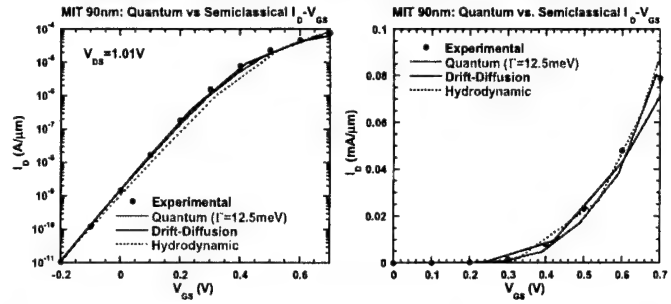

- Hydrodynamic model shows minor current discrepancy in sub-threshold regime
- Drift-diffusion model shows minor current discrepancy for saturation biases
- ***Quantum-mechanical simulation using single parameter rate-based scattering model shows good overall fit with experimental data***

CMOS Effective Mobility

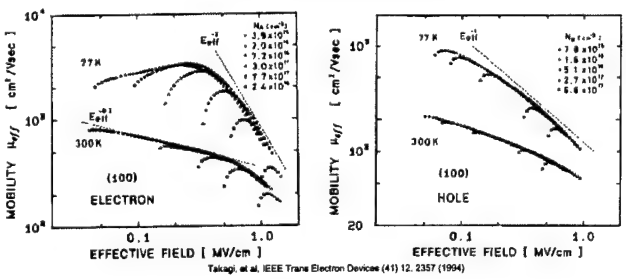

Takagi, et al, IEEE Trans Electron Devices (41) 12, 2357 (1994)

- **Effective mobility is a measure of the local mobility averaged over the vertical carrier density in the channel**
- **Both nMOS and pMOS show a decrease in effective mobility with increasing effective field (inversion charge density)**
- **Roll-off of mobility has been generally attributed to interface roughness**
- **Atomistic interpretation has been lacking**

Non-Equilibrium Quantum Field Theory Calibration
Mobility Model

- **Linear Response Conductivity**

$$\langle\sigma_z\rangle = \lim_{\omega\to 0}\mathrm{Im}\left\{\frac{\Pi(\vec{x},\vec{x}^{+})}{\omega}\right\} \quad \text{(Current-Current Response Function)}$$

$$= \frac{e^2\hbar^3}{8m^2}\lim_{\vec{r}'_\perp\to\vec{r}_\perp}\left[\nabla_{z'}-\nabla_z\right]\int\frac{dE}{2\pi}\frac{\partial f(E)}{\partial E}\int\frac{dk_x}{2\pi}\int d\vec{r}_{\perp 1}\lim_{\vec{r}_{\perp 2}\to\vec{r}_{\perp 1}}\left[\nabla_{z_2}-\nabla_{z_1}\right]A(\vec{r}'_\perp,\vec{r}_{\perp 1},k_x,E)A(,\vec{r}_{\perp 2},\vec{r}_\perp,k_x,E)$$

- **Conductivity: Final Form**

$$\sigma_j^z = \frac{2e^2}{h}\int dE\frac{\partial f(E)}{\partial E}\int\frac{dk_x}{2\pi}\sum_m\phi_{jm}\phi_{mj}^{*}a\,\mathrm{Re}\left\{\frac{\left(e^{i\lambda_m}-e^{-i\lambda_m}\right)^2}{v_m\Gamma_m(E)}+\frac{\left(e^{i2\lambda_m}-e^{-i2\lambda_m}\right)}{v_m^2}\right\}$$

- **Effective Mobility and Corresponding MOSFET Test Structure**

$$\mu_{eff} = \frac{\sum_j\sigma_j^z}{e\sum_j n_j}$$

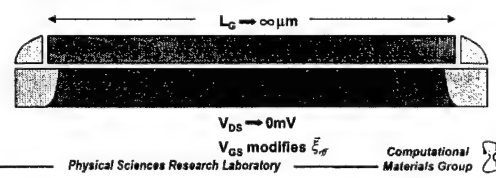

Non-Equilibrium Quantum Field Theory Mobility Model
Single Parameter Scattering

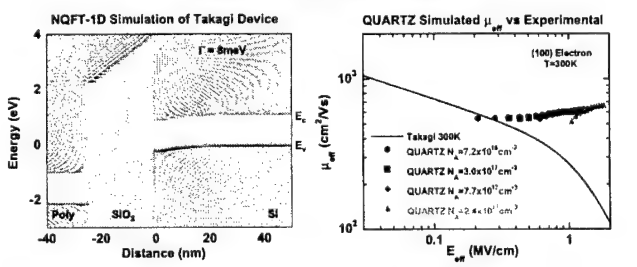

- Single-parameter scattering model brings mobility into empirical range for Γ=8meV
- *Univsersal mobility behavior is exhibited with the NQFT mobility model*
- Strong disagreement with empirical universal mobility curve begins to occur for high effective fields (E_{eff} > 0.3 MV/cm)
- ***Single-parameter scattering model alone is insufficient for capturing effective mobility behavior***

Quantum Transport Simulated Mobility:
Bulk + Interface Scattering Model

$$\Sigma_{ij}^{R}(E,\vec{k}_\perp) = \frac{\lambda_o}{E-\varepsilon_D+i\gamma}\delta_{ij}$$

Parameters:

λ_o = 1.5eV (coupling strength)

ε_D = 0.42 (defect energy above E_c)

$\gamma = \frac{\hbar}{\tau}$ = 90meV linewidth (lifetime)

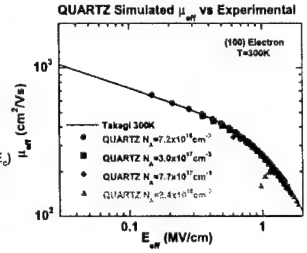

- **Interface model assumes a strong peak of localized states exists in the Si conduction band due to atoms in the Si-SiO_2 transition layer**
- **Qualitative view of the interface suggests that there should be a transition layer that averages Si and SiO_2 conduction/valence band properties**
- ***Bulk + interface scattering model produces universal mobility behavior***

90nm MIT MOSFET Comparison

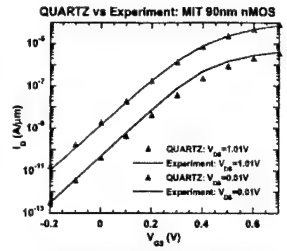

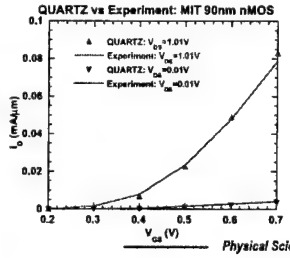

- Calibrated bulk+interface scattering model shows good agreement between theory and experiment
- Band-gap re-normalization leads to states extending into the Si band-gap
- Model agrees with recent gap-state measurements by Lacaita, Pacelli, et al.

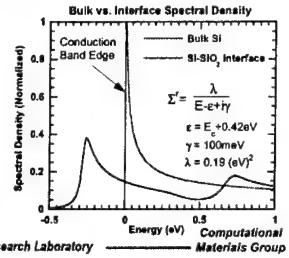

90nm MIT MOSFET Comparison

Calibrated localized interface scattering model shows poor agreement with both experimental data and drift-diffusion simulation for high V_{GS}

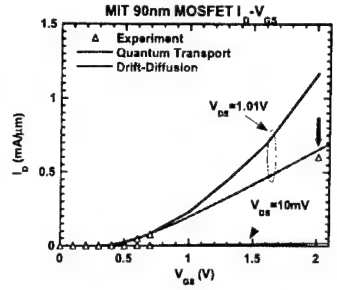

Si-SiO_2 Mobility Model Validation

Validation:

- Direct experimental validation is difficult due to mixing of interface and bulk states
- Density Functional Theory (DFT) electronic structure calculations can provide information on structure and density of states
- Existing DFT work has not focused on the detailed interface properties

DFT Calculations (Liu and Stumpf)

- Performed using VASP on CMG Linux cluster
- Examined three interface structures:
  - Si - SiO_2 (β-quartz)
  - Si - SiO_2 (trydimite)
  - Si - SiO_2 (β-crystalobalite)
- Two basic interface Si-O-Si bonding structures observed:
  - Si-O-Si Bridging bonds
  - Si-O-Si Extended bonds
- *The bridging and extended interface bonds are present in all SiO_2 structures and are periodically distributed along the interface*

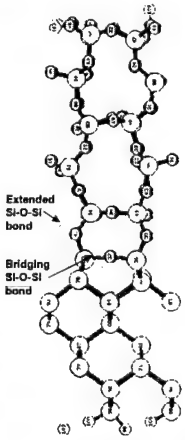

β Quartz SiO_2 / Si interface: Idos plots

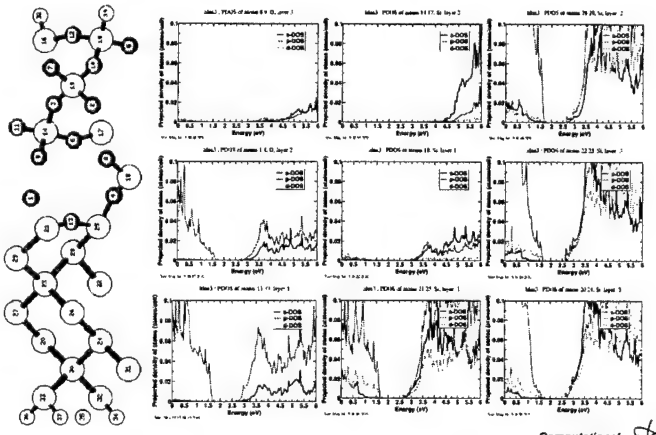

Tridymite SiO_2 / Si interface: Idos plots

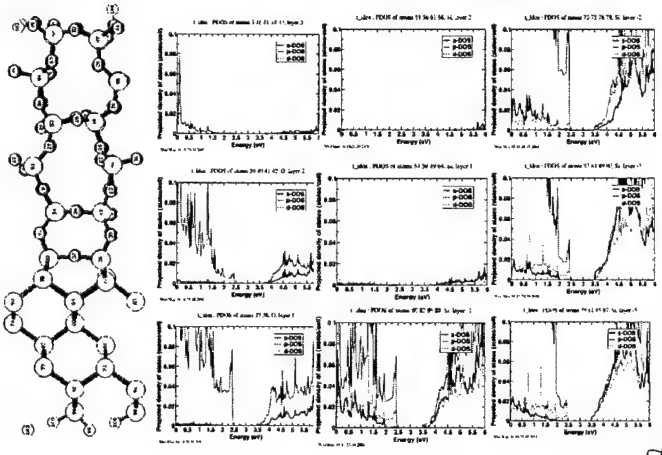

Si(001)/SiO_2 β-cristobalite

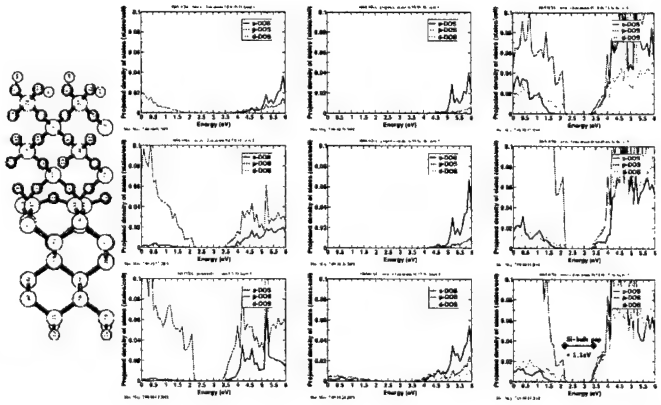

Effective Mobility Dependence on Si Orientation

- Interface scattering may depend on
  - Non-tetrahedral atomic arrangement of bridging and extended interfacial O atoms
  - Distortion of Si atomic positions below the Si-SiO_2 interface
- If interfacial O and/or distorted Si atomic positions are responsible for high-field μ_{eff} behavior, there should be some correlation to Si areal density (ρ_{Si})
- Takagi's data shows that (110) Si orientation should have the strongest interface scattering followed by (111) then (100)

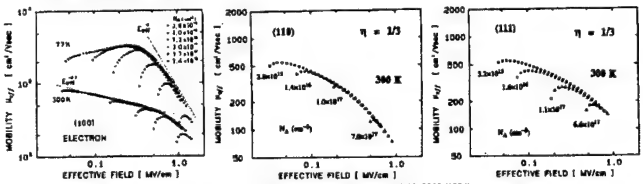

Takagi, et al, IEEE Trans Electron Devices (41) 12, 2363 (1994)

$$\rho_{Si}(100) = \frac{2}{a^2} \qquad \rho_{Si}(110) = \frac{2\sqrt{2}}{a^2} = 1.41\rho_{Si}(100) \qquad \rho_{Si}(110) = \frac{4}{\sqrt{3}a^2} = 1.15\rho_{Si}(100)$$

Scattering from interfacial O and/or distorted Si lattice as the cause of interfacial μ_{eff} degradation is supported by experimental data for orientation dependence

Proposed Model for Effective Mobility Degradation due to Atomic Interface Scattering

The Coherent Picture

- As V_{GS} increases, carriers are increasingly driven into the interfacial O layers where there is a modification to the crystalline periodicity and DOS leading to coherent back-scattering
- As V_{GS} increases, carriers are also increasingly driven into the region with interfacial Si distortion where there is additional modification to the crystalline periodicity and DOS leading to coherent back-scattering
- Long range distortion of the interfacial atomic positions corresponds to interface roughness which may also play role ...

The Incoherent Picture

- Phonon-assisted trapping in the interfacial O atoms de-phases electrons and leads to incoherent backscattering
- Other mechanisms ??

- Model is supported by Si orientation studies on μ_{eff} behavior
- Anomalous enhancement of nMOS mobility in strained Si devices may be explained by modification of interfacial atomic position leading to μ_{eff} enhancement

Quantum Transport Simulated Mobility: Atomistic Interface Scattering Model Calibration

Interface scattering model calibration:

- A monotonically increasing Σ^R is used to account for the increasing interfacial O and distorted Si DOS
- The interface model is spatially extended 0.5nm into both the SiO2 and Si to account for the spatial extent of the interfacial O and distorted Si
- Model is calibrated to effective mobility data

$$\Sigma^R_{i,i'}(E,\vec{k}_x) \equiv \alpha\sqrt{E_z - E_c}\,\theta(E_z - E_c)\delta_{i,i'}$$

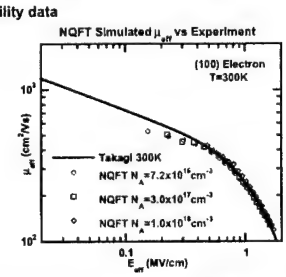

Quantum Transport Simulated Mobility: Atomistic Interface Scattering Model Calibration

- Incorporation of the effective mobility calibrated interface model leads to excellent theory-experiment agreement for 2D MOSFET quantum transport simulation
- Quantum transport MOSFET simulation can now serve as the basis for TCAD device simulator calibration and device engineering studies

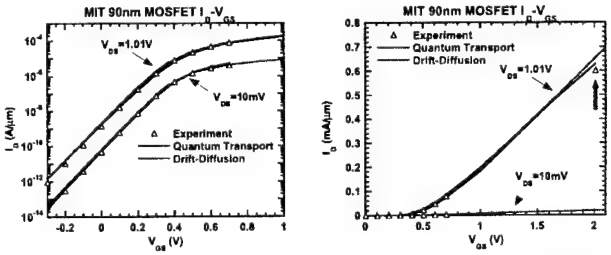

Quantum Transport Simulated Mobility: Ballistic Transport vs Scattering

- Ballistic quantum transport simulations reveal that the MIT 25nm device is operating at ~30% of the ballistic limit
- Interface scattering dominates 25nm MIT device I_{Dsat}
- If the atomic interface scattering model is to be believed, there is little hope of ever achieving ballistic performance in MOSFETs

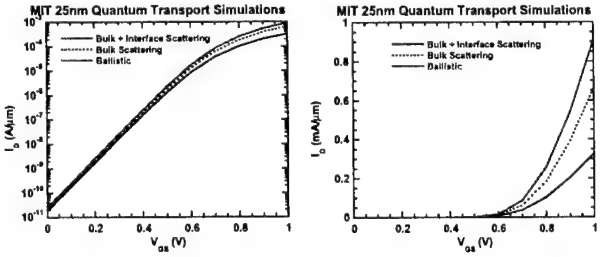

MIT MOSFET Simulation Comparison

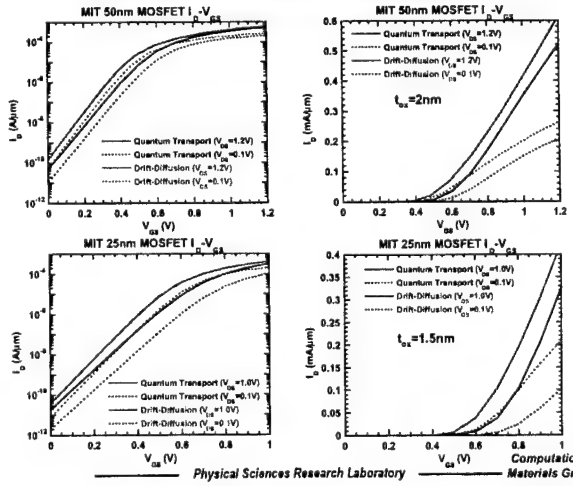

MIT MOSFET Simulation Comparison Eliminating V_t Shift

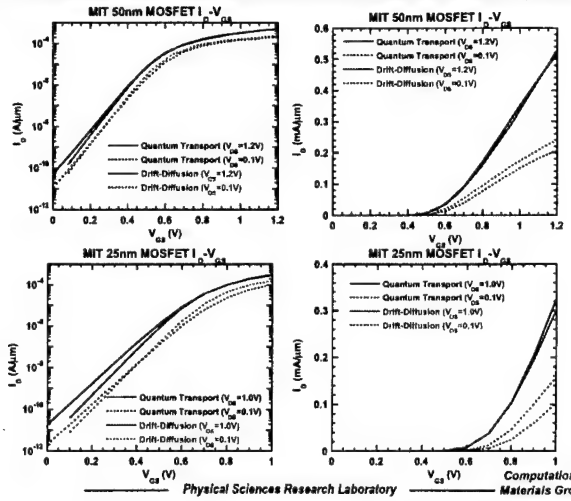

MIT MOSFET Simulation Comparison

Comparison Summary

- Centroid induced V_t shift is approximately 50meV for the 50nm MIT MOSFET (t_{ox}=2nm) and 100mev for the 25nm MIT MOSFET (t_{ox}=1.5nm) as compared to drift diffusion data
- Increasing DIBL, sub-threshold slope, and I_{off} are observed with decreasing L_{poly} (and t_{ox}) indicating the centroid shift may be compromising resistance to short channel effects
- Sub-threshold slope and I_{off} increase are also influenced by increasing sub-threshold tunneling with decreasing L_{poly} ... further study into relative effects of sub-threshold tunneling and centroid shift is required
- Drift-diffusion model show excellent agreement with calibrated quantum transport theory in predicting post-threshold behavior

Conclusion

Appropriately calibrated effective potential corrections applied to drift diffusion models will provide all the essential physics required for TCAD device simulation for the forseeable future

Quantum kinetics and the femtosecond time scale in optical excitation of semiconductors

Tilmann Kuhn

V.M. Axt, M. Glanemann, M. Herbst, J. Schilp, T. Wolterink

WESTFÄLISCHE WILHELMS-UNIVERSITÄT MÜNSTER

Institut für Festkörpertheorie

Work supported by the European Commission (TMR network "Ultrafast Quantum Optoelectronics") and by the Deutsche Forschungsgemeinschaft (Schwerpunktprogramm "Quantenkohärenz in Halbleitern")

Quantum kinetics in semiconductors
introduction

Semiclassical transport and kinetics

Free flights
- electrons accelerated by local electric field ($\sim$ grad V)

Scattering processes
- instantaneous in time
- local in space
- between well-defined k-states
- different mechanisms additive

Dynamical equation
- Boltzmann equation

Quantum kinetics in semiconductors
introduction

Quantum effects on short time and length scales

Energy-time uncertainty
- single-particle energies not conserved on short time-scales

Momentum-position uncertainty
- no local transitions between well-defined momentum states

Memory effects
- dynamics of distribution functions and polarizations non-local in time and space

Quantum-mechanical correlations
- scattering between renormalized states
- phonon-assisted transitions
- intracollisional field effect

Quantum kinetics in semiconductors
overview

Introduction

Phonon quantum kinetics in homogeneous systems
- density-matrix theory
- relation to NGFs
- energy-time uncertainty
- nonequilibrium phonons
- scattering between renormalized states
- phonon quantum beats
- intracollisional field effect

Phonon quantum kinetics in inhomogeneous systems
- different representations
- wave-packet dynamics
- coherent phonons
- carrier-trapping dynamics

Conclusions

Carrier-phonon interaction
1-band model

Hamiltonian

$$H = \sum_{\mathbf{k}} \epsilon_{\mathbf{k}}^{e} c_{\mathbf{k}}^{\dagger} c_{\mathbf{k}} + \sum_{\mathbf{q}} \hbar\omega_{\mathbf{q}} b_{\mathbf{q}}^{\dagger} b_{\mathbf{q}} + \sum_{\mathbf{k},\mathbf{q}} \left(g_{\mathbf{q}}^{e} c_{\mathbf{k}+\mathbf{q}}^{\dagger} b_{\mathbf{q}} c_{\mathbf{k}} + h.c. \right)$$

dynamical variables

distribution functions

$$f_{\mathbf{k}}^{e} = \langle c_{\mathbf{k}}^{\dagger} c_{\mathbf{k}} \rangle \qquad n_{\mathbf{q}} = \langle b_{\mathbf{q}}^{\dagger} b_{\mathbf{q}} \rangle$$

phonon-assisted density matrix

$$S_{\mathbf{k}+\mathbf{q},\mathbf{k}}^{e} = \frac{i}{\hbar} g_{\mathbf{q}}^{e} \langle c_{\mathbf{k}+\mathbf{q}}^{\dagger} b_{\mathbf{q}} c_{\mathbf{k}} \rangle$$

$\Rightarrow$ correlations between electrons and phonons

equations of motion

$$\frac{d}{dt} f_{\mathbf{k}}^{e} = \sum_{\mathbf{q}} \left[2\mathrm{Re}\left\{ S_{\mathbf{k}+\mathbf{q},\mathbf{k}}^{e} \right\} - 2\mathrm{Re}\left\{ S_{\mathbf{k},\mathbf{k}-\mathbf{q}}^{e} \right\} \right]$$

$$\frac{d}{dt} n_{\mathbf{q}} = \sum_{\mathbf{k}} 2\mathrm{Re}\left\{ S_{\mathbf{k}+\mathbf{q},\mathbf{k}}^{e} \right\}$$

Electron-phonon quantum kinetics
hierarchy

equation of motion for S

involves expectation values of 4 operators

$$\langle c_{\mathbf{k}-\mathbf{q}}^{\dagger} c_{\mathbf{k}'+\mathbf{q}'}^{\dagger} c_{\mathbf{k}'} c_{\mathbf{k}} \rangle \qquad \langle c_{\mathbf{k}'-\mathbf{q}'}^{\dagger} c_{\mathbf{k}} b_{\mathbf{q}'}^{\dagger} b_{\mathbf{q}} \rangle$$

$\Rightarrow$ hierarchy of equations of motion

truncation by factorization

$$\langle c_{\mathbf{k}'-\mathbf{q}'}^{\dagger} c_{\mathbf{k}} b_{\mathbf{q}'}^{\dagger} b_{\mathbf{q}} \rangle \approx f_{\mathbf{k}}^{e} n_{\mathbf{q}} \delta_{\mathbf{k},\mathbf{k}'-\mathbf{q}} \delta_{\mathbf{q},\mathbf{q}'}$$

$\Rightarrow$ neglecting higher order correlations

factorized equation of motion

$$\frac{d}{dt} S_{\mathbf{k}',\mathbf{k}}^{e} = \frac{i}{\hbar} \left(\epsilon_{\mathbf{k}'}^{e} - \epsilon_{\mathbf{k}}^{e} - \hbar\omega_{\mathbf{q}} \right) S_{\mathbf{k}',\mathbf{k}}^{e}$$

$$+ \frac{1}{\hbar^2} |g_{\mathbf{q}}^{e}|^2 \left[f_{\mathbf{k}'}^{e} (1 - f_{\mathbf{k}}^{e}) (n_{\mathbf{q}} + 1) - (1 - f_{\mathbf{k}'}^{e}) f_{\mathbf{k}}^{e} n_{\mathbf{q}} \right]$$

$\Rightarrow$ quantum kinetic second Born approximation

Electron-phonon quantum kinetics
memory effects and Markov limit

formal solution

$$S^{\epsilon}_{\mathbf{k}',\mathbf{k}}(t) = S^{0}_{\mathbf{k}',\mathbf{k}} \exp\left[\frac{i}{\hbar}\left(\epsilon^{\epsilon}_{\mathbf{k}'} - \epsilon^{\epsilon}_{\mathbf{k}} - \hbar\omega_{\mathbf{q}}\right) t\right]$$

$$+\frac{1}{\hbar^2}|g^{\epsilon}_{\mathbf{q}}|^2 \int_0^t d\tau \exp\left[\frac{i}{\hbar}\left(\epsilon^{\epsilon}_{\mathbf{k}'} - \epsilon^{\epsilon}_{\mathbf{k}} - \hbar\omega_{\mathbf{q}}\right)\tau\right]$$

$$\times\left[f^{\epsilon}_{\mathbf{k}'}(1-f^{\epsilon}_{\mathbf{k}})(n_{\mathbf{q}}+1) - (1-f^{\epsilon}_{\mathbf{k}'}) f^{\epsilon}_{\mathbf{k}} n_{\mathbf{q}}\right]_{(t-\tau)}$$

$\Rightarrow$ Dynamics with memory

Markov limit

$$\frac{d}{dt} f^{\epsilon}_{\mathbf{k}} = \frac{2\pi}{\hbar}\sum_{\mathbf{q},\pm} |g^{\epsilon}_{\mathbf{q}}|^2 \Big\{\delta(\epsilon^{\epsilon}_{\mathbf{k}} - \epsilon^{\epsilon}_{\mathbf{k}-\mathbf{q}} \mp \hbar\omega_{\mathbf{q}})$$

$$\times\left[(1-f^{\epsilon}_{\mathbf{k}})\left(n_{\mathbf{q}} + \frac{1}{2} \mp \frac{1}{2}\right) f^{\epsilon}_{\mathbf{k}-\mathbf{q}} - f^{\epsilon}_{\mathbf{k}}(1-f^{\epsilon}_{\mathbf{k}-\mathbf{q}})\left(n_{\mathbf{q}} + \frac{1}{2} \pm \frac{1}{2}\right)\right]$$

$$\frac{d}{dt} n_{\mathbf{q}} = \frac{2\pi}{\hbar}\sum_{\mathbf{k}} |g^{\epsilon}_{\mathbf{q}}|^2 \delta(\epsilon^{\epsilon}_{\mathbf{k}} - \epsilon^{\epsilon}_{\mathbf{k}-\mathbf{q}} - \hbar\omega_{\mathbf{q}})$$

$$\times\left[(1-f^{\epsilon}_{\mathbf{k}}) n_{\mathbf{q}} f^{\epsilon}_{\mathbf{k}-\mathbf{q}} - f^{\epsilon}_{\mathbf{k}}(1-f^{\epsilon}_{\mathbf{k}-\mathbf{q}})(n_{\mathbf{q}}+1)\right]$$

$\Rightarrow$ Boltzmann equations

Electron-phonon quantum kinetics
two-particle correlations

including deviations from factorization:

$$T^{(1)}_{\mathbf{k},\mathbf{k}',\mathbf{q}} = \frac{g_{\mathbf{q}} g^*_{\mathbf{k}'-\mathbf{k}}}{\hbar^2}\left[\langle c^\dagger_{\mathbf{k}+\mathbf{q}} b^\dagger_{\mathbf{k}'-\mathbf{k}} b_{\mathbf{q}} c_{\mathbf{k}'}\rangle - \delta_{\mathbf{k}',\mathbf{k}+\mathbf{q}} f^{\epsilon}_{\mathbf{k}} n_{\mathbf{q}}\right]$$

$$T^{(2)}_{\mathbf{k},\mathbf{k}',\mathbf{q}} = \frac{g_{\mathbf{q}} g_{\mathbf{k}'-\mathbf{k}}}{\hbar^2}\langle c^\dagger_{\mathbf{k}+\mathbf{q}} b_{\mathbf{k}-\mathbf{k}'} b_{\mathbf{q}} c_{\mathbf{k}'}\rangle$$

$$T^{(3)}_{\mathbf{k},\mathbf{k}',\mathbf{q}} = \frac{|g_{\mathbf{q}}|^2}{\hbar^2}\left[\langle c^\dagger_{\mathbf{k}+\mathbf{q}} c^\dagger_{\mathbf{k}'} c_{\mathbf{k}'+\mathbf{q}} c_{\mathbf{k}}\rangle + \delta_{\mathbf{k}',\mathbf{k}} f^{\epsilon}_{\mathbf{k}} f^{\epsilon}_{\mathbf{k}+\mathbf{q}}\right]$$

exact equation of motion for S

$$\frac{d}{dt} S^{\epsilon}_{\mathbf{k}',\mathbf{k}} = \frac{i}{\hbar}\left(\epsilon^{\epsilon}_{\mathbf{k}'} - \epsilon^{\epsilon}_{\mathbf{k}} - \hbar\omega_{\mathbf{q}}\right) S^{\epsilon}_{\mathbf{k}',\mathbf{k}}$$

$$+\frac{1}{\hbar^2}|g^{\epsilon}_{\mathbf{q}}|^2\left[f^{\epsilon}_{\mathbf{k}'}(1-f^{\epsilon}_{\mathbf{k}})(n_{\mathbf{q}}+1) - (1-f^{\epsilon}_{\mathbf{k}'}) f^{\epsilon}_{\mathbf{k}} n_{\mathbf{q}}\right]$$

$$+\sum_{\mathbf{k}''}\left[T^{(1)}_{\mathbf{k},\mathbf{k}'',\mathbf{q}} - T^{(1)}_{\mathbf{k}'',\mathbf{k},\mathbf{q}} + T^{(2)}_{\mathbf{k},\mathbf{k}'',\mathbf{q}} - T^{(2)}_{\mathbf{k}'',\mathbf{k},\mathbf{q}} + T^{(3)}_{\mathbf{k},\mathbf{k}'',\mathbf{q}}\right]$$

(with $\mathbf{q} = \mathbf{k} - \mathbf{k}'$)

required: equations of motion for $T^{(i)}$

Electron-phonon quantum kinetics
two-particle correlations

truncation by factorization on 5-point level

$$\langle c^\dagger_{\mathbf{k}} b^\dagger_{\mathbf{q}} b_{\mathbf{q}} b_{\mathbf{q}'} c_{\mathbf{k}'}\rangle \approx \delta_{\mathbf{q},\mathbf{q}'} n_{\mathbf{q}} \langle c^\dagger_{\mathbf{k}} b_{\mathbf{q}'} c_{\mathbf{k}'}\rangle + \delta_{\mathbf{q},\mathbf{q}'} n_{\mathbf{q}} \langle c^\dagger_{\mathbf{k}} b_{\mathbf{q}'} c_{\mathbf{k}'}\rangle$$

factorized equation of motion for T

$$\frac{d}{dt} T^{(1)}_{\mathbf{k},\mathbf{k}',\mathbf{q}} = \frac{i}{\hbar}\left(\epsilon^{\epsilon}_{\mathbf{k}+\mathbf{q}} - \epsilon^{\epsilon}_{\mathbf{k}'} + \hbar\omega_{\mathbf{q}'} - \hbar\omega_{\mathbf{q}}\right) T^{(1)}_{\mathbf{k},\mathbf{k}',\mathbf{q}}$$

$$+\frac{1}{\hbar^2}|g^{\epsilon}_{\mathbf{q}'}|^2\left[(1+n_{\mathbf{q}'} - f^{\epsilon}_{\mathbf{k}+\mathbf{q}}) S^{\epsilon}_{\mathbf{k}'+\mathbf{q},\mathbf{k}'} - (n_{\mathbf{q}'} + f^{\epsilon}_{\mathbf{k}'}) S^{\epsilon}_{\mathbf{k}+\mathbf{q},\mathbf{k}}\right]$$

$$+\frac{1}{\hbar^2}|g^{\epsilon}_{\mathbf{q}}|^2\left[(1+n_{\mathbf{q}} - f^{\epsilon}_{\mathbf{k}'}) S^{\epsilon *}_{\mathbf{k}'+\mathbf{q},\mathbf{k}+\mathbf{q}} - (n_{\mathbf{q}} + f^{\epsilon}_{\mathbf{k}+\mathbf{q}}) S^{\epsilon *}_{\mathbf{k}',\mathbf{k}}\right]$$

(with $\mathbf{q}' = \mathbf{k}' - \mathbf{k}$)

formal solution yields $T^{(1)}_{\mathbf{k},\mathbf{k}',\mathbf{q}}(t) = T^{(1)}_{\mathbf{k},\mathbf{k}',\mathbf{q}}\left[f^{\epsilon}_{\mathbf{k}'}, n_{\mathbf{q}}, S^{\epsilon}_{\mathbf{k},\mathbf{k}'}\right]_{(t-\tau)}$

$\Rightarrow$ closed integro-differential equation for S

$\Rightarrow$ quantum kinetic fourth Born approximation

Electron-phonon quantum kinetics
diagonal approximation

Classification of higher-order contributions

equation of motion for $S_{\mathbf{k},\mathbf{k}'}$ involves terms

(a) $\sim S_{\mathbf{k},\mathbf{k}'}$ (b) $\sim \sum_{\mathbf{q},\mathbf{q}'} S_{\mathbf{k}+\mathbf{q},\mathbf{k}'+\mathbf{q}'}$

assumption: (b) small due to random phases of S

$\Rightarrow$ diagonal approximation: k-components decoupled

Markov approximation for $T^{(i)}$

$$\frac{d}{dt} S^{\epsilon}_{\mathbf{k}',\mathbf{k}} = \left[\frac{i}{\hbar}\left(\epsilon^{\epsilon}_{\mathbf{k}'} - \epsilon^{\epsilon}_{\mathbf{k}} - \hbar\omega_{\mathbf{q}}\right) - \Gamma_{\mathbf{k}'} - \Gamma_{\mathbf{k}}\right] S^{\epsilon}_{\mathbf{k}',\mathbf{k}}$$

$$+\frac{1}{\hbar^2}|g^{\epsilon}_{\mathbf{q}}|^2\left[f^{\epsilon}_{\mathbf{k}'}(1-f^{\epsilon}_{\mathbf{k}})(n_{\mathbf{q}}+1) - (1-f^{\epsilon}_{\mathbf{k}'}) f^{\epsilon}_{\mathbf{k}} n_{\mathbf{q}}\right]$$

with

$$\Gamma_{\mathbf{k}} = \frac{\pi}{\hbar}\sum_{\mathbf{q},\pm} |g^{\epsilon}_{\mathbf{q}}|^2 \delta(\epsilon^{\epsilon}_{\mathbf{k}} - \epsilon^{\epsilon}_{\mathbf{k}+\mathbf{q}} \pm \hbar\omega_{\mathbf{q}})$$

$$\times\left[(n_{\mathbf{q}} + \frac{1}{2} \pm \frac{1}{2}) f^{\epsilon}_{\mathbf{k}+\mathbf{q}} + (n_{\mathbf{q}} + \frac{1}{2} \mp \frac{1}{2})(1 - f^{\epsilon}_{\mathbf{k}+\mathbf{q}})\right]$$

$\Rightarrow$ polaron self energy (real part neglected)

$\Rightarrow$ quantum kinetics with damped memory

Electron-phonon quantum kinetics
density matrices and Greens functions

Generalized Kadanoff-Baym Equation

$$\frac{d}{dt} f^{\epsilon}_{\mathbf{k}}(t) = -i\frac{d}{dt} G^{<}_{\mathbf{k}}(t,t)$$

$$= -\int_{-\infty}^{t} dt'\Big[\Sigma^{>}_{\mathbf{k}}(t,t') G^{<}_{\mathbf{k}}(t',t) - \Sigma^{<}_{\mathbf{k}}(t,t') G^{>}_{\mathbf{k}}(t',t)$$

$$- G^{>}_{\mathbf{k}}(t,t') \Sigma^{<}_{\mathbf{k}}(t',t) + G^{<}_{\mathbf{k}}(t,t') \Sigma^{>}_{\mathbf{k}}(t',t)\Big]$$

self-energy

$$\Sigma^{\lessgtr}_{\mathbf{k}}(t,t') = \frac{i}{\hbar^2}\sum_{\mathbf{q}} |g^{\epsilon}_{\mathbf{q}}|^2 D^{\lessgtr}_{\mathbf{k}}(t,t') G^{\lessgtr}_{\mathbf{k}-\mathbf{q}}(t,t')$$

Generalized Kadanoff-Baym Ansatz (GKBA)

$$G^{<}_{\mathbf{k}}(t,t') = -G^{r}_{\mathbf{k}}(t,t') f^{<}_{\mathbf{k}}(t') + f^{<}_{\mathbf{k}}(t) G^{a}_{\mathbf{k}}(t,t')$$

second Born approximation:

GKBA with $G^{r(0)}, G^{a(0)}$ (no Σ)

fourth Born approximation, diagonal terms:

GKBA with G^r, G^a including Σ

Carrier-phonon interaction
1-band model

Boltzmann

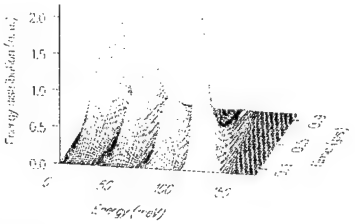

quantum kinetic

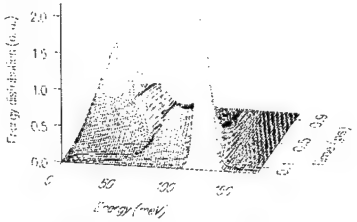

relaxation from given initial distribution

$\Rightarrow$ time-dependent broadening

Carrier-phonon interaction
1-band model

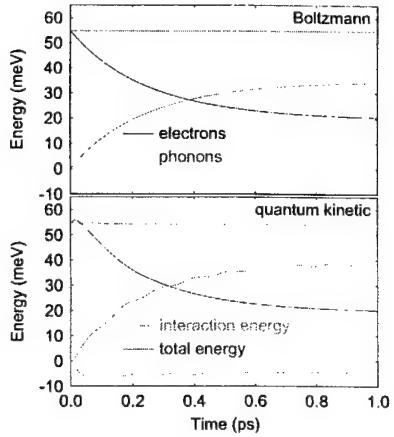

mean energy per electron
⇒ energy conservation with interaction

Carrier-phonon interaction
2-band model

dynamical variables

distribution functions

$$f_k^e = \langle c_k^\dagger c_k \rangle \qquad f_k^h = \langle d_k^\dagger d_k \rangle \qquad n_q = \langle b_q^\dagger b_q \rangle$$

interband polarization

$$p_k = \langle d_{-k} c_k \rangle$$

phonon-assisted density matrices

$$S^e_{k',k} = \frac{i}{\hbar} g^e_q \left\langle c_{k'}^\dagger b_q c_k \right\rangle \qquad S^h_{-k',-k} = \frac{i}{\hbar} g^h_q \left\langle d_{-k'}^\dagger b_q d_{-k} \right\rangle$$

$$T^{(+)}_{-k',k} = \frac{i}{\hbar} g^e_q \langle d_{-k'} b_q c_k \rangle \qquad T^{(-)}_{-k',k} = \frac{i}{\hbar} g^e_q \langle c_{k'}^\dagger b_q d_{-k}^\dagger \rangle$$

Equations of motion
distribution functions and polarization

$$\frac{d}{dt} f_k^e = 2\Re\{i\bar{\mu}_k^* p_k\} + \sum_q \left[2\Re\{S^e_{k+q,k}\} - 2\Re\{S^e_{k,k-q}\}\right]$$

$$\frac{d}{dt} f_{-k}^h = 2\Re\{i\bar{\mu}_k^* p_k\} + \sum_q \left[2\Re\{S^h_{-k+q,-k}\} - 2\Re\{S^h_{-k,-k-q}\}\right]$$

$$\frac{d}{dt} n_q = \sum_k \left[2\Re\{S^e_{k+q,k}\} + 2\Re\{S^h_{-k+q,-k}\}\right]$$

$$\frac{d}{dt} p_k = -i\Omega_k^p p_k - i\bar{\mu}_k (1 - f_k^e - f_{-k}^h) + \sum_q \left[T^{(+)}_{-k-q,k} - T^{(-)*}_{-k+q,k} - T^{(+)}_{-k,k-q} + T^{(-)*}_{-k,k+q}\right]$$

⇒ semiconductor Bloch equations

with
$$\hbar\bar{\mu}_k = \mathbf{M}_k \cdot \mathbf{E}_0(t) e^{-i\omega_l t} - \sum_q V_q p_{k+q}$$

$$\hbar\Omega_k^p = \bar{\epsilon}_k^e + \bar{\epsilon}_k^h$$

$$\bar{\epsilon}_k^{e,h} = \epsilon_k^{e,h} - \sum_q V_q f_{k+q}^{e,h}$$

Equations of motion
phonon-assisted density matrices

$$\frac{d}{dt} S^e_{k',k} = \frac{i}{\hbar}\left(\bar{\epsilon}^e_{k'} - \bar{\epsilon}^e_k - \hbar\omega_{op}\right) S^e_{k',k}$$
$$+ i\,\bar{\mu}_{k'}^* T^{(+)}_{-k',k} - i\,\bar{\mu}_k T^{(-)}_{-k,k'}$$
$$+ \frac{1}{\hbar^2}|g^e_q|^2 \left[(n_q+1)(1-f^e_{k'}) f^e_k - n_q f^e_{k'}(1-f^e_k)\right]$$
$$- \frac{1}{\hbar^2} g^e_q g^h_q \langle b_q b_q \rangle$$

with
$$\hbar\bar{\mu}_k = \mathbf{M}_k \cdot \mathbf{E}_0(t) e^{-i\omega_l t} - \sum_q V_q p_{k+q}$$

$$\bar{\epsilon}_k^{e,h} = \epsilon_k^{e,h} - \sum_q V_q f_{k+q}^{e,h}$$

cross terms (renormalizations)

"Boltzmann" terms (scattering processes)

polarization scattering (eh-coherence)

Carrier-phonon interaction
2-band model

Boltzmann generation and scattering

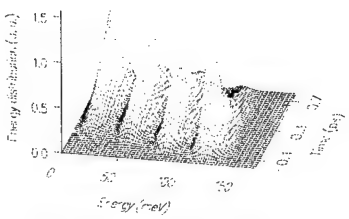

coherent generation, Boltzmann scattering

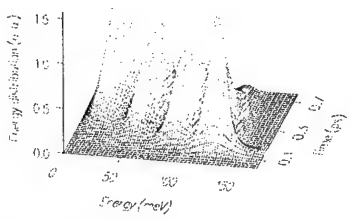

excitation with 100 fs pulse
⇒ broadening of generation

Carrier-phonon interaction
2-band model

quantum kinetic

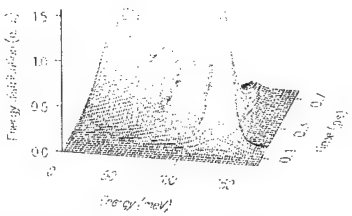

quantum kinetic with renormalizations

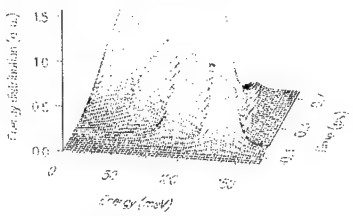

excitation with 100 fs pulse
⇒ time-dependent broadening

Carrier-phonon interaction
2-band model

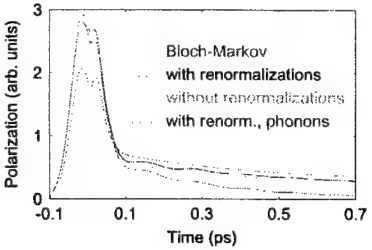

decay of incoherently summed polarization
($P = \sum |p_k|$)
⇒ phonon quantum beats

2-band model with constant field
equations of motion

$$\frac{d}{dt} f_{\mathbf{k}}^{e} = \frac{eE}{\hbar}\frac{\partial}{\partial k_z} f_{\mathbf{k}}^{e} + 2\mathrm{Re}\left\{i\tilde{\mu}_{\mathbf{k}}^{*} p_{\mathbf{k}}\right\} + \sum_{\mathbf{q}}\left[2\mathrm{Re}\left\{S_{\mathbf{k}+\mathbf{q},\mathbf{k}}^{e}\right\} - 2\mathrm{Re}\left\{S_{\mathbf{k},\mathbf{k}-\mathbf{q}}^{e}\right\}\right]$$

$$\frac{d}{dt} p_{\mathbf{k}} = \frac{eE}{\hbar}\frac{\partial}{\partial k_z} p_{\mathbf{k}} - i\left(\tilde{\epsilon}_{\mathbf{k}}^{e} + \tilde{\epsilon}_{\mathbf{k}}^{h}\right) p_{\mathbf{k}} - i\tilde{\mu}_{\mathbf{k}}\left(1 - f_{\mathbf{k}}^{e} - f_{-\mathbf{k}}^{h}\right) + \sum_{\mathbf{q}}\left[T_{-\mathbf{k}-\mathbf{q},\mathbf{k}}^{(+)} - T_{-\mathbf{k}+\mathbf{q},\mathbf{k}}^{(-)*} - T_{-\mathbf{k},\mathbf{k}-\mathbf{q}}^{(+)} + T_{-\mathbf{k},\mathbf{k}+\mathbf{q}}^{(-)*}\right]$$

$$\frac{d}{dt} S_{\mathbf{k}',\mathbf{k}}^{e} = \frac{eE}{\hbar}\left(\frac{\partial}{\partial k_z} + \frac{\partial}{\partial k_z'}\right) S_{\mathbf{k}',\mathbf{k}}^{e} + \frac{i}{\hbar}\left(\tilde{\epsilon}_{\mathbf{k}'}^{e} - \tilde{\epsilon}_{\mathbf{k}}^{e} - \hbar\omega_{LO}\right) S_{\mathbf{k}',\mathbf{k}}^{e} + i\,\tilde{\mu}_{\mathbf{k}'}^{*} T_{-\mathbf{k}',\mathbf{k}}^{(+)} - i\tilde{\mu}_{\mathbf{k}} T_{-\mathbf{k},\mathbf{k}'}^{(-)} - \frac{1}{\hbar^2} g_{\mathbf{q}}^{e} g_{\mathbf{q}}^{h*}\, p_{\mathbf{k}'}^{*} p_{\mathbf{k}} + \frac{1}{\hbar^2}\left|g_{\mathbf{q}}^{e}\right|^2 \left[\left(n_{\mathbf{q}}+1\right)\left(1 - f_{\mathbf{k}}^{e}\right) f_{\mathbf{k}'}^{e} - n_{\mathbf{q}} f_{\mathbf{k}}^{e}\left(1 - f_{\mathbf{k}'}^{e}\right)\right]$$

with
$$\hbar\tilde{\mu}_{\mathbf{k}} = -M\cdot E - \mathbf{M}_{\mathbf{k}}\cdot\mathbf{E}_0(t)e^{-i\omega_r t} - \sum_{\mathbf{q}} V_{\mathbf{q}} p_{\mathbf{k}+\mathbf{q}}$$

$$\tilde{\epsilon}_{\mathbf{k}}^{e,h} = \epsilon_{\mathbf{k}}^{e,h} - \sum_{\mathbf{q}} V_{\mathbf{q}} f_{\mathbf{k}+\mathbf{q}}^{e,h}$$

acceleration terms
Zener term

Intracollisional field effect
2-band model, quantum wire

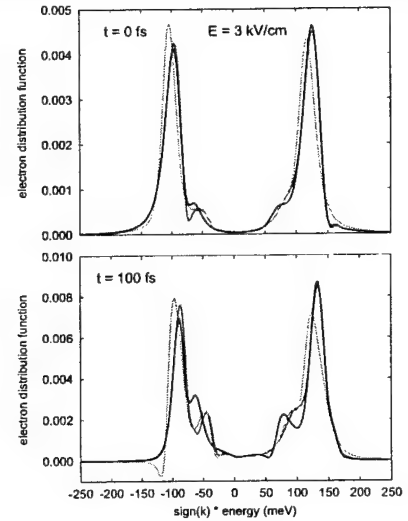

drift term for f, p, S, T
drift term for f, p
drift term for f, S, T

Electron-phonon quantum kinetics
spatially inhomogeneous system

density matrix theory: dynamical variables

distribution functions
$$f_{\mathbf{k}\mathbf{k}'}^{e} = \langle c_{\mathbf{k}}^{\dagger} c_{\mathbf{k}'}\rangle \qquad f_{\mathbf{k}\mathbf{k}'}^{h} = \langle d_{\mathbf{k}}^{\dagger} d_{\mathbf{k}'}\rangle$$
interband polarization
$$p_{\mathbf{k}\mathbf{k}'} = \langle d_{-\mathbf{k}} c_{\mathbf{k}'}\rangle \qquad p_{\mathbf{k}\mathbf{k}'}^{*} = \langle c_{\mathbf{k}}^{\dagger} d_{-\mathbf{k}}^{\dagger}\rangle$$
coherent phonon amplitudes
$$B_{\mathbf{q}} = \langle b_{\mathbf{q}}\rangle \qquad B_{\mathbf{q}}^{*} = \langle b_{\mathbf{q}}^{\dagger}\rangle$$
incoherent phonon distribution function
$$n_{\mathbf{q}\mathbf{q}'} = \langle (b_{\mathbf{q}}^{\dagger} - B_{\mathbf{q}}^{*})(b_{\mathbf{q}'} - B_{\mathbf{q}'})\rangle$$
phonon assisted density matrices

$$S_{\mathbf{k}',\mathbf{q},\mathbf{k}}^{e} = \frac{i}{\hbar} g_{\mathbf{q}} \langle c_{\mathbf{k}'}^{\dagger}(b_{\mathbf{q}} - B_{\mathbf{q}}) c_{\mathbf{k}}\rangle \qquad S_{\mathbf{k}',\mathbf{q},\mathbf{k}}^{h} = -\frac{i}{\hbar} g_{\mathbf{q}} \langle d_{\mathbf{k}'}^{\dagger}(b_{\mathbf{q}} - B_{\mathbf{q}}) d_{\mathbf{k}}\rangle$$

$$T_{\mathbf{k}',\mathbf{q},\mathbf{k}}^{(+)} = \frac{i}{\hbar} g_{\mathbf{q}} \langle d_{-\mathbf{k}'}(b_{\mathbf{q}} - B_{\mathbf{q}}) c_{\mathbf{k}}\rangle \qquad T_{\mathbf{k}',\mathbf{q},\mathbf{k}}^{(-)} = -\frac{i}{\hbar} g_{\mathbf{q}} \langle d_{-\mathbf{k}'}(b_{\mathbf{q}}^{\dagger} - B_{\mathbf{q}}^{*}) c_{\mathbf{k}}\rangle$$

Spatially inhomogeneous system
equations of motion

distribution functions
$$\frac{d}{dt} f_{\mathbf{k}\mathbf{k}'}^{e} = \frac{i}{\hbar}\sum_{\mathbf{k}''}\left[\mathcal{E}_{\mathbf{k}\mathbf{k}''}^{e} f_{\mathbf{k}''\mathbf{k}'}^{e} - \mathcal{E}_{\mathbf{k}''\mathbf{k}'}^{e} f_{\mathbf{k}\mathbf{k}''}^{e} + \mathcal{U}_{\mathbf{k}\mathbf{k}''}^{*} p_{\mathbf{k}''\mathbf{k}'} - \mathcal{U}_{\mathbf{k}''\mathbf{k}'} p_{\mathbf{k}\mathbf{k}''}\right] + \sum_{\mathbf{q}}\left[S_{\mathbf{k}+\mathbf{q},\mathbf{q},\mathbf{k}'}^{e} - S_{\mathbf{k}',\mathbf{q},\mathbf{k}-\mathbf{q}}^{e*} + S_{\mathbf{k}'+\mathbf{q},\mathbf{q},\mathbf{k}}^{e*} - S_{\mathbf{k},\mathbf{q},\mathbf{k}'-\mathbf{q}}^{e}\right]$$

coherent phonon amplitude
$$\frac{d}{dt} B_{\mathbf{q}} = -i\omega_{op} B_{\mathbf{q}} + \frac{i}{\hbar} g_{\mathbf{q}} \sum_{\mathbf{k}}\left[f_{\mathbf{k},\mathbf{k}+\mathbf{q}}^{e} - f_{\mathbf{k},\mathbf{k}+\mathbf{q}}^{h}\right]$$

energy matrices:
$$\mathcal{E}_{\mathbf{k}\mathbf{k}'}^{e,h} = \left[\epsilon_{\mathbf{k}}^{e,h} \pm \frac{ieE}{2}\left(\frac{\partial}{\partial k_z} - \frac{\partial}{\partial k_z'}\right)\right]\delta_{\mathbf{k},\mathbf{k}'} + V_{\mathbf{k}-\mathbf{k}'}^{exp} - \sum_{\mathbf{q}}\left[V_{\mathbf{q}} f_{\mathbf{k}'+\mathbf{q},\mathbf{k}+\mathbf{q}}^{e,h} - V_{\mathbf{k}-\mathbf{k}'}\left(f_{\mathbf{q},\mathbf{k}'-\mathbf{k}+\mathbf{q}}^{e} - f_{\mathbf{q},\mathbf{k}'-\mathbf{k}+\mathbf{q}}^{h}\right)\right] \pm g_{|\mathbf{k}-\mathbf{k}'|}\left(B_{\mathbf{k}-\mathbf{k}'} - B_{\mathbf{k}'-\mathbf{k}}^{*}\right)$$

effective field matrices:
$$\mathcal{U}_{\mathbf{k}\mathbf{k}'} = EM_{\mathbf{k}}\delta_{\mathbf{k},\mathbf{k}'} + \mathbf{M}_{\frac{1}{2}(\mathbf{k}+\mathbf{k}')}\cdot\mathbf{E}_{\mathbf{k}-\mathbf{k}'}^{(+)}(t) - \sum_{\mathbf{q}} V_{\mathbf{q}} p_{\mathbf{k}'+\mathbf{q},\mathbf{k}+\mathbf{q}}$$

single-particle potential
external field (drift and Zener term)
exchange energy and Coulomb enhancement
induced field (Hartree term)
coherent phonons

Spatially inhomogeneous system
equations of motion

phonon assisted density matrices

$$\frac{d}{dt} S_{\mathbf{k},\mathbf{q},\mathbf{k}'}^{e} = \frac{i}{\hbar}\sum_{\mathbf{k}''}\left(\mathcal{E}_{\mathbf{k}\mathbf{k}''}^{e} S_{\mathbf{k}'',\mathbf{q},\mathbf{k}'}^{e} - \mathcal{E}_{\mathbf{k}''\mathbf{k}'}^{e} S_{\mathbf{k},\mathbf{q},\mathbf{k}''}^{e}\right) - i\omega_{op} S_{\mathbf{k},\mathbf{q},\mathbf{k}'}^{e} + \frac{i}{\hbar}\sum_{\mathbf{k}''}\left(\mathcal{U}_{\mathbf{k}\mathbf{k}''}^{*} T_{\mathbf{k}'',\mathbf{q},\mathbf{k}'}^{(+)} - \mathcal{U}_{\mathbf{k}''\mathbf{k}'} T_{\mathbf{k},\mathbf{q},\mathbf{k}''}^{(-)}\right) + \frac{1}{\hbar^2}\sum_{\mathbf{q}',\mathbf{k}''} g_{\mathbf{q}} g_{\mathbf{q}'}^{*}\left[\left(n_{\mathbf{q}'\mathbf{q}} + \delta_{\mathbf{q}'\mathbf{q}}\right) f_{\mathbf{k},\mathbf{k}''+\mathbf{q}}^{e}\left(\delta_{\mathbf{k}''\mathbf{k}'} - f_{\mathbf{k}''\mathbf{k}'}^{e}\right) - n_{\mathbf{q}'\mathbf{q}} f_{\mathbf{k}''\mathbf{k}'}^{e}\left(\delta_{\mathbf{k}'',\mathbf{k}-\mathbf{q}} - f_{\mathbf{k}'',\mathbf{k}-\mathbf{q}}^{e}\right)\right] - \frac{1}{\hbar^2}\left|g_{\mathbf{q}}\right|^2 p_{\mathbf{k}''\mathbf{k}}^{*} p_{\mathbf{k}''-\mathbf{q},\mathbf{k}}$$

renormalization of scattering dynamics due to:
external field (*intracollisional field effect*)
induced field
coherent phonons
exchange energy and Coulomb enhancement
spatial inhomogeneities

Spatially inhomogeneous system
Wigner representation

dynamical variables:

$$f^e(\mathbf{k},\mathbf{r}) = \sum_{\mathbf{q}} e^{i\mathbf{q}\mathbf{r}} \langle c^\dagger_{\mathbf{k}-\frac{1}{2}\mathbf{q}} c_{\mathbf{k}+\frac{1}{2}\mathbf{q}} \rangle$$

$$p(\mathbf{k},\mathbf{r}) = \sum_{\mathbf{q}} e^{i\mathbf{q}\mathbf{r}} \langle d_{-\mathbf{k}+\frac{1}{2}\mathbf{q}} c_{\mathbf{k}+\frac{1}{2}\mathbf{q}} \rangle$$

$$B(\mathbf{r}) = \sum_{\mathbf{q}} e^{i\mathbf{q}\mathbf{r}} B_{\mathbf{q}}$$

spatially resolved variables:

electron density $n^e(\mathbf{r}) = \sum_{\mathbf{k}} f^e(\mathbf{k},\mathbf{r})$

energy density $u^e(\mathbf{r}) = \sum_{\mathbf{k}} \epsilon^e_{\mathbf{k}} f^e(\mathbf{k},\mathbf{r})$

mean kinetic energy per carrier $E(\mathbf{r}) = \frac{u^e(\mathbf{r})}{n^e(\mathbf{r})}$

lattice polarization $\mathbf{P}(\mathbf{r}) = \frac{-i\epsilon_0}{e} \sum_{\mathbf{q}} \mathbf{q} g_{\mathbf{q}} e^{i\mathbf{q}\mathbf{r}} (B_{\mathbf{q}} - B^*_{-\mathbf{q}})$

Spatially resolved kinetics
density and mean energy

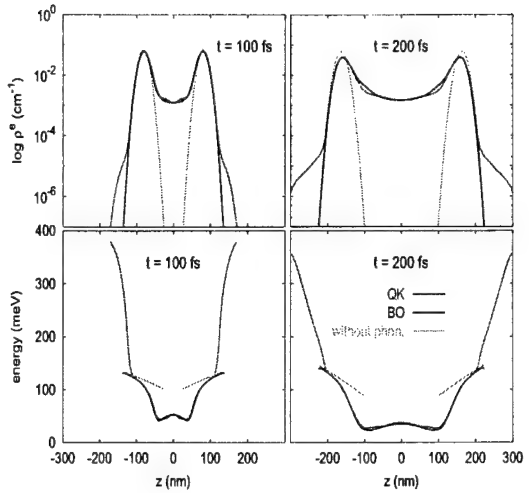

Kinetics of charge separation
coherent phonons

without/with incoherent phonons

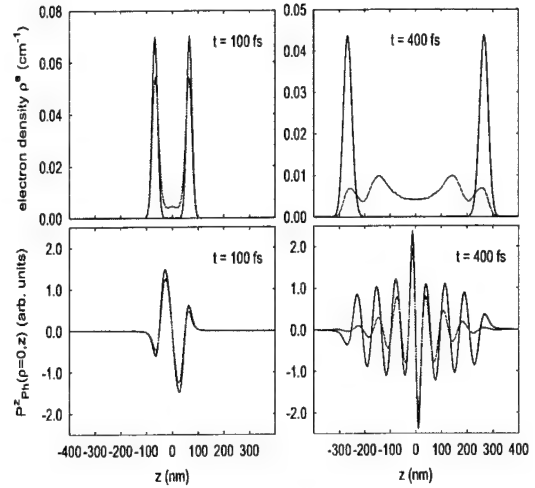

Spatially resolved kinetics
Wigner function

t = 100 fs

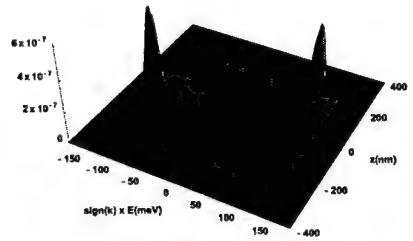

t = 300 fs

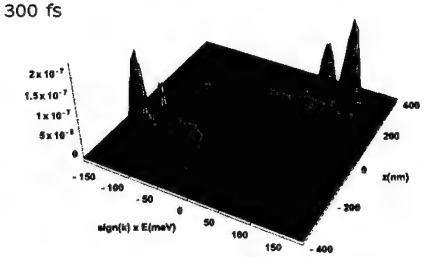

Spatially resolved kinetics
Wigner function

t = 100 fs, quantum kinetic

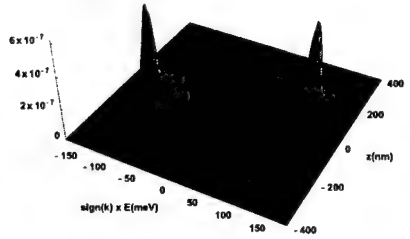

t = 100 fs Boltzmann

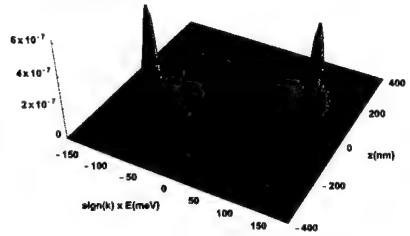

Dynamics with inhomogeneous potential
carrier trapping process

transitions between states of different dimensions

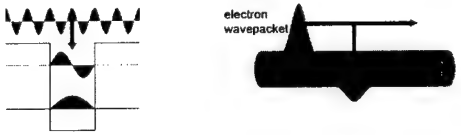

experimental realization & near-field spectroscopy

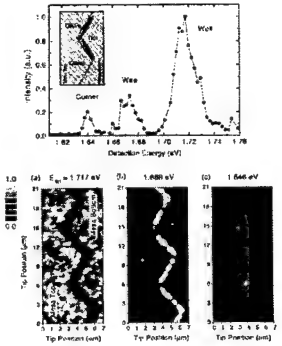

Ch. Lienau et al., phys. stat. sol. (a) **178**, 471 (2000)

Carrier trapping in dot states
shallow smooth potential

initial energy: 18 meV, width: 7.5 meV

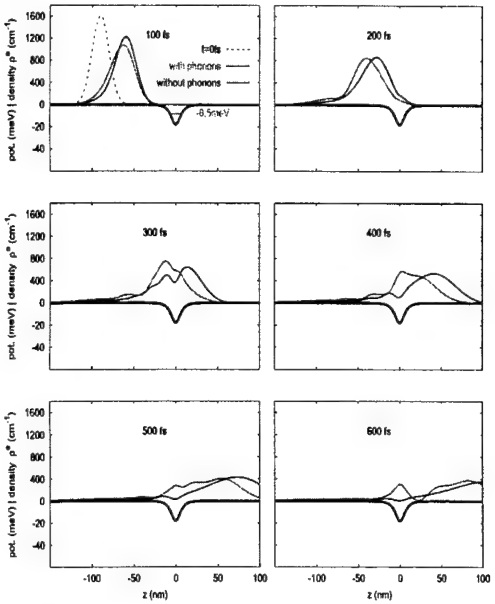

Carrier trapping in dot states
shallow smooth potential

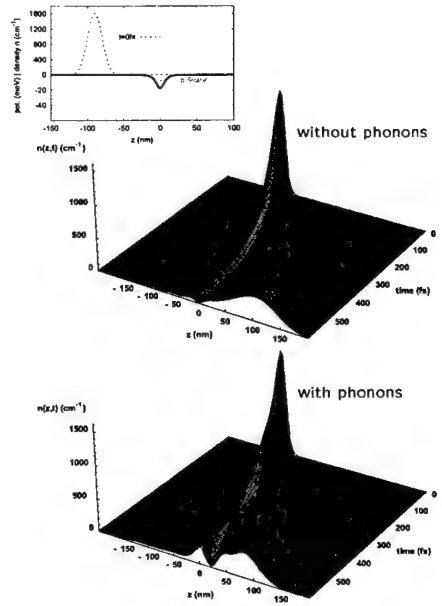

Carrier trapping in dot states
resonant case

initial energy: 18 meV, width: 7.5 meV

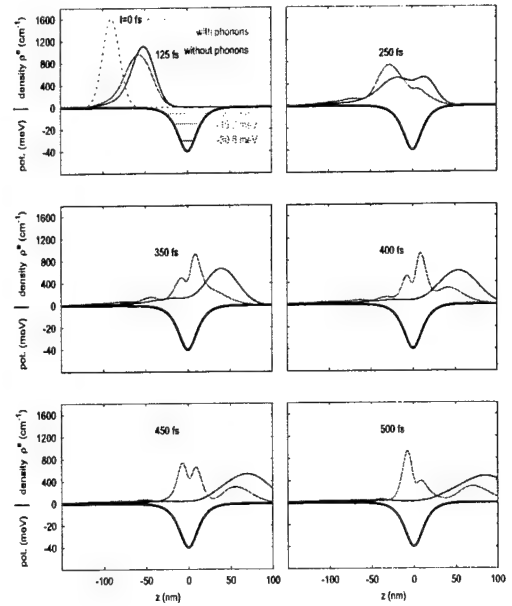

Carrier trapping in dot states
smooth potential, resonant case

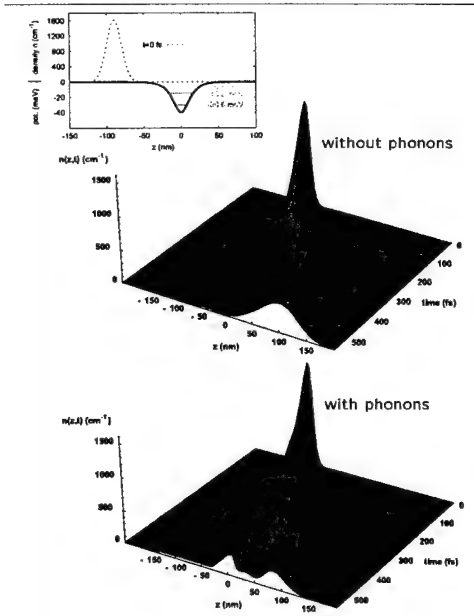

Carrier trapping in dot states
density matrix of bound states

shallow smooth potential, non-resonant case

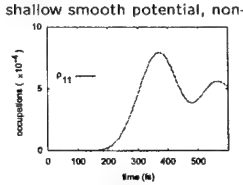

smooth potential, non-resonant case

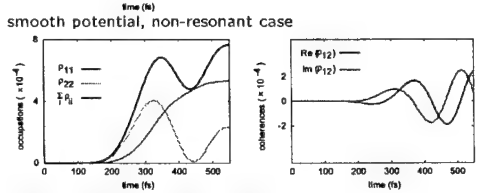

smooth potential, resonant case

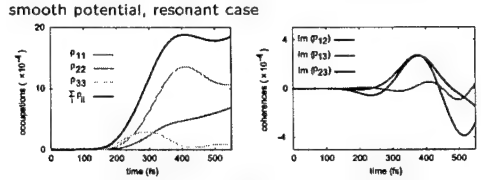

⇒ Non-monotonous behavior of occupations

⇒ Trapping into superposition of eigenstates

Carrier trapping in dot states
square well potential

initial energy: 18 meV, width: 7.5 meV

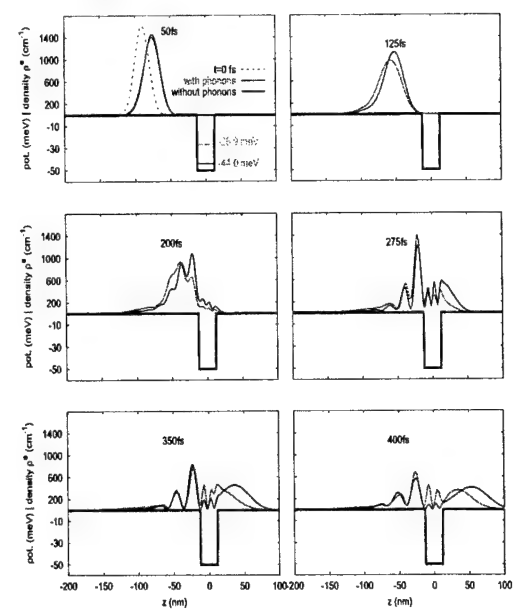

Carrier trapping in dot states

square well potential

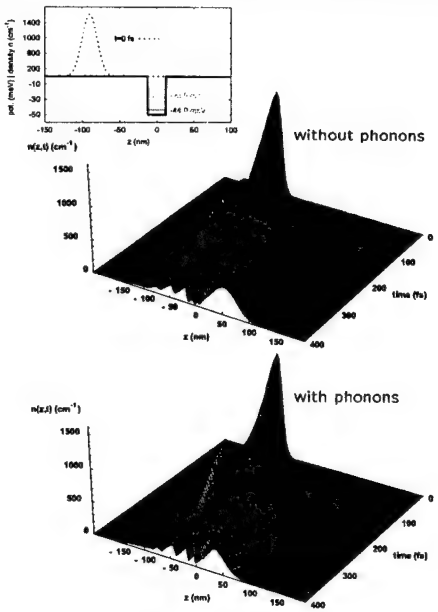

Quantum kinetics in semiconductors

conclusions

Phonon quantum kinetics in homogeneous systems
- density-matrix theory
- relation to NGFs
- energy-time uncertainty
- nonequilibrium phonons
- scattering between renormalized states
- phonon quantum beats
- intracollisional field effect

Phonon quantum kinetics in inhomogeneous systems
- different representations
- wave-packet dynamics
- coherent phonons
- carrier-trapping dynamics

Single-Electron Tunneling through Quantum Dots

(Single-Electron Charging in Quantum Dot Arrays)

Rolf J. Haug

University of Hannover
Germany

Overview:

- Single-Electron Tunneling
- Transport through Quantum Dots
- Spectroscopy
- Influence of Emitter States
- Spin Effects
- Conclusions

Transport through a Quantum Dot:

Tunneling:

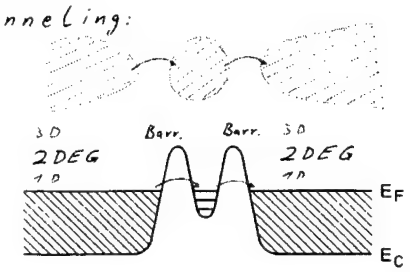

- Discrete Energy Levels (Confinement) ΔE
- Charging Energy (Capacitance C) $E_c = \frac{e^2}{2C}$

Charging Effects

Coulomb Staircase

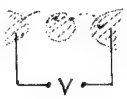

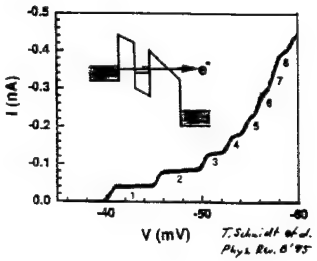

Coulomb Blockade and Single-Electron Tunneling

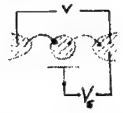

Single-Electron Transistor

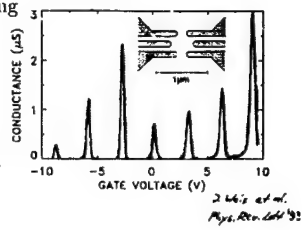

Double-barrier quantum-dot

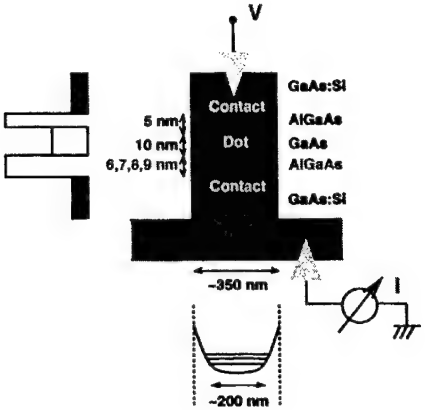

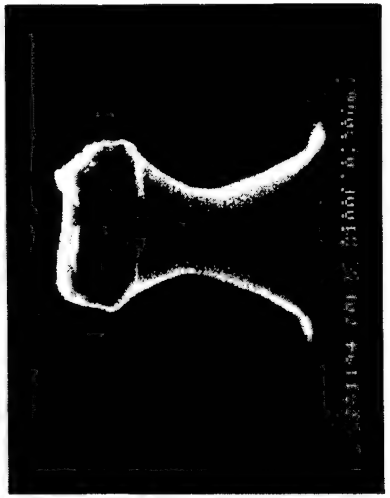

Many-electron ground states E(N)

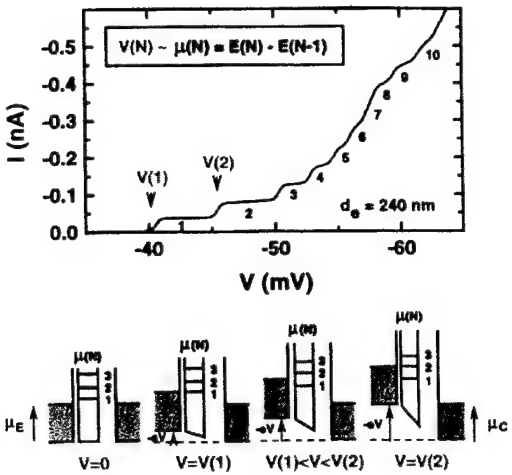

Quantum-dot Helium and Lithium

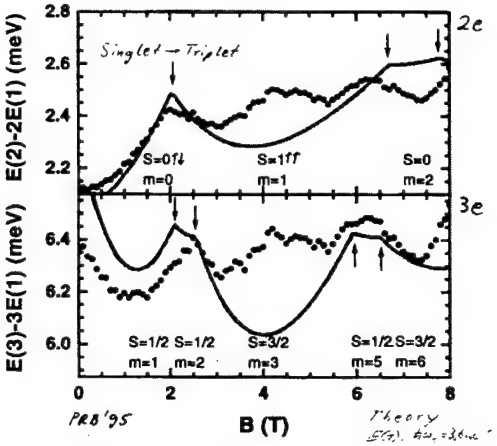

He: S=0 → S=1
↑↓ Singlet
↑↑ Triplet

350 000 T (G. Thummes et al. Phys. Lett. 87A, 133)

Transport Spectroscopy of Artificial 'Atoms'?

in a magnetic field:

Parabolic Confinement Pot.

Single Particle — Fock (1928)

1e

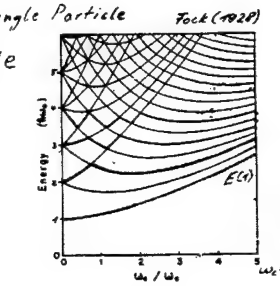

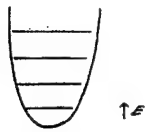

2d Potential:

$V = \frac{1}{2} m^* \omega_0^2 (x^2 + y^2)$

2e

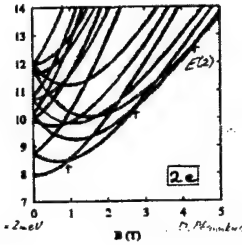

Many Particle
- Groundstate
- Excited States

Coupled Quantum Dots

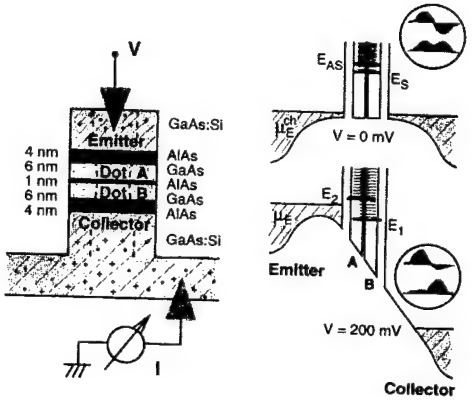

Phys. Rev. Lett. 78, 1544 (1997)

coupled quantum wells
2μm Ø

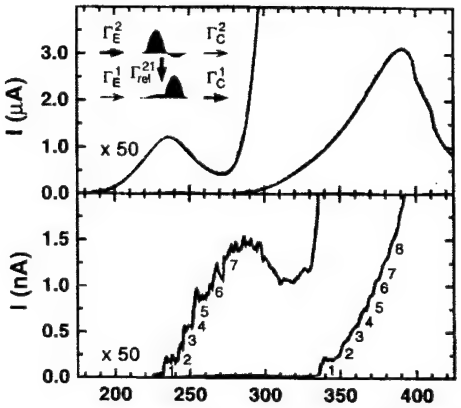

250nm Ø

coupled quantum dots

Phys. Rev. Lett. 78, 1544 (1997)

Lateral Double Quantum Dot

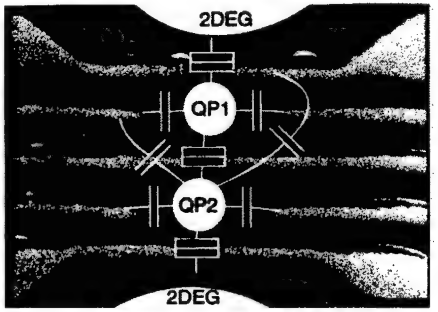

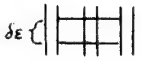

molecular state
Phys. Rev. Lett. 80, 4032 (1998)

Rabi oscillations
Phys. Rev. Lett. 87, 689 (1998)

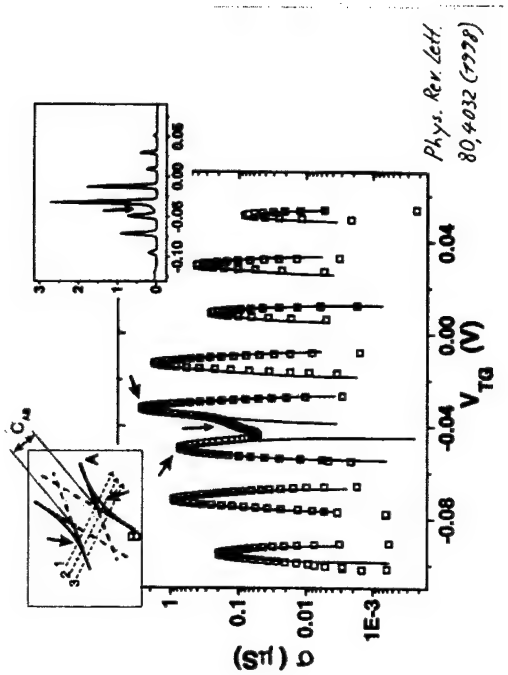

Phys. Rev. Lett. 80, 4032 (1998)

One-Dimensional Superlattice

with a period of 150nm

- Gate level

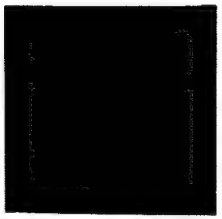

IBM

Transport through Several Quantum Dots

Gate level:

IBM

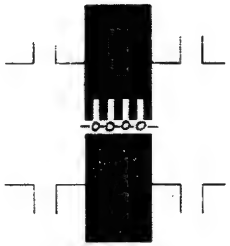

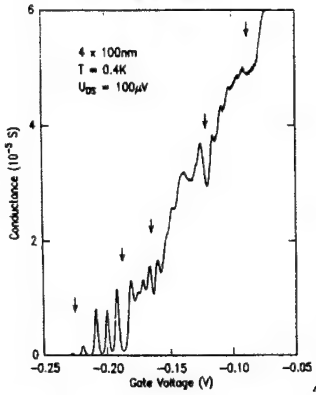

R. J. Haug et al. Proc. of 20th ICPS, 2483 (1990) Mat. Res. Soc. 238-26, 23 (1992) Surf. Sci. 263, 405 (1992) Electronics Lett. '95

Theory: Stafford and Das Sarma Phys. Rev. Lett. 72, 3590 (1994)

Influence of Contacts

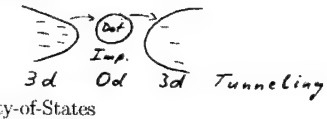

- Density-of-States
- Interaction Effects

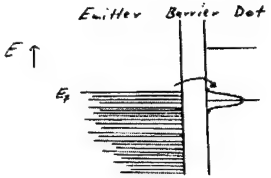

Quantum Dot as Spectrometer

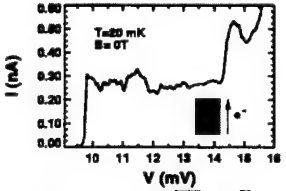

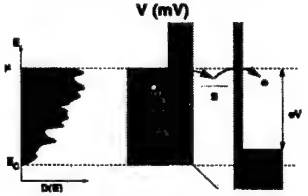

Spectrometer discrete and localized in space (10nm)

➡ **local density of states fluctuations**

nanostrukturen und hannover

Diff. Conductance

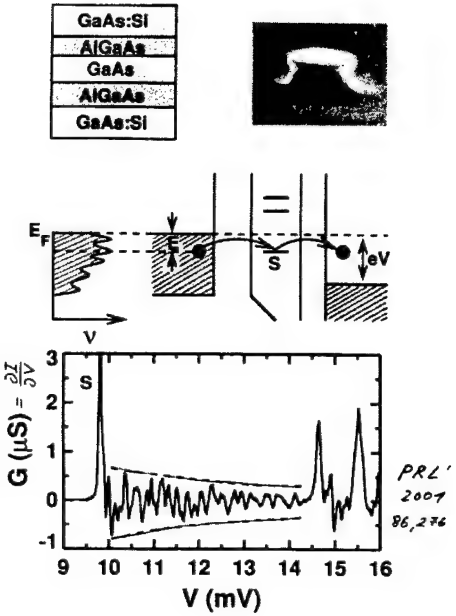

PRL' 2001 86, 276

Magnetic Field B // I

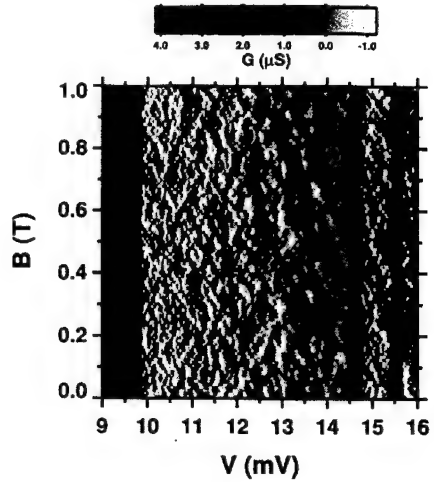

Relaxation

clean System $\sim E^{\frac{1}{2}}$

disordered System $\sim E^{\frac{1}{3}}$

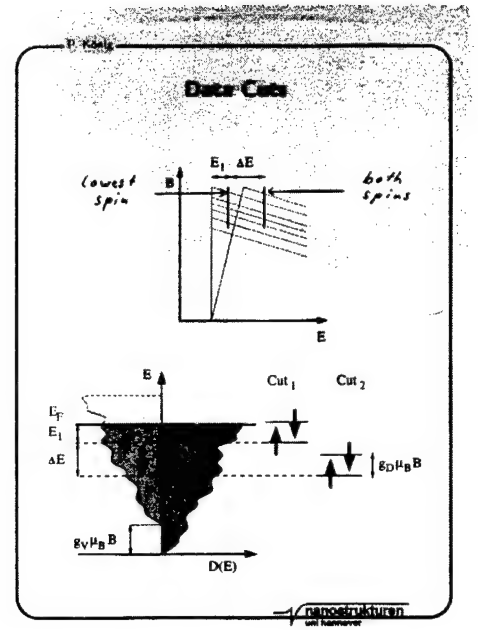

Quantum interference in high magnetic fields

- Magnetic field used for Landau quantization

$$E = \hbar\omega_c(n+\tfrac{1}{2}) + E_{kin}(k_z)$$

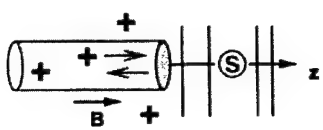

- Interference-induced 1D resonances α

$$E_{kin}(k_z) = E_E^{\alpha}$$

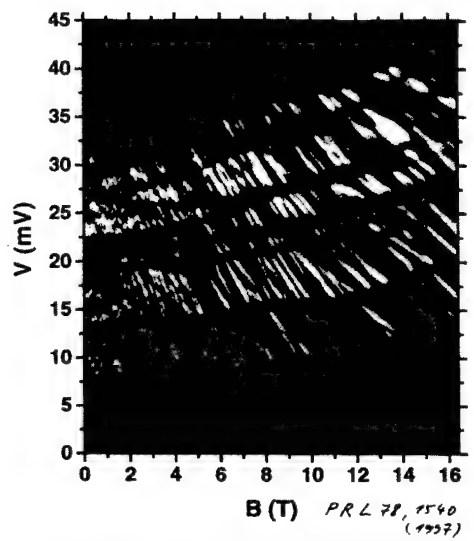

PRL 78, 1540 (1997)

- $\omega_c\tau > 1$, Landau band formation relevant

Magnetic-field dependence of the contact states

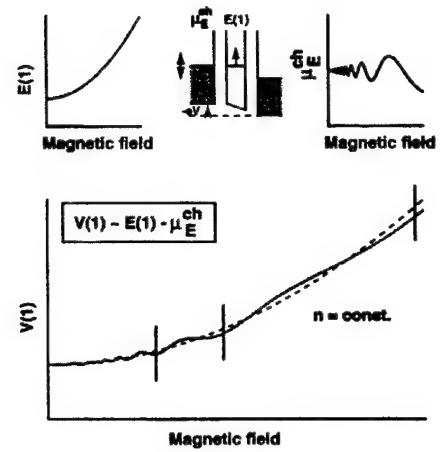

Two Spin-Levels in the Dot

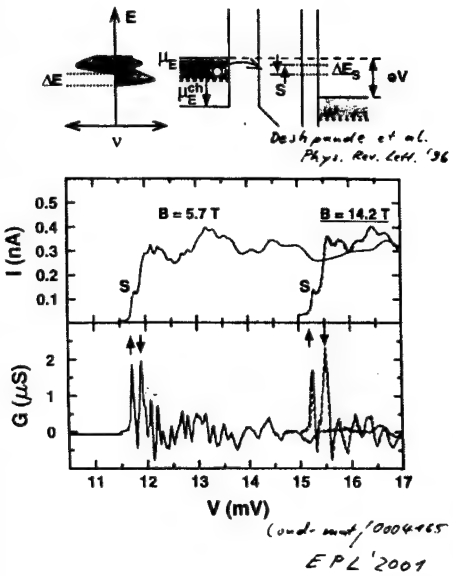

Calculations of I and G for ↑ and ↓ in a magnetic field

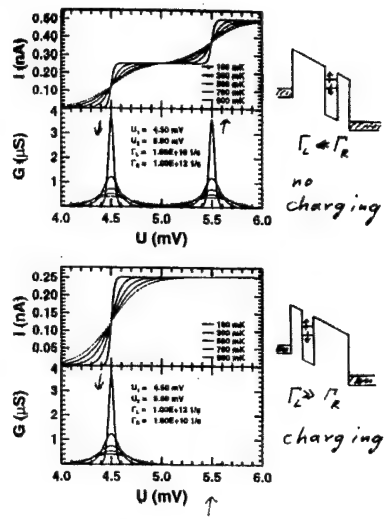

Zeeman Splitting

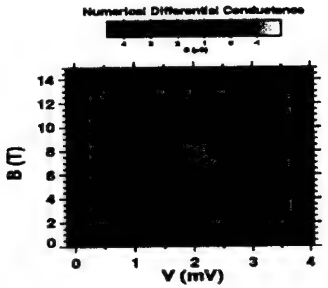

$\Delta V \sim g_s \mu_B B$

sign! (later) $g_s = -0.14$ calc. Kiselev et al. PRB 58, 16353 '98

nanostrukturen uni hannover

P. König

The Reconstructed Current

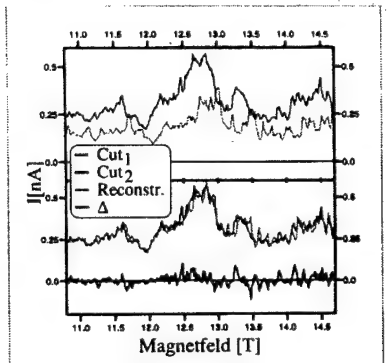

$$I_2 \propto D_\uparrow(E_F - E_1 - \Delta E) + D_\uparrow(E_F - E_1 - \Delta E + g_D\mu_B B - g_V\mu_B B)$$

nanostrukturen uni hannover

with sign! $\Rightarrow g_{Bulk} \approx -0.35$ (Literature value: $g_{Bulk} = -0.44$) see e.g. calc. PRB 44, 4564 (1991) Wolfe & Quinn

Spin effects beyond Zeeman splitting?

$\tau_s \geq 30ps$

Europhys. Lett. '2001 54, 435

InAs Quantum dots

1.8 ML InAs on AlAs and GaAs

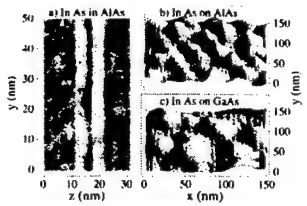

- Lattice mismatch ⇒ Stranski-Krastanov growth
- In situ growth of small quantum dots

InAs on	height (nm)	Ø (nm)	density (μm^{-2})
GaAs	4	30	250
AlAs	4	15	1000

Sample structure

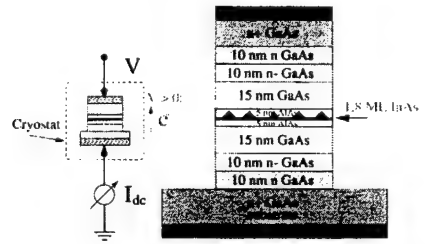

3D-Electrodes(Si-doping):
- undoped GaAs buffer layer
- $n^- = 10^{16}\ cm^{-3}$
- $n = 10^{17}\ cm^{-3}$
- $n^+ = 2 \cdot 10^{18}\ cm^{-3}$

Vertikal tunneling diode: $A = 40 \times 40\ (\mu m)^2$
⇒ $1.6 \cdot 10^8$ InAs quantum dots

Semic. Sci. Tech. 14, L41 (1999)

other works:
- Itskevich et al PRB 54, 16401 (1996)
- Suzuki et al Jpn. J. Appl. Phys 38, 1999 (1999)
- Nakiko et al. Appl. Phys. Lett. 70, 805 (1999)

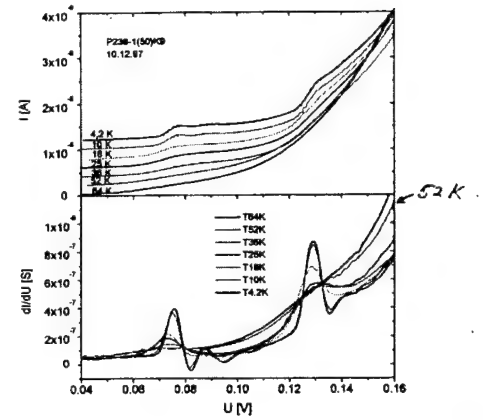

InAs dots Ø = 14 nm (from diamagnetic shift)
(single dots!)

Small magnetic fields $B \parallel I$

Positive bias

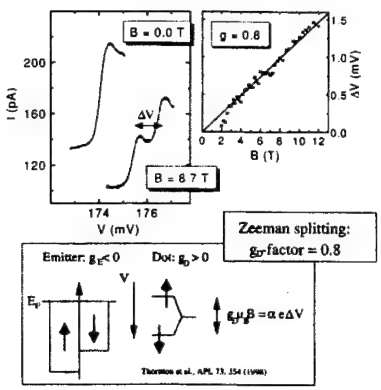

Temperature dependence

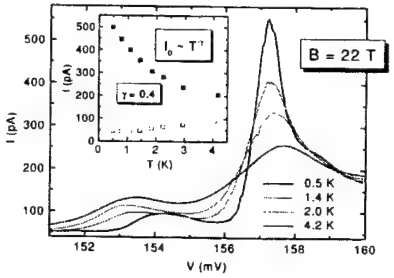

- decrease of majority spin peak
- increase of minority spin peak
- Peak height: $I_0 \sim T^{-\gamma}$ (at $V = V_c$)

Peak form $I \sim (V-V_c)^{-\gamma}\,\Theta(V-V_c)$
$(T=0)$

Exponents

Temperature dependence $I_{Peak} \propto T^{-\alpha}$

Voltage dependence $I \propto (V - V_c)^{-\alpha}$

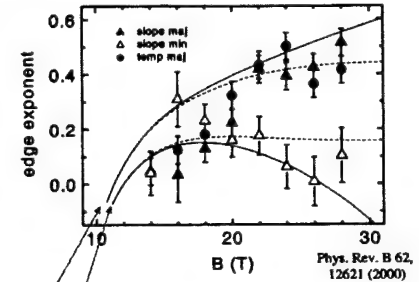

Phys. Rev. B 62, 12621 (2000)

Theory (H. Frahm) ➡ FES

Peaks:

Fermi-Edge Singularity

(Mahan 1967)

Interaction of Charge on Dot with States in the Emitter

FES in Tunneling:
see Geim et al. Phys. Rev. Lett. 72, 2061
Cobden et al. Phys. Rev. Lett. 75, 4274

InAs quantum dots

High magnetic fields
B || I

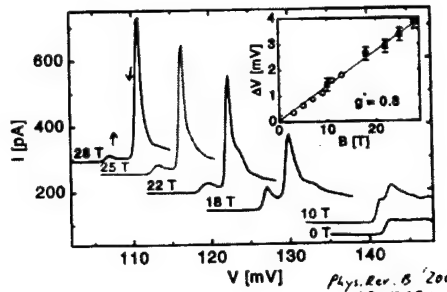

Phys. Rev. B '2000 62, 12621

Theory:

lowest Landau level n=0

wave function $\psi = \psi_m(\rho,\phi)\, e^{ik_z z}$

eig. mom. $m \geq 0$

$\psi_m(\rho,\phi) \sim \rho^m \exp\left(-im\phi - \frac{\rho^2}{4l_0^2}\right)$

$l_0 = \sqrt{\frac{\hbar}{eB}}$

main effect:

FES for tunneling from lowest m-state

(l_0 = dot diameter)

Conclusions

- Transport through
  Quantum Dot Arrays
- Single and Coupled Quantum Dots
- Lateral and Vertical Devices
- Spectroscopy
  Local Density of States of Emitter
  Relaxation
  Spin
- InAs-Quantum Dots
  Interaction Effects (FES)

I. Hapke-Wurst
U.F. Keyser
J. Könemann
P. König
H.W. Schumacher
U. Zeitler
T. Schmidt

H. Frahm
V. Fal'ko
E. McCann

A. G. M. Jansen

K. Pierz
A. Förster, H. Lüth
K. Eberl

Modeling Ballistic Current Flow in Carbon Nanotube Wires

M. P. Anantram

Nanoelectronics & Device Modeling Group

NASA Ames Research Center

Moffett Field, CA
U. S. A.

Acknowledgements:

T. R. Govindan
Jie Han
Supriyo Datta
Liu Yang
Natalio Mingo

Outline:

* Role of Defects
* Bragg reflection
* Metal-nanotube coupling
  - wave vector conservation
  - Armchair versus Zigzag

Topics Studied

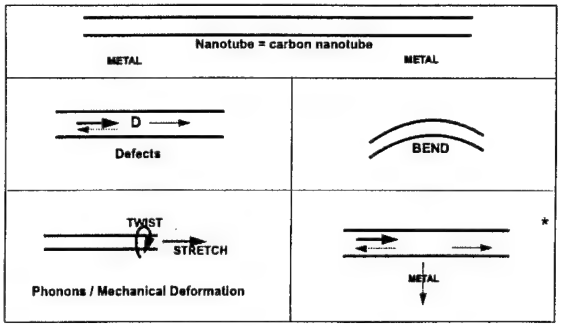

* Bragg reflec.: Intrinsic mechanism, which exists even in an ideal situation

* = This Talk

Transmission vs Energy of a (10,10) Nanotube

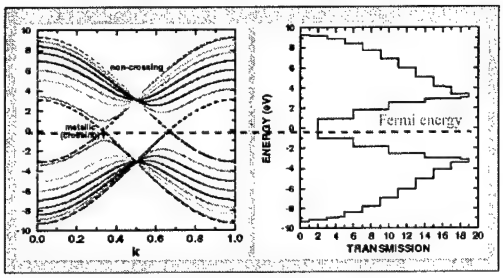

- Close to E=0, Resistance = 6 kΩ; At higher energies, less than 300 Ω
- Experimentally:
  - Max. small bias conductance ~ 12.5 kΩ
  - Max. large bias conductance ~ 4 kΩ

Transmission versus Energy with Defects

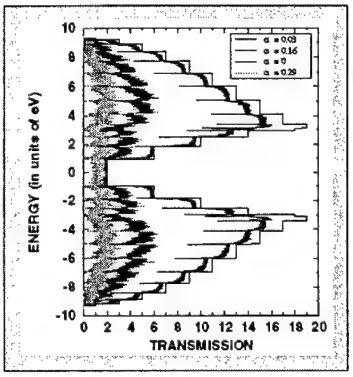

Transmission Probability:

- Decreases with disorder
- Large Dips at some energies
- Very small decrease around E=0 (WIRES?)
- Localization length

Physical explanation of the transmission dips

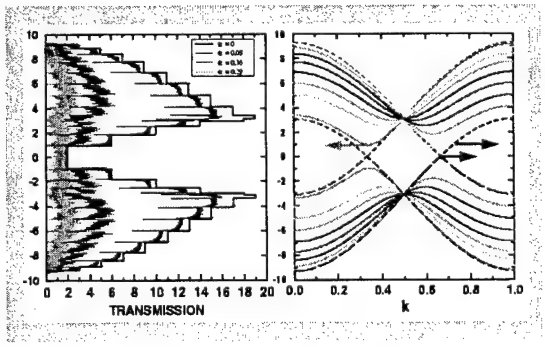

- E=0, Crossing bands: Large velocity (dE/dk)
- Large velocity states (⟶) at higher energies are prone to REFLECTION as they couple to low velocity states (and ⟵)

Conductance vs. Gate Voltage

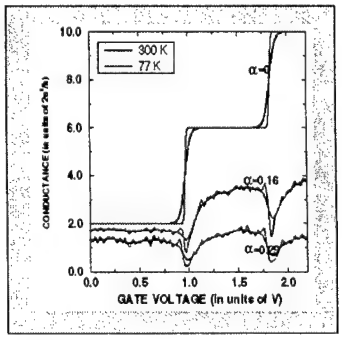

- DIPS IN THE CONDUCTANCE WHEN THE FERMI ENERGY IS CLOSE TO THE SUB-BAND OPENINGS
- FERMI ENERGY AT THE BAND CENTER: GOOD WIRE

Current-carrying capacity of carbon nanotubes

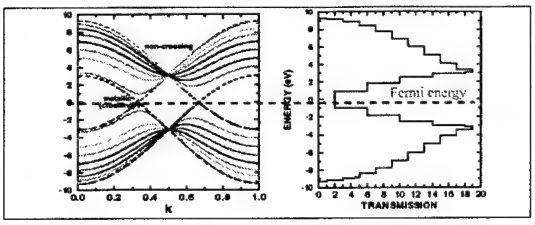

- Close to E=0, only two sub-bands, $Conductance = \frac{4e^2}{h}$ (6 kΩ)
- At higher energies, $Conductance = \frac{(20-30)e^2}{h}$ (< 1kΩ)

An important question is if subbands at higher energies be accessed to drive large currents through these molecular wires?

Experiments by various groups have shown that the differential resistance of a nanotube decreases by small amounts with increase in applied voltage. i.e., the current carrying capacity does not increase better than an ordinary resistor with applied bias.

At what applied voltage are electrons injected into higher subbands?

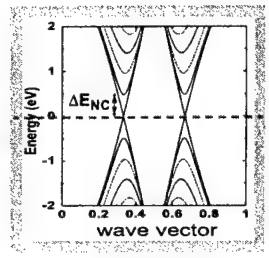

Bias at which electrons are injected into non crossing subbands is ΔE_{NC}

7Å 56Å

size	(5,5)	(10,10)	(20,20)	(40,40)
ΔE_{NC} (eV)	1.9	0.98	0.5	0.25

For example, in a (20,20) nanotube electrons are injected into over 20 subbands at an energy of2.5eV.

The maximum conductance if the Fermi energy is at 2.5 eV is ≈ $40e^2/h$

One exception is the experiment by Frank et. al in Science 280 (1998) which showed a modest decrease in differential resistance with bias.

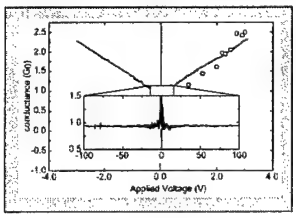

Main experimental features are:

- $V_{APPLIED}$ < 200mV, conductance = G_0
- $V_{APPLIED}$ > 200mV, conductance increases modestly to about 1.75 G_0

- For large diameter nanotubes such as used in the experiments, the non-crossing subbands open at about 100 meV.
- Further there are about 80 subbands at an energy of about 2 eV.

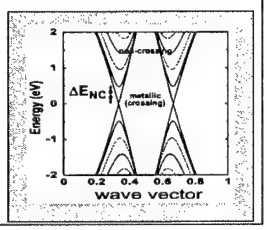

- Yet the conductance is only ~ 1.75 G_0

Semiclassical picture is useful

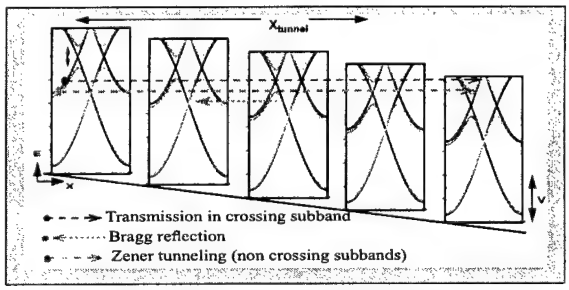

- The strength of the two processes are determined by:
  - Tunneling distance (X_{tunnel}) ➜ Screening length
  - Barrier height, $2\Delta E_{NC}$
  - Scattering and Defects
- ΔE_{NC} α 1/Diameter. So, the importance of Zener tunneling increases with increase in nanotube diameter.

Model

- pi-orbital based tight binding calculation [Phys. Rev. B 58, 4882 (1998)]
- Ideal contacts - reflection less contacts
- Electrostatic potential drop
  - Linear
  - Exponential (Screening length, L_{sc})

$$V(x) = \frac{V_a}{2}\left(1 + \frac{1+e^{\frac{L}{L_{sc}}}}{e^{\frac{L}{L_{sc}}} - e^{-\frac{L}{L_{sc}}}} e^{-\frac{x}{L_{sc}}} - \frac{1+e^{-\frac{L}{L_{sc}}}}{e^{\frac{L}{L_{sc}}} - e^{-\frac{L}{L_{sc}}}} e^{\frac{x}{L_{sc}}}\right)$$

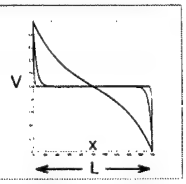

- L=2400 Å, L_{sc}=6, 50, 500 Å
- e-e and e-p scattering are not included

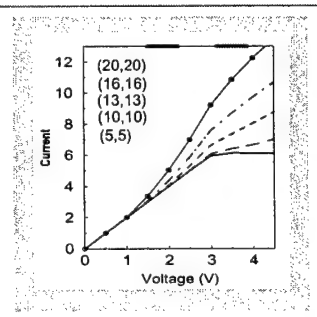

- L=10 Å
- dI/dV ≈ $4e^2/h$ for V_a < $2\Delta E_{NC}$
- Threshold changes with diameter
- Barrier height (ΔE_{NC}) decreases with increase in diameter
- Total Current increases with increase in diameter
- dI/dV > 0 for V_a > 3.1 V, except for the (5,5) nanotube
- (5,5) nanotube ΔE_{NC}≈ 1.9eV

The differential conductance is NOT comparable to the increase in the number of subbands.

For a (20,20) nanotube, there are 35 subbands at E = ± 3.5V.

Bragg reflection severely limits the current carrying capacity

The crossing metallic-type bands conduct current.

The non crossing semiconducotr type bands do not conduct current

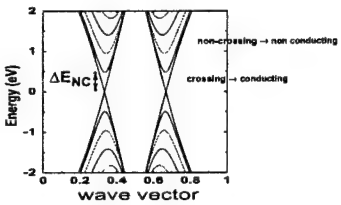

Large diameter nanotubes: non-crossing bands will partially conduct due to Zener-type tunneling.

Coupling of carbon nanotubes to metallic contacts

The electronic properties of nanotubes are closely related to chirality. The metallic versus semicondting nature of nanotubes and the bandgap change with deformation depend on chirality.

Questions:

- Is there a preferable nanotube chirality to maximize current flow?
- Role of wave vector conservation?
- Explain experimentally observed scaling of conductance with contact length

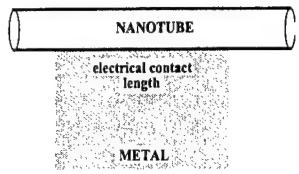

Parameters that influence current flow:

- Strength of coupling to metal
- Length of metal-nanotube contact
- Defects
- Metal Fermi wave vector

How do we model the system?

- Same code as in our MOSFET work
- π electron tight binding model
- Metal is modeled as a free electron gas (k_F)

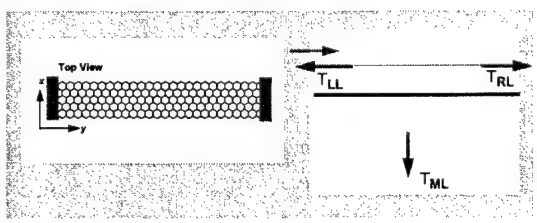

- $T_{RL} + T_{ML} + T_{LL} = 2$.
- Phys. Rev. B, v.58, p. 4882 (1998) and v. 61, p. 14219 (2000)
- Compute self energy due to: (i) metal & (ii) semi-infinite CNT leads

Calculation of the total transmission from nanotube to metal, T_{ML} are presented for armchair and zigzag nanotubes:

Scattering rate

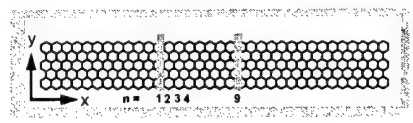

The wave function of a nanotube is $\Psi = e^{ink_x L}\phi$

n is an integer and ϕ is wave func. of atoms in a 1D unit cell

The scattering rate from metal to nanotube (Born approx.) is,

$$1/\tau \;\alpha\; |<\Psi_{nt}|V_{m\text{-}nt}|\Phi_m>|^2$$

$$\delta(k_x - k_x^m) \qquad |<\phi|V_{m\text{-}nt}|\phi_m>|^2$$

This implies that

- k_x is conserved
- k_y conservation is relaxed due to finite *width* of *contact area*

As a result of the difference in k_y corresponding to E=0 (Fermi energy), important differences should arise as a function of chirality.

ARMCHAIR	ZIGZAG
E=0 at $k_y = 2\pi/3a_0 = 0.85$ Å^{-1}	E=0 at $k_y = 0$
Metal with $k_{Fermi} < 0.85$ Å^{-1} couples weakly	No threshold for k_{Fermi}

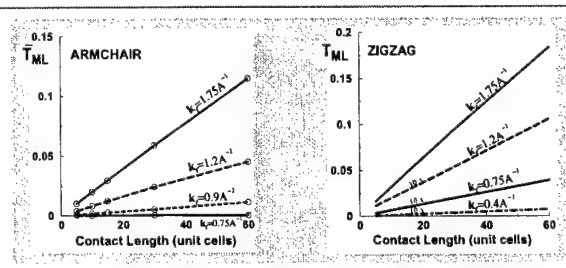

- Note that threshold value is the value of k_f below which the transmission does not scale with contact length

The main differences between the armchair and zigzag case are:

- Threshold value of k_f is $\frac{2\pi}{3a_0}$ =0.85 Å^{-1} for armchair nanotubes (see k_f = 0.75A^{-1}) and is 0 for zigzag nanotubes (see k_f = 0.4Å^{-1}).
- Beyond the threshold k_f, transmission *increases* with contact length as seen in experiment by Tans et. al., Nature, vol. 386, 474 (1997)
- For zigzag tubes, T_{LM} is small for $k_f \leq 1.2$ A^{-1} as a result of the large angular momentum in the circumferential direction.

Diameter dependence of Transmission

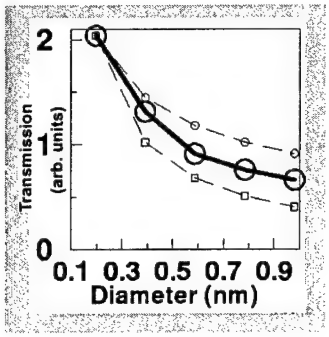

Transmission decreases as the diameter increases because the nanotube tends to a graphite sheet.

The previous values of T are small compared to the maximum possible value of 2. Two possible scenarios to increase T are:

*** Large contact length - Small coupling**

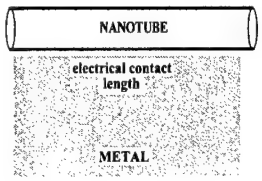

*** Small contact length - Large coupling**

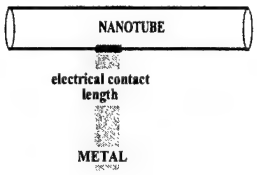

- For nanoelectronics, the second option (right) is better.
- We model a contact length of *30 unit cells* (72 Å for armchair and 125 Å for zigzag nanotubes), and vary the coupling strength. The main results of the calculation are rather surprising and are presented below:

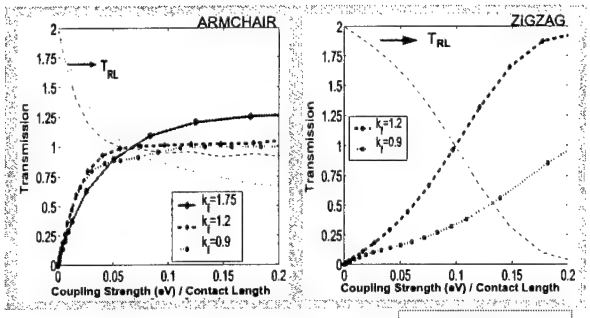

- Armchair:Transmission is pinned at values close to unity for metal k_f of 0.9 and 1.2 $Å^{-1}$
- Zigzag: Transmission increases to two (maximum possible value)
- At small coupling strengths, transmission increases more rapidly in the armchair case

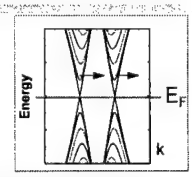

Metallic-zigzag are preferable from metal-nanotube coupling viewpoint

---

Nodes on the cylinder - Shape of NT wave function

$$\Psi = e^{imk_x a_0}\phi$$

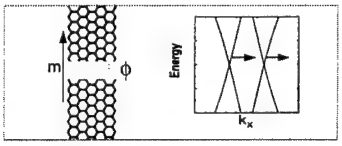

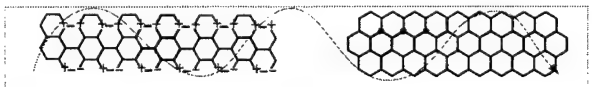

k_x ↑ 0.85 $Å^{-1}$ $\phi(\bullet) + \phi(\bullet) + \phi(\bullet) = 0$ 0 ↑ k_x

metal k_f=0.90 $Å^{-1}$ → distance between nodes 6 Å
Gold k_f=1.20 $Å^{-1}$ → distance between nodes 3.4 Å
Aluminum k_f=1.75 $Å^{-1}$ → distance between nodes 2 Å

Scattering rate from Metal to Nanotube α $\langle\phi_{nanotube} | H_{coupling} | \Psi_{metal}\rangle$ $\langle + - | H_{coupling} | \Psi_{metal}\rangle \sim 0$. Hence, Transmission is pinned close to unity.

- Side-contacted: zigzag nanotube are more desirable (curvature)
- Larger metal Fermi wave vector helps.

Conclusions

- dI/dV versus V does not increase in a manner commensurate with the increase in number of subbands.

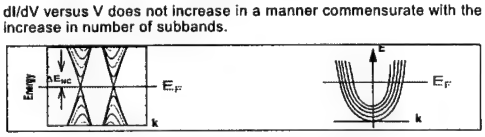

- The increase in dI/dV with bias is much smaller than the increase in the number of subbands - *a consequence of bragg reflection*
- Requirement for axial wave vector conservation:

ARMCHAIR: cut-off $K_{Fermi} = 2\pi/3a_0 = 0.85 Å^{-1}$

ZIGZAG: cut-off $K_{Fermi} = 0$

- Our calculations show an increase in transmission with length of contact, as seen in experiments.
- It is desirable for molecular electronics applications to have a small contact area, yet large coupling. In this case, the circumferential dependence of the nanotube wave function dictates:
  - Transmission in armchair tubes saturates around unity
  - Transmission in zigzag tubes saturates at two

WHAT ARE CNT?

- **STRIP OF A GRAPHENE SHEET ROLLED INTO A TUBE**

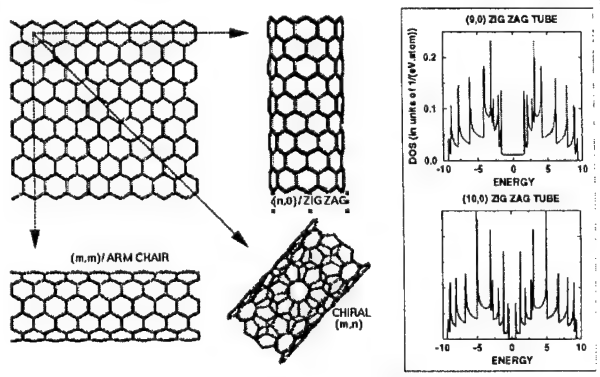

- Varying the diameter and (m,n): metal, semiconductor
- n-m = 3 • integer: metal

WIRE

METAL-SEMICONDUCTOR JUNCTION: RECTIFICATION?

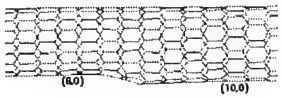

MSM JUNCTION: BARRIER?

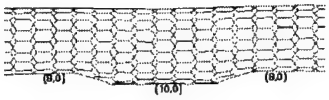

Observed in nature

Branched Nanotube

A POSSIBLE LOOPHOLE IN THE THEOREM OF BELL

Karl Hess[1] and Walter Philipp[2]

[1] Beckman Institute, Department of Electrical Engineering and Department of Physics,University of Illinois, Urbana, Il 61801

[2] Beckman Institute, Department of Statistics and Department of Mathematics, University of Illinois,Urbana, Il 61801

Abstract

The celebrated inequalities of Bell are based on the assumption that local hidden parameters exist. When combined with conflicting experimental results these inequalities appear to prove that local hidden parameters cannot exist. This suggests to many that only instantaneous action at a distance can explain Einstein, Podolsky, Rosen (EPR) type of experiments. The Bell inequalities are based on a simple mathematical model of the EPR- experiments. They have no experimental confirmation since they contradict the results of EPR-experiments. Furthermore, in addition to the assumption that hidden parameters exist, Bell tacitly makes a variety of other assumptions which could contribute to his being able to obtain the desired contradiction. For instance, Bell assumes that the hidden parameters are governed by a single probability measure independent of the analyzer settings. Moreover, we argue that the mathematical model of Bell excludes a large set of local hidden variables and a large variety of probability densities of these local (in the sense of Einstein) variables. These exclusions have neither a physical nor a mathematical basis but are based on Bell's translation of the concept of Einstein locality into the language of probability theory. Our additional set of local hidden variables includes time like correlated parameters and a generalized probability density. We prove that our extended space of local hidden variables does not permit Bell-type proofs to go forward. This opens the possibility to explain EPR-experiments within Einstein's space-time continuum, with a finite velocity of light and without recourse to spooky action at a distance.

1 Introduction

Einstein, Podolsky and Rosen (EPR) [1] challenged Bohr [2] and the completeness of quantum mechanics by designing a "Gedanken" experiment that suggested the existence of "hidden parameters" and of a theory that was more complete than quantum mechanics. The

EPR design was later realized in various implementations [3] with experimental results close to the quantum mechanical prediction. These experimental results by themselves do not have any bearing on the EPR claim that quantum mechanics was incomplete, nor on the existence of hidden parameters. However, inequalities derived by Bell [4] that are based on the assumption that local hidden parameters exist, taken together with the experimental results that happen to be inconsistent with the result of the Bell inequalities, do appear to prove that local hidden parameters cannot exist. This has been discussed in great detail in [5] and [6].

The Bell theorem is based on a mathematical model of the EPR- experiments. It has, by itself, no experimental confirmation since its result contradict the results of the EPR-experiments. The standing of the Bell theorem has therefore unique features in the history of modern physics: the mathematical model and the theorem of Bell are taken to be correct and seen by many as valid as the second law of thermodynamics is, while there exists no experimental confirmation. However, instead of discarding altogether a mathematical model that contradicts experiment, the contradiction to the experiment is used to prove that the basic assumption of the theorem, the existence of local hidden parameters is incorrect. The framework of research that has developed around the Bell theorem claims the necessity of "gross non-localities". In simple words, the correlated spins of the EPR-experiment are in some contact over arbitrary space like distances of our space-time continuum and if one spin is measured in one station, the correlated spin in another station is instantaneously influenced. This contradicts the locality conditions of Einstein and Einstein's very argument for the lack of completeness of quantum mechanics. Einstein called the instantaneous interaction of the spatially separated spins "spukhafte Fernwirkungen (spooky action at a distance)". He did not accept the possibility of such spooky action and since quantum mechanics appeared to demand it, it had to be at least incomplete. The Bell theorem and its standard interpretation has turned the logic around. Its supporters now claim that local hidden parameters do not exist and cannot explain the EPR-experiments. Quantum mechanics does agree with experiments and spooky action at a distance must be accepted as a fact of nature. However, it has been shown in a serious of papers of which we cite only two of the more recent [7] [8], that Bell's theorem does contain more than self-evident locality assumptions. These are related to the role of time in the experiments and the admissibility of more general probability measures.

We show in this paper that the assumption of the existence of local hidden variables is not the only assumption in the proof of the Bell inequalities. We show that the mathematical model of Bell excludes a large set of hidden variables and a large variety of probability densities of these variables that all fulfill Einstein's locality conditions perfectly. This exclusion has neither a physical nor a mathematical basis but is based on Bell's mathematical interpretation of what Einstein locality means in terms of probability theory. Our additional set of hidden variables or, as we will call them, parameter random variables includes time like correlated parameters and a generalized probability density which is a sum of what we later define as setting dependent subspace product measures (SDSPM's). We demonstrate that Bell type proofs cannot go forward using our extended space of hidden variables.

The paper is organized as follows. We first review the theorem of Bell. We then analyze

the restrictions that Bell's proof puts on the parameter space and probability measure and show that a much larger space and a more general probability measure can be constructed without violation of Einstein locality conditions. We demonstrate that a variety of proofs of theorems similar to that of Bell cannot be performed in this larger parameter space and with the more general probability measure, and that these theorems and inequalities are therefore not valid in this space. We finally point toward a mathematical model that uses this larger space and permits the construction of a hidden parameter theory that does agree with EPR-experiments.

2 The theorem of Bell

We first present a short summary of the work of Bell. In EPR experiments, two particles having their spins in a singlet state are emitted from a source and are sent to spin analyzers (instruments) at two spatially separated stations, S_1 and S_2. The spin analyzers are described by Bell using unit vectors $\mathbf{a}, \mathbf{b}, etc.$ of three dimensional Euclidean space and functions $A = \pm 1$ (operating at station S_1) and $B = \pm 1$ (operating at station S_2): furthermore A does not depend on the settings $\mathbf{b}$ of station S_2, nor B on the settings $\mathbf{a}$ of station S_1 (Einstein separability or locality). Bell permits particles emitted from the source to carry arbitrary hidden parameters λ of a set Ω that fully characterize the spins and are "attached" to the particles with a probability density ρ (we denote the corresponding probability measure by μ). Neither the parameters λ nor the probability measure μ are permitted to depend on the settings at the stations. Einstein separability is again cited as the reason for this restriction. The analyzer settings are changed rapidly in the experiments and do change after emission from the source. Therefore the source parameters and their probability measure must not depend on the settings at the time of measurement. Bell further assumes that the values of the functions A and B are determined by the spin analyzer settings and by the parameters such that:

$$A = A_{\mathbf{a}}(\lambda) = \pm 1 \text{ and } B = B_{\mathbf{b}}(\lambda) = \pm 1 \tag{1}$$

Thus $A_{\mathbf{a}}(\lambda)$ and $B_{\mathbf{b}}(\lambda)$ can be considered as stochastic processes on Ω, indexed by the unit vectors $\mathbf{a}$ and $\mathbf{b}$ respectively. Quantum theory and experiments show that, for a given time of measurement for which the settings are equal in both stations, we have for singlet state spins

$$A_{\mathbf{a}}(\lambda) = -B_{\mathbf{a}}(\lambda) \tag{2}$$

with probability one. Bell further defines the spin pair expectation value $P(\mathbf{a}, \mathbf{b})$ by

$$P(\mathbf{a}, \mathbf{b}) = \int_{\Omega} A_{\mathbf{a}}(\lambda) B_{\mathbf{b}}(\lambda) \rho(\lambda) d\lambda = -\int_{\Omega} A_{\mathbf{a}}(\lambda) A_{\mathbf{b}}(\lambda) \mu(d\lambda) \tag{3}$$

From Eqs.(1)-(3), Bell derives his celebrated inequality [4]

$$1 + P(\mathbf{b}, \mathbf{c}) \geq \mid P(\mathbf{a}, \mathbf{b}) - P(\mathbf{a}, \mathbf{c}) \mid \tag{4}$$

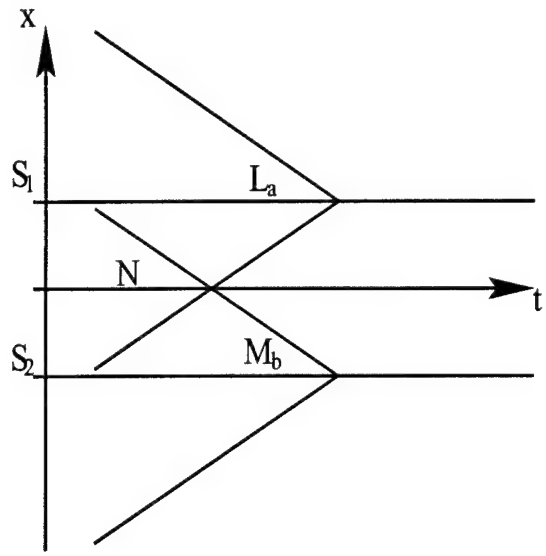

Figure 1: Light cone used by Bell. X denotes the space coordinate and t the time

and observes that this inequality is in contradiction with the result of Quantum Mechanics:

$$P(\mathbf{a}, \mathbf{b}) = -\mathbf{a} \cdot \mathbf{b} \tag{5}$$

Here $\mathbf{a} \cdot \mathbf{b}$ is the scalar product of $\mathbf{a}$ and $\mathbf{b}$.

The proof of Bell's inequality is based on the obvious fact that for $x, y, z = \pm 1$ we have

$$|xz - yz| = |x - y| = 1 - xy \tag{6}$$

Substituting $x = A_{\mathbf{b}}(\lambda)$, $y = A_{\mathbf{c}}(\lambda)$, $z = A_{\mathbf{a}}(\lambda)$ and integrating with respect to the measure μ one obtains Eq.(4) in view of Eq.(3). Thus, from the vantage point of mathematics, the Bell inequality is a straight-forward consequence of the set of hypotheses and assumptions that are imposed.

3 Extension of Bell's parameter space and probability measure

We are going to argue below that Bell's parameter space is not general enough and excludes without any necessity a manifold of parameters that has at least the cardinality of the continuum. Bell's probability measure is, correspondingly, not as general as the physics of relativity would permit. To show this we start with a discussion of the parameter space and corresponding probabilities out of Bell's book [9].

Bell [9] defines the following parameter sets that are in the backward light cone, as defined by relativity and as illustrated in Fig. 1. He lets N denote the specification of all entities that are represented by parameters and belong to the overlap of the backward light cones

of both space-like separated stations S_1 and S_2. In addition he considers sets of parameters $L_{\mathbf{a}}$ (our notation) that are in the remainder of the backward light cone of S_1 and $M_{\mathbf{b}}$ for S_2 respectively. Bell (see p56 of ref. [9]) denotes the conditional probability that the function $A_{\mathbf{a}}$ assumes a certain value with $A_{\mathbf{a}} = \pm 1$ by $\{A_{\mathbf{a}}|L_{\mathbf{a}}, N\}$ and similarly for $B_{\mathbf{b}} = \pm 1$. Then he claims that in a local causal theory we have:

$$\{A_{\mathbf{a}}|L_{\mathbf{a}}, N, B_{\mathbf{b}}\} = \{A_{\mathbf{a}}|L_{\mathbf{a}}, N\} \text{ and } \{B_{\mathbf{b}}|M_{\mathbf{b}}, N, A_{\mathbf{a}}\} = \{B_{\mathbf{b}}|M_{\mathbf{b}}, N\} \tag{7}$$

Eq.(7) appears entirely plausible as a consequence of the finite speed of light: whatever happens at station S_1 to the result of $A_{\mathbf{a}}$ cannot be causally connected to the result of $B_{\mathbf{b}}$ in station S_2 within a local theory. When the switching of the settings is fast enough, the probability that $A_{\mathbf{a}}$ assumes a certain value must be the same no matter what value $B_{\mathbf{b}}$ might assume. While this conclusion is undoubtedly correct at a given instance of measurement, Bell's use of Eq.(7) as identical and valid for all times of measurement with a given setting is fatally flawed. The reason is the possible dependence of $A_{\mathbf{a}}$ and $B_{\mathbf{b}}$ on time-like correlated parameters that may be setting dependent. The mathematics of Bell-type proofs requires complete statistical independence of $A_{\mathbf{a}}$ and $B_{\mathbf{b}}$ for the whole set of measurements and not only at a given time. It also contains the assumption of identical $L_{\mathbf{a}}$ and $M_{\mathbf{b}}$ for all measurements of a run. This, however, cannot be guaranteed because physical phenomena other than the setting of the polarizer by the experimenter can occur in the stations and these can be correlated.

Consider, for example, two clocks, one in each station. These clocks may have different settings (e.g. pendulum length and/or starting time etc.). The time that one clock shows is certainly not the causal reason for the time of the other clock. It is the same physical law that is at work in both stations and that causes a correlation in the periodicity of the processes in the clocks or in some general periodic processes for that matter. It is, of course well known that two gyroscopes in the two stations could also be used as clocks as they may indicate the rotation of the earth. As mentioned, there may be also other periodic processes that cause correlations and these correlations may be influenced by the settings **a** and **b**. Although there are clear analogies of gyroscopes and spin properties, we do not wish to push this comparison too far. We do, however, wish to point out the dangers of using of Eq.(7) without proper caution. Bell's argument resulting in Eq.(7) does not include the vital fact that the experiments are made in a time sequence and that the backward light cones change and evolve with time. The situation is illustrated in Fig.2 which shows that for each instant of measurement there is a different light cone. Fig. 2 illustrates our point for measurements at two different times t_1 and t_2.

The backward light cones contain sets of parameters $L_{\mathbf{a},t_1}$, $M_{\mathbf{b},t_1}$, N_{t_1} and $L_{\mathbf{a},t_2}$, $M_{\mathbf{b},t_2}$, N_{t_2} respectively. It is clear, that the set $L_{\mathbf{a},t_1}$ and the set $L_{\mathbf{a},t_2}$ may contain setting dependent parameters $\lambda^*_{\mathbf{a}}$ with different probability densities. It is also clear from the discussion with clocks that the sets $L_{\mathbf{a},t_1}, L_{\mathbf{a},t_2}$, $M_{\mathbf{b},t_1}, M_{\mathbf{b},t_2}$ etc. need not be statistically independent. This has several consequences that do not permit Bell-type proofs to go forward. We outline below the most crucial problems.

Bell uses combinations of Eq.(7) for different settings in his proofs as follows (see e.g.

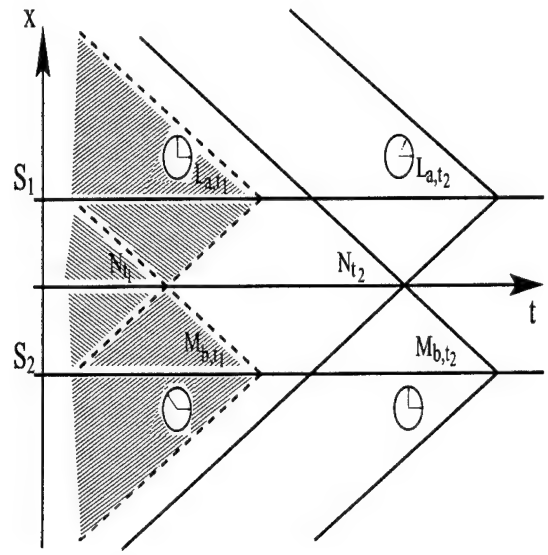

Figure 2: Light cones at randomly chose times t_1 and t_2 of the measurements. The clocks indicate time-like and setting dependent correlations of parameters in stations S_1 and S_2 (in this example, the difference between the times indicated by the clocks in the two stations stays constant).

Bell's Eq.(10) of ref. [9] on page 56):

$$\{A_{\mathbf{a}}|L_{\mathbf{a}}, N, B_{\mathbf{b}}\} = \{A_{\mathbf{a}}|L_{\mathbf{a}}, N, B_{\mathbf{c}}\} = \{A_{\mathbf{a}}|L_{\mathbf{a}}, N\} \tag{8}$$

However, since the measurements with setting **b** and **c** are necessarily taken at different times, this needs to be written in the form:

$$\{A_{\mathbf{a}}|L_{\mathbf{a},t_1}, N_{t_1}, B_{\mathbf{b},t_1}\} = \{A_{\mathbf{a}}|L_{\mathbf{a},t_2}, N_{t_2}, B_{\mathbf{c},t_2}\} \tag{9}$$

which is, in general, clearly incorrect.

The above arguments also demonstrate that Bell's use of a single probability density $\rho(\lambda)$ that is valid for all times of a run of measurements is in contradiction to physical intuition and facts: the parameter space related to light cones changes and evolves, in general, with time. To describe this physical reality (if this word is permitted), one needs at least to admit a time dependence of $\rho(\lambda)$ i.e. one needs to replace $\rho(\lambda)$ by

$$\sum\nolimits_{t_i} \rho_{t_i}(\lambda) \tag{10}$$

In addition one needs to include, again in general, setting dependent parameters denoted e.g. by $\lambda^*_{\mathbf{a}}(t)$ in station S_1 and by $\lambda^{**}_{\mathbf{b}}(t)$ in station S_2 with

$$\lambda^*_{\mathbf{a}}(t) = \lambda^{**}_{\mathbf{a}}(t) \tag{11}$$

if $\mathbf{b} = \mathbf{a}$ in order to make it possible to fulfill Eq.(2). Bell has included into his later proofs (after publication of reference [10]) setting dependent parameters. However, he and everyone

else assumed that the $\lambda_{\mathbf{a}}^{*}$ and $\lambda_{\mathbf{b}}^{**}$ be statistically independent. He argued this independence from the fact that the parameters are in different stations and he did not consider time-like correlations as described above. Bell assumes that setting dependent parameters in the stations analyzers (called instruments by Bell) must be statistically independent or do not exist. This is explicitly stated in his book ([9] p 38): "..it is necessary that the equality holds in (8) (which is equal to our Eq.(1)), i.e. for this case the possibility of the results depending on hidden variables in the instruments can be excluded from the beginning ..". Of course, in a run with all different settings that still would be true. However, $P(\mathbf{a},\mathbf{b})$ is evaluated from measurements with fixed $\mathbf{a}$ and $\mathbf{b}$. Therefore a possible time dependence can cause statistical correlations. To visualize this, assume that the parameters $\lambda_{\mathbf{a}}^{*}$ and $\lambda_{\mathbf{b}}^{**}$ are identified with the the hour pointers of two clocks in the two stations. The clock in station S_1 is connected to a plane that is perpendicular to the setting $\mathbf{a}$ and the clock in station S_2 to a plane perpendicular to $\mathbf{b}$. Let the direction of the pointers be idealized by unit vector $\lambda_{\mathbf{a}}^{*}$ in station S_1 and $\lambda_{\mathbf{b}}^{**}$ in S_2 at each instant of measurement. Clearly, these parameters will exhibit time correlations. Note that it is of no concern that the measurements are taken at random times. It is the time correlation in the two stations at any given time that matters.

In addition to the generalization of Bell's probability densities shown in Eq.(10), one needs a further generalization and replace $\rho(\lambda)$ by

$$\sum\nolimits_{t_i} \rho_{t_i}(\lambda, \lambda_{\mathbf{a}}^{*}, \lambda_{\mathbf{b}}^{**}) \tag{12}$$

Of course, to obey Einstein locality, $\lambda_{\mathbf{a}}^{*}$ and $\lambda_{\mathbf{b}}^{**}$ must be station specific and can only be correlated by time like correlations i.e. by some relation to local periodic processes. It is also important to note that the station parameters $\lambda_{\mathbf{a}}^{*}$ and $\lambda_{\mathbf{b}}^{**}$ cannot be emulated by the parameter pair $\mathbf{a},\lambda$ or $\mathbf{b},\lambda$, as always implied by Bell by use of his functions A and B. The source parameters λ of Bell appear with a given probability density. Since the parameters $\lambda_{\mathbf{a}}^{*}$ and $\lambda_{\mathbf{b}}^{**}$ can have different probability distributions for different $\mathbf{a}$ and $\mathbf{b}$, that are not related in any way to the parameters λ, it becomes clear that the joint density $\rho_{t_i}(\lambda, \lambda_{\mathbf{a}}^{*}, \lambda_{\mathbf{b}}^{**})$ can depend, a priori, on the setting vectors $\mathbf{a}$ and $\mathbf{b}$. It is irrelevant that by lucky coincidence, the triples $(\mathbf{a},\lambda,\lambda_{\mathbf{a}}^{*})$ and $(\mathbf{b},\lambda,\lambda_{\mathbf{b}}^{**})$ could perhaps be written as $\mathbf{a},\Lambda$ and $\mathbf{b},\Lambda$ for some Λ incorporating λ and the station parameters. The probability density that must be considered, in general, for all these parameters is therefore also different from that of Bell and must exhibit a time dependence. This implies the necessity of a more general probability measure that includes time-like correlated parameters.

We have shown [8], that a properly chosen sum of what we call setting dependent subspace product measures (SDSPM) does not violate Einstein-separability and does lead to the quantum result of Eq.(5) while still always fulfilling Eq.(2). By this we mean the following. The probability space Ω is partitioned into a finite number M of subspaces Ω_m

$$\Omega = \cup_{m=1}^{M} \Omega_m \tag{13}$$

For given $\mathbf{a}$ and $\mathbf{b}$, a setting dependent measure $(\mu_{\mathbf{ab}})_m$ is defined on each subspace Ω_m. This measure can be extended to the entire space Ω by setting

$$(\mu_{\mathbf{ab}})_m(\Omega_j) = 0 \text{ if } j \neq m \tag{14}$$

The final measure μ is then defined on the entire space Ω by

$$\mu = \sum_{m=1}^{M} (\mu_{\mathbf{ab}})_m \tag{15}$$

and the index m indicates the time correlations. In the above notation we would have $m = t_i$. We have shown in reference [8] that a product measure can be found such that

$$(\mu_{\mathbf{ab}})_m = (\mu_{\mathbf{a}} \times \mu_{\mathbf{b}})_m \tag{16}$$

This is of minor concern for the main argument presented here but does provide flexibility to completely avoid any hint of spooky action within our system of setting dependent subspace product measures (SDSPM's).

It is clear that Bell's proof does not go through with such a probability measure since integrating Eq.(6)to obtain Eq.(4) works only with a single setting independent probability measure. In addition, one can show in a rather intricate proof [8] that the quantum result of Eq.(5) can be obtained with a probability measure as in Eq.(15). In other words hidden parameters are possible if the parameter space is properly extended. We also have shown in [8] that the parameters that are considered that way show no trace of spooky action.

4 Conclusions

We have presented a mathematical framework that is more extensive than that of Bell and permits the possibility of describing the spin-pair correlation in EPR-type experiments by use of hidden parameters. A key-element of our approach is contained in the introduction of time-like correlated parameter random variables that also depend on the setting of the station in which they influence the measurements. This leads in a natural way to a setting dependent probability measure composed of subspace product measures (SDSPM's). Use of such SDSPM's does not permit the proof of Bell to go forward (nor any other proofs of similar theorems known to us as given e.g. in references [9] and [11]). We conclude that setting and time dependent parameter random variables present a possible loophole in theorems a la Bell.

5 Acknowledgement

The work was supported by the Office of Naval Research N00014-98-1-0604.

References

[1] A. Einstein, B. Podolsky, and N. Rosen, Phys. Rev. Vol. 47, 777 (1935).

[2] N. Bohr, Phys. Rev. Vol. 48, 696 (1935).

[3] A. Aspect, J. Dalibard and G.Roger, Phys. Rev. Letters Vol. 49, 1804 (1982)

[4] J. S. Bell, Physics, Vol. 1, 195 (1964).

[5] N. D. Mermin, Physics Today, Vol. 38, No. 4, 38-47 (1985).

[6] A. J. Leggett, The Problems of Physics, Oxford University Press (1987).

[7] Y. Aharonov, A. Botero and M. Scully, Z. Naturforsch. Vol. 56 a, 5-15 (2001).

[8] Karl Hess and Walter Philipp, quant-ph, see http//xxx.lanl.gov/abs/quant-ph/0103028, March 7 (2001).

[9] J.S. Bell, "Speakable and Unspeakable in Quantum Mechanics", Cambridge University Press, 1993

[10] L.E. Ballentine and Jon P. Jarrett, Am. J. Phys. Vol. 55, 696 (1987)

[11] D. M. Greenberger, M. A. Horne, A. Shimony and A. Zeilinger, Am. J. Phys. Vol. 58, 1131 (1990)

First principles modelling of electron transport in atomic-scale systems

Antti-Pekka Jauho
MIC, Technical University of Denmark

1) Motivation: Atomic/Molecular-scale Electronics
2) Modelling: Challenges
3) Nonequilibrium Green function formalism
4) The *Tran*SIESTA *ab initio* transport program.
5) Results for atomic gold wires.
6) A toy molecular device.

Collaboration of several groups:
Mads Brandbyge, Kurt Stokbro, Jeremy Taylor, MIC, Denmark
Pablo Ordejon, Jose-Luis Mozos, UAB, Spain

ICMAB

Molecular-scale Electronics - Why ??

Smallest functional unit: The single molecule (Aviram & Ratner, 1974)

- "Top-down" silicon technology cannot continue to shrink in component size (dissipation, tunneling,cost of fabs...)
"End of the road map"

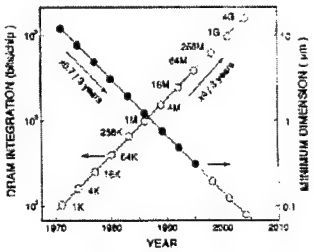

- "Bottom-up": The single molecule = Smallest functional unit
- Chemists can synthesize organic molecules with a range of properties
- Use novel quantum effects

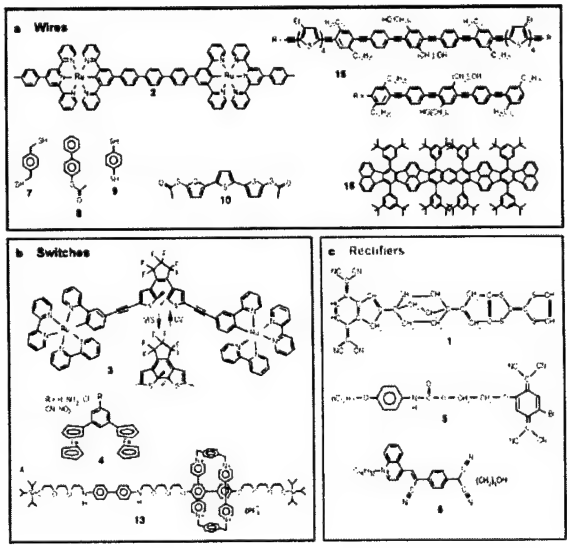

J. Reichert[1], R. Ochs[1], D. Beckmann[1], H. B. Weber[1], M. Mayor[1], and H. v. Löhneysen[2,3]
[1] *Forschungszentrum Karlsruhe, Institut für Nanotechnologie, D-76021 Karlsruhe*
[2] *Forschungszentrum Karlsruhe, Institut für Festkörperphysik, D-76021 Karlsruhe*
[3] *Physikalisches Institut, Universität Karlsruhe, D-76128 Karlsruhe*
(June 12, 2001)

We investigate electronic transport through two types of conjugated molecules. Mechanically controlled break-junctions are used to couple thiol endgroups of single molecules to two gold electrodes. Current-voltage characteristics (IVs) of the metal-molecule-metal system are observed. These IVs reproduce the spatial symmetry of the molecules with respect to the direction of current flow. We hereby unambigously detect an intrinsic property of the molecule, and are able to distinguish the influence of both the molecule and the contact to the metal electrodes on the transport properties of the compound system.

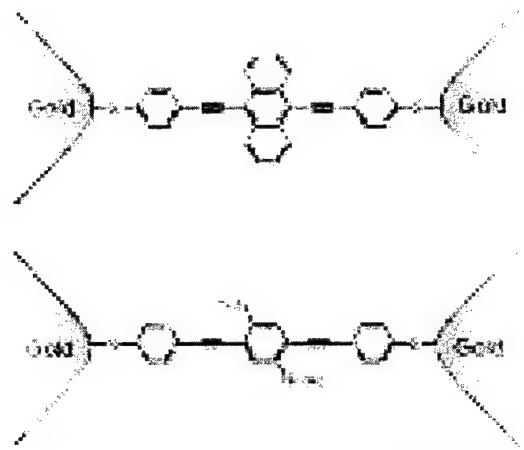

FIG. 1. Scheme of the experimental setup: a spatially symmetric (9,10-Bis((2'-para-mercaptophenyl)-ethinyl)-anthracene) and an asymmetric molecule (1,4-Bis((2'-para-mercaptophenyl)-ethinyl)-2-acetyl-amino-5-nitro-benzene) in between two gold electrodes.

FIG. 2. Scanning electron microscope picture of the lithographically fabricated break junction. The setup consists of a metallic plate, covered by an insulating layer of polyimide. On top of this, a gold film with a small constriction (smallest diameter 50*50 nm^2) is deposited, laterally structured by e-beam lithography. Two electrodes lead outside to connect the bridge electrically. The polyimide is partially etched away so that in the constriction region, the bridge is freely suspended over the polyimide substrate.

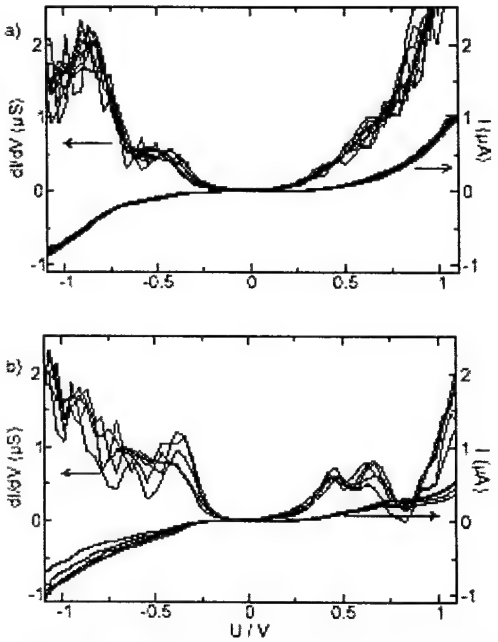

FIG. 3. Transport data of the asymmetric molecule. a) Current-voltage (IV) raw data (dashed lines, nine subsequent voltage sweeps) on a stable junction and the numerically differentiated data dI/dV (solid lines) from the above IV. b) Data from a subsequent junction.

Mechanical Break Junction Experiments

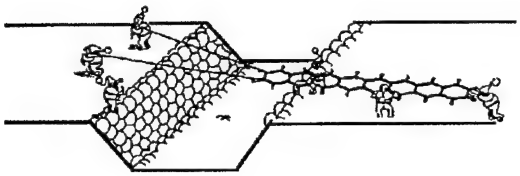

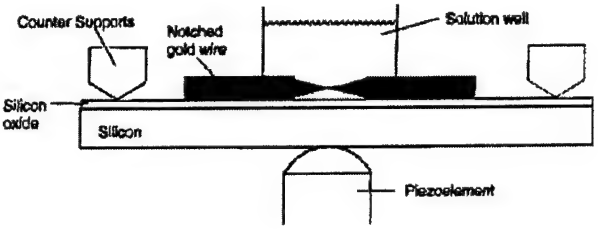

No Molecules/Solution

Conductance Quantization: Atomic short circuit

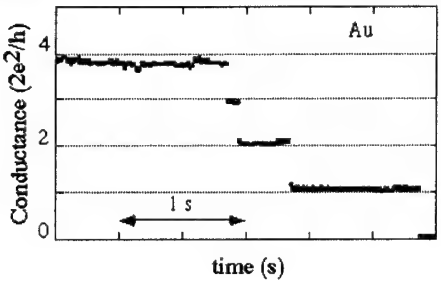

Molecules in solution

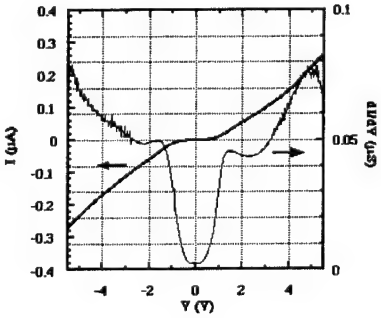

"Conductance of a Molecular Junction," M.A. Reed et al., Science, 278, 252 (1997).

"Single" Molecule Experiments

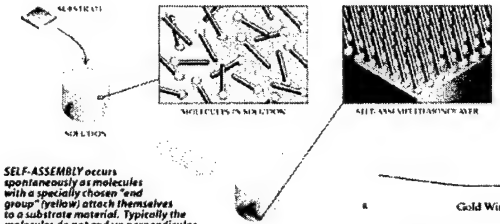

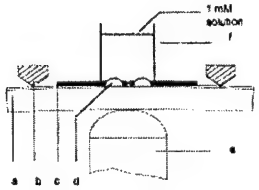

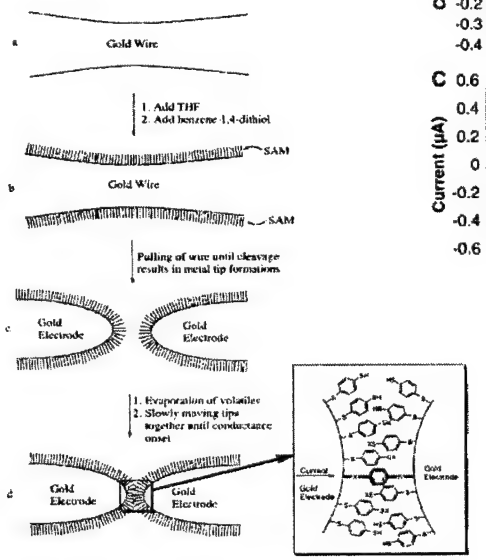

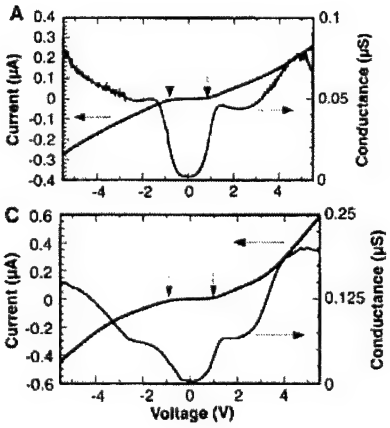

"Conductance of a Molecular Junction," M.A. Reed et al., Science, 278, 252 (1997).

Nano-pore

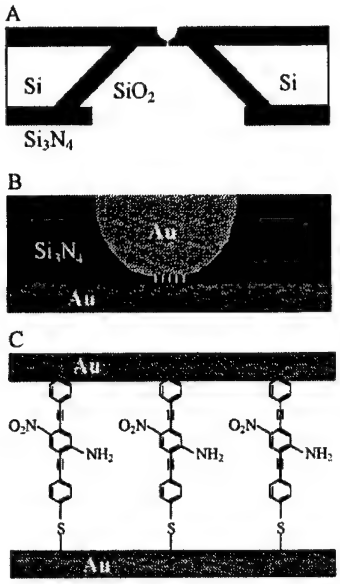

Diode behavior

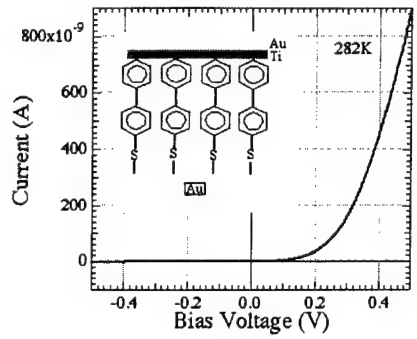

Negative Differential Resistance

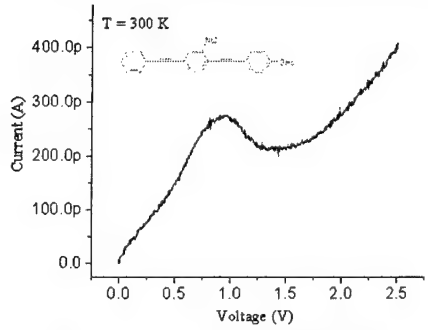

C. Zhou et al., "Nanoscale Metal/Self-Assembled Monolayer/Metal Heterostructures", Appl. Phys. Lett., 71, 611 (1997)

J. Chen et al., "Room-Temperature Negative Differential Resistance in Nanoscale Molecular Junctions", Appl. Phys. Lett., 21, 1224 (2000)

The Tour wire: "Giant" NDR

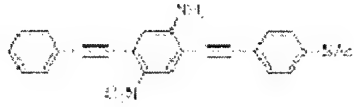

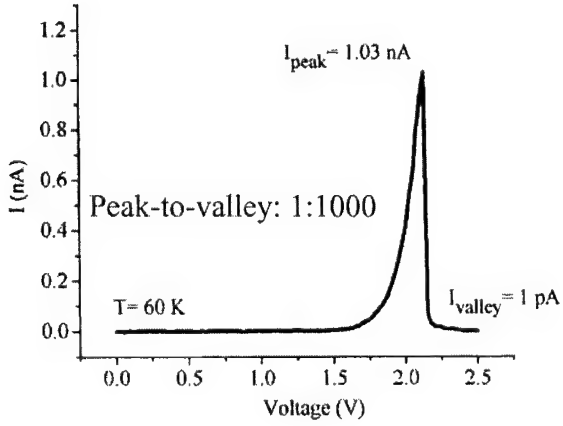

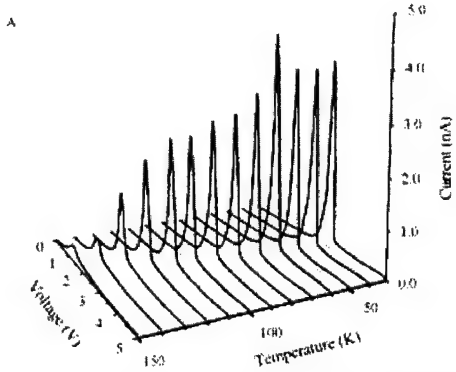

NDR has strange temperature dependence

J. Chen et al., "Observation of a Large On-Off Ratio and Negative Differential Resistance in an Electronic Molecular Switch,", Science, 286, 1550 (1999).

The Tour wire: Mechanism ???

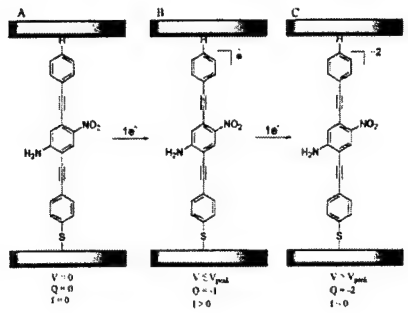

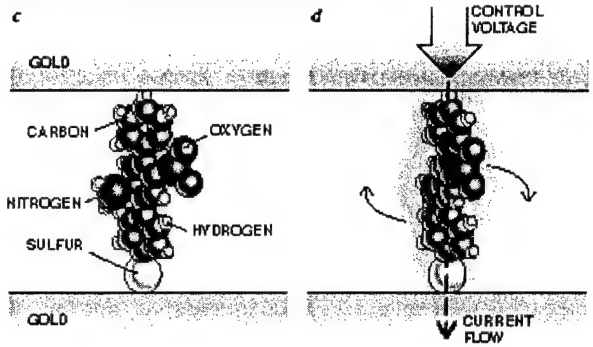

No explanation yet

From Mark A. Reed and James M. Tou, Scientific Am. June 2000

Possible factors:
A) Change in molecular states
B) Change in geometry
C) Change in charge states
D) Interaction of molecular dipole with external field

Only calculations for the *isolated* molecule has been published

Modelling atomic-scale conducters: Challenges

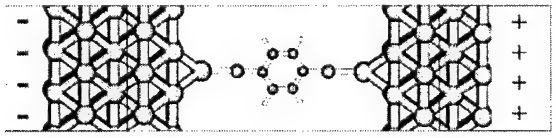

- Model a molecule coupled to bulk (infinite) electrodes
- Model the molecule-electrode system from "first principles":
  No parameters fitted to the particular system
- Include finite bias voltage/current
- Calculate the conductance (quantum transmission through the molecule)
- Determine geometry: Relax the atomic positions to an energy minimum

Density Functional Theory

Challenge: Many **interacting** electrons

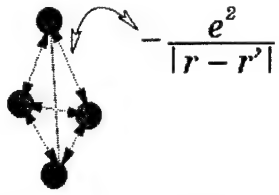

Interacting electrons
+ real potential

Way out: DFT

If the electron density is correct so is the total energy,
W. Kohn, Nobel prize 1998.

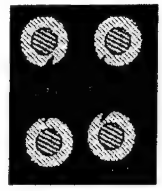

Non–interacting, fictitious
particles + effective potential(V_{eff})
$V_{eff}[n(r)]$, *$n(r)$ is the electron density*

DFT gives a good
description of energy and geometry
of isolated molecules and perfect
crystals

Schrödingers equation

$$\mathbf{H}\Psi = E\Psi, \quad \mathbf{H} = \mathbf{T} + \mathbf{V}_{eff}$$

instead of solving this we solve for G:

$$\mathrm{G}(\mathbf{z}) = (\mathbf{z} - \mathbf{H})^{-1}$$

We can get the density from G

Open/infinite System

Challenge: Coupling to *infinite* electrodes

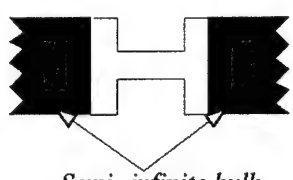

Semi–infinite bulk

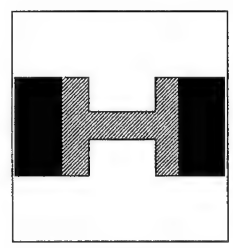

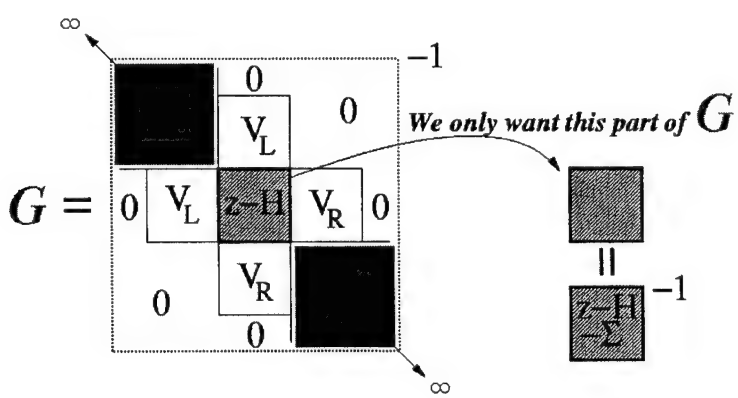

The selfenergy: $\Sigma = \Sigma_L + \Sigma_R$

(can be calculated from $1/(z-H^{bulk})$)

Summary of important relations from Nonequilibrum Green Function Theory

We consider the Hamiltonian:

$$H = \sum_{k,\alpha} \epsilon_\alpha(t) c^\dagger_{k,\alpha} c_{k;\alpha} + \sum_{k,\alpha;n} \left[V_{k,\alpha;n}(t) c^\dagger_{k,\alpha} d_n + \text{h.c.} \right] + H_{\text{cen}}[\{d_n\}, \{d^\dagger_n\}, t]$$

Current is calculated as follows (Caroli et al.(70's), Meir and Wingreen (1992), Jauho et al. (1994)):

$$\begin{aligned} J_L(t) &= \langle (-e)\dot{N}_L(t) \rangle \\ &= \frac{2e}{\hbar} \text{Re} \left\{ \sum_{k,\alpha;n} V_{k,\alpha;n}(t) G^<_{n,k\alpha}(t,t) \right\} \\ &= -\frac{2e}{\hbar} \int_{-\infty}^{t} dt_1 \int d\epsilon \text{Im} \text{Tr} \Big\{ e^{-i\epsilon(t_1-t)} \mathbf{\Gamma}^L(\epsilon, t_1, t) \\ &\qquad \left[\mathbf{G}^<(t,t_1) + f^0_L(\epsilon) \mathbf{G}^r(t,t_1) \right] \Big\} . \end{aligned}$$

Here the Green functions are *matrices* in the indices (m,n), and the linewidth functions $\mathbf{\Gamma}$ are defined as (here given for time-independent situation)

$$[\mathbf{\Gamma}^L(\epsilon_k)]_{mn} = 2\pi \sum_{\alpha \in L} \rho_\alpha(\epsilon_k) V^*_{\alpha;m}(\epsilon_k) V_{\alpha;n}(\epsilon_k)$$

Time-independent case (Meir-Wingreen):

$$\begin{aligned} J &= \frac{ie}{2h} \int d\epsilon \text{Tr} \Big\{ \left[\mathbf{\Gamma}^L(\epsilon) - \mathbf{\Gamma}^R(\epsilon) \right] \mathbf{G}^<(\epsilon) \\ &\quad + \left[f^0_L(\epsilon) \mathbf{\Gamma}^L(\epsilon) - f^0_R(\epsilon) \mathbf{\Gamma}^R(\epsilon) \right] \left[\mathbf{G}^r(\epsilon) - \mathbf{G}^a(\epsilon) \right] \Big\} \\ &= \frac{e}{h} \int d\epsilon \left[f^0_L(\epsilon) - f^0_R(\epsilon) \right] \text{Tr} \Big\{ \mathbf{G}^a \mathbf{\Gamma}^R \mathbf{G}^r \mathbf{\Gamma}^L \Big\} , \end{aligned}$$

where the second line holds, if the central region can be described in terms of an *effective one-body potential* (such as in density-functional theory).

Finite Voltage Bias/Current

Challenge: non-equilibrium electron distribution

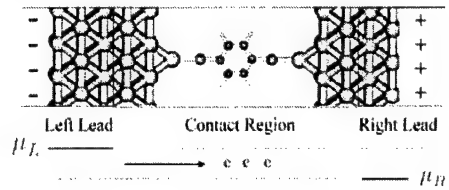

The Non-equilibrium Density Matrix

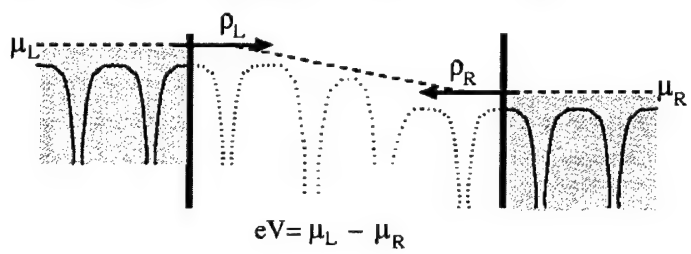

$$\mathbf{D}_{\alpha,\beta} = \int_{-\infty}^{\infty} dE\, \rho^L_{\alpha,\beta}(E) n_F(E-\mu_L) + \rho^R_{\alpha,\beta}(E) n_F(E-\mu_R)$$

$$\rho^L_{\alpha,\beta}(E) = \frac{1}{\pi}(\mathrm{G}(\mathbf{E}+\mathbf{i}\delta)\,\mathrm{Im}\,[\Sigma_\mathrm{L}(\mathbf{E}+\mathbf{i}\delta)]\;\mathrm{G}^\dagger(\mathbf{E}+\mathbf{i}\delta))_{\alpha,\beta}$$

Selfconsistent solution

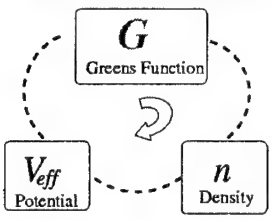

Conductance = Transmission

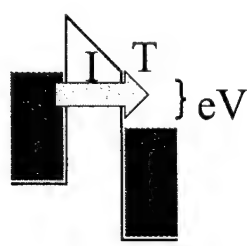

Conductance (Landauer-Büttiker)

$$I = \frac{2e^2}{h} \int dE (f_R(E) - f_L(E)) T_{\mathrm{tot}}(E)$$

$T_{\mathrm{tot}}(E)$: Total Quantum Transmission

$$T_{\mathrm{tot}}(E) = \mathrm{Tr}[\mathbf{t}^\dagger \mathbf{t}](E)$$

$$\mathbf{t}(E) = (\mathrm{Im}\,[\Sigma_\mathrm{R}]\,(E))^{1/2}\,\mathrm{G}(E)\,(\mathrm{Im}\,[\Sigma_\mathrm{L}]\,(E))^{1/2}$$

Implementation: TranSIESTA

- **SIESTA**
  - Density Functional Theory
  - LCAO, numerical orbitals w. finite range
  - Pseudopotentials

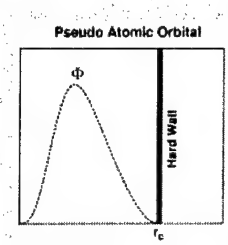

D

H

- ***Transport***
  - Coupling to electrodes using self-energies
  - Non-equilibrium electron distribution using NEGF

Setup

Physical system:

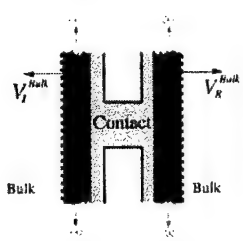

Representation (PBC in x,y):

Example:
3-atom Au chain connecting Au(100) electrodes.

Periodic Boundary Conditions in (x,y)
3◇3 unit cell, ☝-point approximation

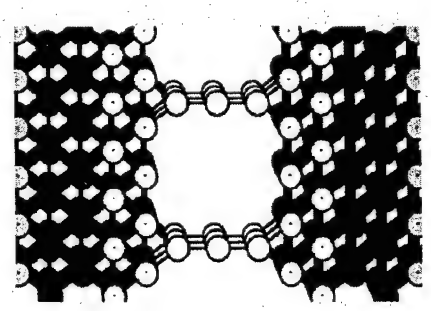

Benchmark atomic-scale conductors: Single-atom gold contacts

- Good statistics:
  1 atom=1 conductance quantum

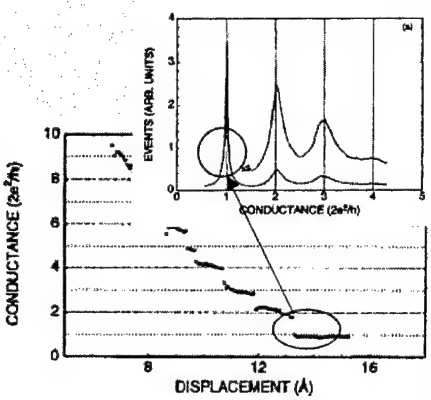

• Brandbyge et al., PRB 52, 8499 (1995)

- Structures directly imaged

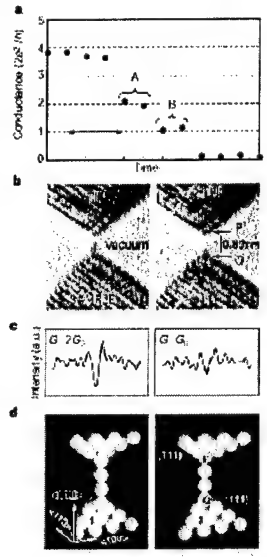

• Ohnishi et al., Nature 395, 780 (1998)

- Single channel transport

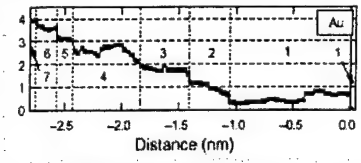

• Scheer et al., Nature 394, 154 (1998)

- Linear I-V characteristic

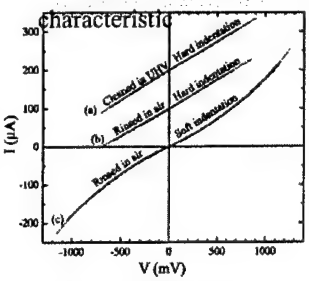

• Hansen et al., APL 77, 708 (2000)

Atomic short circuit: Single-atom contact

3-atom Au chain connecting
Au(100) electrodes.
3◇3 unit cell, ∅-point approximation

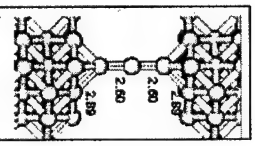

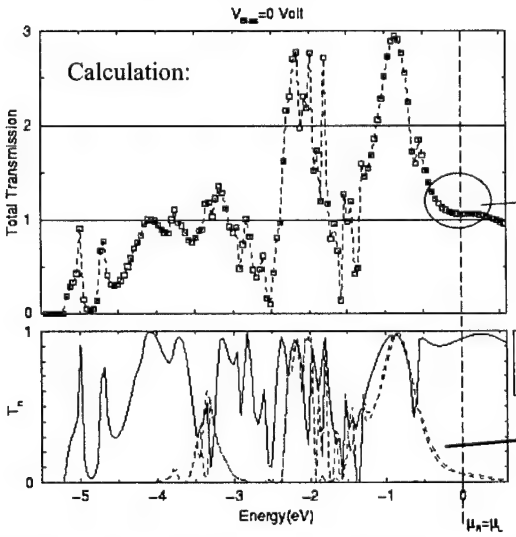

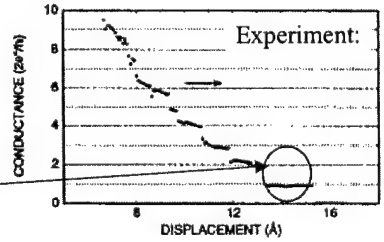

dzx,dyz

Bandstructure of infinite chain

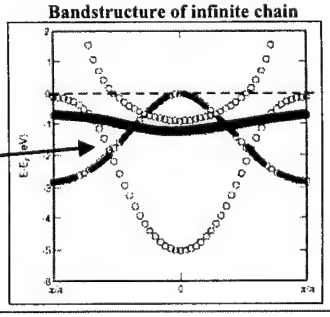

Single atomic contact: 1 Volt Bias

Voltage drop through the contact

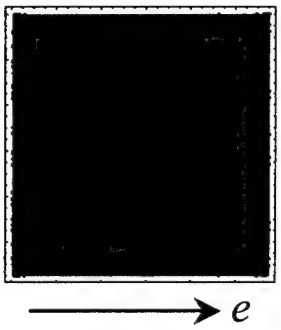

Almost linear IV

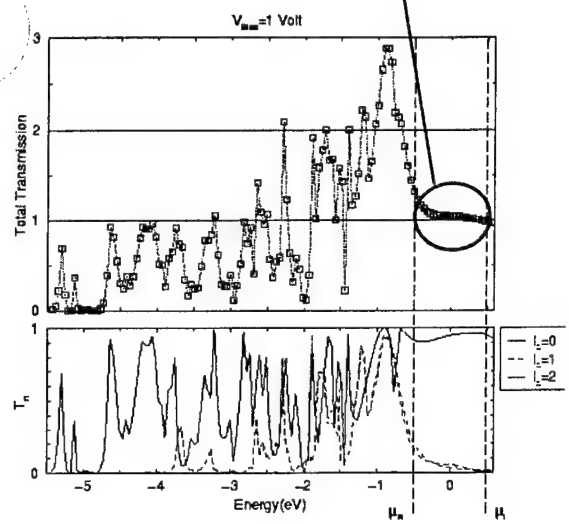

Density

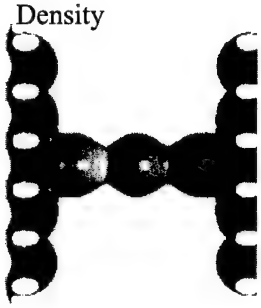

Change in Density

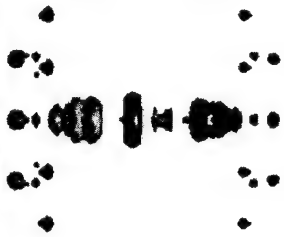

Zig-zag chains

VOLUME 83, NUMBER 19 PHYSICAL REVIEW LETTERS 8 NOVEMBER 1999

Stiff Monatomic Gold Wires with a Spinning Zigzag Geometry

Daniel Sanchez-Portal,[1] Emilio Artacho,[2] Javier Junquera,[2] Pablo Ordejón,[1] Alberto Garcia,[4] and José M. Soler[2]

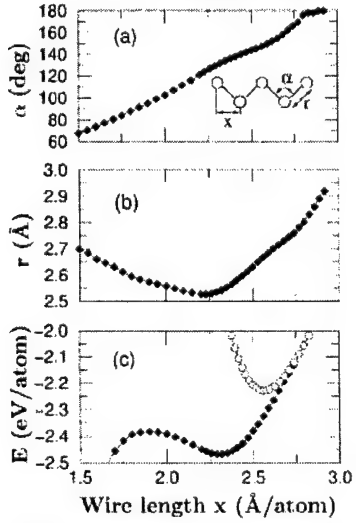

FIG. 1. First-principles, density-functional results for the bond angle α (a), and bond length r (b) in a monatomic gold wire with zigzag geometry, as a function of its length per atom. (c) Binding energy E in the zigzag (solid symbols) and linear wires (open symbols).

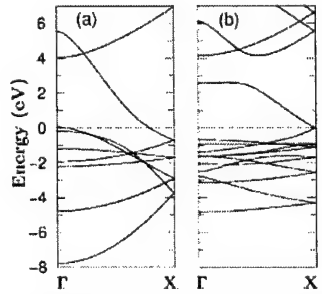

FIG. 2. Electronic band structure of the linear (a) and zigzag (b) wires for a length of 2.32 Å/atom. The linear-wire bands have been folded onto a two-atom Brillouin zone to facilitate the comparison. The energies are relative to the Fermi level.

Zig-zag wires on Au(111)

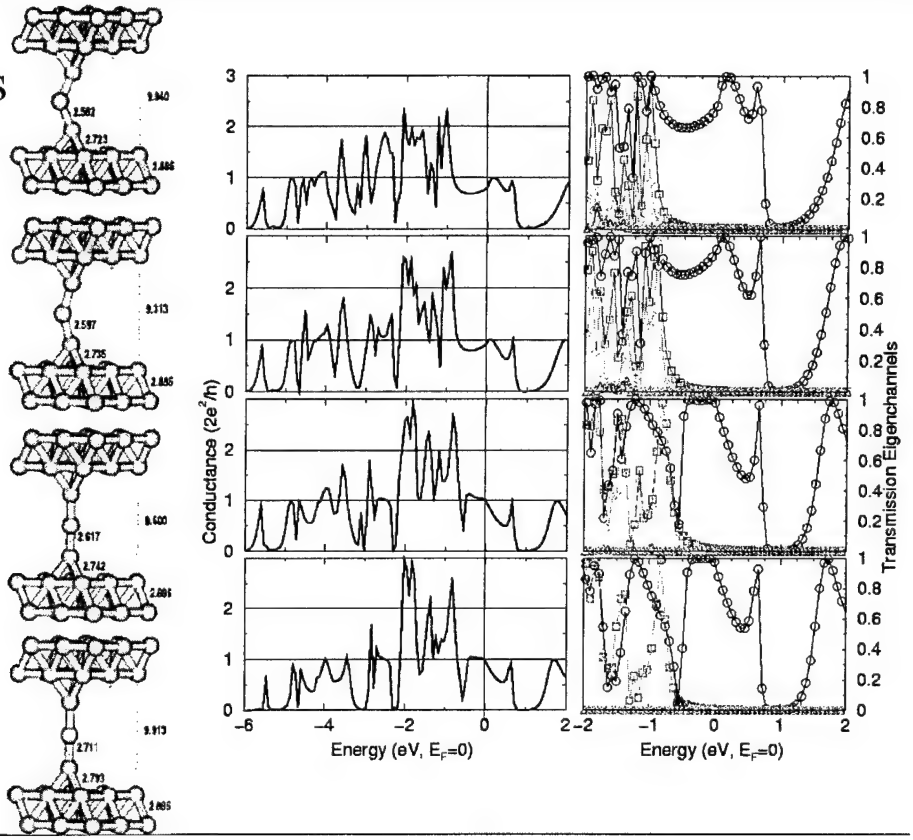

5 atom long gold chain

Chains of at least 4 gold atoms has been observed

Last plateau length = 12 Å

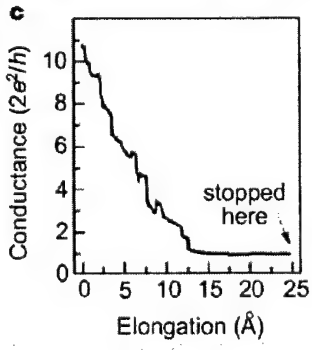

Yanson et al., Nature **395**, 783 (1998)

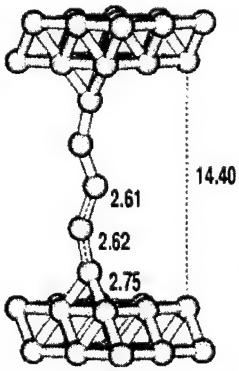

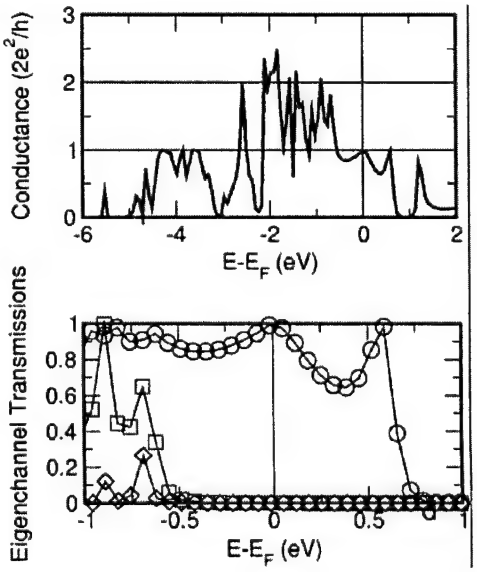

"Toy model"

Benzene-1,4-dithiolate coupled to gold chains

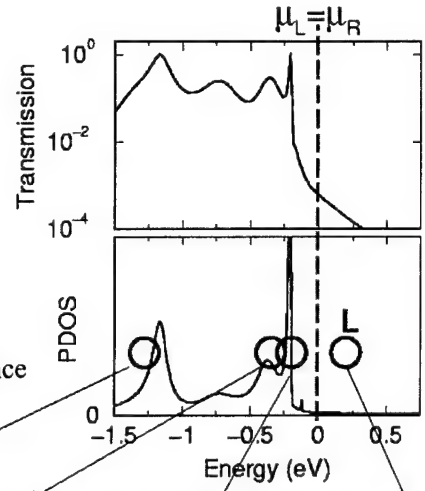

- The molecular states have a node plane
- The chain band states are rot. symmetric at the Fermi energy

} Low conductance

Brandbyge et al., Proceedings MRS fall meeting 2000, D9.25

Benzene-1,4-dithiolate coupled to gold chains: Finite Bias

Change in effective potential and density for 1Volt bias

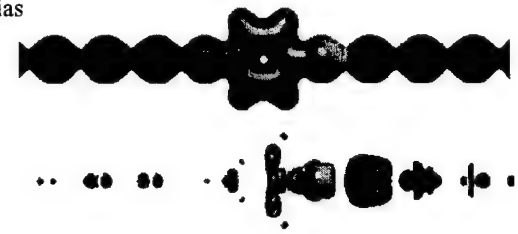

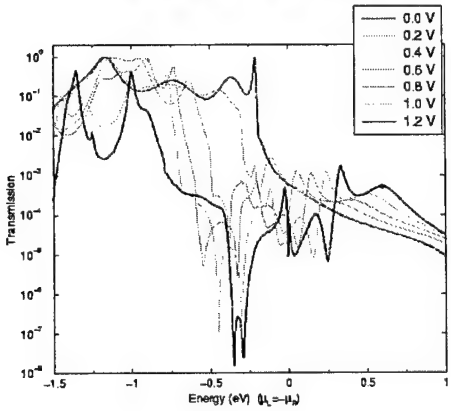

Calculated IV

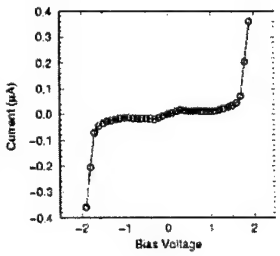

Measured IV

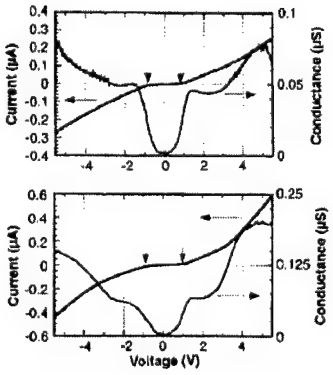

From Reed et al., Science 278, 252 (1997)

Summary

♦ Many exciting and promising experiments on atomic/molecular scale conductors.

♣ Many unknown factors in most experiments.

♥ We are developing a tool for first principles modelling (*Tran*SIESTA)

Preliminary Platinum

• **Linear**

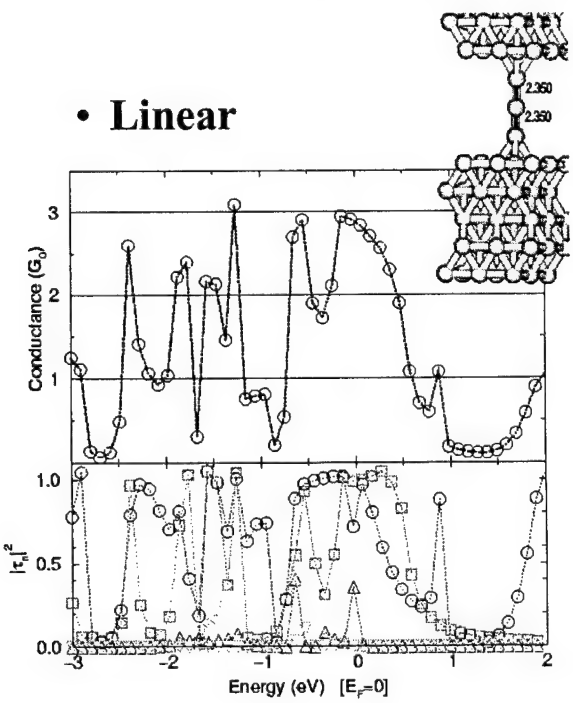

• **Bend**

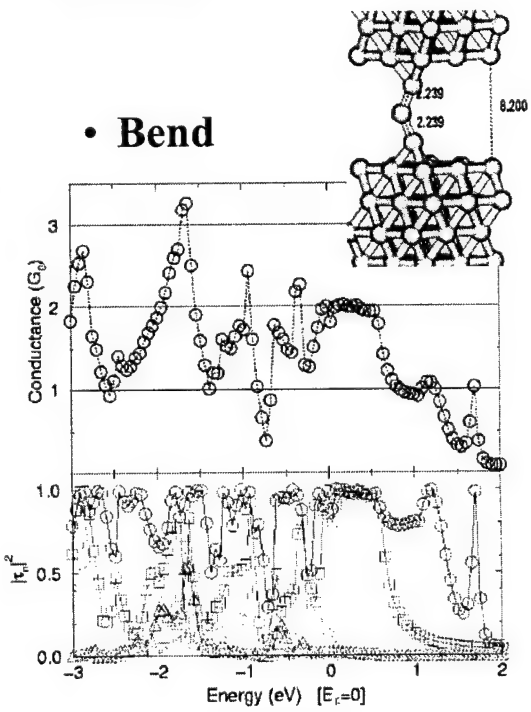

Landauer / McKelvey Approach to MOSFET Modeling

Mark Lundstrom
Electrical and Computer Engineering
Purdue University, West Lafayette, IN

1. Introduction
2. Landauer/McKelvey Theory of the MOSFET
3. The Ballistic MOSFET
4. Back-scattering in MOSFET's
5. Discussion
6. Summary

Acknowledgements

Professor Supriyo Datta

students:

Zhibin Ren, Ramesh Venugopal, Jung-Hoon Rhew
Dave Rumsey, Anisur Rahman, Jing Guo, Sayed Hasan

sponsors:

NSF
SRC
MARCO/DARPA
Indiana 21st Century Research and Technology Fund

1. Introduction

nanoscale MOSFETs

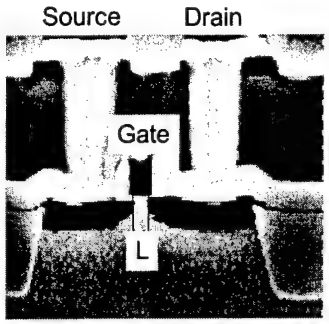

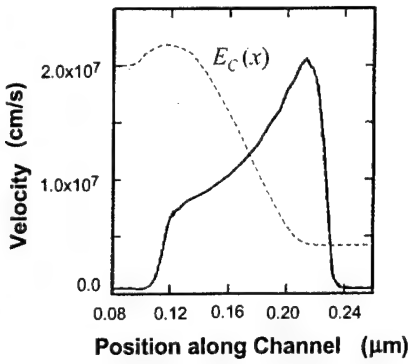

1. Introduction

conceptual approach

Landauer, 1959

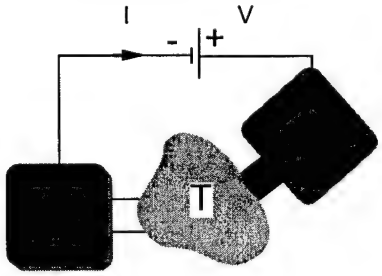

$$G = \frac{2e^2}{h} TM$$

McKelvey, 1961

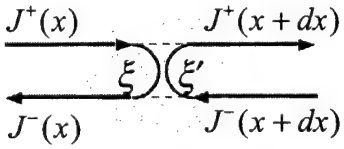

$$\frac{dJ^+}{dx} = -\xi J^+ + \xi' J^-$$

$$\frac{dJ^-}{dx} = -\xi J^+ + \xi' J^-$$

2. Landauer/McKelvey Theory of the MOSFET

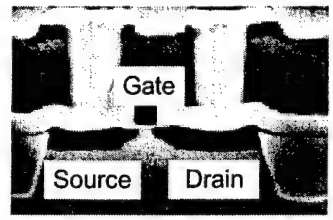

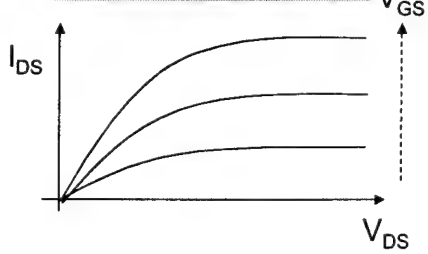

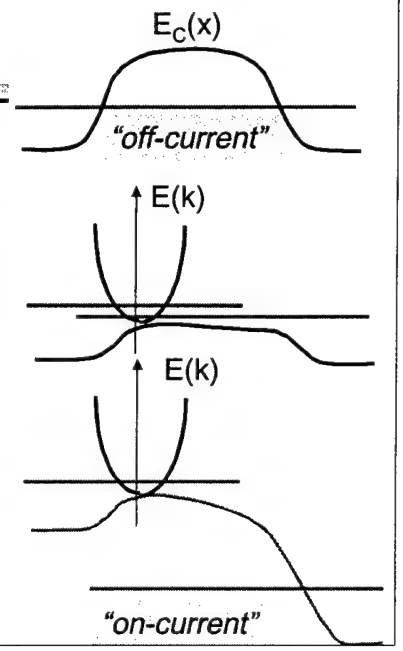

2. Landauer/McKelvey Theory of the MOSFET

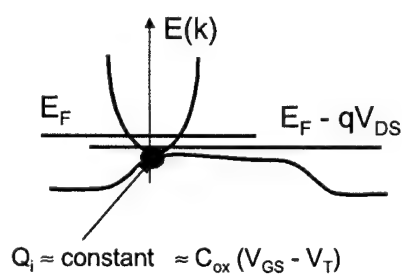

$$J^+ = n^+ \tilde{\upsilon}_T^+$$

$$n^+ = \frac{m}{2\pi\hbar^2} \ln\left(1 + e^{\eta_F}\right)$$

$$\tilde{\upsilon}_T^+ = \sqrt{\frac{2k_B T}{\pi m}} \frac{F_{1/2}(\eta_F)}{F_0(\eta_F)}$$

$$I_D = Wq\left(J^+ - J^-\right)$$

$$Q_i(V_{GS}) = q\left(n^+ + n^-\right)$$

$$I_{DS} = WQ_i(V_{GS})\tilde{\upsilon}_T \times \left\{ \frac{1 - \dfrac{F_{1/2}(\eta_F - U_{DS})}{F_{1/2}(\eta_F)}}{1 + \dfrac{F_0(\eta_F - U_{DS})}{F_0(\eta_F)}} \right\}$$

2. Landauer/McKelvey Theory of the MOSFET

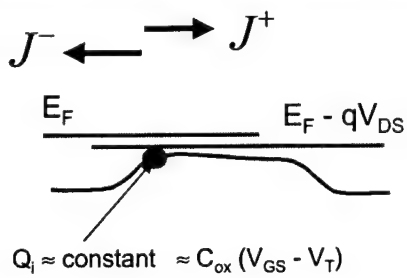

$$J^+ = n^+ \tilde{\upsilon}_T^+$$

$$J^- = (1-T)J^+ + TJ_{ball}^-$$

$$I_D = Wq\left(J^+ - J^-\right)$$

$$Q_i(V_{GS}) = \frac{q\left(J^+ + J^-\right)}{\tilde{\upsilon}_T^+}$$

$$I_{DS} = WQ_i(V_{GS})\tilde{\upsilon}_T\left(\frac{T}{2-T}\right)\times\left\{\frac{1-\dfrac{F_{1/2}(\eta_F - U_{DS})}{F_{1/2}(\eta_F)}}{1+\left(\dfrac{T}{2-T}\right)\dfrac{F_0(\eta_F - U_{DS})}{F_0(\eta_F)}}\right\}$$

2. Landauer/McKelvey Theory of the MOSFET

NEGF Simulations

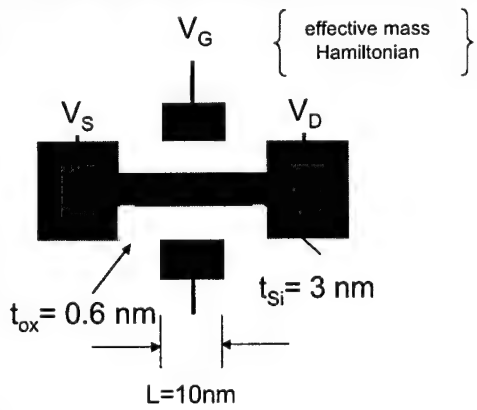

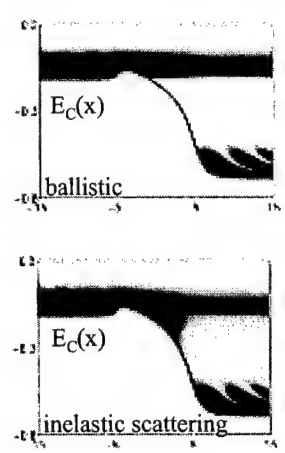

Zhibin Ren and Ramesh Venugopal (Purdue)
Dejan Jovanovic (Motorola, Los Alamos)

2. Landauer/McKelvey Theory of the MOSFET

Landauer/McKelvey model

$$I_{DS} = WC_{ox}(V_{GS} - V_T)\tilde{\upsilon}_T\left(\frac{T}{2-T}\right)\times$$

$$\frac{F_{1/2}(\eta_F)}{\ln(1+e^{\eta_F})}\times\left\{\frac{1-\dfrac{F_{1/2}(\eta_F - U_{DS})}{F_{1/2}(\eta_F)}}{1+\left(\dfrac{T}{2-T}\right)\dfrac{\ln(1+e^{\eta_F - U_{DS}})}{\ln(1+e^{\eta_F})}}\right\}$$

$$T = \frac{\lambda_o}{\lambda_o + (k_B T/eV_{DS})^{\alpha}}$$

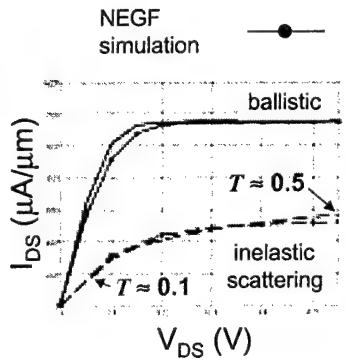

3. The Ballistic MOSFET..... *thermionic emission*

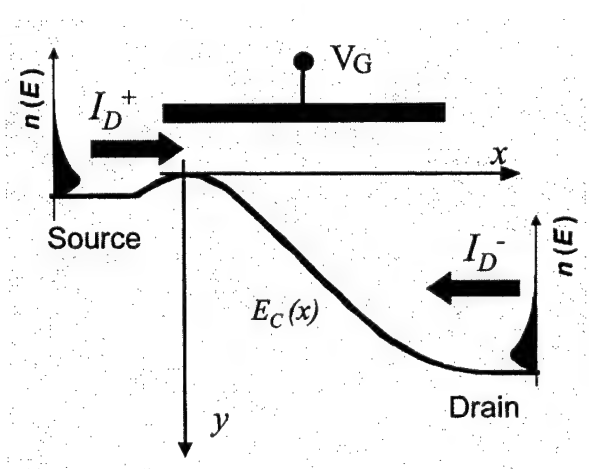

3. The Ballistic MOSFET.....

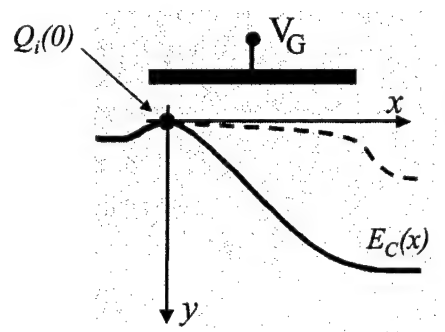

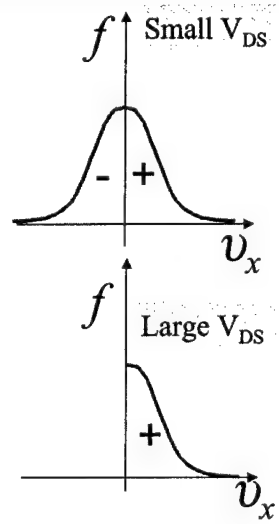

$$f_o = e^{-E/k_BT} \sim e^{-m^*\upsilon_x^2/2k_BT}$$

Lundstrom

3. The Ballistic MOSFET.....

$Q_i(0) \approx C_{ox}(V_{GS} - V_T)$

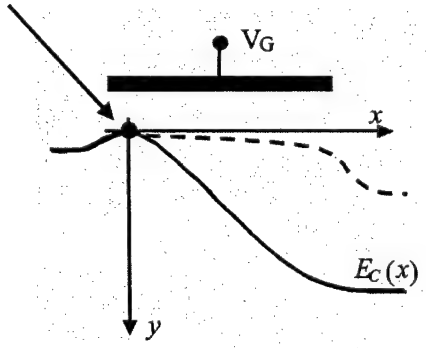

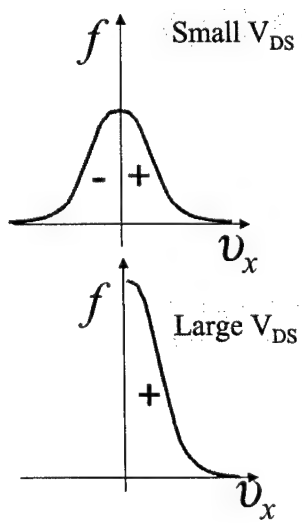

Lundstrom

3. The Ballistic MOSFET..... *numerical solution of the ballistic BTE*

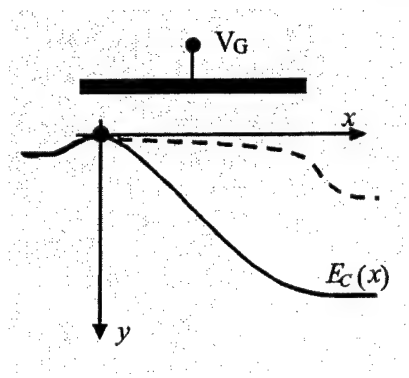

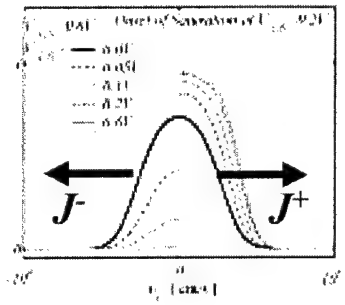

$$R \equiv J^- / J^+$$

Lundstrom Purdue

3. The Ballistic MOSFET..... *numerical solution of the ballistic BTE*

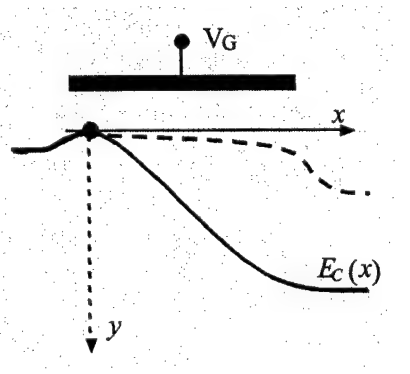

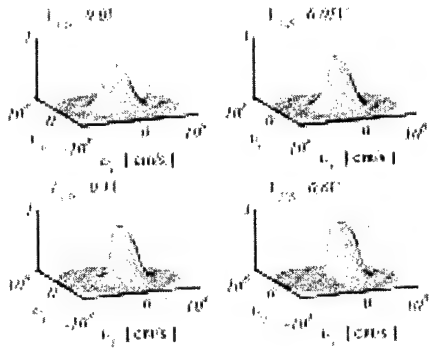

Lundstrom Purdue

3. The Ballistic MOSFET.....

i) $Q_i(0) \approx$ constant
ii) $\langle \upsilon(0) \rangle \rightarrow \upsilon_T$

E_C vs. x for $V_{GS} = 0.5V$

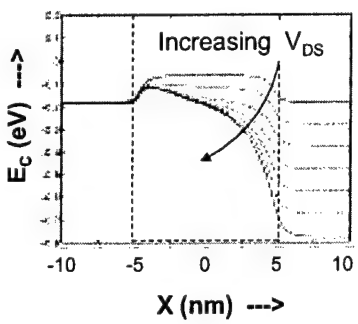

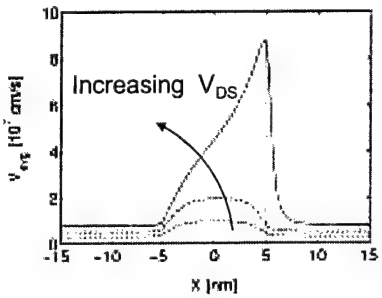

3. The Ballistric MOSFET..... velocity saturation in a ballistic FET

i) $Q_i(0) \approx$ constant
ii) $\langle \upsilon(0) \rangle \rightarrow \upsilon_T$

E_C vs. x for $V_{GS} = 0.5V$

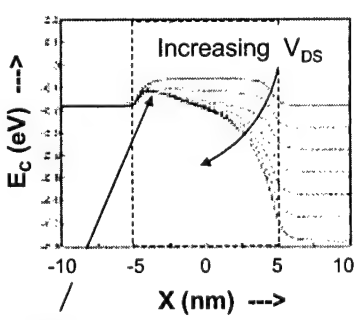

$\upsilon(0) \rightarrow \upsilon_T$

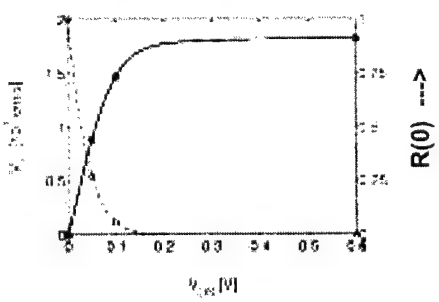

E_C vs. x for V_{GS} = 0.5V

i) $Q_i(0) \approx$ constant
ii) $\langle \upsilon(0) \rangle \rightarrow \upsilon_T$

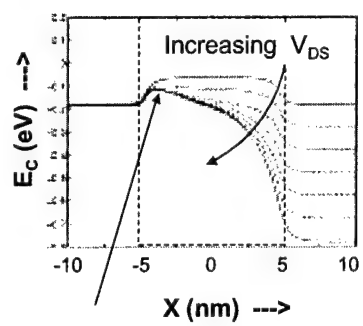

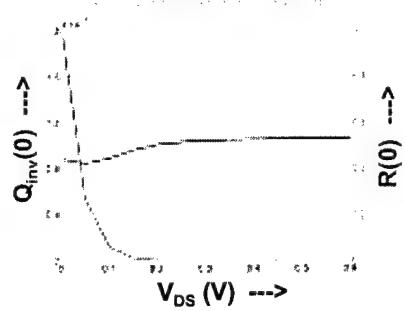

The (2-T) effect: Q_{inv} ~ constant

quasi-equilibrium

$n_S(V_{GS}) = C_{eff}(V_{GS} - V_T)$

(Gradual Channel Approximation + DIBL)

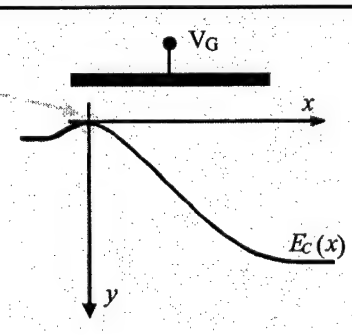

$$I_{DS} = W C_{ox} \upsilon_T (V_{GS} - V_T) \left[\frac{1 - e^{-qV_{DS}/k_BT}}{1 + e^{-qV_{DS}/k_BT}} \right] \quad \upsilon_T = \sqrt{\frac{2k_BT}{\pi m^*}}$$

(Boltzmann statistics and one subband)

3. The Ballistic MOSFET.....

$$I_{DS}(on) = W C_{ox} \upsilon_T (V_{GS} - V_T)$$

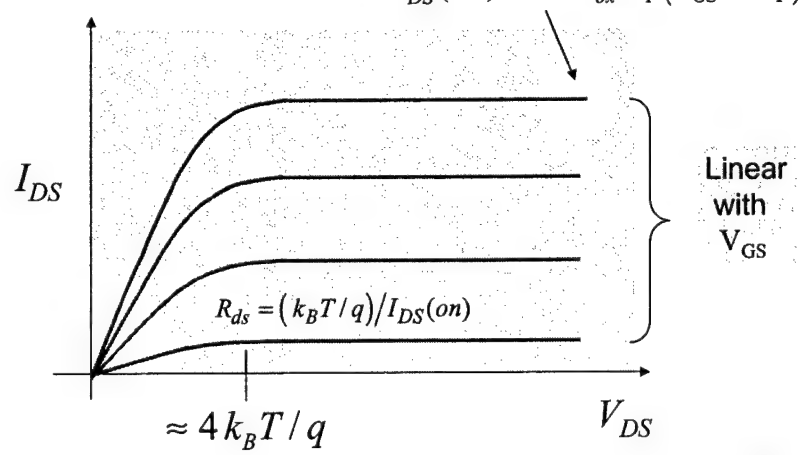

3. The Ballistic MOSFET.....

Why does a ballistic MOSFET have a finite channel resistance?

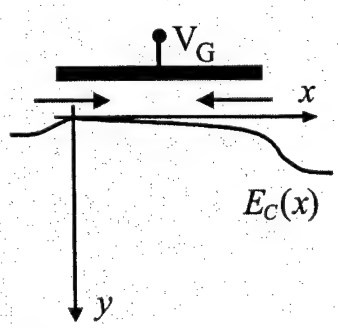

$$I_D^- = I_D^+ e^{-qV_{DS}/k_B T}$$

$$I_{DS} = I_D^+ - I_D^-$$

$$I_{DS} = I_D^+ \left(1 - e^{-qV_{DS}/k_B T}\right)$$

$$I_{DS} \approx \frac{I_D^+}{(k_B T / q)} V_{DS}$$

3. The Ballistic MOSFET.....

100 nm technology node....

tox = 1.5 nm $N_A = 2 \times 10^{18}$ cm^{-3} V_{DD} = 1V DIBL = 100 mV/V

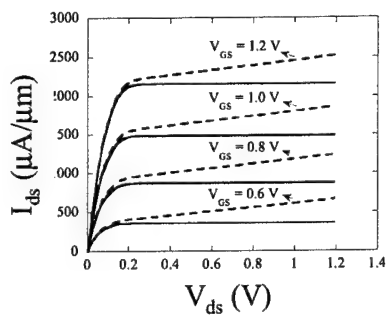

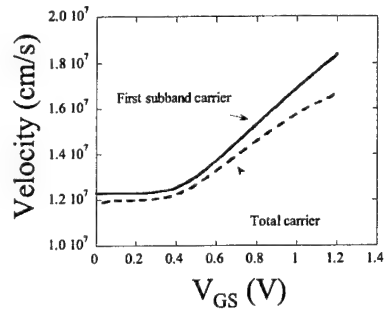

$$I_{DS} \propto (V_{GS} - V_T)^{\alpha}$$

$$1 \le \alpha \le 1.5$$

$$I_{DS}(on)/W = q\, n_S\, \upsilon_T$$

Lundstrom Purdue

3. The Ballistic MOSFET.....

comparison with measurements.....

L_{eff} = 115/125 nm technology

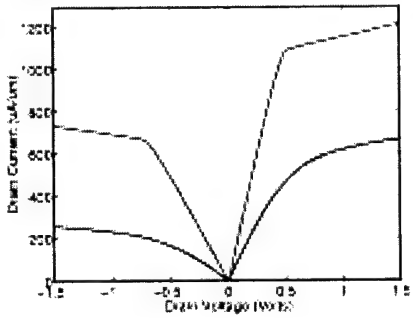

ballistic
(with measured Rs)

NMOS: ~ 55% of limit

PMOS: ~ 33% of limit

How can a device with L_{eff} ~ 6 mfps operate at ~50% of the ballistic limit?

- Farzin Assad, et al. (1999 IEDM)
- Dave Rumsey
- G. Timp, J. Bude, et al., (1999 IEDM)
- A. Lochtefeld, D. Antoniadis (EDL, Feb 2001)

Lundstrom Purdue

Channel resistance vs. V_{GS}

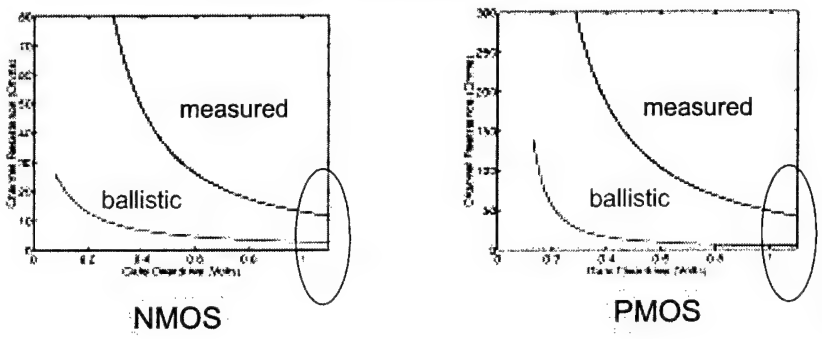

$$R_{SD} = R_{par} + R_{ballistic} + R_0 \frac{L}{W}$$

- the ballistic I-V is readily computed and the ballistic MOSFET is readily understood
- present day devices operate at ~ 50% of the ballistic limit
- future devices will have to operate even closer
- **backscattering** limits the performance of realistic devices

4. Back-Scattering in MOSFETs.....

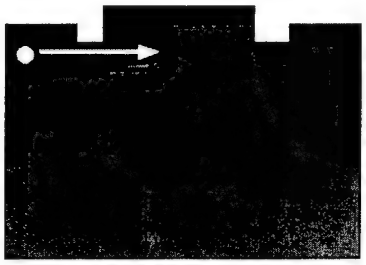

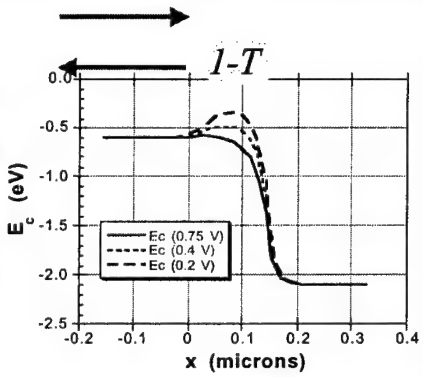

carriers at the top of the barrier: MOS electrostatics
carriers that cross the channel: backscattering, *R=1-T*

4. Back-Scattering in MOSFETs.....

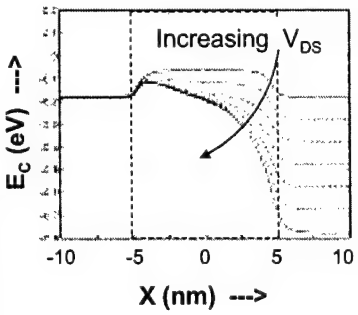

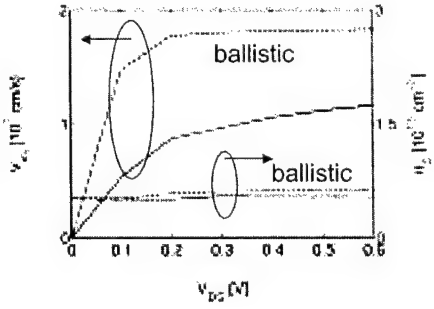

4. Back-Scattering in MOSFETs.....

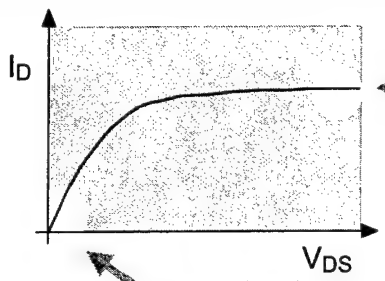

$$I_D = W C_{ox} \upsilon_T \left(\frac{T}{2-T} \right) (V_{GS} - V_T)$$

Note: $T(V_{DS}, V_{GS})$

$$I_D = W C_{ox} \left(\frac{\upsilon_T}{2 k_B T / q} \right) (1-T)(V_{GS} - V_T) V_{DS}$$

M.S. Lundstrom, "Elementary scattering theory of the MOSFET," *EDL*, **18** , 361, 1997
S. Datta, et. al, "The MOSFET from a Tranmission Viewpoint," Superlatrtices and Microstructures, 1998

4. Back-Scattering in MOSFETs.....

computing T: low V_{DS}

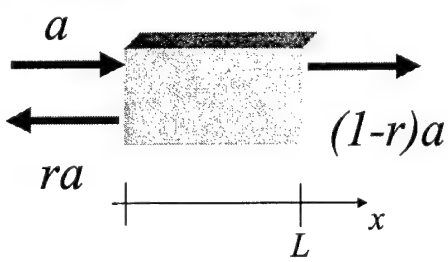

$$T = \frac{\lambda_0}{L + \lambda_0}$$

$$I_{DS} = W C_{ox} \left(\frac{\upsilon_T}{k_B T / q} \right) T (V_{GS} - V_T) V_{DS}$$

$$I_{DS} = \mu_{eff} C_{ox} \left(\frac{W}{L + \lambda_0} \right) (V_{GS} - V_T) V_{DS}$$

4. Back-Scattering in MOSFETs.....

computing T: high V_{DS}

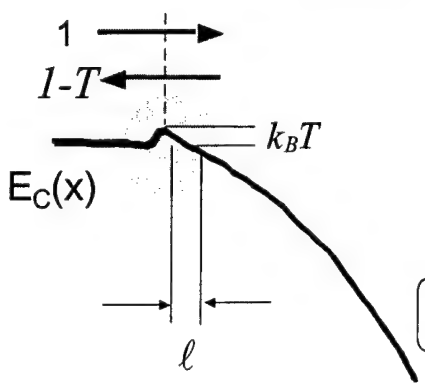

$$T = \frac{\lambda_o}{\ell + \lambda_o}$$

Bethe condition for a MOSFET:

ballistic current: $\ell < \lambda$

[not: $L < \lambda$]

☆ mobility is important for nanoscale FETs

4. Back-Scattering in MOSFETs.....

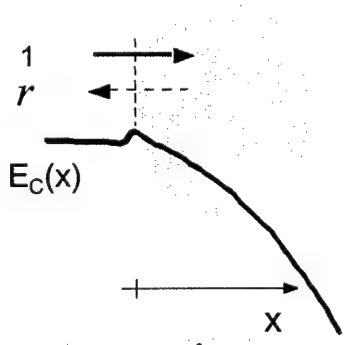

$$r = \frac{\ell}{\ell + \lambda_o}$$

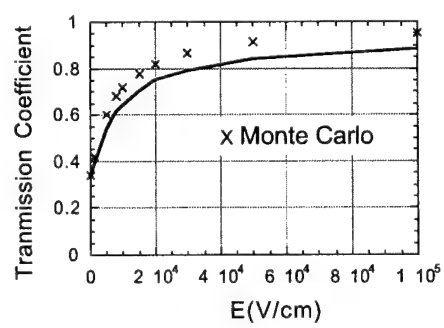

See:
P.J. Price, *Semiconductors and Semimetals*, **14**, 249-334, 1979
H. U. Baranger and J.W. Wilkins, *Phys. Rev. B*, **36**, 1487-1502, 1987.

4. Back-Scattering in MOSFETs..... Landauer/McKelvey model

$$I_D = W C_{ox} \upsilon_T \left(\frac{T}{2-T} \right) (V_{GS} - V_T)$$

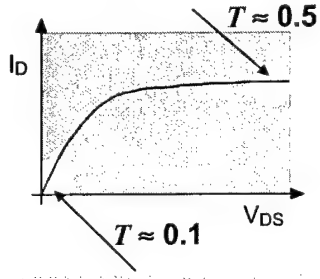

$$I_{DS} = W C_{ox} (V_{GS} - V_T) \tilde{\upsilon}_T \left(\frac{T}{2-T} \right) \times$$

$$\frac{F_{1/2}(\eta_F)}{\ln(1+e^{\eta_F})} \times \left\{ \frac{1 - \frac{F_{1/2}(\eta_F - U_{DS})}{F_{1/2}(\eta_F)}}{1 + \left(\frac{T}{2-T} \right) \frac{\ln(1+e^{\eta_F - U_{DS}})}{\ln(1+e^{\eta_F})}} \right\}$$

$$I_D = W C_{ox} \left(\frac{\upsilon_T / 2}{k_B T / q} \right) T (V_{GS} - V_T) V_{DS}$$

Lundstrom Purdue

Landauer / McKelvey Approach to MOSFET Modeling

Mark Lundstrom
Electrical and Computer Engineering
Purdue University, West Lafayette, IN

1. Introduction
2. Landauer/McKelvey Theory of the MOSFET
3. The Ballistic MOSFET
4. Back-scattering in MOSFET's
5. **Discussion**
6. Summary

Lundstrom Purdue

5. Discussion....

essential physical picture.....

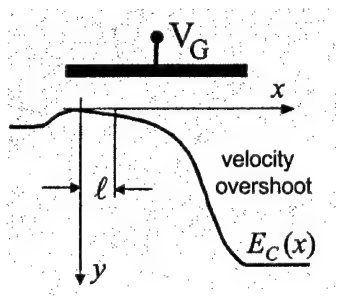

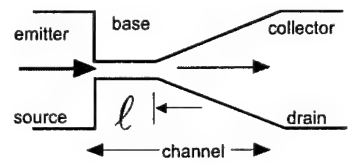

$$r = (1-t) = \frac{\ell}{\ell + \lambda_o}$$

See: "Essential physics of carrier Transport in nanoscale MOSFETs," M. Lundstrom, et al.

$$r \approx 50\% \Rightarrow \ell \approx \lambda_o$$

Lundstrom

Purdue

5. Discussion....

interpreting simulations

$$\langle \upsilon(0) \rangle = \left(\frac{T}{2-T} \right) \upsilon_T$$

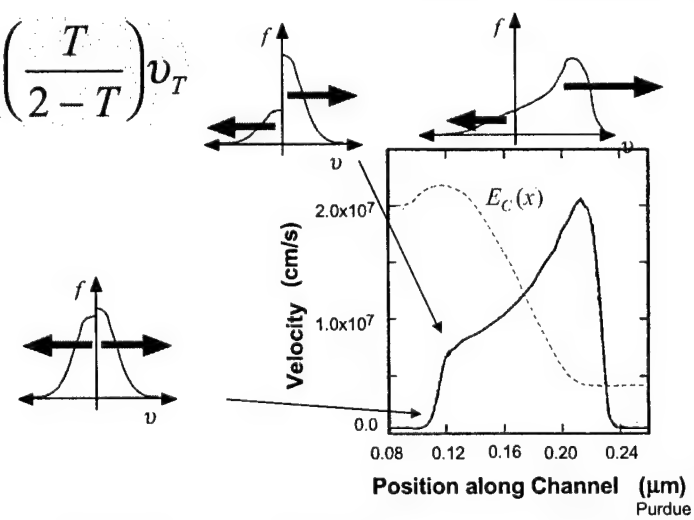

Lundstrom

Purdue

5. Discussion.... *how does T scale?*

$$T = \frac{\lambda}{\ell + \lambda} \approx 50\%$$

$$\ell \approx \lambda$$

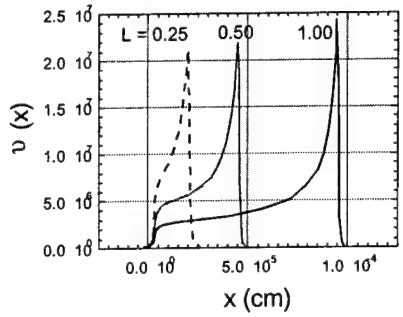

How does T scale?

as $L \downarrow$ ... $\ell \downarrow$ and $\lambda \downarrow$

Scaling maintains a constant T (at min L)

Lundstrom Purdue

5. Discussion.... *How to increase T?*

To reduce backscattering:

1) increase mfp λ (μ)

2) decrease ℓ

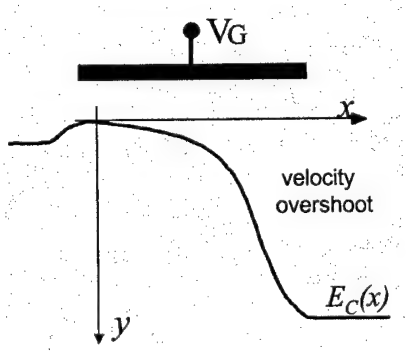

Lundstrom Purdue

Backscattering is related to λ_o and λ_o is related to mobility

Scattering theory gives:

$$\frac{\delta I_D}{I_D} = \frac{\delta \mu}{\mu}(1-B)$$

$$B \equiv \frac{I_D}{I_D(ballistic)}$$

i) linear region: $B \approx 0.2$

$$\frac{\delta I_D}{I_D} \approx \frac{\delta \mu}{\mu}$$

ii) saturated region: $B \approx 0.5$

$$\frac{\delta I_D}{I_D} \approx 0.5\frac{\delta \mu}{\mu}$$

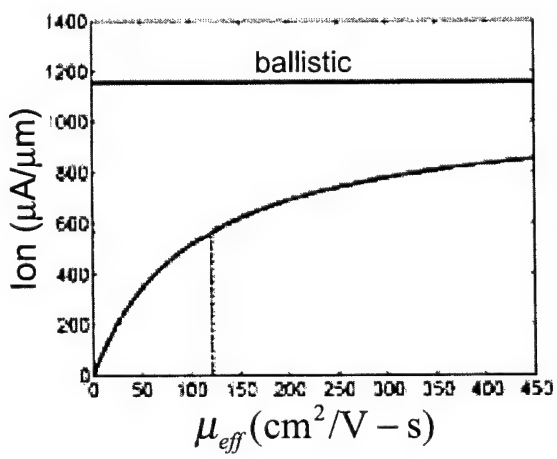

5. Discussion.... *connections to traditional theory*

$$I_D = C_{ox} W \upsilon_{sat} \left(V_{GS} - V_T \right)$$

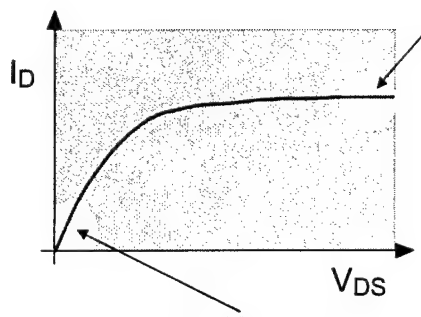

$$I_D = C_{ox} \mu_{eff} \left(\frac{W}{L} \right) \left(V_{GS} - V_T \right) V_{DS}$$

Lundstrom Purdue

5. Discussion.... *connections to traditional theory*

Scattering theory

Linear (low V_{DS}) drain current

$$\left(\begin{array}{l} I_D = W C_{ox} \left(\dfrac{\upsilon_T}{2 k_B T / q} \right) T \left(V_{GS} - V_T \right) V_{DS} \\ T = \dfrac{\lambda_o}{L + \lambda_o} \end{array} \right)$$

Conventional theory

$$\left(I_D = W \mu_{eff} C_{ox} \frac{W}{\left(L + \lambda_o \right)} \left(V_{GS} - V_T \right) V_{DS} \right)$$

Lundstrom

5. Discussion....

connections to traditional theory

Scattering theory

on-current

$$I_D = W C_{ox} \upsilon_T \left(\frac{T}{2-T} \right) (V_{GS} - V_T)$$

$$T = \frac{\lambda_o}{\ell + \lambda_o} \qquad \ell = \left(\frac{k_B T / q}{V_{DS}} \right) L$$

Conventional theory

$$I_D = \frac{W C_{ox} \upsilon_T m (V_{GS} - V_T) V_{DS}}{1 + m V_{DS}}$$

$$m = \left(\frac{\mu}{2 L \upsilon_T} \right)$$

Veeraraghavan and Fossum
IEEE TED, **35**, p. 1866, 1988

6. Summary

- Nanoscale transistor physics is simply understood by beginning at the ballistic limit
- Scattering theory provides a simple, physical view of nanotransistors and compact, analytical models
- Useful for interpreting simulations and guiding experiments
- A bridge to post-CMOS devices

Diffusion and Clustering of Impurities – "a Problem that Cannot be Ignored"

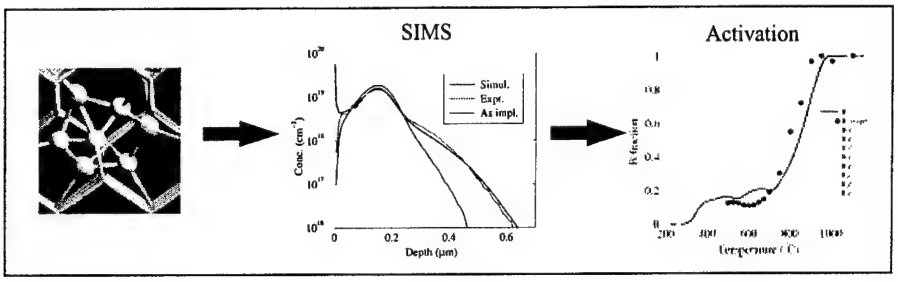

Wolfgang Windl

Digital DNA™ Laboratories, Motorola, Inc.
Austin, TX

in collaboration with

Benjamin Liu, Dejan Jovanovic, Mike Masquelier (Motorola Labs)
Blas Uberuaga, Hannes Jónsson, Scott Dunham (UW)

© 2001 Wolfgang Windl (Motorola, Inc.). All rights reserved.

MOSFET Basics

Metal Oxide Semiconductor Field Effect Transistor

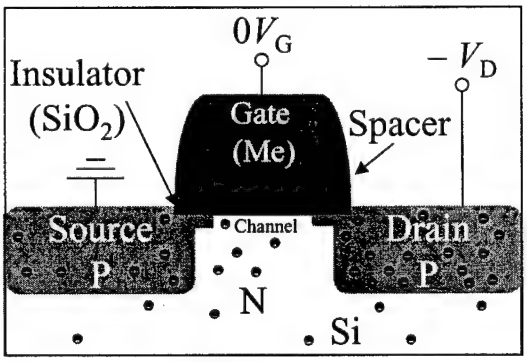

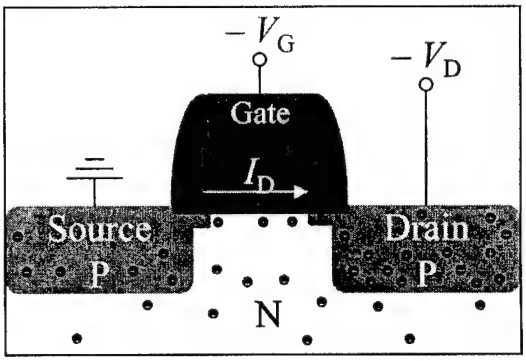

Doping:
N: e^-, e.g. As (Donor)
P: holes, e.g. B (Acceptor)

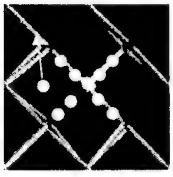

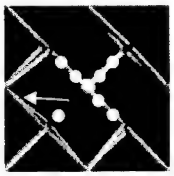

- Analog: Amplification
- Digital: Logic gates

Semiconductor Technology Scaling

- Feature size shrinks on average by 12% p.a. ($f = 0.88$)

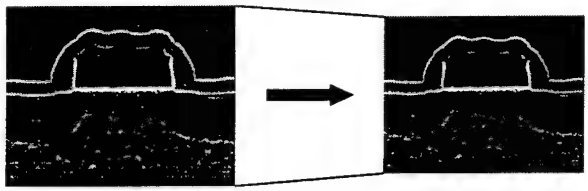

- Chip size increases on average by 2.3% p.a. ($d = 1.023$)

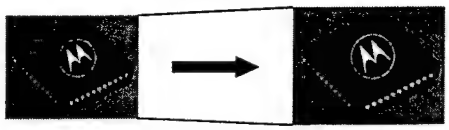

# of transistors / area ($\sim d^2 / f^2$) ↑ by 35% p.a.
Switching speed ($\sim 1 / f$) ↑ by 14% p.a.

Overall performance: ↑ by ~55% p.a. or
~ doubling every 18 months ("Moore's Law")

MOSFET Scaling Challenges

Shorter Channel

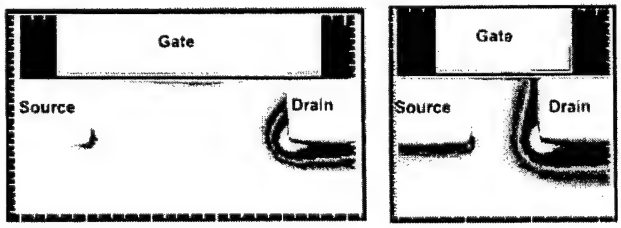

Potential across channel (on)

Higher Doping

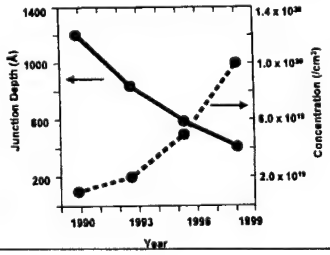

To get enough current with shallow source & drain

Shallower Implant

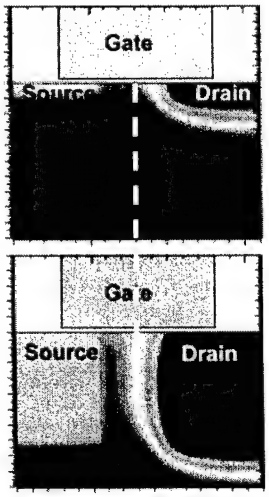

Better insulation (off)

*P. Packan, MRS Bulletin

ITRS Requirements & Solubility Limit

Solid Solubility of Si Dopants

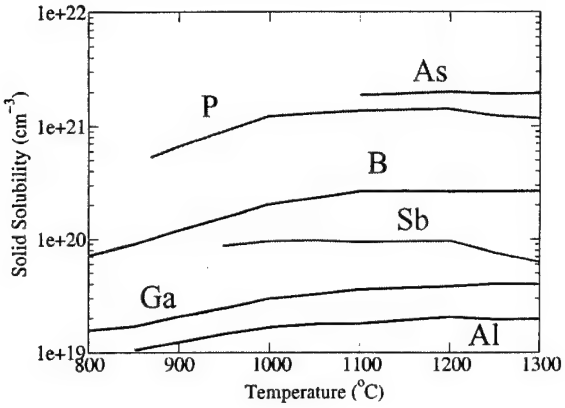

ITRS & Solubility Limit

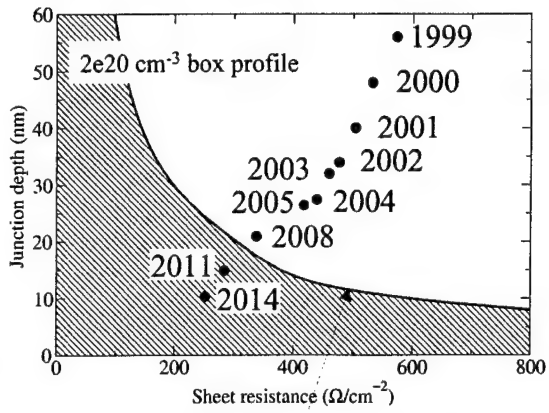

- Electrically active concentrations may be much lower
- "Practical" solubility ~ 2e20 cm^{-3}

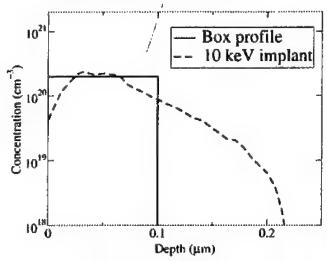

How Are We Doing?

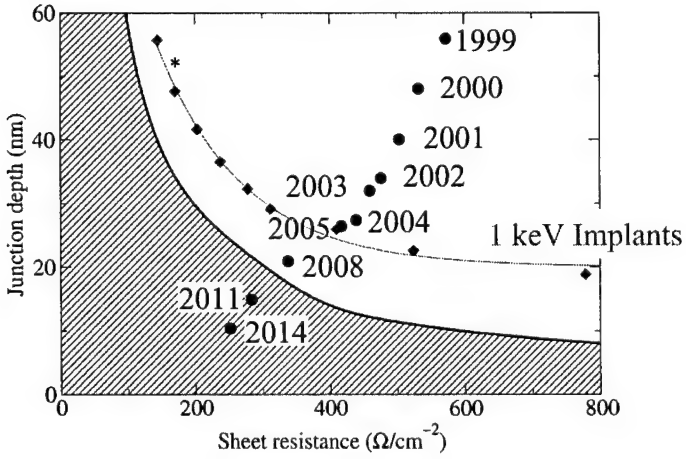

- 1 keV implants + optimum anneals can meet 2005 ITRS requirements (100 nm).
- Further reduction in implant energy can perhaps meet 70 nm (2008) needs, but cannot meet needs beyond this node.
- Need to find way to exceed 2e20 cm^{-3} concentration limit for *n* and *p* dopants, or need new device structures (double gate, surround gate, superhalo, etc.).

*Plummer (Stanford)

Ion Implantation and Annealing

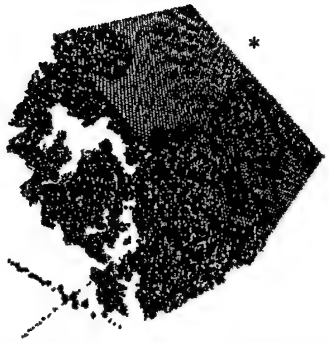

- Dopants inserted by ion implantation damage
- Damage healed by annealing
- During annealing, dopants diffuse fast (assisted by defects)
  important to optimize anneal

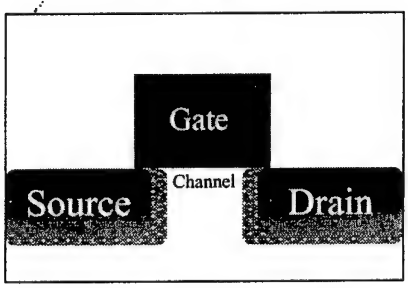

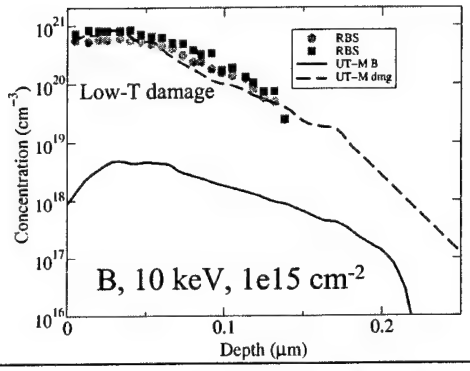

TED & Deactivation

What you expect:
Intrinsic diffusion

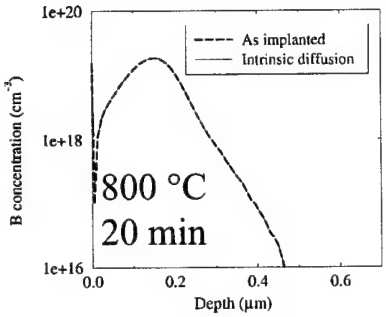

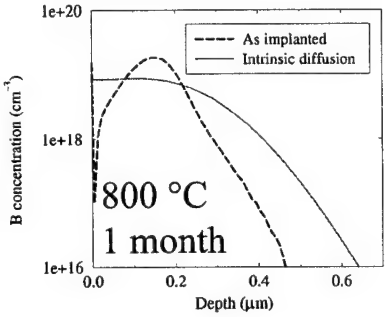

What you get:
TED:
- fast diffusion
- immob. peak

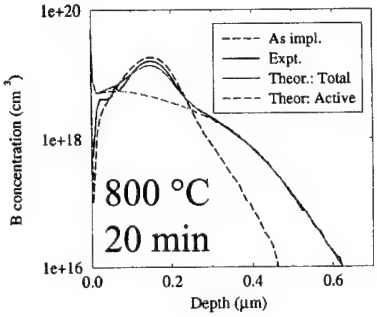

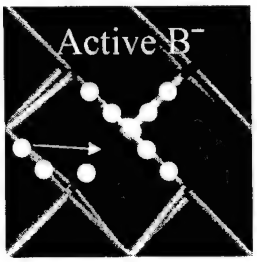

B Diffusion in Bulk Si: Qualitative Picture

- B diffusion exclusively mediated by Si self-interstitials*
- B diffusion limited by self-interstitial diffusion**

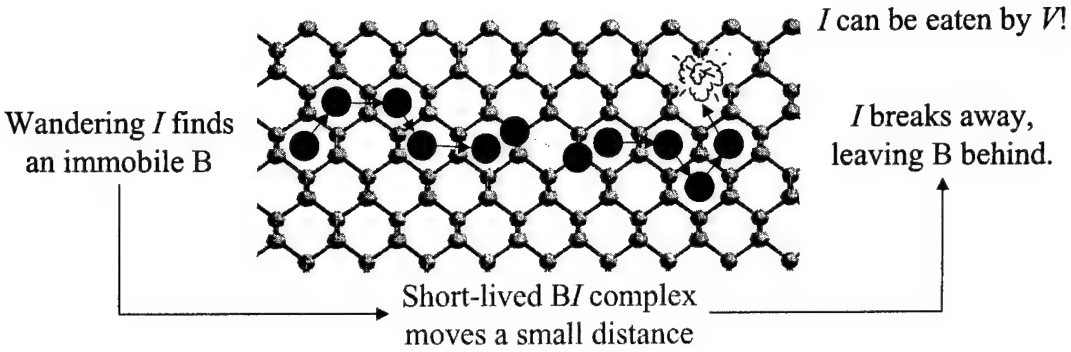

*A. Ural, P. B. Griffin, and J. D. Plummer, J. Appl. Phys. **85**, 6440 (1999)
** W. Windl, M.M. Bunea, R. Stumpf, S.T. Dunham, and M.P. Masquelier, Proc. MSM99 (Cambridge, MA, 1999), p. 369; MRS Proc. **568**, 91 (1999); Phys. Rev. Lett. **83**, 4345 (1999).

Reason for TED: Implant Damage

Interstitial assisted two-step mechanism:

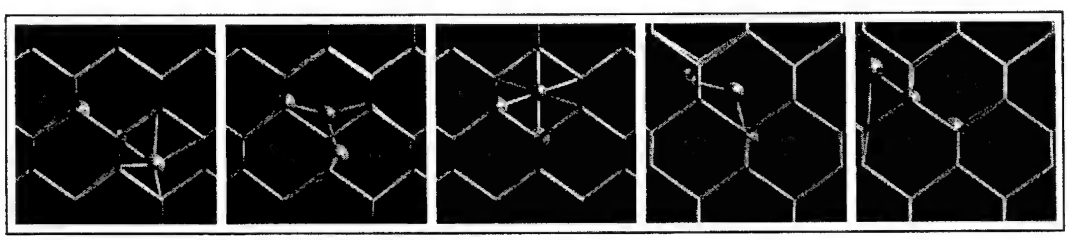

Intrinsic diffusion:

Create interstitial, B captures interstitial, diffuse together

Diffusion barrier: $E_{form}(I) - E_{bind}(BI) + E_{mig}(BI)$

4 eV 1 eV 0.6 eV ~ 3.6 eV

After implant:

Interstitials for "free" diffusion barrier ~ 0.6 eV

W. Windl, M.M. Bunea, R. Stumpf, S.T. Dunham, and M.P. Masquelier, Proc. MSM99 (Cambridge, MA, 1999), p. 369; MRS Proc. **568**, 91 (1999); Phys. Rev. Lett. **83**, 4345 (1999).

Reason for Deactivation?

Phenomenological considerations:

- Boron is smaller than Si substitutional B strains Si lattice
- Boron crystal structure: Icosahedron (buckyball), threefold coord.
  at higher B concentrations: New structures form,
  bind & deactivate B

Experimental findings:

- Structures too small to be seen in EM only "few" atoms
- Clustering dependent on B concentration and *I* concentration
  formation of $B_m I_n$ clusters postulated;
  experimental estimate: $m / n \sim 1.5$*

Approach:

Calculate clustering energies from first principles up to "max." *m*, *n*
Build kinetic Monte Carlo / continuum model from it

*S. Solmi *et al.*, J. Appl. Phys. **88**, 4547 (2000).

Previous Work - More Motivation

De la Rubia's group (LLNL) predicts with *ab intio* based kMC model* (up to $B_4 I_2$) a B "activation window" for annealing activation

*M. J. Caturla et al, APL **72**, (1998) p. 2736

However:

Experiment* finds ***no*** activation window, once activated stays activated.

*Mokhberi, Griffin, Plummer (Stanford).

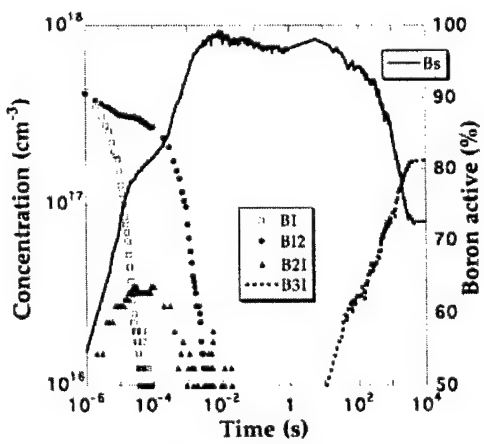

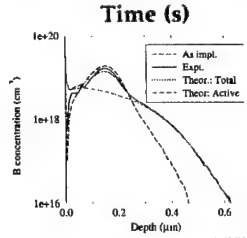

Calculation of the Clustering Energies

- DFT plane-wave code VASP (Technische Universität Wien), LDA and GGA
- Simulation cells of 64 atoms (converged ~7% vs. 216 atoms), E_{cut} = 230 eV, 4^3 k-points
- Relax many different, "guessed" initial structures for each cluster; dangerous, can miss groundstate!

B-I Cluster Structures from *Ab Initio* Calculations

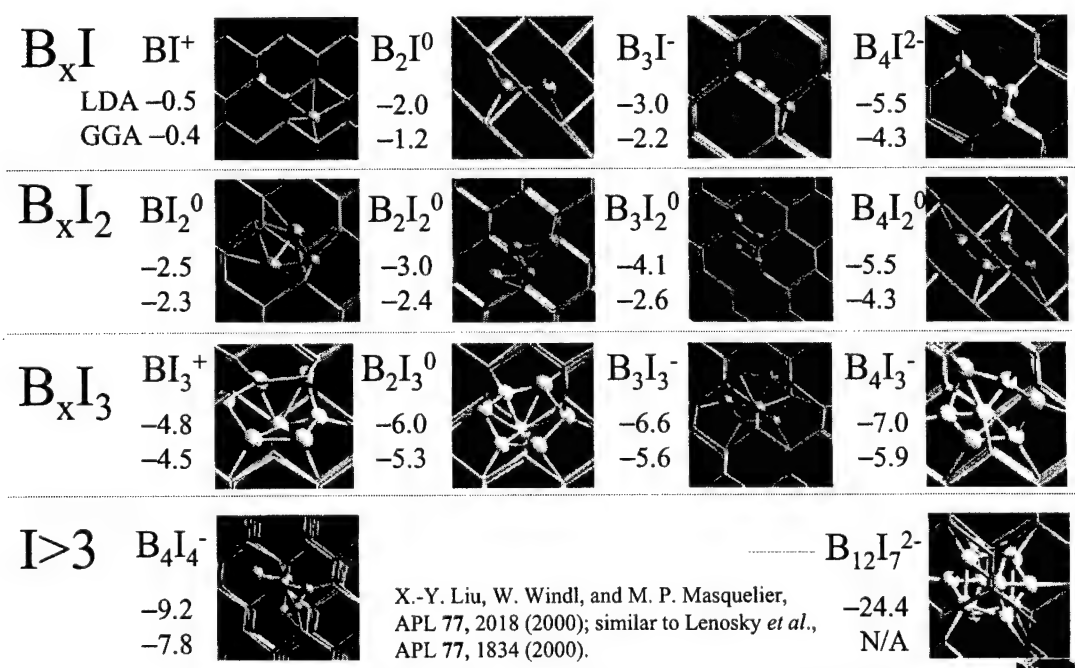

X.-Y. Liu, W. Windl, and M. P. Masquelier, APL **77**, 2018 (2000); similar to Lenosky *et al.*, APL **77**, 1834 (2000).

Influence of B Clustering on *I* Clustering!?

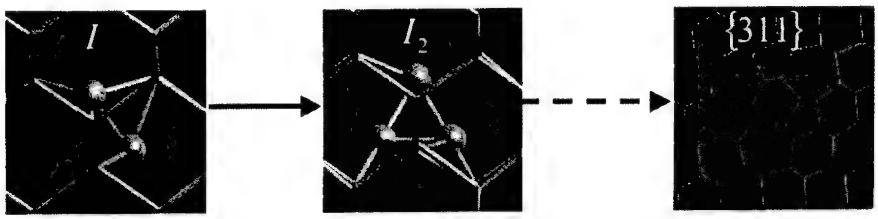

(e.g. Kim, Wilkins,... PRB 1997)

BI_3^+

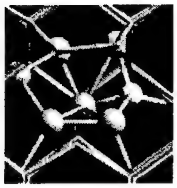

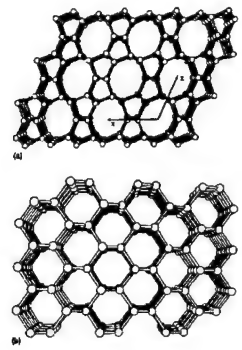

New ring structure for I_3:

- *Without B:* Ring ~ 0.2 eV higher than more compact I_3 structures.
- *With B:* Ring has lowest energies B promotes ring growth!?

"Silisils"

(Demkov, Windl, Sankey, PRB 1996)

B-I Clustering Reaction Paths & Binding Energies

(GGA values, in eV)

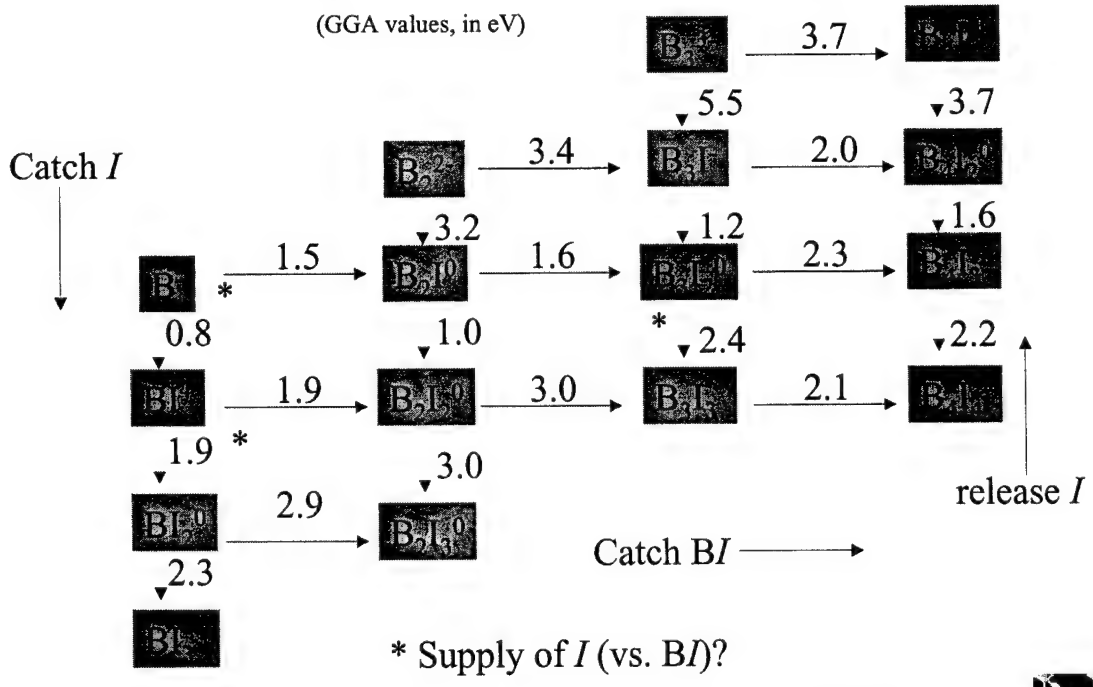

DFT Flavors: GGA and LDA

"real"

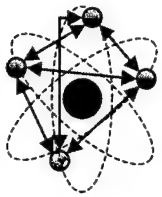

DFT

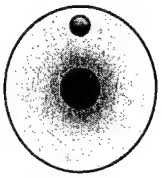

effective potential

$$E_{xc} = E_{real} - E_{eff}$$

For some cases, energetics differ considerably:

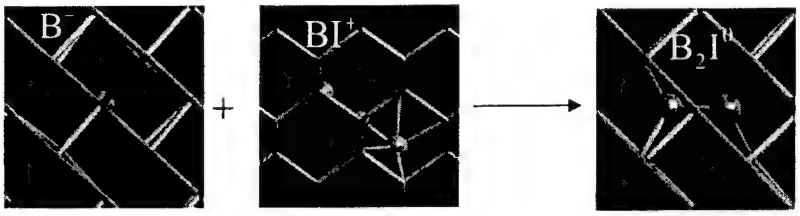

Reaction binding energy: 1.5 eV GGA

0.9 eV LDA.

Calibration with SIMS Measurements

- Continuum model recalibration of ab initio numbers necessary
- Genetic Algorithm:
  - Start with many random parameter sets within boundaries
  - Select pairs of parameter sets ("parents"), biased by χ^2
  - Mate parents (mix parameters randomly), add child to population
- Nearly all fitted parameters between LDA and GGA values

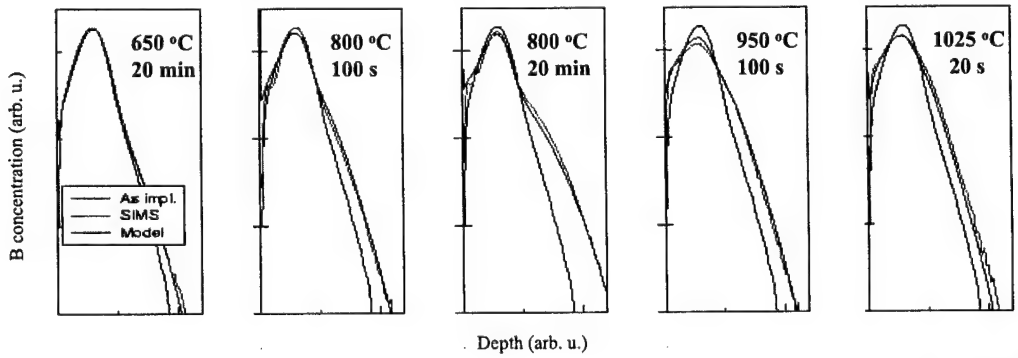

Activation Results

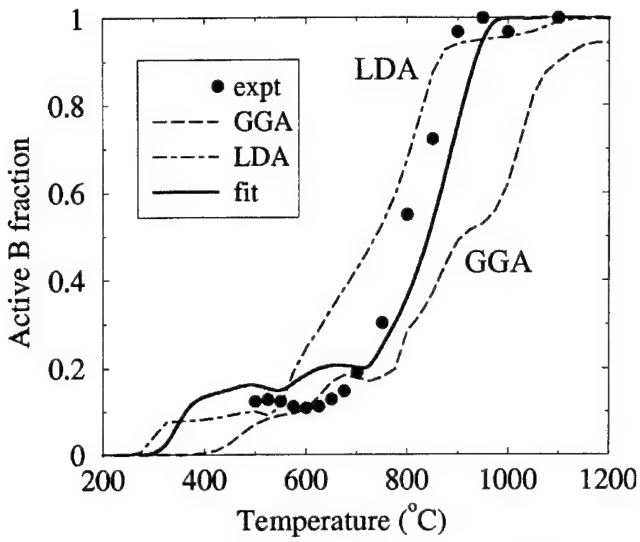

Expt: A. Mokhberi, P. B. Griffin, J. D. Plummer
fit from SIMS

- *No* activation window in agreement with expt.
- SIMS calibration leads to good prediction of activation model (hopefully) reasonably physical.
- Assume only B_s active

Activation and Clusters

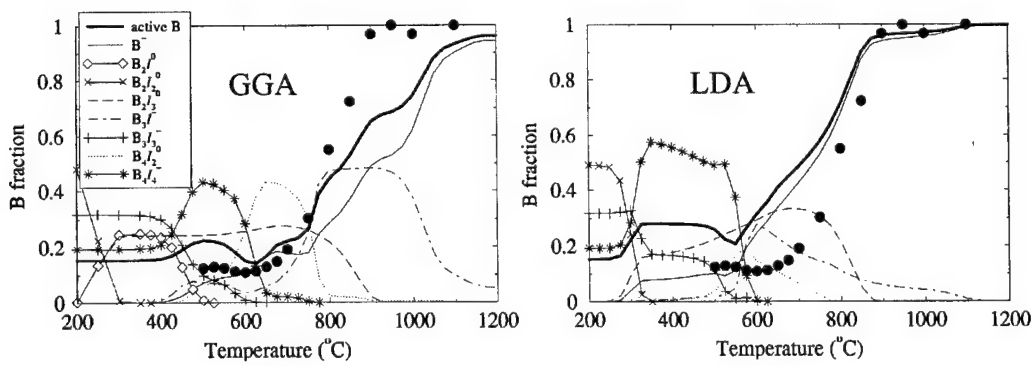

- LDA, GGA, fit do not give consistent clustering pattern:
- GGA: Dominated by B_3I^- cluster (also $B_2I_3^0$)
- LDA: Dominated by $B_2I_3^0$ cluster (also B_3I^-)
- Fit: Dominated by $B_4I_2^0$

Uniqueness of Clustering Model!?

"You can fit an elephant with 21 parameters."
(Ulrich Schröder)

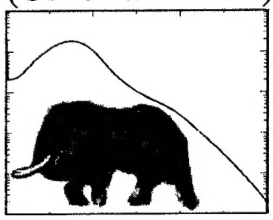

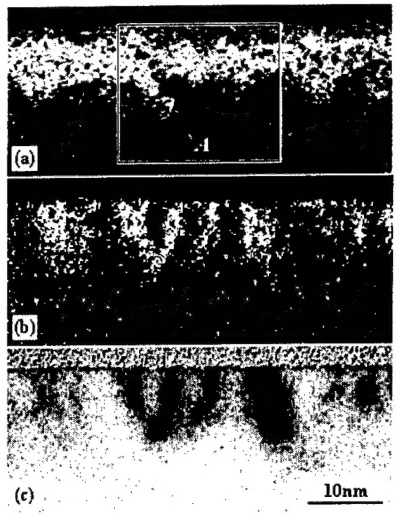

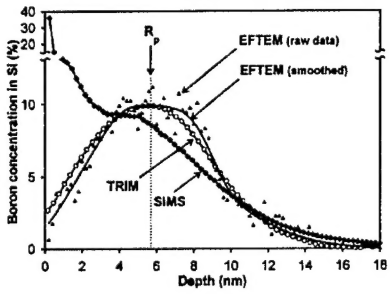

Energy filtered TEM B maps from (a) as-implanted (1 keV, 5e15 cm^{-3}) and (b) 900 °C annealed sample; (c) bright field image of (b). [Wang *et al.*, APL 77, 3586 (2000)].

Application: Well Tempered MOSFET (MIT)

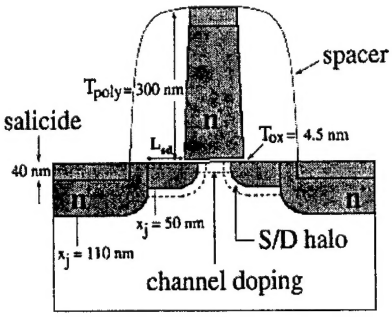

B profile

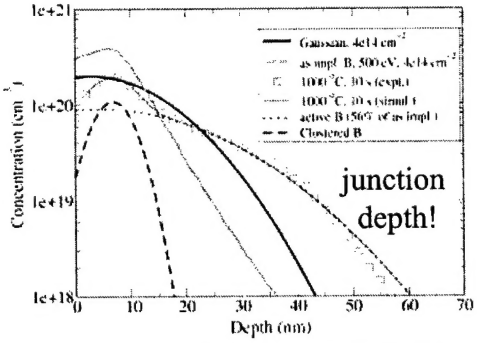

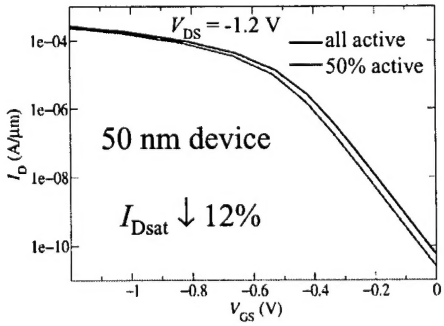

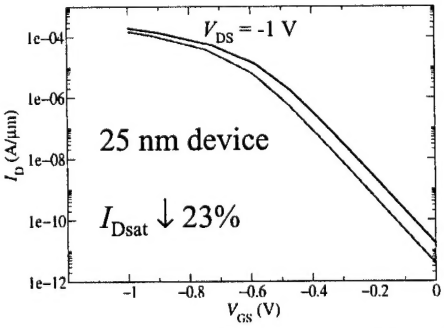

Cluster Energy and Band Structure

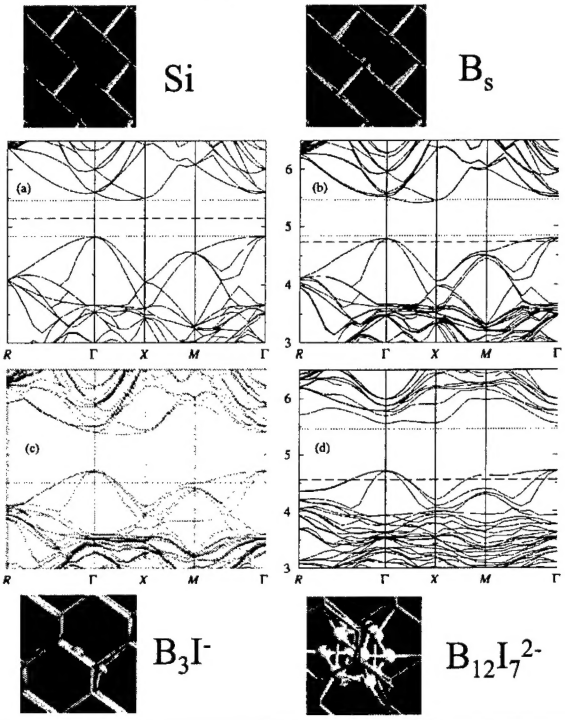

DFT gap too small (0.6 eV)

Cells too small (exciton wave function ~42 Å)

No defect states ⇔ more stable

Evidence of Stress Effect under Metal Gate

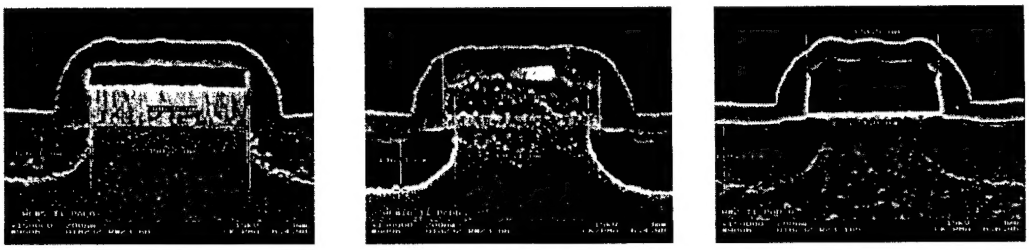

1000Å TiN/600Å poly-Si **250Å TiN/1300Å poly-Si** **Poly-Si**

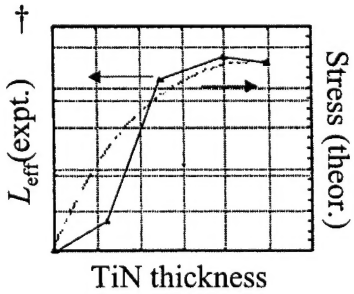

Experiments by Maiti *et al.*:*

- L_{eff} function of TiN thickness
- Stress estimate ~ L_{eff}
  Stress effect

*B. Maiti *et al.*, IEDM, Session 29, 1998.

†M. Laudon, N. N. Carlson, M. P. Masquelier, M. S. Daw, and W. Windl, APL**78** (2001).

Stress Dependence of Diffusivities

- Diffusivity: $D = D_0 \exp(-E/kT)$
- Under hydrostatic pressure: $E \rightarrow E + p\Delta V$

Perfect Si (or reference sys.): Create defect (B_s, I, V,...) ΔV:

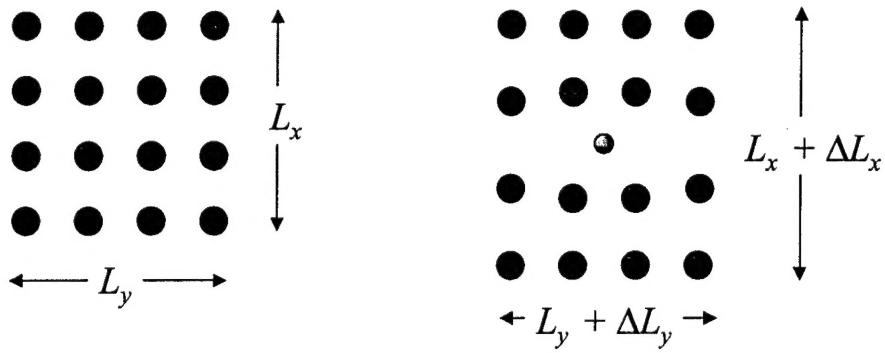

*M. S. Daw, W. Windl, N. N. Carlson, M. Laudon, and M. P. Masquelier (PRB July 2001).

Cell Volume and Charge in Si

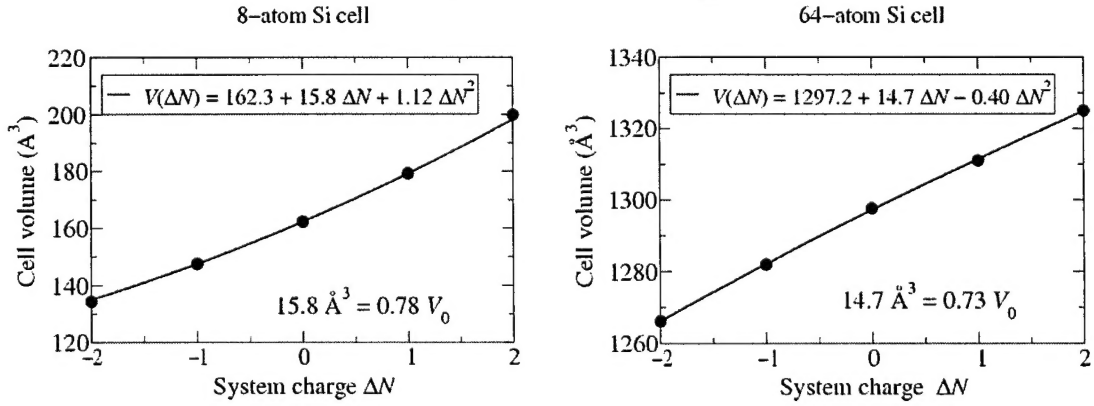

- For all defects, cell sizes, etc., every additional electron adds ~ 15 Å^3 to the volume
- Is this real or an artifact of the charged calculation?

Electron Volume and Maxwell Relations

- Maxwell relation: $\frac{\partial V}{\partial N} = \frac{\partial \mu}{\partial p}$ $\qquad E_F(p) = E_F(0) + V_e p$

- Pressure dependence of bands can be calculated in good agreement with experiment.

TABLE IV. First- and second-order coefficients describing the dependence of the direct band gap at Γ (E_0) under hydrostatic pressure [$E_0(P) = E_0 + aP + bP^2$] for Si, Ge, and GaAs. The experimental results are from Goñi, Syassen, and Cardona (Ref. 1).

	E_0		a (meV/GPa)		b (meV/GPa^2)	
Semiconductor	Theor.	Expt.	Theor.	Expt.	Theor.	Expt.
Si	3.273		100.8		0.05	
Ge	−0.084	0.795	125.4	121	0.2	0.2
GaAs	0.41	1.43	99.1	108	−0.1	−0.1

Alouani and Wills, PRB **54** (1996).

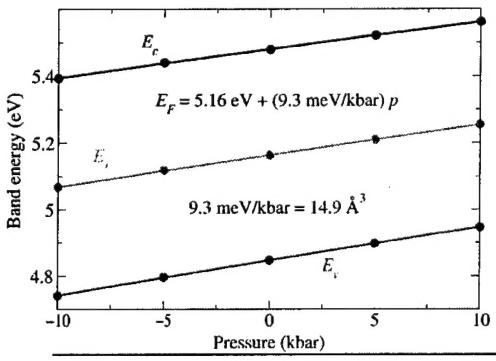

- We calculate again 15 Å^3 for the electron volume in Si

  seems to be real

- Ferry* ~ 5 nm (de Broglie).

*D. K. Ferry and H. L.Grubin, IEEE 1998.

Conclusions & Outlook

- Ab-initio methods are being used to provide predictive capability for dopant/defect profile evolution.

- With recalibration, boron clustering model can predict quantitatively activation and SIMS over a wide range of temperatures and annealing times.

- Dopant deactivation can easily be 50%; concentrations > 2e20 cm^{-3} not achievable. Deactivation can easily change I_{Dsat} by 10s of percents.

- TED can change junction depth substantially (factor 2 even at "good" annealing conditions) short channel effects; resistance.

- We calculate the volume of an electron in Si to be 15 Å^3.